DEVELOPING AN EVOLUTIONARY ROADMAP TO HIGH LIPID ACCUMULATING DIATOMS: A SYSTEMATIC APPRAISAL OF *AMPHORA SENSU LATO*

by

JOSHUA G STEPANEK

B.S., St. Cloud State University, 2008

M.S., St. Cloud State University, 2010

A thesis submitted to the

Faculty of the Graduate School of the

University of Colorado in partial fulfillment

Of the requirement for the degree of

Doctor of Philosophy

Department of Ecology and Evolutionary Biology

2016

This thesis entitled:

Developing an evolutionary roadmap to high lipid accumulating diatoms: a systematic appraisal of *Amphora sensu lato*

Written by Joshua G Stepanek

Has been approved for the Department of Ecology and Evolutionary Biology

Patrick Kociolek

Carrie Eckert

William Lewis

Andrew Martin

Steven Schmidt

Date_____

The final copy of this thesis has been examined by the signatories, and we find that both the content and the form meet acceptable presentation standards of scholarly work in the above mentioned discipline

Stepanek, Joshua G (Ph.D., Ecology and Evolutionary Biology)

Developing an evolutionary roadmap to high lipid accumulating diatoms: a systematic appraisal of *Amphora sensu lato*

Thesis directed by Professor Patrick Kociolek

Products derived from microalgal lipids have long been touted as an efficient and renewable alternative to the plant, animal and petroleum based products currently available. The great promise provided by algae as a biomass feedstock stems from their ubiquitous distribution, metabolic diversity, high productivity and ability to be grown on non-agricultural lands utilizing brackish and saltwater sources. Although promising, commercial production of algal products has not reached levels predicted by early investigators. Despite 40 years of algal biomass research, our basic understanding of the diversity and evolutionary history of these organisms remains in its infancy. If the great potential of algal derived products are to be realized, a biologically relevant approach to strain selection must be adopted. Presented here is a systematic investigation into the taxonomic, evolutionary and lipid accumulation diversity within the oleaginous diatom genus *Amphora sensu lato*. This is approached by first examining the taxonomic diversity of *Amphora* present within coastal and inland waters. From environmental collections made at these sites, a molecular phylogeny is produced to serve as the backbone for lipid accumulation experiments and comparisons. Based on the taxonomic and phylogenetic results, the *Halamphora* group within *Amphora sensu lato* was selected for a phylogenetically based appraisal of lipid production across cultured strains. This appraisal has demonstrated that ecological preference and cellular lipid accumulation within *Halamphora* exhibits a significant phylogenetic signal and therefore evolutionary relationships can be used as predictors of trait expression. The ecological and lipid data taken together with the taxonomic and phylogenetic data make for a predictive evolutionary based tool for the selection of high lipid accumulating lineages within *Halamphora* as well as laying the groundwork for future comparative research.

CONTENTS

SECTION III

LIPID ACCUMULATION WITHIN THE GENUS HALAMPHORA

TABLES

Table

FIGURES

Figure

CHAPTER I

INTRODUCTION

BIOFUELS FROM MICROALGAE

A great potential exists for the efficient and renewable production of algal lipid derived products. These include food and food supplements (Kay & Barton 1991, Barclay et al. 1994, Becker 2007), pharmaceuticals (Lincoln et al. 1990, Berg et al. 1999, Prestegard et al. 2009), fuels (Sheehan et al. 1998, Graham et al. 2012, Scholz & Liebezeit 2013) and other high value products (Jin et al. 2003, Singh & Gu 2010, Scranton et al. 2015). The advantage of algal sources over conventional petroleum, plant and animal based sources lies in microalgae's high per acre biomass productivity (Sheehan et al. 1998, Chisti 2007), ecological and metabolic diversity (Sheehan et al. 1998, Hildebrand et al. 2012) and the ability of many algal strains to dedicate a significant portion of their cellular volume to the storage of high value neutral lipids in the form of triacylglycerides (TAGs) (Sheehan et al. 1998, Chisti 2007, Graham et al. 2012, Hildebrand et al 2012, Scholz & Liebezeit 2013, Chtourou et al. 2015, d'Ippolito et al. 2015, Fields & Kociolek 2015).

Although the diversity of products from algal biomass sources is rapidly expanding (Bassi et al. 2014, Hudek et al. 2014, Scranton et al. 2015), the majority of algal biomass and lipid research over the last 40 years has centered on renewable sources of transportation fuel, collectively known as 'biofuels'. Biofuels as a whole are often touted as a promising alternative to fossil fuels as they are renewable, have a lower net release of greenhouse gases, and can be processed and burned in conventional infrastructure (Gavrilescu & Chisti 2005, Luque et al. 2010, Pienkos & Darzins 2009, Schenk et al. 2008, Scott et al. 2010). Because of this promise, first generation biofuels have been in commercial production for over 50 years (Chisti 2007). These fuels have largely taken the form of alcohols fermented from plant sugars and

cellulose or biodiesel produced from the transesterification of neutral lipids, especially TAGs, from oil seed crops, animal fats and used cooking oils (Chisti 2007, Luque et al. 2010, Nigam & Singh 2010). Biodiesel has been an especially appealing alternative to conventional diesel fuel as it is sulfur free, non-toxic, biodegradable and can be used in existing infrastructure with little or no modification (Sheehan et al. 1998, Demirbas 2009, Luque et al. 2010). Additionally, when combusted biodiesel exhaust has a fraction of the carcinogens of conventional diesel exhaust (Luque et al. 2008, 2010). Despite these advantages, the environmental and social concerns over first generation fuel crops have limited their impact as an alternative to fossil fuels (Luque et al. 2010, Nigam & Singh 2010).

Currently, bioethanol and biodiesel production are dominated by the widely cultivated food-crops corn and soybean (Chisti 2007), respectively, with the bioethanol crops sugarbeet and sugarcane, and the biodiesel crops canola, coconut and oil palm making up much of the remainder (Sheehan et al. 1998, Chisti 2007, Brennan & Owende 2010, Mata et al. 2010, Nigam & Singh 2010). Although currently in production, it has been well documented that even the highest producing terrestrial crop does not have the capacity to substantially displace fossil fuels at current or future usage levels (Table 1.1) (Chisti 2007, Brennan & Owende 2010, Mata et al. 2010) and an attempt to do so may have dire environmental and social implications (Luque et al. 2010, Nigam & Singh 2010).

Table 1.1. Potential yield and land area requirements for conventional and algal biofuel feedstocks to replace 50% of the U.S. transportation fuel needs (reproduced from Chisti 2007).

Feedstock	Potential yield (l/ha)	Land area required (M ha)	Percent of existing US cropland
Corn	172	1540	846
Soybean	446	594	326
Canola	1190	223	122
Jatropha	1892	140	77
Coconut	2689	99	54
Oil Palm	5950	45	24
Microalgae (30% oil PDW)	58,700	4.5	2.5
Microalgae (70% oil PDW)	136,900	2	1.1

Due to land and water use issues, as well as social concerns of the use of food crops for fuel production, attention has turned to microalgae as an alternative to first generation feedstocks (Sheehan et al. 1998). The advantages of microalgae as a fuel feedstock include per acre lipid productivity potential of 10–100 fold greater than conventional terrestrial crops (Table 1.1), they are a non-food based crop and can be grown in non-arable land utilizing brackish and salt waters (Sheehan et al. 1998, Dismukes et al. 2008, Groom et al. 2008, Pienkos & Darzins 2009). This becomes particularly important when considering that to replace 50% of our 2007 fuel requirements with the most productive terrestrial feedstock, oil palm, would require the utilization of nearly 25% of the current cropland in the United States, compared to the 1–3% potentially required by moderate and high lipid producing algae (Table 1.1).

Although promising, microalgae as a fuel crop have not yet achieved the theoretical yields predicted by early investigators (Weyer et al. 2009). Although research in design and engineering for algal growth and lipid extraction (Bajpai et al. 2014, Doucha & Lívanský 2014, Holland & Dragavon 2014) and the genetics and engineering of specific algal strains (Roessler et al. 1994, Dunahay et al. 1996, Rosenber et al. 2008, Beer et al. 2009, Radakovits et al. 2010, Cheng et al. 2014, Ma et al. 2014, Tanaka et al. 2015) continues to increase, basic biological research and screening has lagged behind (Sheehan et al. 1998, Pienkos & Darzins 2009, Brennan & Owende 2010, U.S. DOE 2010). Current biofuels literature continues to report a range of micro-algal cellular lipid levels of between 2 and 75 percent of the total dry weight of the cells (Chisti 2007, Huerliman et al. 2010, Singh et al. 2011, Fields & Kociolek 2015), demonstrating the variability between algal taxa. This variation is less surprising when one considers the evolutionary breadth encompassed by the common classification ‘algae’, which includes all aquatic chlorophyll-a containing organisms that are not ‘higher plants’. Put into perspective, ‘algae’ as previously defined spans two domains, 15 divisions, and 54 classes of life (Guiry 2012), each with distinct structure, physiologies and evolutionary histories. This diversity when combined with the observed variability in lipid production creates enormous challenges for the biofuels industry concerning taxon screening and selection.

The most extensive algal screening project undertaken was the United States Department of Energy (US DOE) aquatic species program (ASP). From 1978 to 1996 the US DOE's office of fuels development funded the ASP whose aim was "the development of transportation fuels from high-oil-producing algae" (Sheehan et al. 1998). Over the course of 18 years, the ASP collected and examined over 3000 strains of algae. These collections included taxa from the green algae (Chlorophyta), diatoms (Bacillariophyta), golden-brown algae (Chrysophyta), haptophyte algae (Haptophyta), and cyanobacteria (Cyanophyta). After the examination of these strains, the investigators concluded that diatoms were one of the best choices for continued biofuels research (Sheehan et al. 1998, p.248). This finding was based on their demonstrated high productivity (up to ca. 3 divisions per day), ability to grow in large-scale culture, and high cellular oil accumulation (accounting for 40-60% of the cell's mass in some taxa). Although small when compared to overall algal diversity, the research summarized in the ASP final report lays the groundwork for a focused biological and evolutionary approach to algal biofuels strain selection.

With general screening performed, one of the top recommendations of the ASP final report for future biofuels research was to "put less emphasis on outdoor field demonstrations and more on basic biology" (Sheehan et al. 1998, p. 20), a recommendation that was echoed in the US DOE national algal biofuels technology roadmap (U.S. DOE 2010). This lack of fundamental biological research has the potential to create profound inefficiencies in the utilization of these organisms. Since the publication of the ASP final report (Sheehan et al. 1998), although data has been reviewed and reprinted many times (Dismukes et al. 2008, Brennan & Owende 2010, Kumar et al. 2010, Hildebrand et al. 2012), only a small number of studies have generated new diatom lipid accumulation data (Garcia et al. 2000, Gatenby et al. 2003, Mansour et al 2005, de la Peña 2007, Rodolfi 2008, Griffiths & Harrison 2009, Chen 2012, Scholz & Liebezeit 2013, Fields & Kociolek 2015). With the exception of Fields and Kociolek (2015), who selected diatoms from across known evolutionary lineages, no study has approached their screening efforts systematically from either a taxonomic or evolutionary perspective.

Although limited screening continues, the current trend in biofuels research involves the investigation and genetic manipulation of a handful of well-studied strains (Beer et al. 2009, Radakovits

et al. 2010, Singh & Gu 2010, Cheng et al. 2014, Ma et al. 2014, Tanaka et al. 2015) in an attempt to engineer the best strain for universal production. An alternative approach, put forth in the ASP final report and others (Sheehan et al. 1998, Pienkos & Darzins 2009, Brennan & Owende 2010), contends that the most desirable algal strains are likely to be different for each growing site depending on the specific local growth conditions (temperature, salinity, pH, etc.) and therefore will require a suite of available taxa adapted to the specific conditions required. The most efficient approach to obtaining such a dataset is the systematic investigation of a group of known high lipid producing diatoms that are also found across a wide range of environments and habitats (Sheehan et al. 1998).

DIATOMS AS A LIPID FEEDSTOCK

Diatoms are a lineage of single celled and colony forming primary producers, within the Heterokont algae, found in virtually all aquatic habitats. Diatoms are characterized by their primary photosynthetic pigments chlorophyll's -*a* and -*c* acquired through a secondary endosymbiotic event with a red alga (Baurain et al. 2010) and the presence of an ornate silica cell wall termed a frustule, comprised of two interconnecting halves referred to as valves (Fig. 1.1). Diatoms are particularly important in the aquatic ecosystem as they potentially account for over 40% of all aquatic primary production (Werner 1977, Nelson et al. 1995) and are the preferred food source for many aquatic grazers (Werner 1977, Round et al. 1990).

Diatoms have received attention as a feedstock for biofuels production (Sheehan et al. 1998, Christi 2007, Graham et al. 2012, Scholz & Liebezeit 2013, Hildebrand et al. 2012, Fields & Kociolek 2015) due to their photosynthetic storage product consisting primarily of 16 and 20 carbon fatty acids (Orcutt & Patterson 1975, Mortensen et al. 1988) in the form of TAGs. In addition to high lipid accumulation, diatoms are extremely diverse taxonomically, with total extant diversity estimates at approximately 100,000 (Mann & Vanormelingen 2013). With this taxonomic diversity comes with a great deal of environmental and habitat diversity, with diatom communities found in abundance in aquatic environments ranging from freshwater to hyper saline from the tropics to the poles (Round et al. 1990) as

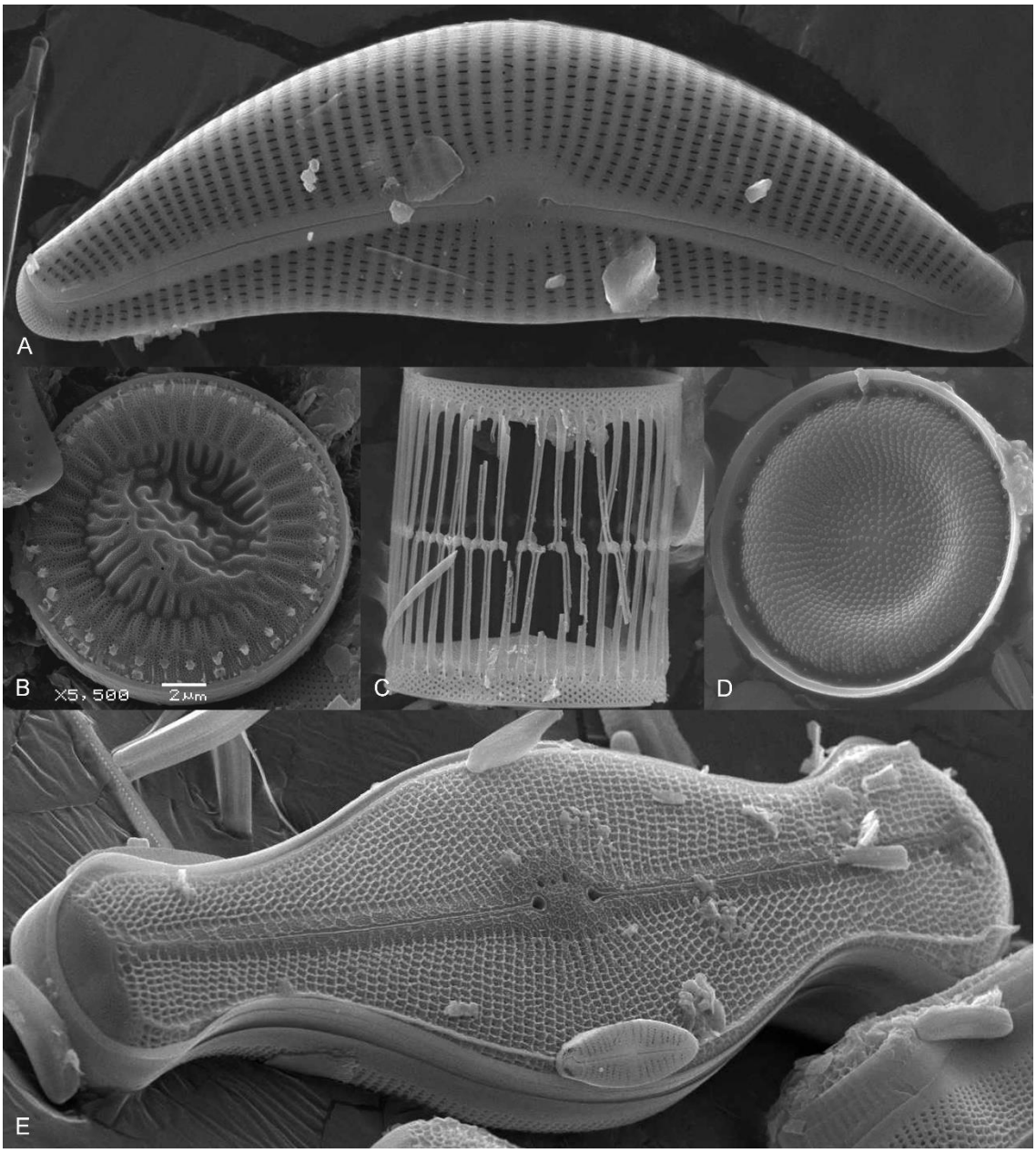

Figure 1.1. Scanning electron micrographs of diatom silica cell walls showing variation in shape and fine structure. **A.** Representative from the raphid diatom genus *Cymbella*. **B.** Representative from the centric genus *Cyclotella*. **C.** Representative from the centric genus *Skeletonema*. **D.** Representative from the centric genus *Stephanodiscus*. **E.** Representative from the raphid genus *Didymosphenia*.

well as moist soils (Van de Vijver & Beyens 1998), subaerial habitats (Lowe et al. 2014) and caves (Kociolek et al. 2013). In addition to this available diversity, diatoms photosynthetic efficiency in both high and low light environments (Wagner et al. 2006, Hildebrand et al. 2012), large nutrient storage vacuoles (Raven 1987), extremely efficient carbon fixation system (utilizing C3 and C4 pathways)

(Haimovich-Dayan et al. 2013) and a high efficiency form of the CO2 fixing enzyme Ribulose-1,5-bisphosphate carboxylase/oxygenase (RUBISCO) (Badger et al. 1998, Whitney et al. 2001) make them superior producers when compared to terrestrial plants and other algal groups.

Of the diatom taxa studied, members of the raphe bearing class of diatoms (raphid diatoms) have been shown to be well suited for continued lipid production research (Sheehan et al. 1998, Scholz & Liebezeit 2013, Fields & Kociolek 2015). In addition to standard screening efforts within the group, a recent phylogenetically based investigation into the lipid production of the major lineages within diatoms (Fields & Kociolek 2015) demonstrated that the raphid group, although understudied when compared to other lineages of diatoms, had a greater proportion of high lipid accumulating strains than other major lineages. These raphid diatoms represent a large (11 orders and 37 families, Round et al. 1990) monophyletic (Theriot et al. 2015) lineage that is primarily characterized by two longitudinally oriented slit-like openings through the frustule (Figs 1.2, 1.3) through which polymeric materials are extruded for attachment and locomotion (Drum & Hopkins 1966, Wustman et al. 1997).

Within the raphid diatoms, members of the genus *Amphora sensu lato* Ehrenberg ex Kützing have been shown to accumulate some of the highest levels of cellular oils (Orcutt & Patterson 1975, Sheehan et al. 1998, Chen 2012, Scholz & Liebezeit 2013) (Fig. 1.4), exhibit high productivity (Sheehan et al. 1998, Scholz & Liebezeit 2013) and are found in a wide range of conductivities from the arctic to the tropics (Patrick & Freese 1961, Hohn & Hellerman 1966, Stoermer & Yang 1971, Bérard-Therriault et al. 1986, Wachnicka & Gaiser 2007). Although *Amphora* taxa have been shown to exhibit favorable biofuel characteristics, significant hurdles remain before their utility as a largescale biomass feedstock can be realized.

One of these challenges is a generally poor understanding of the taxonomic diversity within the genus, a situation that is especially acute in understudied coastal and inland waters of the United States. This situation has persisted, in part, due to many of the widely distributed and commonly reported inland and marine taxa having been described throughout the 1800's (Agardh 1827, Kützing 1844, Rabenhorst

1864, Smith 1873, Cleve 1896, Peragallo & Peragallo 1897, Schmidt et al. 1874–1959). These early line drawings tended to be poor and the descriptions vague, leaving the majority of *Amphora* taxonomy

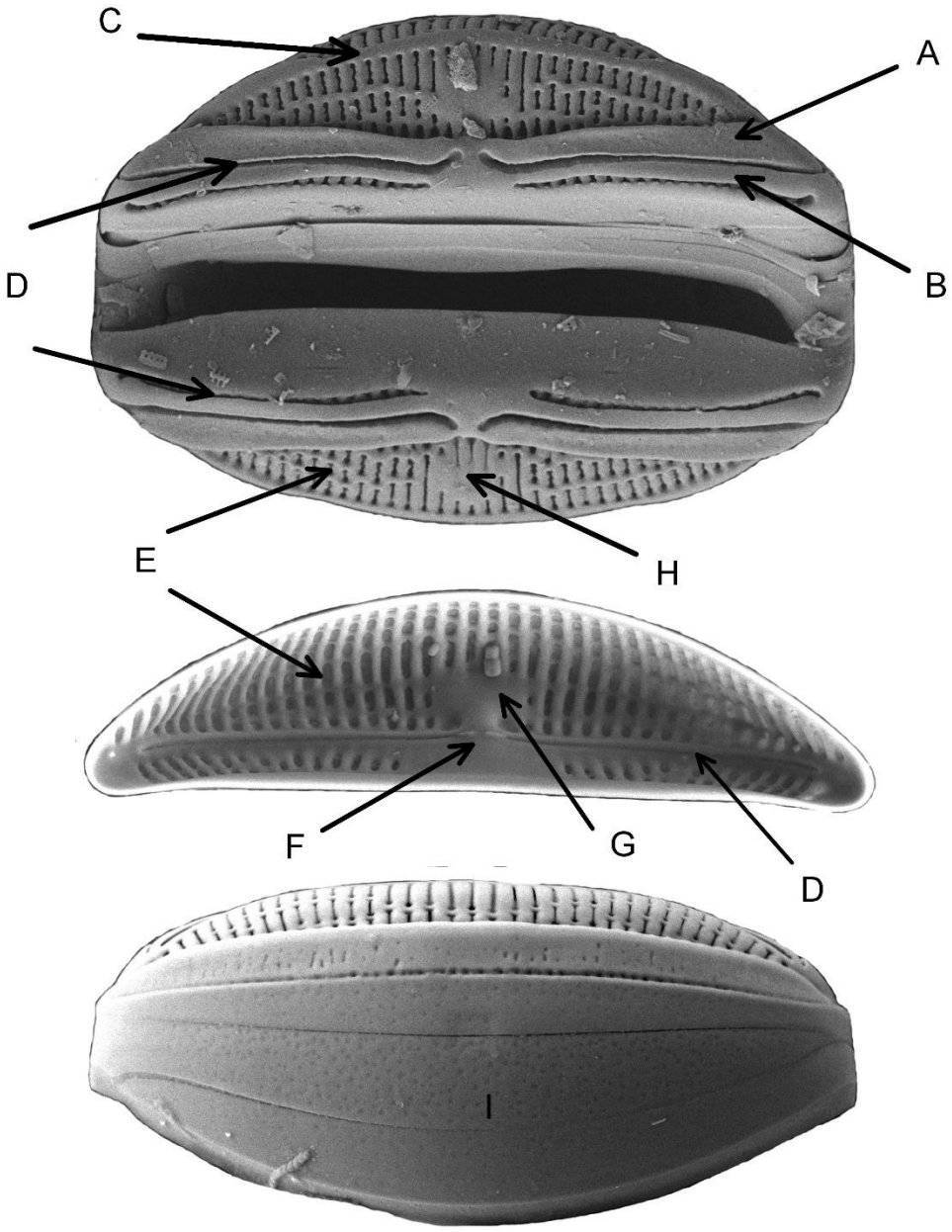

Figure 1.2. Explanation of common terminology associated with *Amphora* morphological features. Upper image: external view of whole frustule viewed from the valve side. Middle image: internal view of a single valve. Lower image: External view of a whole frustule viewed from the girdle side. **A.** Dorsal raphe ledge. **B.** Ventral raphe ledge. **C.** Dorsal marginal ridge. **D.** Raphe. **E.** Striae with areolae. **F.** Separate internal central helictoglossae. **G.** Internal semi-stauros. **H.** External central fascia. **I.** Girdle area with non-areolate girdle bands.

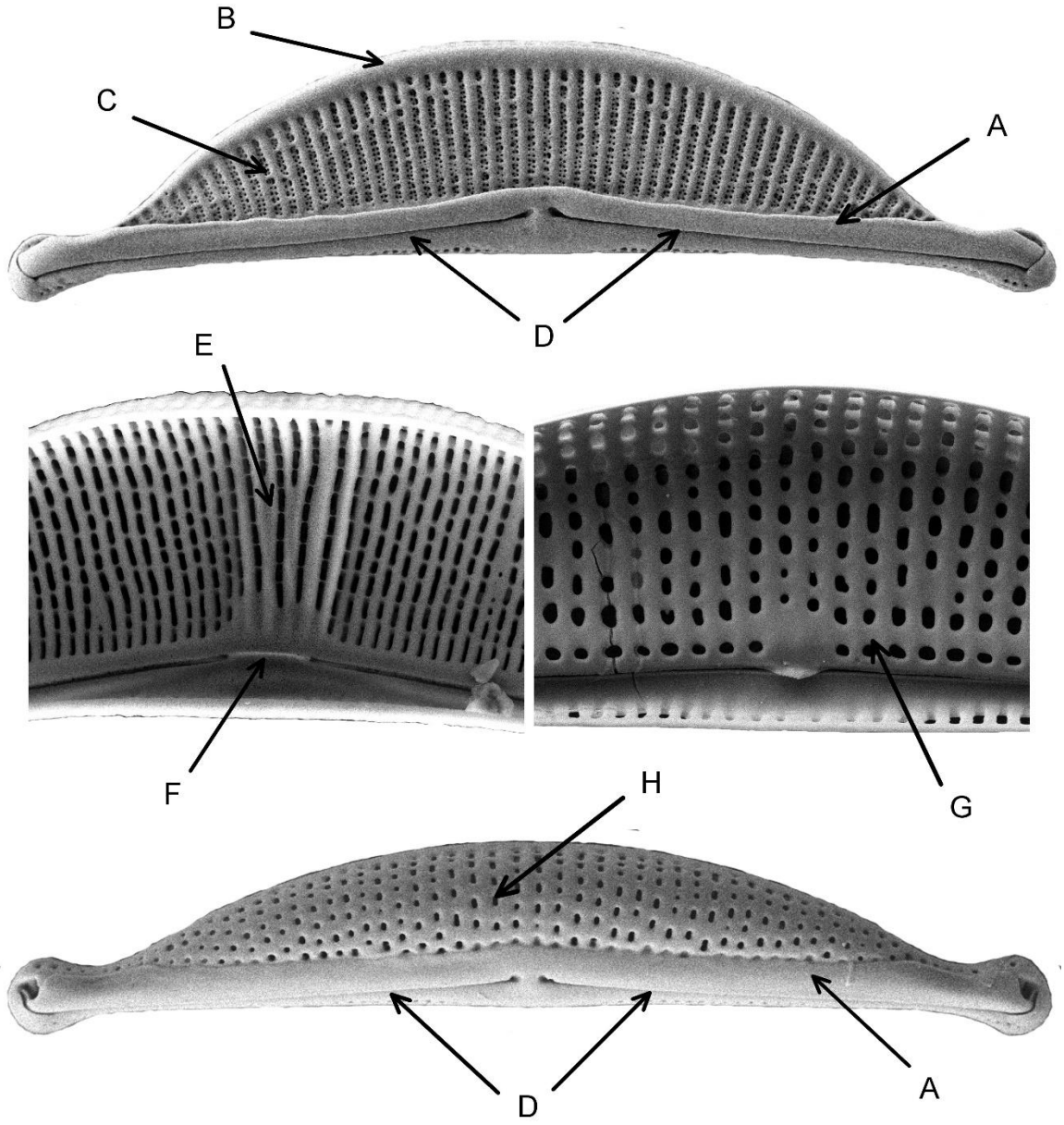

Figure 1.3. Explanation of common terminology associated with *Halamphora* morphological features. Upper image: external view of a single valve. Middle images: internal view of the central portions of single valves. Lower image: external view of a single valve. **A.** Dorsal raphe ledge. **B.** Dorsal marginal ridge. **C.** Biseriate striae. **D.** Raphe. **E.** Internal thickened central virgae. **F.** Internal fused central helictoglossae. **G.** Internal axial longitudinal line. **H.** Areolate striae.

largely relegated to a handful of commonly cited taxa. This condition persisted through the publishing of Patrick and Reimer's (1975) *Diatoms of the United States*, in what is still the last attempt at a freshwater *Amphora* flora of the United States.

Amphora taxonomy took a large step forward in the 1970s and 1980s with a number of important works utilizing the light and electron microscopy. Foremost among these were works by Schoeman and Archibald re-examining British museum type material across six *Amphora* subgenera (Schoeman & Archibald 1986a, b, c, 1987a, b, Schoeman et al. 1986). Along with this came studies focused on thorough taxonomic investigations of several of the most widely reported but poorly understood taxa, including *A. ovalis* (Lee & Round 1987), *A. copulata* (Lee & Round 1988), *A. pediculus* (Schoeman & Archibald 1978, Lee & Round 1989), *H. coffeaeformis* (Schoeman & Archibald 1984), *Halamphora montana* (Krasske) Levkov (Carter & Round 1993), *H. normanii* (Schoeman & Archibald 1978, Carter & Round 1993), and *H. veneta* (Schoeman & Archibald 1978). These studies along with several recent

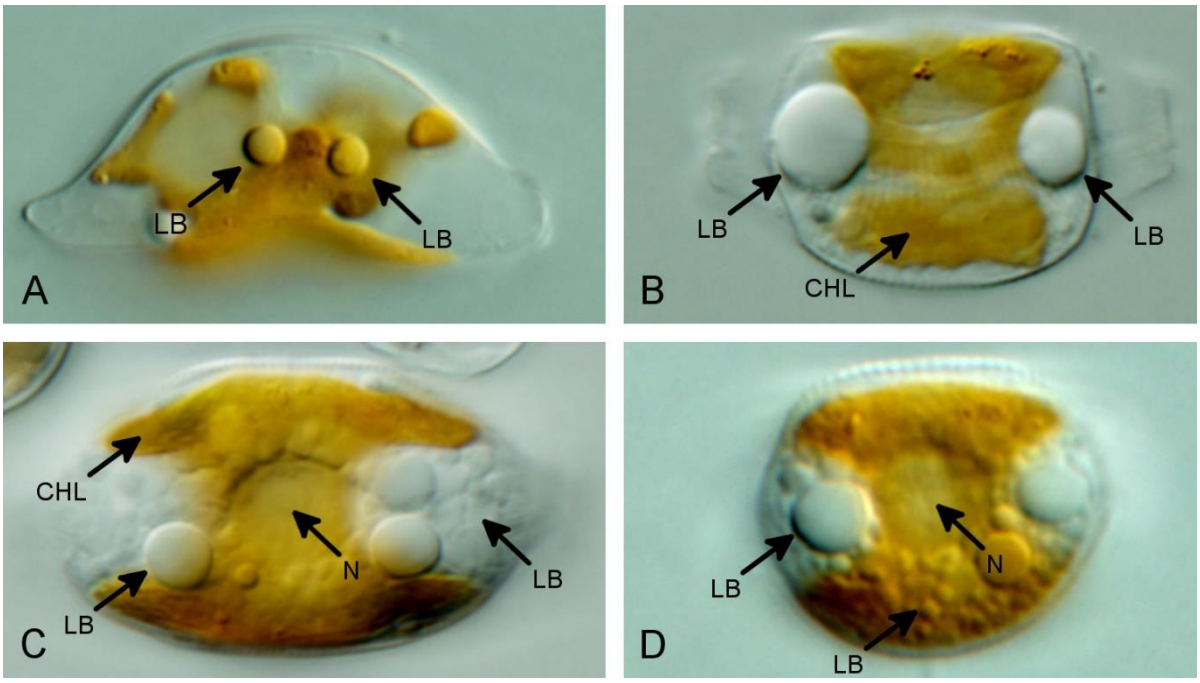

Figure 1.4. Light micrographs showing lipid accumulation in *Halamphora elongata* over four days of silica depravation. **A.** Day 1. **B.** Day 2. **C.** Day 3. **D.** Day 4. LB = Lipid bodies, CHL = Chloroplast, N = Nucleus.

investigations from Japan (Nagumo 2003), coastal Florida, USA (Wachnicka & Gaiser 2007) and Europe (Levkov 2009) have set the stage for a re-evaluation of the *Amphora s.l.* diversity present in coastal and inland waters of the United States.

As with the taxonomy of the group, *Amphora* systematics has been equally challenging. The genus, which was diagnosed by a distinct frustule asymmetry placing both valve faces on a single plane (Fig. 1.2), has for 120 years been plagued by questions as to the validity of this diagnostic feature and the monophyly of the group as a whole (Cleve 1895, Mereschkowsky 1903, Krammer 1980, Mann 1994). Through this time small taxonomic efforts have transferred taxa out of *Amphora* into new or existing genera (Paddock & Sims 1980, Mann in Round et al. 1990, Mann & Cox in Round et al. 1990, Williams & Reid 2006) with largest effort being Levkov's (2009) elevation of the *Amphora* subgenus *Halamphora* Cleve to generic status. Although transfers of taxa out of the genus *Amphora* are ongoing, there continues to be little or no understanding of the phylogenetic relationships within the genus or between the historical and newly created groups of amphoroid diatoms.

Added to this general lack of taxonomic and phylogenetic knowledge is that, of the over 700 currently described species of *Amphora s.l.*, only eight have been closely examined for growth and lipid production (Orcutt & Patterson 1975, Sheehan et al. 1998, Chen 2012, Scholz & Liebezeit 2013). Given the promise and challenges presented here, three areas of research must be addressed if the genus *Amphora* is to be successfully utilized as a biomass feedstock. First, the taxonomic diversity within the group must be understood. Second, the phylogeny of the group must be understood and issues concerning monophyly and relationships within the genus must be addressed. Third, a biologically and evolutionary relevant system must be developed for the selection of promising and well adapted strains.

The work presented here will address these three areas in the first integrated systematic approach for the evaluation of lipid production within a group of microalgae. Due to the broad scope of topics presented, this work will be divided into three sections. Section I will address the taxonomy of *Amphora s.l.* from waters of the United States and Japan. This was accomplished through the investigation of 1,010 environmental samples collected from coastal and inland waters of California, Colorado, Georgia,

Florida, Hawaii, Michigan, Nevada, North Carolina, North Dakota, South Carolina, Utah, USA and Japan from 2011–2015. This work represents the largest taxonomic effort undertaken for the genus *Amphora* in U.S. waters, and, although ongoing, has culminated in the description of 45 species as new to science. Section II will utilize cultured taxa from these environmental collections for a phylogenetic investigation of *Amphora s.l.* utilizing a multi-gene molecular phylogeny. This phylogeny will be used to address the monophyly of *Amphora s.l.*, the relationships between major morphological groups as well as taxon relationships within these groups. The phylogeny along with detailed morphological observations from Section I will be used to lay the groundwork for a new and stable systematic classification for the group. Section III will examine lipid accumulation across the monophyletic *Halamphora* group of amphoroid diatoms. This screening will take a biological and evolutionary approach to the evaluation of high lipid accumulating strains by proposing new biologically relevant lipid metrics as well taking a predictive, comparative phylogenetic approach to the discovery of high lipid accumulating lineages. These sections taken together will create the tools necessary for an evolutionary based roadmap to the high lipid accumulating lineages within the *Amphora s.l.* group *Halamphora*.

SECTION I

AMPHORA *AND* HALAMPHORA *TAXONOMY*

CHAPTER II

SEVERAL NEW SPECIES OF *AMPHORA* AND *HALAMPHORA* FROM THE WESTERN UNITED STATES

Adapted from: Stepanek, J.G. & Kociolek, J.P. 2013. Several new species of *Amphora* and *Halamphora* from the western USA. *Diatom Research* 28: 61–76.

ABSTRACT

Amphora Ehrenberg ex Kützing *sensu lato* incorporates a large and diverse group of diatoms. Although having its greatest taxonomic diversity in marine environments, inland waters of the United States appear to hold a large amount of undescribed taxa diversity requiring thorough taxonomic investigation. Presented here are descriptions and illustrations of seven new species collected from inland waters of the western United States, based on light and scanning electron microscope observations. Species described include *A. copulatoides*, *A. manifesta* and *A. waldeniana* from the genus *Amphora* subgenus *Amphora* and *H. coloradiana*, *H. latecostata*, *H. punctata* and *H. subtilis* from the genus *Halamphora* (Cleve) Levkov. This work represents the first steps in a larger taxonomic and systematic investigation into *Amphora sensu lato* from inland waters of the United States.

INTRODUCTION

Amphora Ehrenberg ex Kützing *sensu lato* is a large and widely distributed group of diatoms that generally has been agreed to represent a heterogeneous collection of taxa (Cleve 1895, Krammer 1980, Round et al. 1990, Mann 1994, Edlund & Stoermer 1999), currently classified within the order *Thalassiophysales* Mann. Although the genus *Amphora* has historically been grouped together by a strong asymmetry along the valvar plane, at the time of the generic description (Kützing 1844) the overall

structure of the *Amphora* frustule was not well understood. Smith (1873) was the first to elucidate and illustrate the asymmetric form of the *Amphora* frustule (Smith 1873, figs 1–9) and likened their asymmetry along valvar and apical planes to their being "exaggerated Cymbelleae" (Smith 1873). Although this asymmetry became the *de facto* characteristic uniting the group, Cleve (1895) warned that "the asymmetrical form is not a sufficient characteristic for a natural family, but is merely a facies, which may occur in groups of very different types and seem to depend on the method of growth". This concern appears to have been warranted as, with the addition of new data, taxa within *Amphora sensu lato* have been transferred to several other genera, including *Undatella* Paddock & Sims (1980), *Biremis* Mann & Cox (Round et al. 1990), *Seminavis* Mann (Round et al. 1990), *Eunophora* Vyverman, Sabbe & Mann (Vyverman et al. 1998), *Colliculoamphora* Williams & Reid (2006), and the recent elevation of the subgenus *Halamphora* Cleve to generic status (Levkov 2009).

The taxonomy of the genus *Amphora* has been equally difficult. Many of the widely distributed and commonly reported inland taxa were described in the early to mid-1800s, including *A. affinis* Kützing, *A. copulata* (Kützing) Schoeman & Archibald, *A. ovalis* (Kützing) Kützing, *A. pediculus* (Kützing) Grunow, *H. coffeaeformis* (Agardh) Levkov, *H. normanii* (Rabenhorst) Levkov and *H. veneta* (Kützing) Levkov. However, these early species illustrations tended to be poor and the descriptions vague. Later, comprehensive works covering the genus *Amphora* by Smith (1873), Schmidt et al. (1874–1959), Cleve (1895) and Peragallo & Peragallo (1897–1908) focused primarily on marine species, leaving freshwater taxa largely relegated to a handful of poorly described species. This condition largely persisted through Patrick & Reimer (1975), in what is still the last attempt at a freshwater flora of the genus *Amphora* for the United States.

The taxonomy of *Amphora* took a large step forward in the 1970s and 1980s with a number of important studies using electron microscopy. Foremost among these studies were the re-examination of British Museum type material across six *Amphora* subgenera by Schoeman & Archibald (1986a–c, 1987a,b) and Schoeman et al. (1986). Along with these came studies focusing on thorough taxonomic investigations of a number of widely reported but poorly understood taxa, e.g., *A. copulata* (Lee & Round

1988), *A. ovalis* (Lee & Round 1987), *A. pediculus* (Schoeman & Archibald 1978, Lee & Round 1989), *H. coffeaeformis* (Schoeman & Archibald 1984), *H. montana* (Krasske) Levkov (Carter & Round 1993), *H. normanii* (Schoeman & Archibald 1978, Carter & Round 1993) and *H. veneta* (Schoeman & Archibald 1978).

Recent investigations from Japan (Nagumo 2003), coastal Florida, USA (Wachnicka & Gaiser 2007), coastal St. Lawrence Estuary, eastern Canada (Bérard-Therriault et al. 1986) and Europe (Levkov 2009) have greatly expanded and refined our taxonomic understanding of the group, but thorough investigation from inland waters continues to be lacking for USA. At present only 14 extant *Amphora* and *Halamphora* taxa have been described from the inland waters of the continental USA (Kociolek 2006, Fourtanier & Kociolek 2011). With the exception of four taxa described by Levkov (2009), the entirety of the new species literature from inland waters in the USA is comprised of five studies from 1975 or earlier (Thomas & Chase 1886, Hohn 1961, Hohn & Hellerman 1963, Stoermer & Yang 1971, Patrick & Reimer 1975), with more than half of the taxa described from Lake Michigan and surrounding waters (Stoermer & Yang 1971).

There is a general understanding that *Amphora sensu lato* is predominantly a marine genus with a few freshwater representatives (Lee & Round 1987, Round et al. 1990). While it certainly cannot be argued that the majority of currently described taxa are from marine or brackish water environments, this assertion and a certain degree of taxonomic ambiguity has probably led to an under-representation of the freshwater diversity of this genus. Complicating matters further is the difficulty in drawing clear distinctions between freshwater and marine taxa, an issue that is likely to become more difficult as our understanding of the diversity and distribution of the group continues to grow. *Amphora* has been reported from a wide range of conductivities from coastal (Hohn & Hellerman 1966, Riznyk 1973, Wachnicka & Gaiser 2007) to inland waters (Fritz & Battarbee 1988, Fritz 1990, Blinn 1993), creating difficulty in where to draw the line between freshwater, brackish and marine taxa.

Recently, Levkov (2009) described 79 new taxa from the genera *Amphora* and *Halamphora*, 63 of which were collected from freshwater environments. With this in mind, a closer look at the freshwater

flora of *Amphora sensu lato* for the USA seems warranted. Presented here are descriptions and illustrations of three new species from the genus *Amphora sensu stricto* and four from the genus *Halamphora*, collected from inland waters of California and Colorado, and based on light and scanning electron microscopy. The taxa presented here represent a preliminary effort toward a larger taxonomic and systematic investigation into *Amphora sensu lato* of the United States.

MATERIALS AND METHODS

Materials examined were collected for the Southern California Coastal Water Research Project (SCCWRP) from 2004–2008 (www.sccwrp.org), the United States Environmental Protection Agency's (US EPA) National Lakes Assessment (NLA) from California in 2007, as well as recent Colorado collections. All materials are permanently held in the University of Colorado, Museum of Natural History Diatom Herbarium, Boulder, Colorado.

Type locations in California include three streams, Adobe Creek, Agua Hedionda Creek and San Diego Creek located in Southern California between Los Angeles and San Diego, and Vasona Reservoir located ca. 20 km south of the San Francisco Bay area of Central California. The Adobe Creek sampling site is located ca. 30 km upstream from the Pacific coast at an elevation of 553 m above sea level, and it has a mean depth of 7.25 cm and a mean discharge of 0.00210 $m^3 s^{-1}$. Agua Hedionda Creek is a small coastal stream that drains into the tidal influenced Agua Hedionda Lagoon in San Diego County, California. The Agua Hedionda Creek sampling site is located ca. 9 km upstream from the lagoon at an elevation of 90 m above sea level, and it has a mean depth of 16 cm and a mean discharge of 0.00788 $m^3 s^{-1}$. San Diego Creek is located in a residential area southeast of Los Angeles in Orange County, California and drains to the Pacific Ocean via Newport Bay. The San Diego Creek sampling site is ca. 12 km upstream from the Pacific coast at an elevation of 16 m above sea level, and it has a mean depth of 4.5 cm and a mean discharge of 0.0508 $m^3 s^{-1}$. All California stream sampling was performed in November 2008. Depth, stream flow, conductivity and pH measurements were obtained from SCCWRP, averaging across four sampling events from fall 2007 through summer 2008. The Vasona Reservoir has a surface

area of 1.6 km^2 and is located in Santa Clara County ca. 20 km south of the southern extent of the San Francisco Bay and ca. 30 km inland from the Pacific coast. Surface sediments were collected by the US EPA in July 2007 as part of the EPA NLA program. Conductivity and pH values were measured by the EPA at the time of collection. These measurements as well as additional chemical and site information for the EPA NLA lake sites are publically available at http://water.epa.gov/type/lakes/NLA_data.cfm.

Type locations in Colorado include two ponds, Bass Pond and Cottonwood Marsh, in a series of reclaimed gravel pits, now part of Walden Ponds Wildlife Habitat, Boulder County. Sediment samples were collected from Bass Pond in September 2010. The Cottonwood Marsh collection consisted of near shore epiphytes sampled in January 2011. Conductivity and pH measurements for the Colorado collections were made near shore using a YSI 556 multi-probe (YSI Incorporated, Yellow Springs, Ohio) at the time of sampling. All materials examined, along with locality, conductivity and pH data are presented in Table 2.1.

Materials were cleaned of organic matter by boiling it in nitric acid followed by repeated rinses with distilled water until neutral pH was reached. Cleaned material was permanently mounted in Naphrax® for light microscope (LM) observations. Permanent slides were examined using an Olympus BX-51 LM (Olympus America Inc., Center Valley, Pennsylvania) and images were taken using an Olympus DP 71 digital camera. For scanning electron microscope (SEM) observations, cleaned material was air-dried onto glass coverslips, sputter coated with 1 nm gold using a Cressington 108 sputter coater (Cressington Scientific Instruments Ltd., Watford, UK) and examined using a JEOL JSM 6480LV low vacuum SEM (JEOL Ltd., Tokyo, Japan) at an acceleration voltage of 15 kV and a JEOL JSM 7401 field emission SEM (JEOL Ltd., Tokyo, Japan) at an acceleration voltage of 5 kV. The terminology of the valve ultrastructure associated with *Amphora* and *Halamphora* follows that of Nagumo (2003) and Levkov (2009).

Table 2.1. List of diatom material examined including habitat, geographical coordinates, pH and conductivity measurements. ANSP: Academy of Natural Sciences, Philadelphia, COLO: Kociolek Collection at University of Colorado Museum of Natural History, CA: California, CO: Colorado, MN: Minnesota, TX: Texas, n.d.: no data.

Accession number	Habitat	Latitude North	Longitude West	pH	Conductivity ($\mu S\ cm^{-1}$)
ANSP GC 64903	Adobe Creek, Riverside County, CA	33.51272°	117.27038°	7.10	376–504
ANSP GC 64904	Adobe Creek, Riverside County, CA	33.51272°	117.27038°	7.10	376–504
ANSP GC 64900	Agua Hedionda Creek, San Diego County, CA	33.15013°	117.24843°	7.55	2227–2400
ANSP GC 64899	Bass Pond, Boulder County, CO	40.04527°	105.18882°	7.89	409
ANSP GC 64905	Cottonwood Marsh, Boulder County, CO	40.00342°	105.25104°	8.91	1235
COLO JPK 8357	Lake Itasca, Clearwater County, MN	47.21706°	95.207623°	n.d.	n.d.
COLO JPK 2834	Rattlesnake Creek, Santa Barbara County, CA	34.45701°	119.69357°	7.78	832–1205
ANSP GC 6560a	Sabine River, Orange County, TX	n.d.	n.d.	n.d.	n.d.
ANSP GC 64902	San Diego Creek, Orange County, CA	33.68637°	117.81625°	8.10	1978–2467
ANSP GC 64901	Vasona Reservoir, Santa Clara County, CA	37.24531°	121.96623°	8.56	361

RESULTS

Amphora waldeniana Stepanek & Kociolek sp. nov. (Figs 2.1, 2.2)

Description: Valves are semi-elliptical with the dorsal margin smoothly rounded near the apices, becoming straight over the central portion of the valve. The ventral margin is straight and deflected ventrally near the apices. Valve length 27–45 µm, valve breadth 6.5–7.0 µm. Valve ends are narrowly rounded and deflected ventrally. The raphe is biarcuate and positioned centrally along the valve. The proximal raphe ends are deflected dorsally. The axial area is narrow throughout. Dorsal and ventral fasciae are present, with the ventral fascia somewhat wider. The dorsal fascia is elliptical. A row of short

striae often separate the dorsal fascia from the axial area, although this feature appears somewhat variable. The dorsal striae are parallel near the valve center, becoming radiate at the apices, 12–13 in 10 µm. They are composed of two rows of ovoid areolae, becoming a single areola near the apices. The ventral striae are radiate near the valve center, becoming convergent near the apices. The radiate ventral striae are composed of a single areola, while the convergent striae are composed of two smaller areolae. A prominent, hyaline area is present between the ventral striae and the ventral margin.

In SEM, the raphe is biarcuate with proximal and distal ends deflected dorsally. The raphe ledge is well-developed consisting of a thin siliceous flap. The ledge is continuous along the dorsal side of the axial area nearly completely covering the first row of dorsal areolae. The ventral ledge is intermittent, most prominent near the apices. The dorsal and ventral areolae are opened externally by distinctive narrow slit-like openings dilated at both ends and covered internally by a sieve membrane. A dorsal marginal ridge is distinct externally.

Holotype: Slide and material ANSP GC 64899, Academy of Natural Sciences, Philadelphia, USA. Holotype specimen illustrated in Fig. 2.1B.

Isotype: Slide and material JPK 8358, Kociolek collection at the University of Colorado Museum of Natural History, Boulder, USA.

Type locality: Bass Pond (40.04527°N, 105.18882°W), shoreline benthic sample, Walden Ponds Wildlife Habitat, Boulder County, Colorado, USA. Collected by J.G. Stepanek, January 2011.

Taxonomic remarks: *Amphora waldeniana* resembles the widespread freshwater taxa *A. copulata* and *A. affinis*, sharing a biarcuate raphe, a clear dorsal fascia and dorsal striae composed of 2–3 rows of elongate areolae. However, it can be distinguished from both taxa in LM by a more linear valve outline, a centrally positioned raphe and ventral striae composed of a single areola near the valve center and two areolae near

the poles. This ventral stria pattern contrasts with the ventral uni- and biareolate striation present throughout the valve in *A. copulata* and *A. affinis*, respectively. In SEM, *A. waldeniana* is distinguished by the narrow slit-like external areola coverings and the continuous dorsal raphe ledge running uninterrupted the length of the valve.

Other taxa with similar ventral striae include *A. affinis* var. *sabiniana* Levkov described from the Sabine River, Texas, *A. birnirkiana* Patrick & Freese described from an Alaskan lagoon and *A. crawfordii* Levkov described from Lake Ohrid, Macedonia. *Amphora waldeniana* is distinguished from *A. affinis* var. *sabiniana* by its linear outline through the central portion of the valve and a prominent hyaline area between the ventral striae and valve margin. In Levkov's (2009, pl. 70, figs 13–21) illustration of *A. affinis* var. *sabiniana*, specimens shown in figs 13 and 16 appear to exhibit a more linear valve outline resembling *A. waldeniana*; additional investigation is necessary to determine if these specimens represent variation within the species or a separate taxon. The description of the illustrated holotype specimen of *A. affinis* var. *sabiniana* (Levkov 2009, pl. 70, fig. 15) was used for comparison with *A. waldeniana*. *Amphora waldeniana* can be distinguished from *A. birnirkiana* by the presence of a clear dorsal fascia. It can also be distinguished from *A. crawfordii* by its relatively narrow valves and the lack of a wide ventral axial area (Levkov 2009, pl. 35, figs 1–6).

Amphora waldeniana resembles *A. cruciferoides* Stoermer & Yang described from Lake Michigan in having linear valves and to some extent the appearance of the ventral striae. *Amphora waldeniana* is distinguished from *A. cruciferoides* by its more narrow valves (6.5–7.0 µm), finer striation and dorsal striae composed of two rows of elongate areolae. *Amphora waldeniana* resembles another new species, *A. copulatoides* Stepanek & Kociolek described below, sharing ventral striae changing from uni- to biareolate. *Amphora waldeniana* is distinguished by its more linear valve shape with straight ventral margin, and the prominent unornamented area between the ventral striae and ventral margin.

Distribution: Known only from Bass Pond and surrounding ponds within the Walden Ponds Wildlife Habitat, Boulder County, Colorado, USA.

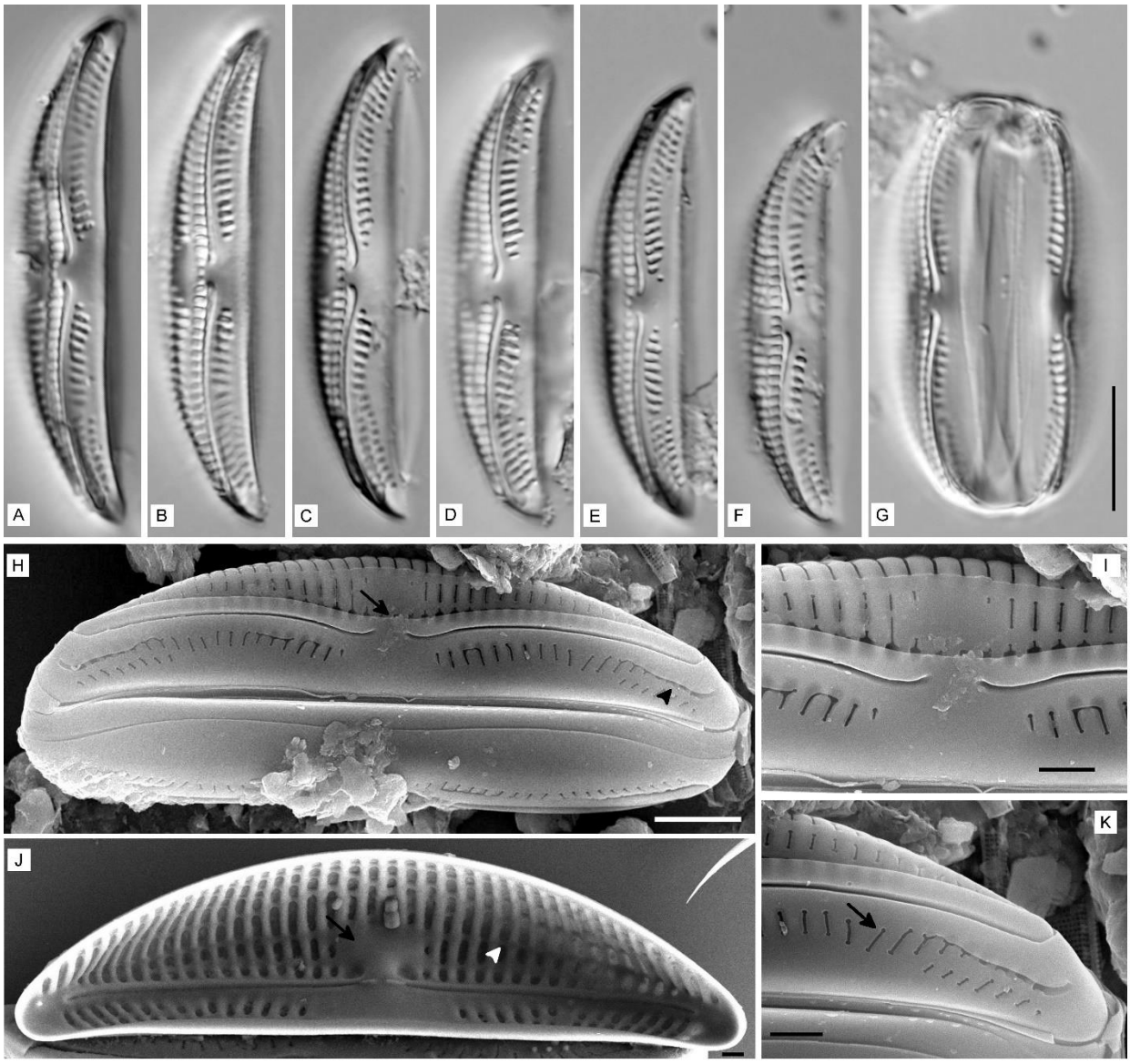

Figure 2.1. Type material of *Amphora waldeniana* from Bass Pond, Boulder County, Colorado, USA, LM (A–G) and SEM (H–K). **A–G.** Single valves showing size range. **B.** Holotype specimen. **G.** Whole frustule. **H.** External view of whole frustule showing biarcuate raphe with continuous dorsal raphe ledge (arrow) and ventral raphe ledge intermittent and most prominent near the apices (arrowhead). **I.** Internal view of whole valve, note thickened dorsal fascia (arrow) and intercostal ribs breaking striae into rows of oblong areolae (arrowhead). **J.** External view of valve center showing a siliceous ridge near the dorsal valve margin and the first row of dorsal areolae obscured by the dorsal raphe ledge. **K.** External view of apex showing dorsal and ventral raphe ledges, and narrow slit-like areola openings (arrow). Scale bars = 10 µm (A–G), 5 µm (H), 2 µm (J, K), 1 µm (I).

Amphora copulatoides Stepanek & Kociolek sp. nov. (Fig. 2.2)

Description: Valves are semi-elliptical, moderately dorsiventral with a smoothly rounded dorsal margin and a slightly concave ventral margin. The ventral margin is often tumid near the valve center in large specimens. Valve length 27–45 µm, valve breadth 5.0–7.5 µm. Apices are narrowly rounded. The raphe is biarcuate, with the proximal raphe ends slightly deflected dorsally. The axial area is narrow throughout. Dorsal and ventral fasciae are present. The dorsal fascia is ovoid to rectangular, the presence or absence of a row of short striae along the axial and marginal edges of the fascia appears variable. The ventral fascia is typically wider than the dorsal fascia. The dorsal striae are composed of two rows of areolae, parallel to slightly radiate near the valve center, becoming more radiate near the apices, 12–13 in 10 µm. The ventral striae are radiate near the valve center becoming convergent near the apices. The ventral striae are composed of single elongate areolae near the valve center, changing to two small round areolae per stria near the apices.

In SEM, the raphe is biarcuate with the proximal and distal ends weakly and strongly deflected toward the dorsal valve margin, respectively. The raphe ledge is prominent on the dorsal side of the axial area, nearly completely covering the first row of areolae although not continuing through the fascia. The ventral raphe ledge is only evident near the poles. A distinct marginal ridge separates the valve face from the dorsal mantle. The dorsal areolae are opened externally by a narrow elongate slit with dilated ends and covered internally by a sieve membrane. The ventral striae abruptly change from a single areola in the radiate striae to two small circular areolae in the convergent striae.

Holotype: Slide and material ANSP GC 64900, Academy of Natural Sciences, Philadelphia, USA. Holotype specimen illustrated in Fig. 2.2A.

Isotype: Slide and material JPK 8359, Kociolek collection at the University of Colorado, Museum of Natural History, Boulder, USA.

Type locality: Agua Hedionda Creek (33.15013°N, 117.24843°W), rock scrape, San Diego County, California, USA. Collected by J.P. Kociolek, November 2008.

Taxonomic remarks: This taxon can be distinguished from others in the *A. copulata–affinis* group by the ventral striae changing from uni- to biareolate, whereas one and two rows of areolae forming the ventral striae characterize *A. copulata* and *A. affinis*, respectively. In SEM, *A. copulatoides* is distinguished by the narrow slit-like openings of the dorsal and ventral areolae. The valve outline and ventral striae of *A. birnirkiana* are similar to *A. copulatoides*, but the latter has a clear dorsal fascia which is absent in *A. birnirkiana*. *Amphora copulatoides* also differs from *A. affinis* var. *sabiniana* by having straight to tumid ventral margin and uni- to biareolate ventral striae.

Distribution: Present in Agua Hedionda Creek, San Diego County and San Diego Creek, Orange County, California.

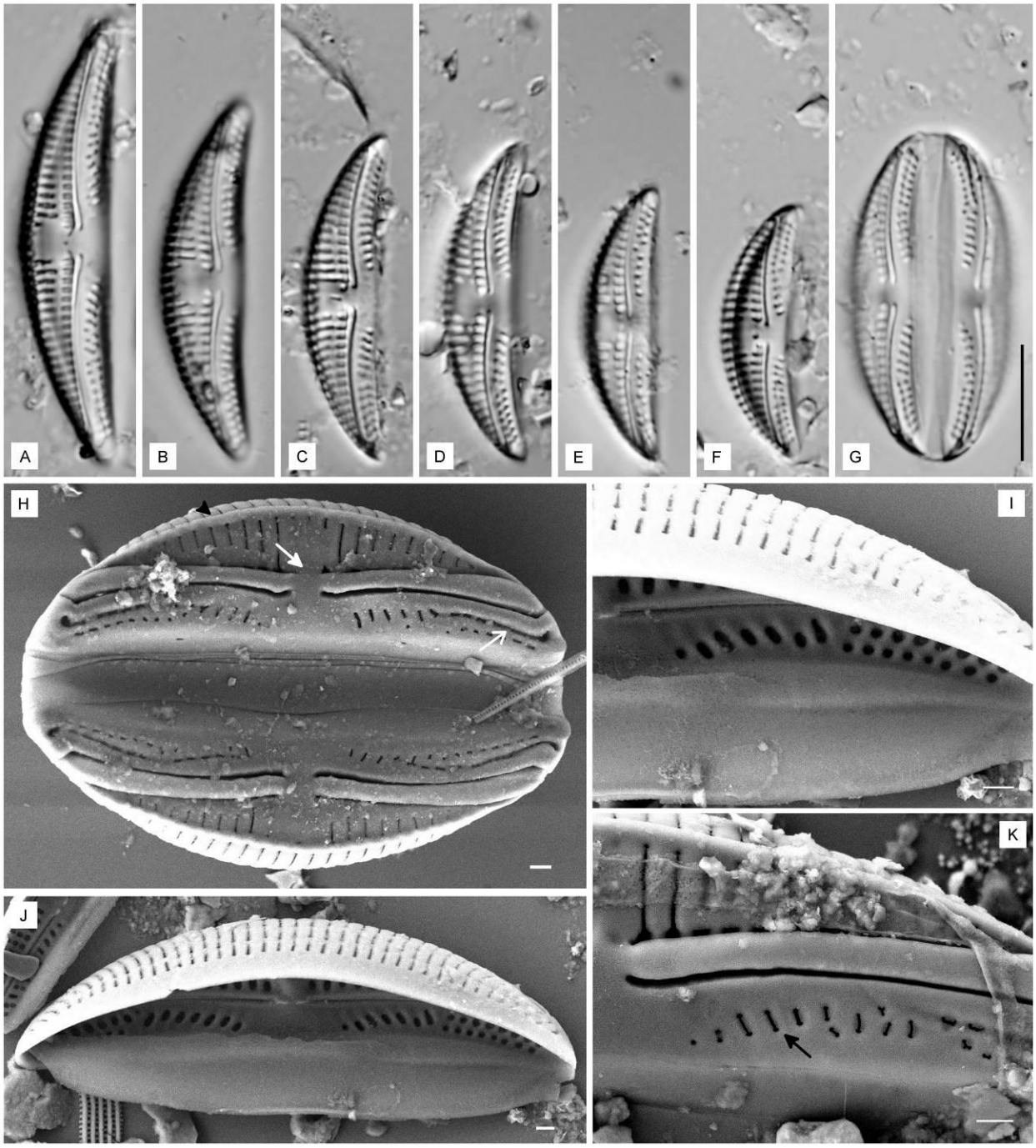

Figure 2.2. Type material of *Amphora copulatoides* from Agua Hedionda Creek, San Diego County, California, USA, LM (A–G) and SEM (H–K). **A–G.** Single valves showing size range. **A.** Holotype specimen. **G.** Whole frustule. **H.** External view of whole frustule showing the dorsal raphe ledge interrupted by the dorsal fascia (arrow), the ventral raphe ledge present only near the poles (thin arrow) and a prominent dorsal marginal ridge (arrowhead). **J.** Oblique view of internal valve showing the ventral margin and striae. **I.** Oblique view of internal valve showing uni- and biareolate striation of the ventral striae. **K.** External view of the valve face showing narrow slit-like areolae (arrow). Scale bars = 10 µm (A–G), 1 µm (H–K).

Amphora manifesta Stepanek & Kociolek sp. nov. (Fig. 2.3)

Description: Valves are semi-elliptical and moderately dorsiventral. The dorsal margin is smoothly arched, sometimes flattened over the valve center in larger specimens. The ventral margin is straight to slightly concave. Valve length 22–50 µm, valve breadth 5–7 µm. The valve ends are broadly rounded. The raphe is straight to weakly biarcuate with proximal raphe ends straight to slightly dorsally deflected. The axial area is typically narrow throughout, expanded slightly in some larger specimens. Dorsal and ventral fasciae are present. The dorsal fascia is rectangular near the axial area and is wider near the dorsal margin, creating a distinctive Y-shaped fascia which typically opens on the axial and marginal sides. The ventral fascia extends to the margin and is wider than the dorsal fascia. The dorsal striae, 15–17 in 10 µm, are distinctly areolate, parallel to slightly radiate near the center and becoming more radiate near the apices. The ventral striae, 15–17 in 10 µm, are radiate near the center and composed of one or two areolae, becoming convergent near the apices.

In SEM, the raphe appears straight to slightly biarcuate, with external proximal ends weakly dilated and slightly dorsally deflected. The external distal raphe ends are strongly deflected dorsally. The raphe ledge is continuous on the dorsal side. The dorsal and ventral striae are distinctly areolate with intercostal ribs forming round to ovoid areolae. Externally the presence of areolate-like depressions gives the dorsal fascia an ovoid outline; the characteristic Y-shaped fascia is only evident internally.

Holotype: Slide and material ANSP GC 64901, Academy of Natural Sciences, Philadelphia, USA. Holotype specimen illustrated in Fig. 2.3A.

Isotype: Slide and material JPK 8360, Kociolek collection at the University of Colorado, Museum of Natural History, Boulder, USA.

Type locality: Vasona Reservoir (37.24531°N, 121.96623°W), surface sediment sample, Santa Clara County, California, USA. Collected by EPA, July 2007.

Taxonomic remarks: The robust valves and coarsely areolate striae of *A. manifesta* easily distinguish it from many related taxa. In LM, *A. manifesta* resembles *A. edlundii* Levkov reported from an unnamed Alaskan lake, but is quite dissimilar in the structure of the external areolae (see Levkov 2009, pl. 182, figs 3–4). In SEM, *A. manifesta* more closely resembles *A. vetula* Levkov described from Lake Ohrid, Macedonia and *A. paracopulata* Levkov & Edlund described from Lake Hövsgöl, Mongolia. *Amphora manifesta* can be distinguished from these two taxa by its narrower valves and finer striation. Levkov (2009) reported a breadth of 7.5–11.5 µm and 7.0–11 µm, and stria density of 12–13 and 11–12 in 10 µm for *A. vetula* and *A. paracopulata*, respectively.

Distribution: Present in Vasona Reservoir, Santa Clara County, California and Lake Itasca, Clearwater County, Minnesota, USA.

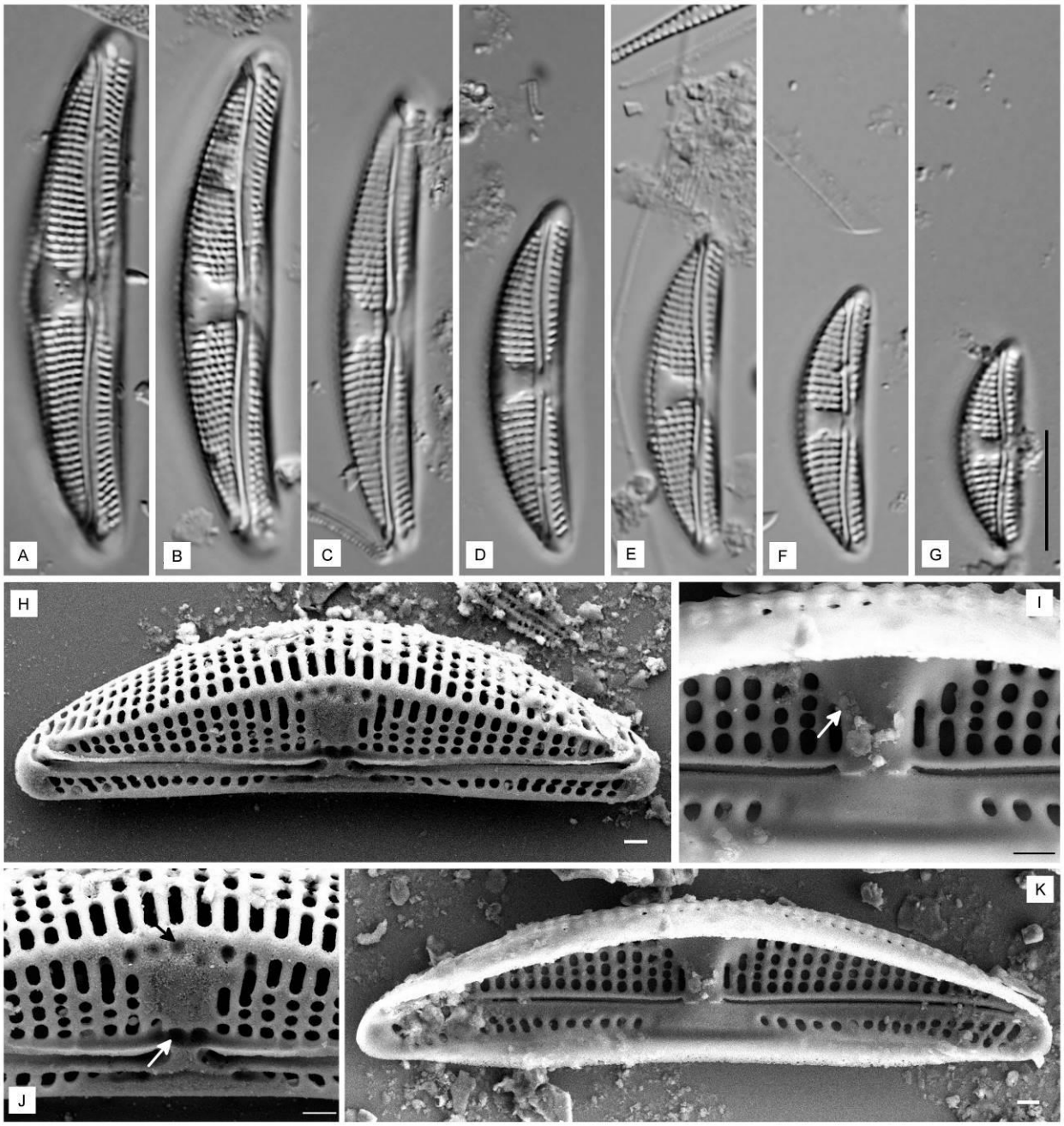

Figure 2.3. Type material of *Amphora manifesta* from Vasona Reservoir, Santa Clara County, California, USA, LM (Figs A–G) and SEM (Figs H–K). **A–G.** Single valves showing size range. **A.** Holotype specimen. **H.** External view of valve showing straight to slightly arched external raphe fissures, dorsal marginal ridge and areolate dorsal striae formed by several rows of intercostal ribs. **J.** External view of valve center showing the continuous dorsal raphe ledge and dorsal fascia appearing rounded due to depressions on its marginal and axial edges (white and black arrows). **K.** Internal view of valve showing straight internal raphe fissures and ventral striae changing from uni- to biareolate. **I.** Internal view of valve center with thickened Y-shaped dorsal fascia (arrow). Scale bars = 10 µm (A–G), 1 µm (H–K).

Halamphora latecostata Stepanek & Kociolek sp. nov. (Fig. 2.4)

Description: Valves are semi-elliptical and dorsiventral with a smoothly arched dorsal margin and a tumid ventral margin. Valve length 25–40 µm, valve breadth 5.5–7.0 µm. Apices are protracted, capitate and ventrally deflected. The raphe is arched with straight to slightly curved branches, with the proximal ends slightly inflated. The axial area is narrow dorsally, more expanded on the ventral side. Only a ventral fascia is present, extending to the margin. The dorsal striae are uninterrupted and radiate throughout, appearing more widely spaced in the valve center, with 10 in 10 µm compared to 14–15 in 10 µm at apices. No dorsal marginal ridge is present. The ventral striae, 18–22 in 10 µm, are small and difficult to see due to their position near the ventral margin.

In SEM, the raphe is arched with proximal raphe ends straight and dilated. Externally, the distal raphe ends are dorsally deflected, while internally they are ventrally deflected. The dorsal raphe ledge is small but continuous across the valve. The dorsal striae are uninterrupted and separated by thick costal ribs. Externally, the striae are bi- to triseriate with the areolae irregular in size and position, while internally striae are biseriate. The internal dorsal costae are distinctly thickened near the valve center, fusing near the axial area to form a small central area. Near the dorsal margin, striae are crossed by thin and somewhat variable intercostal ribs.

Holotype: Slide and material ANSP GC 64902, Academy of Natural Sciences, Philadelphia, USA. Holotype specimen illustrated in Fig. 2.4B.

Isotype: Slide and material JPK 8361, Kociolek collection at the University of Colorado, Museum of Natural History, Boulder, USA.

Type Locality: San Diego Creek (33.68637°N, 117.81625°W), rock scrape, Orange County, California, USA. Collected by J.P. Kociolek, November 2008.

Taxonomic remarks: The robust size and coarse striation of this taxon easily distinguish it from many taxa in the *H. coffeaeformis* group. *Halamphora latecostata* is similar in LM to the brackish-marine *H. turgida* (Gregory) Levkov, but is distinguished by its more narrow valves and widely spaced dorsal striae near the valve center. In SEM, the external dorsal striae are finely biseriate in *H. turgida* (see Levkov 2009, pl. 236), whereas they are irregularly bi- to triseriate in *H. latecostata*. *Halamphora latecostata* closely resembles *A. acutiuscula* Kützing *sensu* Patrick & Reimer (1975, pl. 14, figs 9–10). Their reference slide (ANSP GC 6560a, Sabine River, Orange County, Texas, labeled to contain *A. acutiuscula*) was examined and illustrated a taxon closely resembling that of *H. latecostata* (Fig. 2.5). In their description of *A. acutiuscula*, Patrick & Reimer (1975) were unable to check their concept of this taxon with Kützing's specimens at the British Museum. Since that time, Levkov (2009) has re-examined the type material for *A. acutiuscula* (type slide BM 18173) and illustrated four specimens from this slide (Levkov 2009, pl. 265, figs 12–15). Kützing's *A. acutiuscula* is clearly different from the Sabine River specimens, exhibiting a narrower valve, distinct longitudinal line crossing the dorsal striae near the axial area and parallel, evenly spaced dorsal striae. In light of the taxonomic clarification of *A. acutiuscula* and the similarity between *A. latecostata* and the Sabine River taxa, *A. acutiuscula sensu* Patrick & Reimer (1975) is considered as a synonym of *A. latecostata*. It is worth noting that the Sabine River population appears to contain larger specimens than the ones recorded from the California collections. Patrick & Reimer (1975) reported the size range of the Sabine River specimens as 30–60 µm in length and 6–9 µm in breadth, as opposed to 25–40 µm in length and 5.5–7.0 µm in breadth for the California taxa.

Distribution: Recorded from San Diego Creek, Orange County and Rattlesnake Creek, Santa Barbara County, California, and Sabine River, Orange County, Texas. Patrick & Reimer (1975) reported *A. acutiuscula* as widely distributed in waters of high conductivity throughout the New England, Middle Atlantic, Gulf Coast and East Central states as well as California and Washington.

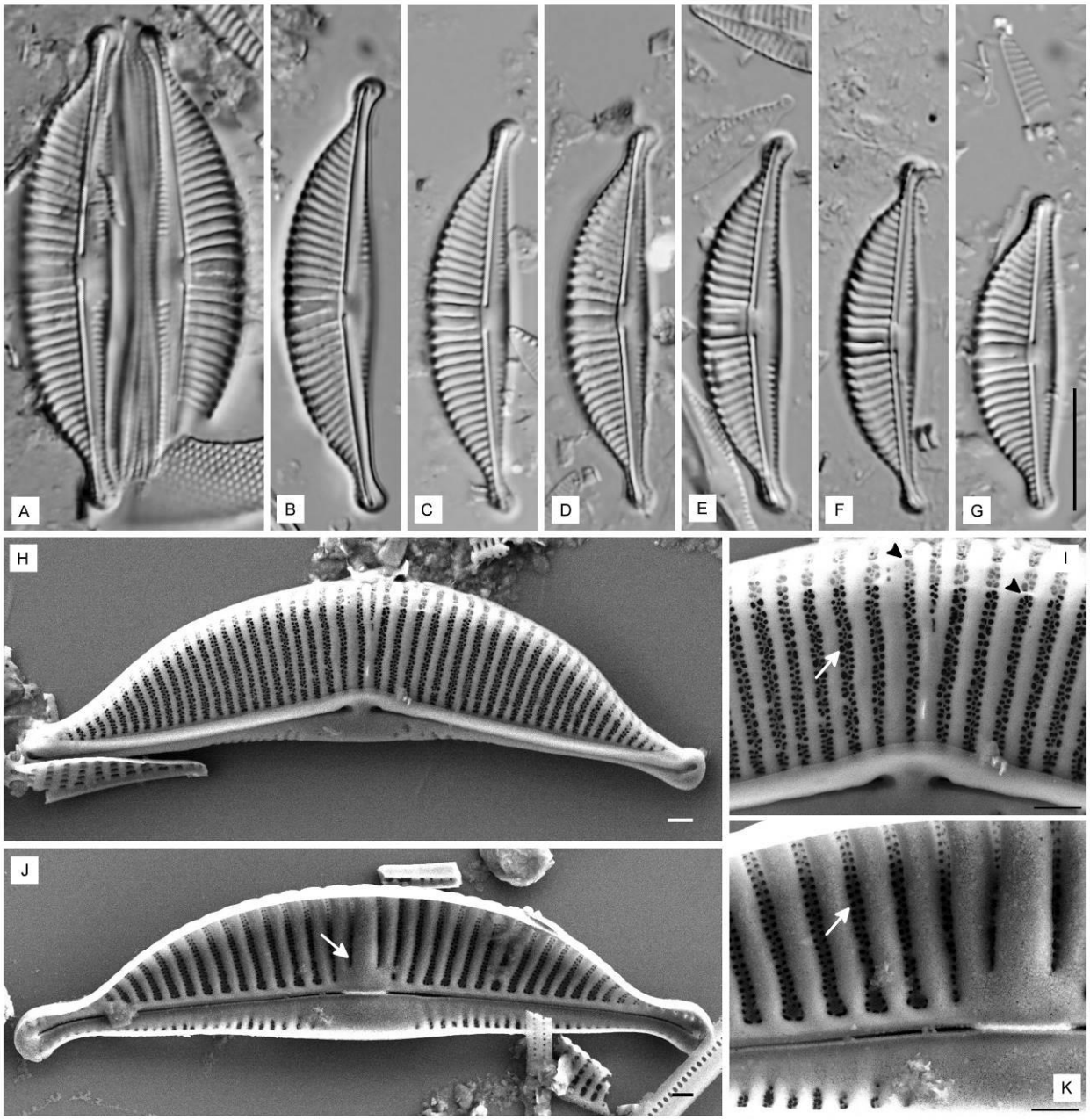

Figure 2.4. Type material of *Halamphora latecostata* from San Diego Creek, Orange County, California, USA, LM (A–G) and SEM (H–K). **A.** Whole frustule. **B.** Holotype specimen. **B–G.** Single valves showing size range. **H.** External view of valve showing the continuous dorsal raphe ledge, uninterrupted dorsal striae, inflated proximal raphe fissures and weakly deflected distal raphe ends. **J.** Internal view of valve showing thickened central dorsal costae (arrow), fusing near the axial area to form a small central area. **I.** External view of valve center showing the irregularly uni- to triseriate dorsal striae (arrow) and thin intercostal ribs near the dorsal margin (arrowheads). **K.** Internal view of valve center showing the biseriate dorsal striae (arrow) and thickened central dorsal costae. Scale bars = 10 µm (A–G), 1 µm (Figs H–K).

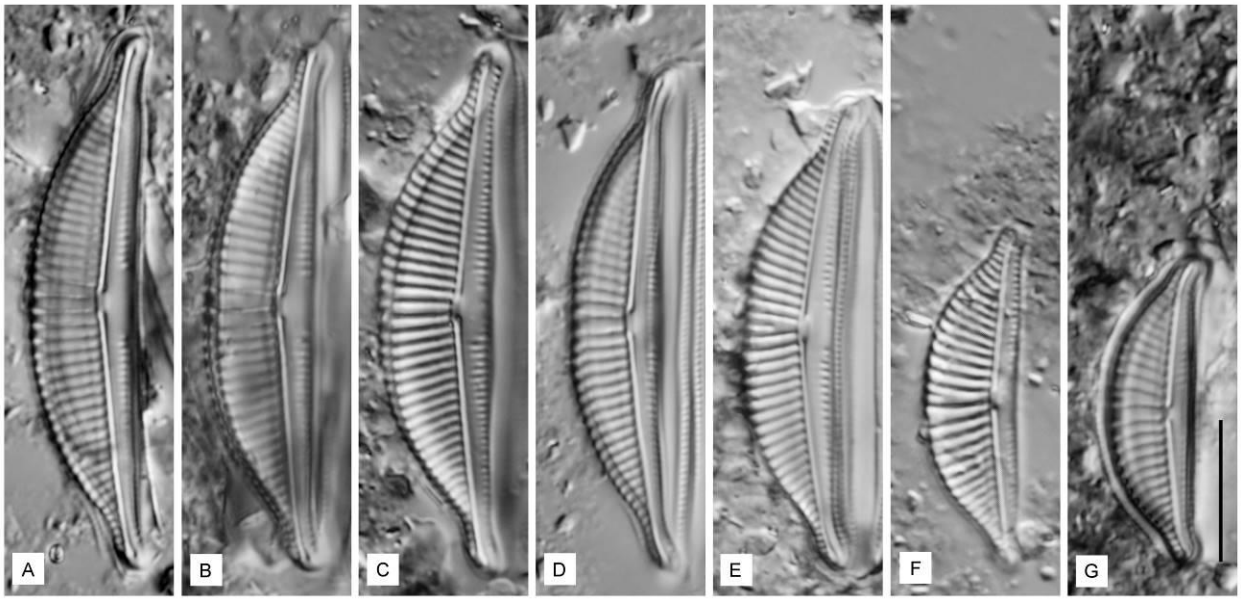

Figure 2.5. Single valves of *Amphora acutiuscula sensu* Patrick & Reimer (1975) showing size range from slide ANSP GC 6560a. Scale bar = 10 µm.

Halamphora subtilis Stepanek & Kociolek sp. nov. (Fig. 2.6)

Description: Valves are narrowly semi-elliptical and dorsiventral. The dorsal margin is smoothly arched near the apices, becoming flat over the center and the ventral margin is tumid. Valve length 14–18 µm, valve breadth 2.5–3.5 µm. Apices are protracted, capitate and weakly deflected ventrally. The raphe is straight, with straight to weakly dorsally deflected proximal raphe ends. The axial area is narrow throughout. Only a ventral fascia is present and extends to the margin. The dorsal striae, 21–25 in 10 µm, are uninterrupted, radiate throughout and more widely spaced near the valve center. The ventral striae, 46–48 in 10 µm, are difficult to resolve in LM.

In SEM, the raphe is straight both internally and externally, with the external proximal ends nearly straight and the distal ends sharply hooked dorsally. The dorsal raphe ledge is prominent, composed of a thin siliceous flap running uninterrupted the length of the valve. The dorsal striae are separated by thick costal ribs and are coarsely and somewhat irregularly uni- to triseriate both externally

and internally. The dorsal costae at center are distinctly thickened both externally and internally. No dorsal marginal ridge is present, although striae are crossed by thin, irregularly placed intercostal ribs near the dorsal margin. The ventral striae are small and fine.

Holotype: Slide and material ANSP GC 64903, Academy of Natural Sciences, Philadelphia, USA. Holotype specimen illustrated in Fig. 2.6B.

Isotype: Slide and material JPK 8362, Kociolek collection at the University of Colorado, Museum of Natural History, Boulder, USA.

Type locality: Adobe Creek (33.51272°N, 117.27038°W), rock scrape, Riverside County, California, USA. Collected by J.P. Kociolek, November 2008.

Taxonomic remarks: This taxon is similar to the small brackish to marine taxa *H. tenerrima* (Aleem & Hustedt) Levkov and *H. tenuissima* (Hustedt) Levkov (see Clavero et al. 2000), but is distinguished from both by its thickened dorsal costae. *Halamphora subtilis* shares a siliceous thickening of the dorsal valve center with *H. sabiniana* (Reimer) Levkov, but is distinguished by its small size and fine ventral striation. *Distribution*: Known only from the type locality.

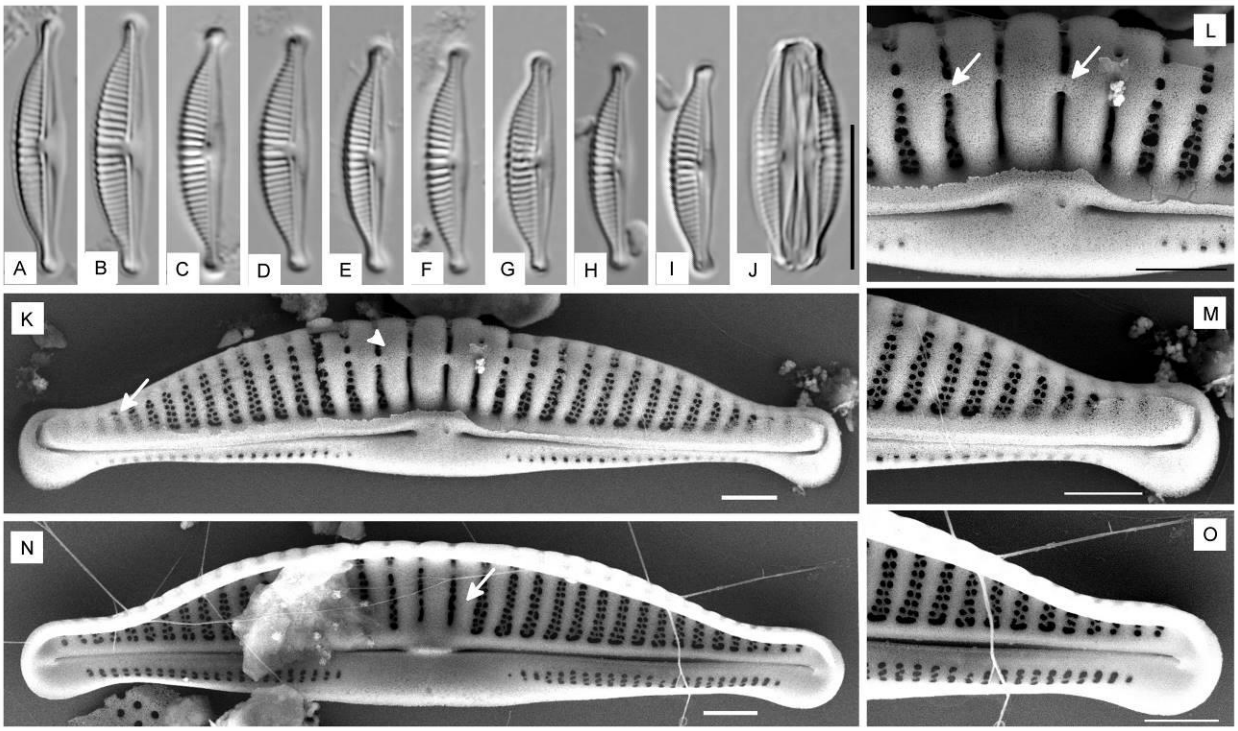

Fig. 2.6. Type material of *Halamphora subtilis* from Adobe Creek, Riverside County, California, USA, LM (A–J) and SEM (K–O). **A–J.** Single valves showing size range. **B.** Holotype specimen. **J.** Whole frustule. **K.** External view of valve showing a portion of the broad raphe ledge (arrow), straight raphe fissures with straight proximal ends and sharply hooked distal ends, and continuous dorsal striae with costae distinctly thickened at center (arrowhead). **L.** External view of valve center showing thickened costae crossed near the dorsal margin by thin intercostal ribs (arrows). **M.** External view of apex showing sharply hooked raphe end and irregularly biseriate dorsal striae. **N.** Internal view of valve showing thickened central dorsal costae (arrow) and fine ventral striae. **O.** Internal view of apex showing irregularly biseriate dorsal striae. Scale bars = 10 µm (A–J), 1 µm (K–O).

Halamphora punctata Stepanek & Kociolek sp. nov. (Fig. 2.7)

Description: Valves are semi-elliptical and dorsiventral. The dorsal margin is smoothly arched, flattening near the valve center. The ventral margin is weakly tumid. Valve length 15–25 µm, valve breadth 3.5–4.5 µm. The valve ends are protracted, subcapitate to capitate and ventrally deflected. The raphe is weakly arched with the proximal ends slightly dorsally deflected. The axial area is narrow on the dorsal side, more pronounced on the ventral side and expanding into a wide central area. The dorsal striae are

distinctly areolate, 20–23 in 10 µm. No dorsal marginal ridge is present. The ventral striae, 24 in 10 µm, consist of a short row of areolae near the ventral margin and can be difficult to see in LM.

In SEM, the raphe is arched with proximal and distal ends deflected dorsally. The dorsal raphe ledge is continuous along the length of the valve. The ventral axial area widens quickly from the apices towards the valve center, creating a semi-lanceolate axial area. The dorsal striae are distinctly areolate externally, composed of widely spaced areolae formed by irregularly spaced intercostal ribs. The first row of axial dorsal areolae are elongate and biseriate. Internally, the striae are not interrupted by intercostal ribs and are biseriate, although the external intercostal ribs can be seen through the internal covering. The internal costae at center are strongly thickened and fused near the axial area. The ventral striae are composed of a single row of small areolae running along the margin.

Holotype: Slide and material ANSP GC 64904, Academy of Natural Sciences, Philadelphia, USA. Holotype specimen illustrated in Fig. 2.7A.

Isotype: Slide and material JPK 8363, Kociolek collection at the University of Colorado, Museum of Natural History, Boulder, USA.

Type locality: Adobe Creek (33.51272°N, 117.27038°W), rock scrape, Riverside County, California, USA. Collected by J.P. Kociolek, November 2008.

Taxonomic remarks: *Halamphora punctata* is distinguished from other similar taxa such as *H. aponina* (Kützing) Levkov by its distinctly areolate dorsal striae. *Halamphora punctata* shares distinctly areolate dorsal striae with the taxa *H. borealis* (Kützing) Levkov, *H. holsatica* (Hustedt) Levkov and *H. subholsatica* (Krammer) Levkov. *Halamphora punctata* is distinguished from *H. borealis* by its thickened dorsal costae near the valve center and from *H. holsatica* and *H. subholsatica* by its smaller size and fine striation.

Distribution: Recorded from Adobe Creek, Riverside County and Agua Hedionda Creek, San Diego County, California.

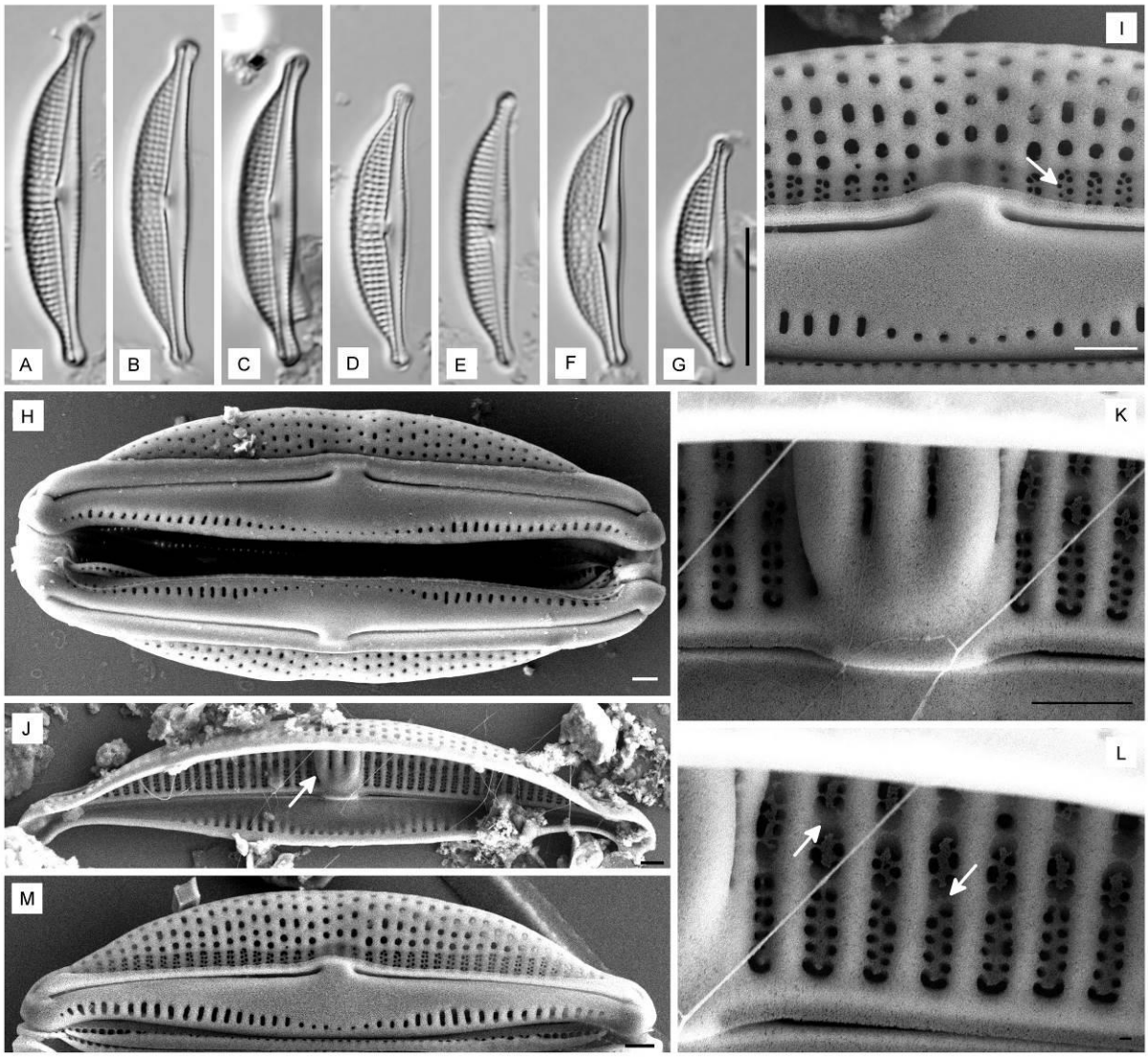

Figs 2.7. Type material of *Halamphora punctata* from Adobe Creek, Riverside County, California, USA, LM (A–G) and SEM (H–L). **A.** Holotype specimen. **Figs A–G.** Single valves showing size range. **H.** Frustule in external view showing the prominent dorsal raphe ledge, broad semi-lanceolate ventral axial area and areolate striae. **J.** Internal view of valve showing the distinctly thickened central dorsal costae (arrow). **M.** External view of whole valve with no dorsal raphe ledge present. **I.** External view of valve center with no dorsal raphe ledge present, showing the first row of elongate and biseriate dorsal striae (arrow). **K.** Internal view of valve center showing thickened dorsal costae fusing near the axial area. **L.** Detail of biseriate striae from internal view showing intercostal ribs (arrows). Scale bars = 10 µm (Fig. 2.7A–H, J, M), 1 µm (Fig. 2.7I, K), 100 nm (Fig. 2.7L).

Halamphora coloradiana Stepanek & Kociolek sp. nov. (Fig. 2.8)

Description: Valves are semi-elliptical and strongly dorsiventral, with a smoothly arched dorsal margin and a straight ventral margin. Valve length 12–25 µm, valve breadth 2.5–4.5 µm. Valve ends are protracted, almost rostrate in larger specimens, and weakly ventrally bent. The raphe is straight to slightly arched, with external proximal ends straight to slightly dorsally deflected. The axial area is narrow on the dorsal side and not well defined on the ventral side. No fascia present. The dorsal striae are distinctly areolate, more so near the valve center, with 23–24 in 10 µm at center and 29–41 in 10 µm near the apices. Due to their position near the ventral margin, the ventral striae are often difficult to see in LM.

In SEM, the external raphe system appears straight with proximal and distal ends weakly deflected dorsally and proximal ends slightly inflated. Internally, the raphe appears straight. The dorsal raphe ledge is small and continuous across the length of the valve. The dorsal striae are interrupted by many irregularly spaced intercostal ribs forming elongate areolae of variable size. The ventral striae are composed of a single row of small areolae. A prominent marginal ridge separates the valve face from the dorsal mantle. This ridge appears to wrap around the distal raphe ends to the ventral margin. The dorsal central costae are slightly thickened both externally and internally.

Holotype: Slide and material ANSP GC 64905, Academy of Natural Sciences, Philadelphia, USA. Holotype specimen illustrated in Fig. 2.8A.

Isotype: Slide and material JPK 8364, Kociolek collection at the University of Colorado, Museum of Natural History, Boulder, USA.

Type locality: Cottonwood Marsh (40.00342°N, 105.25104°W), shoreline epiphytes, Walden Ponds Wildlife Habitat, Boulder County, Colorado. Collected by J.G. Stepanek, September 2010.

Taxonomic remarks: This taxon is morphologically similar to *H. veneta* and *H. oligotraphenta* (Lange-Bertalot) Levkov. This taxon appears most similar to *H. veneta* although occupying the lower end of the reported size range for US specimens (*H. veneta* valve length 10–45 µm, valve breadth 4–6 µm according to Patrick & Reimer 1975). *Halamphora coloradiana* is distinguished from *H. veneta* by its comparatively narrow valves, protracted valve ends, closely spaced proximal raphe ends and finer striation. This taxon is distinguished from *H. oligotraphenta* by its smaller size, fine striation, narrowly rounded valve ends and closely spaced proximal raphe ends.

Distribution: Known only from Cottonwood Marsh and ponds within the Walden Ponds Wildlife Habitat, Boulder County, Colorado, USA.

DISCUSSION

The new species of *Amphora* and *Halamphora* described here appear morphologically similar to several distinct groups within *Amphora sensu lato*. *Amphora waldeniana* and *A. copulatoides* are closely allied with one another and share features that would suggest a close relationship between them and the common freshwater taxa *A. affinis* and *A. copulata*. The most distinct differences between these taxa can be seen in the SEM where both *A. waldeniana* and *A. copulatoides* exhibit narrow slit-like external areola openings. This is in contrast to the absence of any external areola coverings in both *A. affinis* (Schoeman & Archibald 1986c, Levkov 2009) and *A. copulata* (Krammer 1980, Lee & Round 1988).

External areola coverings are observed within *Amphora* taxa, with *A. ovalis* the most notable example. In the case of *A. ovalis*, the external openings are continuous from the axial area to the dorsal margin (Lee & Round 1987, figs 2–7) and along the dorsal margin (Lee & Round 1987, figs 3, 6–7), with the areolae partitioned by intercostal ribs internally only (Krammer 1980, fig. 10). This is in contrast with the areolae in *A. waldeniana* and *A. copulatoides* being partitioned internally and externally, with a narrow opening corresponding to each areola. This feature along with differences in the ventral raphe ledge and striae (see Lee & Round 1987 for thorough discussion of *A. ovalis*) clearly distinguish these

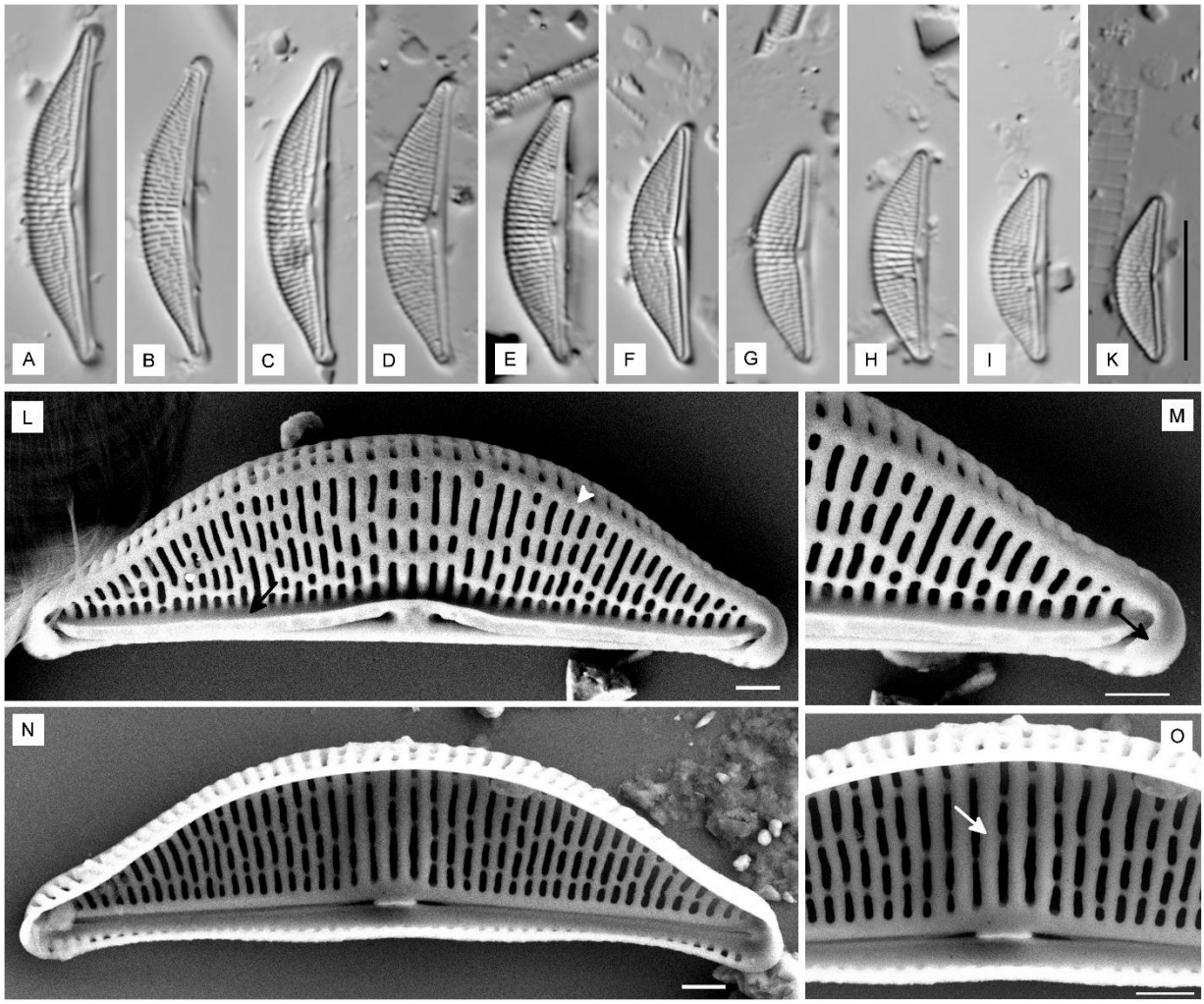

Figure 2.8. Type material of *Halamphora coloradiana* from Cottonwood Marsh, Boulder County, Colorado, USA, LM (A–K) and SEM (L–O). **A.** Holotype specimen. **A–K.** Single valves showing size range. **L.** External view of valve showing small dorsal raphe ledge (arrow), prominent dorsal marginal ridge (arrowhead) and striae interrupted by irregularly spaced intercostal ribs. **M.** External view of apex showing the weakly deflected distal raphe end and dorsal marginal ridge continuing to the ventral margin (arrow). **N.** Internal valve view. **O.** Internal view of valve center showing thickened dorsal costae (arrow). Scale bars = 10 µm (A–K), 1 µm (L–O).

taxa from *A. ovalis* and closely related taxa. Several new *Amphora* species described and illustrated by Levkov (2009), such as *A. accomoda* Levkov, *A. skvortzowii* Levkov, *A. subrobusta* Hustedt, *A. ohridana* Levkov and *A. sancti-naumii* Levkov & Metzeltin, exhibit a range of narrow single areolate external openings and similar raphe features to *A. waldeniana* and *A. copulatoides*. However, at present none of

these species have been reported from the US and further investigation will be required to determine if these features place these taxa into a natural group or if they are variable throughout the genus.

In contrast to *A. waldeniana* and *A. copulatoides*, *A. manifesta* appears similar in form to several new distinctly areolate *Amphora* taxa described by Levkov (2009) from Europe, namely *A. vetula*, *A. lange-bertalotii* Levkov & Metzeltin and *A. recens* Levkov & Nakov. These taxa all share similar valve shape, coarsely areolate striae and distinct Y-shaped dorsal fascia. In contrast to these taxa, *A. manifesta* is smaller and exhibits finer striation (see discussion under *A. manifesta* description).

In SEM, *H. latecostata* and *H. subtilis* are quite similar to one other in having uninterrupted irregularly seriate dorsal striae and distinctly thickened central dorsal costae (more pronounced in *H. subtilis*). *Halamphora latecostata* and *H. subtilis* both appear to be most closely allied with the *H. coffeaeformis* group within the genus *Halamphora*, all of which share similarities in valve outline and uninterrupted multi-seriate dorsal striae (Schoeman & Archibald 1984). These last authors present several taxa that appear to exhibit some slight thickening and fusing of central dorsal costae (Schoeman & Archibald 1984, figs 117–118, 129–130), but the extent to which this occurs in *H. latecostata* and *H. subtilis* would appear to group these taxa together to the exclusion of *H. coffeaeformis* and its closely related species.

In LM, *H. punctata* with its strongly dorsiventral valve shape and distinctly areolate dorsal striae would appear most closely allied with the group of areolate *Halamphora* which include *H. subholsatica* and *H. borealis*. In SEM, the biseriate axial row of striae, broad ventral axial area and thickened central dorsal costae suggest that *H. punctata* may be more closely related to *H. acutiuscula* (*sensu* Levkov 2009, pl. 96, figs 10–18, pl. 109, figs 1–4), *H. rugosa* (Hustedt) Levkov and *H. schroederi* (Hustedt) Levkov (see Sala et al. 2006), all of which share these features.

Halamphora coloradiana shows a strong morphological affinity to *H. veneta*. These taxa share a strongly dorsiventral valve shape, distinct areolae of irregular size and spacing, a prominent dorsal marginal ridge and thickening of the central dorsal costae (see Schoeman & Archibald 1978 for thorough morphological treatment of *H. veneta*).

Finally, it is worth noting that all of these taxa were collected from waters with elevated conductivity (361–2302 µS cm^{-1}; see Table 1), and it may be that continued examination of higher conductivity inland waters will be the most fruitful in future taxonomic investigations. Although this work may represent the largest effort to describe new *Amphora sensu lato* taxa from inland waters of the United States since the 1970s, it surely represents only a small portion of the undescribed taxonomic diversity present. Whereas US coastal waters have received some attention by taxonomic investigators (Hustedt 1955, Hohn & Hellerman 1966, Wachnicka & Gaiser 2007), only a small area of inland environments of the continental US have been thoroughly investigated for *Amphora* diversity. Of the 14 extant taxa currently described from US inland waters, nine were described from Lake Michigan and surrounding waters (Thomas & Chase 1886, Stoermer & Yang 1971, Levkov 2009), two from the Potomac River, Maryland (Hohn & Hellerman 1963) and the Gulf Coast rivers (Patrick & Reimer 1975, Levkov 2009), and one from Central Florida (Hohn 1961). With this in mind, the high conductivity waters of the western United States have been largely unexplored. Continued investigation of inland waters of the western United States remains important to increase our understanding of the diversity of amphoroid diatoms.

ACKNOWLEDGEMENTS

The authors would like to thank Marina Potapova and the Academy of Natural Sciences, Philadelphia for providing the Sabine River collection slide.

CHAPTER III

THREE NEW SPECIES OF THE DIATOM GENUS *HALAMPHORA* (BACILLARIOPHYTA) FROM THE PRAIRIE POTHOLE LAKES REGION OF NORTH DAKOTA, USA

Adapted from: Stepanek, J.G. & Kociolek, J.P. 2015. Three new species of the diatom genus *Halamphora* (Bacillariophyta) from the prairie pothole lakes region of North Dakota, USA. *Phytotaxa* 197: 27–36.

ABSTRACT

The prairie pothole region of North America is characterized by a large number of lakes and wetlands created during the last glacial retreat. These waterbodies are characterized by their generally small sizes (70% of waterbodies are less than 0.4 ha), high densities (as many as 40 waterbodies km $^{-2}$) and elevated but variable conductivities, ranging between 230–70,000 µS cm^{-1}. Although this region boasts a great number and diversity of habitats, few studies have investigated the diatom diversity present. Presented here are descriptions and illustrations of three new species from the genus *Halamphora* based on light microscope and scanning electron microscope observations. *Halamphora pratensis* was collected from Long Lake, Burleigh County, with a conductivity of 2187 µS cm^{-1}, and appears to be most closely allied with the common freshwater *H. veneta* group within the genus. *Halamphora pertusa* and *H. attenuata* were collected from Salt Alkaline Lake, Kidder County, with an elevated conductivity of 9811 µS cm^{-1}. Both of these taxa, although unique, exhibit some morphological similarity to several marine and estuarine species.

INTRODUCTION

The prairie pothole region (PPR) of North America covers an area of over 700,000 km^2, extending from south central Canada into the north central United States (Sloan 1972, Sethre et al. 2005).

This area marks the furthest extent and end moraine of the Wisconsin glaciation and is characterized by closed basin pothole lakes, which range from freshwater to hypersaline, formed from melting blocks of ice into glacial till and outwash during the glacial retreat (Shjeflo 1968, Sloan 1972). These lakes tend to be small, with approximately 70% of the waterbodies 0.4 ha or smaller (Johnson & Higgins 1997) and can reach densities of 40 waterbodies km^{-2} (Sethre et al. 2005).

Pothole basins are largely composed of poorly permeable glacial till comprised of equal parts clay silt and sand (Shjeflo 1968). Although these waterbodies typically have no stream inputs or outputs, they are in continuous contact with groundwater and the relative conductivity of individual waterbodies is largely determined by seepage inflow and outflow. Because of this groundwater influence and differences in substrate and elevation, there can be a great deal of heterogeneity in waterbody conductivity over small spatial scales, with surface waters ranging between 230–70,000 $\mu S\ cm^{-1}$ (Sloan 1972). This heterogeneity in water chemistry creates a unique diversity of aquatic habitats over relatively small areas.

Although the PPR is expansive in both area and number of lakes, investigations into the diatom diversity present in these habitats is lacking. Currently only three diatom species have been described from the waters of North Dakota, two (Boyer 1914, Elmore 1921) from the often studied Devils Lake (Stoermer et al. 1971, Fritz 1990, Fritz et al. 2000), and one fossil taxon from Moon Lake (Hamilton & Laird 2001). It has previously been suggested that elevated conductivity inland waters of the United States may hold significant undescribed *Amphora* Ehrenberg ex Kützing (1844) and *Halamphora* (Cleve) Levkov (2009) diversity (Stepanek & Kociolek 2013), and this has been evidenced by the recent publication of 11 new species from the western United States (Stepanek & Kociolek 2013, Kociolek et al. 2014).

The number and variety of elevated conductivity habitats available throughout the PPR make it ideal for an investigation into the undescribed diversity of *Halamphora* present in inland waters of the western United States. Presented here are the descriptions and illustrations of three new species of *Halamphora* collected from Long Lake and Salt Alkaline lake in the prairie pothole region of North Dakota based on light microscope and scanning electron microscope observations. Although consisting of

a small sample of lakes from the PPR, this investigation illustrates the potential diversity present in these waters.

MATERIALS AND METHODS

Examined materials include samples collected from two lakes in the prairie pothole region of central and eastern North Dakota. Samples include: near shore periphyton (JPK 7951) from Long Lake, part of the Long Lake State Wildlife Refuge, Burleigh County, ND (N 46.69169°, W 100.19026°), epiphytes (JPK 7977), a benthic sample (JPK 7978), and a composite sample (JPK 7981) from the northwest shore of Salt Alkaline Lake, Kidder County, ND (N 46.95092°, W 99.53915°). These materials were collected as part of a larger collection effort in which 38 waterbodies were sampled from November 3–5, 2011. All collections are currently held in the Kociolek collection at the University of Colorado Boulder. See Table 1 for site, conductivity and pH information for the waterbodies included in this study. Conductivity and pH values for the habitats are based off a single near shore measurement taken at the time of collection using a YSI 556 multi-probe (YSI Incorporated, Yellow Springs, Ohio).

Table 3.1. List of material examined including collection locality, geographical coordinates, pH and conductivity measurements. ANSP: Academy of Natural Sciences Philadelphia, COLO: Kociolek collection at the University of Colorado Boulder.

Accession number	Sample type	Collection locality	Latitude North	Longitude West	pH	Conductivity (µS cm−1)
ANSP GC 65212	Periphyton	Long Lake, Burleigh County, ND	46.69169	100.19026	8.79	2187
ANSP GC 65213	Epiphyton	Salt Alkaline Lake, Kidder County, ND	46.95092	99.53915	8.89	9811
COLO JPK 7978	Benthos	Salt Alkaline Lake, Kidder County, ND	46.95092	99.53915	8.89	9811
ANSP GC 65214	Composite	Salt Alkaline Lake, Kidder County, ND	46.95448	99.52382	8.89	9811

Diatom samples were cleaned of organic matter by boiling in nitric acid, followed by repeated rinses with deionized water until a neutral pH was reached. For light microscope (LM) observations,

cleaned samples were air dried onto glass coverslips and permanently mounted in Naphrax mounting medium (Brunel Microscopes, Chippenham, U.K.). Light microscope observations were conducted using an Olympus BX-51 LM with DIC optics and a 100X (1.40 N.A.) objective (Olympus America Inc., Center Valley, Pennsylvania). Images were taken using an Olympus DP 71 digital camera. For scanning electron microscope (SEM) observations cleaned material was air dried onto glass coverslips and sputter coated with 1 nm gold using a Cressington 108 sputter coater (Cressington Scientific Instruments Ltd., Watford, UK). Materials were examined using a JEOL JSM 7401 field emission SEM (JEOL Ltd., Tokyo, Japan) at an acceleration voltage of 3 kV.

Valve ultrastructure terminology follows that of Cox and Ross (1981), Nagumo (2003) and Levkov (2009).

RESULTS

Halamphora pratensis Stepanek & Kociolek sp. nov. (Figs 3.1, 3.2)

Valves are semi-elliptical with a smoothly rounded dorsal margin and a straight to slightly concave ventral margin, the ventral margin in larger specimens is often slightly tumid. Valve length 13.0–35.0 µm, valve breadth 4.5–6.0 µm. Valve ends are protracted, narrowly rounded and slightly bent ventrally. The raphe is arched with nearly straight raphe branches. Proximal raphe ends are straight and the distal raphe ends deflect dorsally. The axial area is narrow throughout. Dorsal striae are areolate, slightly radiate throughout, becoming more so near the apices. Dorsal striae are distinctly more widely spaced near the valve center, with 23–27 striae in 10 µm and 31–34 in 10 µm near the apices. Ventral striae are difficult to see in the LM. A dorsal marginal ridge is not apparent.

In the SEM, externally, the raphe is straight with proximal ends straight to slightly deflected dorsally and the distal ends are weakly deflected dorsally. The dorsal raphe ledge is small and continuous across the length of the valve, ending before the proximal raphe ends. The axial area is narrow on the dorsal side, more pronounced on the ventral side and expanded near the valve center. The dorsal striae are separated by thin virgae and are crossed, externally and internally, by thick irregularly placed vimines

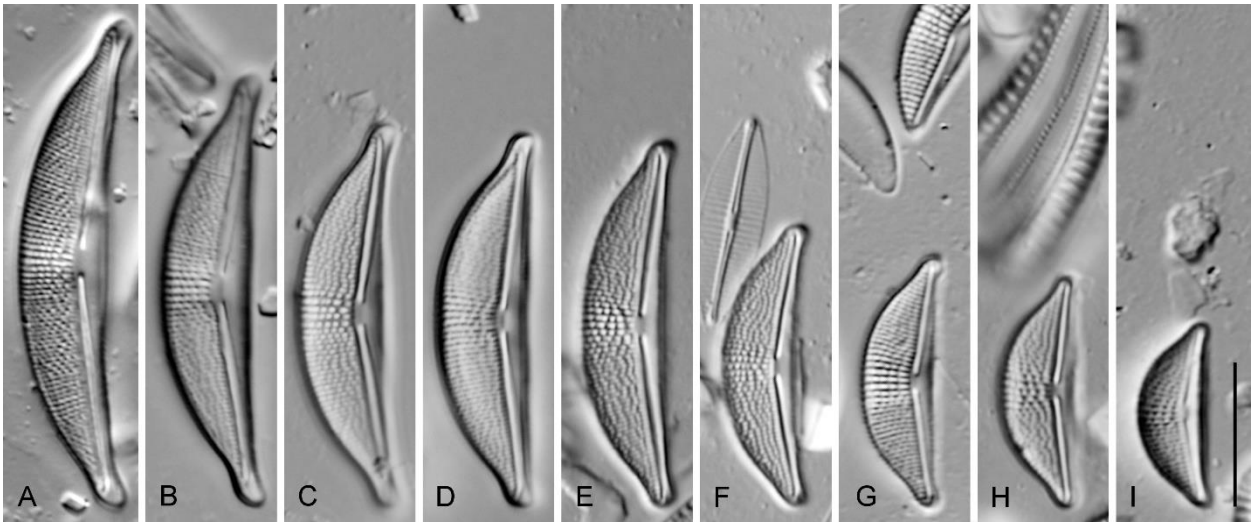

Figure 3.1 A–I. LM. *Halamphora pratensis* sp. nov. Single valves showing size range. **A.** Holotype specimen. Scale bar = 10 µm.

creating round to ovoid areolae of varying size. The dorsal virgae are thickened near the valve center, a feature that is more pronounced internally. The dorsal marginal ridge is variable. Externally, the ridge is well defined only near the apices, where it wraps around the distal raphe end to merge with the ventral margin, but becomes much less defined over the central portion of the valve. The ventral striae are difficult to see externally due to their marginal position, but can be observed internally as a single continuous row of elongate areolae. The girdle area consists of six bands, each having two rows of elongate areolae running their length.

Type. USA. North Dakota, Burleigh County: Long Lake, N46.69169°, W100.19026°, 3 November 2011, Holotype: Slide ANSP GC 65212, Fig. 3.1A; Isotypes: Cleaned material ANSP GCM 5690, slide and cleaned material JPK 7951, Kociolek Collection at COLO.

Observations. Halamphora pratensis resembles several taxa in the *Halamphora veneta* (Kützing) Levkov group, including, *H. veneta*, *Halamphora veneta* var. *somalica* (Frenguelli) Levkov, *Halamphora oligotraphenta* (Lange-Bertalot) Levkov (2009), *Halamphora coloradiana* Stepanek & Kociolek and

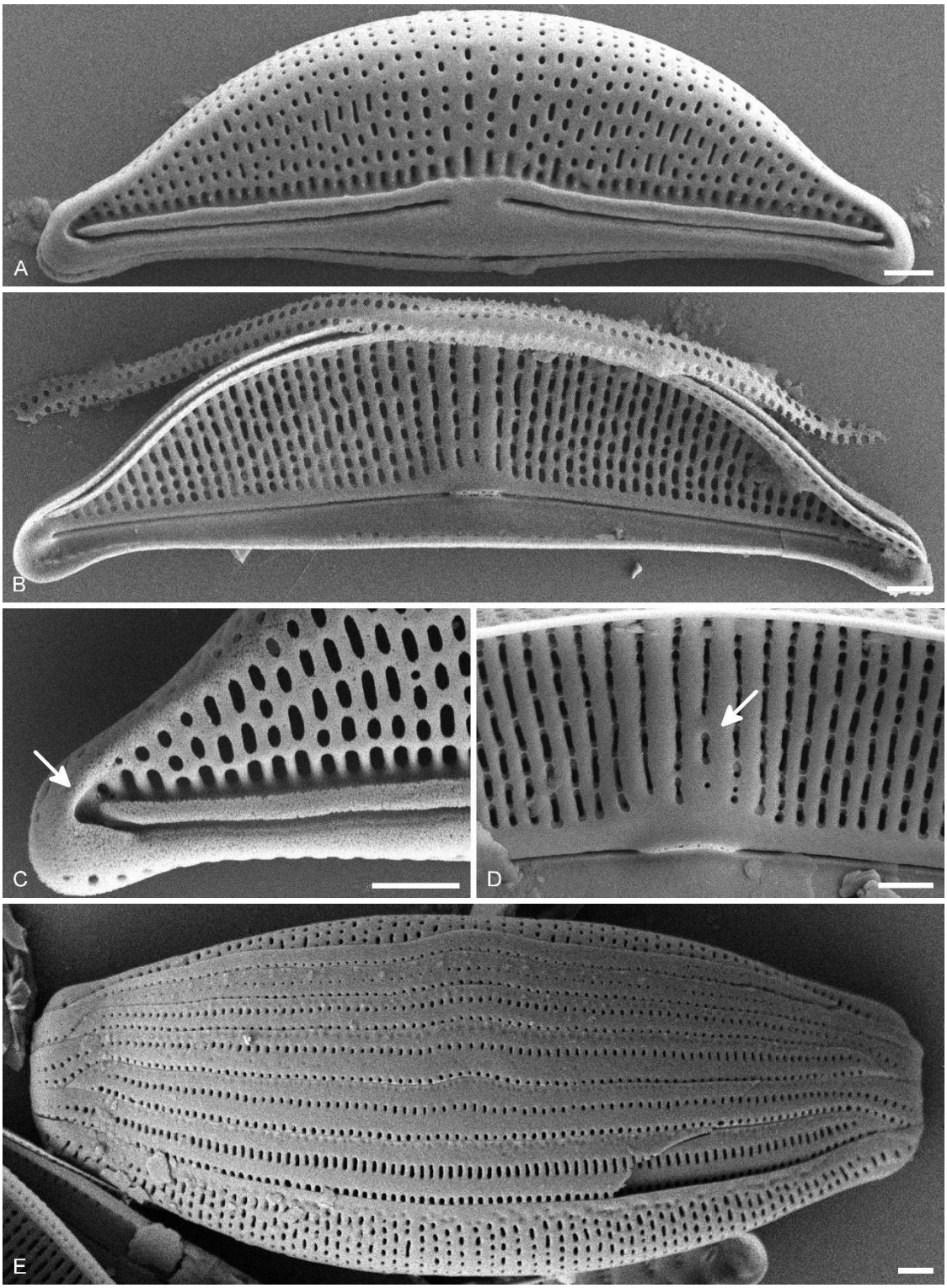

Figure 3.2. SEM *Halamphora pratensis* sp. nov. **A.** External whole valve view. **B.** Internal whole valve view. **C.** Detail of valve apex showing marginal ridge wrapping around distal raphe end to the ventral margin (arrow). **D.** Detail of internal valve center showing thickened central virgae (arrow). **E.** Whole frustule in dorsal girdle view showing girdle bands with two rows of poroids. Scale bars = 1 µm.

Halamphora coraensis (Foged) Levkov. *Halamphora pratensis* can be distinguished from *H. veneta* by its distinctly protracted and narrowly rounded valve ends, its finer striation (Patrick and Reimer 1975, give 14–20 striae in 10 µm at center valve and 26 in 10 µm near the apices) and the more closely spaced proximal raphe ends. In the SEM, *H. pratensis* exhibits a less well defined marginal ridge than is seen in *H. veneta*. *Halamphora pratensis* shares protracted valve ends with *H. veneta* var. *somalica*, *H. oligotraphenta* and *H. coloradiana*. *Halamphora pratensis* can easily be distinguished from these taxa by its larger and comparably wider valves. *Halamphora pratensis* is quite similar to *H. coraensis* in valve dimensions and striae count (Levkov 2009, gives length 26–36 µm, breadth 4.5–6.5 µm and a dorsal striae count of 24–26 in 10µm). Unlike *H. pratensis*, *H. coraensis* exhibits distinctly capitate valve ends (Levkov 2009: pl. 107, Figs 33–37) and is found in freshwater oligotrophic waters of northern Europe. *Halamphora pratensis* also shares similar valve dimensions and striae counts with the punctate taxon *Halamphora ausloosiana* Van de Vijver & Kopalová (Van de Vijver *et al*. 2014 give length 22–34, breadth 4.0–6.5, and 22–28 dorsal striae in 10 µm for this taxon) recently described from an Antarctic Island. In the LM *H. ausloosiana* can be distinguished from *H. pratensis* by its sub-capitate valve ends and lack of more widely spaced dorsal central striae. In the SEM *H. ausloosiana* exhibits a broad dorsal raphe ledge and biseriate dorsal striae, both absent in *H. pratensis*.

Halamphora pertusa Stepanek & Kociolek sp. nov. (Figs 3.3, 3.4)

Valves are semi-elliptical, with a smoothly arched dorsal margin and a straight to slightly concave ventral margin. Valve length 17.0–34.0, valve breadth 5.0–6.0. Valve ends are protracted, narrowly rounded to sub-capitate and slightly bent ventrally. The raphe is arched, with straight raphe branches. Proximal raphe ends are straight to slightly dorsally deflected, the distal raphe ends are difficult to see in the LM. The axial area is narrow throughout, widening slightly near the ventral valve center. Dorsal striae are distinctly areolate, nearly parallel at the valve center, becoming radiate near the apices. Dorsal striae number 17–19 in 10 µm. Ventral striae are fine and number 29–31 in 10 µm.

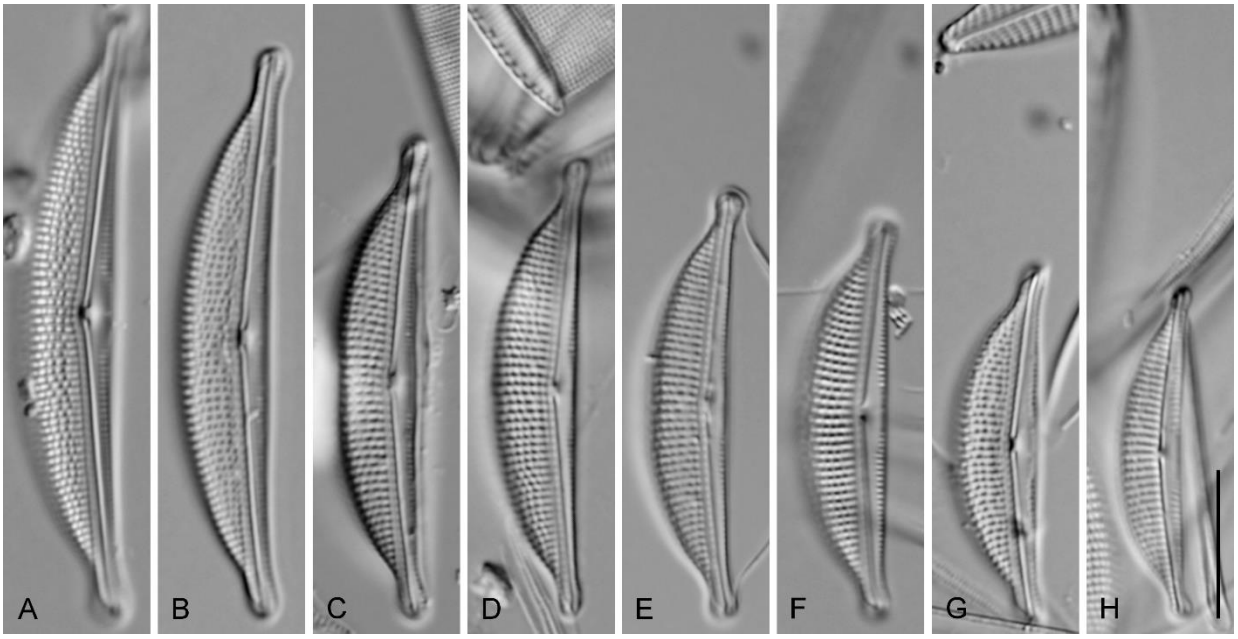

Figure 3.3. LM. *Halamphora pertusa* sp. nov. Single valves showing size range. **A.**. Holotype specimen. Scale bar = 10 µm.

In the SEM, externally, the raphe branches are straight with the proximal raphe ends slightly dorsally deflected and the distal ends hooked dorsally past the raphe ledge. The dorsal raphe ledge is prominent and is continuous the length of the valve. The dorsal striae are crossed by many irregularly spaces vimines, creating many internally biseriate round to ovoid areolae. The ventral striae consist of a single row of elongate areolae. A marginal ridge is not present and the areolate striae continue uninterrupted to the valve margin. Internally, the dorsal striae appear irregularly biseriate throughout. A distinct longitudinal band of silica runs the length of the valve near the dorsal axial area.

Type. USA. North Dakota, Kidder County: Salt Alkaline Lake, N46.95092°, W99.53915°, 3 November 2011, Holotype: Slide ANSP GC 65213, Fig. 3.3A; Isotypes: Cleaned material ANSP GCM 5691, slide and cleaned material JPK 7977, Kociolek Collection at COLO.

Observations. Halamphora pertusa is similar in valve outline and areolate striae to the freshwater species *Halamphora punctata* Stepanek & Kociolek, and to the brackish/marine species *Halamphora acutiuscula*

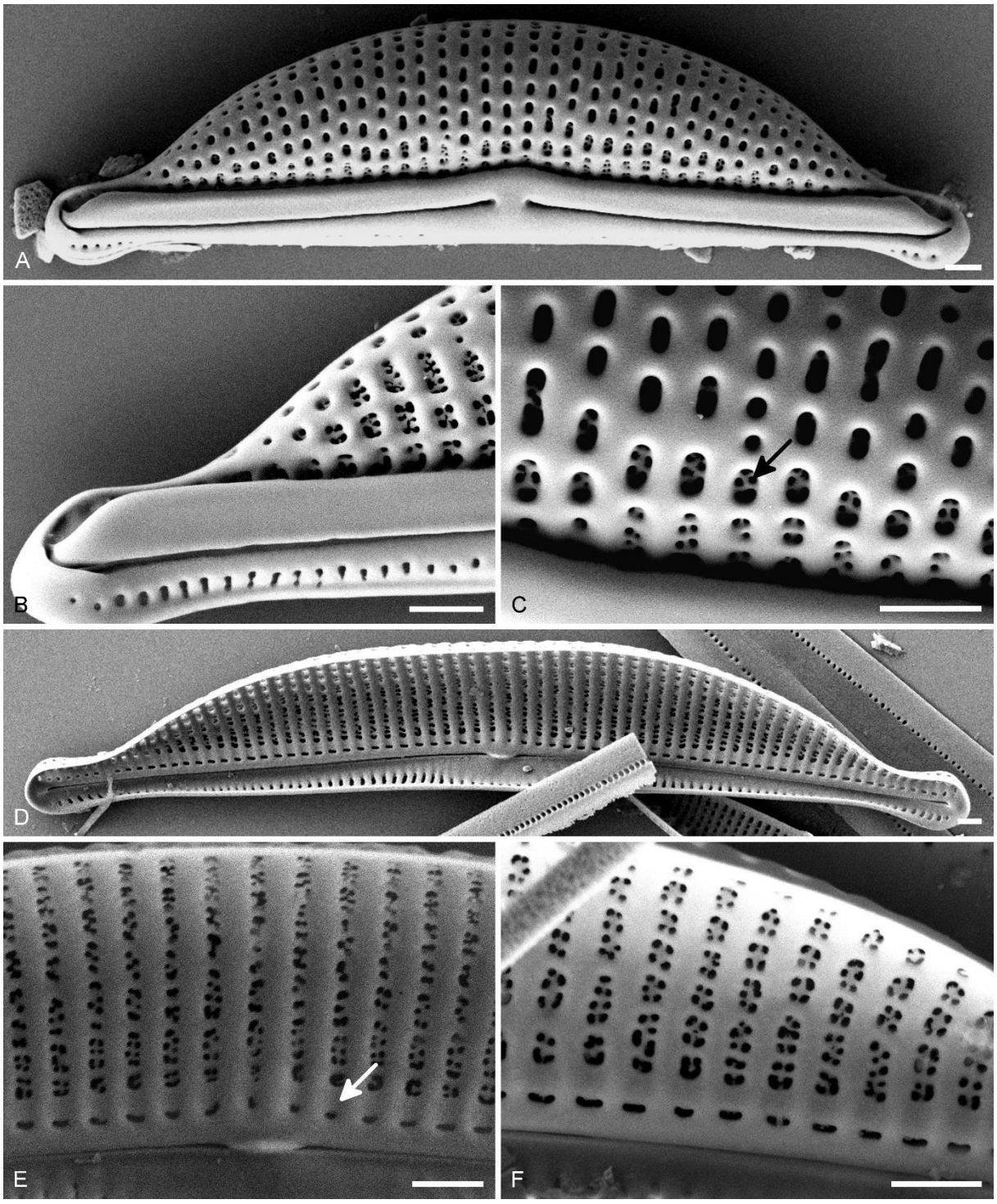

Figure 3.4. SEM. *Halamphora pertusa* sp. nov. **A.** External whole valve view. **B.** Detail of external valve apex. **C.** Detail of the external areolae structure, showing internal biseriate sieve plate (arrow). **D.** Interior whole valve view. **E.** Detail of interior valve center showing longitudinal band of silica (arrow). **F.** Detail of valve interior showing biseriate striae.

(Kützing) Levkov and *Halamphora subholsatica* (Krammer) Levkov. *Halamphora pertusa* can be distinguished from *H. acutiuscula* by its smaller size, longitudinal band of silica and the absence of distinctly thickened central dorsal virgae that is seen in *H. acutiuscula* (Levkov 2009: pl. 234, Fig. 4). *Halamphora pertusa* shares the internal silica band with *H. subholsatica*, but can be distinguished by its smaller size, finer striation, closely spaced proximal raphe ends, straight to concave ventral margin and lack of any thickening of the dorsal central virgae (Levkov 2009). *Halamphora pertusa* shares biseriate areolate striae with the freshwater species *H. punctata*, but can easily be distinguished by its comparatively broader valves, coarser striation, narrow ventral axial area and lack of any thickening of the dorsal central virgae (Stepanek & Kociolek 2013).

Halamphora attenuata Stepanek & Kociolek sp. nov. (Figs 3.5, 3.6)

Valves are semi-lanceolate with a smoothly arched dorsal margin and a straight to slightly convex ventral margin. Valve length 20.0–33.0 µm, valve breadth 3.5–4.5 µm. The valve ends are protracted, narrowly rounded and slightly bent ventrally. The raphe is arched with nearly straight raphe branches. Proximal raphe ends terminate closely and are slightly deflected dorsally. The distal raphe ends are difficult to see in the LM. The axial area is narrow throughout, expanding slightly near the ventral valve center. Dorsal striae are fine, 23–25 in 10 µm, and are finely areolate and weakly radiate throughout. In many specimens a broad raphe ledge can be seen in the LM, appearing as a 'longitudinal line' or 'shadow' running the length of the dorsal striae. Ventral striae number 26–29 in 10 µm. A light siliceous thickening or 'semi-stauros' can be observed at the dorsal central area in some of the specimens. Depending on the angle at which the valve is lying, the ventral portion of the valve can appear broad or narrow.

In the SEM, externally, the raphe is slightly biarcuate with the proximal ends slightly deflected dorsally and the distal ends hooked past the raphe ledge. The dorsal raphe ledge is very broad, although many specimens exhibited significant dissolution of this feature. The dorsal striae are crossed by many irregularly spaced vimines creating round to ovoid areolae of variable size and spacing. The initial axial

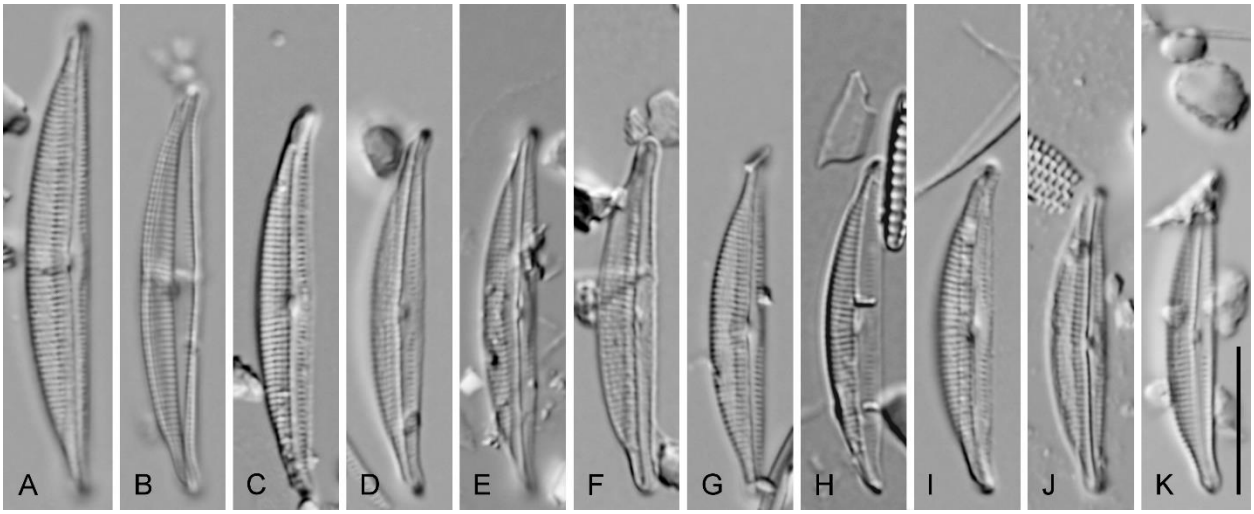

Figure 3.5. LM. *Halamphora attenuata* sp. nov. Single valves showing size range. **C.** Holotype specimen. Scale bar = 10 µm.

row of areolae is elongate and biseriate in contrast to the single areolate structure of the rest of the striae. It appears that this biseriate row of areolae is typically covered by the dorsal raphe ledge, and can only be observed here due to the partial dissolution of the raphe ledge. The ventral striae are composed of a single row of elongate areolae. A marginal ridge is not apparent in this taxon and the areolate striae continue to the valve margin. Internally, the axial row of biseriate dorsal striae make up nearly half of the dorsal striae before being crossed by vimines. The dorsal virgae near the valve center are slightly thickened and fused near the central nodule.

Type. USA. North Dakota, Kidder County: Salt Alkaline Lake, N46.95448°, W99.52382°, 3 November 2011, Holotype: Slide ANSP GC 65214, Fig. 3.5C; Isotypes: cleaned material ANSP GCM 5692, slide and cleaned material JPK 7981, Kociolek Collection at COLO.

Observations. Halamphora attenuata resembles several taxa with fine areolate striae in general valve dimensions and striae counts, including *Halamphora borealis* (Kützing) Levkov (2009) and *Halamphora salinicola* Levkov & Diaz in Levkov (2009). Of these taxa only *H. borealis* is widespread, being found in

brackish waters throughout Europe. *Halamphora attenuata* can be distinguished from these taxa by its broad, often convex, ventral valve, broad raphe ledge, and thickened dorsal virgae near the valve center.

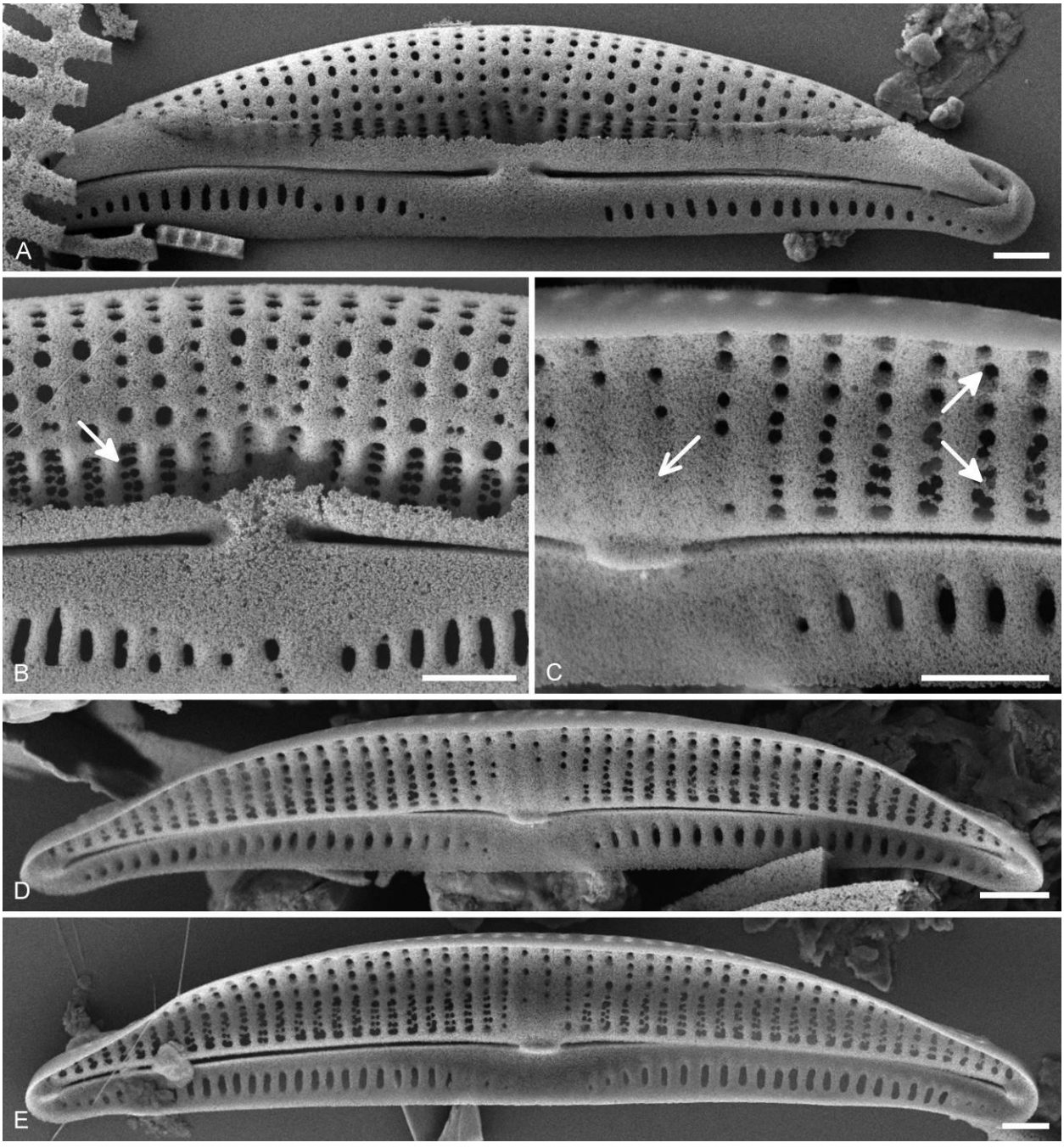

Figure 3.6. SEM. *Halamphora attenuata* sp. nov. **A.** External whole valve view. **B.** Detail of external valve center showing axial row of biseriate striae (arrow). **C.** Detail of the internal valve center showing the transition from biseriate to uniseriate striae (arrows), and fused virgae at the dorsal valve center (thin arrow). **D, E.** Internal whole valve view. Scale bars = 1 µm.

DISCUSSION

Prairie pothole lakes and wetlands represent a rich and varied environment with an understudied diatom flora. The new species described here were collected from elevated conductivity waters, ranging from 2187 to 9811 µS cm^{-1} for Long Lake and Salt Alkaline Lake, respectively. These habitats present interesting challenges for the classification of the genus *Halamphora* and the other groups present. Whereas diatom lineages have historically been thought of as either freshwater or marine (Round & Sims 1980, Mann 1999), this distinction may not be appropriate for many of these and other high conductivity inland waters. Certainly, the concept of a stable evolutionary divide between freshwater and saltwater lineages has been challenged recently, and we are beginning to understand that lineages move between these environments at a greater frequency than previously thought (Alverson et al. 2007, Alverson et al. 2011, Potapova 2011). The genus *Halamphora* is an excellent example of a group of diatoms that blurs the line between these habitat distinctions, being a monophyletic group that exhibits considerable taxonomic diversity in freshwater, marine and inland high conductivity waters (Stepanek & Kociolek 2014).

Largely marine diatom floras have been described from inland elevated conductivity environments including Devils Lake, ND (Stoermer et al. 1971) and Blue Lake warm springs (Kaczmarska & Rushforth 1983) which include a diversity of typical coastal marine and estuarine *Amphora* and *Halamphora* taxa. This does not seem to be the case in the smaller pothole lakes examined in this study, and it may be that these small, high conductivity waters have a unique flora separate from freshwater and coastal marine environments. An important question moving forward is whether these species are derived from largely freshwater lineages that have moved into saltier inland environments, or if they are derived from marine lineages that have moved inland, and if these environments represent an intermediate between these lineages.

Halamphora pratensis is most clearly allied with the common freshwater species *H. veneta*. This group has many freshwater representatives, including *H. coloradiana*, *H. oligotraphenta*, *H. veneta* var. *somalica*, and due to the broad definition of *H. veneta* it is likely that the freshwater diversity of this

group is underrepresented (Schoeman & Archibald 1978). Although the *H. veneta* group is largely thought of as freshwater in ecology, many halophilic species do exist that appear very morphologically similar to *H. veneta* (Levkov 2009) and the relationship between the freshwater and marine species within this group is not currently understood.

Halamphora pertusa and *H. attenuata* are morphologically similar to a number of punctate *Halamphora* taxa that are common and widespread in coastal marine and estuarine environments. This is especially apparent in the case of *H. pertusa*. The valve outline, distinctly punctate dorsal striae and the presence of an internal silica band near the dorsal axial area indicate a close affinity between *H. pertusa* and the brackish to marine taxa *Halamphora holsatica* (Hustedt) Levkov and *H. subholsatica*.

Given the small number of waterbodies examined in this current study (38 lakes and wetlands), it seems likely that the PPR of North America, which covers an area of over 700,000 km^2 (Sloan 1972), may hold a large amount of undescribed *Halamphora* diversity unique to elevated conductivity inland waters. With an estimated 49% of the lakes in the prairie pothole region of North Dakota drained in the last 200 years (Dahl 1990) and the continued loss of small wetlands (Doherty et al. 2013), our continued study of the diversity present within these habitats is especially important.

ACKNOWLWDGMENTS

This research was supported in part by a Seed Grant for Innovation from the University of Colorado Boulder.

CHAPTER IV

IMAGES AND DESCRIPTIONS OF CULTURED *AMPHORA* AND *HALAMPHORA* TAXA, WITH THE DESCRIPTION OF 31 NEW SPECIES

AMPHORA CLADE A

Amphora australiensis John Amph170/174 (Figs 4.1, 4.2)

Valves are broadly semi-elliptical and strongly dorsiventral. The dorsal margin is smoothly arched, the ventral margin is straight. The valve ends are narrowly rounded and ventrally deflected. Valve length 16–35 µm, valve breadth 4.5–8.0 µm. The raphe is straight with straight proximal ends. The ventral axial area is narrow throughout, the dorsal axial area is more or less expanded into a semi-lanceolate hyaline area. A siliceous thickening is observable at the central dorsal margin as a central depression. The dorsal striae are composed of elongate uninterrupted areolae. The ventral striae are composed of a single row of small areolae more or less continuous through the central area. Striae number 17–21 in 10 µm.

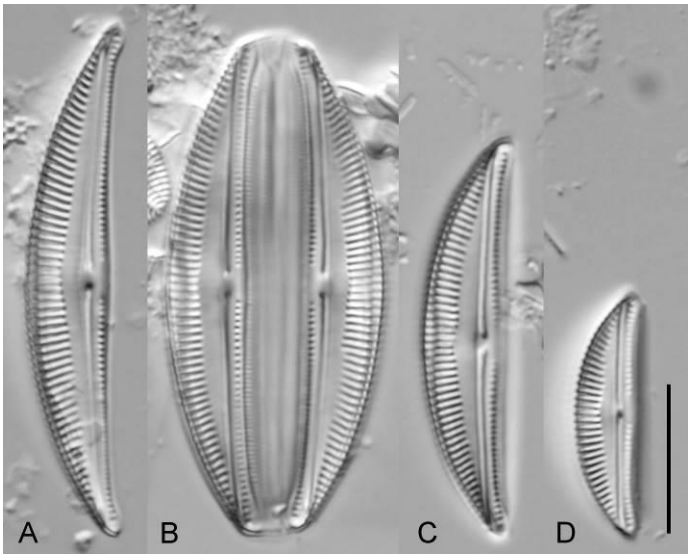

Figure 4.1. A–D. Light micrographs of *Amphora australiensis* showing size range. Scale bar = 10 µm.

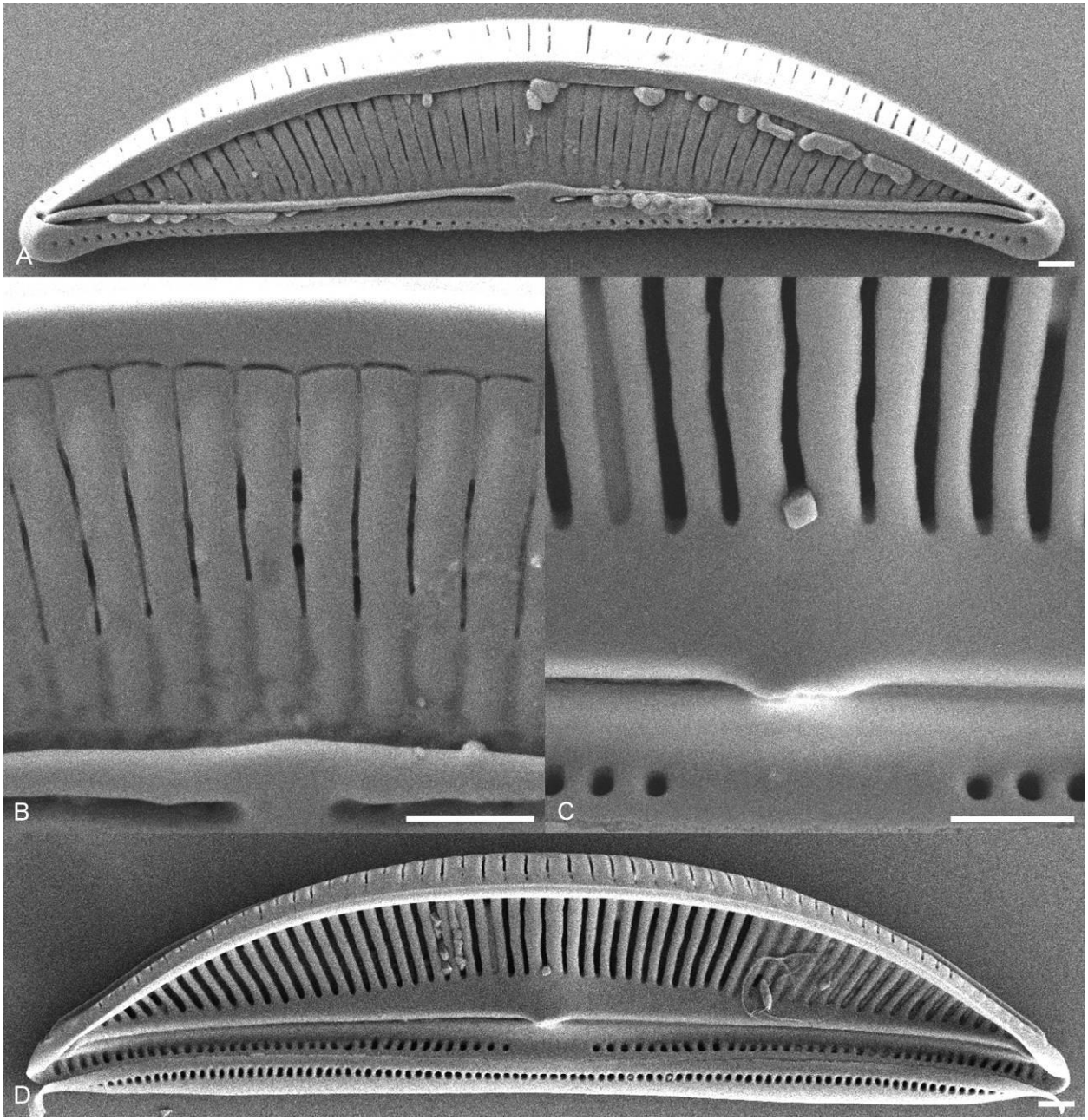

Figure 4.2. Scanning electron micrographs of *Amphora australiensis*. **A.** Whole external valve. **B.** Detail of external valve center. **C.** Detail of internal valve center. **D.** Whole internal valve. Scale bars = 1 µm.

In SEM, externally, the raphe is straight with straight proximal ends and dorsally deflected distal ends. The dorsal raphe ledge is small and continuous across the length of the valve. The dorsal axial area is narrow and semi-lanceolate. The dorsal marginal ridge is broad and developed into a siliceous flap that extends onto the valve face. The dorsal striae are composed of single foramen areolae extending uninterrupted from the axial area to the dorsal margin. The ventral striae are composed of a single row of

small ovoid areolae. Internally, the proximal raphe ends terminate in a weakly developed central helictoglossa. The dorsal and ventral striae are composed of single elongate areolae. The dorsal central virgae are slightly thickened compared to the rest of the valve.

Amphora sp. nov. Amph026 (Figs 4.3, 4.4)

Valves are semi-elliptical to semi-lanceolate and strongly dorsiventral. The dorsal margin is smoothly arched, the ventral margin is straight to slightly convex. The valve ends are narrowly rounded and ventrally deflected. Valve length 20.0–30.0 µm, valve breadth 3.5–5.5 µm. The raphe is ventrally positioned and weakly biarcuate. The axial area is narrow, slightly expanded through the dorsal valve center. The dorsal striae are composed of a single elongate areolae running from the axial area to a distinct marginal ridge. The ventral striae are composed of a single row of small areolae interrupted at the valve center. Striae number 23–25 in 10 µm.

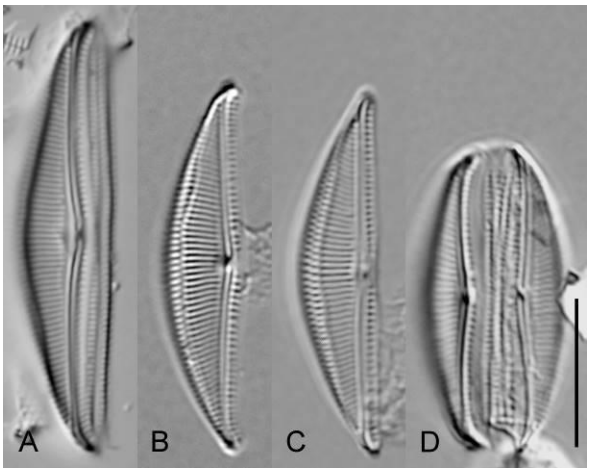

Figure 4.3. A–D. Light micrographs of *Amphora sp. nov.* Amph026 showing observed size range. Scale bar = 10 µm.

In SEM, externally, the raphe is straight with slightly dorsally deflected proximal ends and dorsally hooked distal ends. The dorsal raphe ledge is small and continuous along the length of the valve. A narrow dorsal axial area is present, not as broad as in most taxa. A prominent dorsal marginal ridge runs the length of the valve. The dorsal striae are composed of a single foramen areolae opened externally

as a thin slit. The ventral striae are composed of a single row of small slit-like areolae interrupted at the valve center. The dorsal girdle bands are broad and each have a single row small slit-like areolae.

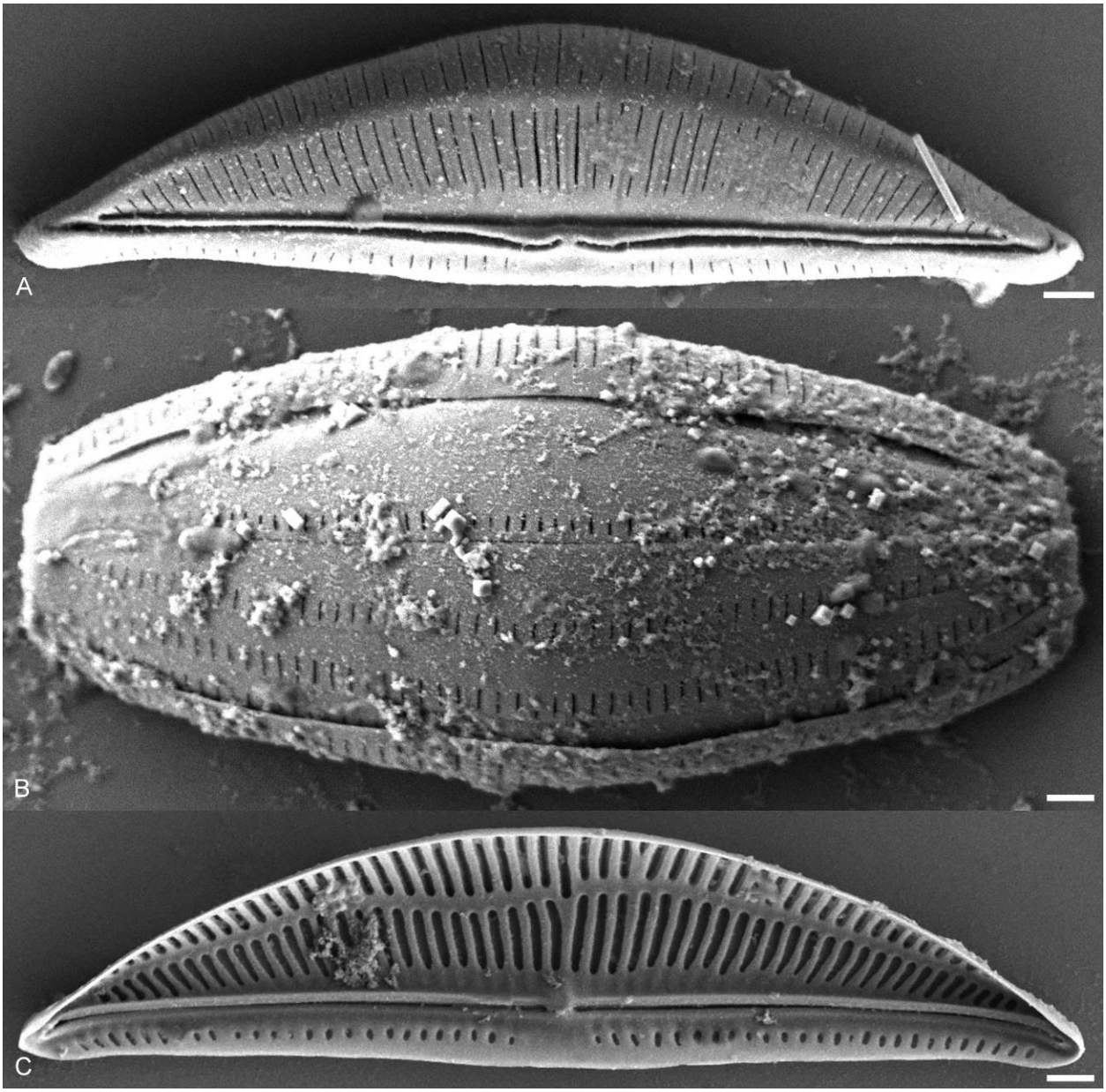

Figure 4.4. Scanning electron micrographs of *Amphora sp. nov.* Amph026. **A.** Whole external valve view. **B.** External whole frustule, girdle view. **C.** Whole internal valve view. Scale bars = 1 µm.

Internally, the proximal raphe ends terminate in a weakly developed fused central helictoglossae. The striae on the dorsal valve face and mantle are composed of single elongate areolae interrupted only by the dorsal marginal ridge.

Amphora sp. nov. Amph066 (Fig. 4.5)

Valves are semi-elliptical and strongly dorsiventral. The dorsal margin is smoothly arched, the ventral margin is slightly biarcuate. The valve ends are acute, narrowly rounded and ventrally deflected. Valve length 29.0–50.0 µm, valve breadth 6.0–7.5 µm. The raphe is slightly biarcuate with slightly dorsally deflected proximal valve ends. The ventral axial area is narrow throughout, the dorsal axial area is slightly expanded more so at the valve center. A distinct dorsal marginal ridge is visible in the LM. The dorsal striae are composed of a single thin areolae running uninterrupted from the axial area to the marginal ridge. The ventral striae are composed of a single row of small areolae. Striae number 25 in 10 µm.

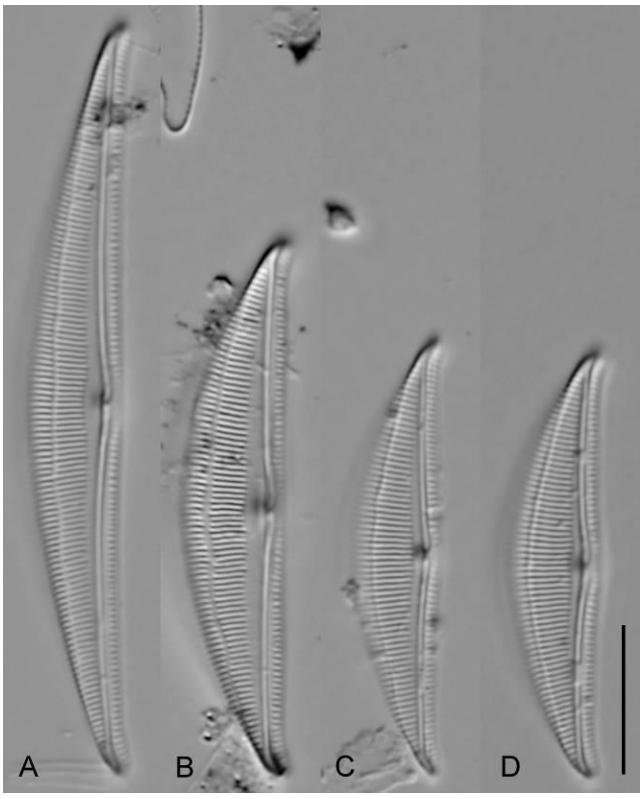

Figure 4.5. A–D. Light micrographs of *Amphora sp. nov.* Amph066 showing the observed size range. Scale bar = 10 µm.

Amphora graeffeana Hendey Amph074 (Figs 4.6, 4.7)

Valves narrowly semi-elliptical and strongly dorsiventral. The dorsal margin is smoothly arched, the ventral margin is straight to slightly convex. The valve ends are narrowly rounded and ventrally deflected. Valve length 23.0–27.0 µm, valve breadth 5.0–6.0 µm. The raphe is ventrally positioned and weakly biarcuate with straight proximal ends. A broad hyaline area is present along the dorsal axial area, ventral striae are not observable in the LM. The dorsal striae are composed of a single row of elongate areolae running along the dorsal margin. A distinct dorsal marginal ridge can be seen depending on the valve angle. Striae number 26–27 in 10 µm.

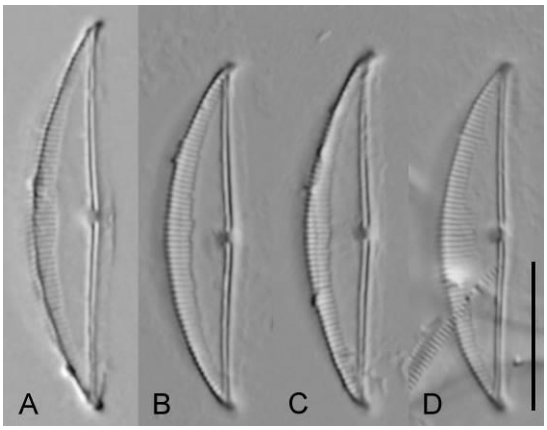

Figure 4.6. A–D. Light micrographs of *Amphora graeffeana* showing observed size range. Scale bar = 10 µm.

In SEM, externally, the raphe is straight with straight proximal ends and dorsally deflected distal ends. The raphe ledge is weakly developed dorsally, not seen ventrally. A large hyline axial area is present and appears as a siliceous infilling in some specimens. The dorsal striae are composed of a single row of elongate areolae ending at a prominent marginal ridge. From the marginal ridge a second row of elongate areolae make up the mantle striae. The ventral striae are irregular and not well developed in some specimens, otherwise a single row of thin slit-like areolae. Internally, the proximal raphe ends µterminate in an extremely weakly developed fused helictoglossae.

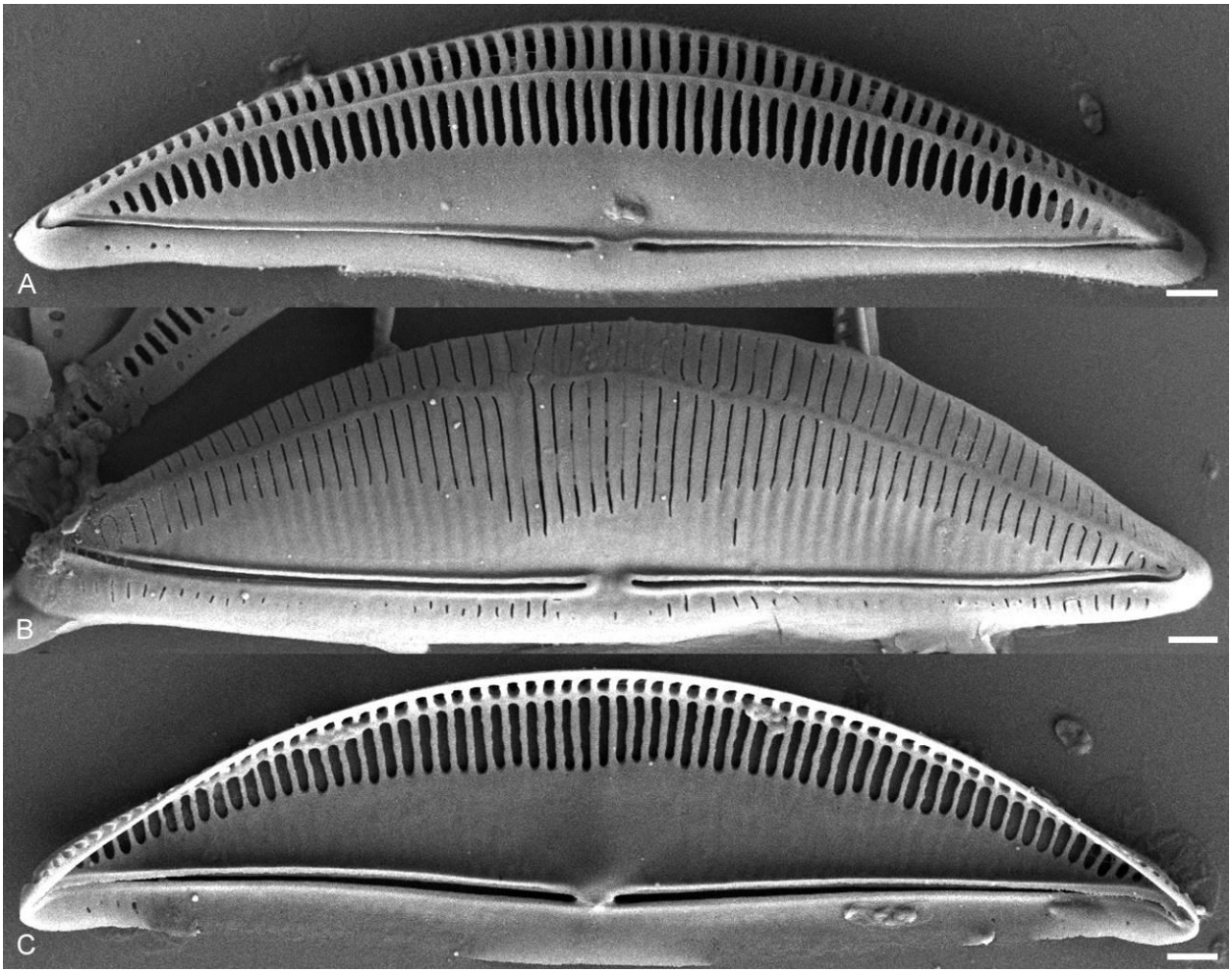

Figure 4.7. Scanning electron micrographs of *Amphora graeffeana*. **A.** Whole valve external view. **B.** Whole valve external view. **C.** Whole valve internal view. Scale bars = 1 µm.

Amphora graeffeana Hendey Amph069 (Figs 4.8, 4.9)

Valves narrowly semi-elliptical and strongly dorsiventral. The dorsal margin is smoothly arched, the ventral margin is straight to slightly convex. The valve ends are narrowly rounded and ventrally deflected. Valve length 30.0–40.0 µm, valve breadth 5.5–7.0 µm. The raphe is ventrally positioned and weakly biarcuate with straight proximal ends. A broad hyaline area is present along the dorsal axial area, ventral striae are not observable in the LM. The dorsal striae are composed of a single row of elongate areolae running along the dorsal margin. A distinct dorsal marginal ridge can be seen depending on the valve angle. Striae number 28 in 10 µm.

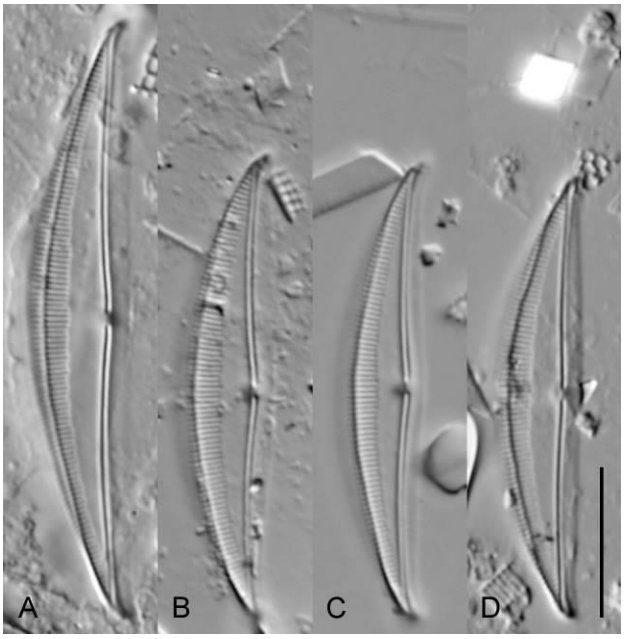

Figure 4.8. A–D. Light micrographs of *Amphora graeffeana* Amph069 showing the observed size range. Scale bar = 10 µm.

In SEM, externally, the raphe is straight with straight proximal ends and straight to slightly dorsally deflected distal ends. The raphe ledge is weakly developed. A large hyline axial area is present. The dorsal striae are composed of a single row of elongate areolae ending at a prominent marginal ridge. From the marginal ridge a second row of elongate areolae make up the mantle striae. The ventral striae are irregular and not well developed. Internally, the proximal raphe ends terminate in an extremely weakly developed fused helictoglossae.

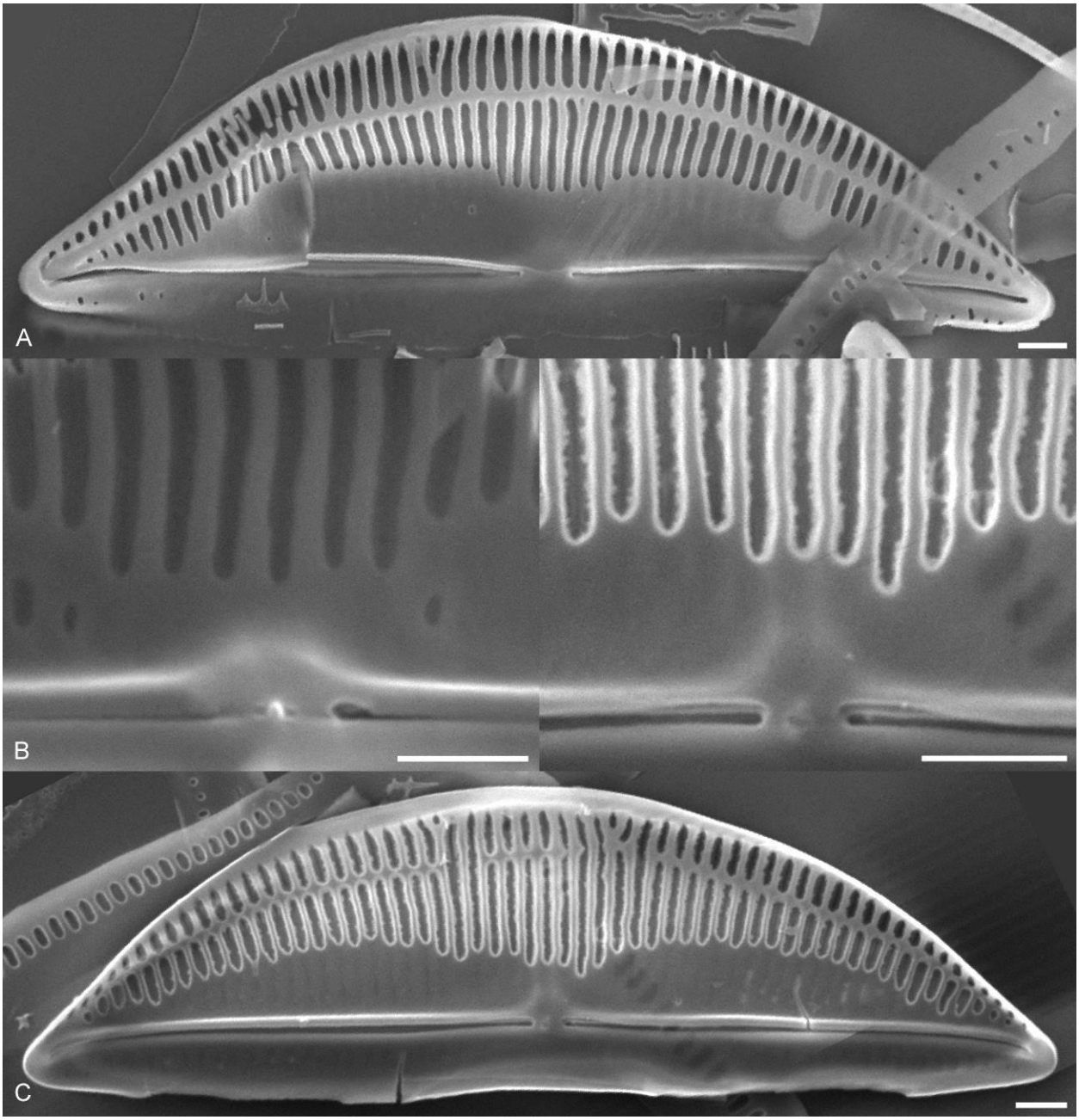

Figure 4.9. Scanning electron micrographs of *Amphora graeffeana* Amph069. **A.** Whole external valve view. **B.** Detail of internal valve center. **C.** Detail of internal valve center. **D.** Whole internal valve. Scale bars = 1 μm.

Amphora sp. nov. Amph044/038 (Figs 4.10, 4.11)

Valves semi-elliptical and strongly dorsiventral. The dorsal margin is smoothly arched and the ventral margin is straight. The valve ends are rounded and slightly ventrally deflected. Valve length 13.0–

29.0 µm, valve breadth 3.5–5.0 µm. The raphe is straight and runs along the ventral margin. The proximal raphe ends terminate closely together. The axial area is narrow throughout. A thin, transapically oriented, siliceous thickening runs from the central axial area to the dorsal margin. The striae are fine and difficult to resolve in the LM.

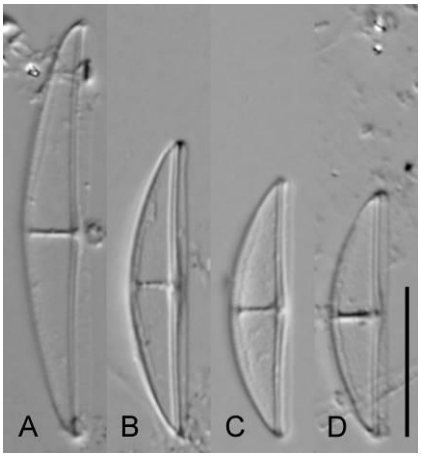

Figure 4.10 A–D. Light micrographs of *Amphora sp. nov.* Amph044/038 showing observed size range. Scale bar = 10 µm.

In SEM, the raphe is straight with dorsally deflected distal ends and proximal ends that dip ventrally before ending in closely spaced dorsally deflected endings. The dorsal raphe ledge is weakly developed but continuous across the length of the valve. The dorsal striae are composed of many small round areolae. These dorsal areolae become elongate at the marginal ridge which is thin and runs the length of the dorsal margin. The ventral striae are composed of small irregularly placed areolae. Internally, a distinct siliceous thickening runs transapically from the central axial area to the dorsa margin. The internal raphe branches are straight and end, proximally, in a highly reduced fused central helictoglossae.

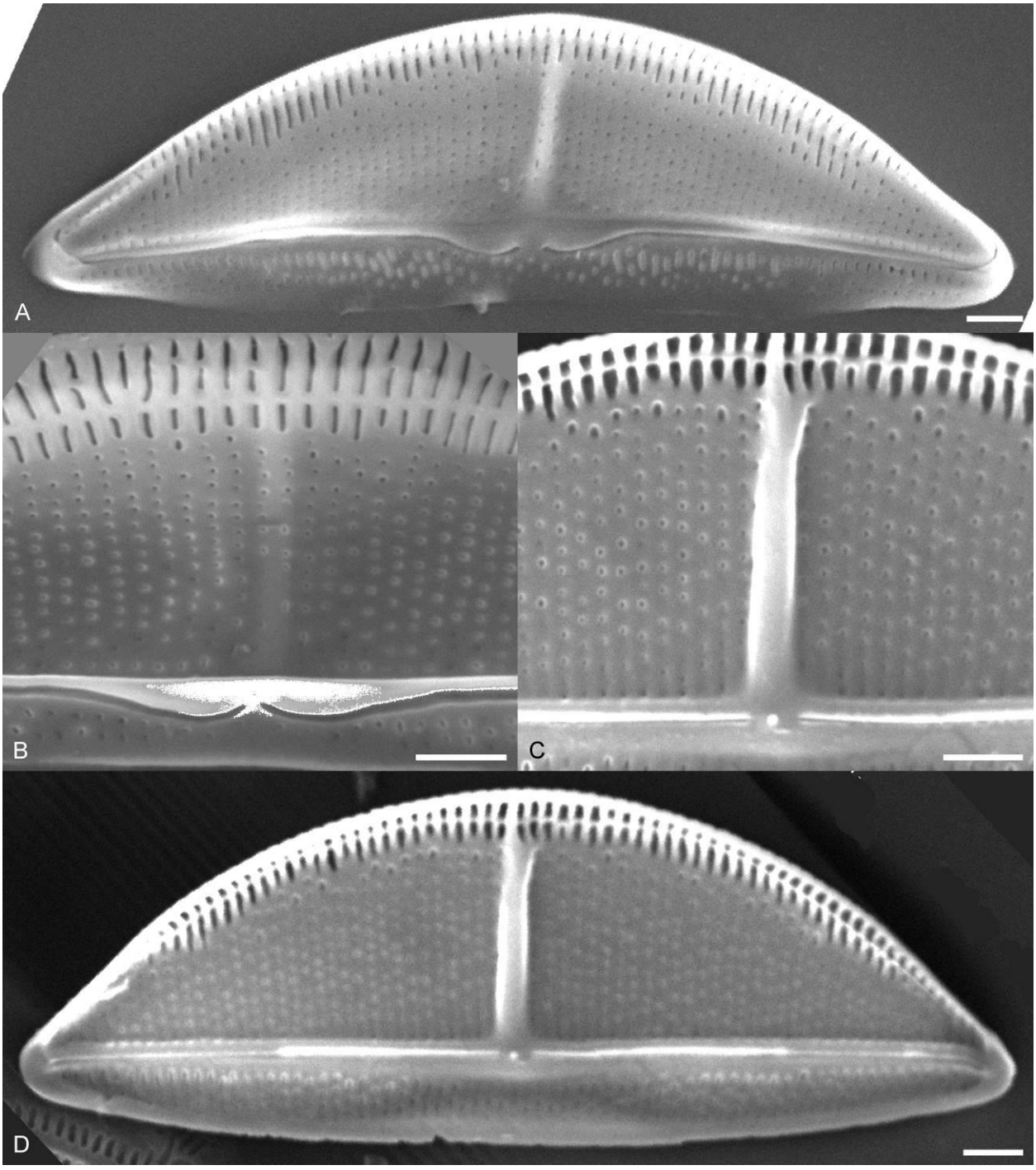

Figure 4.11. Scanning electron micrographs of *Amphora sp. nov.* Amph044/038. **A.** Whole external valve. **B.** Detail of external valve center. **C.** Detail of internal valve center. **D.** Whole internal valve. Scale bars = 1 µm.

Amphora abludens Simonsen Amph072/059 (Figs 4.12, 4.13)

Valves narrowly semi-elliptical and strongly dorsiventral. The dorsal margin is smoothly to shallowly arched and the ventral margin is straight to slightly convex. The valve ends are narrowly rounded. Valve length 14.0–35.0 µm, valve breadth 4.0–5.5 µm. The raphe is straight and positioned along the ventral margin. The proximal raphe ends are straight. The axial area is narrow throughout. A thin siliceous thickening is present at the dorsal valve center running from the axial area to the dorsal margin. A thin marginal ridge is visible in some imaged specimens. The dorsal and ventral striae are extremely fine and are difficult to resolve in the LM.

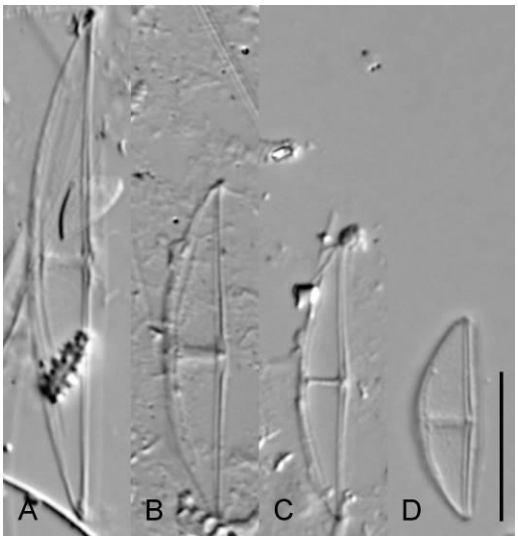

Figure 4.12. A–D. Light micrographs of *Amphora abludens* Amph072/059 showing observed size range. Scale bar = 10 µm.

In SEM, externally, the raphe is straight with dorsally deflected distal ends and proximal ends that dip ventrally before terminating closely in simple endings. The dorsal raphe ledge is small but continuous along the length of the valve. A ventral raphe ledge is not present. The dorsal striae are composed of many small areolae, often becoming more elongate near the dorsal margin. A more or less hyaline fascia is present at the dorsal central valve. A moderately developed marginal ridge runs the length of the valve. The ventral striae consist of a single row of thin, elongate areolae. Internally, a thin siliceous thickening runs transapically from the axial area to the dorsal margin. The proximal raphe ends terminate in a small weakly developed fused central helictoglossae.

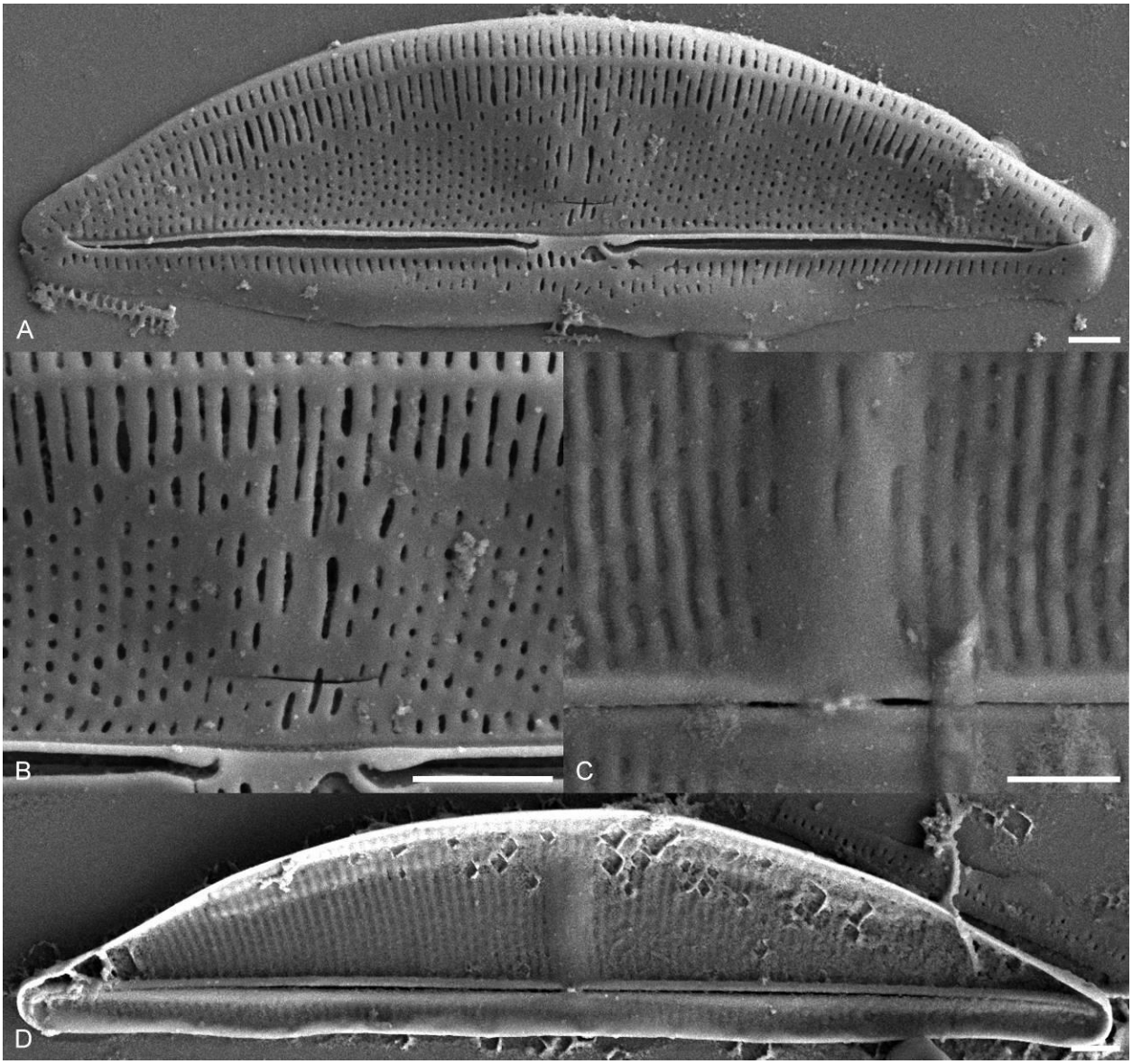

Figure 4.13. Scanning electron micrographs of *Amphora abludens* Amph072/059. **A.** Whole external valve. **B.** Detail of external valve center. **C.** Detail of internal valve center. **D.** Whole internal valve. Scale bars = 1 µm.

Amphora sp. nov. Amph135 (Fig. 4.14)

Valves are narrowly semi-elliptical and strongly dorsiventral. The dorsal margin is shallowly arched and the ventral margin is convex to slightly biarcuate. The valve ends are acute and narrowly rounded. Valve length 26.0–43.0 µm, valve breadth 5.0–5.5 µm. The raphe is positioned along the ventral

margin and is slightly biarcuate. The proximal raphe ends are straight. The axial area is narrow throughout. Dorsal and ventral fascia are not present. The dorsal and ventral striae are fine and difficult to resolve in the LM.

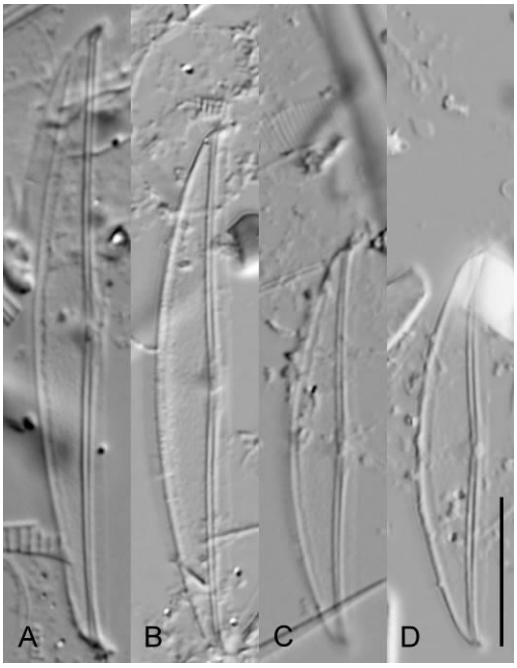

Figure 4.14. A–D. Light micrographs of *Amphora sp. nov.* Amph135 showing the observed size range. Scale bar = 10 µm.

AMPHORA CLADE B

Amphora commutata Grunow in Van Heurck Amph126 (Figs 4.15, 4.16)

Valves semi-elliptical to linear through the valve center. The dorsal margin is arched near the apices, straight to biarcuate through the central portion of the valve. The ventral margin is straight to slightly convex. The valve ends are narrowly rounded and deflected ventrally. Valve length 40.0–60.0 µm, valve breadth 5.5–7.5 µm. The raphe is biarcuate and dorsally positioned so that the majority of the raphe runs along the dorsal margin. The proximal raphe ends are deflected dorsally. The axial area is narrow along the dorsal side, although slightly expanded near the central area. The ventral axial area is not discernable due to the large unornamented ventral valve. Dorsal and ventral fascia are not present. The dorsal striae are difficult to image in the LM, not obviously areolate and parallel through the central

valve, becoming radiate near the apices. No ventral striae are present although a single row of small areolae can be seen running along the ventral margin. Striae number 15–16 in 10 µm.

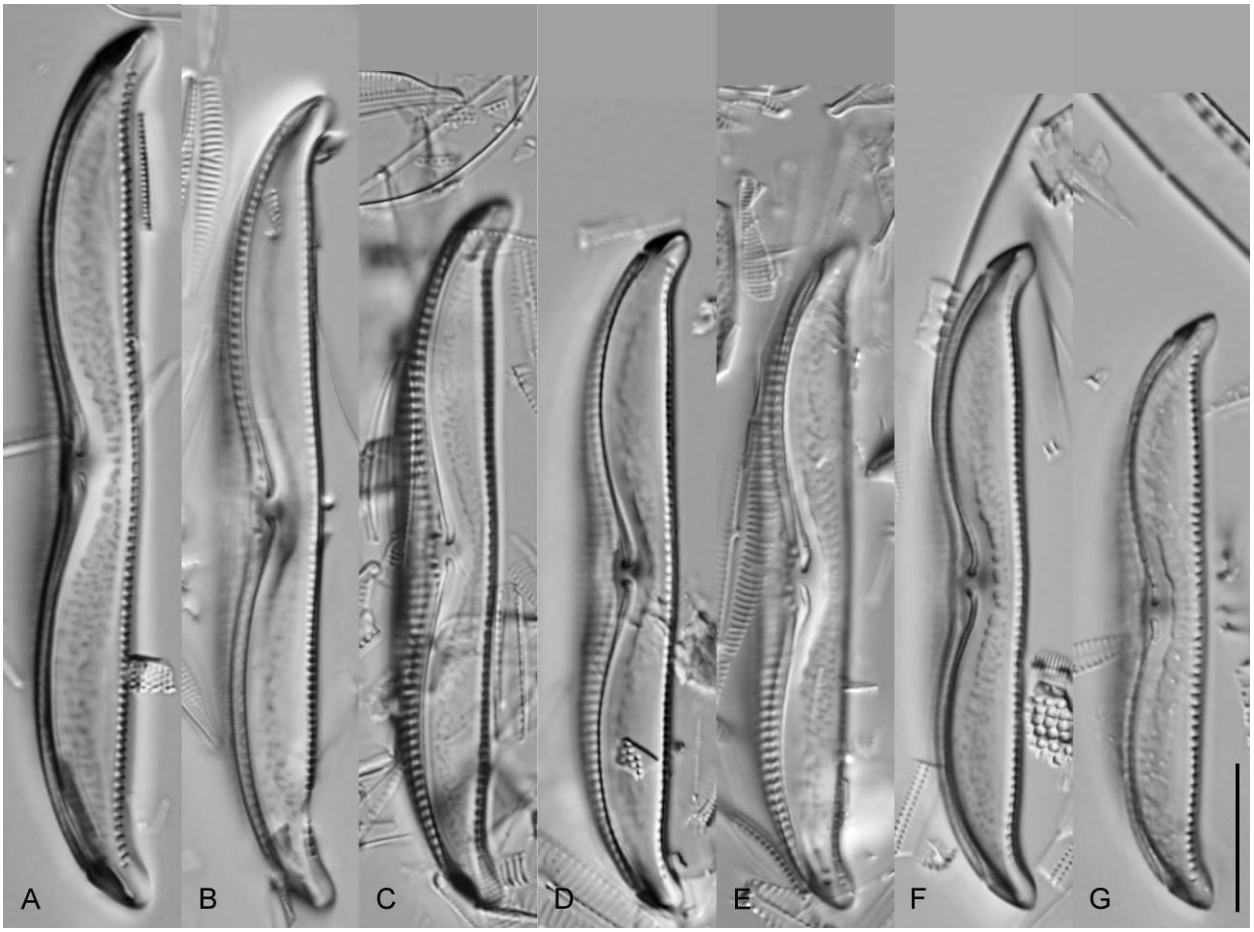

Figure 4.15. A–G. Light micrographs of *Amphora commutata* Amph126 showing observed size range. Scale bar = 10 µm.

In SEM, externally, the raphe is biarcuate with proximal and distal ends deflected dorsally. The dorsal raphe ledge is broad, more so at the central area, and covers the majority of the dorsal striae. No ventral raphe ledge is visible. The dorsal striae are composed of a single row of slit-like foramina. An extremely broad marginal ridge separates the valve face from the dorsal margin. This marginal ridge is ornamented with many irregularly placed indentations. The ventral valve, although not striate, is ornamented in many irregularly placed indentations, as with the marginal ridge. Internally, the dorsal striae are composed of a single row of elongate ovoid areolae. The dorsal axial area is broad and expands into a siliceous thickening at the valve center. As with the external view, the ventral valve is not striate

except for a single row of small areolae running along the ventral margin. The proximal raphe ends terminate in a weakly developed fused central helictoglossa. In cross-section the chambered foramen areolae are evident.

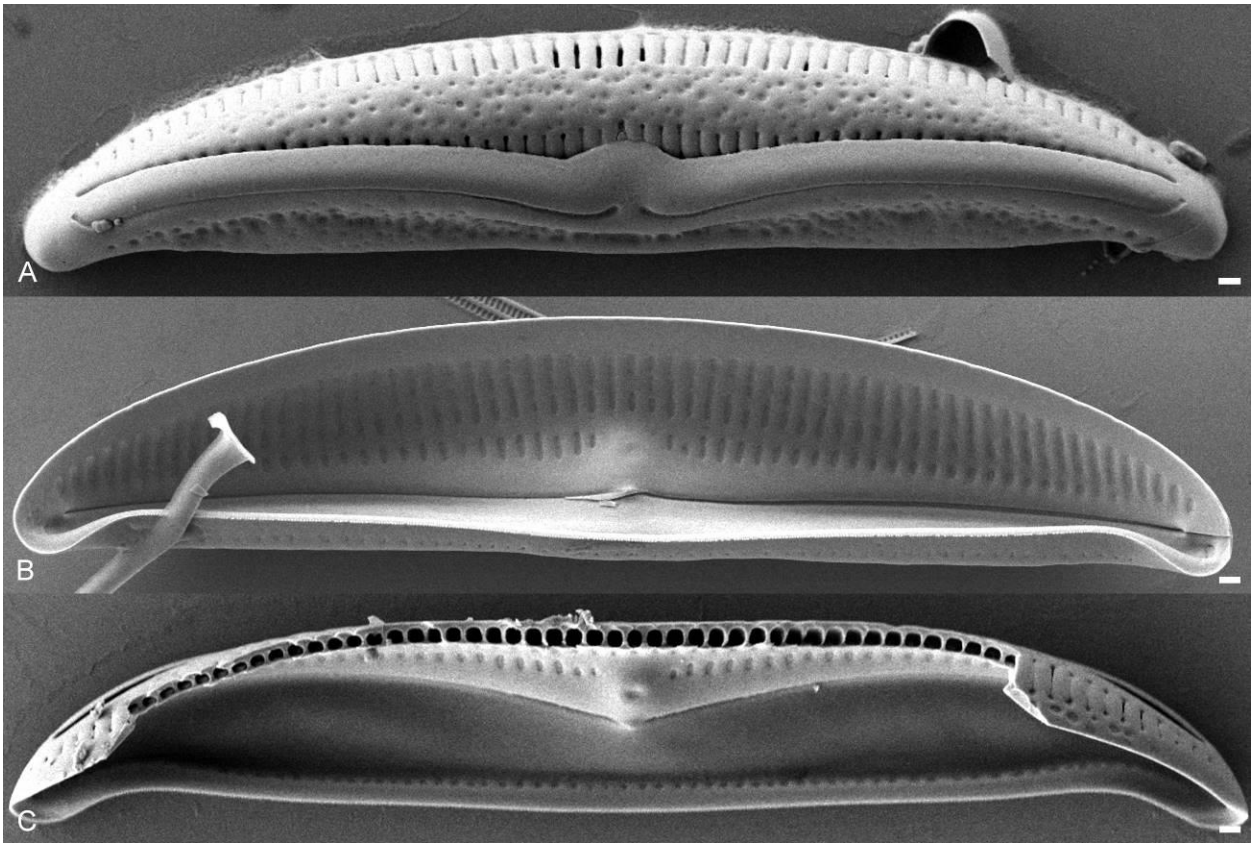

Figure 4.16. Scanning electron micrographs of *Amphora commutata* Amph126. **A.** Whole external valve. **B.** Whole internal valve. **C.** Whole internal valve showing dorsal valve cross-section. Scale bar = 1 µm.

Amphora aliformis Stepanek, Mayama & Kociolek Amph159/177 (Figs 4.17, 4.18)

Frustule elliptical with bluntly truncated ends. Valves semi-elliptical, moderately dorsiventral, with a smoothly arched dorsal margin and a straight to slightly convex ventral margin. Valve length 12.0–24.0 µm, valve breadth 3.5–5.5 µm, although the breadth of this taxon can vary greatly depending on the angle at which the valve is lying. Valve ends are narrowly rounded and slightly deflected ventrally. The raphe is nearly centrally placed on the valve, straight to slightly arched, with straight proximal raphe ends and distal raphe ends that are difficult to observe in the LM. The axial area is narrow throughout dorsally. Dorsal striae are uninterrupted, nearly parallel at the valve center and becoming radiate near the apices.

Dorsal striae number 19–20 in 10 µm. Depending on the valve angle, the dorsal striae are often obscured near the dorsal margin by a distinct hyaline area. Ventral striae are absent, although a broad unornamented ventral area is present.

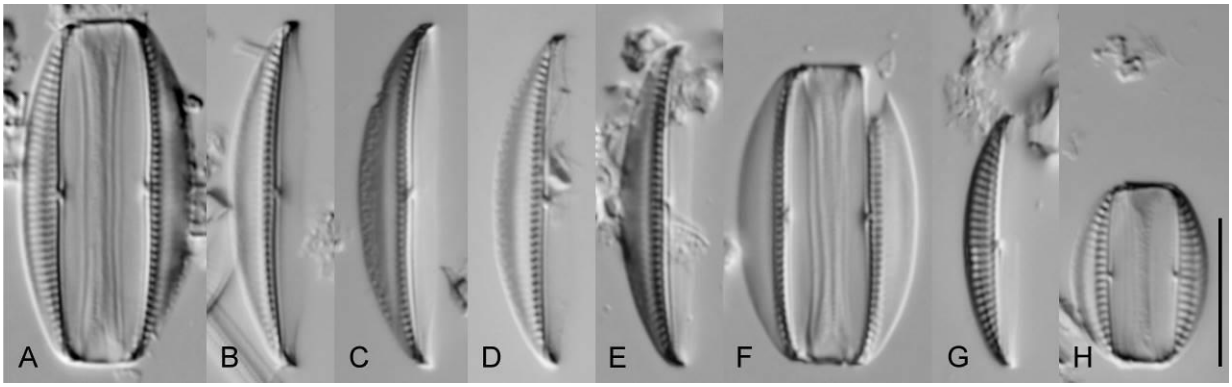

Figure 4.17. A–H. Light micrographs of *Amphora aliformis* Amph159/177 showing the observed size range. Scale bar = 10 µm.

In the SEM, the most prominent feature of *A. aliformis* is a dorsal marginal ridge that extends into a broad "wing" running the length of the dorsal margin. When the whole frustule is viewed from the dorsal margin side, this wing lies flush against the substrate. The wing is broad and unornamented except for small depressions or dimples irregularly spaced throughout the structure. When viewed from the ventral mantle side, the dorsal valve face quickly falls away from the valvar plane before meeting the dorsal wing. This wing then comes back to the valvar plane creating a deep depression or valley between the axial area and the dorsal edge of the wing. This steep curvature of the dorsal valve face combined with the broad unornamented dorsal wing creates the obscured dorsal striae seen in the LM.

The striae are alveolate with the external areolae openings consisting of a narrow slit interrupted only by the dorsal marginal wing. The external areolae openings extend some way onto the protracted wing, past the internal occlusions that make up the internal valve structure. This feature is seen in both the valve face and marginal striae creating a hollow chamber at the base of the wing that is open via the external striae but is closed to the valve interior by the internal valve coverings. Externally, the raphe is weakly arched with proximal ends slightly deflected dorsally. The distal raphe ends are sharply deflected

dorsally past the distal end of the raphe ledge and dorsal marginal wing, continuing onto the dorsal margin. The raphe ledge is continuous on the dorsal side, not apparent on the

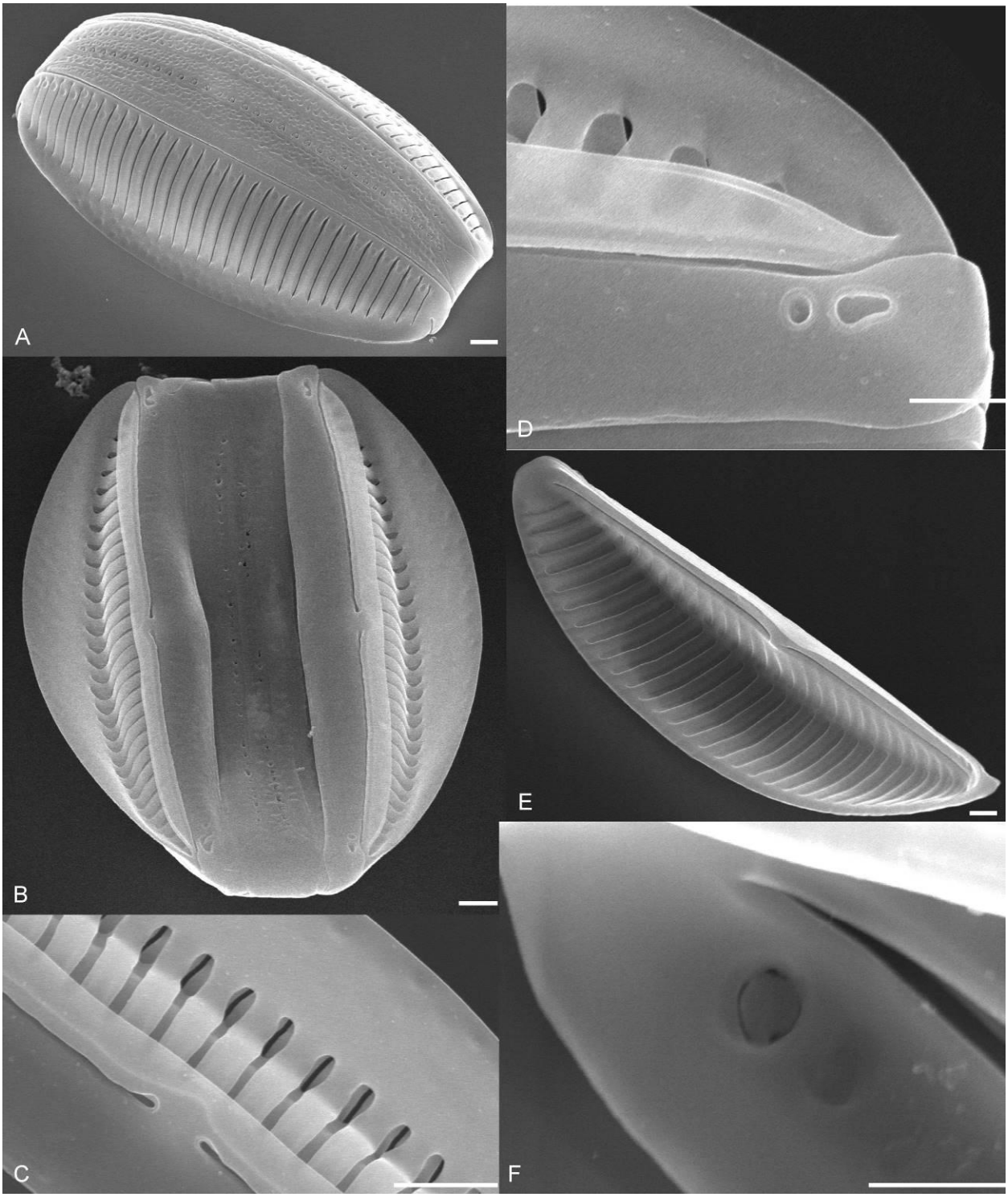

Figure 4.18. Scanning electron micrographs of *Amphora aliformis* Amph159/177. **A.** Whole frustule girdle side. **B.** Whole frustule valve side. **C.** Detail of external valve center. **D.** Detail of external valve end. **E.** Whole internal valve. **F.** Detail of internal valve end. Scale bars = 1 µm.

ventral side. The ventral valve is broad and unornamented aside from several large pores positioned near the valve apices.

The girdle bands are somewhat irregularly areolate, varying between small pores to more complex crescent and horseshoe shaped openings. Along with the pores, many irregular depressions are visible throughout the girdle area.

Internally, the striae are composed of a single elongate areolae interrupted only at the valve margin by a band of silica. The internal raphe terminates proximally at a weakly developed central helictoglossae. The ventral apical pores seen externally are occluded internally by a sieve plate anchored in several places to the ventral valve. Although in the fully developed cell the ventral striae are absent, in early valve development ventral virgae are initially formed and must be filled in later development.

AMPHORA SENSU STRICTO

Amphora gigantea var. *fusca* (Schmidt in Schmidt et al.) Cleve Amph099 (Figs 4.19, 4.20)

Valves semi-elliptical and dorsiventral with a smoothly arched dorsal margin and a straight ventral margin. The valve ends are broadly rounded. Valve length 60.0–75.0 µm, valve breadth 10.5–13.5 µm. The raphe is centrally positioned and strongly biarcuate with dorsally deflected proximal raphe ends. The dorsal raphe ledge is visible in the LM as a faint longitudinal line along the axial area. The axial area on the dorsal side is narrow throughout. The ventral side of the valve face is largely unornamented with striae only visible at the apices. No dorsal fascia is present. The dorsal striae are areolate, parallel near the valve center and becoming radiate near the apices. The ventral striae are convergent and only visible near the apices. Striae number 11–12 in 10 µm.

In SEM, externally, the proximal and distal raphe ends deflect dorsally. The dorsal raphe ledge is broad and continuous along the length of the valve. The dorsal striae are composed of a single unbroken slit-like foramina, running from the axial area through the dorsal mantle. The ventral valve is largely unornamented with striae only near the apices. Internally, the striae are crossed by vimines creating many small round to ovoid areolae. A lanceolate hyaline area is present at the dorsal central axial area. The

ventral apical striae appear to be infilled with silica. The proximal raphe ends terminate in separate central helictoglossae.

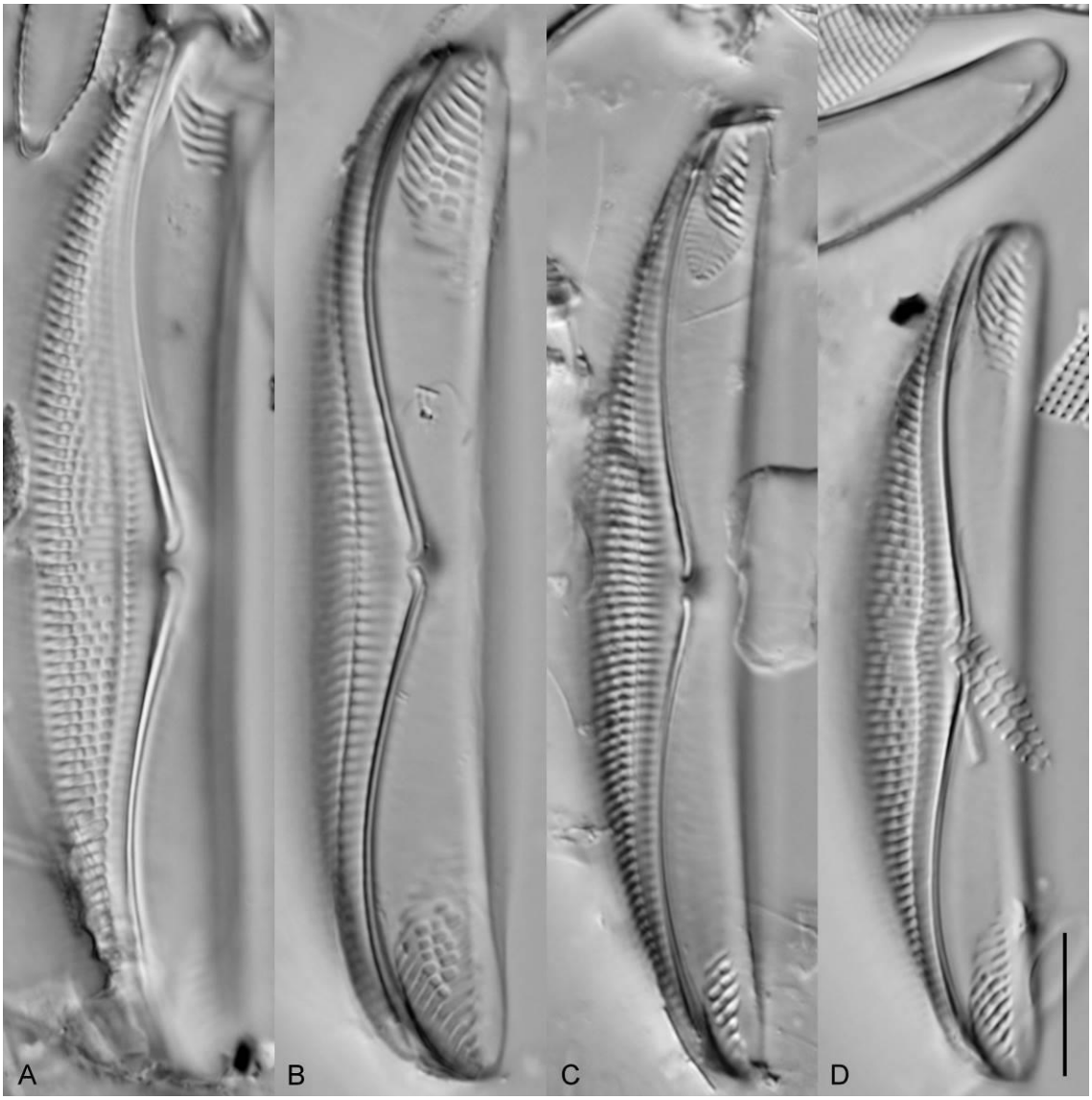

Figure 4.19. A–D. Light micrographs of *Amphora gigantea* var. *fusca* Amph099 showing observed size range. Scale bar = 10 µm.

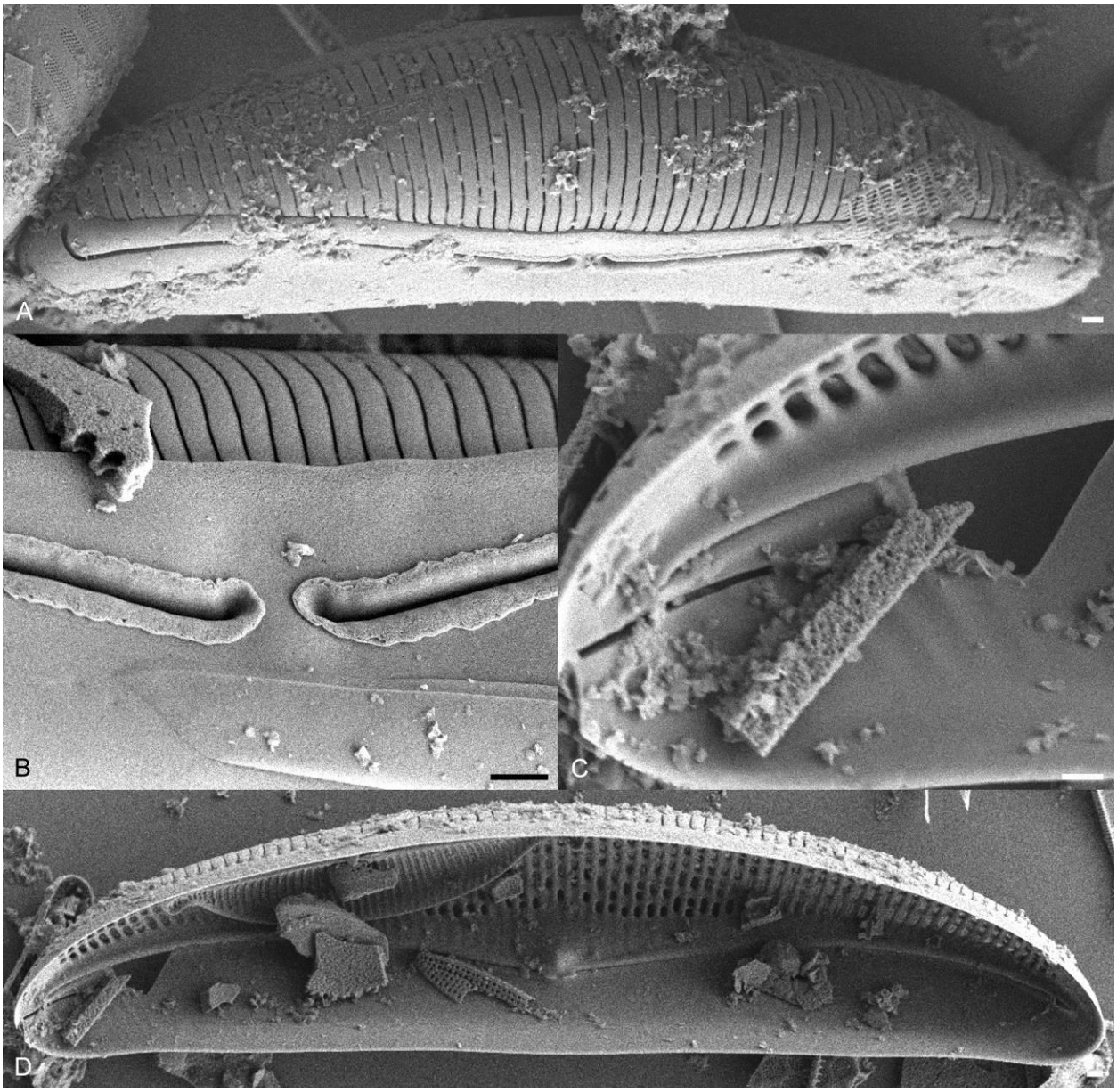

Figure 4.20. Scanning electron micrographs of *Amphora gigantea* var. *fusca* Amph099. **A.** Whole external valve. **B.** Detail of external valve center. **C.** Detail of internal valve end. **D.** Whole internal valve. Scale bars = 1 µm.

Amphora sp. nov. Amph071 (Figs 4.21, 4.22)

Valves are narrowly semi-elliptical and moderately dorsiventral. The dorsal margin is shallowly arched and the ventral margin is straight to slightly concave. The valve ends are broadly rounded. Valve length 35.0–51.0 µm, valve breadth 5.5–7.5 µm. The raphe is centrally placed and biarcuate with proximal ends slightly dorsally deflected. The axial area is narrow along the dorsal side, slightly

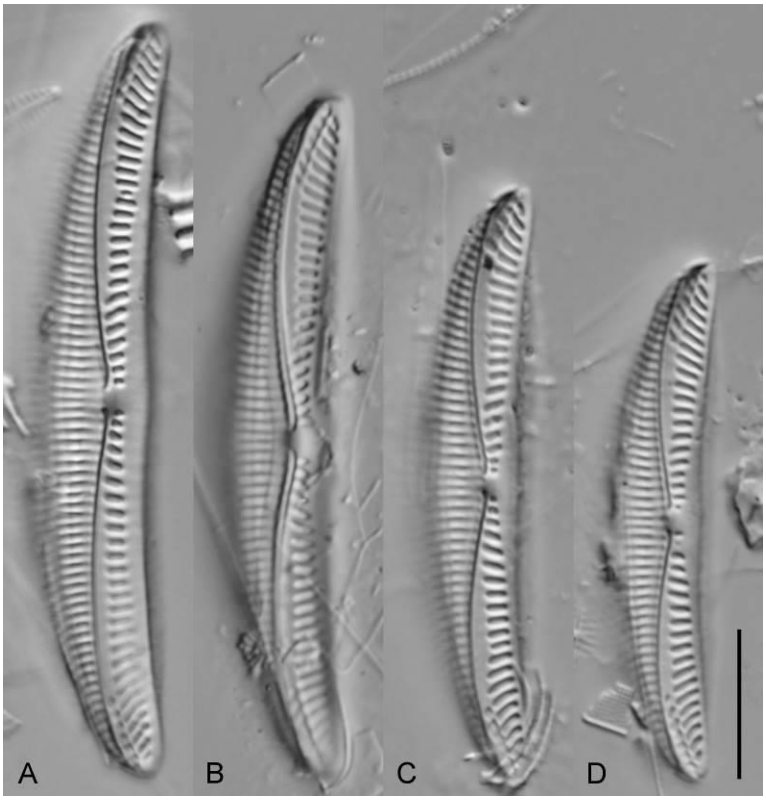

Figure 4.21. A–D. Light micrographs of *Amphora sp. nov.* Amph071 showing observed size range. Scale bar = 10 µm.

expanded along the ventral side. A dorsal fascia is not present. A small ventral fascia is present as a break in the ventral striae. The dorsal striae do not appear areolate, parallel at the valve center and becoming radiate near the apices. The ventral striae are composed of one to two rows of elongate areolae, radiate near the valve center, becoming convergent near the apices. Striae number 13–15 in 10 µm.

In SEM, externally, the proximal and distal raphe ends are dorsally deflected. The dorsal raphe ledge is continuous along the length of the valve. The ventral raphe ledge is only present near the apices. The dorsal striae are composed of a single unbroken foramen slit from the axial area through the dorsal mantle. The ventral areolae are opened individually by thin foramina. Internally, the dorsal striae are composed of several small round to ovoid areolae. There is a lanceolate hyaline area present along the dorsal central axial area. The proximal raphe ends terminate in small weakly developed separate central helictoglossae.

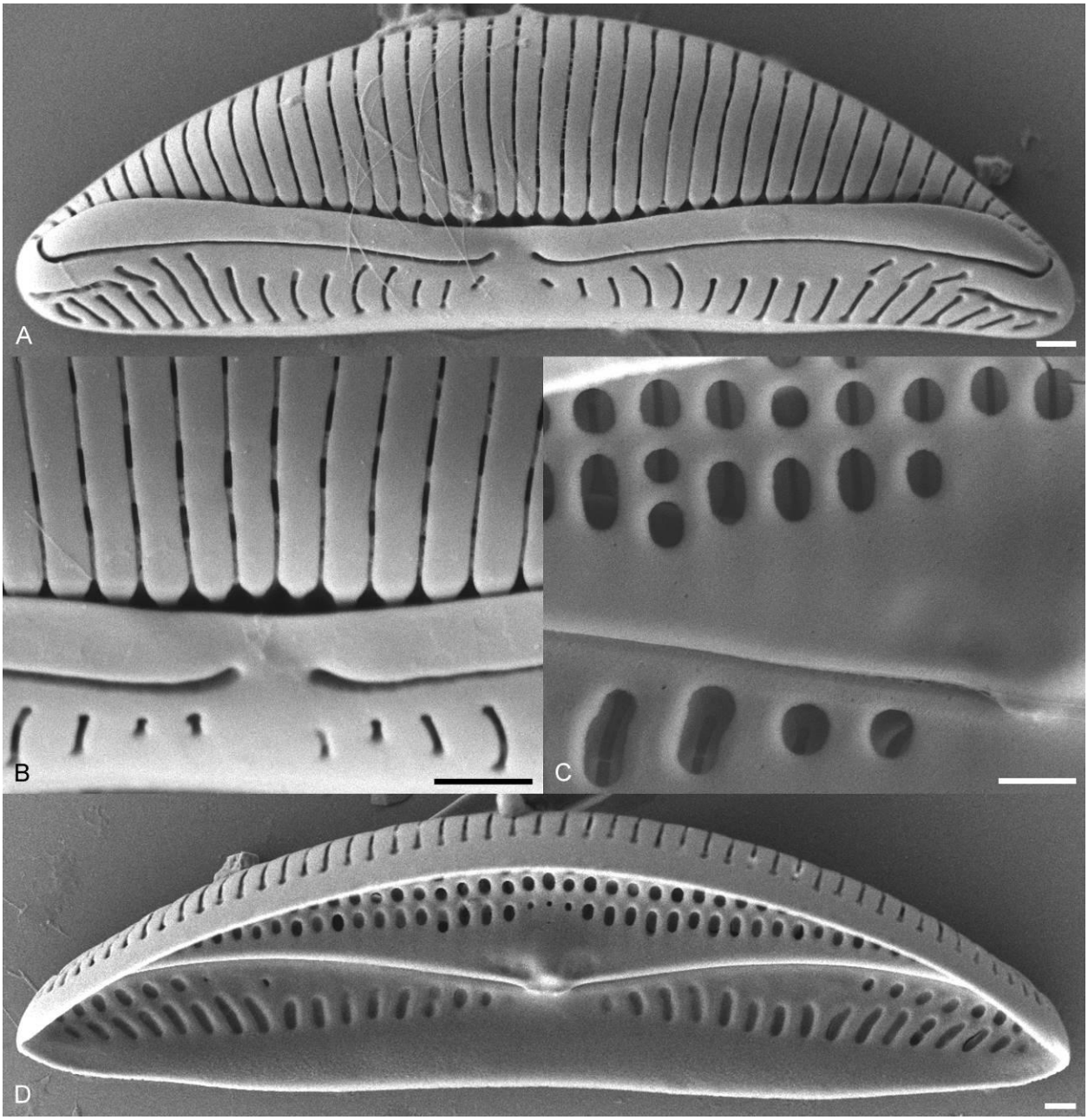

Figure 4.22. Scanning electron micrographs of *Amphora sp. nov.* Amph071. **A.** Whole external valve. **B.** Detail of external valve center. **C.** Detail of internal valve center. **D.** Whole internal valve. Scale bar = 1 µm.

Amphora sp. nov. Amph064 (Fig. 4.23)

Valves semi-elliptical to nearly linear with the ventral valve distinctly larger and more prominent in most views. The dorsal margin is arched near the apices, becoming flat over the central valve in larger specimens. The valve ends are broadly rounded. Valve length 38.0–65.0 µm, valve breadth 8.5–10.5 µm.

The raphe is strongly biarcuate with the branches positioned near the dorsal margin over much of the valve. The proximal raphe ends are deflected dorsally. The dorsal raphe ledge is visible in the LM as a faint longitudinal line running long the axial area. A dorsal fascia is not apparent. A small ventral fascia is produced from a break in the ventral striae. The dorsal striae are difficult to image in the LM due to the curvature of the valve face. The dorsal striae are composed of one to two rows of elongate areolae. The ventral striae are prominent and compose of two rows of large elongate areolae, radiate near the valve center, becoming convergent near the apices. Striae number 11–13 in 10 µm.

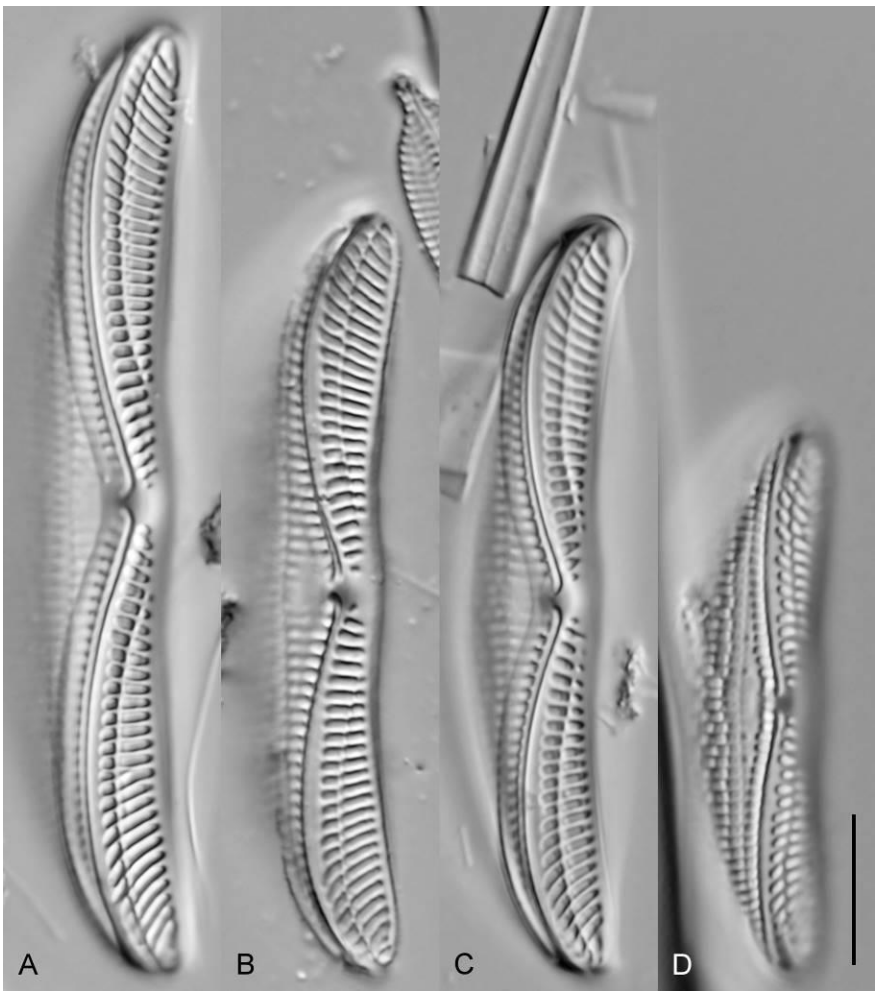

Figure 4.23. A–D. Light micrographs of *Amphora sp. nov.* Amph064 showing observed size range. Scale bar = 10 µm.

Amphora sp. nov. Amph033/097 (Figs 4.24, 4.25)

Valves semi-elliptical and dorsiventral. The dorsal margin is smoothly arched, the ventral margin is straight to slightly concave. The valve ends are broadly rounded and slightly ventrally deflected. Valve length 31.0–41.0 µm, valve breadth 6.5–7.5 µm. The raphe is centrally placed and strongly biarcuate with dorsally deflected proximal ends. The axial area is narrow along the dorsal side and slightly expanded along the ventral side in some specimens. A small lanceolate dorsal fascia is present and appears as a hyaline separation of the dorsal areolae. A small ventral fascia is produced as a break in the ventral striae. The dorsal striae are composed of two rows of small areolae, separated through the valve center. The dorsal striae are parallel through the valve center, becoming radiate near the apices. The ventral striae are composed of one to two rows of distinctly larger areolae than the dorsal striae. The ventral striae are radiate near the valve center, becoming convergent near the apices. Striae number 12–13 in 10 µm.

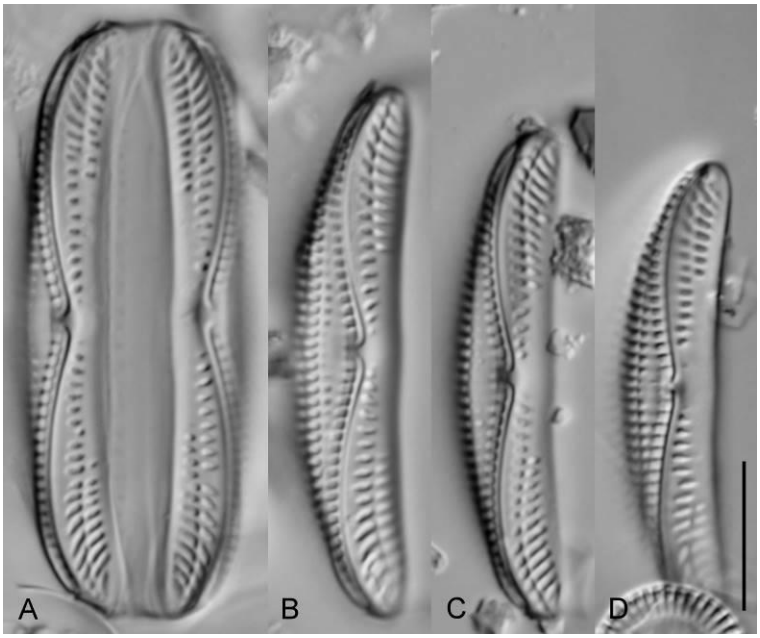

Figure 4.24. A–D. Light micrographs of *Amphora sp. nov.* Amph033/097 showing observed size range. Scale bar = 10 µm.

In SEM, externally, the proximal and distal raphe ends are dorsally deflected. The dorsal raphe ledge is small and continuous along the length of the valve. The ventral raphe ledge is only apparent near the apices. A small dorsal hyaline fascia is more or less observable in imaged specimens. A thin marginal

ridge is present. The dorsal valve face is extremely narrow in this taxon when compared to the ventral valve face and dorsal mantle. The striae are composed of large elongate openings. These areolae are more elongated in the ventral striae than in the dorsal striae. Internally, the proximal raphe ends terminate in small closely spaced central helictoglossae.

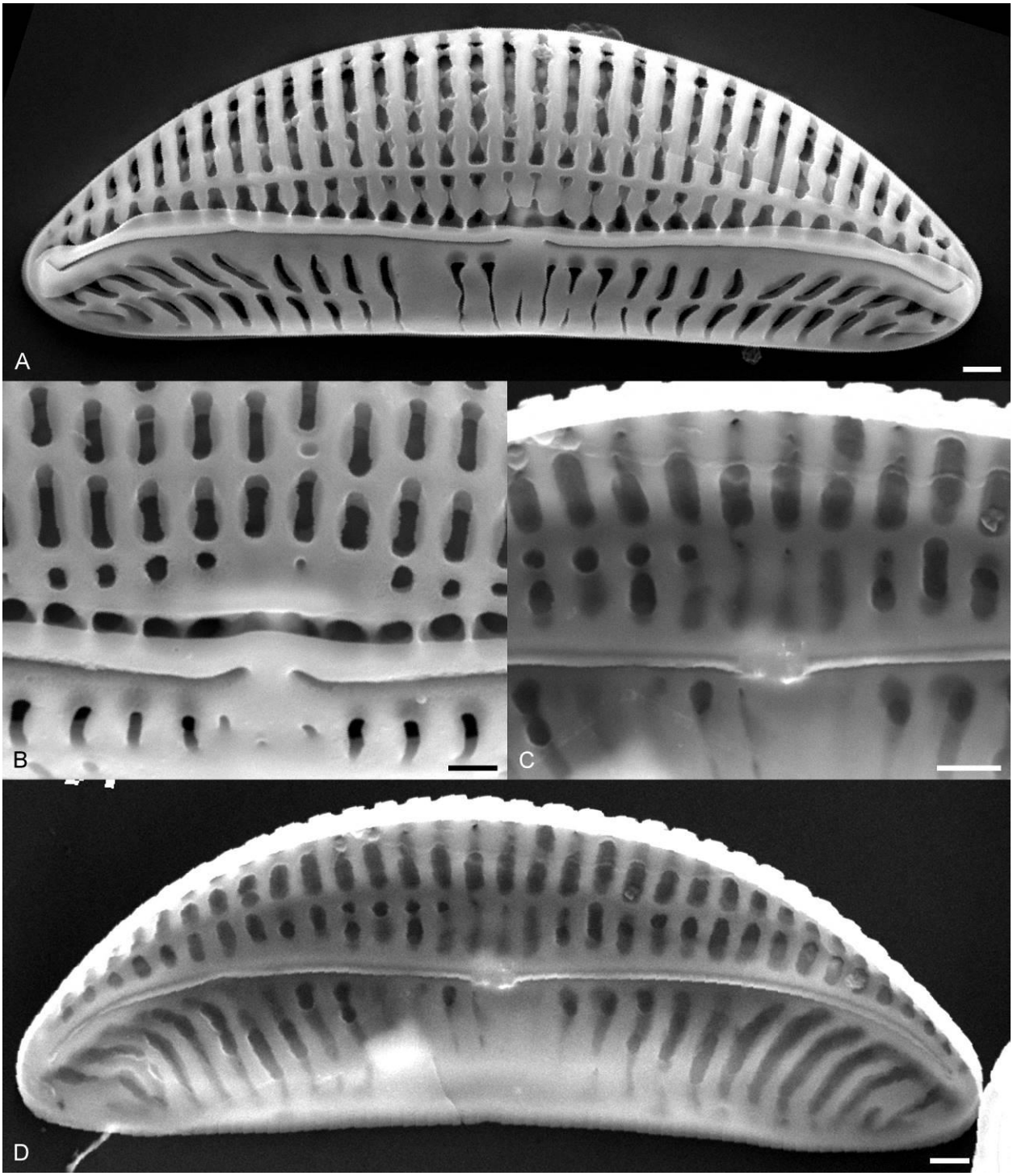

Figure 4.25. Scanning electron micrographs of *Amphora sp. nov.* Amph033/097. **A.** Whole external valve. **B.** Detail of external valve center. **C.** Detail of internal valve center. **D.** Whole internal valve. Scale bars = 1 µm.

Amphora allanta Hohn & Hellerman Amph129 (Figs 4.26, 4.27)

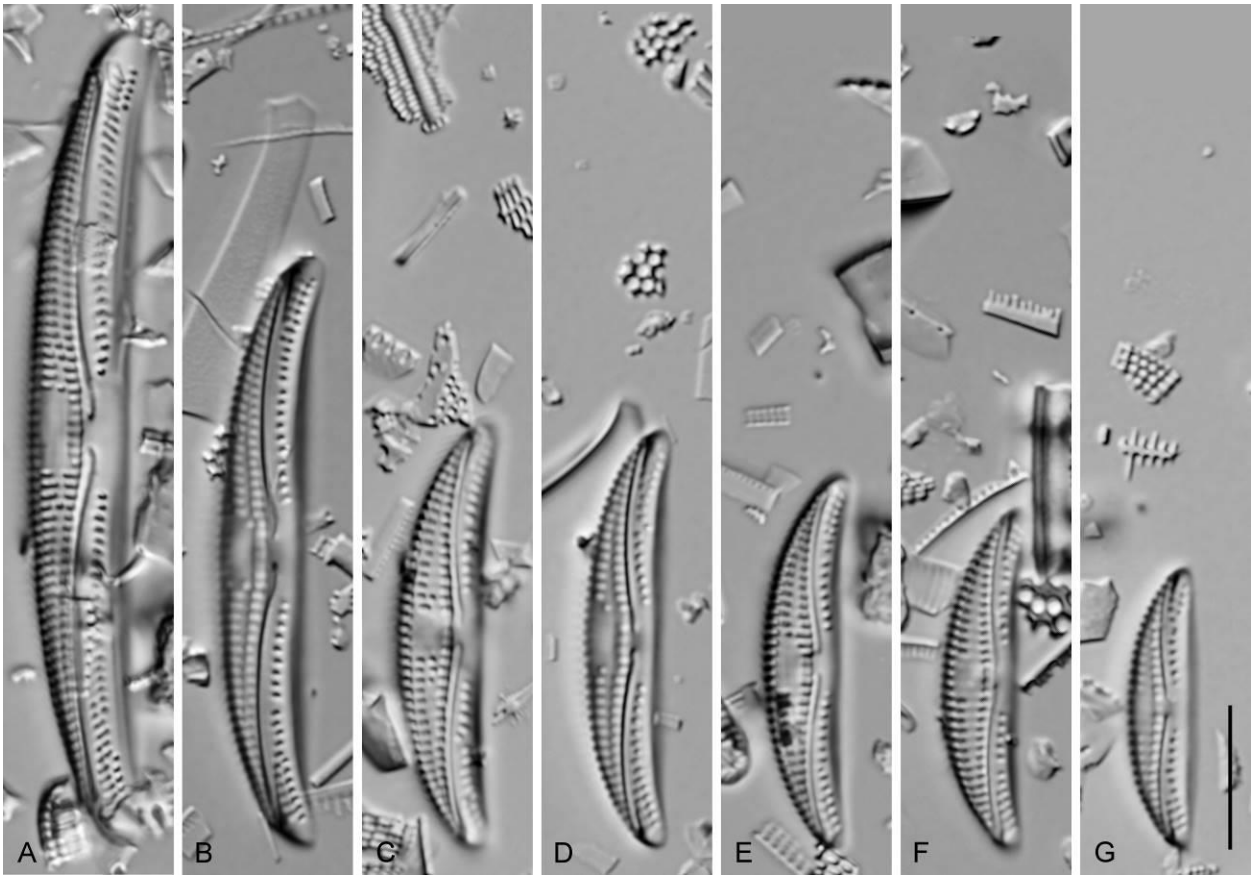

Figure 4.26. A–G. Light micrographs of *Amphora allanta* Amph129 showing observed size range. Scale bar = 10 µm.

Valves narrowly semi-elliptical and moderately dorsiventral. The dorsal margin is shallowly arched, becoming nearly straight over the valve center in some specimens. The ventral margin is weakly concave to slightly tumid. Valve ends are rounded and ventrally deflected. Valve length 20.0–57.0 µm, valve breadth 4.0–7.0 µm. The raphe is biarcuate with proximal ends deflected dorsally. The axial area is narrow, although slightly expanded on the ventral side in some of the larger specimens. A round to ovoid dorsal fascia is present and is separated from the dorsal axial area by a single row of small areolae. A broad ventral fascia is present as a break in the ventral striae. The dorsal striae are composed of two rows of areolae, although a third row can be seen in some specimens. Often the two row are separated by a distinct hyaline area that is most prominent near the valve center. The dorsal striae are parallel near the valve center, becoming radiate near the apices. The ventral striae are composed of a single row of areolae

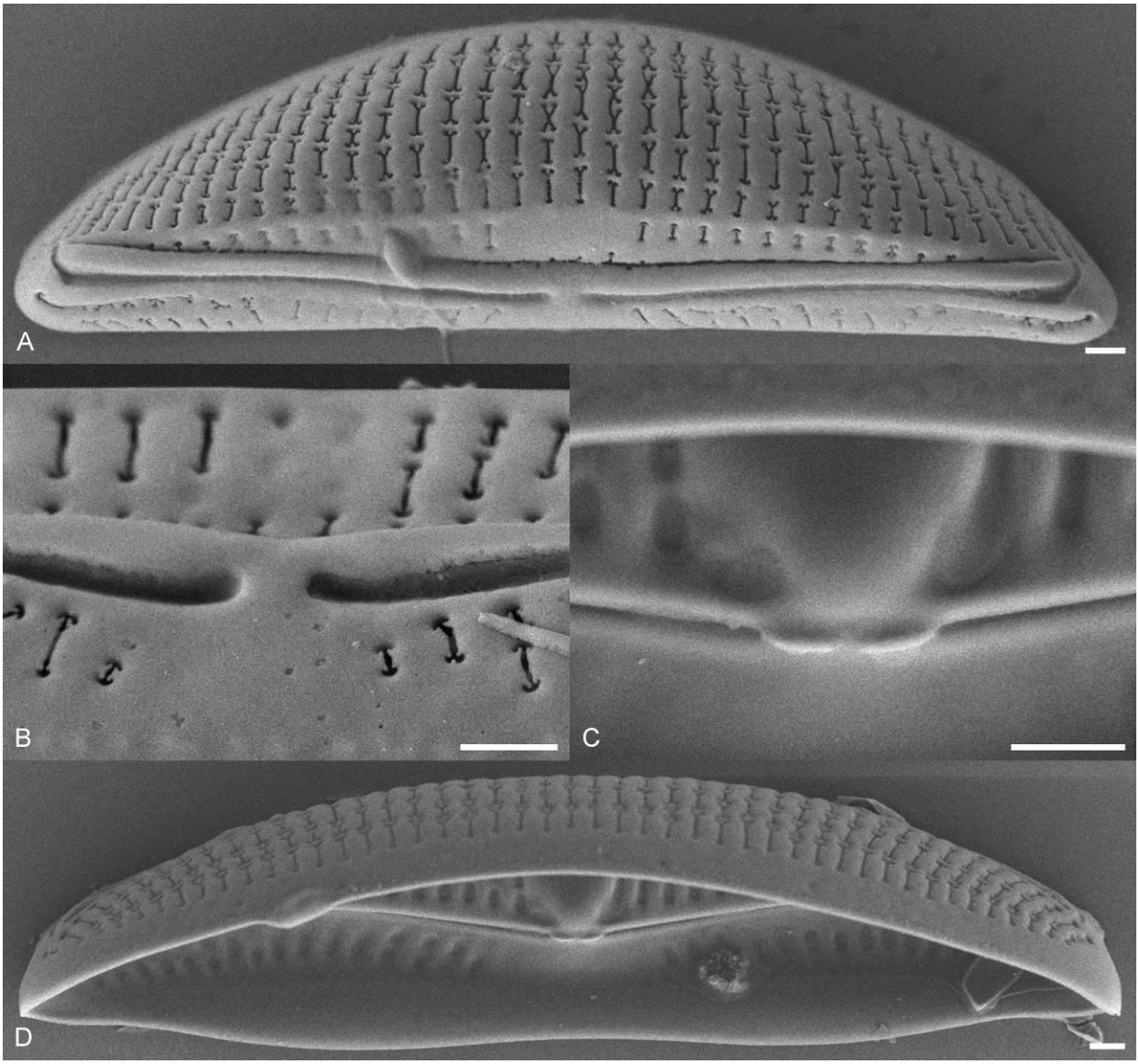

Figure 4.27. Scanning electron micrographs of *Amphora allanta* Amph129. **A.** Whole external valve. **B.** Detail of external valve center. **C.** Detail of internal valve center. **D.** Whole internal valve. Scale bar = 1 µm.

except where they approach the apices when they transition to two areolae per stria. The ventral striae are radiate near the valve center becoming convergent near the apices. Striae number 13–15 in 10 µm.

In SEM, externally, the dorsal raphe ledge is continuous along the length of the valve, the ventral raphe ledge is only apparent near the apices. Although not broad, the dorsal raphe ledge nearly completely obscures the first row of dorsal areolae. A moderately developed dorsal marginal ridge is present. The external foramen openings are narrow and complex in shape. These slit like openings have ends dilated

into “I”, “Y”, “T” and “X” shapes with the mantle areolae more complex than those on the valve face. Internally, the areolae are ovoid in shape. A distinct siliceous thickening is associated with the dorsal fascia. The proximal raphe ends terminate in separate but closely spaced helictoglossae.

Amphora proteoides Hustedt Amph096 (Figs 4.28, 4.29)

Figure 4.28. A, B. Light micrographs of *Amphora proteoides* Amph096 showing observed size range. Scale bar = 10 µm.

Valves semi-elliptical to nearly linear through the central valve and weakly dorsiventral. The dorsal margin is rounded near the apices and nearly flat over the valve center. The ventral margin is straight to slightly concave. The valve ends are broadly rounded and slightly ventrally deflected. Valve length 46.0–51.0 µm, valve breadth 6.5–7.5 µm. The raphe is weakly biarcuate and nearly centrally positioned, with straight proximal ends. The axial area is narrow along the dorsal side, expanded along the ventral side. An ovoid dorsal fascia is present and is separated from the dorsal axial area by a single

row of small areolae. A broad ventral fascia is present as a break in the ventral striae. The dorsal striae are composed of three rows of small ovoid areolae throughout much of the valve, becoming two rows near

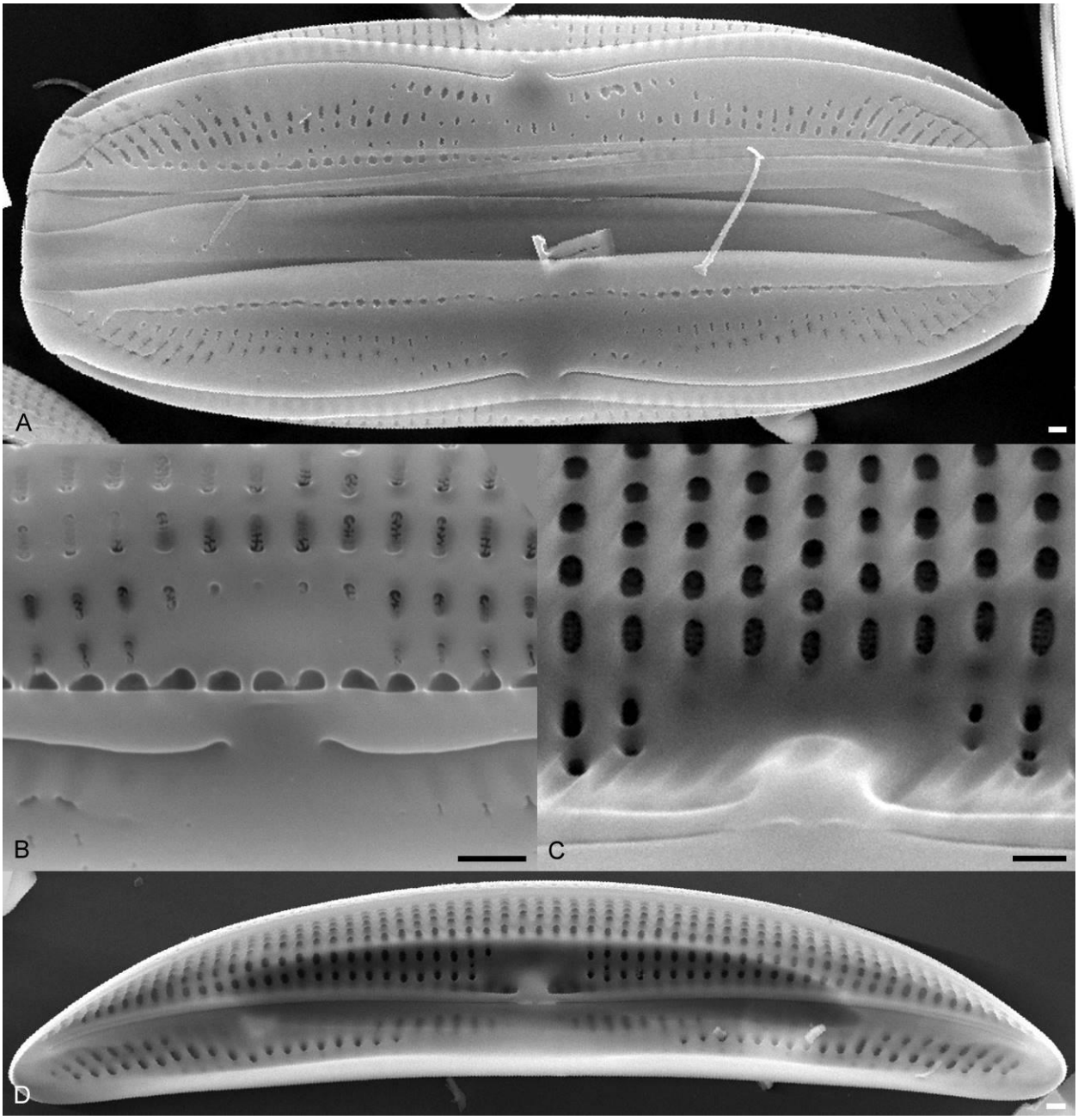

Figure 4.29. Scanning electron micrographs of *Amphora proteoides* Amph096. **A.** External whole frustule, valve side. **B.** Detail of external valve center. **C.** Detail of internal valve center. **D.** Internal whole valve. Scale bars = 1 µm.

the apices. The dorsal striae are parallel at the valve center becoming radiate near the apices. The ventral striae are composed of one or two irregularly placed areolae. Many faint 'ghost areolae' are visible

throughout the ventral portion of the valve. The ventral striae are convergent throughout. Striae number 12 in 10 µm.

In SEM, externally, ventral portion of the valve is distinctly broader than the dorsal portion. The raphe is biarcuate with dorsally deflected proximal and distal ends. The dorsal raphe ledge is broad and continuous across the length of the valve and nearly completely covers the first row of areolae. The ventral raphe ledge is only apparent near the apices. A marginal ridge is present. The areolae are occluded externally by narrow reticulate foramina. The areolae that make up the ventral striae are irregular in size, number and position. Internally, the areolae are small and round to ovoid. Several of the ventral areolae have the appearance of being filled in with silica and could explain the faint areolae seen in the LM. A siliceous thickening is associated with the dorsal fascia. The proximal raphe ends terminated in small, separated helictoglossae.

Amphora waldeniana Stepanek & Kociolek Amph011 (Figs 4.30, 4.31)

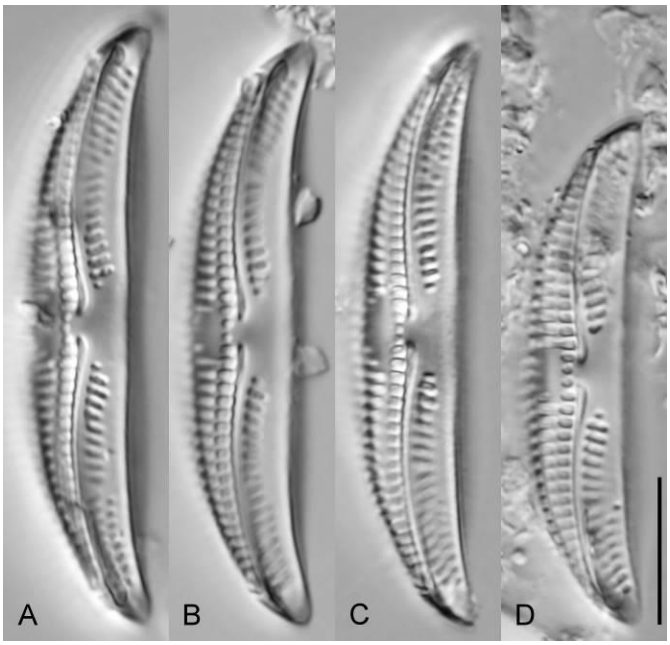

Figure 4.30. A–D. Light micrographs of *Amphora waldeniana* Amph011 showing observed size range. Scale bar = 10 µm.

Valves are semi-elliptical, becoming linear through the central portion of the valve, and weakly dorsiventral. The dorsal margin is flat over the valve center, rounded near the apices. The ventral margin is straight. Valve ends are rounded and ventrally deflected. Valve length 27.0–45.0 µm, valve breadth 6.5–7.0 µm. The raphe is positioned near the center of the valve, biarcuate with dorsally deflected proximal ends. The axial area is narrow throughout. An ovoid dorsal fascia is present, separated from the

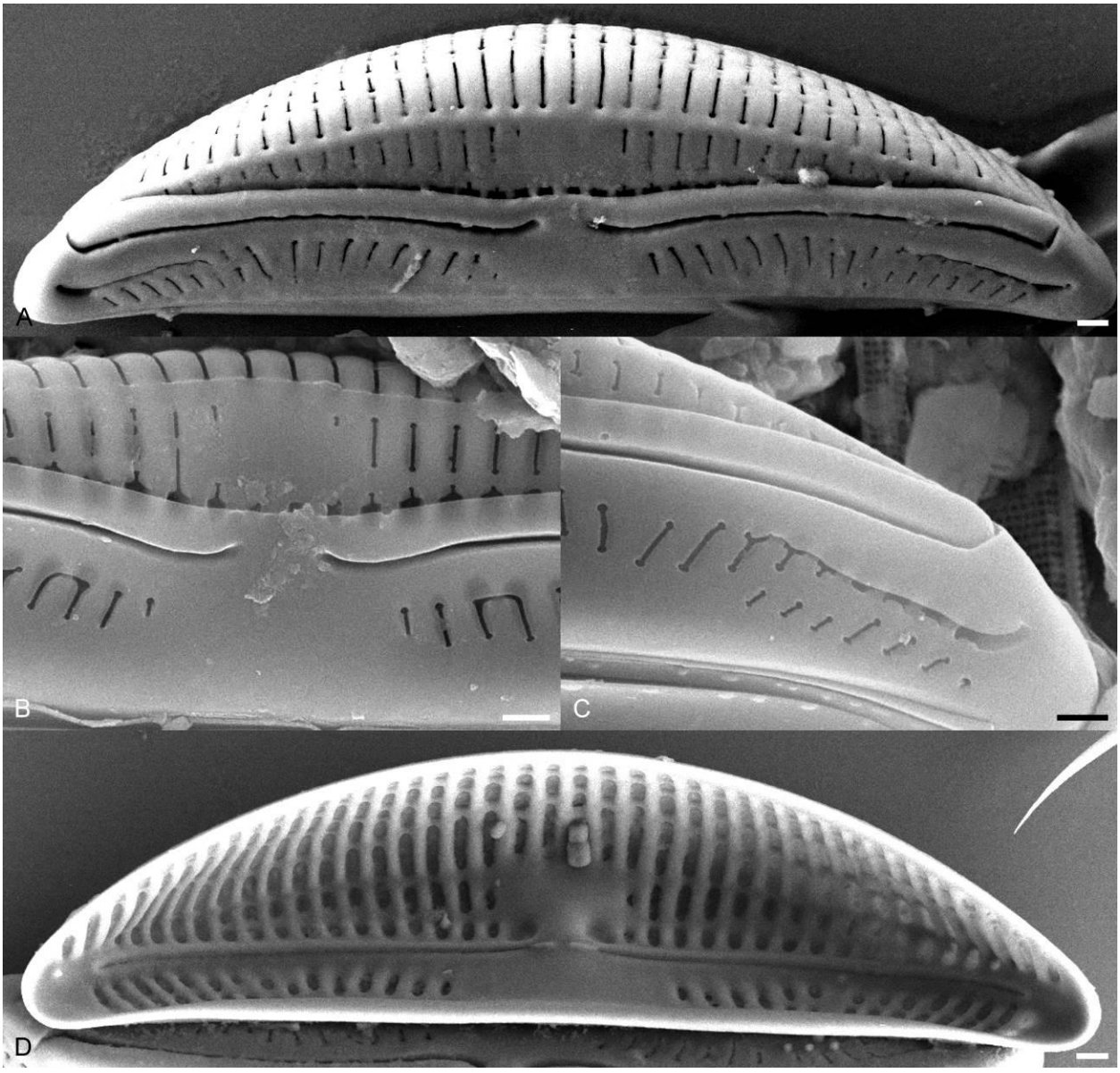

Figure 4.31. Scanning electron micrographs of *Amphora waldeniana* Amph011. **A.** External whole valve. **B.** Detail of external valve center. **C.** Detail of external valve end. **D.** Internal whole valve. Scale bars = 1 µm.

axial area by a single row of small areolae. A broad ventral fascia is present as a break in the ventral striae. The dorsal striae are composed of two rows of transapically elongated areolae, parallel through the central valve becoming radiate near the apices. The ventral striae are composed of a single elongate areolae near the valve center then abruptly transition to two areolae per stria as they near the apices. The single areolate striae are radiate, the striae with two areolae are convergent. Striae number 12–13 in 10 µm.

In SEM, externally, the raphe is weakly biarcuate with dorsally deflected proximal and distal ends. The raphe ledge is continuous along the dorsal side of the raphe and nearly completely obscures the first row of dorsal areolae. Along the ventral side of the raphe the raphe ledge is only apparent near the apices. A distinct marginal ridge is present. The areolae are opened externally by thin foramen slits with dilated ends, creating a "dog-bone" appearance. Internally, the areolae are ovoid in shape. An internal siliceous thickening is associated with the dorsal fascia. The proximal raphe ends end in separated central helictoglossae.

Amphora indistincta Levkov Amph019 (Figs 4.32, 4.33)

Valves narrowly semi-elliptical and moderately dorsiventral. The dorsal margin is smoothly arched and the ventral margin is slightly concave and tumid in the valve center. Valve ends narrowly rounded. Valve length 13.5–16.5 µm, valve breadth 3.0–3.5 µm. The raphe is straight to slightly arched with straight proximal raphe endings. The distal endings are difficult to image in the LM. The axial area is narrow throughout. Rectangular dorsal and ventral fascias are present. The dorsal striae are composed of a single elongate areolae and are parallel throughout. The ventral striae are composed of a single row of small areolae and are radiate near the valve center becoming convergent near the apices. Striae number 18–20 in 10 µm.

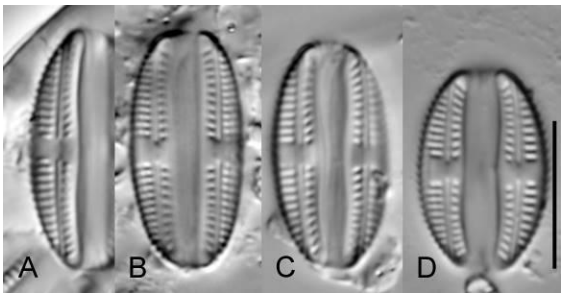

Figure 4.32. A–D. Light micrographs of *Amphora indistincta* Amph019 showing observed size range. Scale bar = 10 µm.

In SEM, externally, the raphe is straight with straight proximal ends and dorsally hooked distal ends. The raphe ledge is barely visible along the dorsal side of the raphe and is absent along the ventral side. A distinct marginal ridge runs the length of the dorsal margin. The dorsal fascia extends from the axial area to the dorsal marginal ridge. Both the dorsal and ventral striae are composed of single rows of elongate areolae. Internally, the proximal raphe ends terminate in separated central helictoglossae.

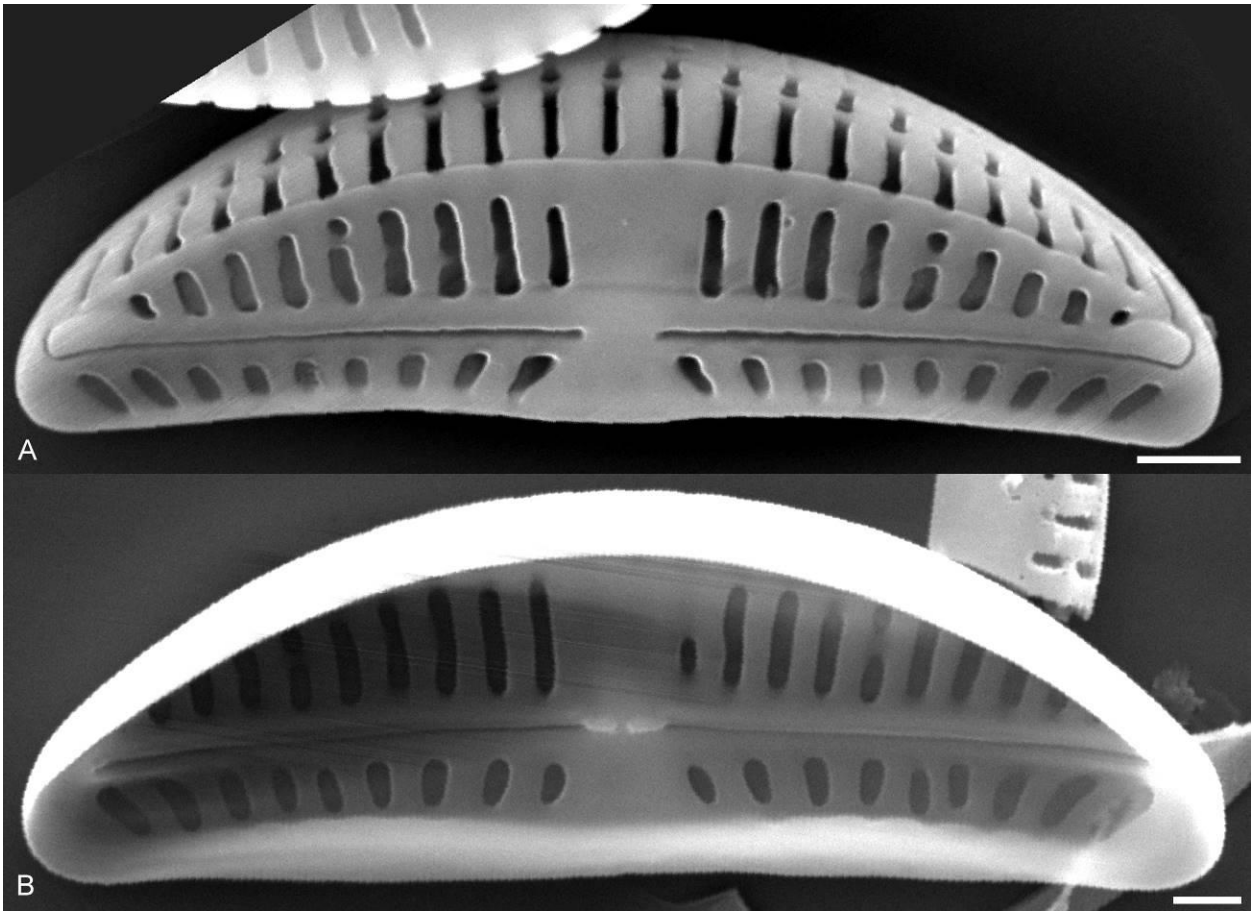

Figure 4.33. Scanning electron micrographs of *Amphora indistincta* Amph019. **A.** External whole valve. **B.** Internal whole valve. Scale bars = 1 µm.

Amphora pediculus (Kützing) Grunow in Schmidt et al. Amph020 (Figs 4.34, 4.35)

Valves narrowly semi-elliptical and strongly dorsiventral with a smoothly arched dorsal margin and a straight ventral margin. Valve ends rounded. Valve length 10.0–17.0 µm, valve breadth 2.5–3.5 µm. The raphe is straight with straight proximal raphe ends. The distal raphe ends are difficult to image in the LM. The axial area is narrow throughout. A rectangular dorsal fascia is present and is open to the axial area. A ventral fascia is present as a break in the ventral striae. The dorsal striae are distinctly areolate, parallel through the central valve becoming slightly radiate near the apices. The ventral striae are composed of a single row of small areolae. Striae number 20–22 in 10 µm.

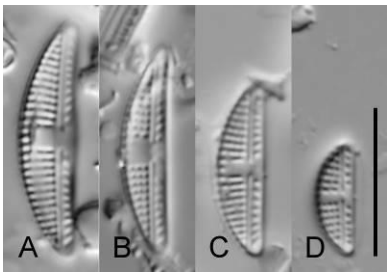

Figure 4.34. A–D. Light micrographs of *Amphora pediculus* Amph020 showing observed size range. Scale bar = 10 µm.

In SEM, externally, the raphe is straight with straight proximal ends and dorsally hooked distal ends. The dorsal raphe ledge is weakly developed and is nearly non-existent on the ventral side. The dorsal striae are composed of small elongated areolae. The ventral striae are composed of a single row of areolae. A distinct dorsal marginal ridge runs the length of the valve. The dorsal fascia extends from the axial area to the dorsal marginal ridge.

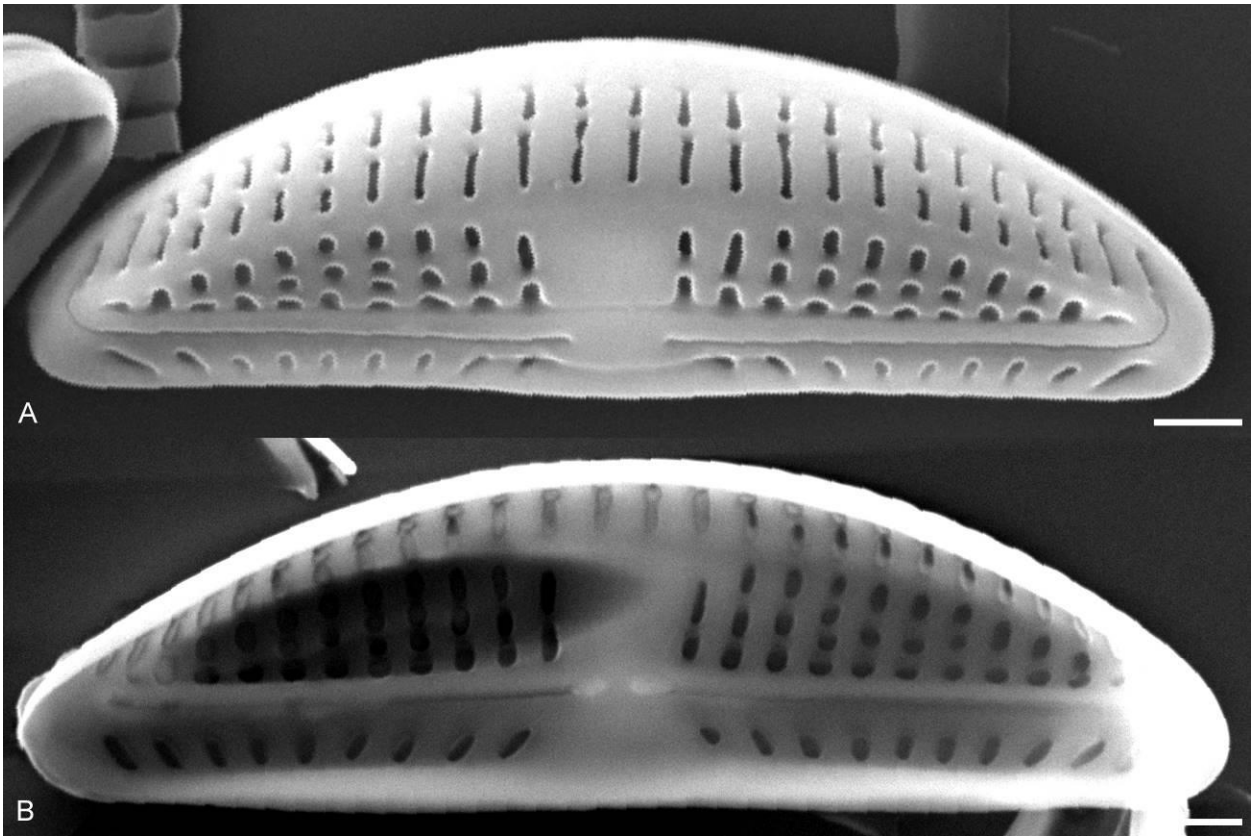

Figure 4.35. Scanning electron micrographs of *Amphora pediculus* Amph020. **A.** External whole valve. **B.** Internal whole valve. Scale bars = 1 µm.

Amphora pediculus (Kützing) Grunow in Schmidt et al. Amph008 (Figs 4.36, 4.37)

Valves narrowly semi-elliptical and strongly dorsiventral with a smoothly arched dorsal margin and a straight ventral margin. Valve ends rounded. Valve length 7.5–16.0 µm, valve breadth 2.5–4.0 µm. The raphe is straight with straight proximal raphe ends. The distal raphe ends are difficult to image in the LM. The axial area is narrow throughout. A rectangular dorsal fascia is present and is open to the axial area. A ventral fascia is present as a break in the ventral striae. The dorsal striae are distinctly areolate, parallel through the central valve becoming slightly radiate near the apices. The ventral striae are composed of a single row of small areolae. Striae number 19–21 in 10 µm.

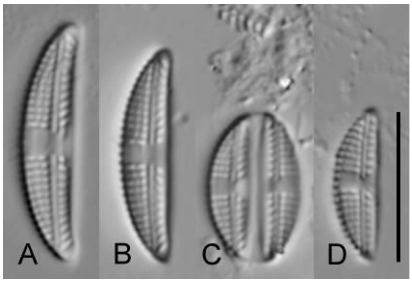

Figure 4.36. A–D. Light micrographs of *Amphora pediculus* Amph008 showing observed size range. Scale bar = 10 µm.

In SEM, externally, the raphe is straight with straight proximal ends and dorsally hooked distal ends. The dorsal raphe ledge is weakly developed and is nearly non-existent on the ventral side. The dorsal striae are composed of small elongated areolae. The ventral striae are composed of a single row of areolae. A distinct dorsal marginal ridge runs the length of the valve. The dorsal fascia extends from the axial area to the dorsal marginal ridge. Internally, the dorsal fascia is distinctly thickened. The internal proximal raphe ends terminate at separated central helictoglossae.

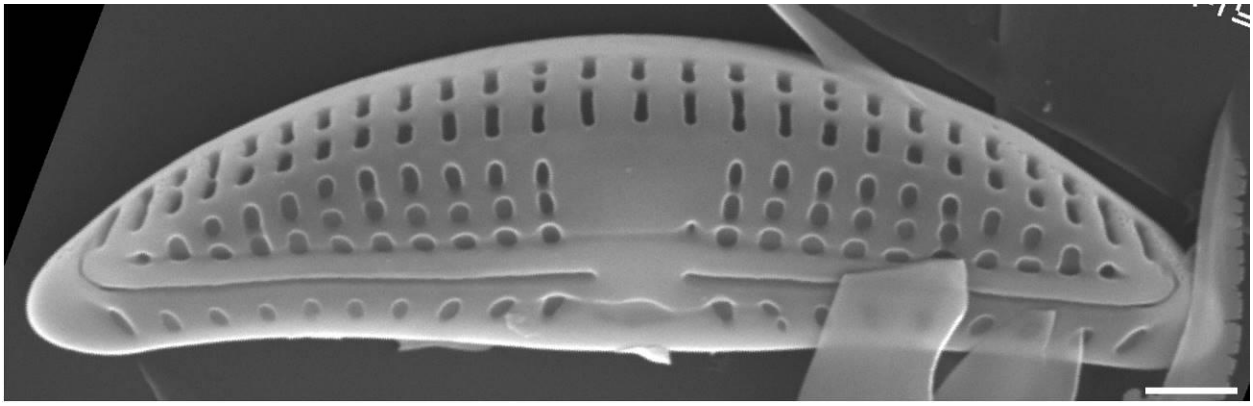

Figure 4.37. Scanning electron micrograph of *Amphora pediculus* Amph008 valve. Scale bar = 1 µm.

Amphora calumetica (Thomas in Thomas & Chase) Peragallo Amph094 (Figs 4.38, 4.39)

Valves semi-elliptical, weakly dorsiventral and dorsally constricted at the valve center. The ventral margin is slightly concave and tumid at the valve center. Valve ends broadly rounded. Valve length 50.0–64.0 µm, valve breadth 10.0–10.5 µm. The raphe is weakly biarcuate with dorsally deflected proximal ends. The distal valve ends are difficult to image in the LM. The dorsal and ventral raphe ledges

are visible in the LM as faint axial longitudinal lines. A thickened central area is present. The axial area is narrow throughout. Depending on the imaged focal plane a siliceous projection is visible extending from the dorsal margin at the valve center. The dorsal and ventral striae are composed of many small areolae except at the dorsal central area where the striae become a single elongate areolae. The striae are nearly parallel throughout, numbering 13–14 in 10 µm.

In SEM, externally, the raphe ledge is broad and continuous both on the dorsal and ventral side. At the valve center the dorsal striae are composed of single elongate slit-like foramen areolae. The dorsal striae become areolate as they move towards the apices. The ventral striae are composed of small areolae and are mostly obscured by the ventral raphe ledge. A distinct marginal ridge is present, extending into a siliceous wing at the valve center. The dorsal mantle striae are composed of a single uninterrupted narrow foramen slit.

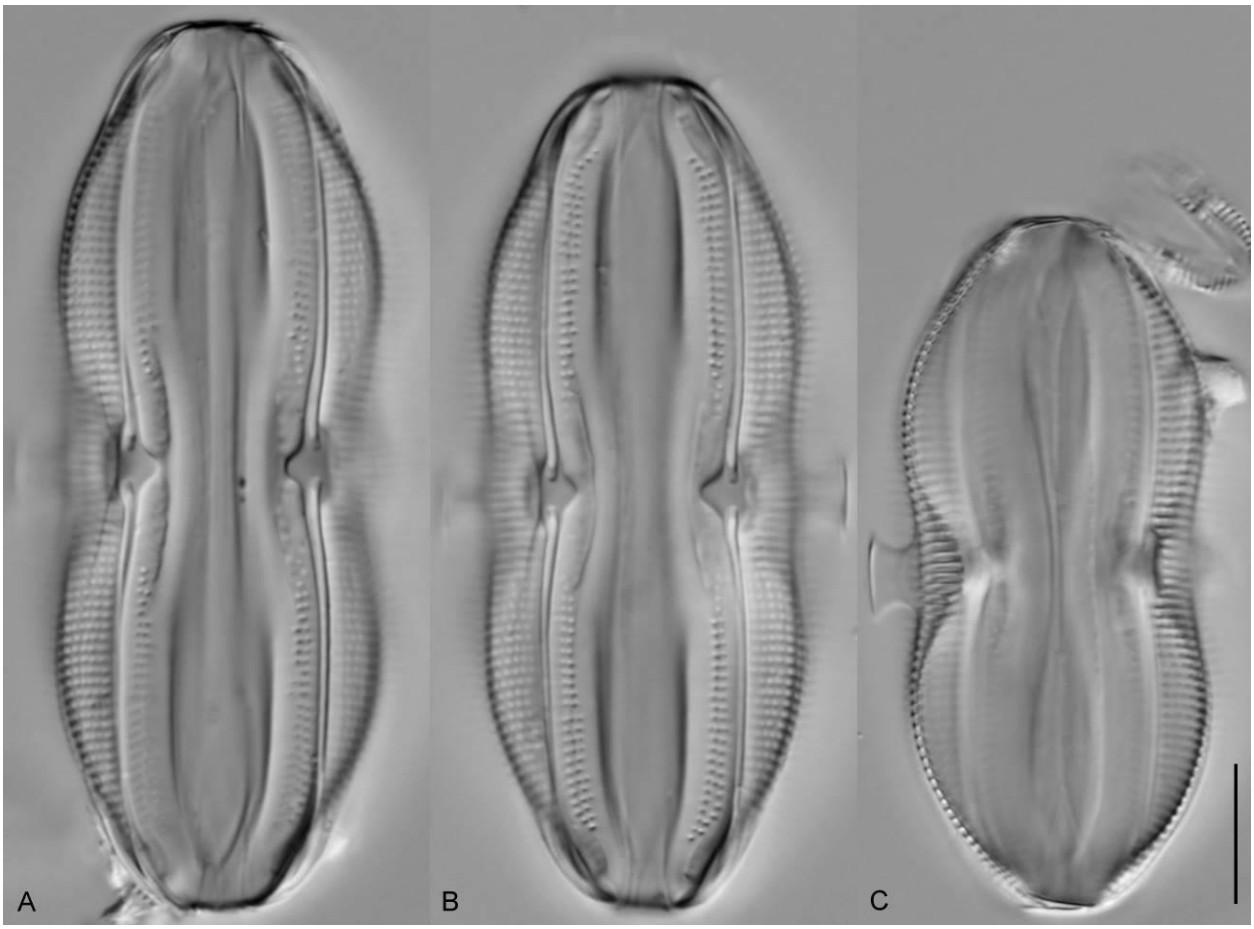

Figure 4.38. A–C. Light micrographs of *Amphora calumetica* Amph094 frustules showing observed size range. Scale bar = 10 µm.

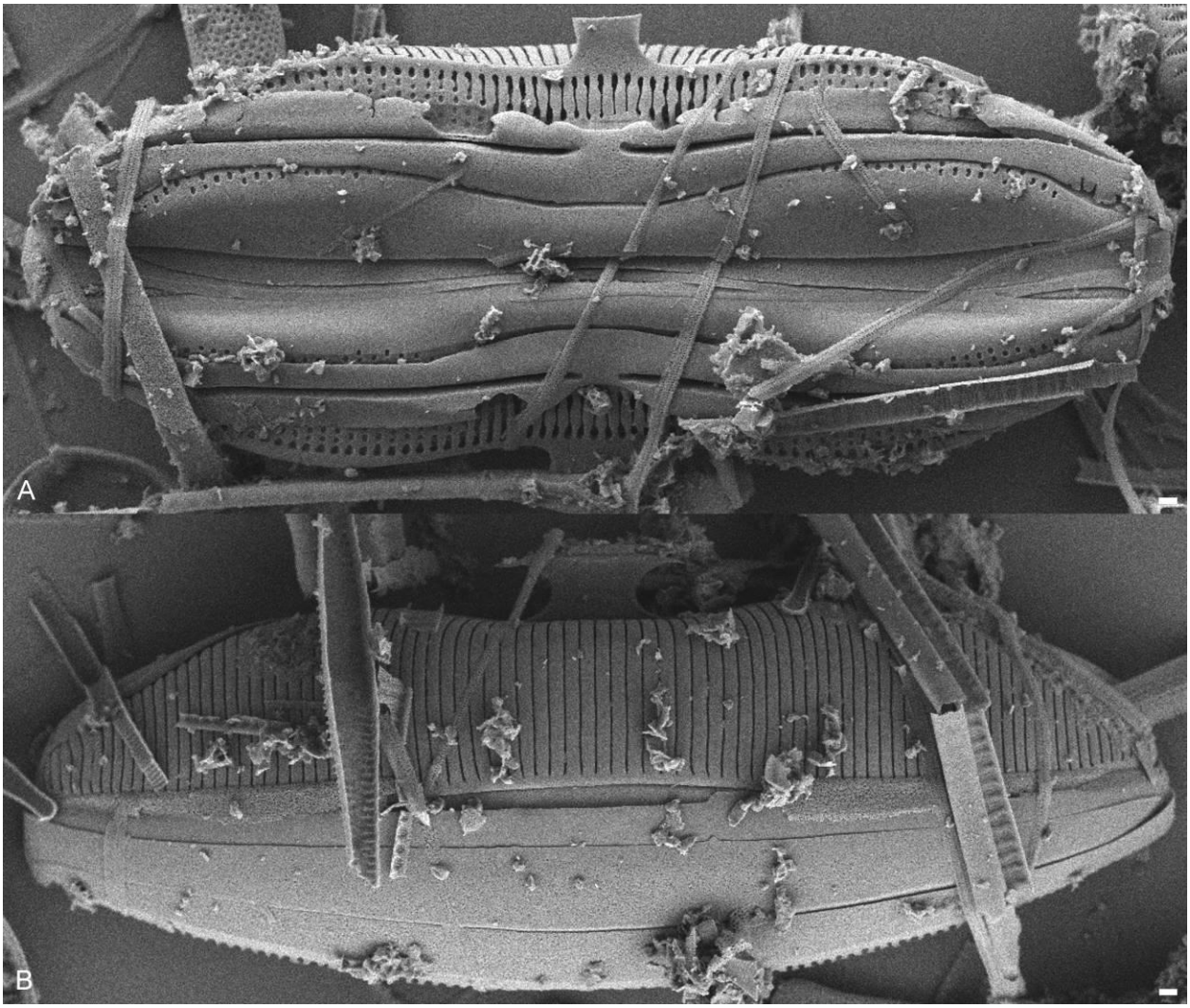

Figure 4.39. Scanning electron micrographs of *Amphora calumetica* Amph094. **A.** External whole frustule, valve view. **B.** External whole frustule, girdle view. Scale bars = 1 µm.

Amphora affinis Kützing Amph016 (Figs 4.40, 4.41)

Valves narrowly semi-elliptical and weakly to moderately dorsiventral. Valves with a smoothly arched dorsal margin and concave to slightly tumid ventral margin. Valve ends rounded. Valve length 22.0–42.0 µm, valve breadth 5.0–7.5 µm. The raphe is biarcuate with dorsally deflected proximal and distal ends. The axial area is narrow throughout. A dorsal fascia is present, separated from the axial area by a row of more or less developed areolae in some imaged specimens. A ventral fascia is present as a break in the ventral striae. A dorsal marginal ridge is visible in some specimens as a hyaline extension of the dorsal fascia. The dorsal striae are composed of transapically elongate areolae, parallel at the valve

center, becoming radiate near the apices. The ventral striae are composed of two rows of small areolae, radiate near the valve center, becoming convergent near the poles. Striae number 14–15 in 10 µm.

In SEM, externally, the raphe is biarcuate with dorsally deflected proximal and distal raphe ends. The raphe ledge is weakly developed. The dorsal raphe ledge is interrupted through the valve center, the ventral raphe ledge is only apparent near the valve center and at the apices. The dorsal striae are separated by virgae crossed by well-developed vimines creating areolae of varying size. The ventral striae are composed of two rows of areolae. The girdle bands are broad and unornamented. Internally, a distinct siliceous thickening is associated with the dorsal fascia. The proximal raphe ends terminate in separated central helictoglossae.

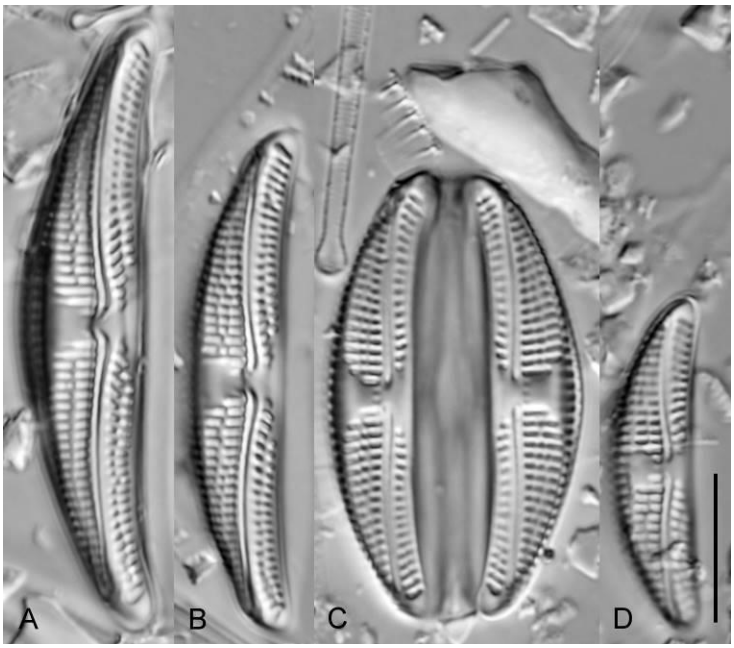

Figure 4.40. A–D. Light micrographs of *Amphora affinis* Amph016 showing observed size range. Scale bar = 10 µm.

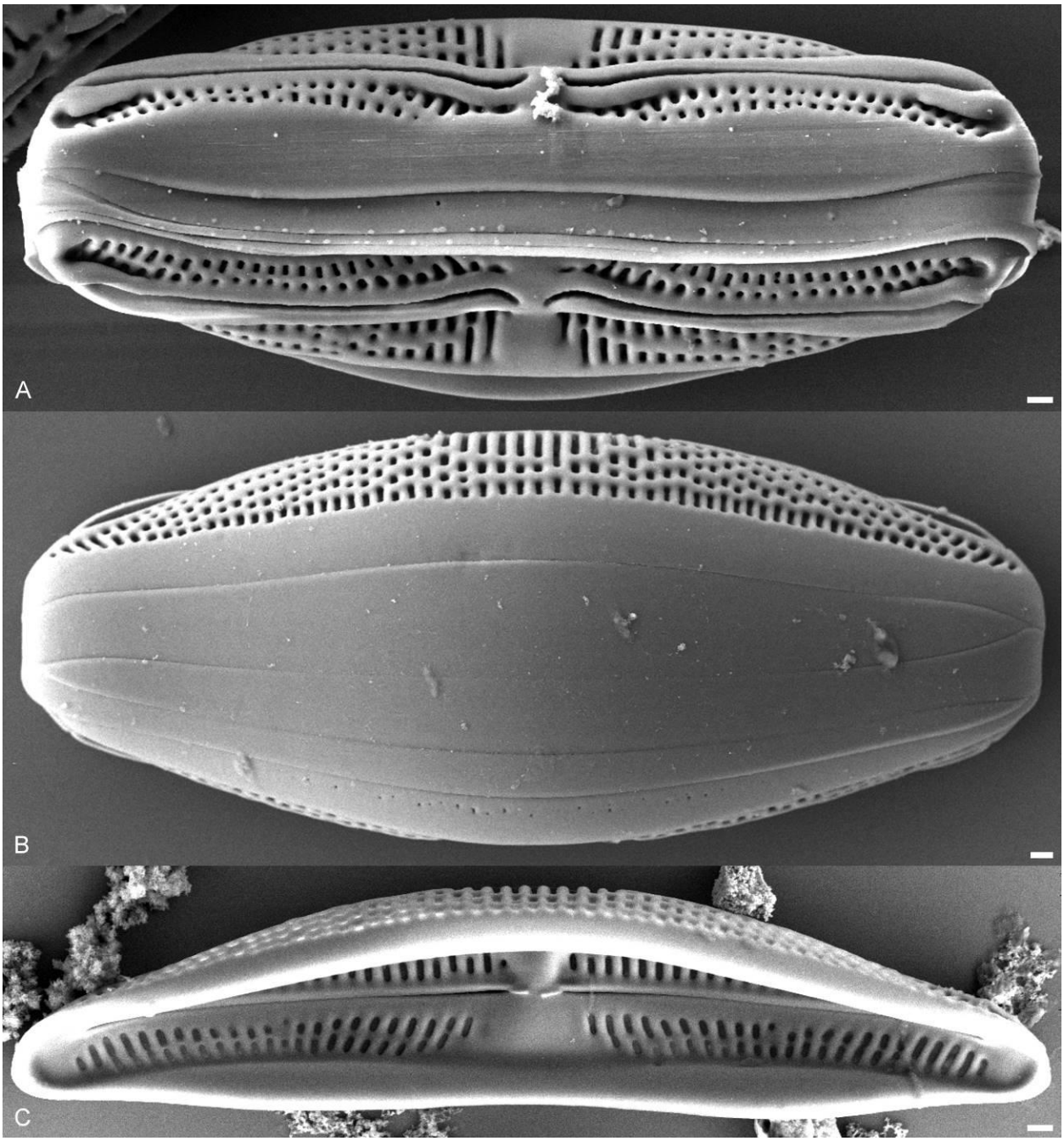

Figure 4.41. Scanning electron micrographs of *Amphora affinis* Amph016. **A.** External whole frustule, valve view. **B.** External whole frustule, girdle view. **C.** Internal whole valve. Scale bars = 1 µm.

Amphora ovalis (Kützing) Kützing Amph013 (Figs 4.42, 4.43)

Valves are semi-elliptical and strongly dorsiventral, with a smoothly arched dorsal margin and slightly concave ventral margin. Valve ends are rounded and ventrally deflected. Valve length 32.0–78.0 µm, valve breadth 9.0–15.0 µm. The raphe is weakly biarcuate with dorsally deflected proximal ends and

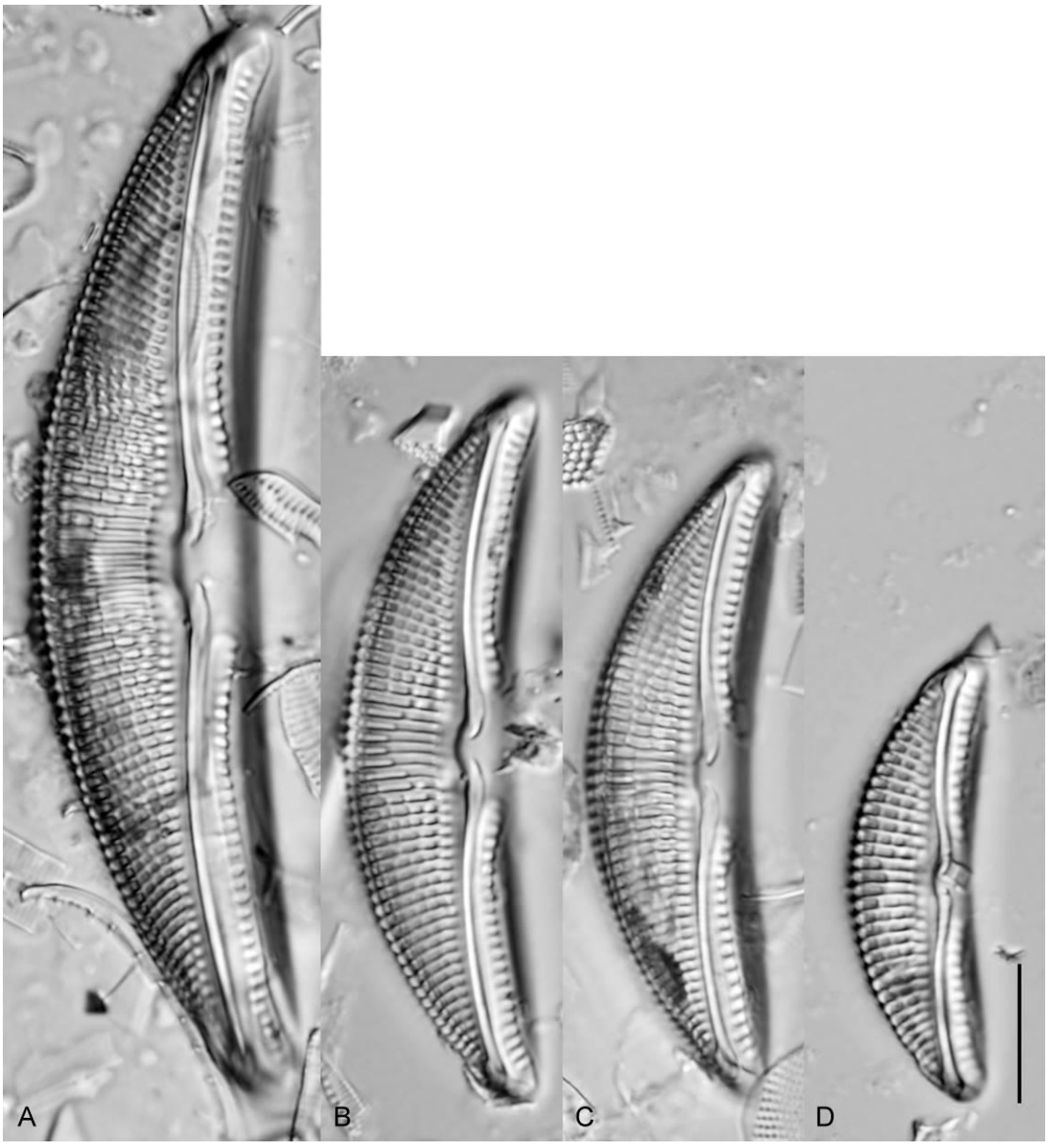

Figure 4.42. A–D. Light micrographs of *Amphora ovalis* Amph013 showing observed size range. Scale bar = 10 µm.

dorsally hooked distal ends. The axial area is narrow dorsally, slightly expanded ventrally. The dorsal and ventral raphe ledges are visible in the LM as faint longitudinal lines. The dorsal striae are composed of many transapically elongate areolae except at the valve center where they appear as a single elongate areola. The ventral striae are composed of a single row of areolae. The dorsal striae are slightly radiate throughout, becoming more so near the apices. The ventral striae are radiate near the valve center becoming convergent near the apices. Striae number 9–11 in 10 µm.

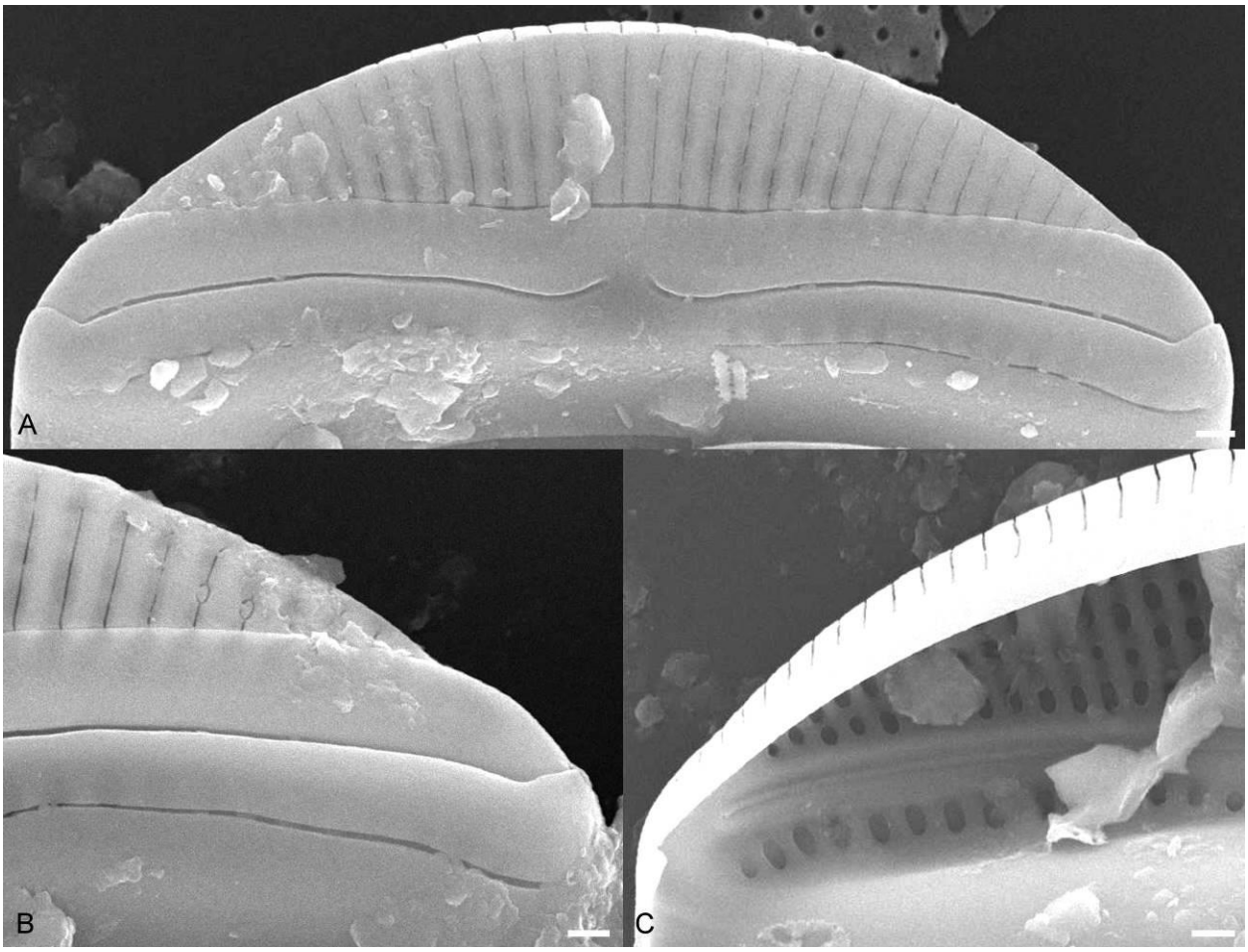

Figure 4.43. Scanning electron micrographs of *Amphora ovalis* Amph013. **A.** External whole valve. **B.** Detail of external valve end. **C.** Detail of internal valve end. Scale bars = 1 µm.

In SEM, externally, the raphe is biarcuate with dorsally deflected proximal and distal ends. The raphe ledge is well developed and broad both dorsally and ventrally. The dorsal raphe ledge is continuous along the length of the valve, the ventral ledge is most prominent near the apices and is interrupted at the valve center. The dorsal striae are composed of a narrow uninterrupted foramen slit running to a distinct

marginal ridge. The ventral striae are completely obscured by the ventral raphe ledge. Internally, the dorsal striae are separated by virgae crossed by well-developed vimines creating ovoid areolae. The ventral striae are composed of a single row of ovoid areolae.

Amphora copulata (Kützing) Schoeman & Archibald Amph095 (Fig. 4.44)

Valves semi-elliptical and strongly dorsiventral with a smoothly arched dorsal margin slightly concave to tumid ventral margin. Valve ends rounded. Valve length 30.0–40.0 µm, valve breadth 6.5–8.5 µm. The raphe is weakly biarcuate with dorsally deflected proximal ends and dorsally hooked distal ends. The axial area is narrow throughout. A circular to ovoid dorsal fascia is present. A row of small areolae separate the dorsal fascia from the axial area. A ventral fascia is present as a break in the ventral striae. The dorsal striae are composed of irregularly sized and positioned elongate areolae. A marginal ridge is visible in the LM as a narrow hyaline area. The dorsal striae are parallel near the valve center becoming radiate near the apices. The ventral striae are composed of a single row of areolae, parallel near the valve center becoming convergent near the apices. Striae number 13–14 in 10 µm.

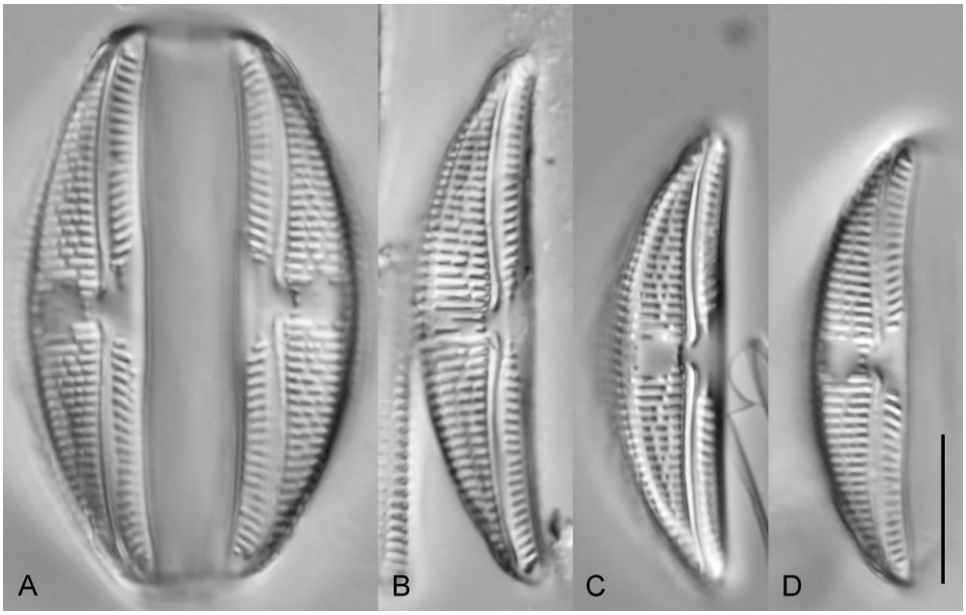

Figure 4.44. A–D. Light micrographs of *Amphora copulata* Amph095 showing observed size range. Scale bar = 10 µm.

Amphora copulata (Kützing) Schoeman & Archibald Amph107 (Figs 4.45, 4.46)

Valves semi-elliptical and strongly dorsiventral with a smoothly arched dorsal margin slightly concave ventral margin. Valve ends rounded. Valve length 24.0–30.0 µm, valve breadth 6.5–7.5 µm. The raphe is weakly biarcuate with dorsally deflected proximal ends and dorsally hooked distal ends. The axial area is narrow throughout. A circular to ovoid dorsal fascia is present. A row of small areolae separate the dorsal fascia from the axial area. A ventral fascia is present as a break in the ventral striae. The dorsal striae are composed of two rows of elongate areolate areolae. A marginal ridge is visible in the LM as a narrow hyaline area. The dorsal striae are parallel near the valve center becoming radiate near the apices. The ventral striae are composed of a single row of areolae, parallel near the valve center becoming convergent near the apices. Striae number 13–14 in 10 µm.

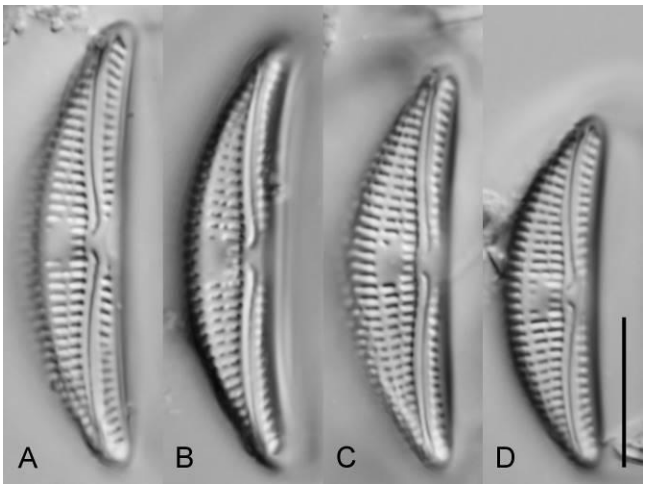

Figure 4.45. A–D. Light micrographs of *Amphora copulata* Amph107 showing the observed size range. Scale bar = 10 µm.

In SEM, externally, the dorsal raphe ledge is continuous along the length of the valve. The ventral raphe ledge is well developed but interrupted at the valve center. The raphe is biarcuate with dorsally deflected proximal ends and dorsally hooked distal ends. An unornamented dorsal fascia is present. The dorsal striae are separated by moderate virgae crossed by vimines, creating two rows of transapically elongate areolae. The marginal ridge is well developed. The ventral striae are composed of a single row of

elongate areolae. Internally, the dorsal fascia is distinctly thickened into a semi-stauros. The proximal raphe ends terminate at separated central helictoglossae.

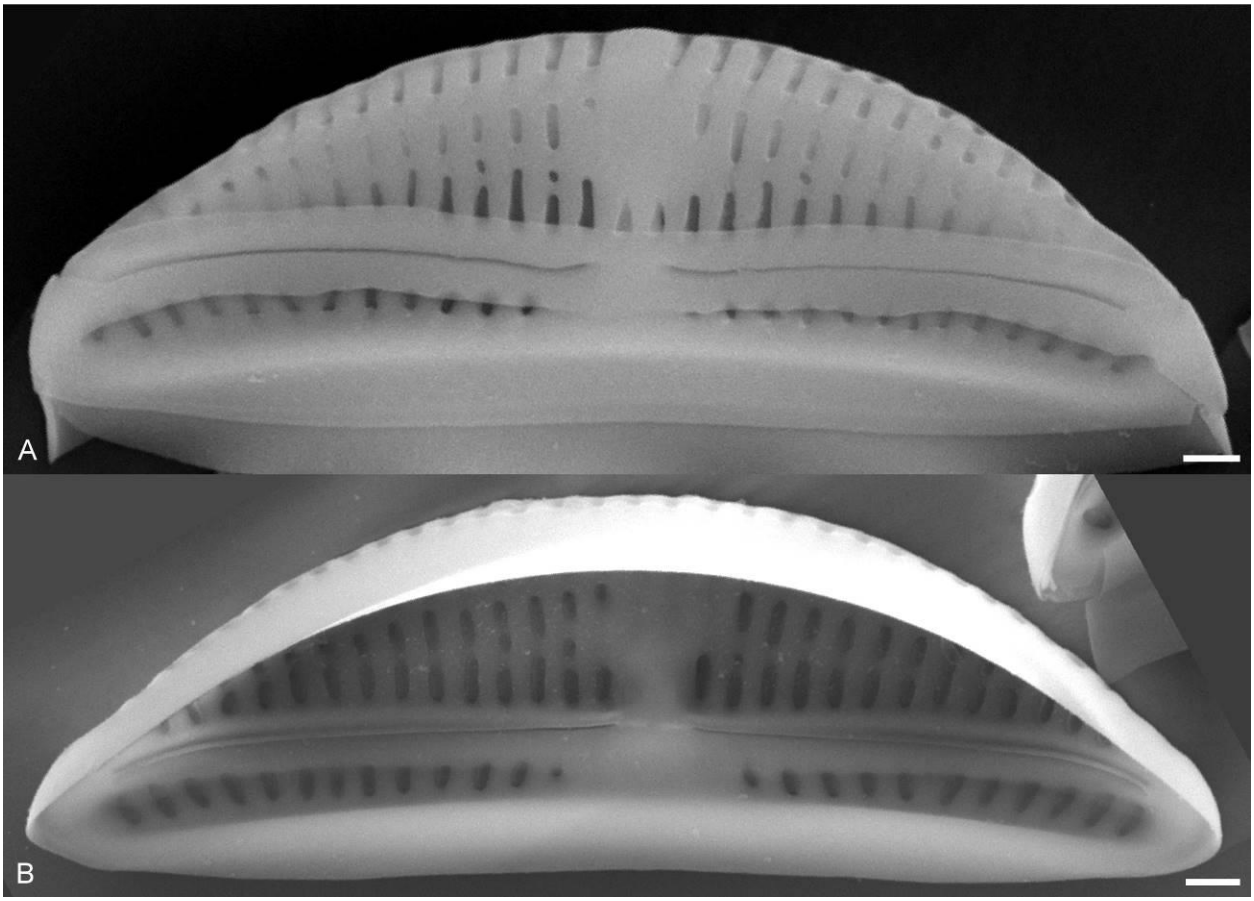

Figure 4.46. Scanning electron micrographs of *Amphora copulata* Amph107. **A.** External whole valve. **B.** Internal whole valve. Scale bars = 1 µm.

Amphora copulata (Kützing) Schoeman & Archibald Amph021 (Fig. 4.47)

Valves semi-elliptical and strongly dorsiventral with a smoothly arched dorsal margin slightly concave ventral margin. Valve ends rounded. Valve length 24.0–33.0 µm, valve breadth 5.5–7.0 µm. The raphe is weakly biarcuate with dorsally deflected proximal ends and dorsally hooked distal ends. The axial area is narrow throughout. A circular to ovoid dorsal fascia is present. A row of small areolae separate the dorsal fascia from the axial area. A ventral fascia is present as a break in the ventral striae. The dorsal striae are composed of two rows of elongate areolae. A marginal ridge is visible in the LM as a

narrow hyaline area. The dorsal striae are parallel near the valve center becoming radiate near the apices. The ventral striae are composed of a single row of areolae, parallel near the valve center becoming convergent near the apices. Striae number 12–13 in 10 µm.

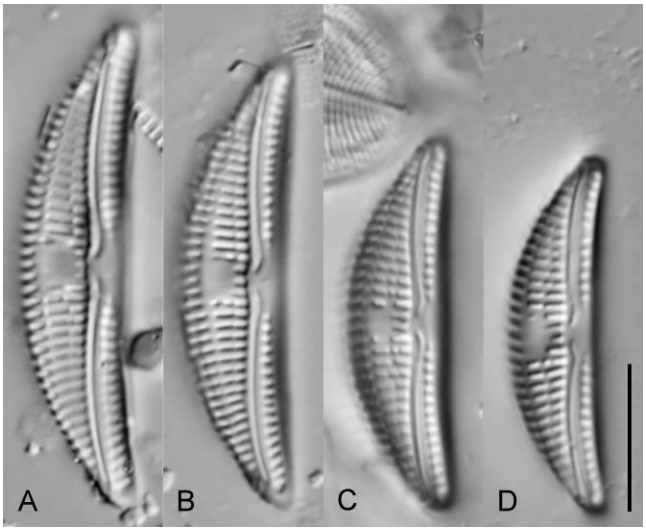

Figure 4.47. A–D. Light micrographs of *Amphora copulata* Amph021 showing the observed size range. Scale bar = 10 µm.

HALAMPHORA CLADE A

Halamphora semperpalorum (Wachnicka & Gaiser) Stepanek & Kociolek comb. nov. Amph142 (Fig. 4.48)

Valves semi-elliptical and strongly dorsiventral. The dorsal margin is shallowly arched, the ventral margin is straight. The valve ends are capitate. Valve length 50.0–53.0 µm, valve breadth 5.5–6.0 µm. The axial area is narrow throughout. The raphe is straight with dorsally deflected proximal raphe ends. Two longitudinal lines are visible in the LM, one near the axial area and one near the dorsal margin. The dorsal striae are fine and only interrupted by the two longitudinal lines. The dorsal striae are parallel at the valve center, becoming weakly radiate as they near the apices. The ventral striae are not continuous through the central portion of the valve. The ventral striae are often difficult to image in the LM due to the narrow ventral valve exhibited by this species. Striae number 28–29 in 10 µm.

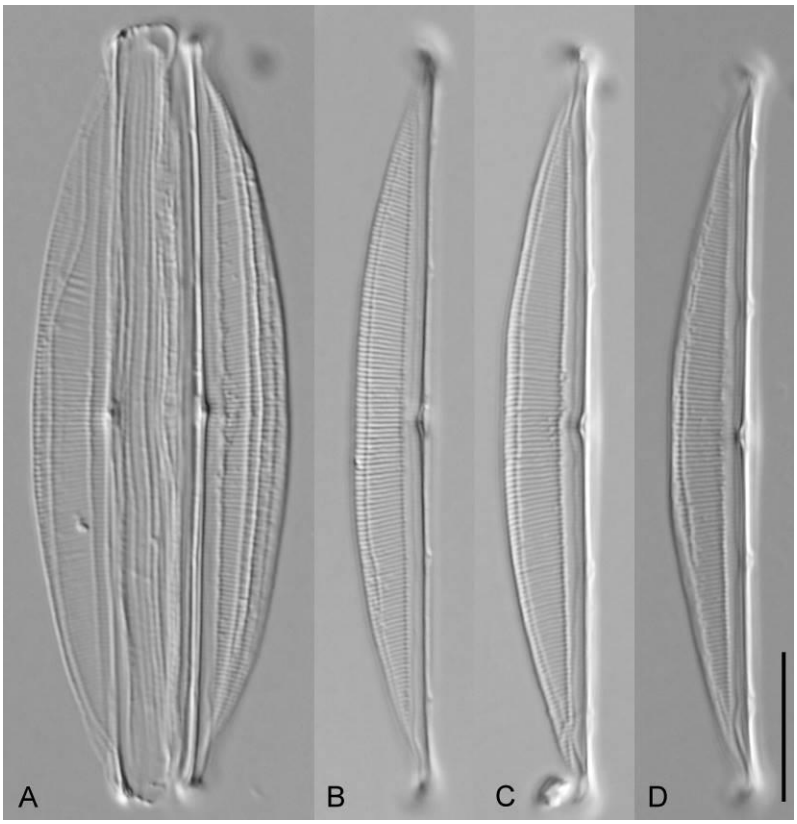

Figure 4.48. A–D. Light micrographs of *Halamphora semperpalorum* Amph142 showing observed size range. Scale bar = 10 µm.

Halamphora semperpalorum (Wachnicka & Gaiser) Stepanek & Kociolek comb. nov. Amph137 (Figs 4.49, 4.50)

Valves narrowly semi-elliptical and strongly dorsiventral. The dorsal margin is smoothly arched, the ventral margin is straight. The valve ends are capitate. Valve length 43.0–56.0 µm, valve breadth 5.0–5.5 µm. The raphe is nearly straight with proximal ends closely terminating and slightly dorsally deflected. The axial area is narrow dorsally and difficult to distinguish ventrally due to the narrow ventral valve. The dorsal striae are not visibly areolate, parallel, becoming radiate only near the apices. The dorsa

striae are crossed by two distinct longitudinal lines, one near the axial area and one near the dorsal margin. The ventral striae are difficult to image in the LM due to the extremely narrow ventral valve.

In SEM, externally, the raphe is straight closely terminating proximal ends. The proximal and distal raphe ends deflect dorsally. The dorsal raphe ledge is moderately broad and continuous along the length of the valve. Two longitudinal ribs of silica are present on the dorsal side of the valve, one runs the length of the valve near the axial area, the other runs along the dorsal margin. The Dorsal striae are

Figure 4.49. A–D. Light micrographs of *Halamphora semperpalorum* Amph137 showing observed size range. Scale bar = 10 µm.

composed of two elongate areolae, one extending from the axial area to the axial longitudinal rib, the other extending from the axial rib to the marginal ridge. A third mantle areolae extends from the marginal ridge to dorsal valve edge. The ventral axial area is narrow throughout. The ventral areolae not continuous through the central portion of the valve and are composed of a single row of elongate areolae. Internally,

the proximal raphe ends terminate in a small fused central helictoglossa. The striae are occluded internally with sieve plates. The axial and marginal longitudinal ribs are visible internally.

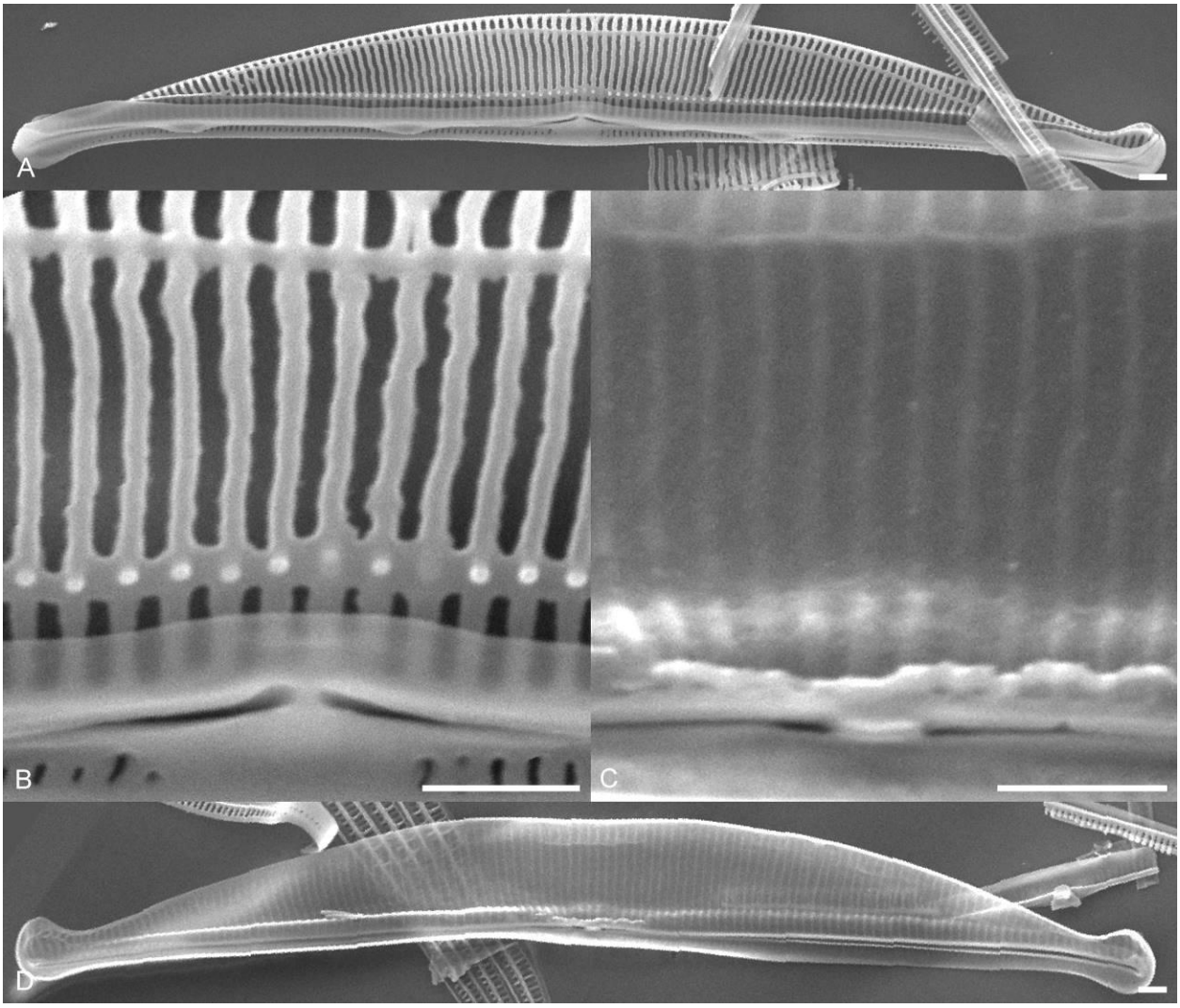

Figure 5.50. Scanning electron micrographs of *Amphora semperpalorum* Amph137. **A.** External whole valve. **B.** Detail of external valve center. **C.** Detail of internal valve center. **D.** Internal whole valve. Scale bars = 1 µm.

Halamphora semperpalorum (Wachnicka & Gaiser) Stepanek & Kociolek comb. nov. Amph047 (Figs 5.51, 5.52)

Valves are narrowly semi-elliptical and strongly dorsiventral. The dorsal margin is smoothly arched, the ventral margin is straight. The valve ends are capitate. Valve length 40.0–56.0 µm, valve 4.5–5.0 µm. The raphe is straight with slightly dorsally deflected proximal ends. The dorsal axial is narrow,

the ventral axial area is difficult to distinguish due to the narrow ventral valve exhibited by this species. The dorsal striae are not visibly areolate parallel at the valve center, becoming slightly radiate towards the apices. The dorsal striae are crossed by two distinct longitudinal lines, one near the axial area, one near

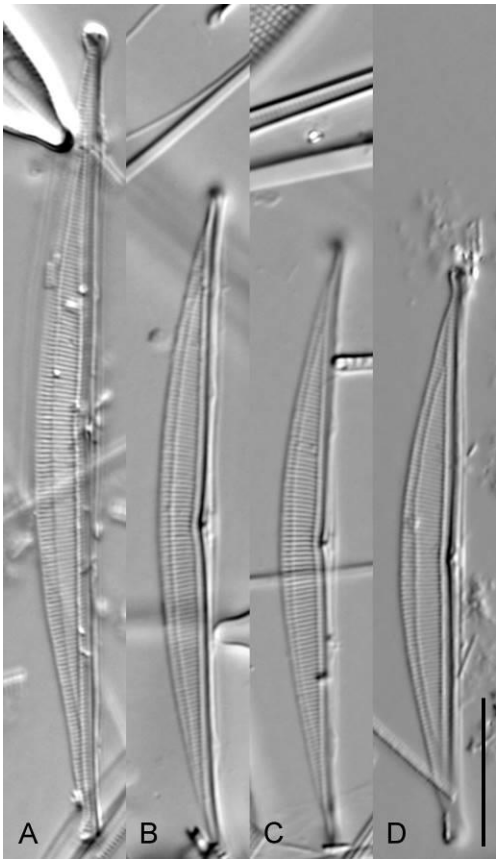

Figure 5.51. A–D. Light micrographs of *Halamphora semperpalorum* Amph047 showing observed size range. Scale bar = 10 µm.

the dorsal margin. The ventral striae are difficult to image in the LM due to the narrow ventral valve. Striae number 30-32 in 10 µm.

In SEM, externally, the raphe branches are straight with closely terminating proximal ends. The proximal and distal raphe ends are deflected dorsally. Two longitudinal bands of silica run the longitudinal length of the valve on the dorsal side. One longitudinal silica band is positioned near the axial area, the other longitudinal band is positioned at the dorsal margin. The dorsal striae are composed of large elongate areolae separated by thin virgae. One row of areole extend from the axial area to the axial longitudinal band, a second row of areolae extend from the axial longitudinal band to the marginal

band, the third row of areolae extend from the marginal band to the dorsal edge of the valve. The axial row of areolae are nearly completely obscured by the dorsal raphe ledge. The ventral striae are not continuous through the central portion of the valve and are composed of a single row of small elongate areolae. Internally, the proximal raphe ends terminate in a very small fused central helictoglossa. The axial and marginal longitudinal silica bands are visible internally and merge near the apices.

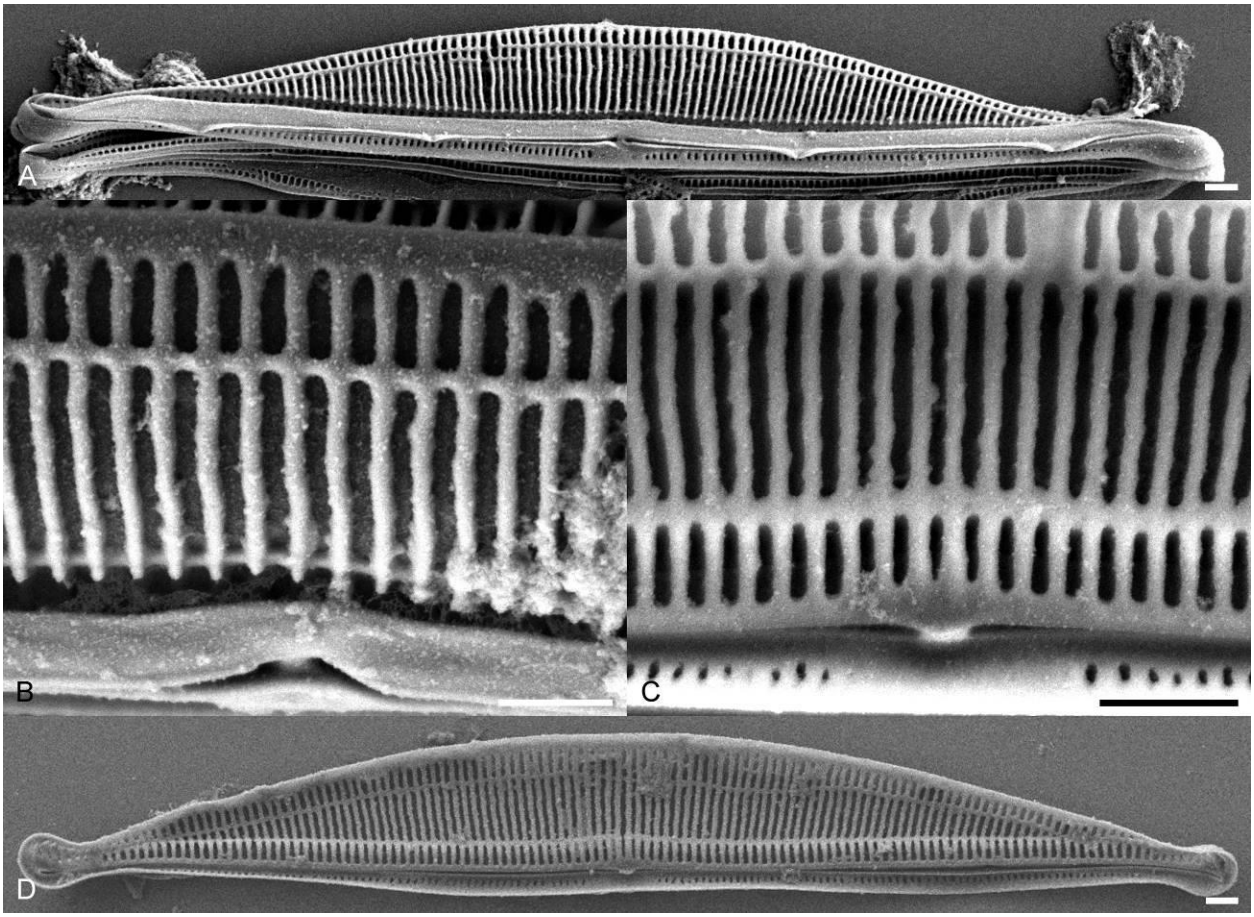

Figure 4.52. Scanning electron micrographs of *Halamphora semperpalorum* Amph047. **A.** External whole valve. **B.** Detail of external valve center. **C.** Detail of internal valve center. **D.** Internal whole valve. Scale bars = 1 µm.

Halamphora sp. nov. Amph081 (Figs 4.53, 4.54)

Valves are semi-elliptical and strongly dorsiventral. The dorsal margin is smoothly arched, the ventral margin is straight. The valve ends are acutely rounded. Valve length 27.0–30.0 µm, valve breadth 7.5–8.0 µm. The raphe is straight becoming dorsally curved as is approaches the central portion of the

valve. The axial area is narrow dorsally and difficult to distinguish ventrally due to the narrow ventral valve. The dorsal raphe ledge is visible in the LM as a faint longitudinal line running along the axial area.

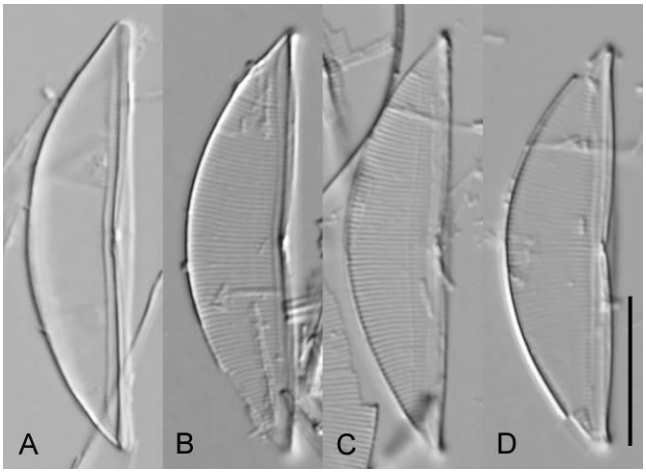

Figure 4.53. A–D. Light micrographs of *Halamphora sp. nov.* Amph081 showing observed size range. Scale bar = 10 µm.

The dorsal striae are very fine, nearly parallel at the valve center, becoming weakly radiate towards the apices. The ventral striae are difficult to resolve in the LM. Dorsal striae number 28–29 in 10 µm.

In SEM, externally, the raphe branches are weakly arched dorsally as they approach the valve center. The proximal raphe ends terminate closely, the distal ends are nearly straight. The dorsal raphe ledge is well developed and continuous along the length of the valve. The dorsal striae are finely biseriate and are uninterrupted along the valve face. A dorsal marginal ridge runs the length of the valve. The dorsal mantle striae appear to be uniseriate. The ventral striae are very fine and ventrally placed. The ventral striae are composed of a single row of closely placed slit-like areolae and are irregular through the central portion of the valve. Internally, the raphe is straight with proximal raphe ends terminating in a small fused central helictoglossa. The dorsal striae are biseriate and separated by thin virgae.

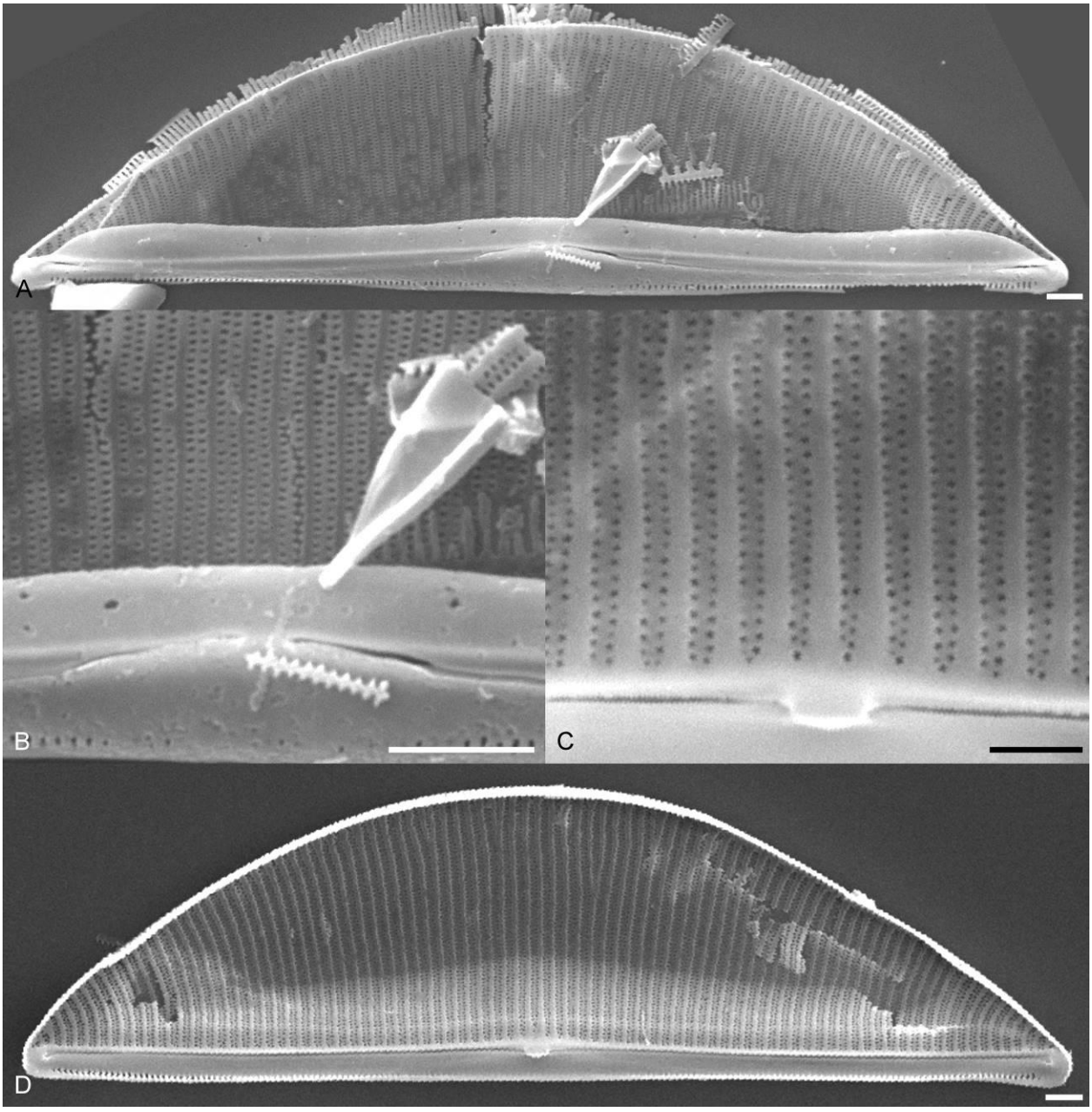

Figure 4.54. Scanning electron micrographs of *Halamphora sp. nov.* Amph081. **A.** External whole valve. **B.** Detail of external valve center. **C.** Detail of internal valve center. **D.** Internal whole valve. Scale bars = 1 µm.

Halamphora hyalina (Ehrenberg) Stepanek & Kociolek Amph037 comb. nov. (Figs 4.56, 4.57)

Valves narrowly semi-elliptical and strongly dorsiventral. The dorsal margin is shallowly arched, the ventral margin is straight. The valve ends are protracted, capitate and deflected ventrally. Valve length 55.0–57.0 µm, valve breadth 4.5–6.0 µm. The raphe is straight with weakly dorsally deflected proximal

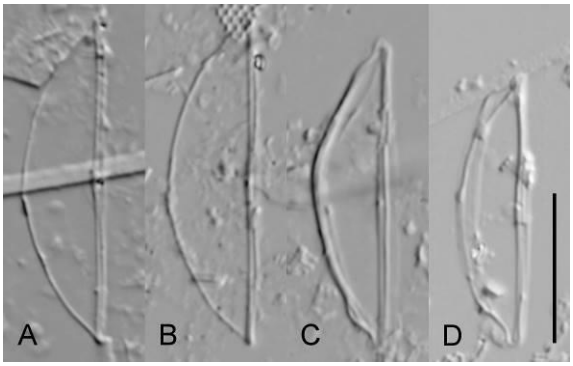

Figure 4.55. A–D. Light micrographs of *Halamphora hyalina* Amph037 showing observed size range. Scale bar = 10 µm.

ends. The axial area appears narrow throughout although it is somewhat difficult to distinguish on the ventral side due to the narrow ventral valve exhibited by this taxon. Two dorsal longitudinal lines running the length of the valve are visible in the LM, one near the axial area, the other near the dorsal margin. The dorsal striae are fine and only interrupted by the two longitudinal lines. The dorsal striae are parallel at the valve center, becoming radiate towards the apices. The ventral striae are difficult to image in the LM due to the narrow ventral valve. Striae number 28–30 in 10 µm.

In SEM, externally, the proximal raphe ends terminate very closely and are weakly deflected dorsally. The distal raphe ends are deflected dorsally. The dorsal raphe ledge is well developed and continuous along the length of the valve. Two longitudinal bands of silica run the length of the valve on the dorsal side. One band of silica runs parallel to the dorsal extent of the raphe ledge along the axial area, the other runs along the dorsal margin. The two longitudinal silica bands merge as they approach the apices. The dorsal striae are composed of large elongate areolae, one row extends from the axial area to the axial longitudinal silica band and the second row extends from the axial silica band to the marginal band. A third row of mantle areolae extends from the marginal band to the dorsal edge of the valve. The axial row of areolae are almost completely covered by the dorsal marginal ridge. The ventral striae are extremely fine and composed of a single row of closely spaced slit-like areolae. The ventral striae are not continuous through the central portion of the valve. Internally, the proximal raphe ends terminate in a small fused central helictoglossa. Both the axial and marginal dorsal silica bands are visible internally.

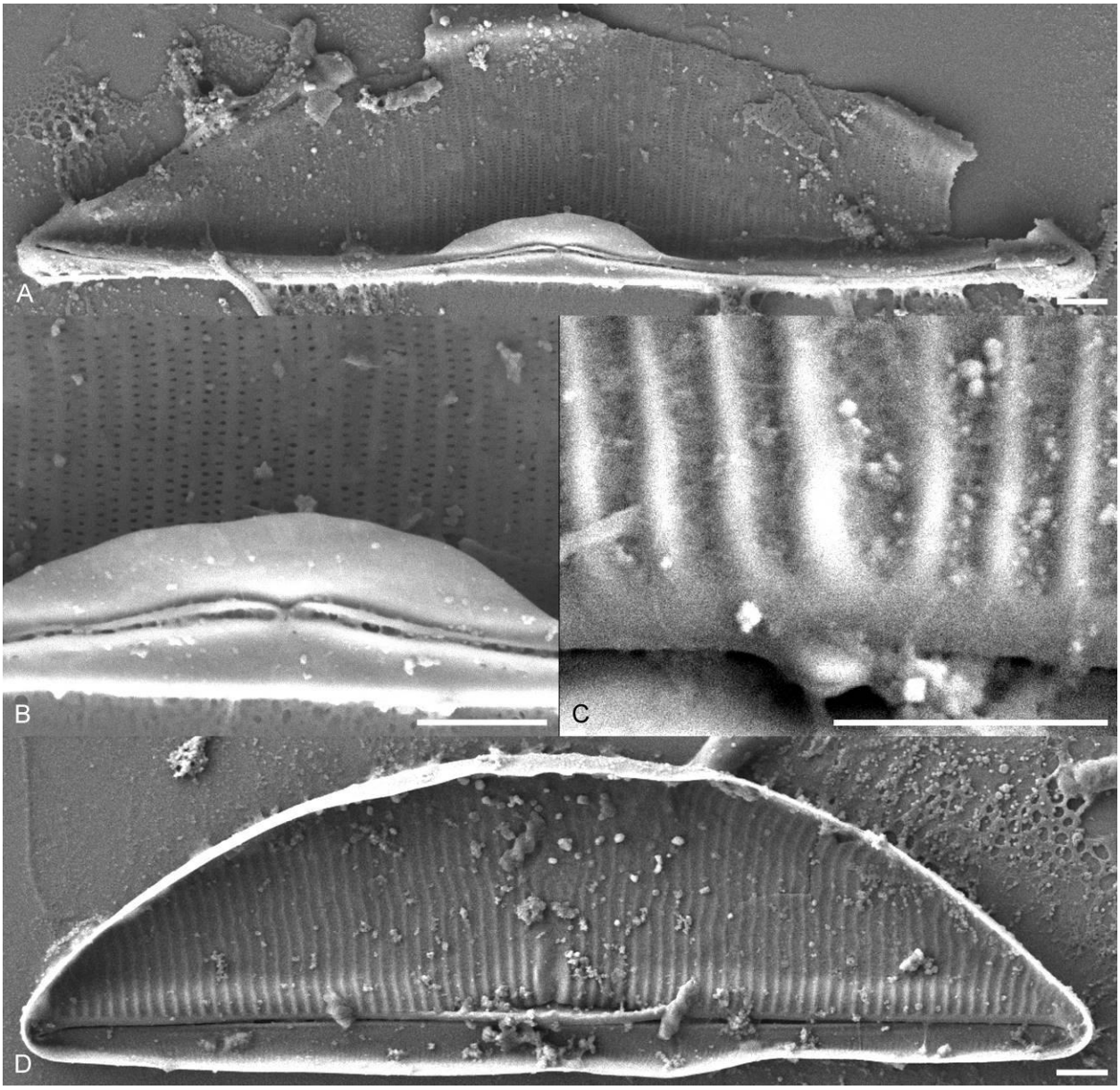

Figure 4.56. Scanning electron micrographs of *Halamphora hyalina* Amph037. **A.** External whole valve. **B.** Detail of external valve center. **C.** Detail of internal valve center. **D.** Internal whole valve. Scale bars = 10 µm.

Halamphora hyalina (Ehrenberg) Stepanek & Kociolek Amph136 comb. nov. (Figs 4.58, 4.59)

Valves broadly semi-elliptical and strongly dorsiventral. The dorsal margin is smoothly arched, the ventral margin is straight. The valve ends are narrowly rounded. Valve length 18.0–23.0 µm, valve

breadth 4.5–6.5 µm. The raphe is straight with straight proximal raphe ends. The axial area appears narrow throughout.. The dorsal and ventral striae are difficult to resolve in the LM.

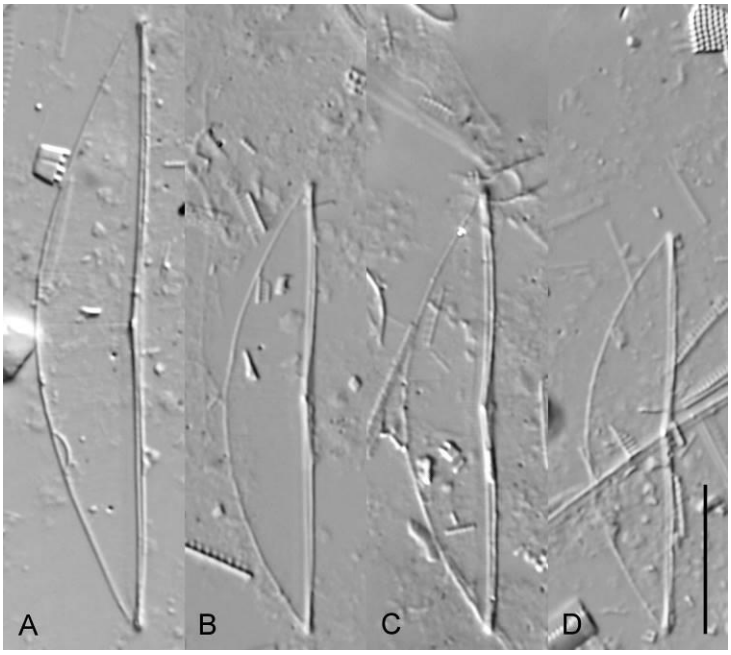

Figure 4.57. A–D. Light micrographs of *Halamphora hyalina* Amph136 showing observed size range. Scale bar = 10 µm.

In the SEM, externally, the proximal raphe ends terminate closely and are slightly curved dorsally, the distal ends are weakly deflected dorsally. The dorsal raphe ledge is narrow through most of the valve, expanded at the valve center. The dorsal striae are finely biseriate. A dorsal marginal ridge is present. Internally, the raphe is straight with proximal ends terminating in a small fused central helictoglossa. The dorsal striae are biseriate and separated by thin virgae. The ventral striae are fine and uniseriate.

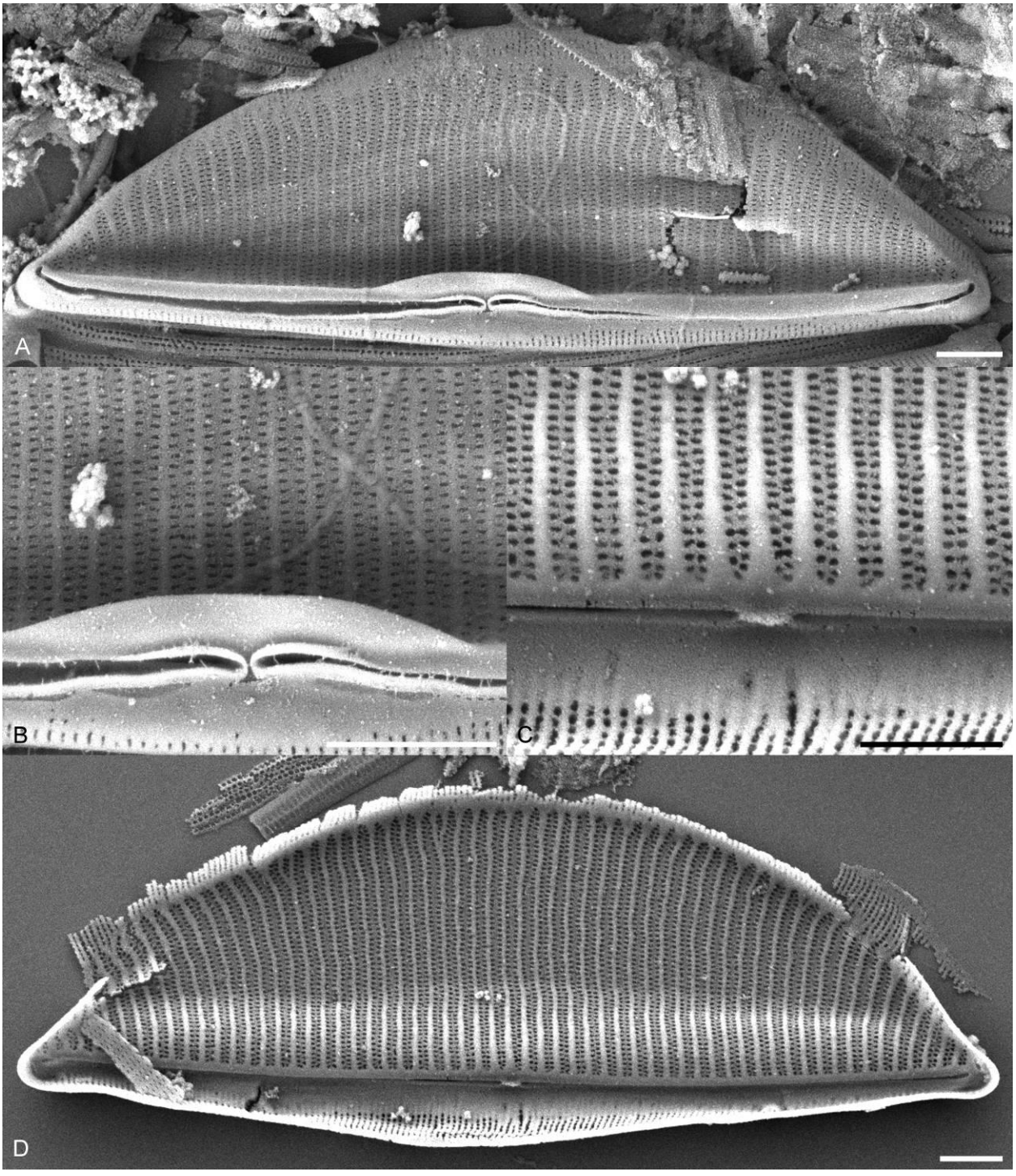

Figure 4.58. Scanning electron micrographs of *Halamphora hyalina* Amph136. **A.** External whole valve. **B.** Detail of external valve center. **C.** Detail of internal valve center. **D.** Internal whole valve. Scale bars = 1 µm.

Halamphora hyalina (Ehrenberg) Stepanek & Kociolek Amph061 comb. nov.

Valves semi-elliptical and strongly dorsiventral. The dorsal margin is smoothly arched, the ventral margin is straight to slightly concave at the valve center. The valve ends are narrowly rounded. Valve length 27.0–42.0 µm, valve breadth 6.0–7.5 µm. The axial area appears narrow throughout. The raphe is straight with the raphe branches curve dorsally as they approach the central portion of the valve. The dorsal and ventral striae are difficult to resolve in the LM.

In SEM, externally, the raphe is slightly biarcuate. The distal raphe ends are weakly dorsally deflected. The dorsal raphe ledge is narrow through the majority of the valve, becoming expanded at the valve center. The dorsal striae are finely biseriate. A dorsal marginal ridge is more or less visible. The ventral striae are continuous through the valve center, fine and uniseriate. Internally, the proximal raphe ends terminate in a very small fused central helictoglossa. The dorsal striae are biseriate and separated by thin virgae. The dorsal marginal ridge is visible internally. The ventral striae are fine and uniseriate.

HALAMPHORA CLADE B

Halamphora holsatica (Hustedt) Levkov Amph154 (Figs 4.60, 4.61)

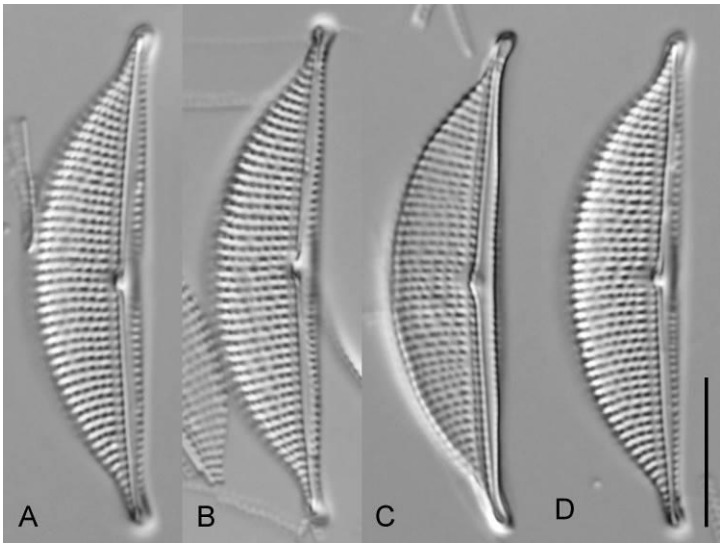

Figure 4.59. A–D. Light micrographs of *Halamphora holsatica* Amph154 showing observed size range. Scale bar = 10 µm.

Valves broadly semi-elliptical and strongly dorsiventral. The dorsal margin is smoothly arched, the ventral margin is nearly straight. The valve ends are protracted, narrowly rounded and ventrally deflected. Valve length 33.0–35.0 µm, 7.5–8.0 µm. The raphe is slightly arched with straight raphe branches. The proximal raphe ends are deflected dorsally deflected. The axial area is narrow slightly expanded at the ventral valve center. The dorsal striae are distinctly areolate, parallel through the central valve, becoming slightly radiate near the apices. The ventral striae are composed of a single row of small areolae, more or less continuous through the valve center. Striae number 14–15 in 10 µm.

In SEM, externally, the proximal raphe ends are slightly dorsally deflected, the distal ends are hooked dorsally. The dorsal raphe ledge is broad and continuous along the length of the valve. The dorsal striae are composed of irregularly positioned round to ovoid areolae. No marginal ridge is present. The ventral striae are small and marginally positioned. The dorsal central virgae are slightly fused into a small hyaline fascia. Internally, the proximal raphe ends terminate in a fused central helictoglossa. A distinct longitudinal band of silica runs the length of the valve near the dorsal axial area. Internally, the dorsal central virgae are slightly fused.

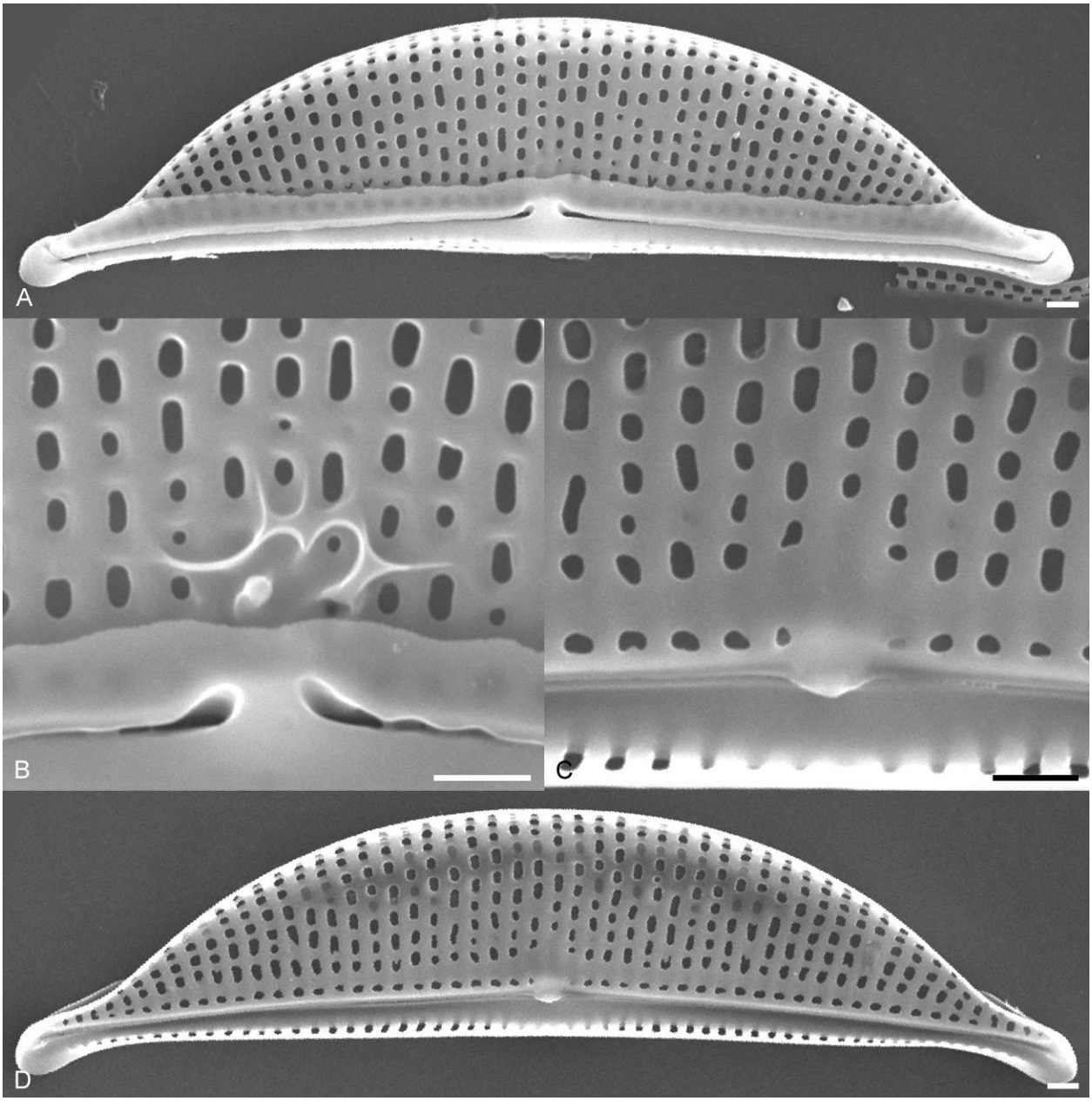

Figure 4.60. Scanning electron micrographs of *Halamphora holsatica* Amph154. **A.** External whole valve. **B.** Detail of external valve center. **C.** Detail of internal valve center. **D.** Internal whole valve. Scale bars = 1 µm.

Halamphora pseudoholsatica (Nagumo & Kobayasi) Stepanek & Kociolek comb. nov. Amph165 (Figs 4.62, 4.63)

Valves semi-elliptical and strongly dorsiventral. The dorsal margin is smoothly arched, the ventral margin is straight to slightly convex. The valve ends are protracted, narrowly rounded and ventrally deflected. Valve length 25.0–26.0 µm, valve breadth 4.5–5.0 µm. The raphe is straight with

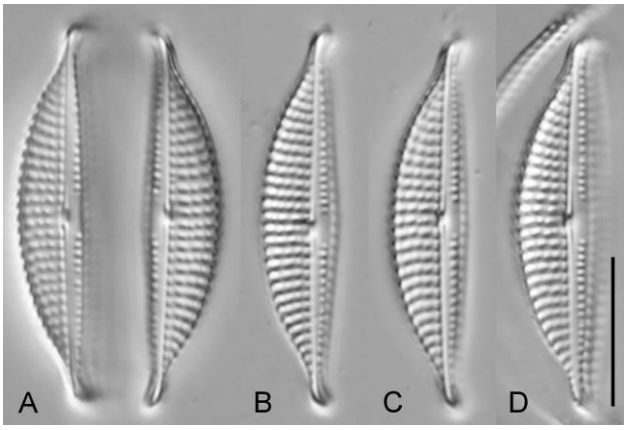

Figure 4.61. A–D. Light micrographs of *Halamphora pseudoholsatica* Amph165 showing observed size range. Scale bar = 10 µm.

straight proximal ends. The axial area is narrow throughout. The dorsal striae are coarse and distinctly areolate, parallel at the valve center and becoming slightly radiate near the apices. The ventral striae are fine and composed of a single row of small areolae. The ventral striae are not continuous through the valve center. Striae number 12–13 in 10 µm.

In SEM, externally, the raphe is straight with dorsally deflected proximal and distal ends. The dorsal raphe ledge is very broad and is continuous across the length of the valve. A well-developed marginal ridge runs the length of the dorsal margin. The dorsal striae are composed of several large round to oval areolae. The ventral striae are composed of a single row of small round areolae. Internally the proximal raphe ends terminate in a well-developed central helictoglossa. Internally, a longitudinal band of silica runs the length of the valve near the axial are on the dorsal valve.

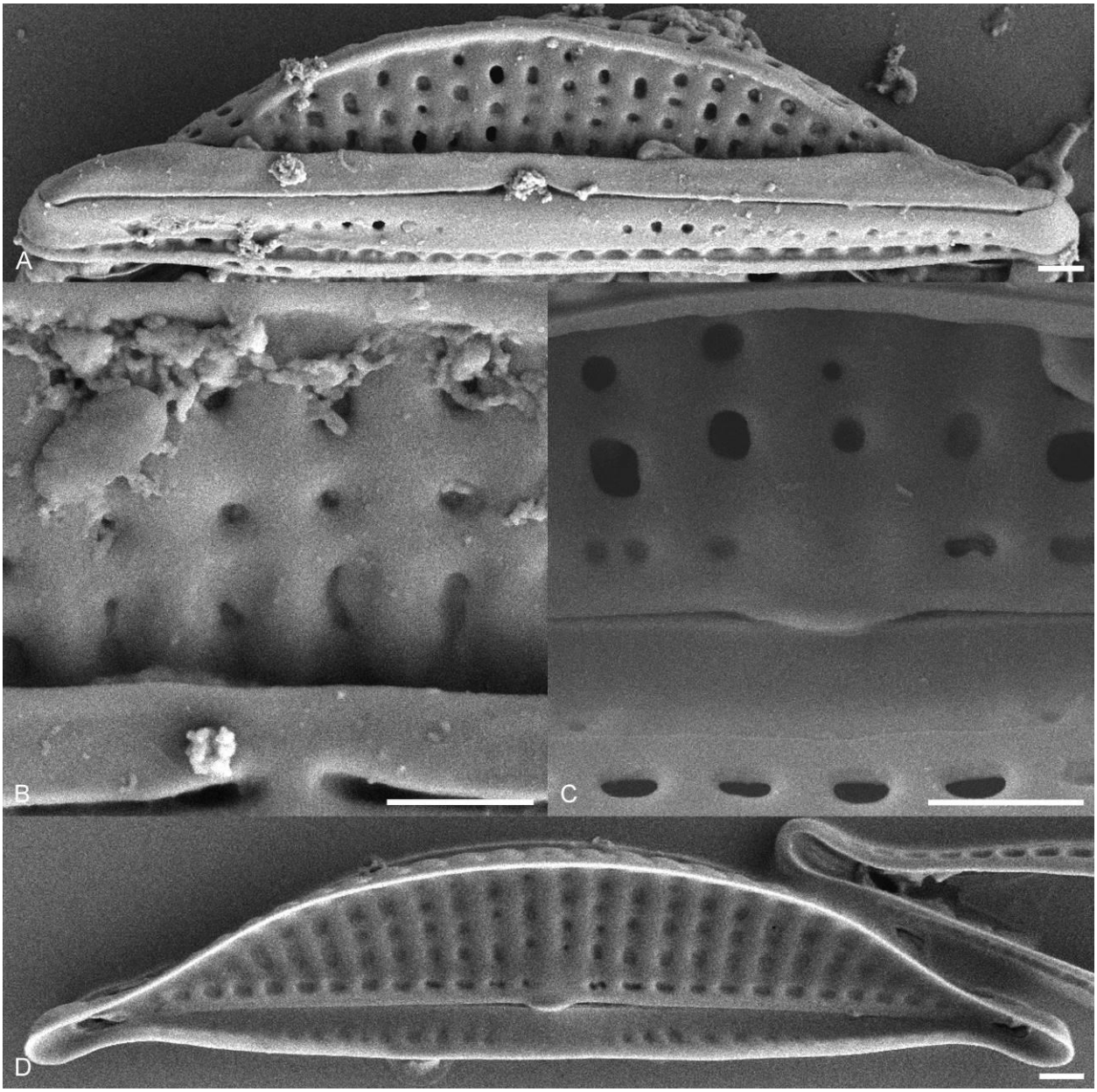

Figure 4.62. Scanning electron micrographs of *Halamphora pseudoholsatica* Amph165. **A.** External whole valve. **B.** Detail of external dorsal valve margin. **C.** Detail of internal valve center. **D.** Internal whole valve. Scale bars = 1 µm.

Halamphora pseudoholsatica (Nagumo & Kobayasi) Stepanek & Kociolek comb. nov. Amph169 (Figs 4.64, 4.65)

Valves are broadly semi-elliptical and strongly dorsiventral. The dorsal margin is smoothly arched, the ventral margin is straight to slightly convex. The valve ends are protracted, narrowly subcapitate and ventrally deflected. Valve length 28.0–43.0 µm, valve breadth 6.0–7.5 µm. The raphe is

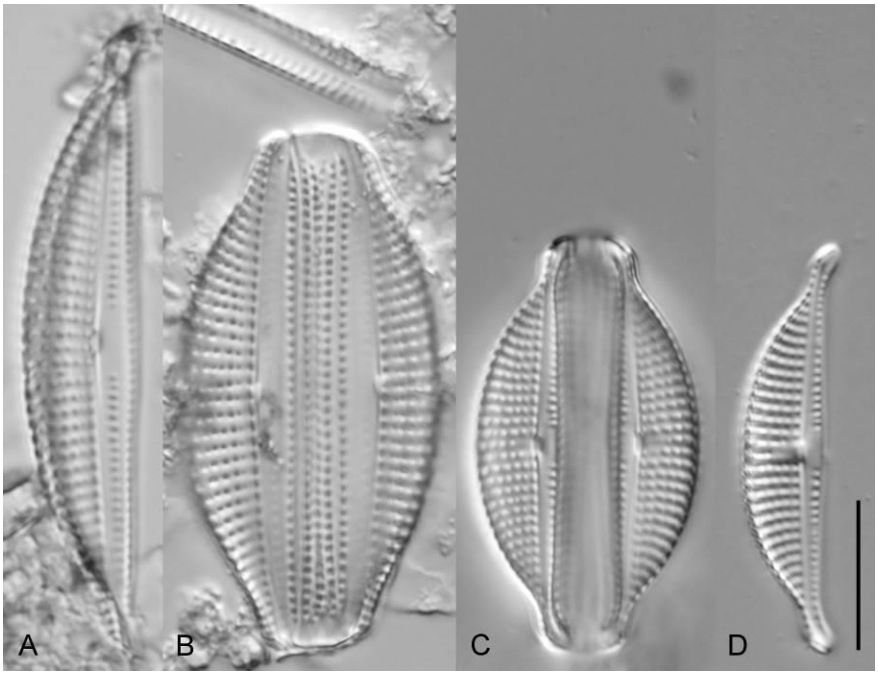

Figure 4.63. A–D. Light micrographs of *Halamphora pseudoholsatica* Amph169 showing observed size range. Scale bar = 10 µm.

slightly arched with the proximal ends weakly deflected dorsally. The axial area is narrow along the dorsal side, slightly expanded through the ventral valve center. The dorsal striae are coarse and distinctly areolate. The dorsal striae are parallel at the valve center, often with the central striae shortened, becoming radiate near the apices. The ventral striae are fine and composed of a single row of small areolae. Striae number 9–12 in 10 µm.

In SEM, externally, the raphe is slightly arched with proximal and distal ends deflected dorsally. The raphe ledge is well developed and continuous along the length of the valve. A well-developed marginal ridge is present, most prominent at the valve center. The ventral axial are is expanded into a narrowly semi-lanceolate hyaline area. The dorsal striae are composed of large round to oval areolae. The

ventral striae are composed of a single row of small areolae. Internally, the proximal raphe ends terminate in a fused central helictoglossa. At the dorsal valve center the central virgae are fused to produce a small siliceous hyaline fascia. No marginal ridge is visible internally.

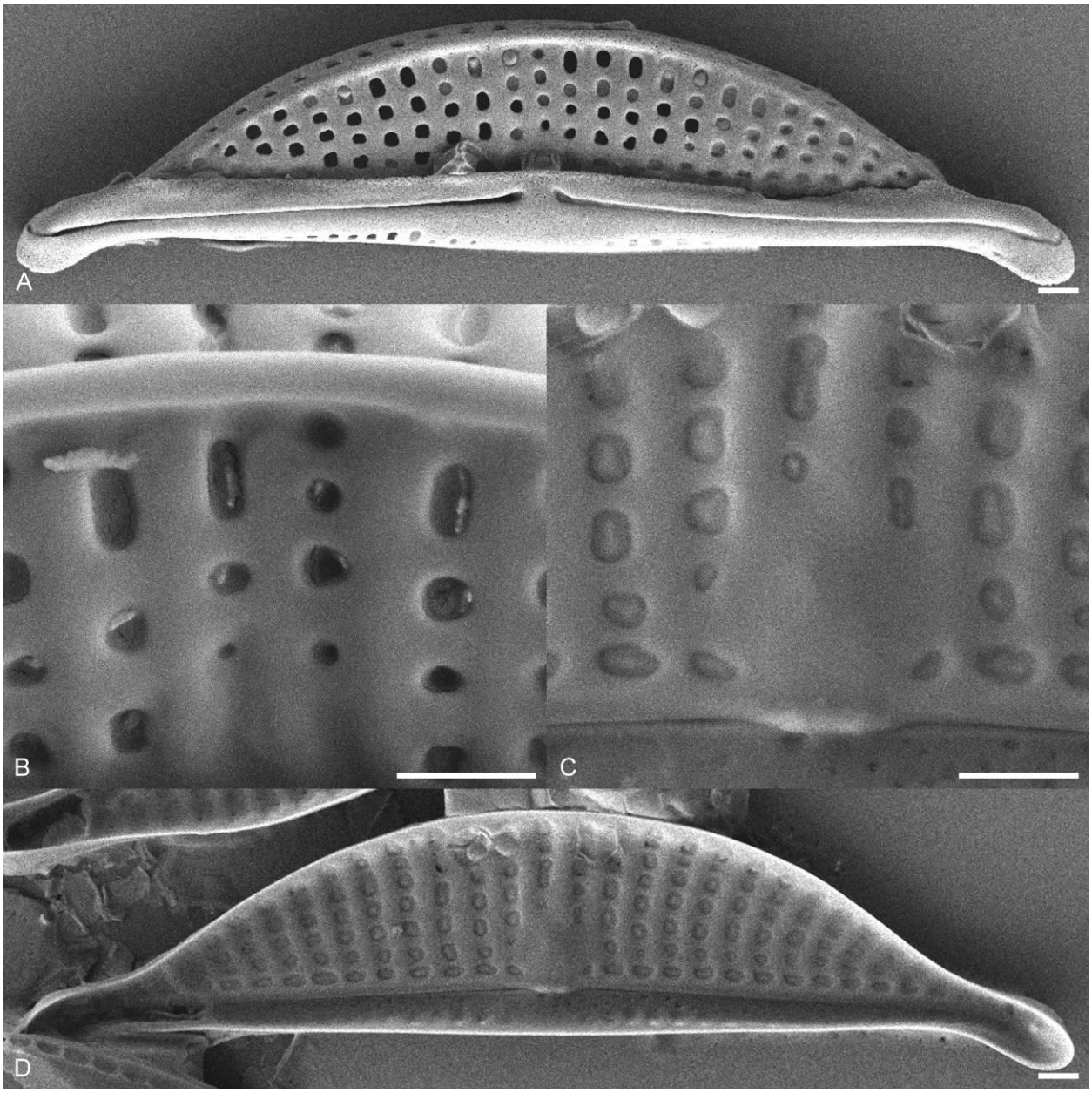

Figure 4.64. Scanning electron micrographs of *Halamphora pseudoholsatica* Amph169. **A.** External whole valve. **B.** Internal whole valve. Scale bars = 1 µm.

Halamphora sp. nov. Amph141 (Figs 4.66, 4.67)

Valves are semi-elliptical and strongly dorsiventral. The dorsal margin is smoothly arched, the ventral margin is straight. The valve ends are weakly protracted, narrowly rounded and slightly ventrally deflected. Valve length 15.0–18.0 µm, valve breadth 4.0–4.5 µm. The raphe is straight with straight proximal raphe ends that terminate closely. The axial area is narrow throughout. A faint longitudinal line is visible in the LM running the length of the valve near the dorsal axial area. The dorsal striae are areolate, parallel at the valve center, becoming weakly radiate near the apices. The ventral striae are fine and continuous through the valve center. Striae number 18–19 in 10 µm.

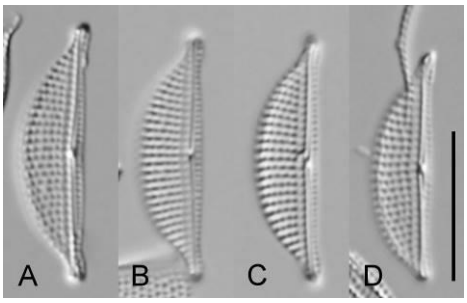

Figure 4.65. A–D. Light micrographs of *Halamphora sp. nov.* Amph141 showing observed size range. Scale bar = 10 µm.

In SEM, the proximal and distal raphe ends are deflected dorsally. The raphe ledge is broad and continuous along the length of the valve. The striae are composed of numerous round or ovoid areolae. A marginal ridge is not well developed. The dorsal striae are marginally positioned and composed of a single row of small areolae. Internally, the proximal raphe ends terminate in a small fused central helictoglossa. A longitudinal band of silica runs the length of the valve near the dorsal axial area.

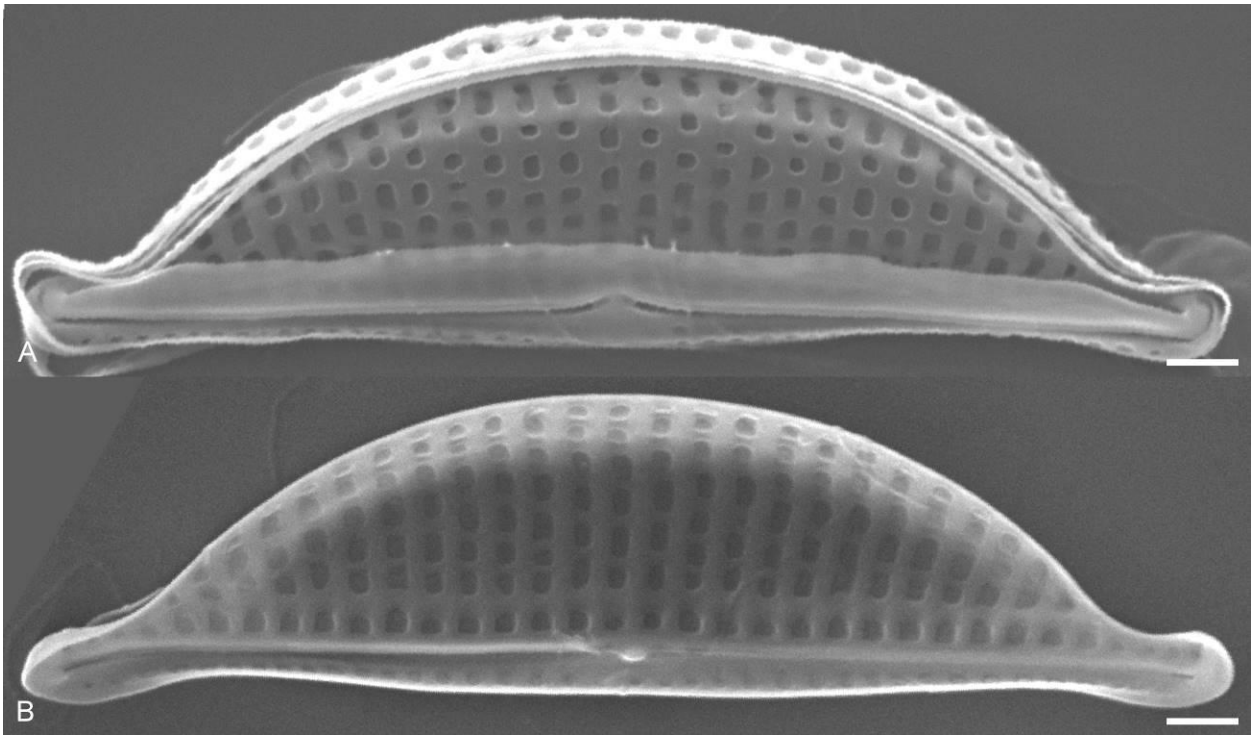

Figure 4.66. Scanning electron micrographs of *Halamphora sp. nov.* Amph141. **A.** External whole valve. **B.** Detail of external valve center. **C.** Detail of internal valve center. **E.** Internal whole valve. Scale bar = 1 µm.

Halamphora sp. nov. Amph060 (Figs 4.68, 4.69)

Valves are narrowly semi-elliptical and strongly dorsiventral. The dorsal margin is shallowly arched becoming flat over the valve center, the ventral margin is nearly straight to slightly concave. The valve ends are protracted and subcapitate. Valve length 33.0 µm, valve breadth 4.0 µm. The raphe is slightly arched with straight to slightly dorsally deflected proximal ends. The axial area is narrow throughout. The dorsal striae are areolate, parallel ate the valve center, becoming radiate near the apices. The ventral striae are fine, difficult to image in the LM and appear to be continuous through the central valve.

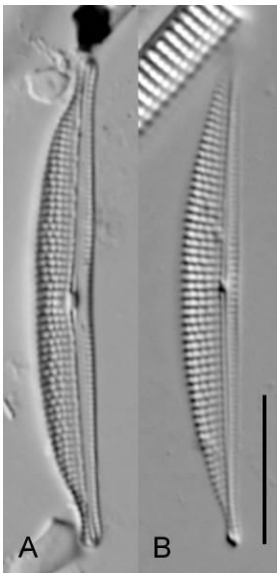

Figure 4.67. A, B. Light micrographs of *Halamphora sp. nov.* Amph060 showing observed size range. Scale bar = 10 µm.

In SEM, externally, the raphe is straight with dorsally deflected proximal ends and dorsally bent distal ends. The dorsal raphe ledge is well developed, distinctly more so near the apices, and continuous along the length of the valve. The ventral axial area is expanded near the central valve, creating a semi-lanceolate hyaline area. No dorsal marginal ridge is present. The dorsal striae are composed of numerous ovoid to rectangular areolae. The ventral striae a fine and composed of a continuous single row of small elongate areolae. Internally, the proximal raphe ends terminate in a small fused central helictoglossa. A longitudinal band of silica runs the length of the valve near the dorsal axial area.

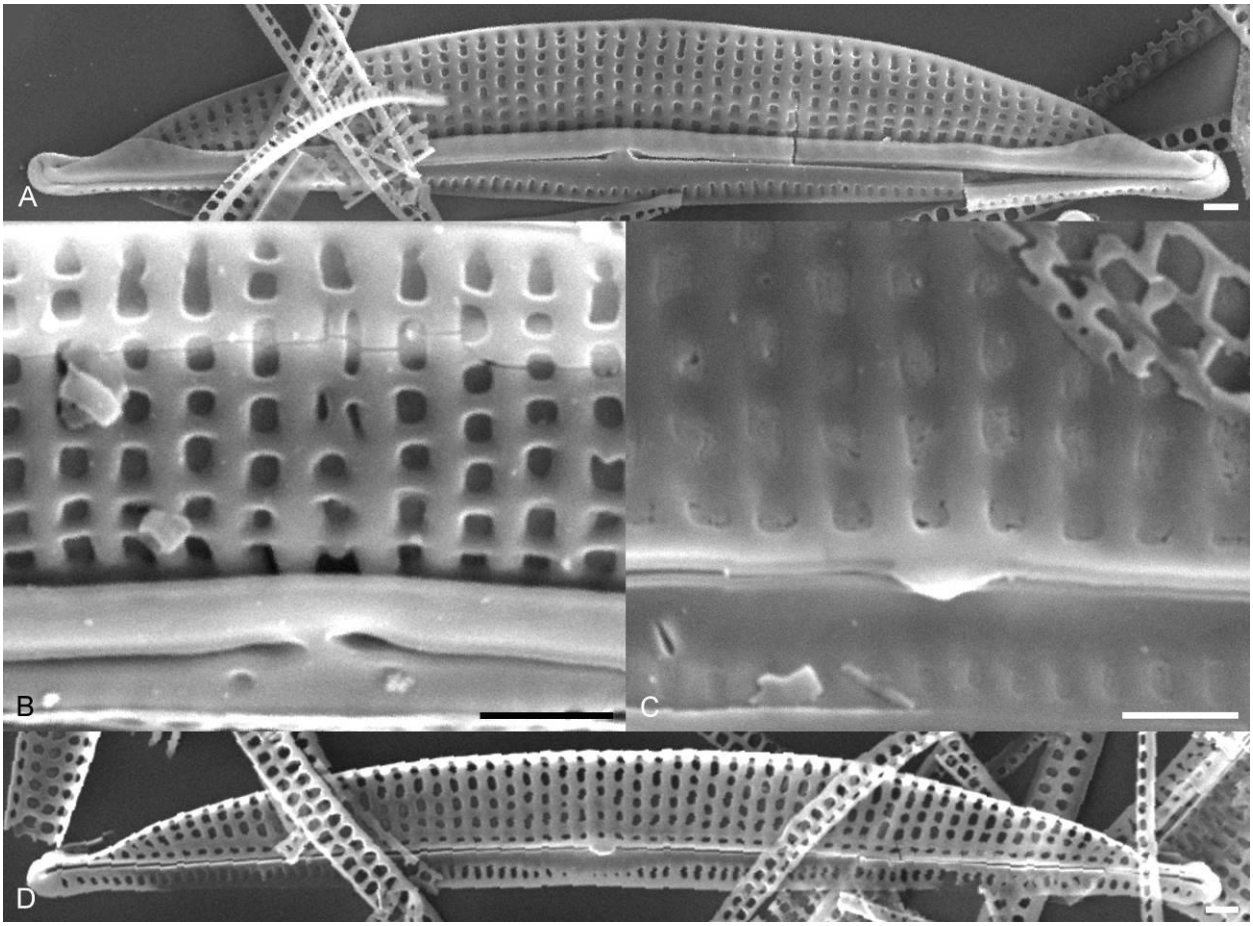

Figure 4.68. Scanning electron micrographs of *Halamphora sp. nov.* Amph060. **A.** External whole valve. **B.** Detail of external valve center. **C.** Detail of internal valve center. **D.** Internal whole valve. Scale bars = 1 µm.

HALAMPHORA CLADE C

Halamphora cymbifera var. *heritierarum* (Wachnicka and Gaiser) Stepanek & Kociolek comb. nov.

Amph082 (Figs 4.70, 4.71)

Valves semi-elliptical with a smoothly arched dorsal margin and a straight to slightly concave ventral margin. Valve length 47.0–49.0 µm, valve breadth 8.5–10.0. Valve ends protracted and weakly subcapitate. Raphe nearly straight to slightly arched with straight raphe branches. Proximal raphe ends straight and slightly dilated, distal ends hooked dorsally. The axial area is narrow throughout. The dorsal

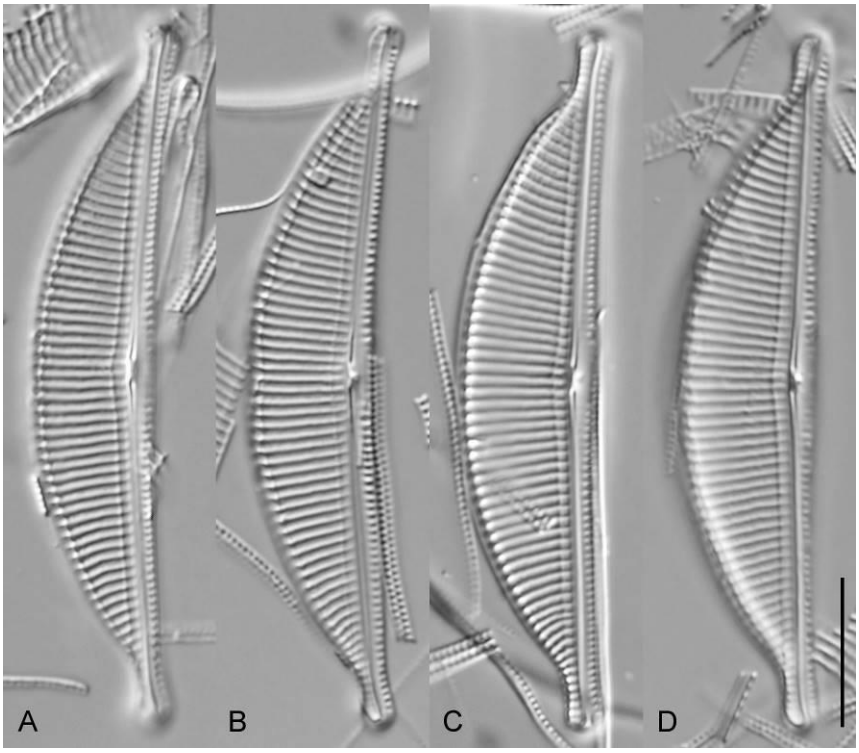

Figure 4.69. A–D. Light micrographs of *Halamphora cymbifera* var. *heritierarum* Amph082 showing observed size range. Scale bar = 10 µm.

raphe ledge is visible in the LM as a longitudinal line near the axial area. Dorsal striae parallel through the valve center, becoming slightly radiate near the apices, 12–13 in 10 µm. The dorsal striae are interrupted at the dorsal margin. Ventral striae are fine and continuous through the central valve.

In SEM, externally, the raphe branches are straight with proximal ends slightly dorsally deflected and distal ends hooked dorsally. The raphe ledge is broad and continuous along the length of the valve. The dorsal striae are uninterrupted, biseriate and separated by thick virgae. A broad marginal ridge, extended into a flap, runs the length of the valve. The ventral striae are thin and finely areolate. Internally, the proximal raphe ends terminate in a fused central helictoglossa, the distal ends in a weakly developed helictoglossa. The dorsal striae are biseriate and the ventral striae are narrow and finely areolate.

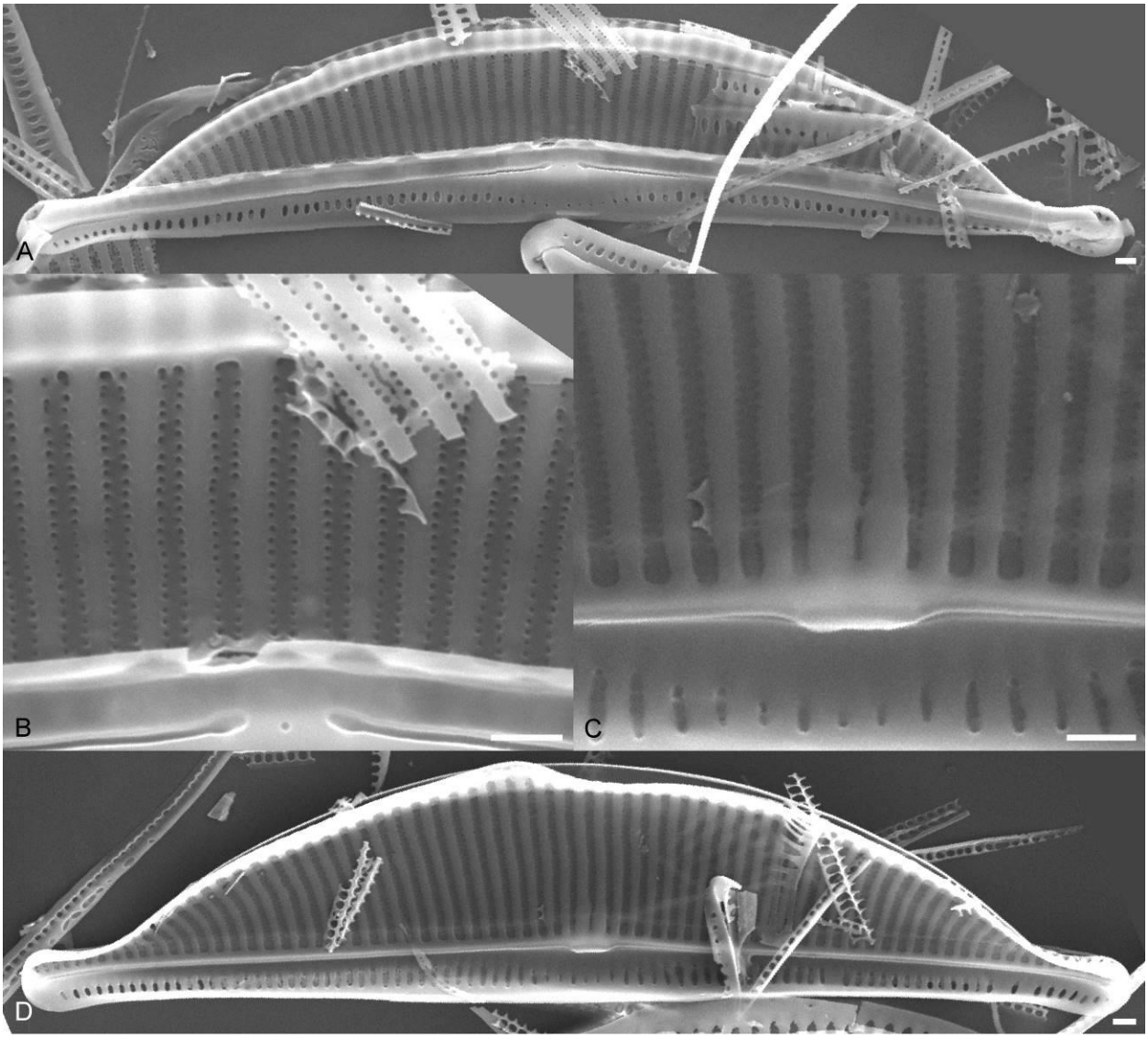

Figure 4.70. Scanning electron micrographs of *Halamphora cymbifera* var. *heritierarum* Ammph082. **A.** External whole valve. **B.** Detail of external valve center. **C.** Detail of internal valve center. **D.** Internal whole valve. Scale bars = 1 µm.

Halamphora sp. nov. Amph124/192 (Figs 4.72, 4.73)

Valves semi-elliptical with the dorsal margin smoothly arched in smaller specimens becoming centrally constricted in larger specimens. The ventral margin is slightly concave. Valve length 40.0–65.0 µm, valve breadth 7.0–9.0 µm. The valve ends are protracted, subcapitate and slightly ventrally bent. The raphe is weakly arched with straight raphe branches. Proximal raphe ends terminate closely and are slightly deflected dorsally, the distal ends hook dorsally near the apices. The axial area is narrow

throughout. The raphe ledge is visible in the LM as a faint longitudinal line running the length of the valve dorsal to the raphe. The dorsal striae are coarse, appear finely areolate and run uninterrupted to the margin. The dorsal striae are weakly radiate to nearly parallel at the valve center, becoming more radiate near the apices. The ventral striae are fine and run the length of the valve. Dorsal striae number 13–14 in 10 µm, ventral striae 20–22 in 10 µm.

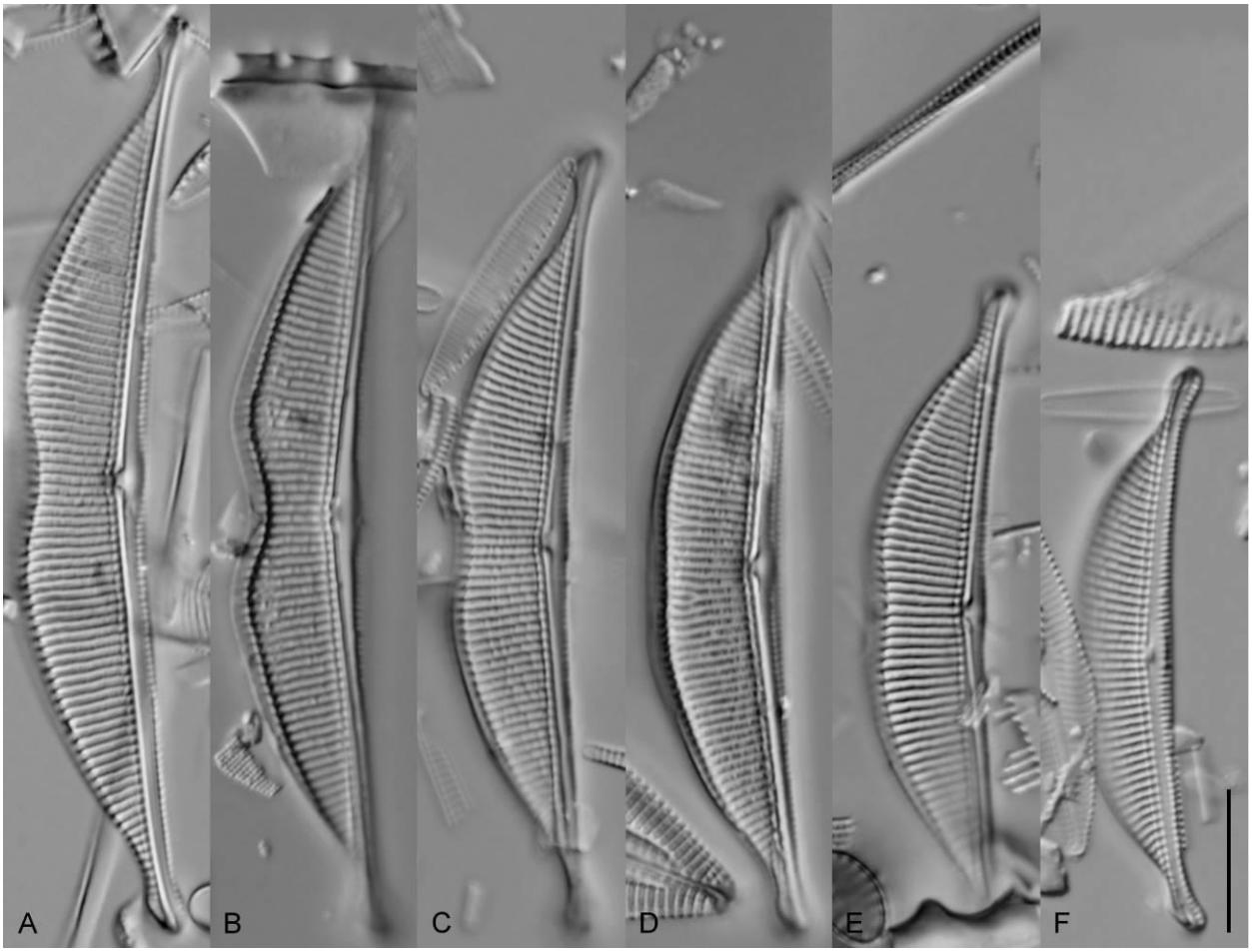

Figure 4.71. A–D. Light micrographs of *Halamphora sp. nov.* Amph124/192 showing observed size range. Scale bar = 10 µm.

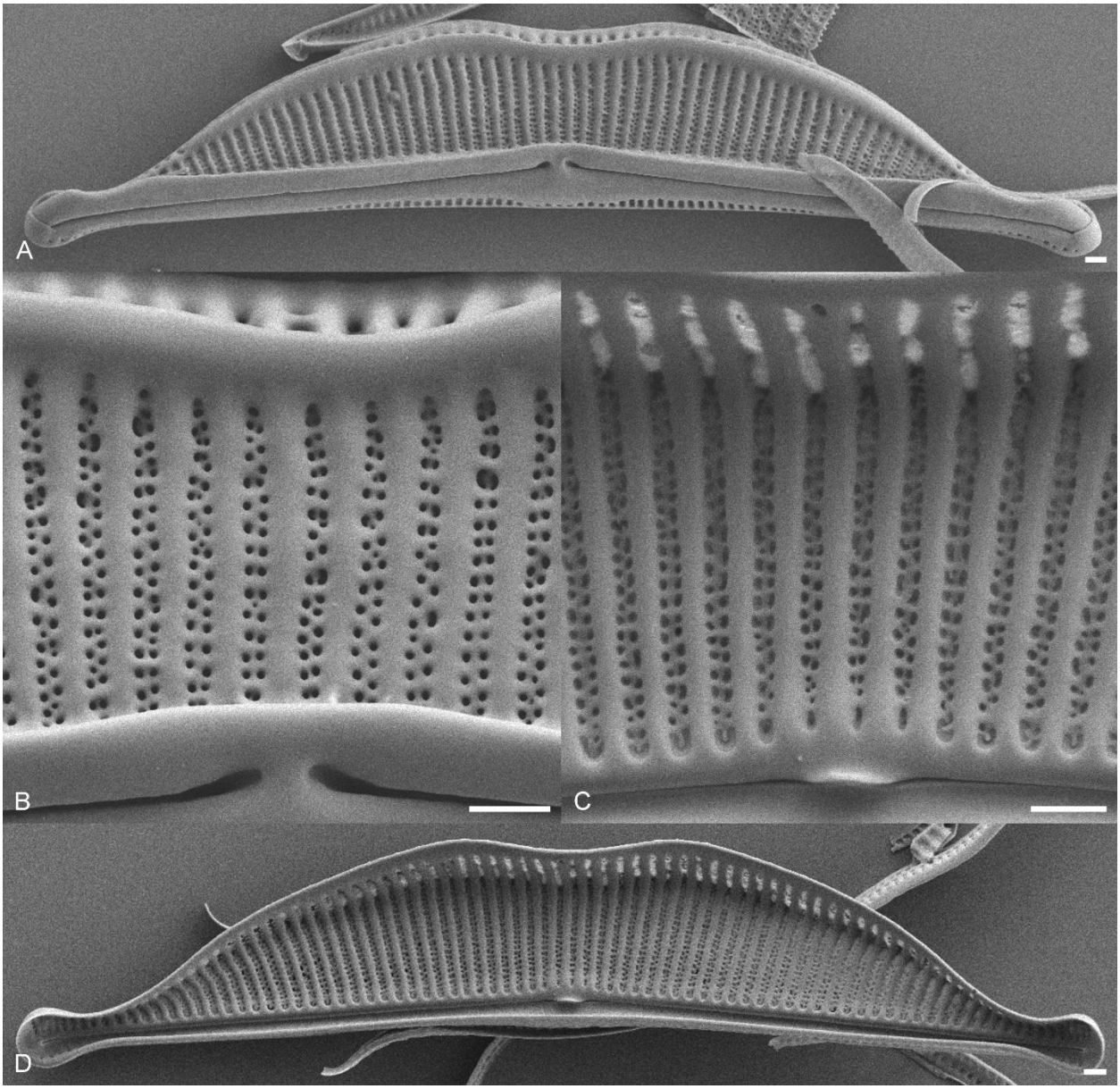

Figure 4.72. Scanning electron micrographs of *Halamphora sp. nov.* Amph124/192. **A.** External whole valve. **B.** Detail of external valve center. **C.** Detail of internal valve center. **D.** Internal whole valve. Scale bars = 1 µm.

In SEM, externally, the raphe branches are straight with proximal end slightly inflated and dorsally deflected and ventral ends hooking dorsally. The dorsal raphe ledge is narrow but thickly silicified. A distinct marginal ridge runs the length of the dorsal margin and is most pronounced near the valve center. The dorsal striae are biseriate. The ventral striae are composed of a row of single elongate areolae. Internally, the proximal raphe ends terminate in a fused central helictoglossa and the distal ends

in a simple helictoglossa. The dorsal striae are biseriate and, although prominent externally, the marginal ridge is not apparent.

Halmphora sp. nov. Amph117 (Figs 4.74, 4.75)

Valves narrowly semi-elliptical to semi-lanceolate with an arched dorsal margin and slightly concave ventral margin. Valve ends protracted, subcapitate in large specimens to narrowly rounded in smaller specimens. Valve length 49.0–68.0 µm, valve breadth 6.0–7.5 µm. The raphe is moderately arched with raphe branches straight to dorsally arched. The proximal raphe ends are straight, the ventral raphe ends hook dorsally The axial area is narrow, becoming slightly expanded at the ventral central area. The dorsal striae are coarse, distinctly areolate and slightly radiate throughout. The dorsal areolae are transapically elongated and are irregular in size and position. The ventral striae are fine and less distinctly areolate. Dorsal striae number 14–17 in 10 µm.

In SEM, externally, the raphe ledge is moderately developed. The raphe branches are straight and terminated in simple proximal raphe ends. The dorsal striae are separated by thin virgae irregularly crossed by more or less developed vimines and are irregularly uni- to biseriate. A weakly developed marginal ridge is present, most pronounced near the apices. The ventral striae are fine and irregularly areolate. Internally, the striae are irregularly uni- to biseriate. The raphe is arched and terminates proximally at a fused central helictoglossa.

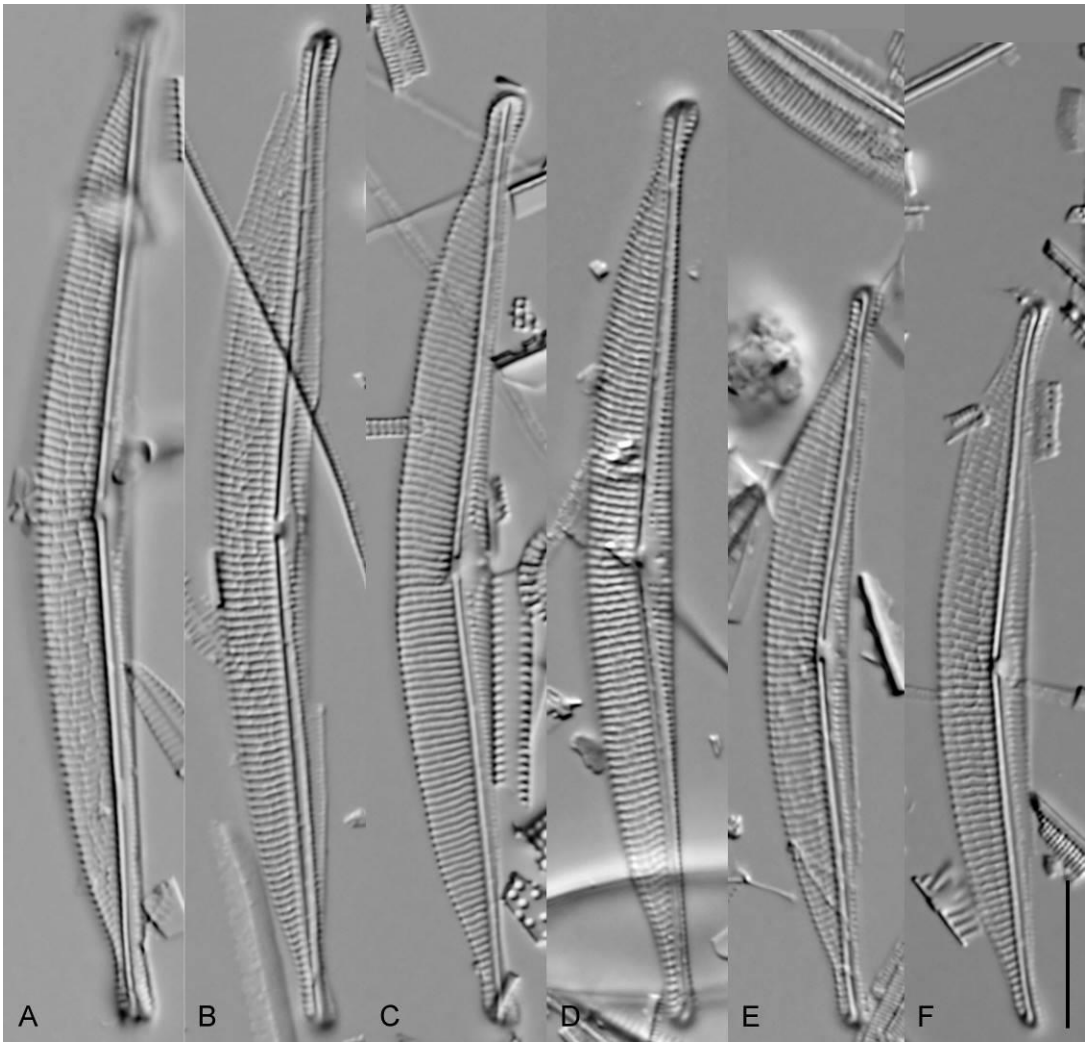

Figure 4.73. A–F. Light micrographs of *Halamphora sp. nov.* Amph117 showing observed size range. Scale bar = 10 µm.

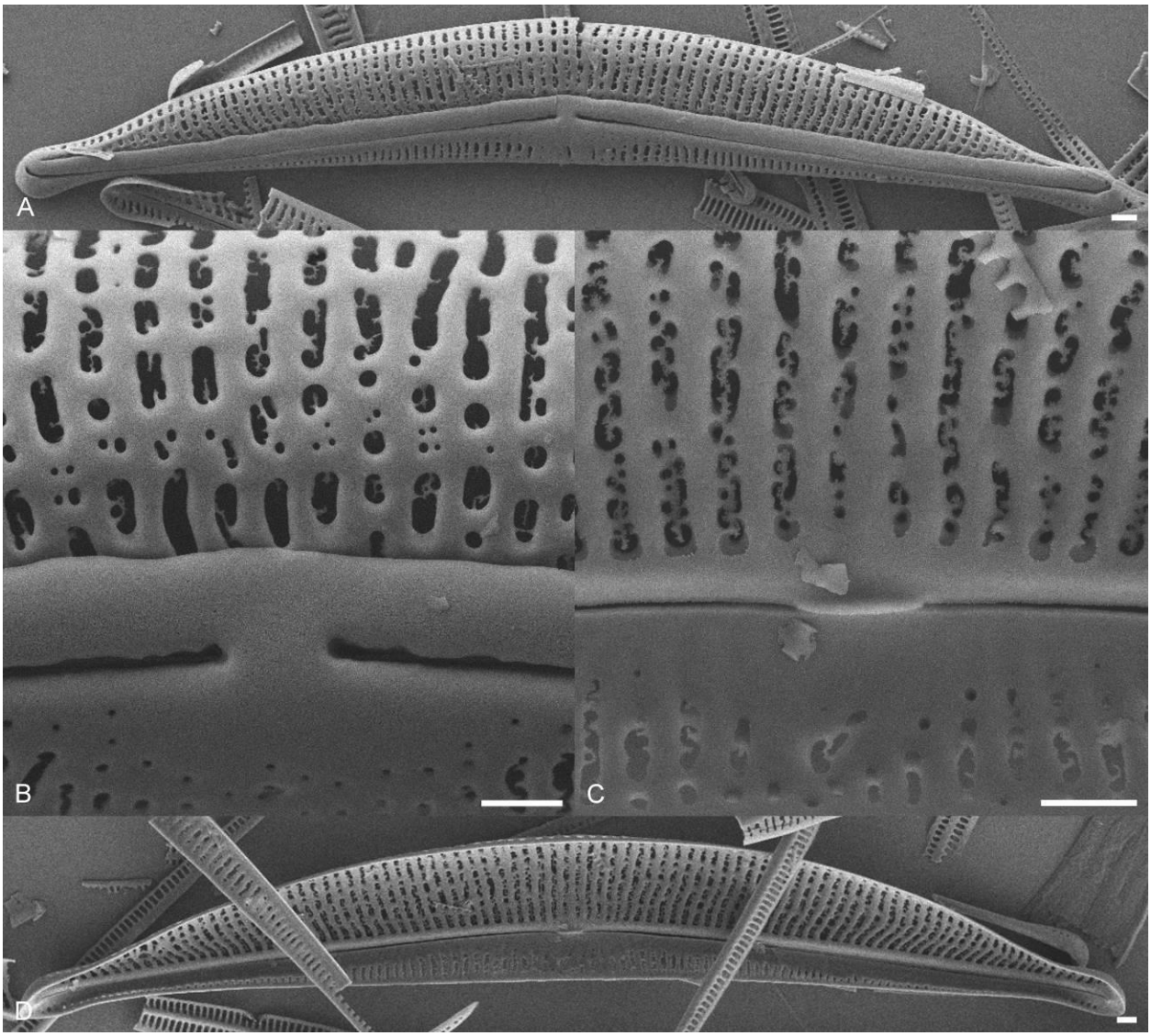

Figure 4.74. Scanning electron micrographs of *Halamphora sp. nov.* Amph117. **A.** External whole frustule. **B.** Detail of external valve center. **C.** Detail of internal valve center. **D.** Internal whole valve. Scale bars = 1 µm.

Halamphora sp. nov. Amph181 (4.76, 4.77)

Valves narrowly semi-elliptical to semi-lanceolate with an arched dorsal margin and slightly concave ventral margin. Valve ends protracted, subcapitate in large specimens to narrowly rounded in smaller specimens. Valve length 68.0–75.0 µm, valve breadth 8.5–9.0 µm. The raphe is moderately arched with raphe branches straight to dorsally arched. The proximal raphe ends are straight, the ventral raphe ends hook dorsally The axial area is narrow, becoming slightly expanded at the ventral central area.

Figure 4.75. A–D. Light micrographs of *Halamphora sp. nov.* Amph181 showing the observed size range. Scale bar = 10 µm.

The dorsal striae are coarse, distinctly areolate and slightly radiate throughout. The dorsal areolae are transapically elongated and are irregular in size and position. The ventral striae are fine and less distinctly areolate. Dorsal striae number 14–17 in 10 µm.

In SEM, externally, the raphe ledge is moderately developed. The raphe branches are straight and terminated in simple proximal raphe ends. The dorsal striae are separated by thin virgae irregularly crossed by more or less developed vimines and are irregularly uni- to biseriate. A weakly developed marginal ridge is present, most pronounced near the apices. The ventral striae are fine and irregularly

areolate. Internally, the striae are irregularly uni- to biseriate. The raphe is arched and terminates proximally at a fused central helictoglossa.

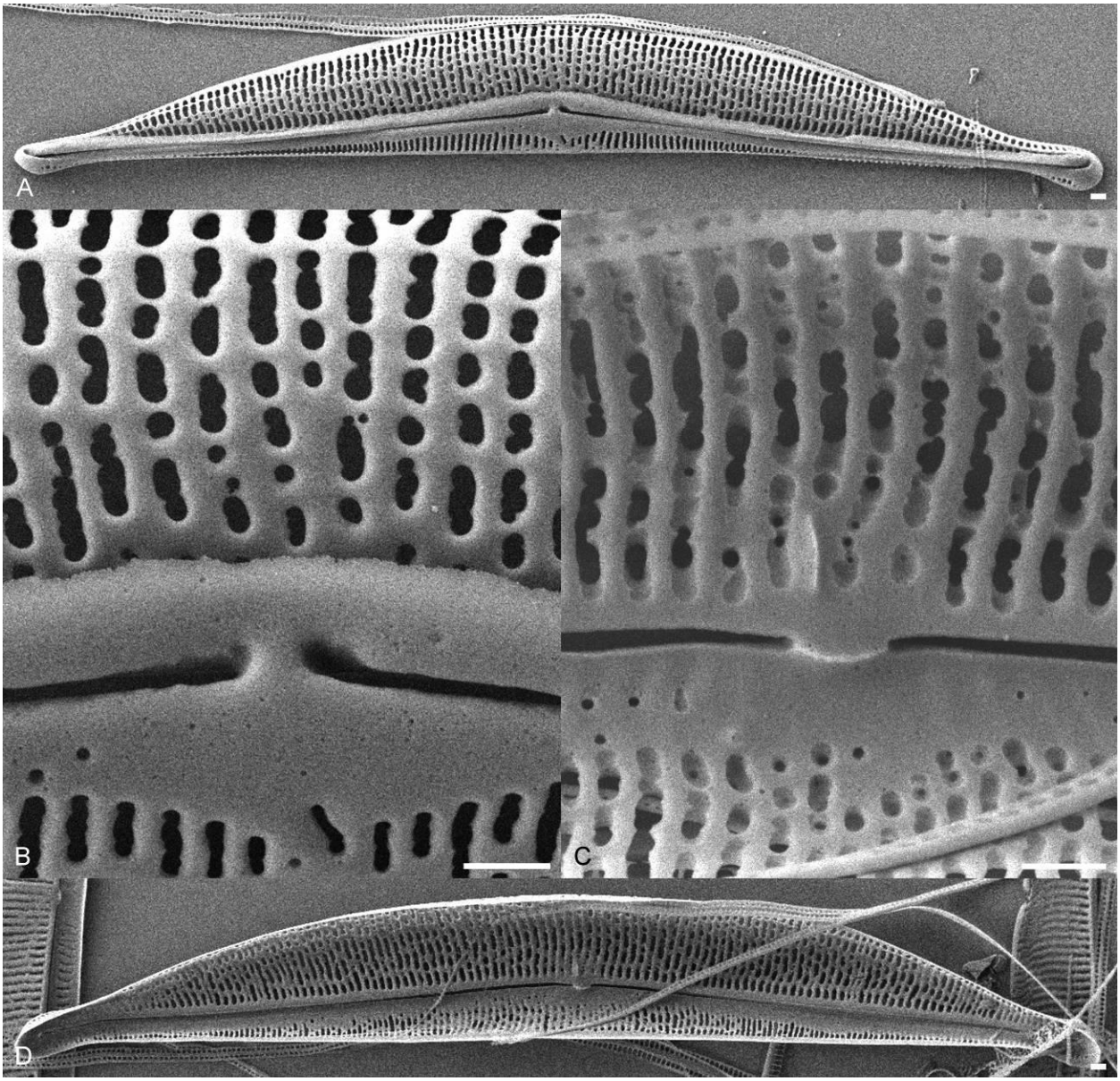

Figure 4.76. Scanning electron micrographs of *Halamphora sp. nov.* Amph181. **A.** External whole valve. **B.** Detail of external valve center. **C.** Detail of internal valve center. **D.** Internal whole valve. Scale bars = 1 µm.

Halamphora coffeaeformis (Agardh) Levkov Amph104/105 (4.78, 4.79)

Valves are semi-elliptical with a smoothly arched dorsal margin and a straight to slightly concave ventral margin. Valve length 25.0–40.0 µm, valve breadth 6.0–7.5 µm. The valve ends are protracted and ventrally deflected. The raphe is slightly arched with straight raphe branches. Proximal raphe ends are straight, distal ends hook dorsally. The axial area is narrow dorsally, slightly expanded at the ventral valve center. Dorsal striae are uninterrupted and not obviously areolate, parallel near the valve center, becoming radiate near the apices. The ventral striae are fine and can be difficult to image in the LM. Dorsal striae number 16–19 in 10 µm.

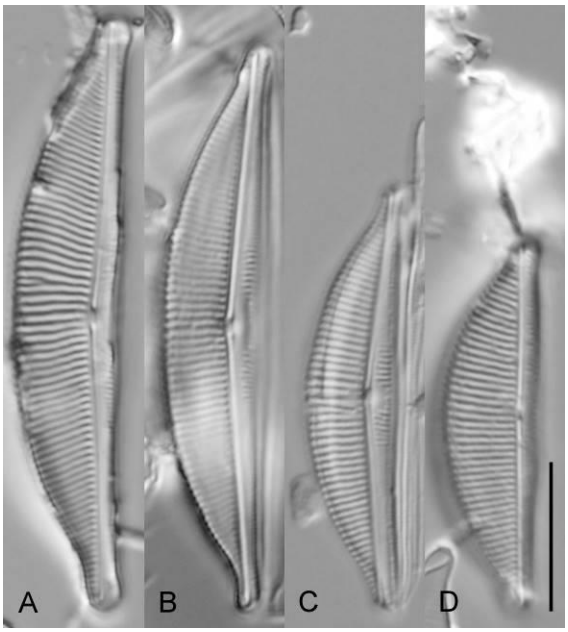

Figure 4.77. A–D. Light micrographs of *Amphora coffeaeformis* Amph104/105 showing the observed size range. Scale bar = 10 µm.

In SEM, externally, the raphe branches are straight with proximal ends slightly inflated and deflected dorsally and distal ends hooked dorsally. The dorsal raphe ledge is moderately developed and expanded near the valve center. The dorsal striae are biseriate and separated by distinct virgae. The marginal ridge is not well developed in imaged specimens. The ventral striae are fine and uniseriate. Internally, the striae are biseriate. The proximal raphe ends terminate in a prominent fused central helictoglossa.

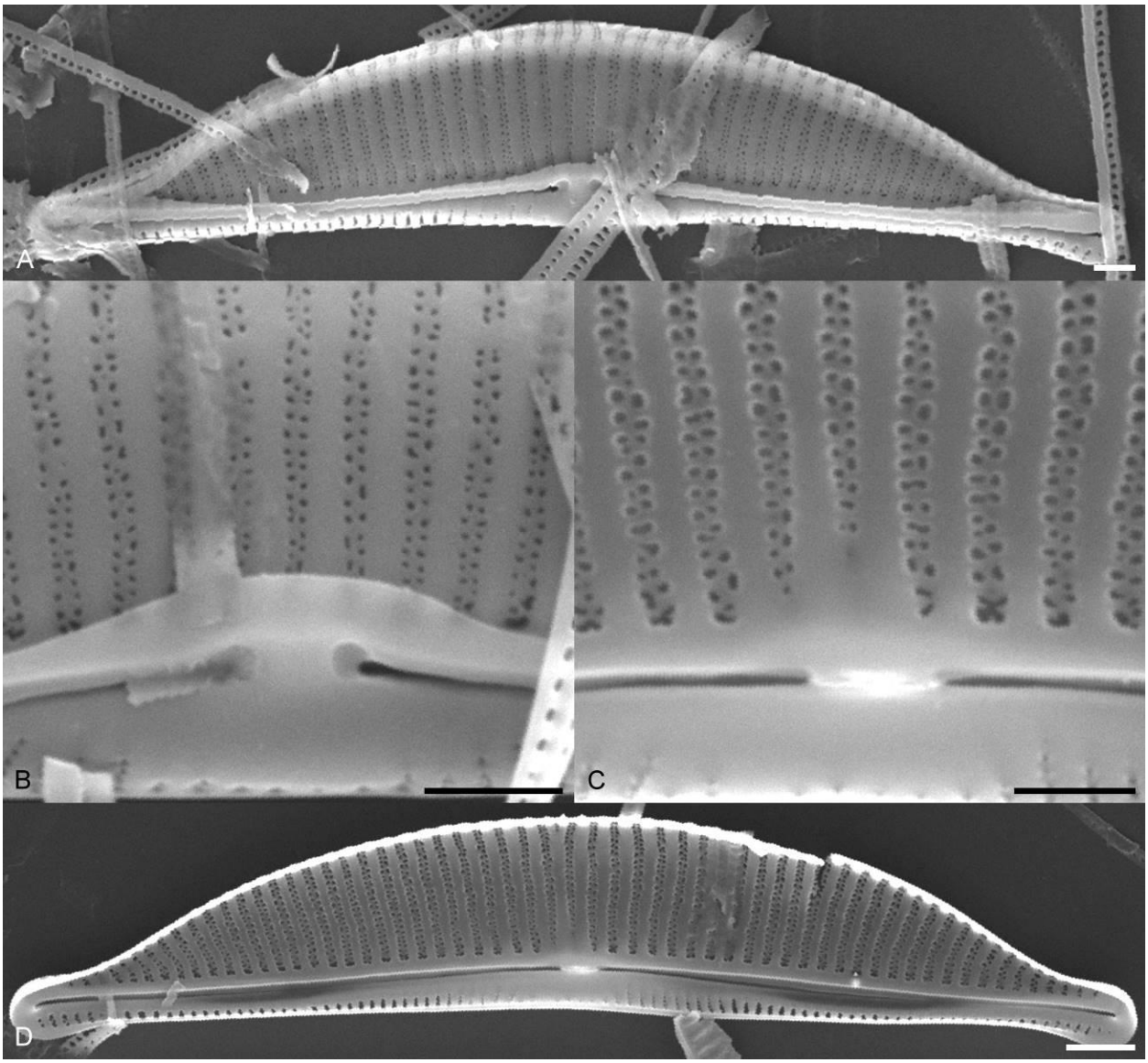

Figure 4.78. Scanning electron micrographs of *Halamphora coffeaeformis* Amph104/105. **A.** External whole valve. **B.** Detail of external valve center. **C.** Detail of internal valve center. **D.** Internal whole valve. Scale bars = 1 µm.

Halamphora coffeaeformis (Agardh) Levkov Amph023 (Figs 4.80, 4.81)

Valves are semi-elliptical with a smoothly arched dorsal margin and a straight to slightly concave ventral margin. Valve length 32.0–34.0 µm, valve breadth 5.5–6.0 µm. The valve ends are protracted and ventrally deflected. The raphe is slightly arched with straight raphe branches. Proximal raphe ends are straight, distal ends hook dorsally. The axial area is narrow dorsally, slightly expanded at the ventral valve center. Dorsal striae are uninterrupted and not obviously areolate, parallel near the valve center,

becoming radiate near the apices. The ventral striae are fine and can be difficult to image in the LM. Dorsal striae number 16–18 in 10 µm.

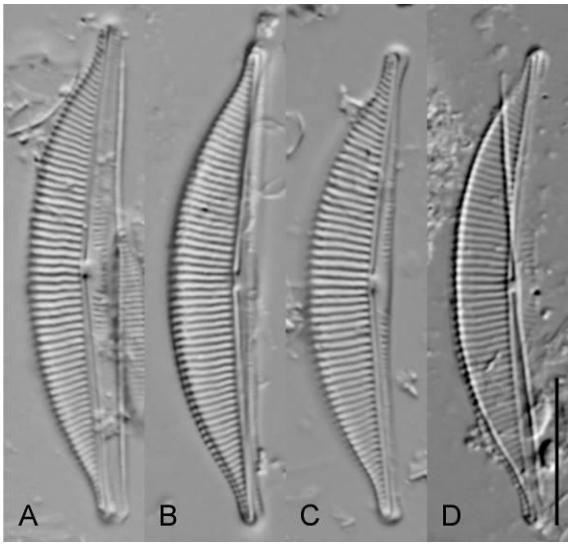

Figure 4.79. A–D. Light micrographs of *Halamphora coffeaeformis* Amph023 showing the observed size range. Scale bar = 10 µm.

In SEM, externally, the raphe branches are straight with proximal ends slightly inflated and deflected dorsally and distal ends hooked dorsally. The dorsal raphe ledge is moderately developed and expanded near the valve center. The dorsal striae are biseriate and separated by distinct virgae. A more or less developed marginal ridge is present. The ventral striae are fine and uniseriate. Internally, the striae are biseriate. The proximal raphe ends terminate in a prominent fused central helictoglossa.

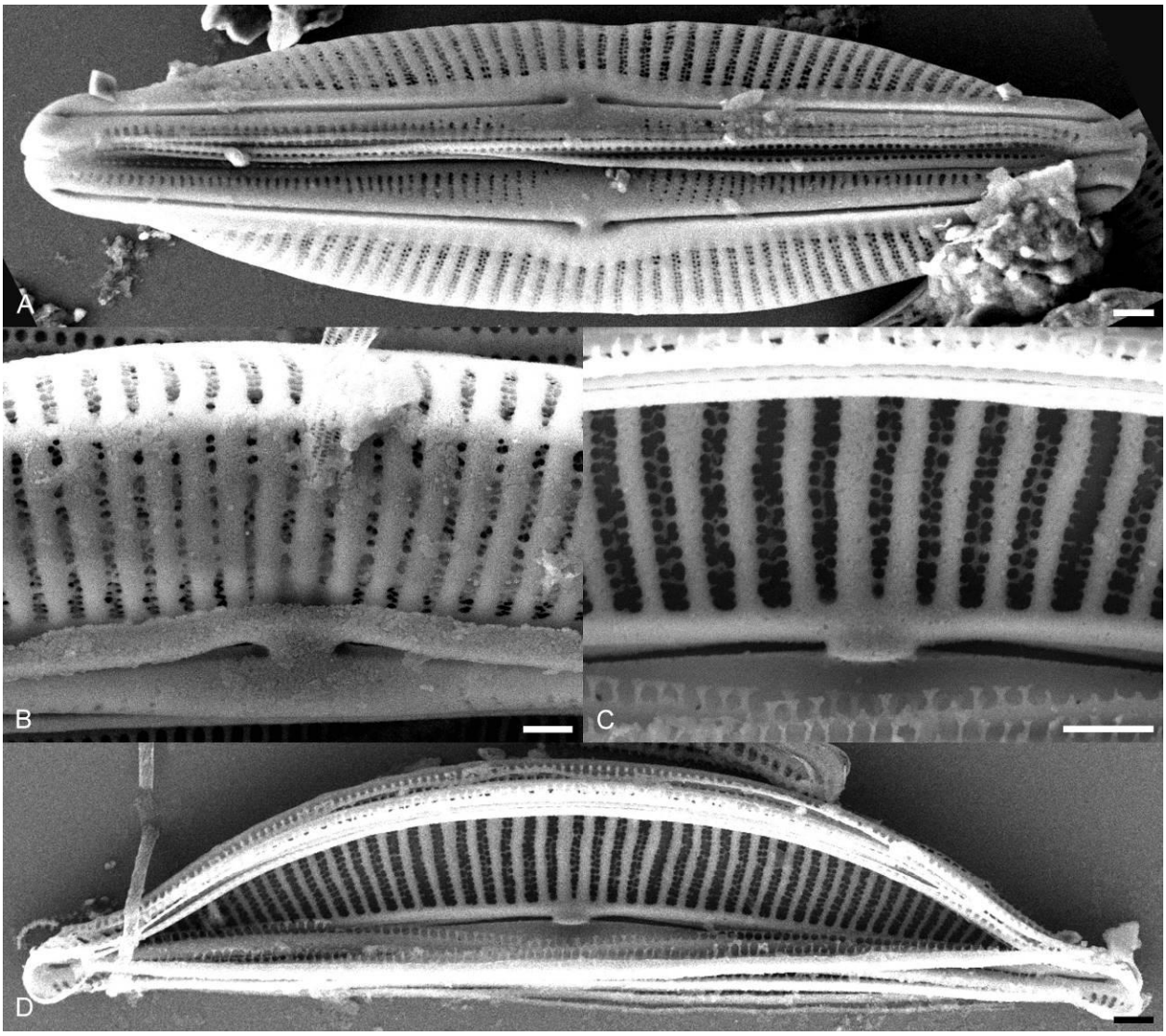

Figure 4.80. Scanning electron micrographs of *Halamphora coffeaeformis* Amph023. **A.** External whole frustule, valve view. **B.** Detail of external valve center. **C.** Detail internal valve center. **D.** Internal whole valve. Scale bars = 1 µm.

Halamphora coffeaeformis (Agardh) Levkov Amph101 (Figs 4.82, 4.83)

Valves are semi-elliptical with a smoothly arched dorsal margin and a straight to slightly concave ventral margin. Valve length 35.0–37.0 µm, valve breadth 5.5–6.0 µm. The valve ends are protracted and ventrally deflected. The raphe is slightly arched with straight raphe branches. Proximal raphe ends are straight, distal ends hook dorsally. The axial area is narrow dorsally, slightly expanded at the ventral valve center. Dorsal striae are uninterrupted and not obviously areolate, parallel near the valve center,

becoming radiate near the apices. The ventral striae are fine and can be difficult to image in the LM. Dorsal striae number 18–19 in 10 µm.

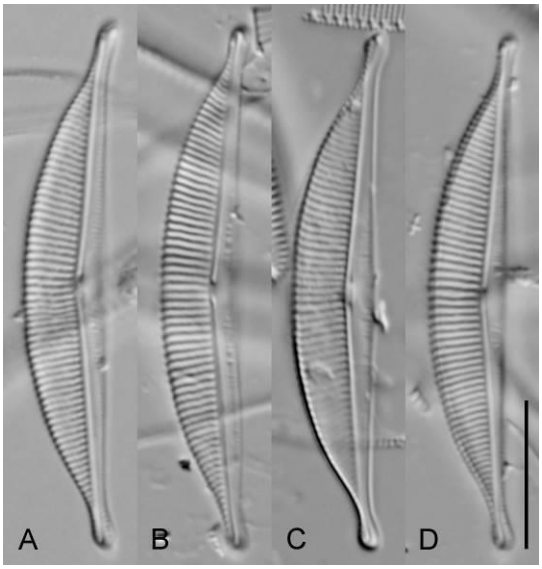

Figure 4.81. A–D. Light micrographs of *Halamphora coffeaeformis* Amph101 showing observed size range. Scale bar = 10 µm.

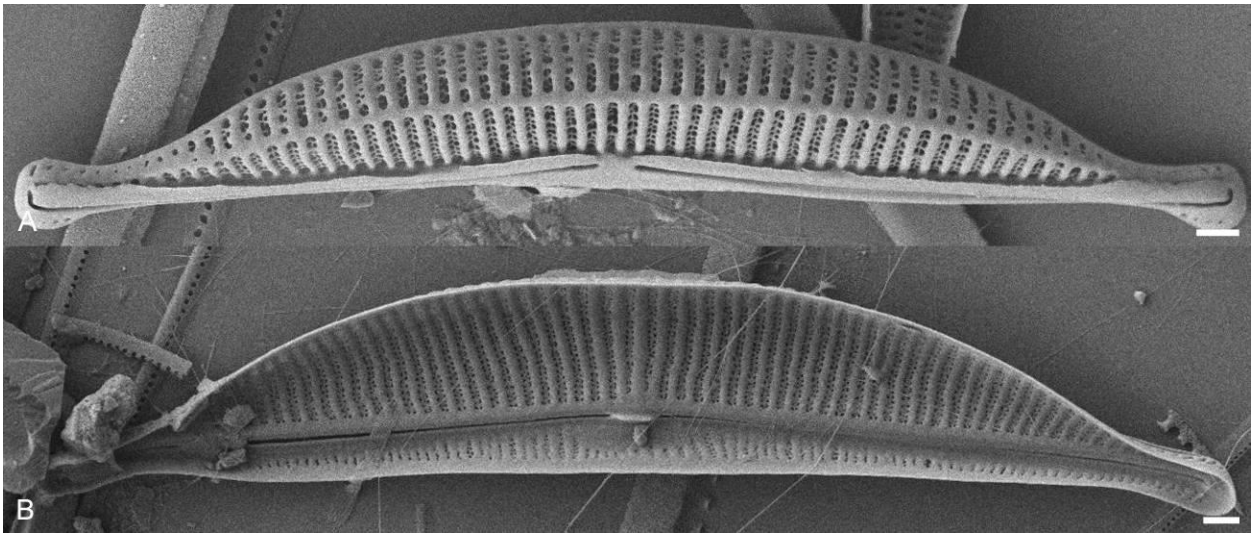

Figure 4.82. Scanning electron micrographs of *Halamphora coffeaeformis* Amph101. **A.** External whole valve. **B.** Internal whole valve. Scale bars = 1 µm.

In SEM, externally, the raphe branches are straight with proximal ends deflected dorsally and distal ends hooked dorsally. The dorsal raphe ledge is moderately developed. The dorsal striae are

biseriate and separated by distinct virgae. A well-developed marginal ridge is present. The ventral striae are fine and uniseriate. Internally, the striae are biseriate. The proximal raphe ends terminate in a prominent fused central helictoglossa.

Halamphora turgida (Gregory) Levkov Amph087 (Figs 4.84, 4.85)

Valves semi-elliptical with a smoothly rounded dorsal margin, becoming nearly parallel over the valve center, and a straight ventral margin. Valve length 40.0–53.0 µm, valve breadth 6.5–9.0 µm. Valve ends protracted, subcapitate and ventrally deflected. The raphe is weakly arched with straight raphe branches. The proximal raphe ends are straight, the ventral raphe branches are difficult to observe in the LM. The axial area is narrow throughout. Dorsal striae uninterrupted and without obvious punctation,

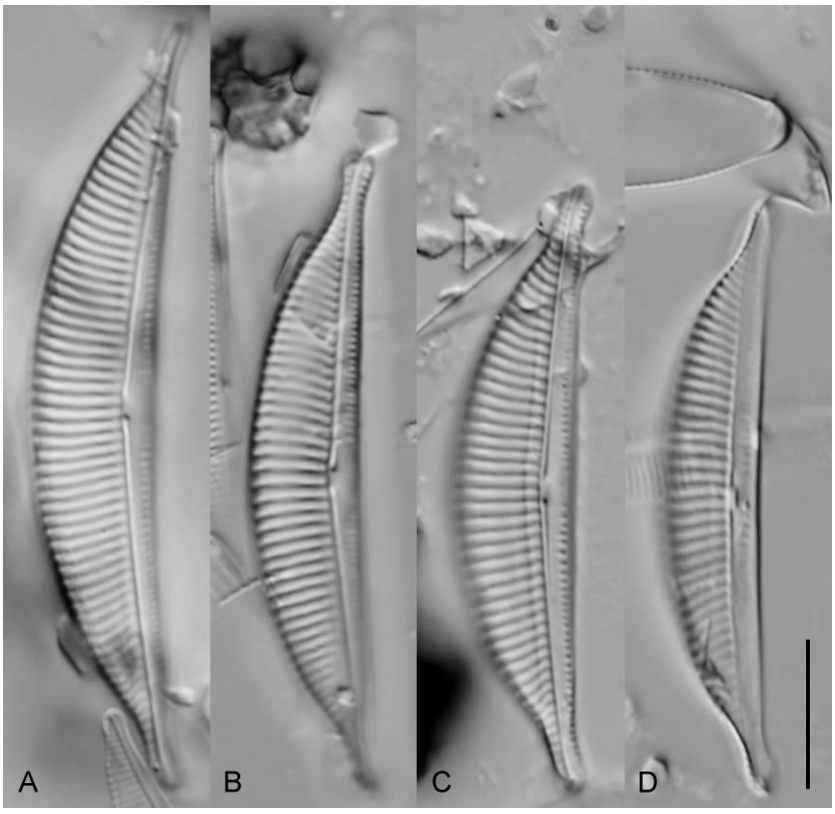

Figure 4.83. A–D. Light micrographs of *Halamphora turgida* Amph087 showing observed size range. Scale bar = 10 µm.

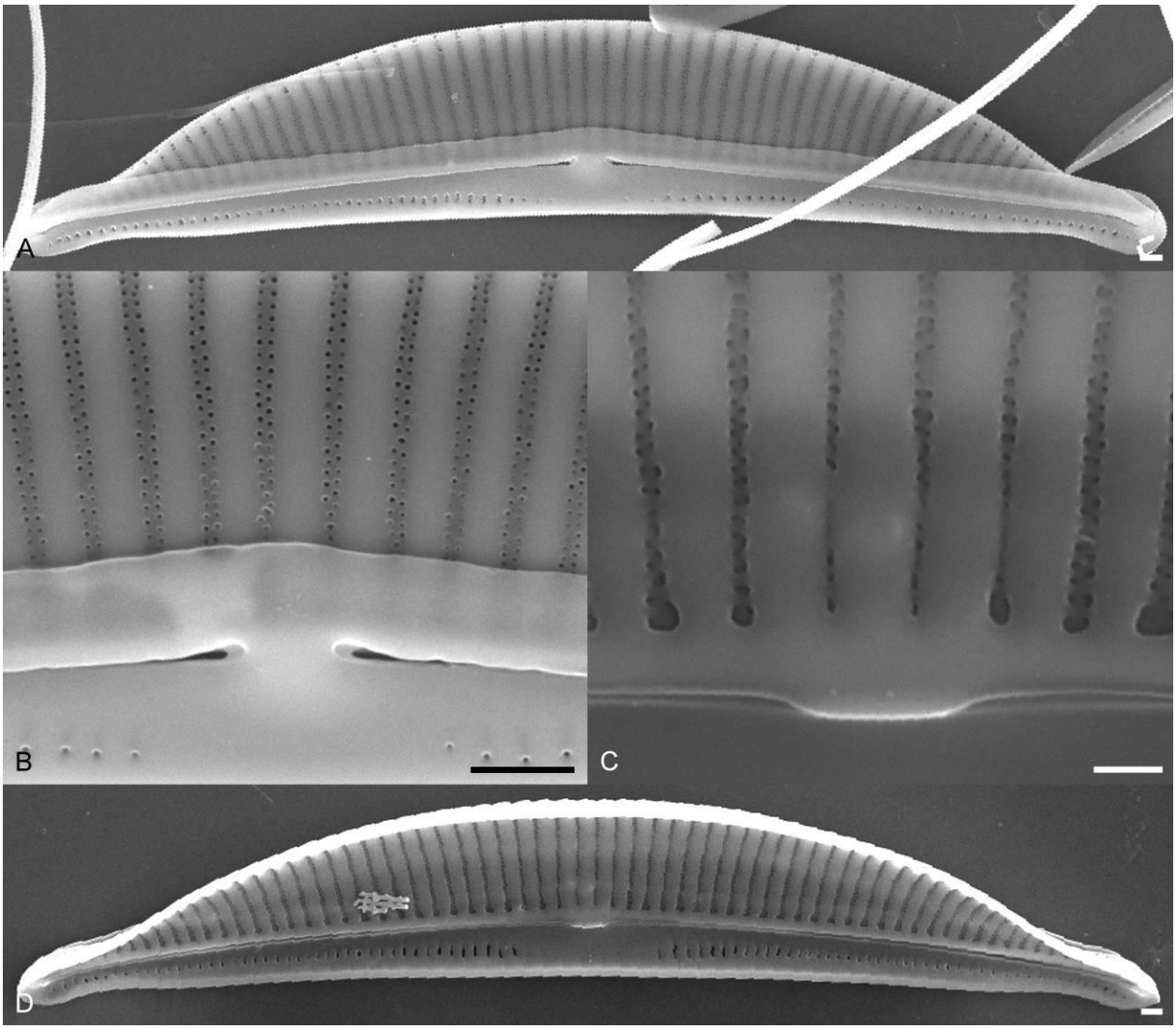

Figure 4.84. Scanning electron micrographs of *Halamphora turgida* Amph087. **A.** External whole valve. **B.** Detail of external valve center. **C.** Detail of internal valve center. **D.** Internal whole valve. Scale bars = 1 µm.

nearly parallel at the valve center radiate near the apices. Dorsal striae more widely spaced near the vale center, 10–11 striae in 10 µm. The ventral striae are fine, interrupted at the valve center, 18–21 in 10 µm.

In SEM, externally, valves semi-elliptical and heavily silicified. The raphe branches are straight with proximal raphe ends slightly dorsally deflected and distal ends hooked dorsally. The dorsal raphe ledge is robust and continuous across the valve. The dorsal striae are finely biseriate and separated by thick virgae. The dorsal striae are not continuous to the dorsal margin but are separated by a thin marginal ridge. The ventral striae are composed of small and finely biseriate. Internally, the raphe branches are

straight with proximal ends ending in a fused central helictoglossae and distally in a weakly developed helictoglossa. The dorsal striae are finely biseriate and are separated by thick virgae. The dorsal virgae are slightly thicker through the valve center. The ventral striae are thin and finely biseriate.

Halamphora cf. *turgida* (Gregory) Levkov Amph124 (Figs 4.86, 4.87)

Valves semi-elliptical with a smoothly rounded dorsal margin, becoming nearly parallel over the valve center, and a straight ventral margin. Valve length 39.0–48.0 µm, valve breadth 6.0–8.0 µm. Valve ends protracted, subcapitate and ventrally deflected. The raphe is weakly arched with straight raphe branches. The proximal raphe ends are straight, the ventral raphe branches are difficult to observe in the LM. The axial area is narrow throughout. Dorsal striae uninterrupted and without obvious punctation, nearly parallel near the valve center becoming radiate near the apices. Dorsal striae more widely spaced

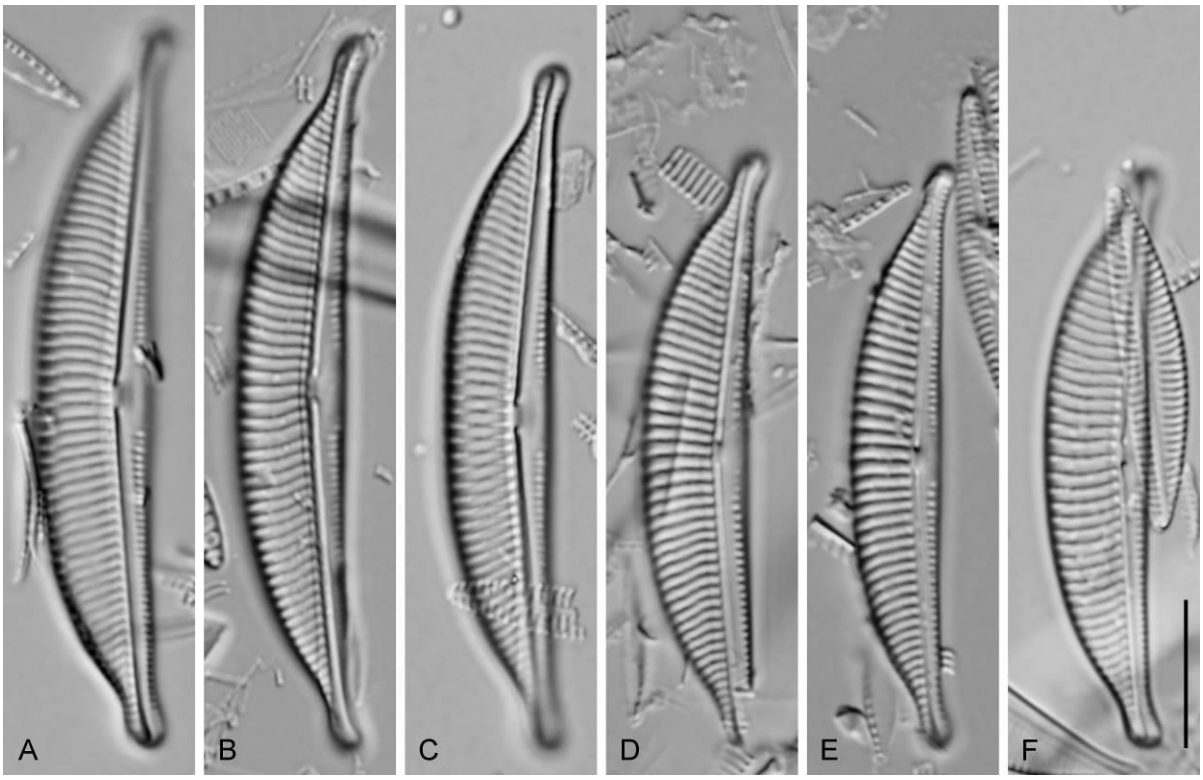

Figure 4.85. A–F. Light micrographs of *Halamphora* cf. *turgida* Amph122 showing the observed size range. Scale bar = 10 µm.

near the vale center, 10–11 striae in 10 µm, 14–15 striae in 10 µm near the apices. The ventral striae are fine, interrupted at the valve center, 18–21 in 10 µm.

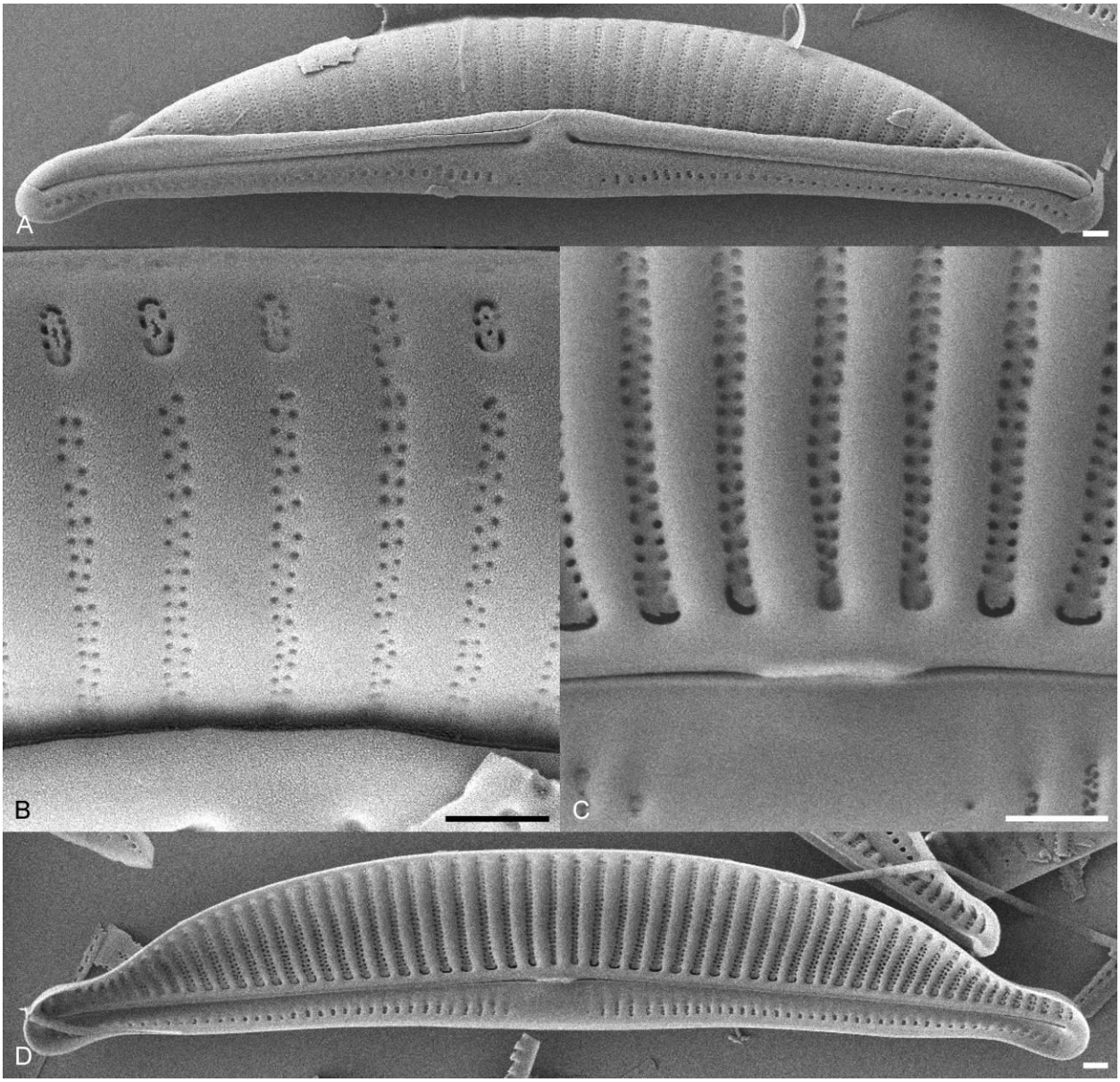

Figure 4.86. Scanning electron micrographs of *Halamphora* cf. *turgida* Amph122. **A.** External whole valve. **B.** Detail of external valve center. **C.** Detail of internal valve center. **D.** Internal whole valve. Scale bars = 1 µm.

In SEM, externally, valves semi-elliptical and heavily silicified. The raphe branches are straight with proximal raphe ends slightly dorsally deflected and distal ends hooked dorsally. The dorsal raphe ledge is robust and continuous across the valve. The dorsal striae are finely biseriate and separated by

thick virgae. The dorsal striae are not continuous to the dorsal margin but are separated by a thin marginal ridge. The ventral striae are composed of small and finely biseriate. Internally, the raphe branches are straight with proximal ends ending in a fused central helictoglossae and distally in a weakly developed helictoglossa. The dorsal striae are finely biseriate and are separated by thick virgae. The dorsal virgae are slightly thicker through the valve center. The ventral striae are thin and finely biseriate.

Halamphora turgida (Gregory) Levkov Amph192 (Figs 4.88, 4.89)

Valves semi-elliptical with a smoothly rounded dorsal margin, becoming nearly parallel over the valve center, and a straight ventral margin. Valve length 27.0–37.0 µm, valve breadth 6.5–7.5 µm. Valve ends protracted, subcapitate and ventrally deflected. The raphe is weakly arched with straight raphe branches. The proximal raphe ends are straight, the ventral raphe branches are difficult to observe in the LM. The axial area is narrow throughout. Dorsal striae uninterrupted and without obvious punctation, nearly parallel at the valve center radiate near the apices. Dorsal striae more widely spaced near the vale center11 striae in 10 µm The ventral striae are fine, interrupted at the valve center, 18–21 in 10 µm.

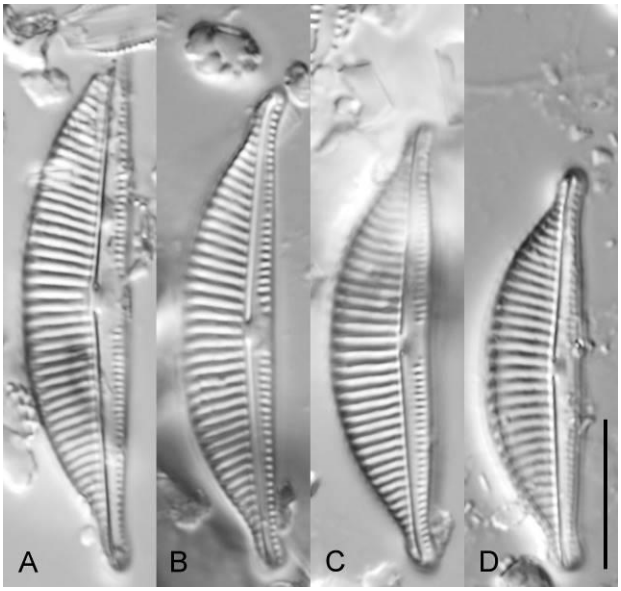

Figure 4.87. A–D. Light micrographs of *Halamphora* cf. *turgida* Amph192 showing observed size range. Scale bar = 10 µm.

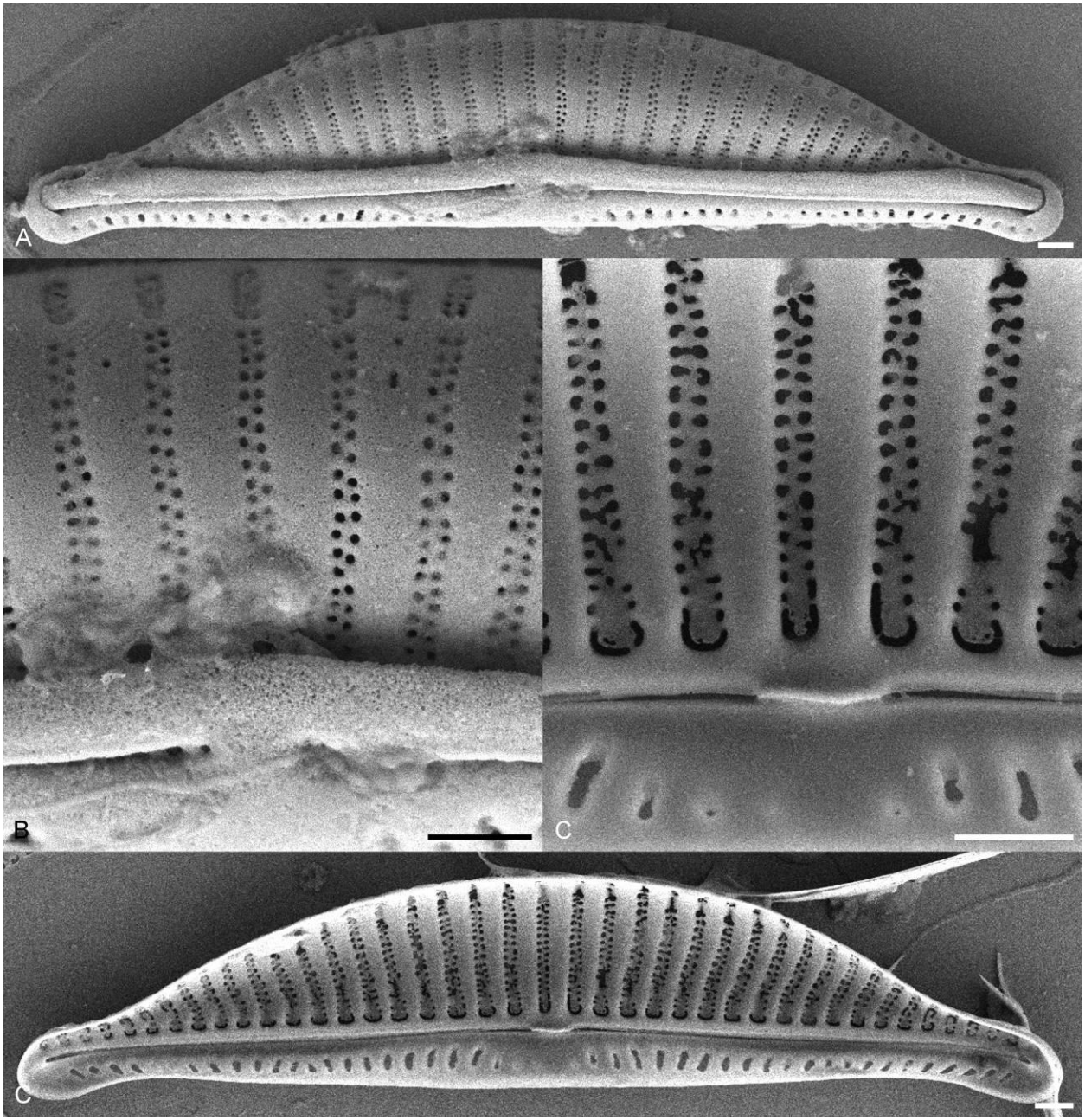

Figure 4.88. Scanning electron micrographs of *Halamphora* cf. *turgida* Amph192. **A.** External whole valve. **B.** Detail of external valve center. **C.** Detail of internal valve center. **D.** Internal whole valve. Scale bars = 1 µm.

In SEM, externally, valves semi-elliptical and heavily silicified. The raphe branches are straight with proximal raphe ends slightly dorsally deflected and distal ends hooked dorsally. The dorsal raphe ledge is robust and continuous across the valve. The dorsal striae are finely biseriate and separated by thick virgae. The dorsal striae are not continuous to the dorsal margin but are separated by a thin marginal

ridge. The ventral striae are composed of small and finely biseriate. Internally, the raphe branches are straight with proximal ends ending in a fused central helictoglossae and distally in a weakly developed helictoglossa. The dorsal striae are finely biseriate and are separated by thick virgae. The dorsal virgae are slightly thicker through the valve center. The ventral striae are thin and finely biseriate.

HALAMPHORA CLADE D

Halamphora sp. nov. Amph034 (Figs 4.90, 4.91)

Valves narrowly semi-elliptical and strongly dorsiventral. The dorsal margin is smoothly arched to slightly concave at the valve center in larger specimens. The ventral margin is straight. The valve ends are protracted, subcapitate and ventrally deflected. Valve length 13.0–19.0 µm, valve breadth 2.5–3.0 µm. The raphe is straight, positioned very near the ventral margin, with straight proximal raphe ends. The axial area is narrow throughout. The dorsal striae are very fine, appearing slightly more widely spaced at the valve center and parallel throughout. The ventral striae are difficult to resolve in the LM. Striae number 31–32 in 10 µm.

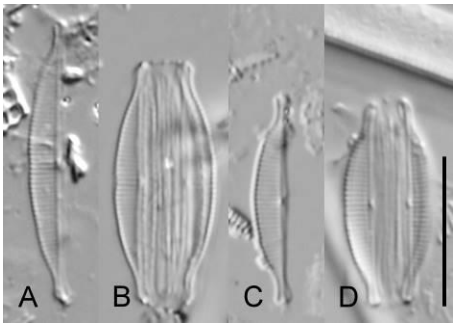

Figure 4.89. A–D. Light micrographs of *Halamphora sp. nov.* Amph034 showing the observed size range. Scale bar = 10 µm.

In SEM, externally, the raphe is straight with nearly straight to dorsally deflected proximal ends and dorsally deflected distal ends. The raphe ledge is moderately developed and continuous across the length of the valve. A marginal ridge is weakly developed and more or less visible along the length of the valve margin. The dorsal striae are biseriate and separated by thin virgae. The ventral striae are fine and

uniseriate. Internally the proximal raphe ends terminate in a weakly developed central helictoglossa. The internal striae are biseriate.

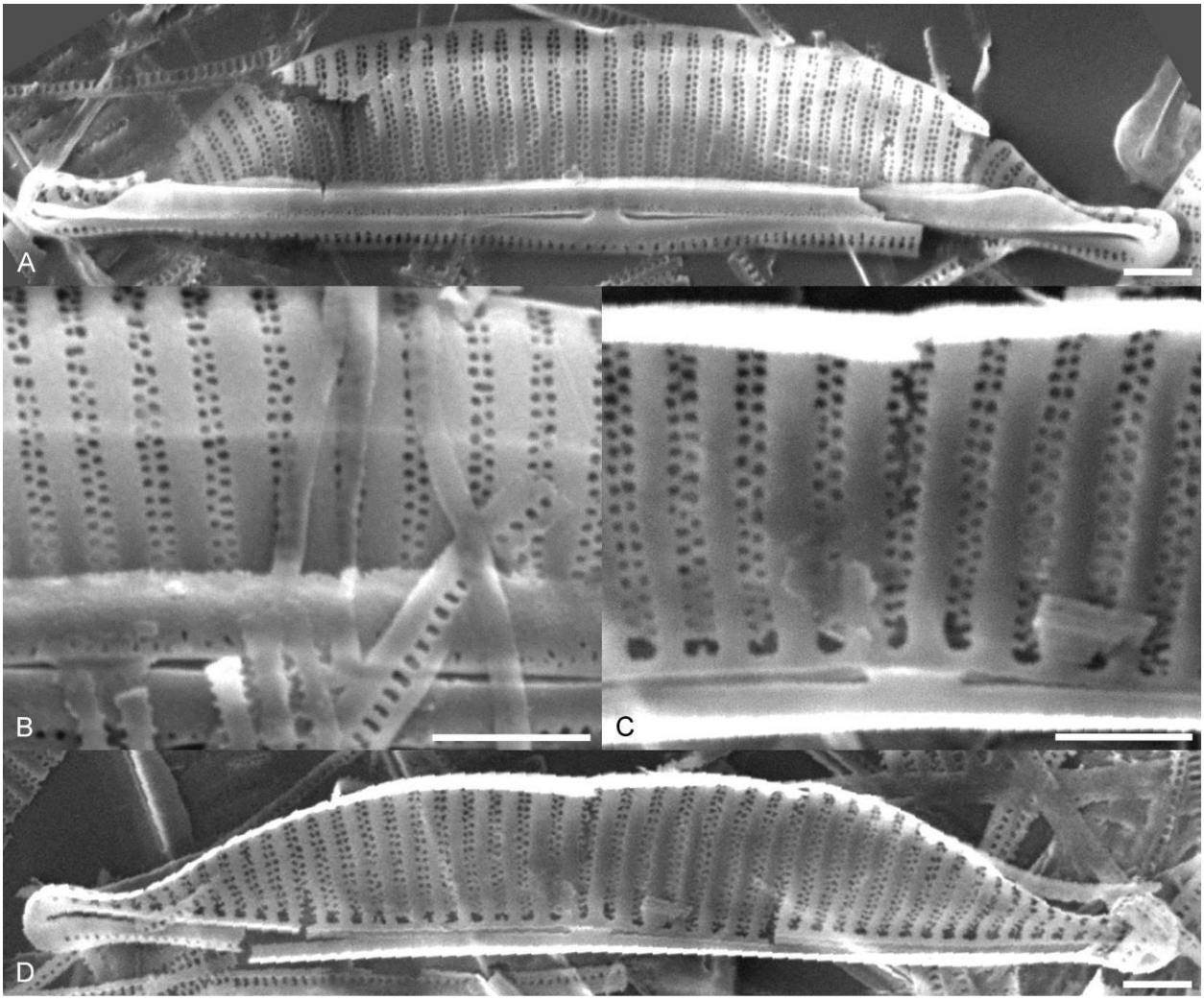

Figure 4.90. Scanning electron micrographs of *Halamphora sp. nov.* Amph034. **A.** External whole valve. **B.** Detail of external valve center. **C.** Detail of internal valve center. **D.** Internal whole valve. Scale bars = 1 µm.

Halamphora taylori (Grunow in Van Heurck) Stepanek & Kociolek comb. nov. Amph119 (Figs 4.92, 4.93)

Valves semi-elliptical and strongly dorsiventral with a smoothly arched dorsal margin and a straight ventral margin. The valve ends are protracted subcapitate to capitate. Valve length 22.0–30.0 µm, valve breadth 4.0–5.0 µm. The raphe is straight with straight proximal raphe ends. The axial area is

narrow throughout. The dorsal striae are fine, not visibly areolate and parallel throughout. The ventral striae are difficult to image in the LM. Striae number 22–23 in 10 µm.

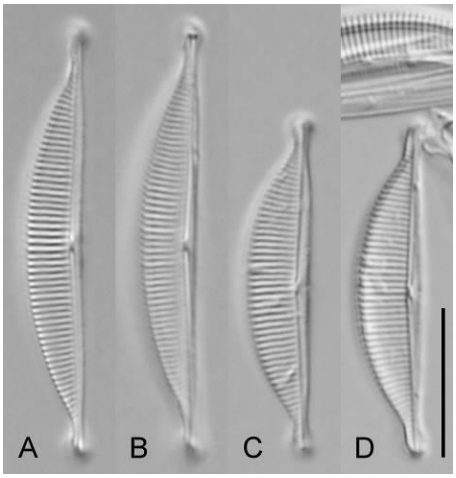

Figure 4.91. A–D. Light micrographs of *Halamphora taylori* Amph119 showing observed size range. Scale bar = 10 µm.

In SEM, externally, the raphe is straight with dorsally deflected proximal raphe ends and dorsally hooked distal ends. The dorsal raphe ledge is well developed and continuous along the length of the valve. The marginal ridge is absent. The dorsal striae are biseriate and separated by thin virgae. The ventral striae are fine, uniseriate and uninterrupted through the valve center. Internally, the proximal raphe ends terminate in a well-developed central helictoglossa. The internal striae are biseriate.

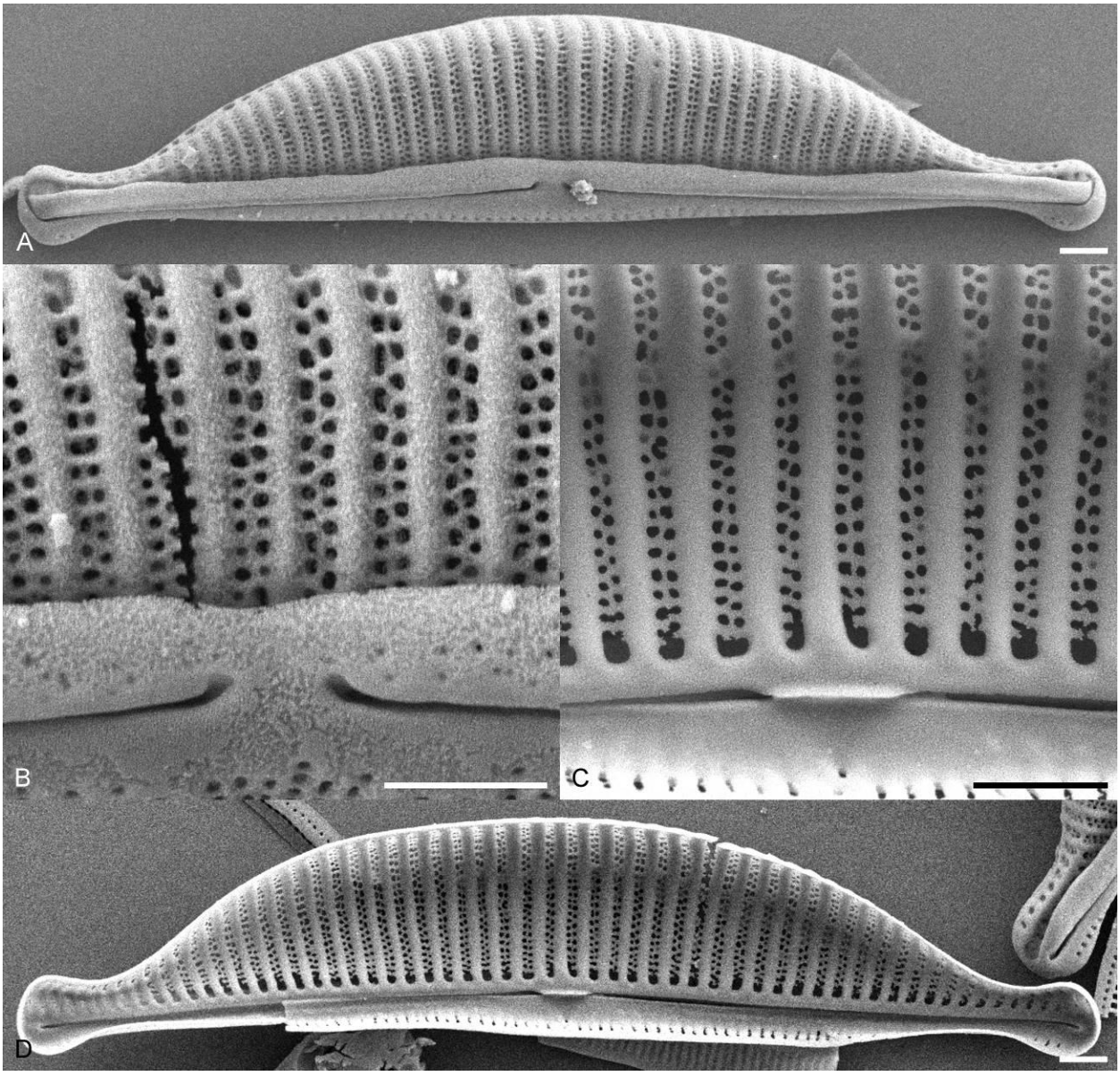

Figure 4.92. Scanning electron micrographs of *Halamphora taylori* Amph119. **A.** External whole valve. **B.** Detail of external valve center. **C.** Detail of internal valve center. **D.** Internal whole valve. Scale bars = 10 µm.

Halamphora acutiuscula (Kützing) Levkov Amph042 (Figs 4.94, 4.95)

Valves are semi-elliptical and strongly dorsiventral. The dorsal margin is smoothly rounded, the ventral margin is straight. The valve ends are protracted, subcapitate to capitate. Valve length 23.0–30.0 µm, valve breadth 4.5–5.0 µm. The raphe is slightly arched with straight raphe branches. The proximal raphe ends are slightly dorsally deflected. The axial are is narrow throughout. A longitudinal line is often

seen running along the dorsal axial area. The dorsal striae are not areolate, nearly parallel at the valve center, becoming radiate near the apices. The ventral striae are fine and are continuous across the central area. Striae number 17–19 in 10 µm.

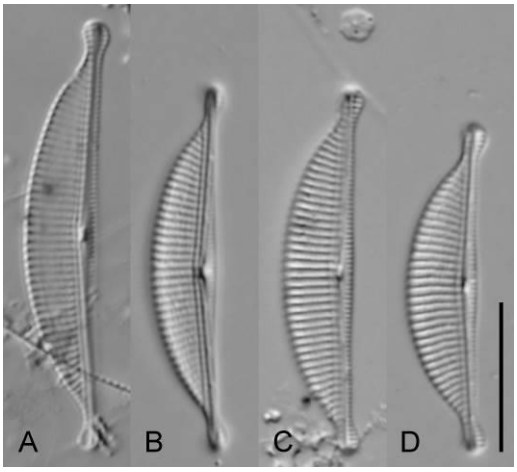

Figure 4.93. A–D. Light micrographs of *Halamphora acutiuscula* Amph042 showing observed size range. Scale bar = 10 µm.

In SEM, externally, the proximal and distal raphe ends deflect dorsally. The dorsal raphe ledge is moderately developed and continuous across the length of the valve. A marginal ridge is weakly developed and more or less visible along the dorsal margin. The dorsal striae are coarsely biseriate, separated by fine virgae. The ventral striae are fine and uniseriate. Internally, the proximal raphe ends terminate in a well-developed fused central helictoglossa. A longitudinal band of silica runs the length of the dorsal axial area. The internal dorsal striae are biseriate.

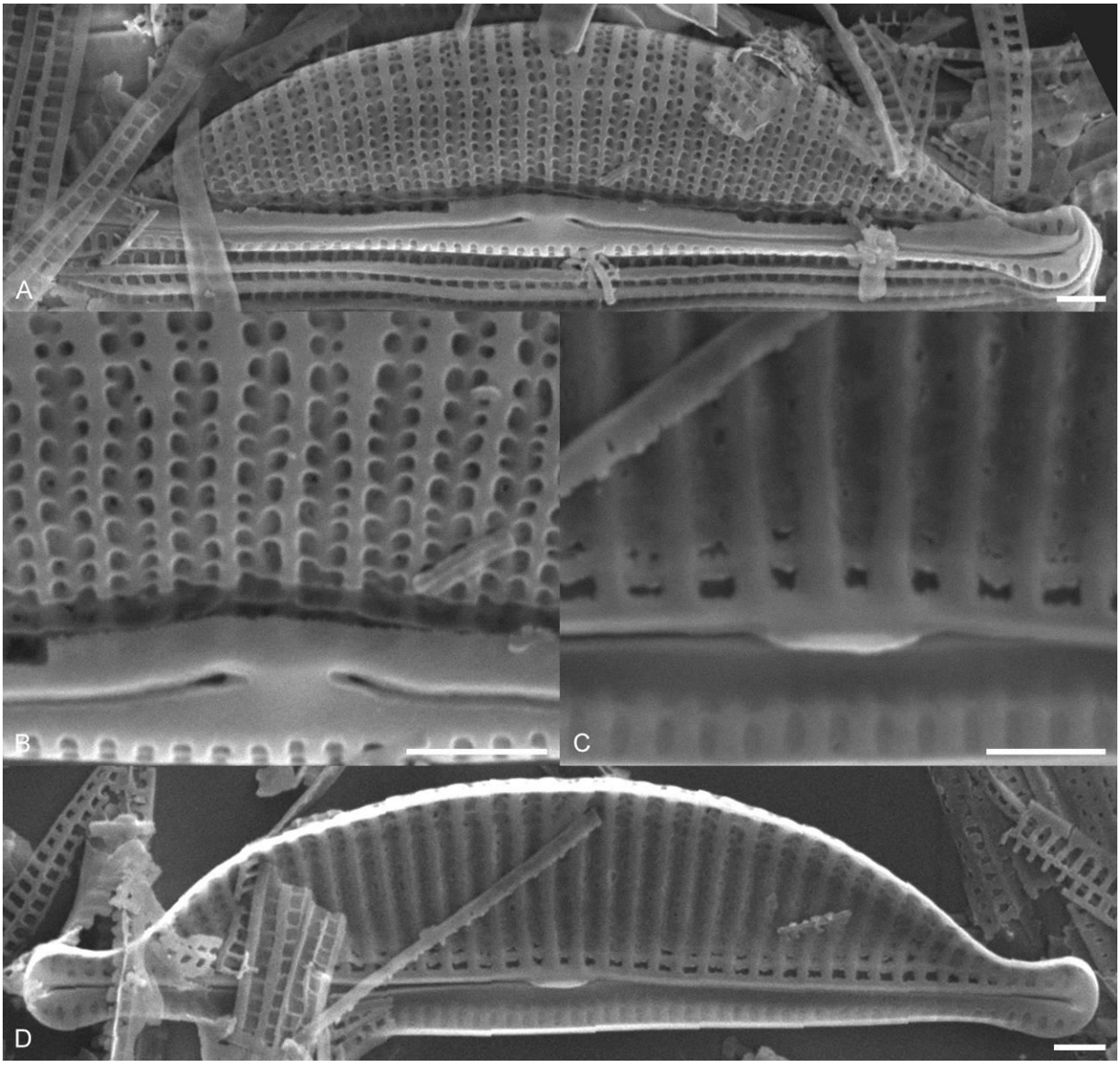

Figure 4.94. Scanning electron micrographs of *Halamphora acutiuscula* Amph042. **A.** External whole valve. **B.** Detail of external whole valve. **C.** Detail of internal whole valve. **D.** Internal whole valve. Scale bar = 1 µm.

Halamphora aponina (Kützing) Levkov Amph049 (Figs 4.96, 4.97)

Valves are narrowly semi-elliptical and strongly dorsiventral. The dorsal margin is arched near the apices, nearly flat over the valve center in some specimens. The ventral margin is straight. The valve ends are protracted, subcapitate and slightly ventrally deflected. Valve length 23.0–30.0 µm, valve breadth 3.0–3.5 µm. The raphe is slightly arched with straight raphe branches. The proximal raphe ends

are straight. The axial area is narrow throughout. The dorsal striae are fine and not areolate, parallel through most of the valve, becoming slightly radiate near the apices. The ventral striae are difficult to observe in the LM. Striae number 21–22 in 10 µm.

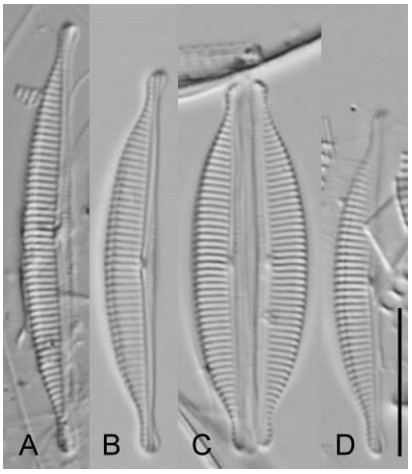

Figure 4.95. A–D. Light micrographs of *Halamphora aponina* Amph049 showing the observed size range. Scale bar = 10 µm.

In SEM, externally, the proximal raphe ends are slightly dorsally deflected and the distal ends are bent dorsally. The dorsal raphe ledge s moderately developed and continuous across the length of the valve. A continuous dorsal marginal ridge runs the length of the valve. The dorsal striae are biseriate and separated by thin virgae. The ventral striae are fine and uniseriate. Internally, the proximal raphe ends terminate in a fused central helictoglossa. The dorsal striae are finely biseriate.

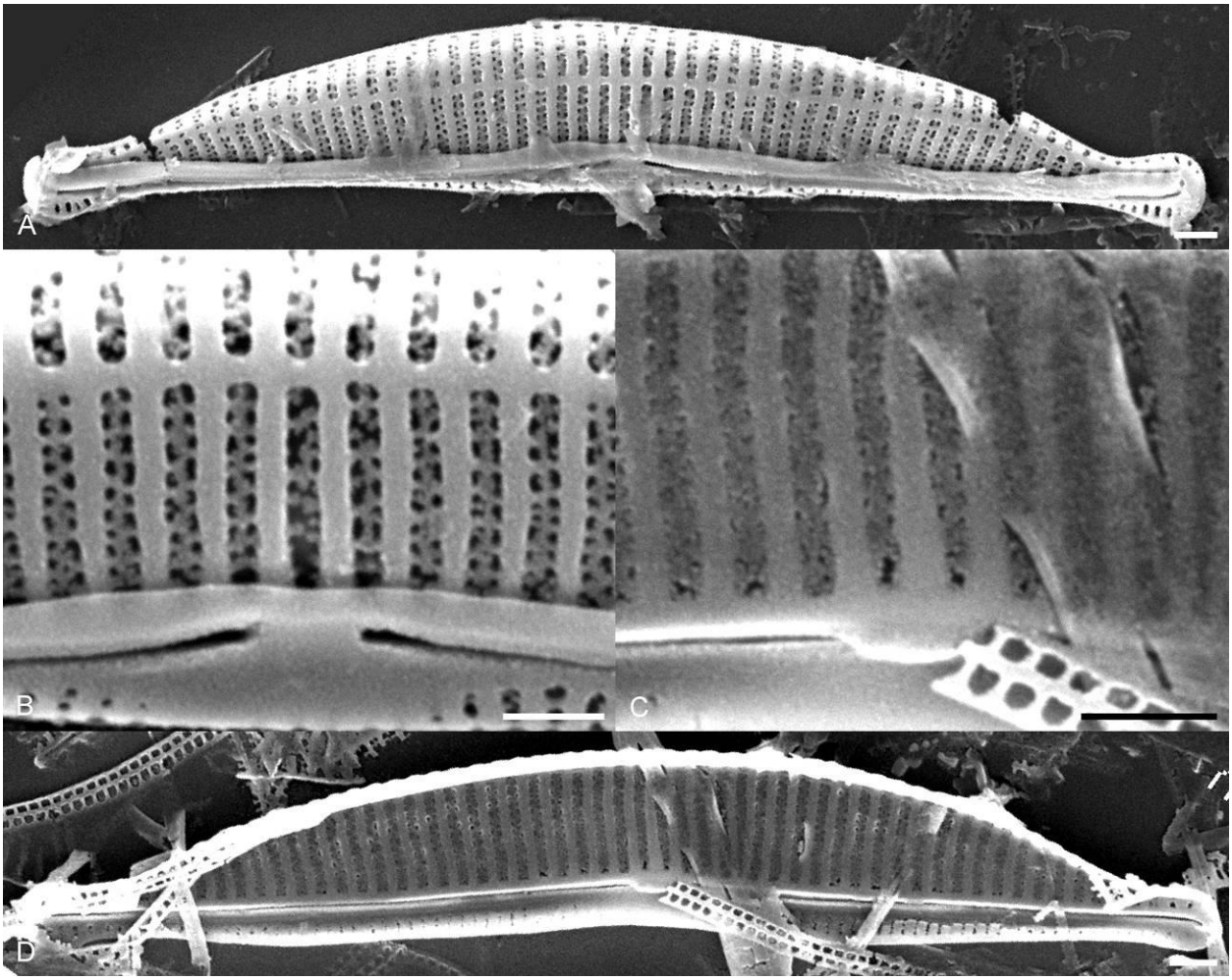

Figure 4.96. Scanning electron micrographs of *Halamphora aponina* Amph049. **A.** External whole valve. **B.** Detail of external valve center. **C.** Detail of internal valve center. **D.** Internal whole valve. Scale bar = 1 µm.

Halamphora aponina (Kützing) Levkov Amph102 (Figs 4.98, 4.99)

Valves narrowly semi-elliptical and strongly dorsiventral. The dorsal margin is smoothly arched becoming somewhat flat over the valve center in some specimens. The ventral margin is straight to slightly concave. The valve ends are protracted, subcapitate and slightly ventrally deflected. Valve length 23.0–31.0 µm, valve breadth 3.5–4.0 µm. The raphe is arched with straight raphe branches. The proximal raphe ends are straight. The axial area is narrow throughout. The dorsal striae are fine, not areolate, parallel through the valve center, becoming slightly radiate near the apices. The ventral striae are difficult to observe in the LM. Striae number 20–21 in 10 µm.

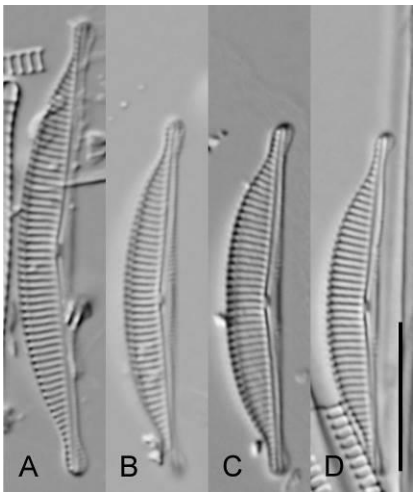

Figure 4.97. A–D. Light micrographs of *Halamphora aponina* Amph102 showing observed size range. Scale bar = 10 µm.

In SEM, externally, the raphe is straight with proximal ends gently curved dorsally and distal ends nearly straight. The dorsal raphe ledge is moderately developed and continuous across the length of the valve. A thin marginal ridge is present and runs the length of the valve. The dorsal striae are finely biseriate and separated by thin virgae. The ventral striae are composed of a single row of small areolae. Internally, the proximal raphe ends terminate in a weakly developed central helictoglossa. The internal dorsal striae are biseriate.

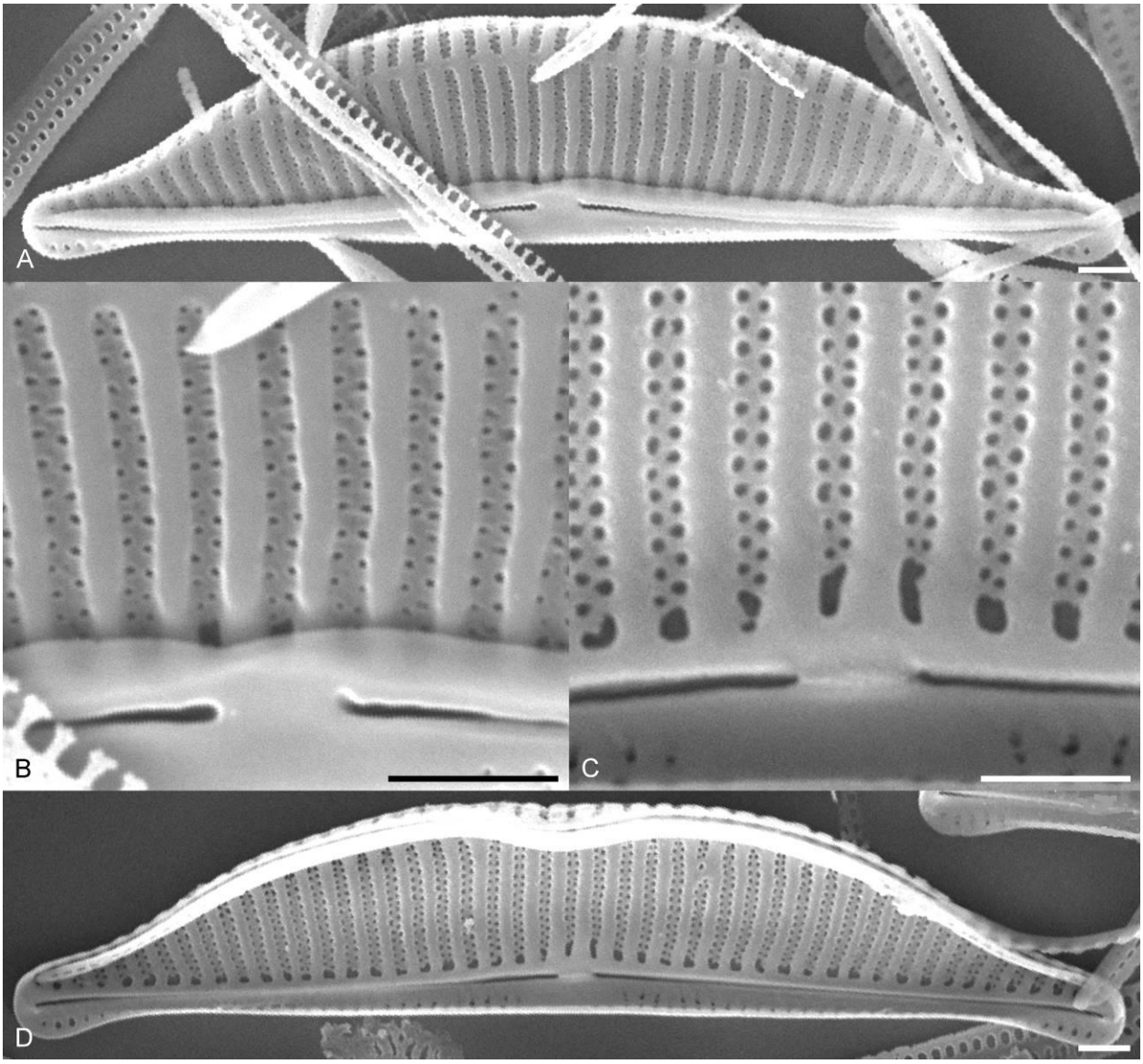

Figure 4.98. Scanning electron micrographs of *Halamphora aponina* Amph102. **A.** External whole valve. **B.** Detail of external valve center. **C.** Detail of internal valve center. **D.** Internal whole valve. Scale bar = 10 µm.

Halamphora sp. nov. Amph018

Valves are small, semi-elliptical and strongly dorsiventral. The dorsal margin is smoothly arched, the ventral margin is slightly concave. The valve ends are slightly protracted and narrowly rounded. Valve length 10–13 µm, valve breadth 2.5–3.5 µm. The raphe is arched with straight raphe branches. The proximal raphe ends are straight. The axial area is narrow throughout. The dorsal striae are fine, not

areolate, parallel at the valve center, becoming radiate near the apices. The ventral striae are difficult to see in the LM. Striae number 27–28 in 10 µm.

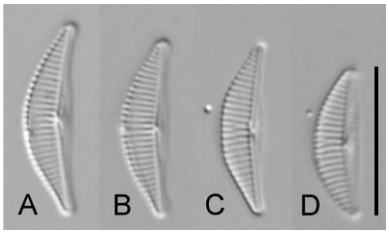

Figure 4.99. A–D. Light micrographs of *Halamphora sp. nov.* Amph018 showing observed size range. Scale bar = 10 µm.

HALAMPHORA CLADE E

Halamphora borealis (Kützing) Levkov Amph077/079 (Figs 4.101, 4.102)

Valves narrowly semi-elliptical and strongly dorsiventral. The dorsal margin is arched, somewhat flattened over the central portion of the valve, the ventral margin is straight. The valve ends are narrowly rounded. Valve length 16–27 µm, valve breadth 3.0–4.0 µm. The raphe is slightly arched with straight raphe branches. The proximal raphe ends are slightly dilated and straight. The axial area is narrow throughout. The dorsal striae are composed of several rows of elongate areolae, parallel near the valve center becoming radiate near the apices. The ventral striae are difficult to resolve in the LM. Dorsal striae 19–22 in 10.

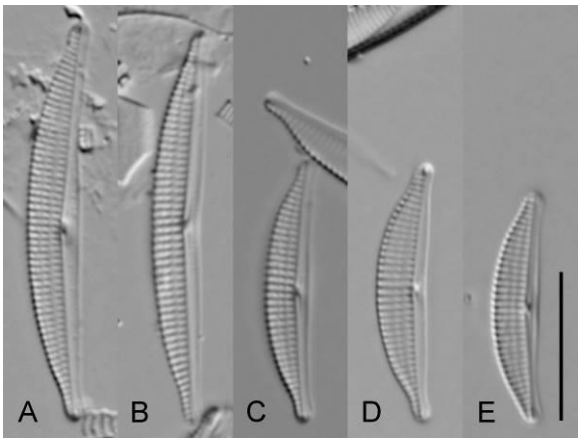

Figure 4.100. A–E. Light micrographs of *Halamphora borealis* Amph077/079. Scale bar = 10 µm.

In SEM, externally, the raphe branches are straight with slightly deflected proximal ends and dorsally deflected distal raphe ends. The dorsal raphe ledge is narrow and continuous along the length of the valve. The dorsal striae are composed of several rows of elongate areolae. The ventral striae are fine and composed of a single row of narrow elongate areolae. The ventral striae are not continuous through the valve center. Internally, the proximal raphe ends terminate in a central helictoglossa. The dorsal areolae are organized into distinct longitudinal rows.

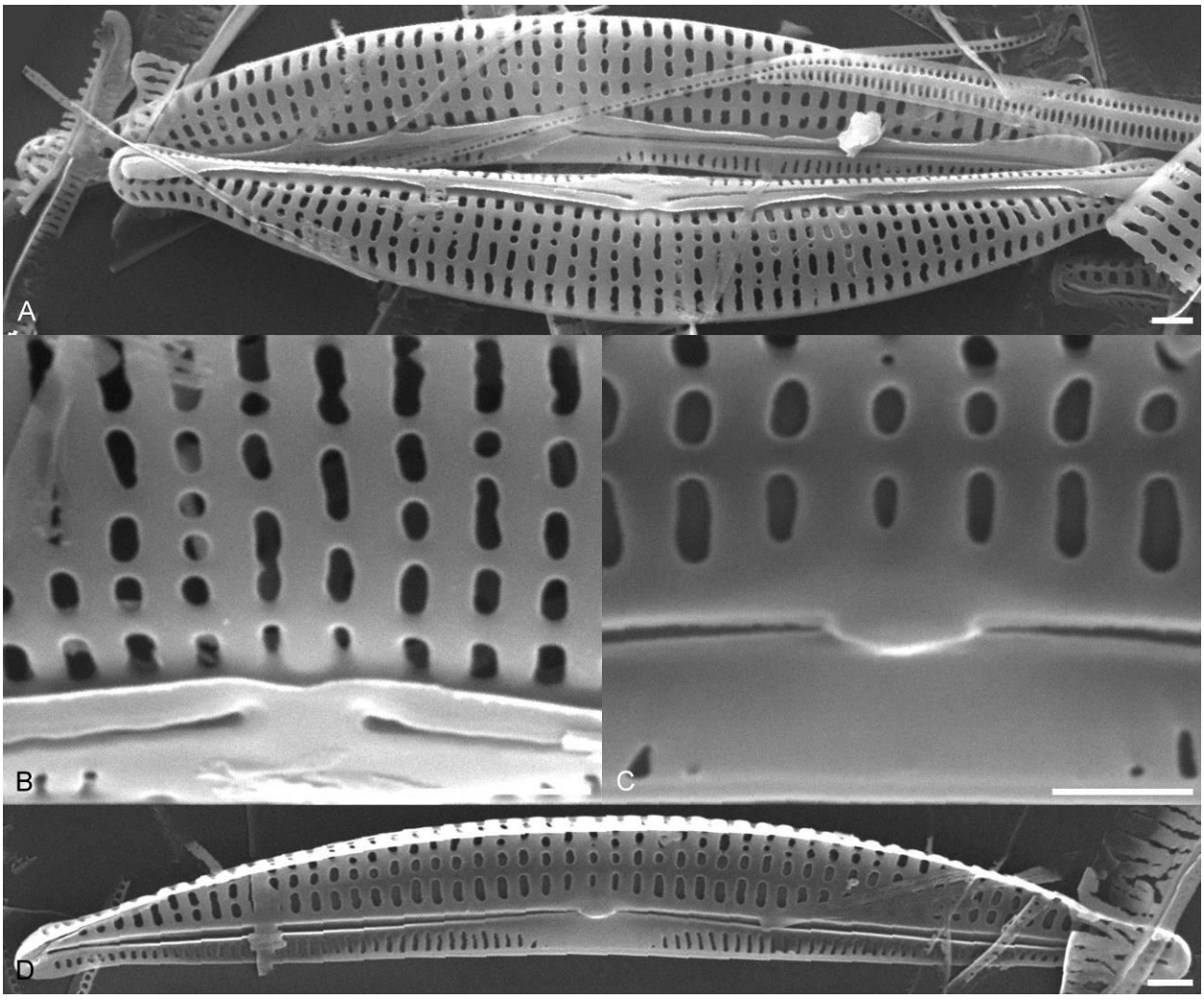

Figure 4.101. Scanning electron micrographs of *Halamphora borealis* Amph077/079. **A.** External whole valve. **B.** Detail of external valve center. **C.** Detail of internal valve center. **D.** Internal whole valve. Scale bars = 1 µm.

Halamphora sp. nov. Amph185 (Figs 4.103, 4.104)

Description: Valves are semi-elliptical and moderately dorsiventral. The dorsal margin is arched, somewhat flattened over the valve center. The ventral margin is more or less straight. The ventral valve is broad. The valve ends are weakly protracted, rounded and ventrally deflected. Valve length 29.0–33.0 µm, valve breadth 4.5–5.0 µm. The axial area is narrow on the dorsal side, difficult to differentiate along the ventral side. The raphe is slightly arched with dorsally deflected proximal ends. The dorsal side are finely areolate, parallel through the valve center becoming radiate near the apices. The ventral striae are difficult to resolve in the LM. Striae number 21–22 in 10 µm.

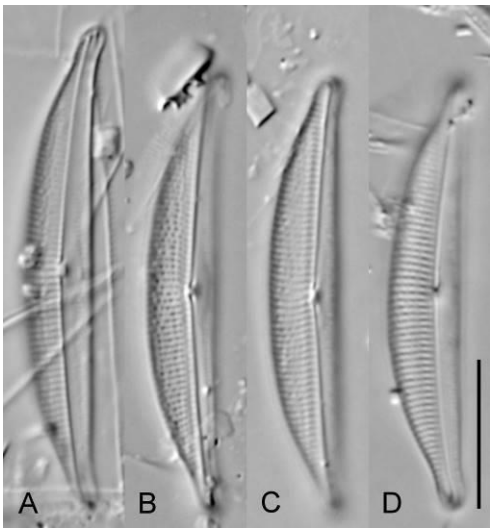

Figure 4.102. A–D. Light micrographs of *Halamphora sp. nov.* Amph185 showing observed size range. Scale bar = 10 µm.

In SEM, externally, the raphe branches are straight with dorsally deflected proximal ends and dorsally hooked distal ends. The dorsal raphe edge is broad and continuous along the length of the valve. A dorsal marginal ridge is absent. The dorsal striae are composed of many small round to ovoid areolae. The ventral axial area is expanded at the valve center. The ventral striae are fine and finely areolate. Internally, the proximal raphe ends terminate in a small fused central helictoglossa. The dorsal striae begin finely biseriate near the axial are transitioning to small elongate areolae for the remainder of the dorsal valve. The ventral valve is broad. The ventral striae are fine and finely areolate.

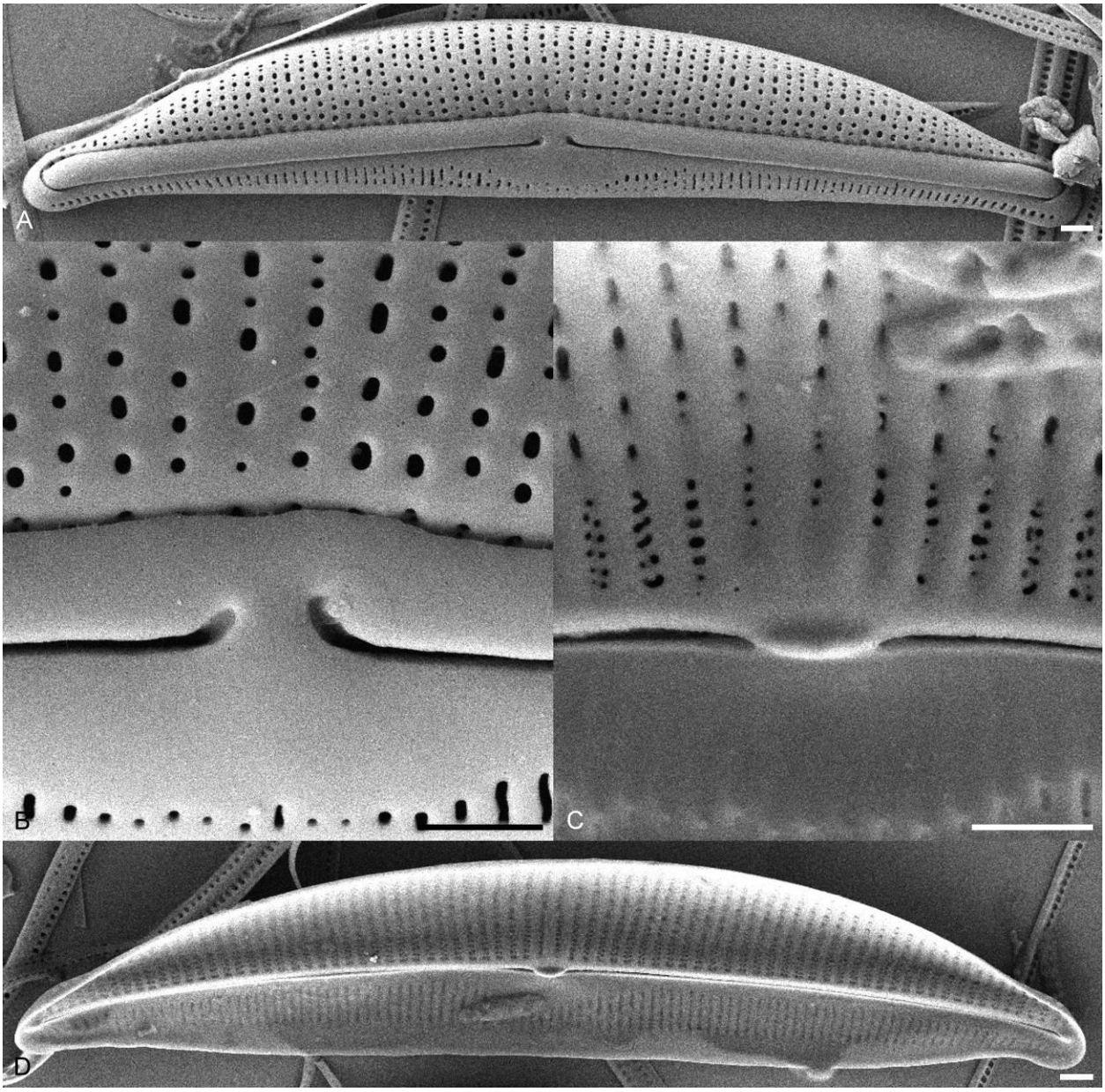

Figure 4.103. Scanning electron micrographs of *Halamphora sp. nov.* Amph185. **A.** External whole valve/ **B.** Detail of external valve center. **C.** Detail of internal valve center. **D.** Internal whole valve. Scale bars = 1 µm.

Halamphora adumbrata (Hohn & Hellerman) Stepanek & Kociolek comb. nov. Amph041 (Figs 4.105, 4.106)

Valves are narrowly semi-lanceolate and strongly dorsiventral. The dorsal margin is arched, the ventral margin is straight. Valve ends are narrowly rounded to weakly subcapitate in larger specimens.

Valve length 10.0–18.0 µm, valve breadth 1.5–2.5 µm. The raphe is straight with straight proximal raphe ends. The axial area is not easily distinguished. The striae are not easily resolved in the LM.

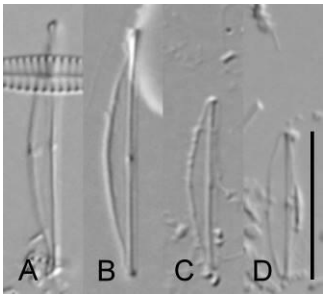

Figure 4.104. A–D. Light micrographs of *Halamphora adumbrata* Amph041 showing observed size range. Scale bar = 10 µm.

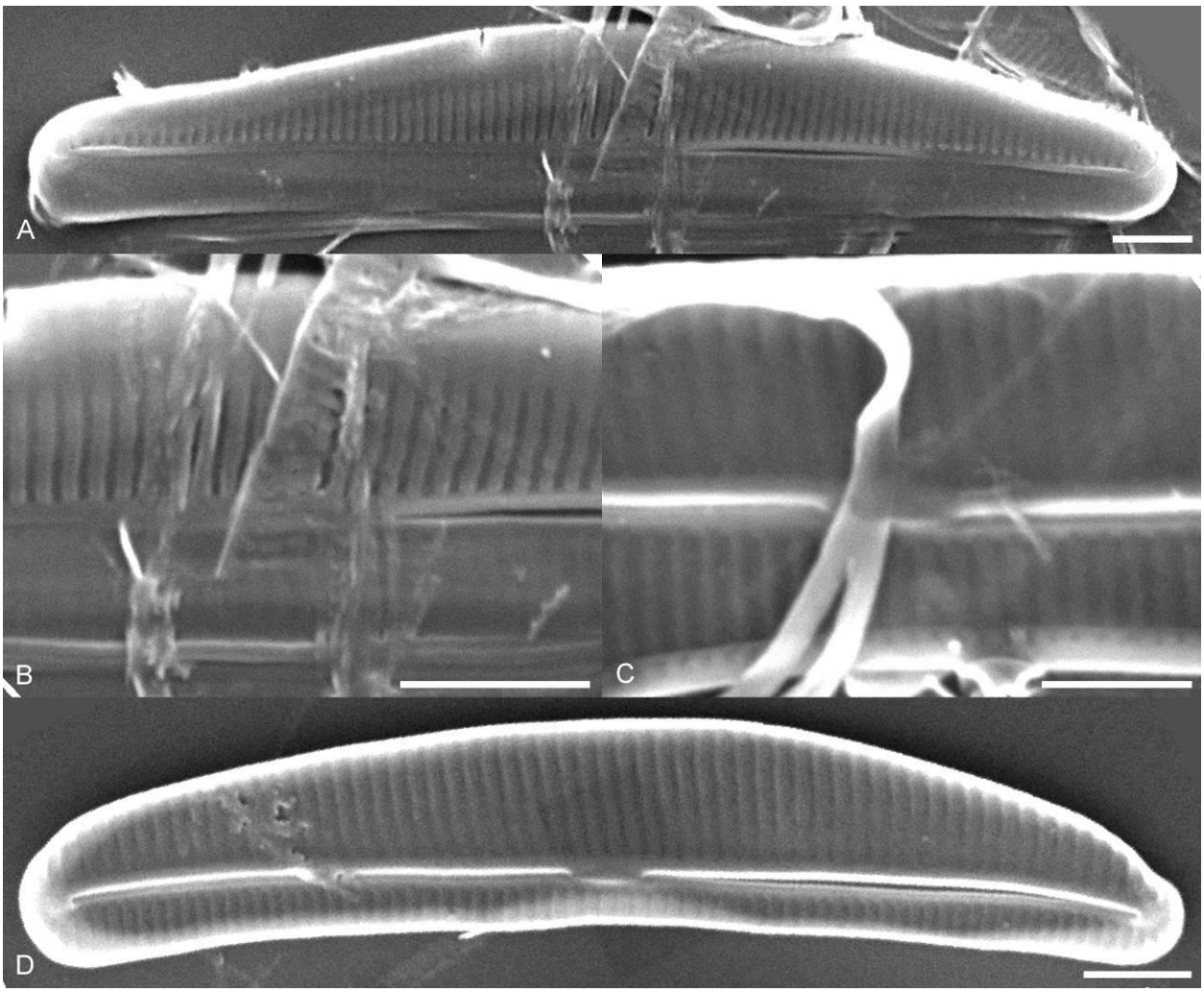

Figure 4.105. Scanning electron micrographs of *Halamphora adumbrata* Amph041. **A.** External whole valve. **B.** Detail of external valve center. **C.** Detail of internal valve center. **D.** Internal whole valve. Scale bars = 1 µm.

In SEM, externally, the raphe is straight with straight proximal raphe ends that terminate widely. The distal raphe ends are deflected dorsally. The dorsal raphe ledge is nearly absent, especially through the valve center. A thin dorsal marginal ridge is present. The dorsal and ventral striae are composed of a single row of thin interrupted areolae. The ventral striae are continuous through the valve center. Internally, the proximal raphe ends terminate in a broad fused central helictoglossa.

Halamphora sp. nov. Amph134 (Figs 4.107, 4.108)

Valves semi-elliptical and strongly dorsiventral. The dorsal margin is broadly arched, the ventral margin is straight to slightly convex. The valve ends are protracted, subcapitate and ventrally deflected. Valve length 10.0–12.0 µm, valve breadth 2.5–3.5 µm. The raphe is arched with dilated and straight proximal raphe ends. The axial area is not well defined. The dorsal and ventral striae are difficult to resolve in the LM, although a dorsal marginal ridge can be seen in some specimens.

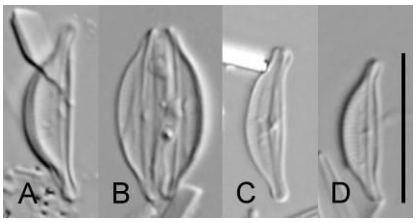

Figure 4.106. A–D. Light micrographs of *Halamphora sp. nov.* Amph134 showing observed size range. Scale bar = 10 µm.

In SEM, externally, the raphe branches are straight with nearly straight to slightly dorsally deflected proximal ends and dorsally deflected ventral ends. The dorsal raphe ledge is very broad and continuous along the length of the valve. An irregularly positioned dorsal marginal ridge runs the length of the valve. The dorsal striae are composed of a single elongate areolae running from the axial area to the thin marginal ridge. The ventral striae are continuous through the central valve and are composed of a single row of narrow elongate areolae. Internally, the proximal raphe ends terminate in a central fused helictoglossa. The dorsal and ventral striae are composed of single elongate areolae. The dorsal mantle striae are also composed of a single row of elongate areolae.

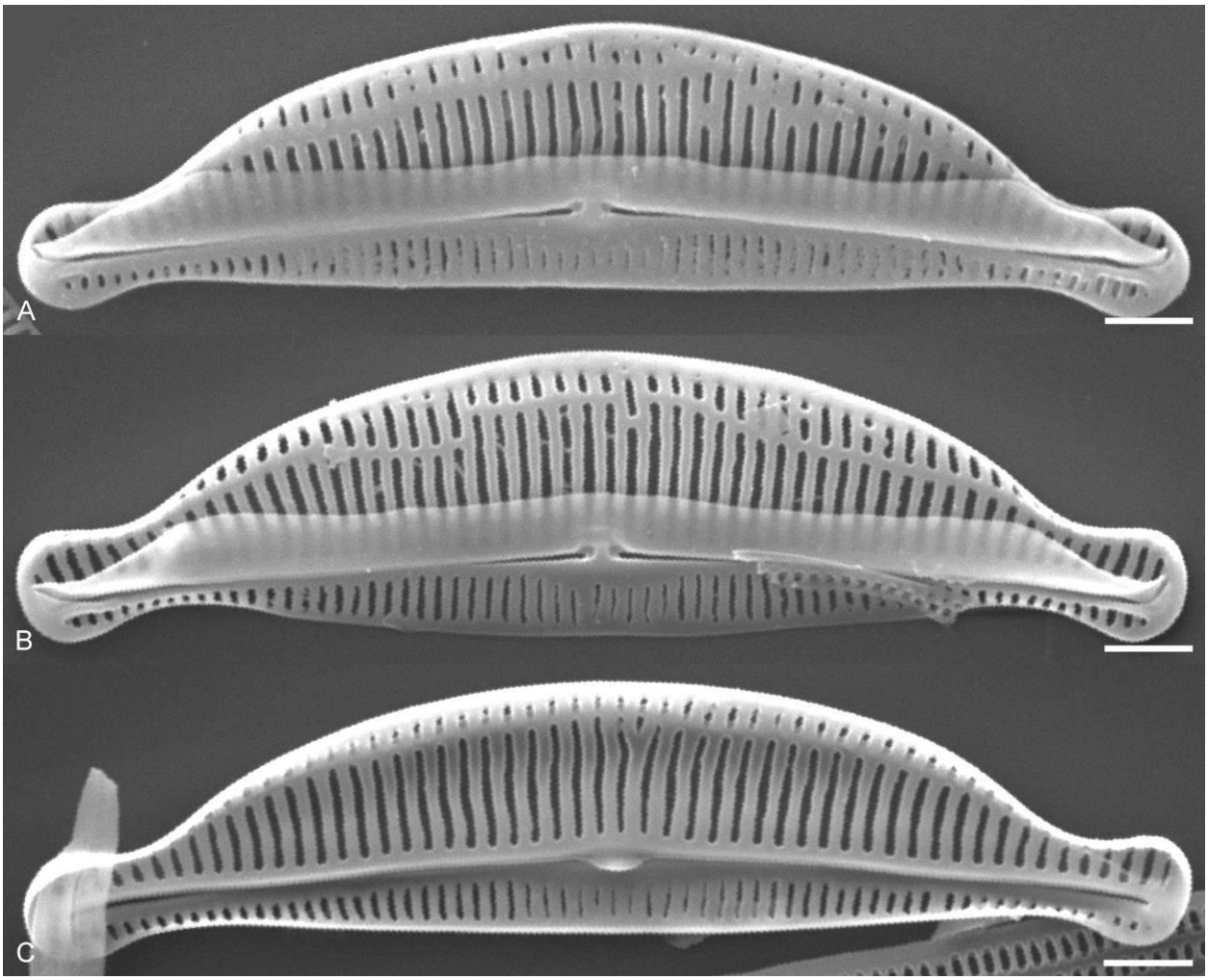

Figure 4.107. Scanning electron micrographs of *Halamphora sp. nov.* Amph134. **A.** External whole valve. **B.** External whole valve. **C.** Internal whole valve. Scale bars = 1 µm.

Halamphora sp. nov. Amph153 (Figs 4.109, 4.110)

Valves are semi-elliptical and strongly dorsiventral. The dorsal margin is smoothly arched and the ventral margin is straight to slightly concave. The valve ends are protracted narrowly rounded to subcapitate and slightly ventrally deflected. Valve length 17.0–18.0 µm, valve breadth 3.0–3.5 µm. The raphe is slightly arched to straight with straight proximal ends. The axial area is not easily distinguished. The dorsal and ventral striae are difficult to resolve in the LM. A dorsal marginal ridge is can be seen in the LM near the valve margin.

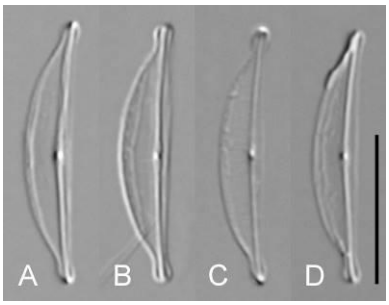

Figure 4.108. A–D. Light micrographs of *Halamphora sp. nov.* Amph153 showing observed size range. Scale bar = 10 µm.

In SEM, externally, the proximal and distal raphe ends are dorsally deflected. The dorsal raphe ledge is narrow and continuous along the length of the valve. A thin marginal ridge runs the length of the valve. The dorsal and marginal striae are composed of single elongate areolae separated by thin virgae and interrupted only by the marginal ridge. The ventral striae are continuous through the valve center and are composed of a single row of thin elongate areolae. Internally, the proximal raphe ends terminate in a small fused central helictoglossa.

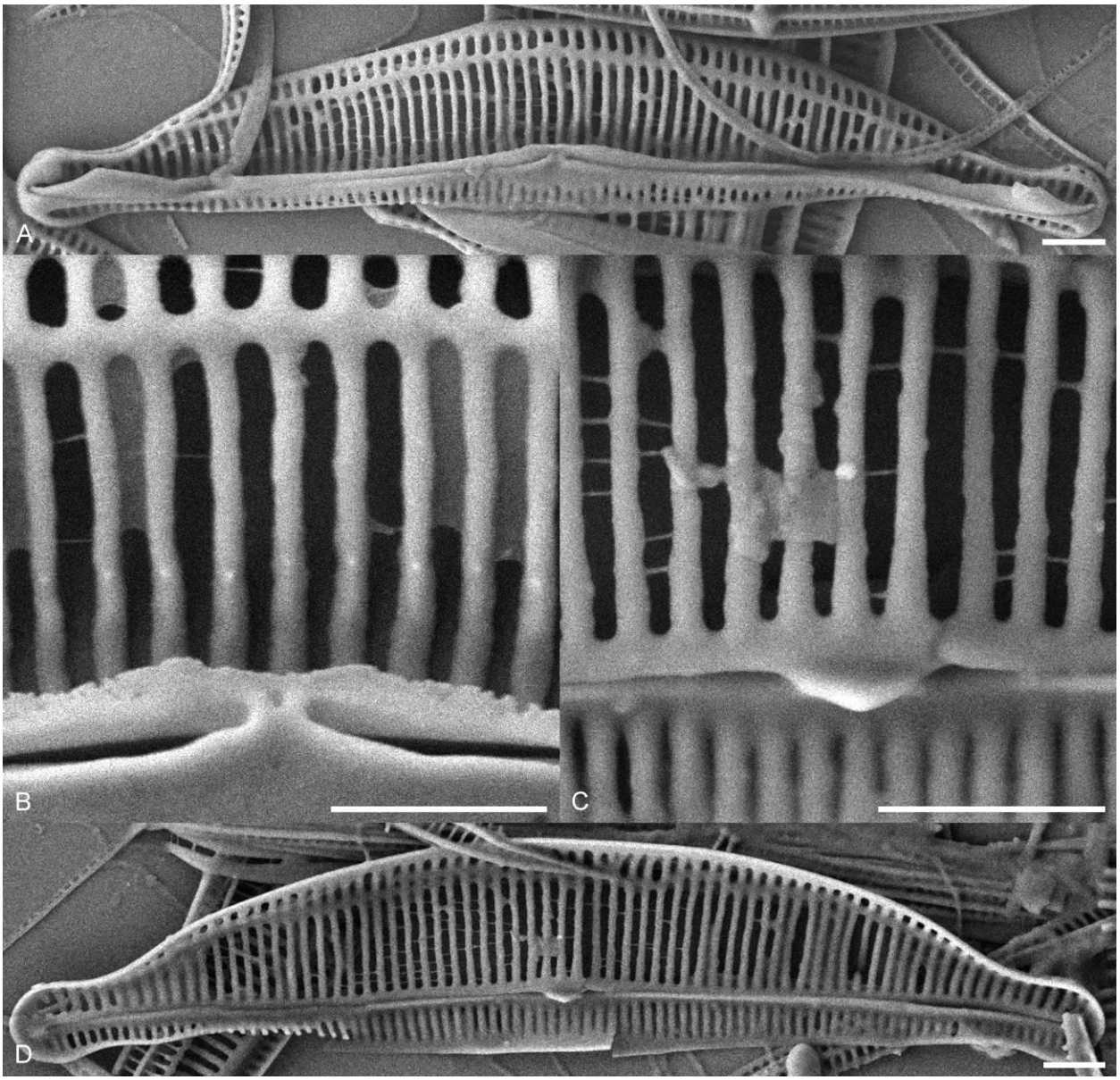

Figure 4.109. Scanning electron micrographs of *Halamphora sp. nov.* Amph153. **A.** External whole valve. **B.** Detail of external valve center. **C.** Detail of internal valve center. **D.** Internal whole valve. Scale bars = 1 µm.

HALAMPHORA CLADE F

Halamphora sp. nov. Amph164 (4.111, 4.112)

Valves are narrowly semi-elliptical and strongly dorsiventral. The dorsal margin is arched near the apices, becoming flattened over the valve center. The ventral margin is straight. The valve ends are

protracted, subcapitate and slightly ventrally deflected. Valve length 28.0–29.0 µm, valve breadth 4.0–4.5 µm. The raphe is nearly straight with straight proximal raphe ends. The axial area is narrow dorsally and not distinguishable ventrally. The dorsal striae are not visibly areolate, parallel at the valve center, becoming radiate near the apices. The ventral striae are difficult to image in the LM. Striae number 16 in 10 µm.

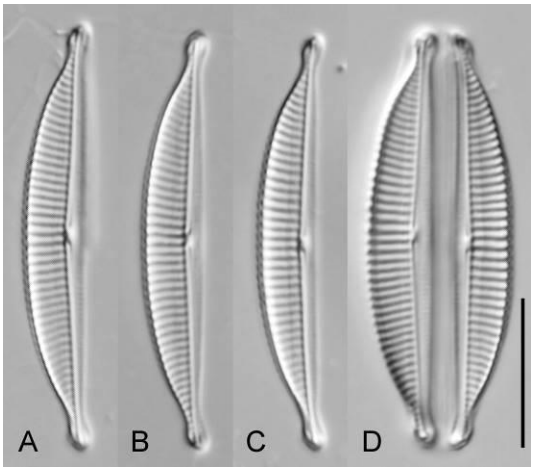

Figure 4.110. A–D. Light micrographs of *Halamphora sp. nov.* Amph164 showing observed size range. Scale bar = 10 µm.

In SEM, externally, the raphe is straight with dilated proximal raphe ends that are slightly deflected dorsally. The distal raphe ends are dorsally deflected. The dorsal raphe ledge is broad and continuous along the length of the valve. The dorsal striae are biseriate and separated by thick virgae. A well-developed dorsal marginal ridge is present. The ventral striae are fine and uniseriate. The ventral striae are not continuous through the valve center creating a broad ventral fascia. Internally, the proximal raphe ends terminate in a small fused central helictoglossa. The dorsal striae are biseriate and separated by wide virgae. The ventral striae are fine and uniseriate.

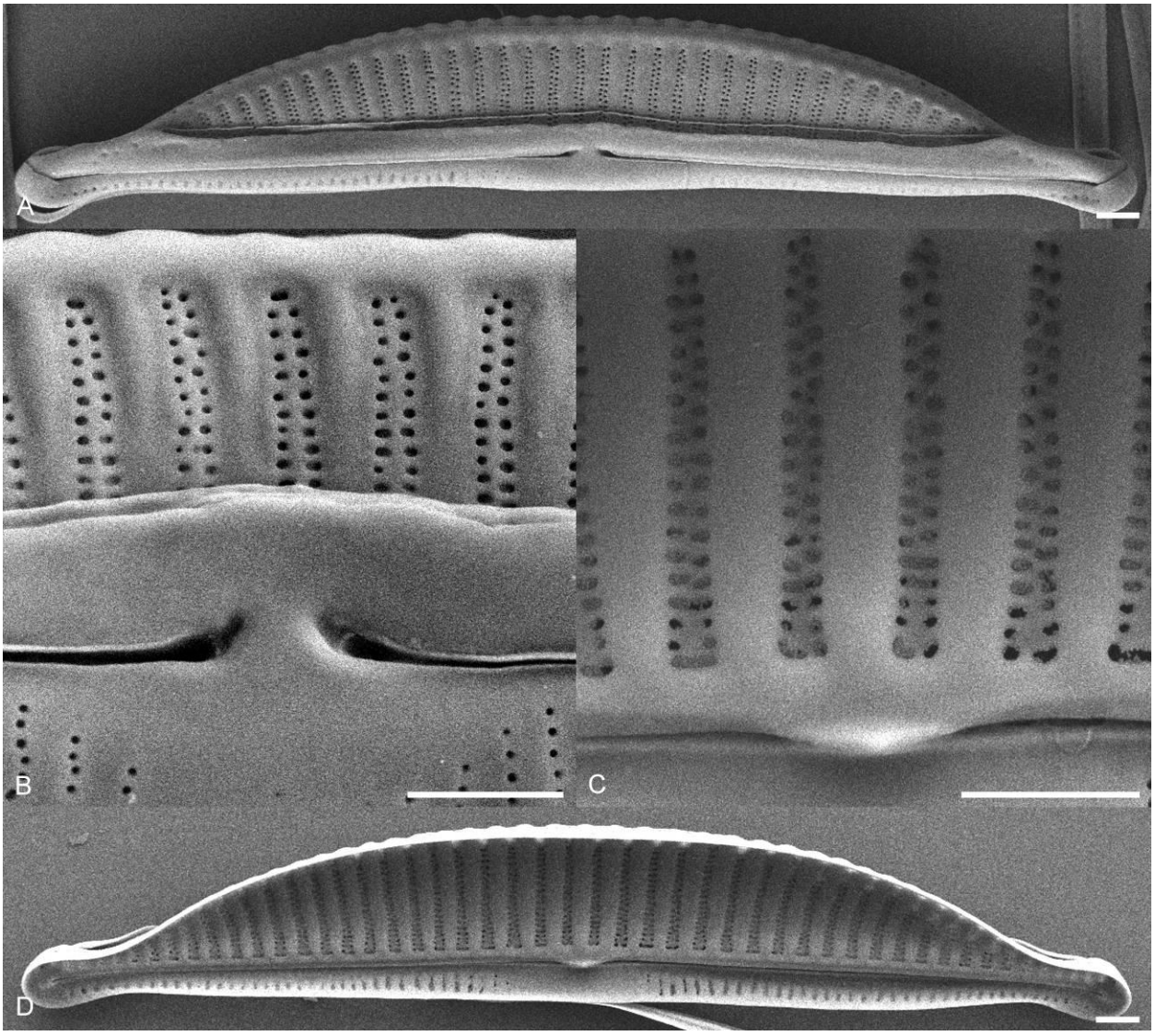

Figure 4.111. Scanning electron micrographs of *Halamphora sp. nov.* Amph164. **A.** External whole valve. **B.** Detail of external whole valve. **C.** Detail of internal valve center. **D.** Internal whole valve. Scale bars = 1 µm.

Halamphora margalefii (Tomàs in Sabater et al.) Stepanek & Kociolek comb. nov. Amph130 (Figs 4.113, 4.114)

Valves are semi-elliptical to nearly linear through the valve center and moderately dorsiventral. The dorsal margin is arched near the apices becoming flat over the valve center. The ventral margin is slightly convex. The valve ends are protracted, narrowly rounded and ventrally deflected. Valve length 15.0–18.0 µm, valve breadth 2.5–3.0 µm. The raphe is straight with straight proximal raphe ends. The

axial area is narrow throughout. The dorsal striae are not visibly areolate and uninterrupted along the valve face. The dorsal striae are parallel through much of the central valve, becoming radiate near the apices. The ventral striae are fine and are interrupted at the valve center. Striae number 23–24 in 10 µm.

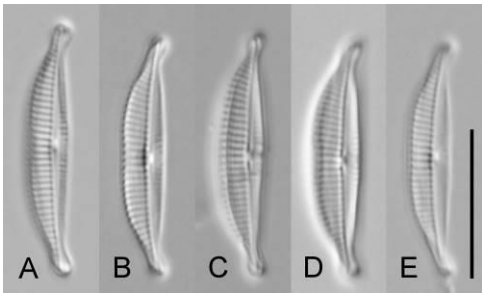

Figure 4.112. A–D. Light micrographs of *Halamphora margalefii* Amph130 showing observed size range. Scale bar = 10 µm.

In SEM, externally, the proximal raphe ends are dilated and slightly deflected dorsally, the distal ends deflect dorsally. The dorsal raphe ledge is very broad, obscuring nearly half of the dorsal valve face and continuous through the valve center. The dorsal striae are biseriate and more or less continuous to the dorsal margin. The ventral striae are fine and uniseriate. A small ventral fascia is present. Internally, the proximal raphe ends terminate in a small fused central helictoglossa. The dorsal striae are biseriate and separated by relatively thick virgae. The ventral striae are fine and uniseriate. A distinct ventral fascia is present.

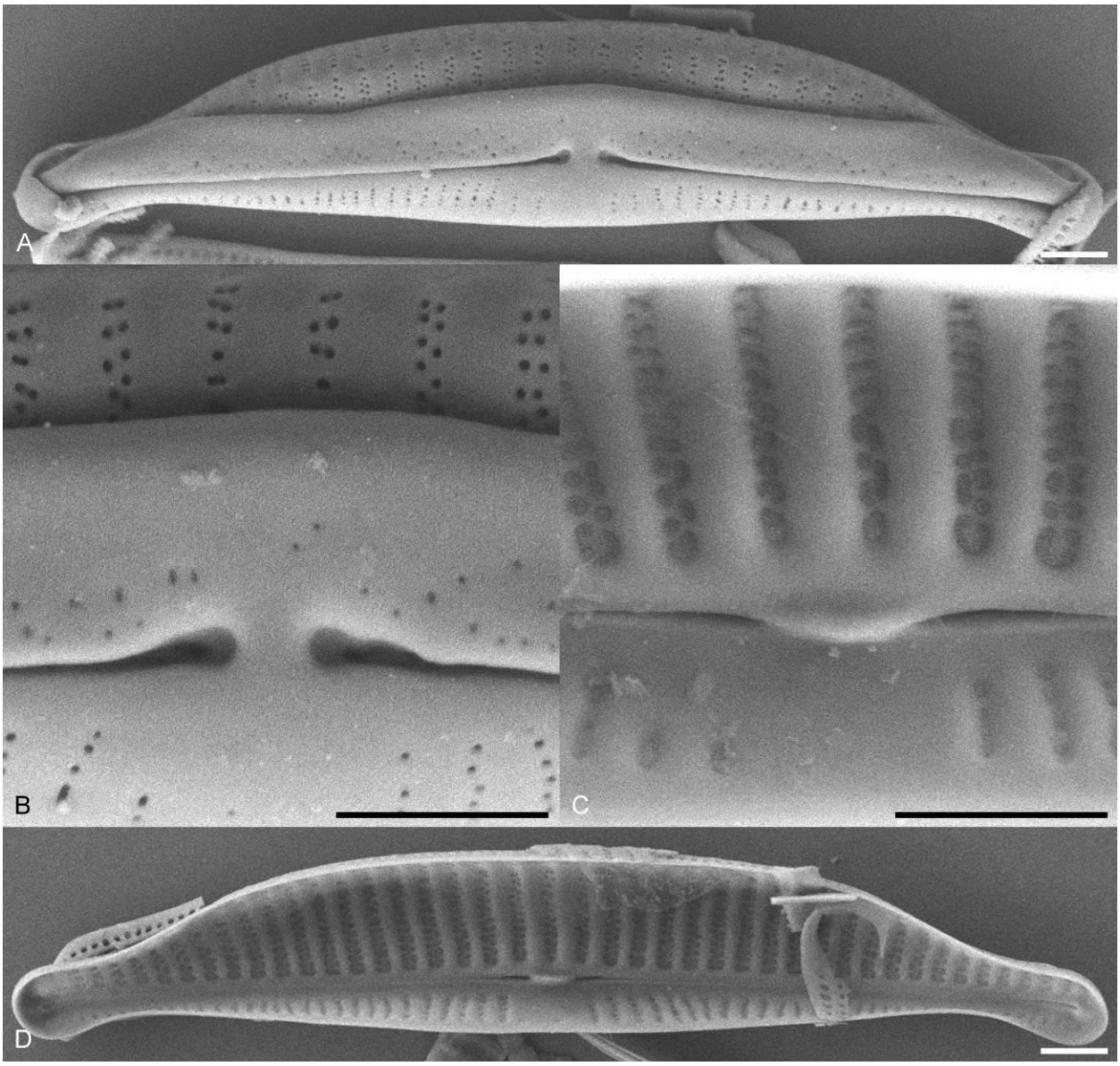

Figure 4.113. Scanning electron micrographs of *Halamphora margalefii* Amph130. **A.** External whole valve. **B.** Detail of external valve center. **C.** Detail of internal valve center. **D.** Internal whole valve. Scale bars = 1 µm.

Halamphora subturgida (Hustedt) Levkov Amph015 (Fig. 4.115)

Valves broadly semi-elliptical and strongly dorsiventral. The dorsal margin is smoothly arched, the ventral margin is slightly convex. The valve ends are protracted subcapitate and ventrally deflected. Valve length 16.0–17.0 µm, valve breadth 3.5–4.0 µm. The raphe is slightly arched with straight raphe branches. The proximal raphe ends terminate widely in straight ends. The dorsal axial area is narrow,

slightly expanded at the central area. The ventral axial area is difficult to differentiate. The dorsal striae are weakly areolate, parallel near the valve center becoming radiate near the apices. The ventral striae are difficult to image in the LM. Striae number 23–25 in 10 µm.

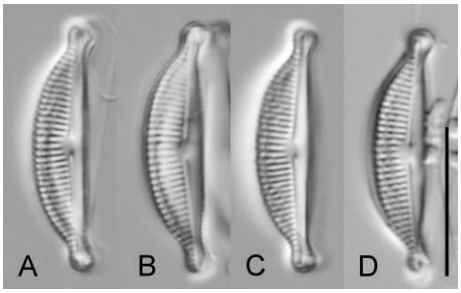

Figure 4.114. A–D. Light micrographs of *Halamphora subturgida* Amph015 showing observed size range. Scale bar = 10 µm.

Halamphora sp. nov. Amph166 (Figs 4.116, 4.117)

Valves are narrowly semi-elliptical and strongly dorsiventral. The dorsal margin is smoothly arched, the ventral margin is straight. The valve ends are weakly protracted, narrowly rounded and deflected ventrally. Valve length 16.0–24.0 µm, valve breadth 3.0–3.5 µm. The raphe is slightly arched with straight proximal raphe ends. The axial area is narrow dorsally and difficult to distinguish ventrally. The dorsal striae are not obviously areolate, parallel through the valve center and becoming radiate near the apices. A dorsal marginal ridge is visible in the LM. The ventral striae are difficult to image in the LM. Striae number 18–20 in 10 µm.

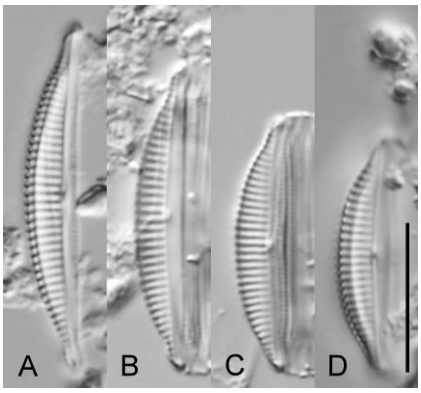

Figure 4.115. A–D. Light micrographs of *Halamphora sp. nov.* Amph166 showing observed size range. Scale bar = 10 µm.

In SEM, externally, the raphe is nearly straight with proximal ends terminating very closely, dilated and slightly dorsally deflected. The distal raphe ends are deflected dorsally. The dorsal raphe ledge is broad and continuous through the central valve. The dorsal striae are biseriate and separated by relatively broad virgae. A dorsal marginal ridge runs the length of the dorsal margin. The ventral striae are composed of a single row of round to ovoid areolae and are more or less continuous through the valve center. The ventral axial area is expanded, more so near the valve center forming a semi-lanceolate hyaline area. Internally, the proximal raphe ends terminate in a small fused central helictoglossa. The dorsal striae are biseriate and separated by relatively broad virgae, the ventral striae are composed of a single row of areolae.

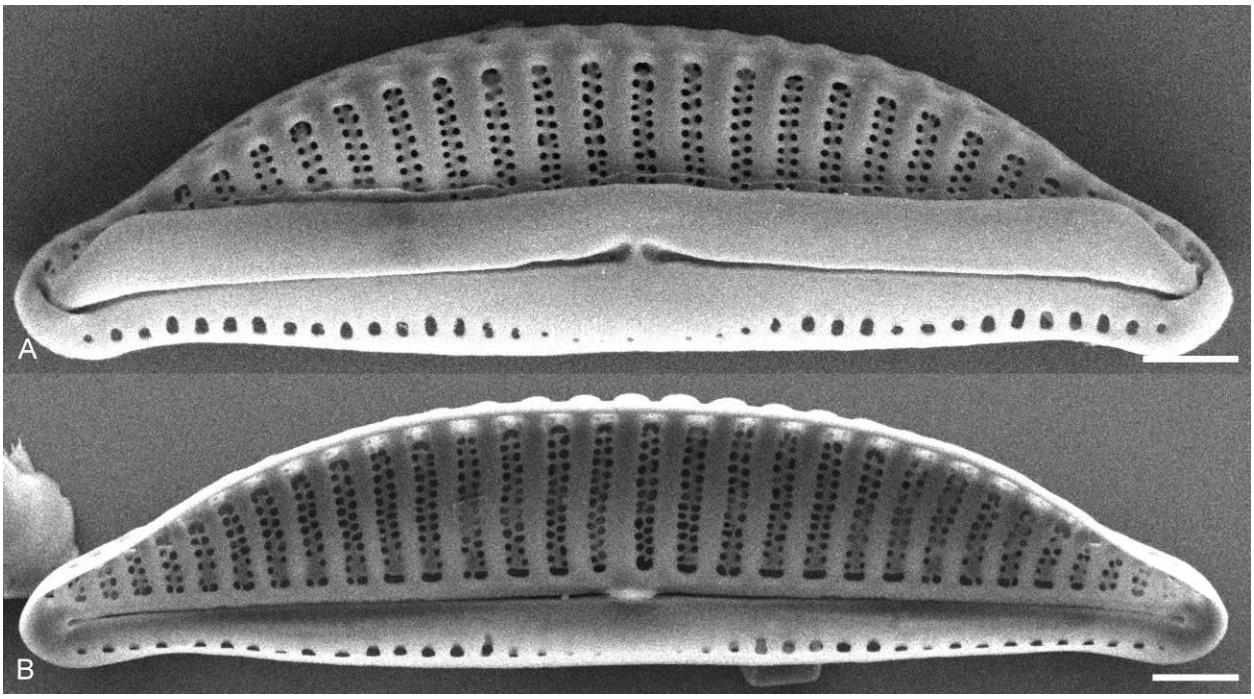

Figure 4.116. Scanning electron micrographs of *Halamphora sp. nov.* Amph166. **A.** External whole valve. **B.** Internal whole valve. Scale bars = 1 µm.

Halamphora bicapitata (Hohn & Hellerman) Stepanek & Kociolek comb. nov. Amph055 (Fig. 4.118)

Valves are broadly semi-elliptical and moderately dorsiventral. The dorsal margin is smoothly arched, the ventral margin is slightly convex. The valve ends are weakly protracted, narrowly rounded and ventrally deflected. Valve length 22.0–33.0 µm, valve breadth 5.0–7.0 µm. The raphe is arched with

straight to slightly dorsally deflected proximal ends. The dorsal axial area is narrow throughout, the ventral axial is broad and semi-lanceolate. A siliceous thickening is visible at the dorsal valve center. The dorsal striae are areolate parallel at the valve center, becoming radiate near the apices. The ventral striae are composed of a single row of marginally positioned small areolae. The ventral striae are continuous along the length of the valve. Striae number 19–21 in 10 µm.

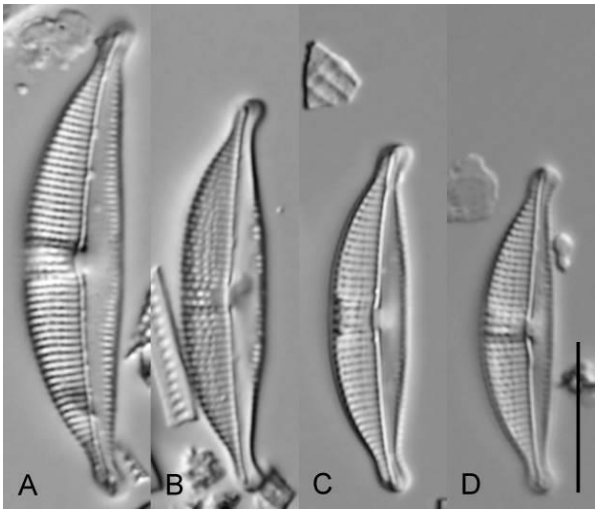

Figure 4.117. A–D. Scanning electron micrographs of *Halamphora bicapitata* Amph055 showing observed size range. Scale bar = 10 µm.

Halamphora fontinalis (Hustedt) Levkov Amph111 (Figs 4.119, 4.120)

Valves are narrowly semi-elliptical and moderately dorsiventral. The dorsal margin is smoothly arched, the ventral margin is straight to slightly convex. The valve ends are protracted, narrowly rounded to subcapitate in larger specimens and ventrally deflected. Valve length 24.0–33.0 µm, valve breadth 4.5–6.0 µm. The raphe is slightly arched with sharply dorsally bent to hooked proximal raphe ends. The dorsal axial area is narrow throughout. The ventral portion of the valve is broad with a wide axial area. A siliceous thickening is apparent at the dorsal valve center. The dorsal striae are areolate and somewhat obscured at the central valve by the distinct siliceous thickening. The dorsal striae are parallel at the valve center becoming radiate near the apices. The ventral striae are positioned very near the ventral valve margin and are composed of a single row of small areolae. The ventral striae are not present through a wide portion of the valve center. Striae number 18–22 in 10 µm.

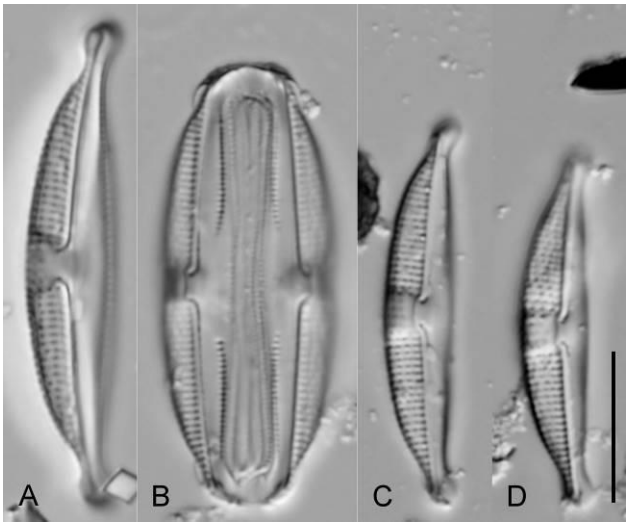

Figure 4.118. A–D. Light micrographs of *Halamphora fontinalis* Amph111 showing observed size range. Scale bar = 10 µm.

In SEM, externally, the raphe is straight with dorsally deflected proximal and distal raphe ends. The dorsal raphe ledge is narrow and not continuous through the valve center. The dorsal striae are composed of rows of small areolae. At the valve center the dorsal areolae are often filled in with silica. A dorsal marginal ridge is absent. Internally, the proximal raphe ends terminate in a broad fused central helictoglossa. The central dorsal virgae are distinctly thickened becoming fused near the central area.

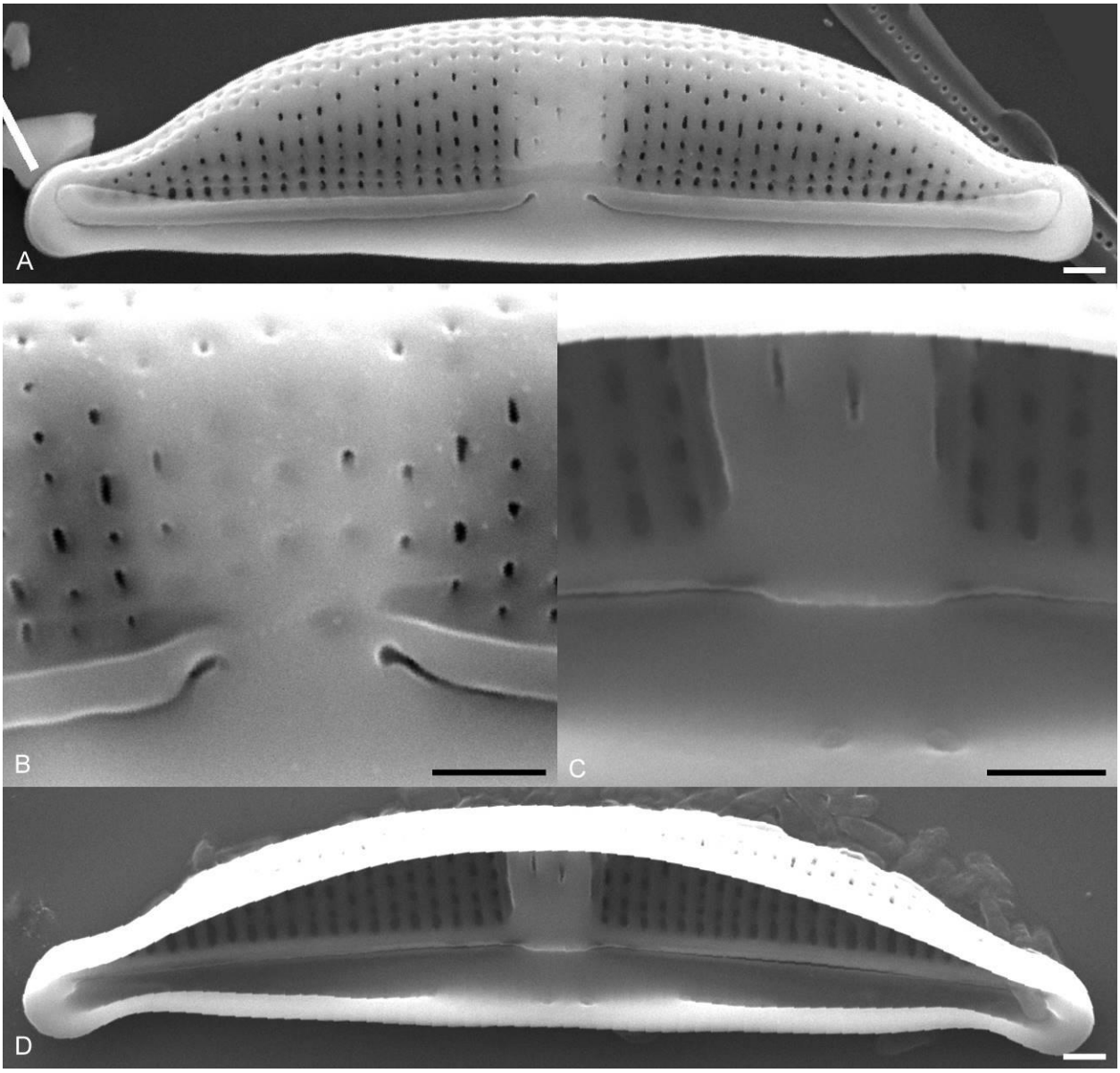

Figure 4.119. Scanning electron micrographs of *Halamphora fontinalis* Amph111. **A.** External whole valve. **B.** Detail of external valve center. **C.** Detail of internal valve center. **D.** Internal whole valve. Scale bars = 1 µm.

HALAMPHORA CLADE G

Halamphora elongata Bennett & Kociolek Amph001 (Figs 4.121, 4.122)

Valves broadly semi-elliptical and strongly dorsiventral. The dorsal margin is broadly arched and somewhat flattened over the central portion of the valve in some specimens, the ventral margin is

concave. The valve ends are protracted and rounded to subcapitate. Valve length 22.0–57.0 µm, valve breadth 7.0–8.5 µm. The raphe is highly arched with nearly straight to dorsally curved raphe branches. The proximal raphe ends are straight, the distal raphe ends are dorsally deflected. The axial area is narrow, somewhat expanded at the valve center. The dorsal striae are areolate and more widely spaced and coarsely areolate at the valve center. The dorsal striae are radiate throughout. The ventral striae are difficult to image in the LM due to the very narrow ventral valve. Striae number 18–21 in 10 µm.

In SEM, externally, the raphe branches are dorsally curved with dorsally curved proximal and distal raphe ends. The dorsal raphe ledge is narrow and continuous along the length of the valve. A small siliceous hyaline area is present at the dorsal central area. The dorsal striae are composed of numerous small elongate areolae. The ventral striae are difficult to image due to their marginal position. A dorsal marginal ridge is not present. Internally, the proximal raphe ends terminate in a wide fused central helictoglossa. The central dorsal virgae are distinctly thickened and become fused near the central area.

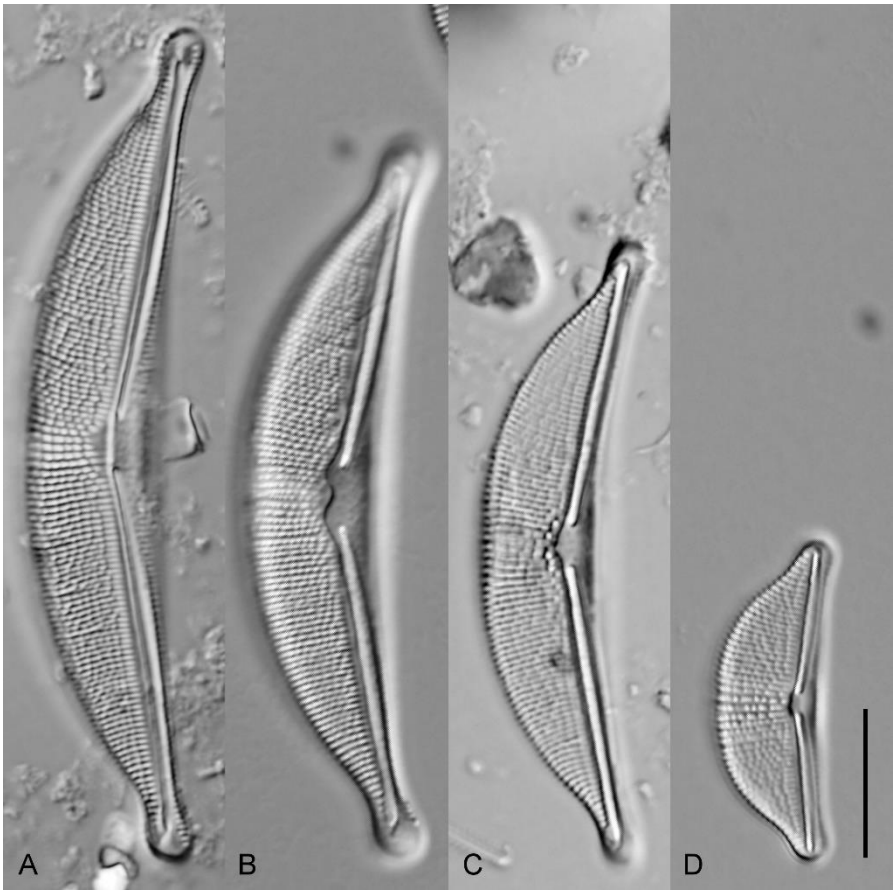

Figure 4.120. A–D. Light micrographs of *Halamphora elongata* Amph001 showing observed size range. Scale bar = 10 µm.

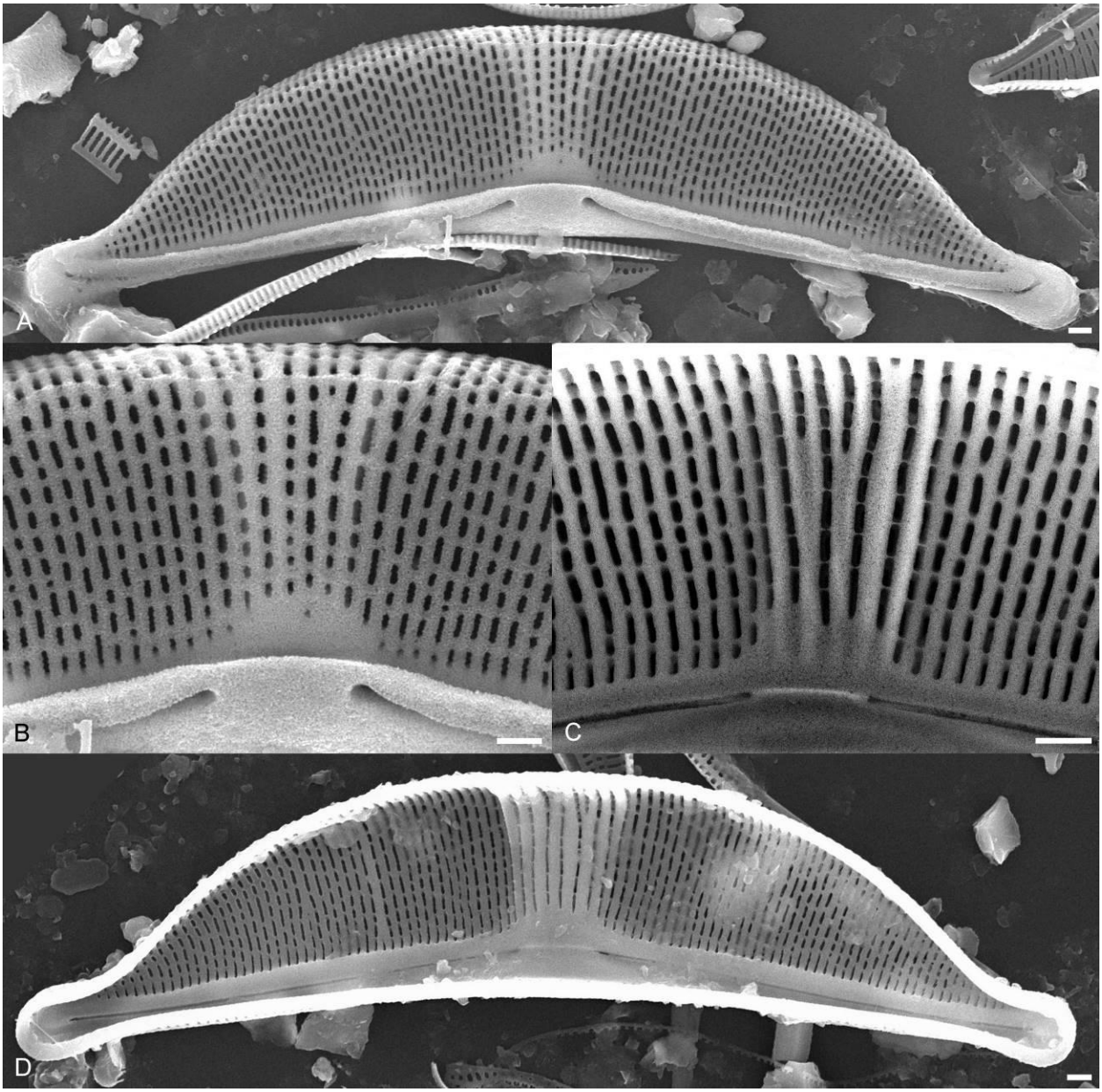

Figure 4.121. Scanning electron micrographs of *Halamphora elongata* Amph001. **A.** External whole valve. **B.** Detail of external valve center. **C.** Detail of internal valve center. **D.** Internal whole valve. Scale bars = 1 µm.

Halamphora oligotraphenta (Lange-Bertalot) Levkov Amph009 (Figs 4.123, 4.124)

Valves narrowly semi-elliptical and strongly dorsiventral. The dorsal margin is arched, somewhat flattened over the central portion of the valve in some specimens, the ventral margin is slightly concave. The valve ends are protracted subcapitate to capitate and slightly ventrally deflected. Valve length 22.0–

29.0 µm, valve breadth 3.5–4.0 µm. The raphe is arched. The proximal raphe ends terminate widely and are slightly dorsally deflected, the distal ends are dorsally deflected. The dorsal axial area is narrow, the ventral axial are is difficult to distinguish due to the narrow ventral valve face. The dorsal striae are finely areolae although more widely spaced and coarsely areolate at the valve center. The dorsal striae are weakly radiate throughout. The ventral striae are difficult to image in the LM due to their marginal position. Striae number 27–29 in 10 µm.

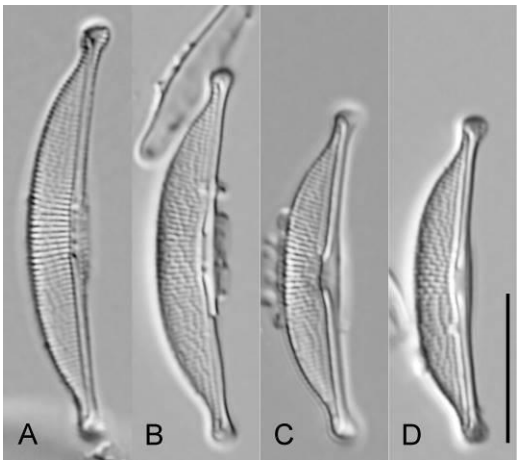

Figure 4.122. A–D. Light micrographs of *Halamphora oligotraphenta* Amph009 showing observed size range. Scale bar = 10 µm.

In SEM, externally, the proximal and distal ends are weakly dorsally deflected. The dorsal raphe ledge is narrow and continuous through the central portion of the valve. The dorsal striae are composed of numerous small elongate areolae. A dorsal marginal ridge is only present near the apices and not through the central portion of the valve. The ventral axial area is relatively broad. The ventral striae are composed of a singly row of small areolae and are often difficult to image due to their marginal position. The ventral striae can be seen to continue uninterrupted through the central portion of the valve.

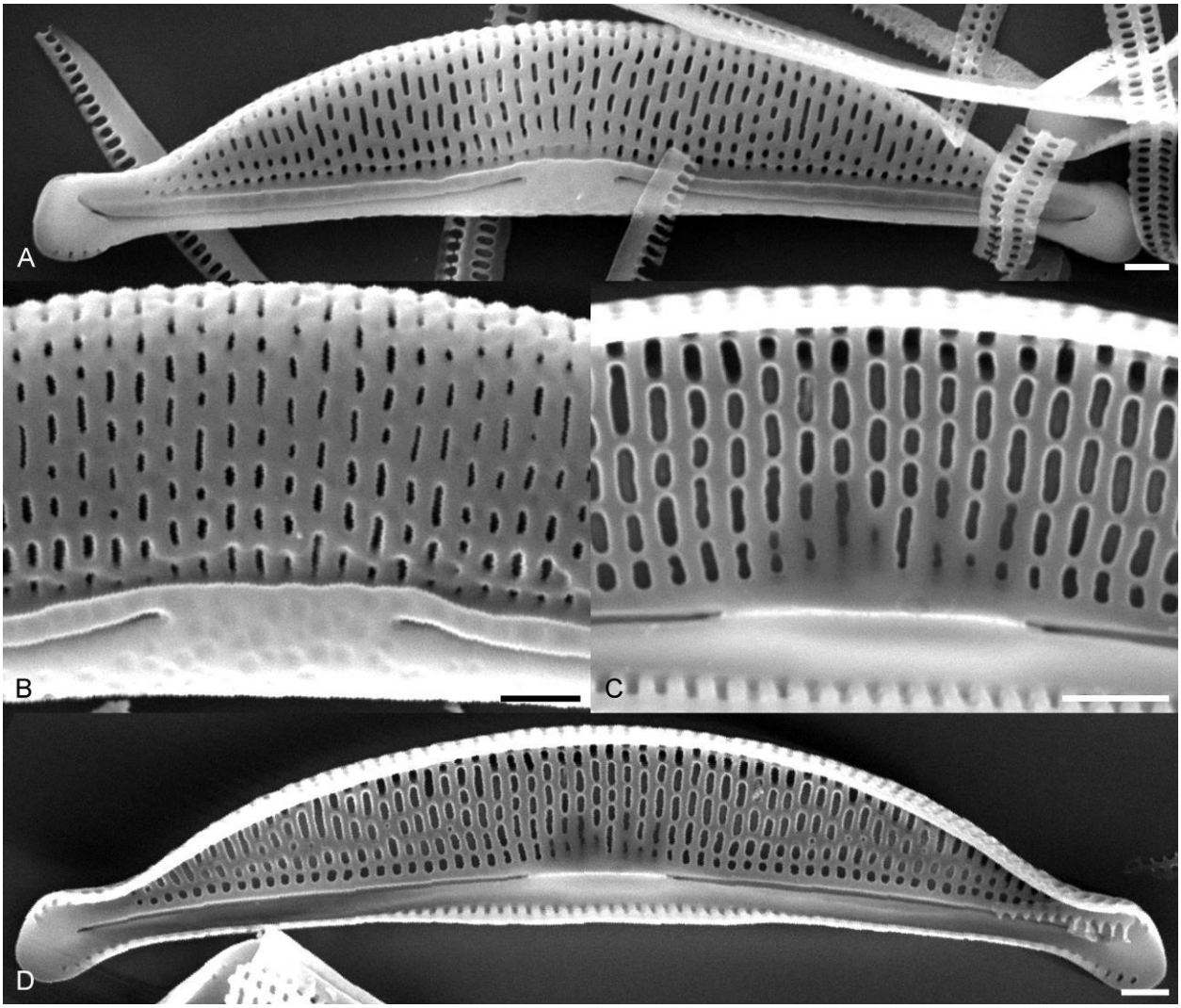

Figure 4.123. Scanning electron micrographs of *Halamphora oligotraphenta* Amph009. **A.** External whole valve. **B.** Detail of external valve center. **C.** Detail of internal valve center. **D.** Internal whole valve. Scale bars = 1 µm.

Halamphora pratensis Stepanek & Kociolek Amph106 (Figs 4.125, 4. 126)

Valves broadly semi-elliptical and strongly dorsiventral. The dorsal margin is broadly arched, the ventral margin is slightly concave to weakly tumid in some specimens. The valve ends are protracted, rounded and ventrally deflected. Valve length 13.0–35.0 µm, valve breadth 4.5–6.0 µm. The raphe is arched with straight raphe branches. The proximal raphe ends terminate widely and are straight. The axial area is narrow dorsally and difficult to distinguish on the ventral side. The dorsal striae are finely areolate and more widely spaced and coarsely areolate at the valve center. The dorsal striae are nearly parallel at

the valve center, weakly radiate across the rest of the valve. The ventral striae are difficult to image in the LM due to their marginal position. The dorsal striae are distinctly more widely spaced at the valve center, with 23–27 striae in 10 µm and 31–34 in 10 µm near the apices.

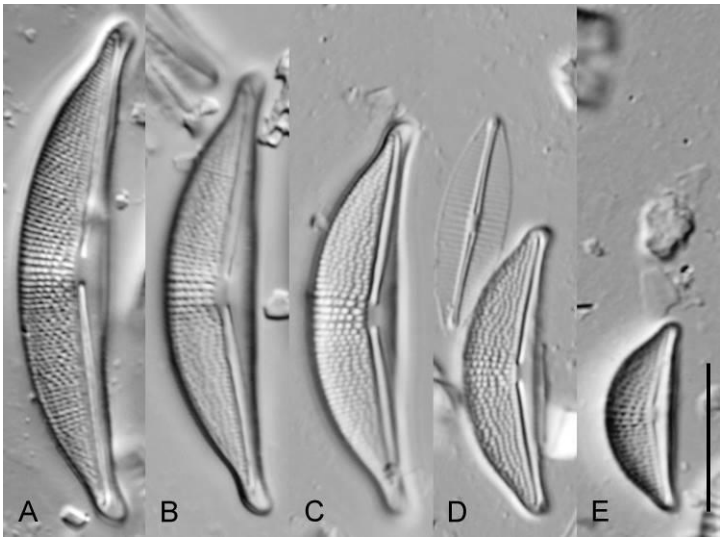

Figure 4.124. A–E. Light micrographs of *Halamphora pratensis* Amph106 showing the observed size range. Scale bar = 10 µm.

In SEM, externally, the proximal raphe ends are straight, the distal ends are weakly dorsally deflected. The raphe ledge is narrow and continuous through the central portion of the valve. The dorsal striae are composed of numerous round to elongate areolae. A dorsal marginal ridge is only visible near the apices, not apparent across the central portion of the valve. The ventral axial area is broad. The ventral striae are composed of small areolae and are difficult to image due to their marginal position. Internally, the proximal raphe ends terminate in a wide fused central helictoglossa. The central dorsal virgae are distinctly thickened.

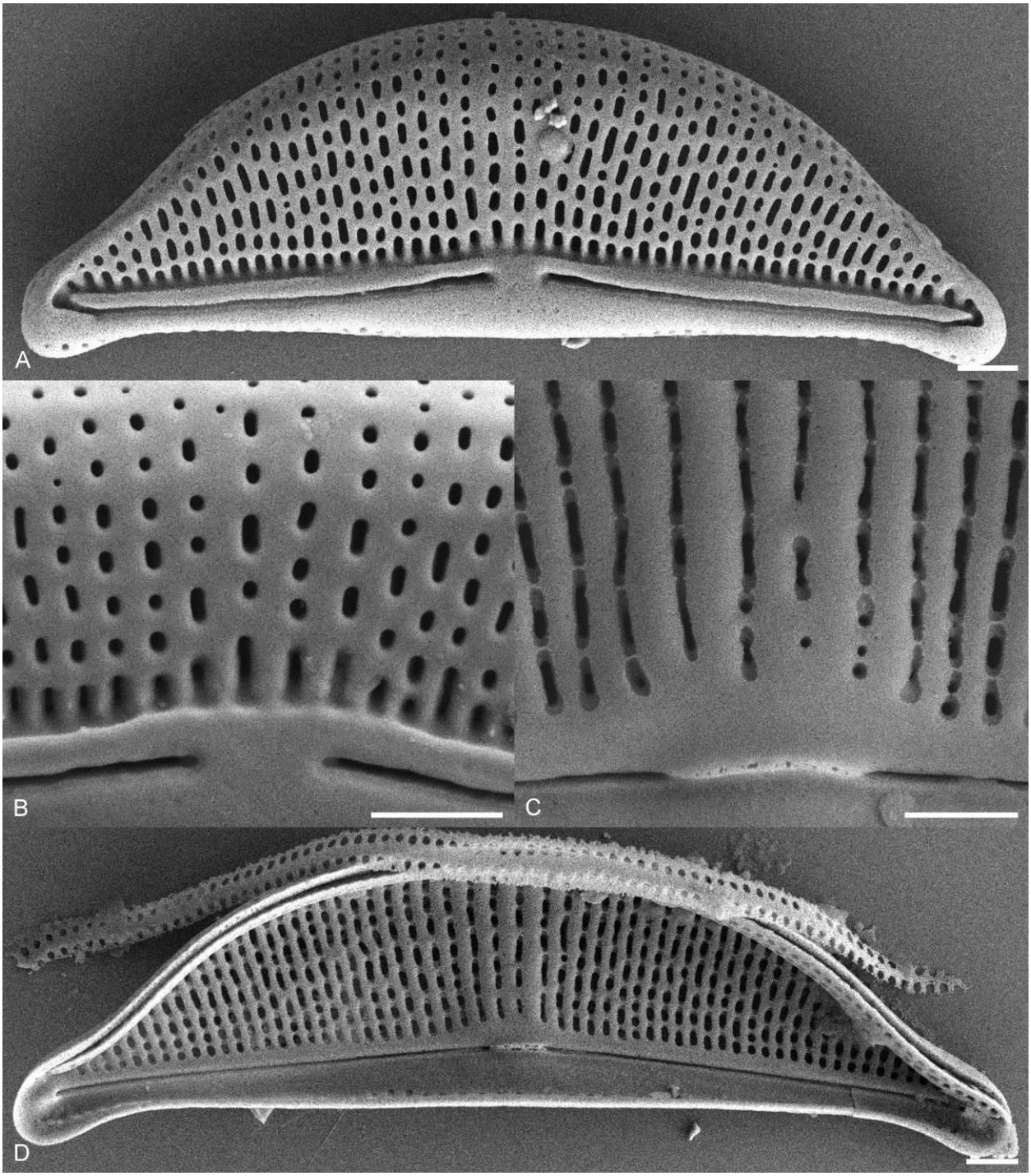

Figure 4.125. Scanning electron micrographs of *Halamphora pratensis* Amph106. **A.** External whole valve. **B.** Detail of external valve center. **C.** Detail of internal valve center. **D.** Internal whole valve. Scale bars = 1 µm.

Halamphora veneta (Kützing) Levkov Amph005 (Figs 4.127, 4.128)

Valves semi-elliptical and strongly dorsiventral. The dorsal margin is smoothly arched, the ventral margin is straight to slightly concave. The valve ends are rostrate. Valve length 12.0–37.0 µm, valve breadth 4.0–5.5 µm. The raphe is slightly arched. The proximal raphe ends terminate widely and are slightly dorsally deflected. The dorsal axial area is narrow, the ventral axial area is difficult to differentiate. The dorsal striae are finely areolate, more widely spaced and coarsely areolate at the valve center. The dorsal striae are weakly radiate throughout. The ventral striae are marginally positioned and difficult to image in the LM. Striae number 20–25 in 10 µm.

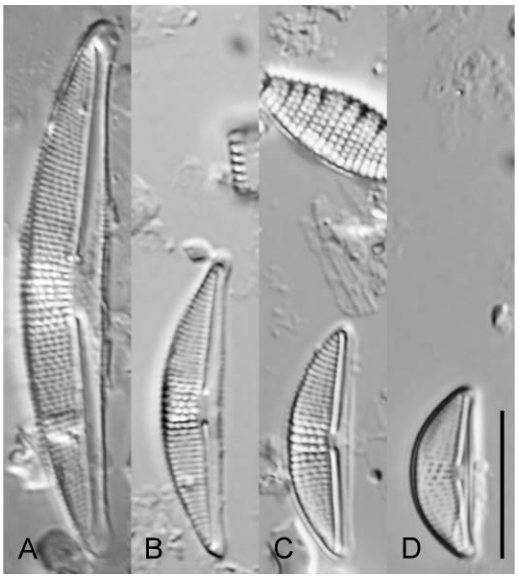

Figure 4.126. A–D. Light micrographs of *Halamphora veneta* Amph005 showing observed size range. Scale bar = 10 µm.

In SEM, externally, the proximal raphe ends terminate widely and are slightly dorsally deflected. The distal ends are dorsally deflected. The dorsal raphe ledge is narrow and continuous across the central portion of the valve. The dorsal striae are composed of numerous elongate areolae of irregular length. A dorsal marginal ridge runs the length of the valve. The ventral striae are difficult to image due to their marginal position. Internally, the proximal raphe ends terminate in a wide fused central helictoglossa. The central dorsal virgae are distinctly thickened.

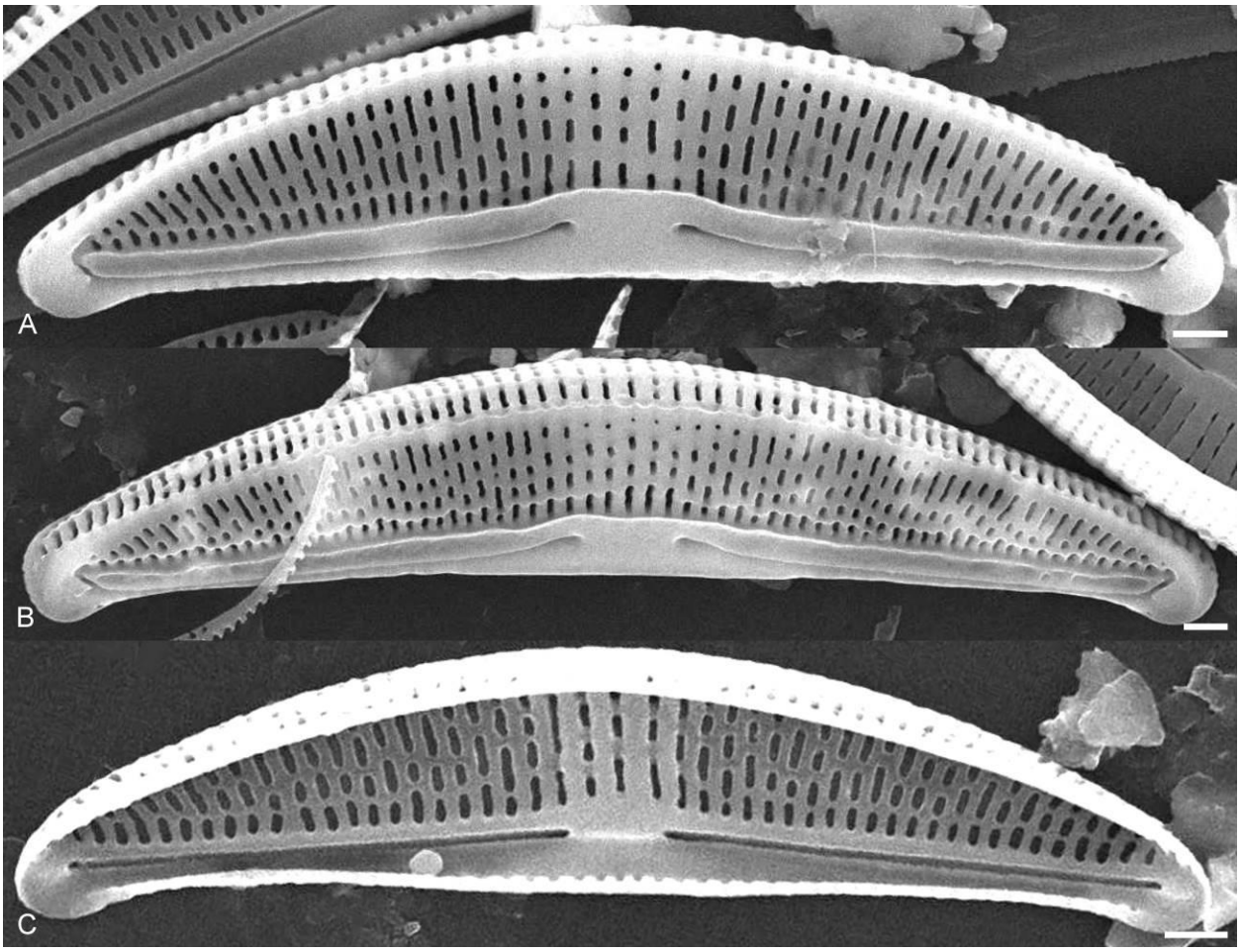

Figure 4.127. Scanning electron micrographs of *Halamphora veneta* Amph005. **A.** External whole valve. **B.** External whole valve. **C.** Internal whole valve. Scale bars = 1 µm.

Halamphora cf. *veneta* (Kützing) Levkov Amph017 (4.129, 4.130)

Valves broadly semi-elliptical and strongly dorsiventral. The dorsal margin is arched, the ventral margin is straight to slightly concave. The valve ends are rostrate. Valve length 18.0–25.0 µm, valve breadth 3.5–5.0 µm. The raphe is arched. The proximal raphe ends terminate widely and are dorsally deflected. The axial area is narrow dorsally and difficult to distinguish ventrally. The dorsal striae are areolate, more widely spaced and coarsely areolate at the valve center. The dorsal striae are weakly radiate throughout. The ventral striae are difficult to image in the LM due to their marginal position. Striae number 20–22 in 10 µm.

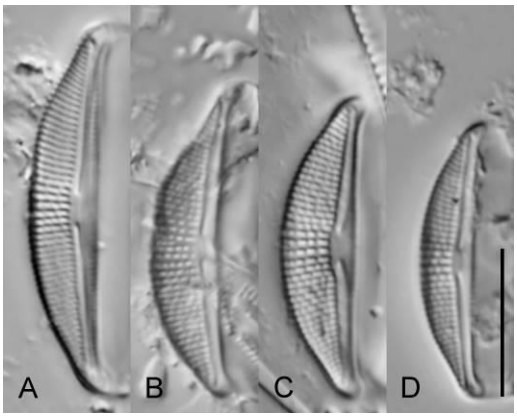

Figure 4.128. A–D. Light micrographs of *Halamphora* cf. *veneta* Amph017 showing observed size range. Scale bar = 10 µm.

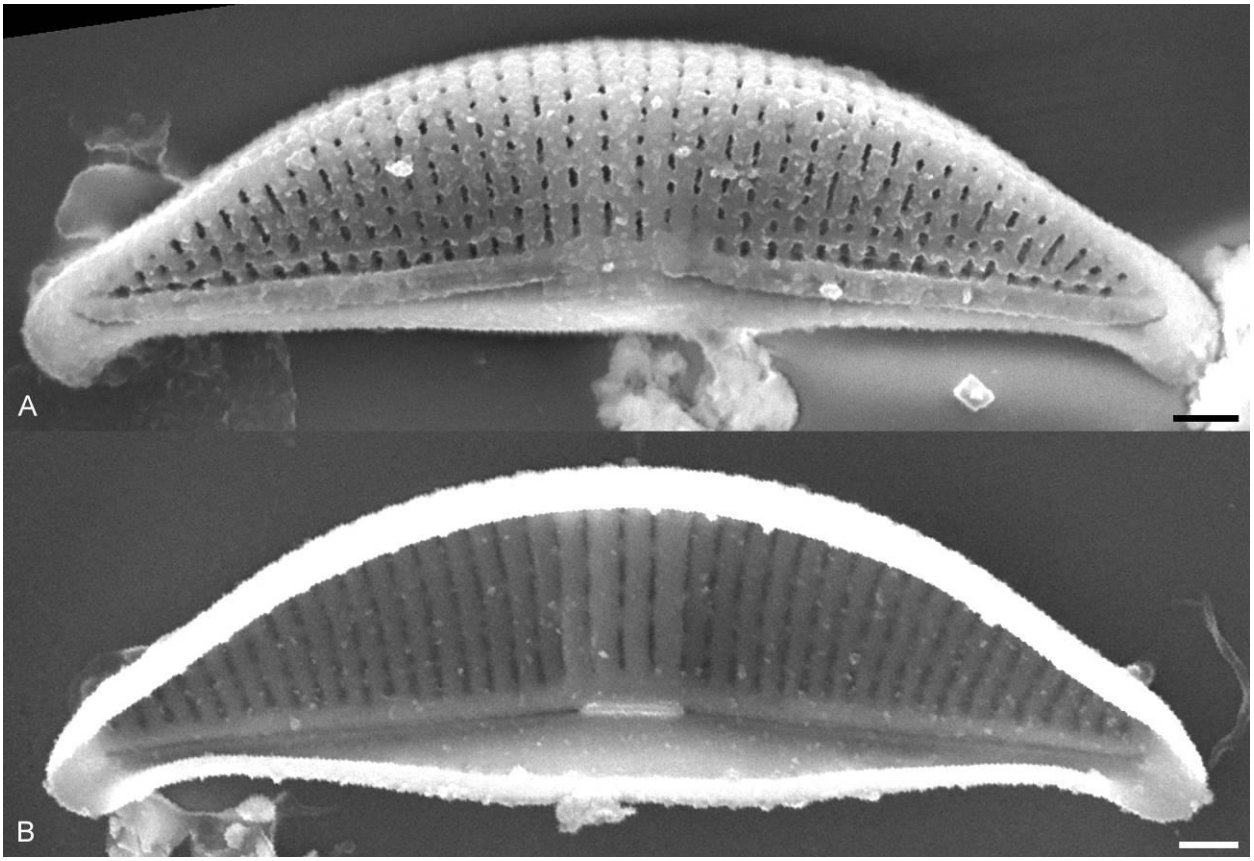

Figure 4.129. Scanning electron micrographs of *Halamphora* cf. *veneta* Amph017. **A.** External whole valve. **B.** Internal whole valve. Scale bars = 1 µm.

In SEM, externally, the proximal and distal raphe ends are weakly dorsally deflected. The dorsal raphe ledge is very narrow and least apparent across the valve center. The dorsal striae are composed of

numerous small elongate areolae. A dorsal marginal ridge is visible near the apices, becoming less apparent across the valve center. The ventral striae are difficult to image due to their marginal position. Internally, the proximal raphe ends terminate in a very broad fused central helictoglossa. The central dorsal virgae are distinctly thickened.

Halamphora coloradiana Stepanek & Kociolek Amph025 (Figs 4.131, 4.132)

Valves semi-elliptical and strongly dorsiventral. The dorsal margin is smoothly arched, the ventral margin is slightly concave. The valve ends are narrowly rounded to rostrate and ventrally deflected in larger specimens. Valve length 12.0–25.0 µm, valve breadth 2.5–4.5 µm. The raphe is arched with slightly dorsally deflected proximal raphe ends. The dorsal axial area is narrow, the ventral axial area is difficult to distinguish. The dorsal striae are areolate, more widely spaced and coarsely areolate at the valve center. The dorsal striae are slightly radiate throughout. The ventral striae are difficult to image in the LM due to their marginal position. Striae number 23–24 in 10 µm.

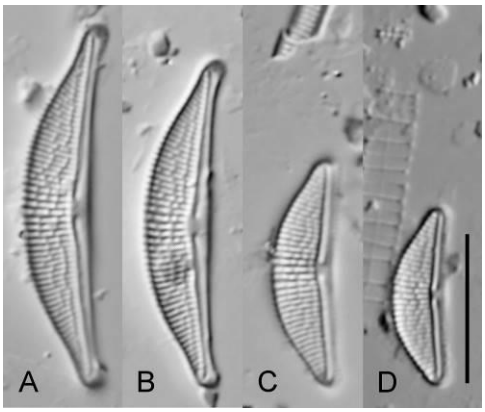

Figure 4.130. A–D. Light micrographs of *Halamphora coloradiana* Amph025 showing observed size range. Scale bar = 10 µm.

In SEM, externally, the proximal raphe ends terminate in slightly expanded pores and are weakly dorsally deflected. The distal raphe ends are dorsally deflected. The dorsal raphe ledge is small and continuous across the valve center. The dorsal striae are composed of numerous elongate areolae of irregular length. A dorsal marginal ridge runs the length of the valve. Internally, the proximal raphe ends

terminate in a well-developed fused central helictoglossa. The dorsal central virgae are distinctly thickened. The ventral striae are marginally positioned, fine and continuous across the valve center.

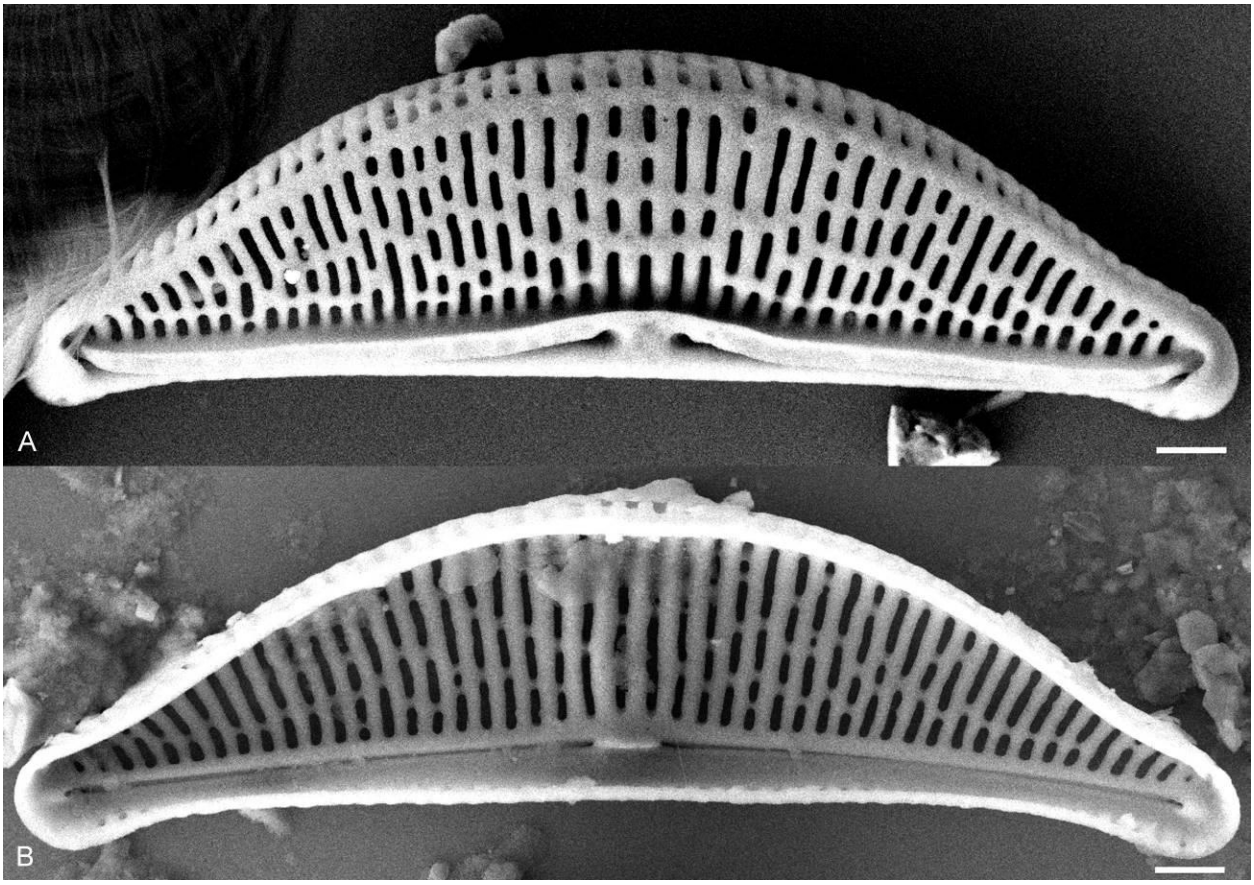

Figure 4.131. Scanning electron micrographs of *Halamphora coloradiana* Amph025. **A.** External whole valve. **B.** Internal whole valve. Scale bars = 1 µm.

HALAMPHORA CLADE H

Halamphora sp. nov. Amph163 (Figs 4.133, 4.134)

Valves are narrowly semi-elliptical and strongly dorsiventral. The dorsal margin is smoothly arched, the ventral margin is straight to slightly convex. The valve ends are protracted narrowly rounded to subcapitate and ventrally deflected. Valve length 18.0–29.0 µm, valve breadth 3.5–4.0 µm. The raphe is slightly arched with straight raphe branches and straight proximal raphe ends. The axial area is narrow dorsally and centrally expanded ventrally. The dorsal striae are finely areolate, parallel through the central

portion of the valve, becoming radiate towards the apices. The ventral striae are fine and continuous along the length of the valve. Striae number 21–23 in 10 µm.

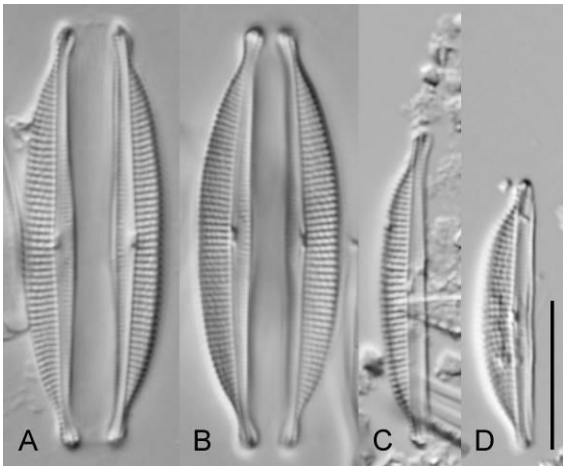

Figure 4.132. A–D. Light micrographs of *Halamphora sp. nov.* Amph163 showing observed size range. Scale bar = 10 µm.

In SEM, externally, the raphe branches are straight with nearly straight and dilated proximal ends and weakly dorsally deflected distal ends. The dorsal raphe ledge is broad and continuous along the length of the valve. The dorsal striae are composed of numerous small elongate areolae. A dorsal marginal ridge is not present. The ventral striae are composed of a single row of small elongate areolae and are continuous along the length of the valve. The ventral axial area is expanded through the central portion of the valve. Internally, the proximal raphe ends terminate in a small fused central helictoglossa. The dorsal and ventral striae are areolate. An axial band of silica runs the longitudinal length of the valve.

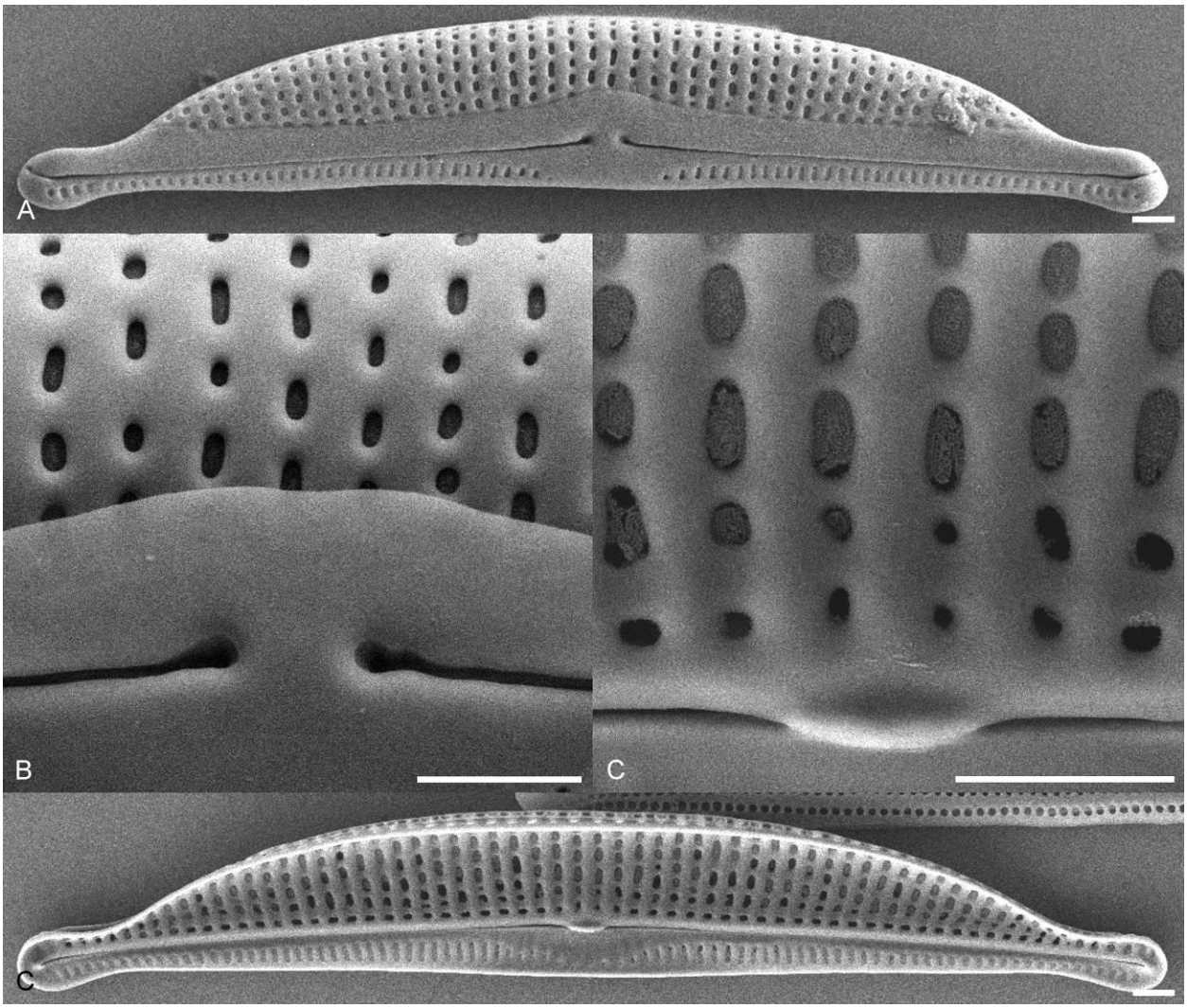

Figure 4.133. Scanning electron micrographs of *Halamphora sp. nov.* Amph163. **A.** External whole valve. **B.** Detail of external valve center. **C.** Detail of internal valve center. **D.** Internal whole valve. Scale bar = 10 µm.

Halamphora sp. nov. Amph110 (Figs 4.135, 4.136)

Valves are semi-elliptical and dorsiventral. The dorsal margin is smoothly arched, the ventral margin is straight. The valve ends are protracted, subcapitate and ventrally deflected. Valve length 23.0–30.0 µm, valve breadth 4.5–5.5 µm. The raphe is weakly arched with straight raphe branches. The proximal raphe ends are slightly dilated and weakly dorsally deflected. The axial area is narrow dorsally, slightly centrally expanded ventrally. The dorsal striae are areolate, parallel at the valve center, becoming

radiate towards the apices. The ventral striae are composed of a single row of small areolae and are continuous along the length of the valve. Striae number 17–19 in 10 µm.

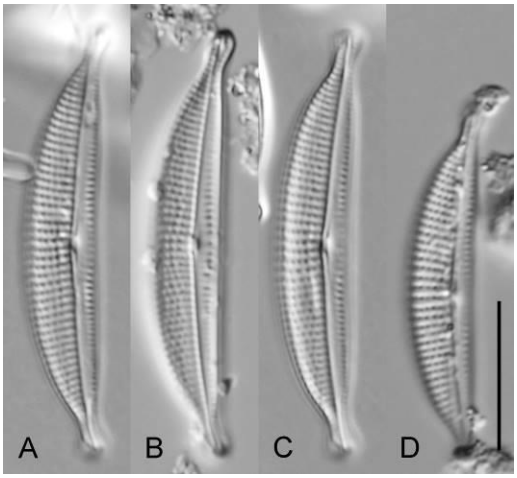

Figure 4.134. A–D. Light micrographs of *Halamphora sp. nov.* Amph110 showing observed size range. Scale bar = 10 µm.

In SEM, externally, the raphe branches are straight with dorsally deflected proximal and distal ends. The dorsal raphe ledge is broad and continuous along the length of the valve. The dorsal striae are composed of numerous small round areolae. A dorsal marginal ridge is not present. The ventral striae are composed of a single row of small round to elongate areolae. The ventral axial area expands from the apices to the valve center creating a semi-lanceolate hyaline area. Internally, the proximal raphe ends terminate in a small fused central helictoglossa. The dorsal and ventral striae are areolate. An axial band of silica runs the longitudinal length of the valve.

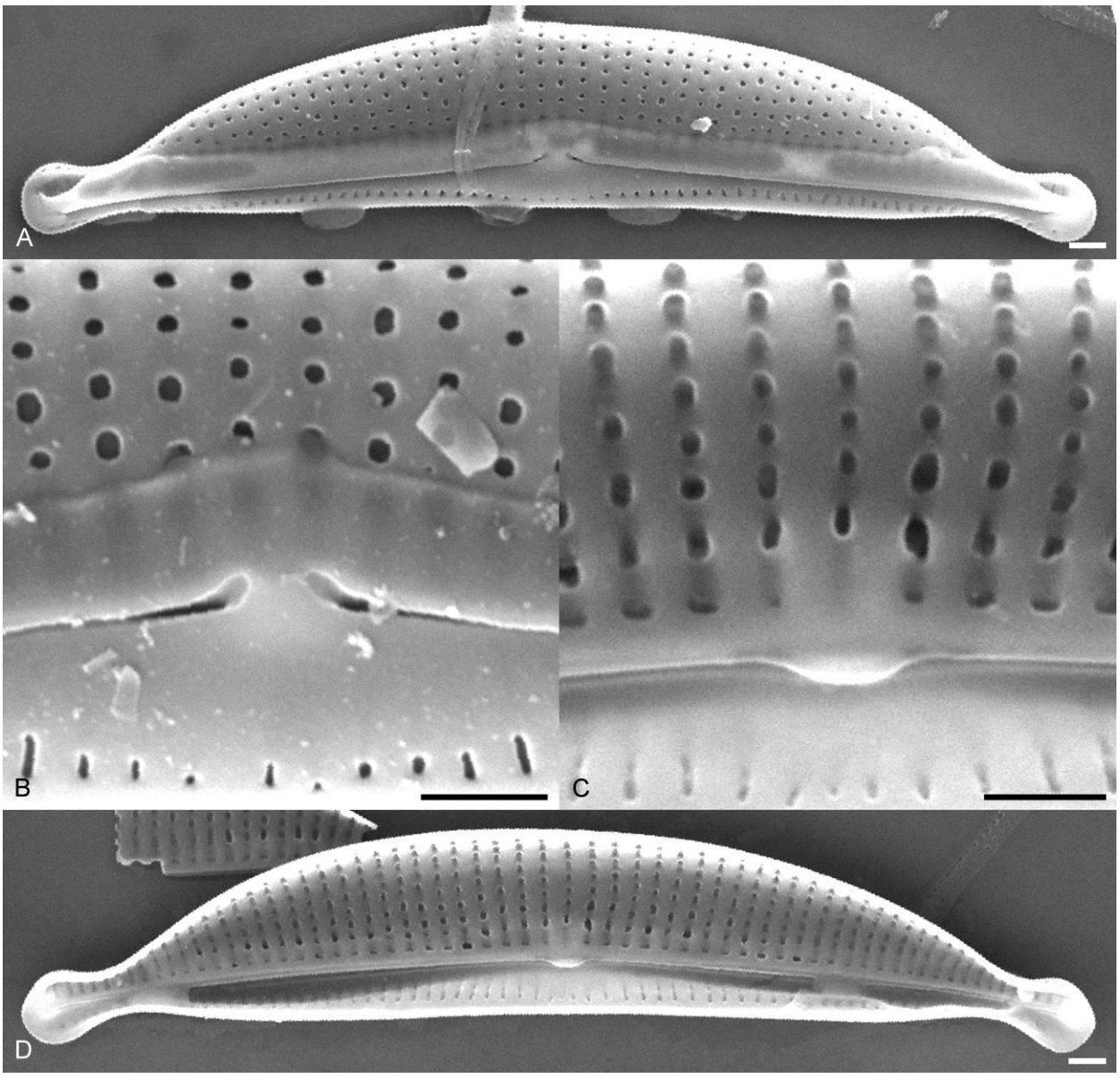

Figure 4.135. Scanning electron micrographs of *Halamphora sp. nov.* Amph110. **A.** External whole valve. **B.** Detail of external valve center. **C.** Detail of internal valve center. **D.** Internal whole valve. Scale bars = 1 µm.

Halamphora sp. nov. Amph086 (Figs 4.137, 4.138)

Valves narrowly semi-elliptical and weakly dorsiventral. The dorsal margin is smoothly arched the ventral margin is straight. The valve ends are narrowly rounded and ventrally deflected. Valve length 21.0–37.0 µm, valve breadth 4.0–4.5 µm. The raphe is near centrally positioned on the valve face. The raphe is arched with closely terminating straight proximal ends. The axial area is narrow dorsally and

centrally expanded ventrally. The dorsal striae are fine, although appearing slightly more widely spaced at the valve center. The dorsal striae are parallel near the valve center, becoming radiate towards the apices. The ventral striae are extremely fine and continuous through the central portion of the valve, Striae number 26–28 in 10 µm.

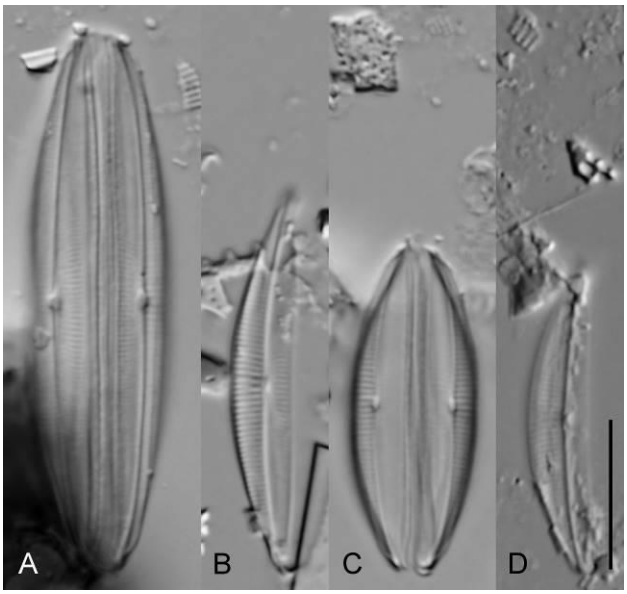

Figure 4.136. A–D. Light micrographs of *Halamphora sp. nov.* Amph086 showing observed size range. Scale bar = 10 µm.

In SEM, externally, the proximal and distal raphe ends are deflected dorsally. The raphe ledge is broad and continuous along the length of the valve. The dorsal striae are biseriate near the raphe ledge, becoming irregularly uni- to biseriate as they progress towards the margin. A marginal ridge is not present. The ventral valve is broad. The ventral striae are finely uniseriate. The ventral axial area is narrow near the apices, becoming expanded at the valve center. Internally, the proximal raphe ends terminate in a small fused central helictoglossa. The dorsal striae are biseriate and separated by thin virgae. The central dorsal virgae are slightly thickened.

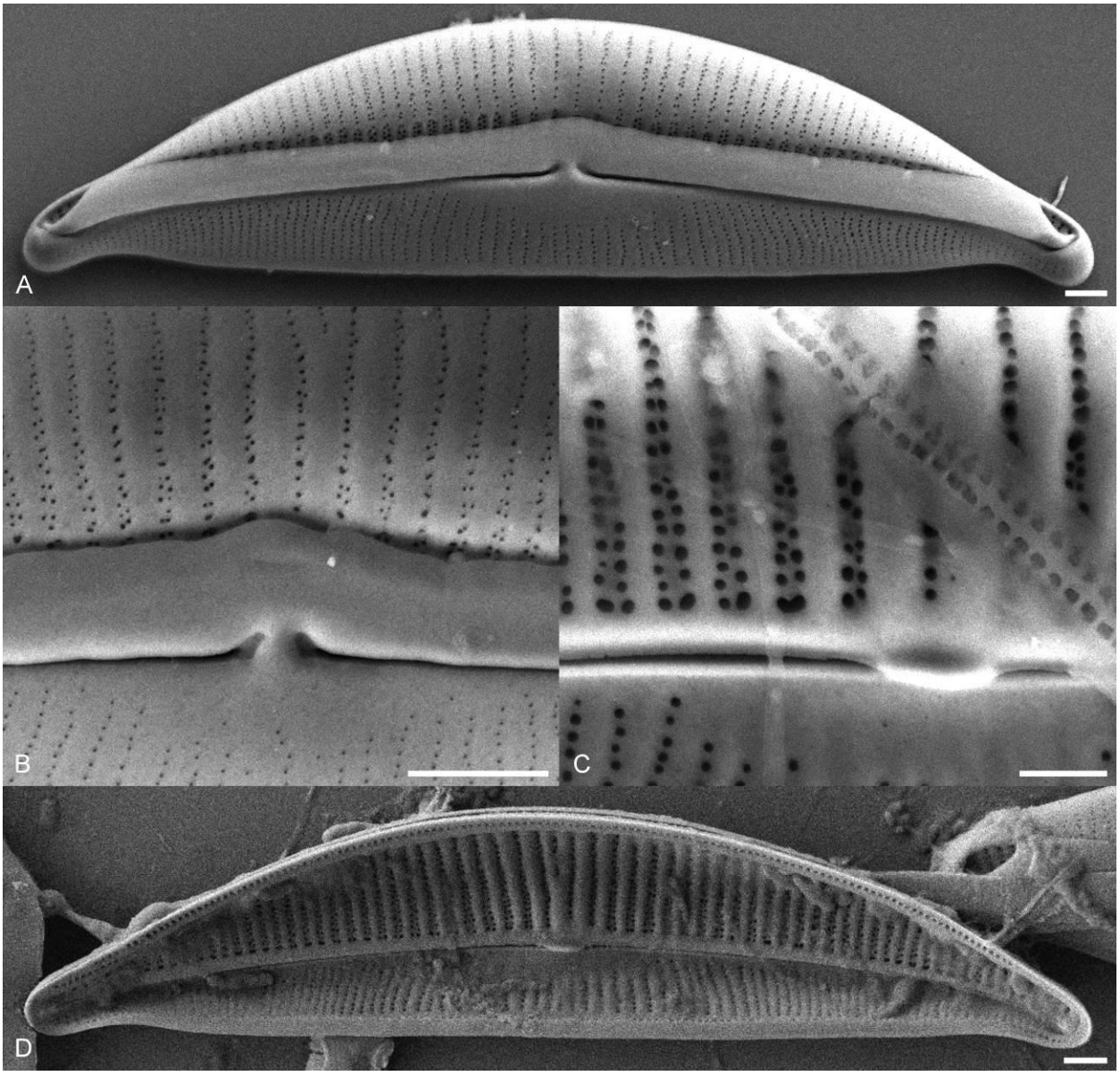

Figure 4.137. Scanning electron micrographs of *Halamphora sp. nov.* Amph086. **A.** External whole valve. **B.** Detail of external valve center. **C.** Detail of internal valve center. **D.** Internal whole valve. Scale bars = 1 µm.

Halamphora sp. nov. Amph109 (Figs 4.139, 4.140)

Valves narrowly semi-elliptical and weakly dorsiventral. The dorsal margin is shallowly arched, the ventral margin is straight. The valve ends are narrowly rounded and ventrally deflected. Valve length 14.0–19.0 µm, valve breadth 2.5–3.0 µm. The raphe is slightly arched with straight closely terminating proximal ends. The raphe is positioned near the valve center creating a broad ventral valve. The dorsal

axial area is narrow, the ventral axial area is difficult to distinguish due to the fine ventral striae. The dorsal striae are fine, parallel at the valve center, becoming radiate towards the apices. The ventral striae are difficult to resolve in the LM. Striae number 24–26 in 10 µm.

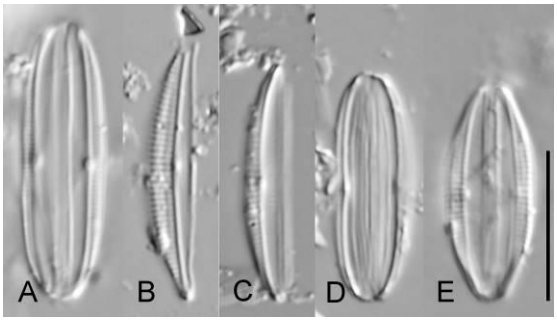

Figure 4.138. A–E. light micrographs of *Halamphora sp. nov.* Amph109 showing observed size range. Scale bar = 10 µm.

In SEM, externally, the proximal raphe ends are slightly dorsally deflected, the distal ends are dorsally deflected past the dorsal raphe ledge. The dorsal raphe ledge is well developed and is continuous through the central portion of the valve. The dorsal striae are composed of numerous more or less round areolae. Close examination shows that each areola is internally biseriate. A dorsal marginal ridge is not present. The ventral striae are extremely finely uniseriate and continuous through the central portion of the valve. The ventral axial area is narrow near the apices and expanding near the valve center to form a semi-elliptical ventral hyaline area. Internally, the proximal raphe ends terminate in a fused central helictoglossa. The dorsal striae are biseriate. The central dorsal virgae are thickened.

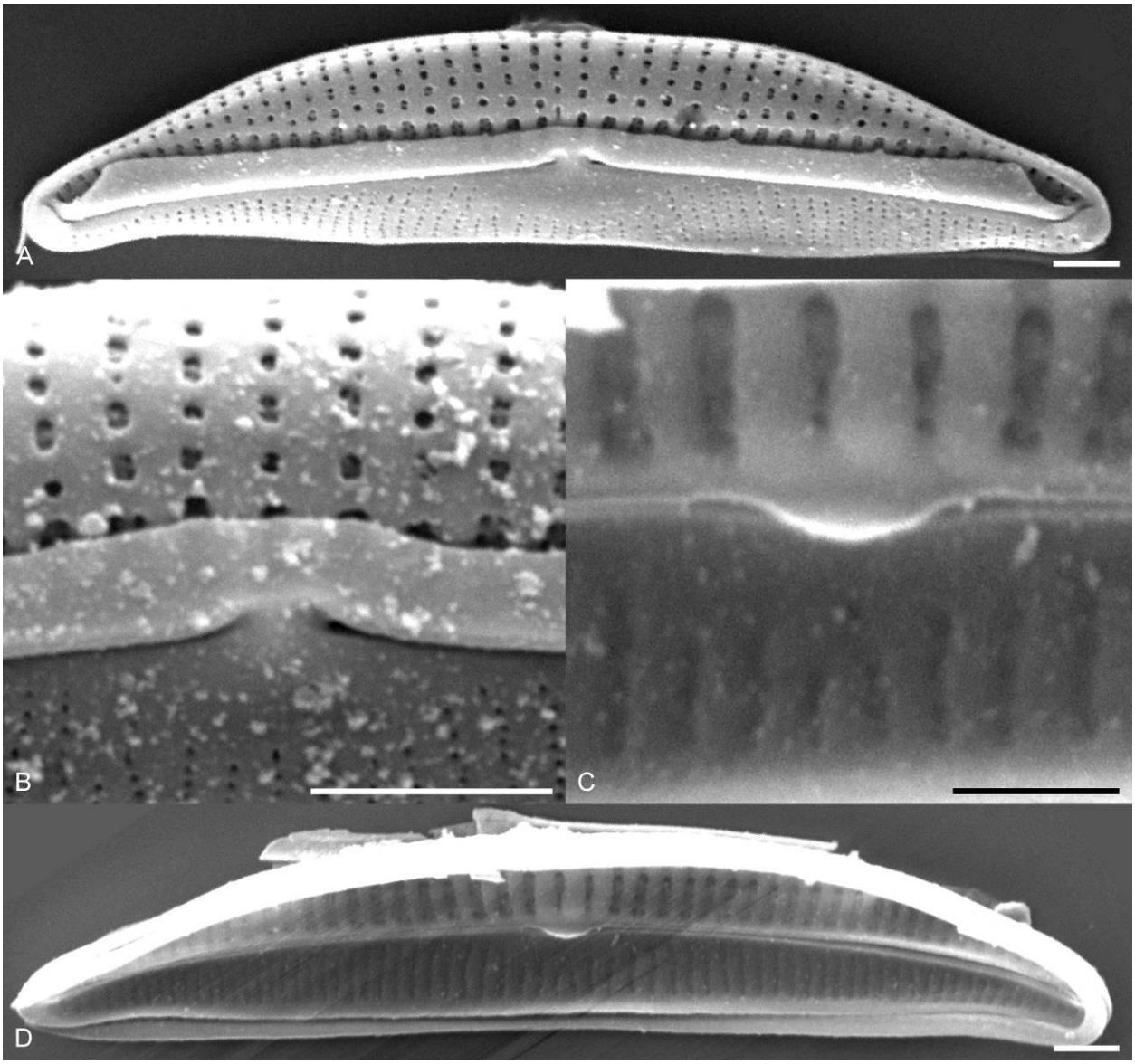

Figure 4.139. Scanning electron micrographs of *Halamphora sp. nov.* Amph109. **A.** External whole valve. **B.** Detail of external valve center. **C.** Detail of internal valve center. **D.** Internal whole valve. Scale bar = 1 µm.

Halamphora sp. nov. Amph112 (Figs 4.141, 4.142)

Valves semi-elliptical to nearly elliptical and weakly dorsiventral. The dorsal margin is arched and somewhat flattened over the valve center in some specimens, the ventral margin is convex. The valve ends are weakly protracted, narrowly rounded and ventrally deflected. Valve length 13.0–17.0 µm, valve breadth 3.0–3.5 µm. The raphe is centrally to slightly dorsally positioned on the valve face. The raphe is

arched with straight to slightly dorsally deflected proximal ends. The axial area is narrow on the dorsal side, centrally expanded on the ventral side. The dorsal striae are fine and do not appear areolate. The dorsal striae are distinctly more widely spaced at the valve center. The ventral striae are very fine and are continuous through the central portion of the valve. Striae number 23–26 in 10 µm.

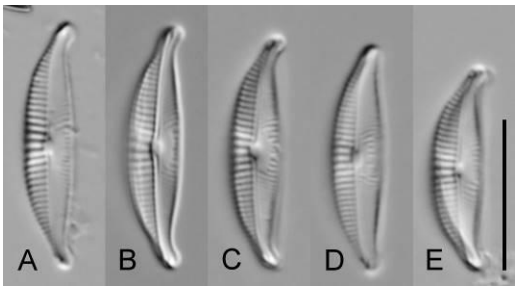

Figure 4.140. A–E. Light micrographs of *Halamphora sp. nov.* Amph112 showing observed size range. Scale bar = 10 µm.

In SEM, externally, the raphe branches are straight with dorsally deflected proximal and distal ends. The raphe ledge is well developed and is continuous along the length of the valve. The dorsal striae are somewhat irregularly biseriate and are crossed, externally, by a single band of silica running the length of the valve just dorsal of the raphe ledge. The central dorsal virgae are thickened to a degree that the central striae appear areolate in some taxa due to siliceous in-filling. The ventral striae are finely uniseriate. The ventral axial area is narrow near the apices, expanding near the valve center. Internally, the proximal raphe ends terminate in a large fused central helictoglossa. The central dorsal virgae are distinctly thickened and fused near the central area.

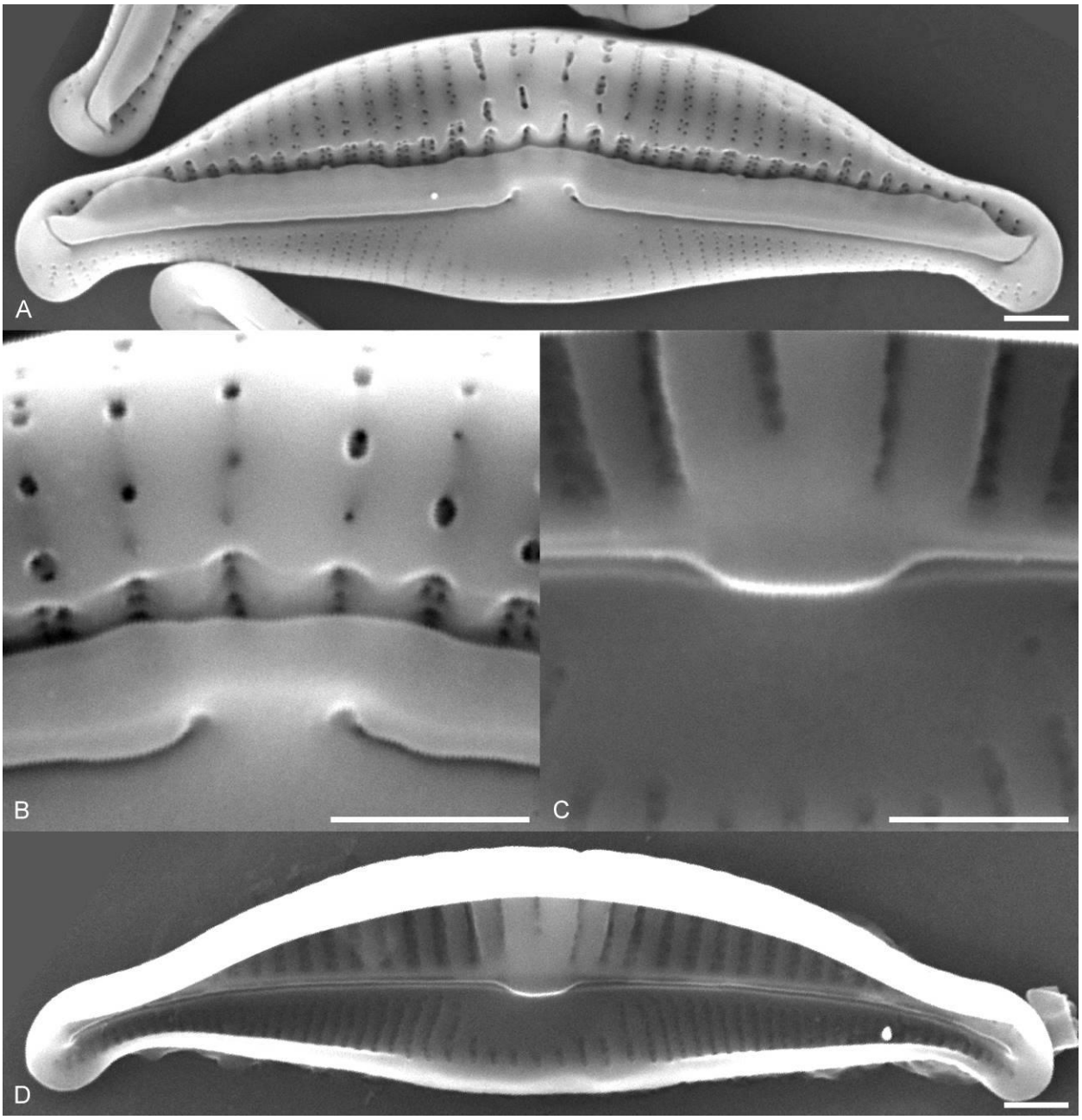

Figure 4.141. Scanning electron micrographs of *Halamphora sp. nov.* Amph112. **A.** External whole valve. **B.** Detail of external valve center. **C.** Detail of internal valve center. **D.** Internal whole valve. Scale bar = 1 µm.

HALAMPHORA CLADE I

Halamphora sp. nov. Amph027/029 (Figs 4.143, 4.144)

Valves are narrowly semi-elliptical and dorsiventral. The dorsal margin is arched, somewhat flattened over the central valve in some specimens, the ventral margin is straight to slightly convex. The valve ends are protracted, subcapitate and slightly ventrally deflected. Valve length 16–23 µm, valve breadth 3.0–4.0 µm. The raphe is arched with straight raphe branches. The proximal raphe ends appear straight to slightly deflected dorsally. The dorsal axial area is narrow, the ventral axial area is expanded at the central valve. The dorsal striae are coarsely areolate, parallel through the valve center, becoming radiate towards the apices. The ventral striae are fine and continuous across the valve center. Striae number 17–23 in 10 µm.

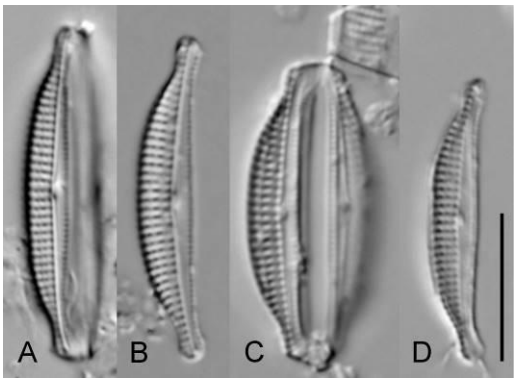

Figure 4.142. A–D. Light micrographs of *Halamphora sp. nov.* Amph027/029 showing observed size range. Scale bar = 10 µm.

In SEM, externally, the proximal raphe ends are slightly deflected dorsally at the terminal pores, the distal ends are weakly dorsally deflected. The raphe ledge is broad and continuous across the valve center. The dorsal striae are composed of many small round to slightly elongate areolae. A dorsal marginal ridge is not present. The ventral striae are continuous across the valve center and are composed of a single row of elongate areolae. Internally, the proximal raphe ends terminate in a fused central helictoglossa. The dorsal and ventral striae are areolate.

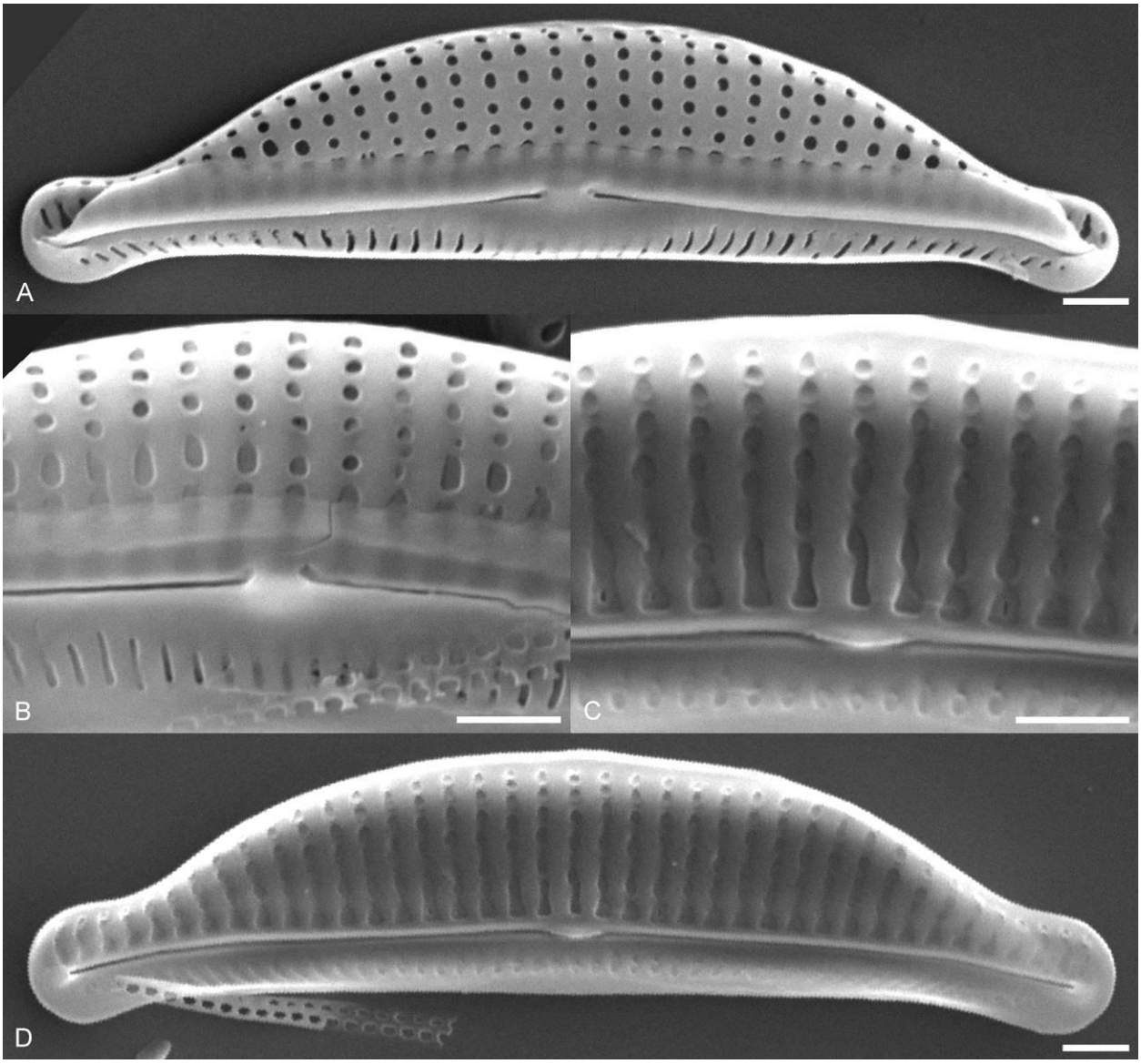

Figure 4.143. Scanning electron micrographs of *Halamphora sp. nov.* Amph027/029. **A.** External whole valve. **B.** Detail of external valve center. **C.** Detail of internal valve center. **D.** Internal whole valve. Scale bars = 1 µm.

Halamphora sp. nov. Amph080 (Figs 4.145, 4.146)

Valves narrowly semi-elliptical and strongly dorsiventral. The dorsal margin is smoothly arched to flattened over the valve center in larger specimens. The ventral margin is straight to slightly concave. The valve ends are protracted, narrowly rounded to subcapitate in larger specimens and ventrally deflected. Valve length 15.0–33.0 µm, valve breadth 3.0–4.0 µm. The raphe is weakly arched with

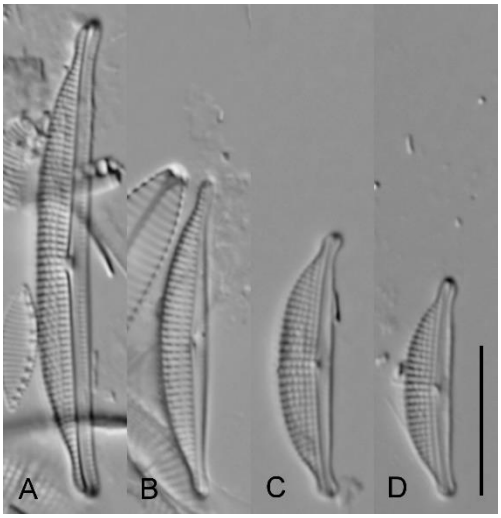

Figure 4.144. A–D. Light micrographs of *Halamphora sp. nov.* Amph080 showing observed size range. Scale bar = 10 µm.

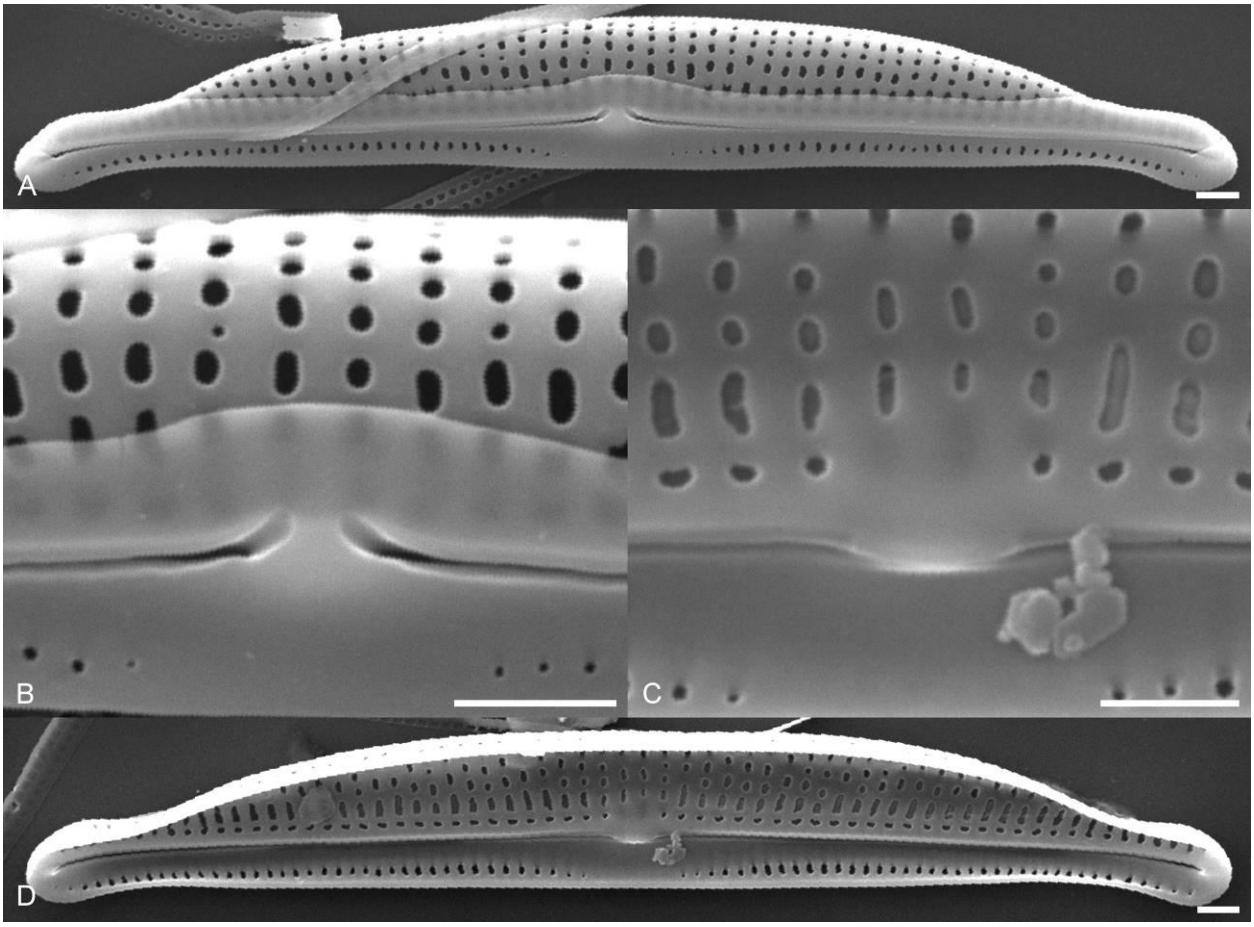

Figure 4.145. Scanning electron micrographs of *Halamphora sp. nov.* Amph080. **A.** External whole valve. **B.** Detail of external valve center. **C.** Detail of internal valve center. **D.** Internal whole valve. Scale bars = 1 µm.

dorsally deflected proximal raphe ends. The axial area is narrow throughout. The dorsal striae are finely areolate, parallel through the central valve and becoming radiate near the apices. The ventral striae are fine and do not continue through the central valve. Striae number 20–22 in 10 µm.

In SEM, externally, the proximal and distal raphe ends are deflected dorsally. The dorsal raphe ledge is broad and continuous through the central valve. The dorsal striae are composed of several round to ovoid areolae. A marginal ridge is not present. The ventral striae do not continue through the central valve and are composed of a single row of small areolae. Internally, the proximal raphe ends terminate in a fused central helictoglossa. The dorsal striae are areolate. A axial band of silica runs the longitudinal length of the valve.

Halamphora sp. nov. Amph162/167 (Figs 4.147, 4.148)

Valves are narrowly semi-elliptical and dorsiventral. The dorsal margin is arched at the apices somewhat flattened over the valve center, the ventral margin is straight. The valve ends are protracted, rounded and ventrally deflected. Valve length 27.0–28.0 µm, valve breadth 4.5–5.0 µm. The raphe is arched with straight proximal raphe ends. The axial area is narrow dorsally, expanded ventrally near the valve center. A dorsal longitudinal line is visible in many specimens. The dorsal striae are distinctly areolate and weakly radiate throughout. The ventral striae are fine, marginally positioned and continuous through the central valve. Striae number 18 in 10 µm.

In SEM, externally, the proximal raphe ends are slightly dilated and dorsally defected, the distal ends are strongly deflected dorsally. The dorsal raphe ledge is moderately broad and continuous along the length of the valve. The dorsal striae are composed of many small round to ovoid areolae. A dorsal marginal ridge is not present. The ventral striae are continuous through the central valve and are composed of a single row of small areolae. The ventral axial area expands as it near s the valve center. Internally, the proximal raphe ends terminate in a small fused central helictoglossa. The dorsal striae are areolate, separated by distinct virgae. A axial band of silica runs the longitudinal length of the dorsal valve.

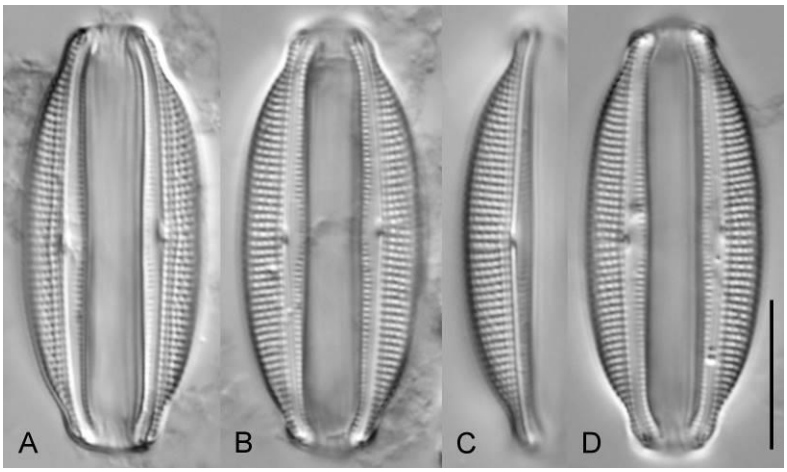

Figure 4.146. A–D. Scanning electron micrographs of *Halamphora sp. nov.* Amph162/167 showing observed size range. Scale bar = 10 µm.

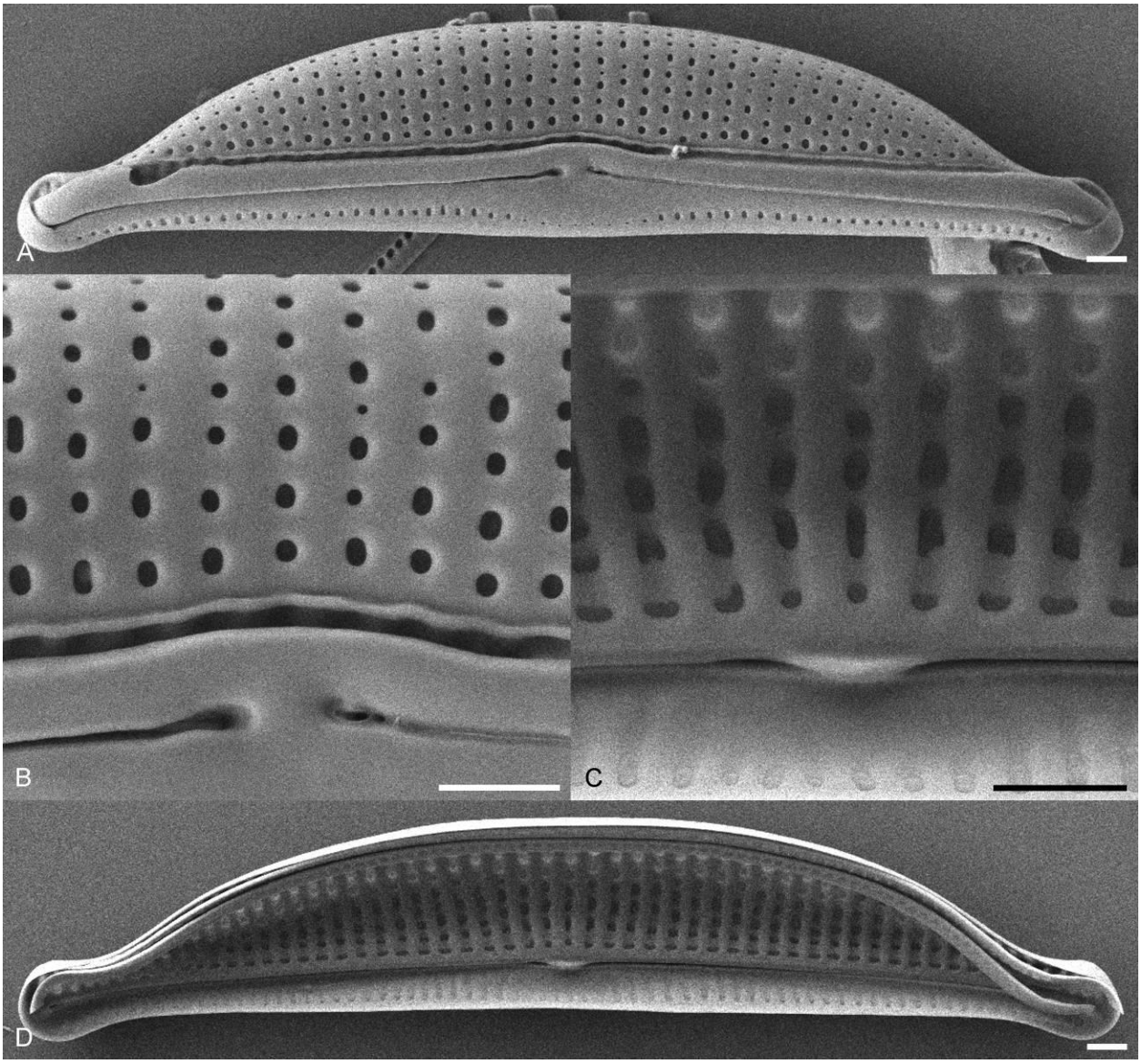

Figure 4.147. Scanning electron micrographs of *Halamphora sp. nov.* Amph162/167. **A.** External whole valve. **B.** Detail of external valve center. **C.** Detail of internal valve center, **D.** Internal whole valve. Scale bars = 1 µm.

Halamphora sp. nov. Amph030/050 (Figs 4.149, 4.150)

Valves broadly semi-elliptical and strongly dorsiventral. The dorsal margin is arched at the apices flattened over the valve center, the ventral margin is straight to slightly concave. The valve ends are strongly protracted, rounded to subcapitate and slightly ventrally deflected. Valve length 34.0–51.0 µm, valve breadth 7.0–8.0 µm. The raphe is arched with straight raphe branches. The proximal raphe ends

appear straight to slightly deflected dorsally. The axial area is narrow dorsally, expanded ventrally at the valve center. A dorsal longitudinal line is visible running the length of the valve near the axial area. The dorsal striae are areolate, parallel over the valve center, becoming radiate near the apices. The ventral striae are fine and continuous through the central valve. Striae number 15–17 in 10 µm.

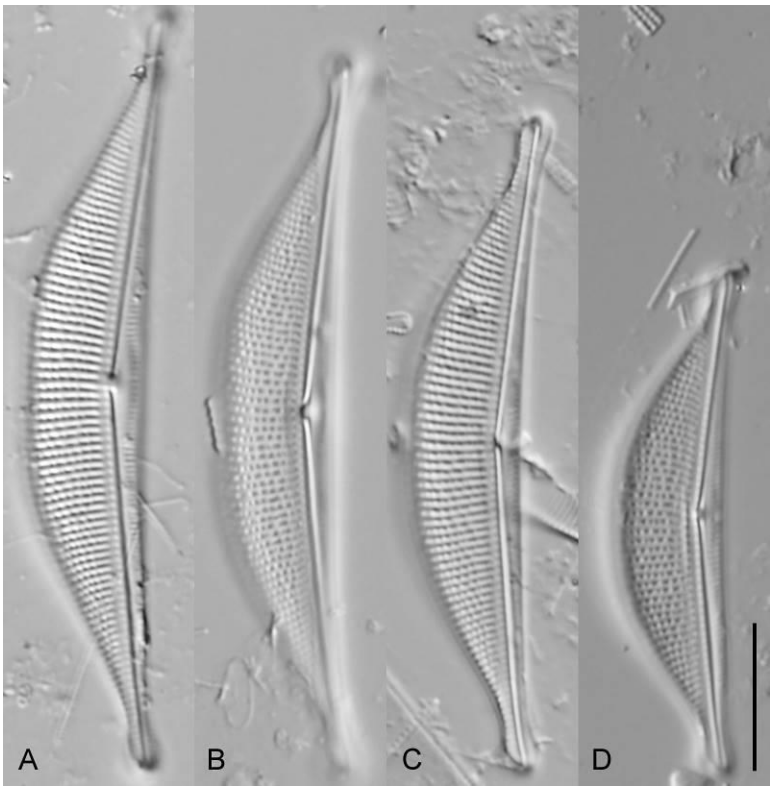

Figure 4.148. A–D. Light micrographs of *Halamphora sp. nov.* Amph030/050 showing observed size range. Scale bar = 10 µm.

In SEM, externally, the proximal raphe ends gently deflect dorsally, the distal ends are strongly deflected dorsally. The dorsal raphe ledge is continuous through the valve center. The dorsal striae are composed of many small round to ovoid areolae. A dorsal marginal ridge is not present. The ventral striae fine, continuous through the valve center and composed of a single row of elongate areolae. The ventral axial are is narrow near the apices, becoming expanded at the valve center. Internally, the proximal raphe ends terminate in a fused central helictoglossa. The dorsal striae are areolate. An axial band of silica runs the longitudinal length of the valve.

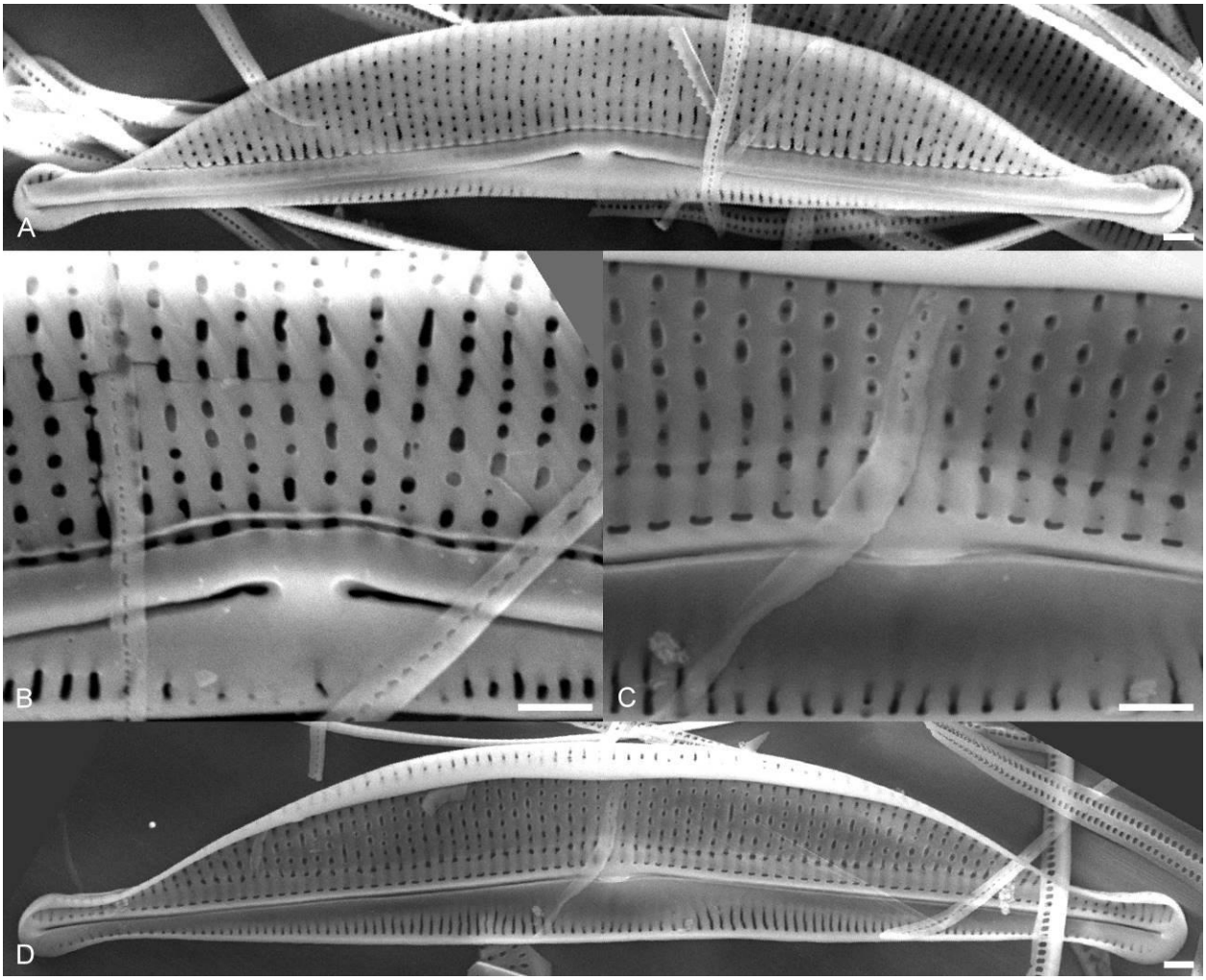

Figure 4.149. Scanning electron micrographs of *Halamphora sp. nov.* Amph030/050. **A.** External whole valve. **B.** Detail of external whole valve. **C.** Detail of internal valve center. **D.** Internal whole valve. Scale bar = 1 µm.

HALAMPHORA CLADE J

Halamphora pertusa Stepanek & Kociolek Amph121/123 (Figs 4.151, 4.152)

Valves narrowly semi-elliptical and dorsiventral. The dorsal margin is shallowly arched, the ventral margin is straight to slightly concave. The valve ends are protracted, narrowly rounded to subcapitate and ventrally deflected. Valve length 20.0–43.0 µm, valve breadth 4.0–6.0 µm. The raphe is weakly arched with straight raphe branches and proximal raphe ends. The axial area is narrow throughout dorsally, centrally expanded on the ventral side. The dorsal striae are coarsely areolate, parallel through

the central portion of the valve, becoming radiate near the apices. The ventral striae are fine and composed of a single row of small areolae. The ventral striae are more or less continuous through the central portion of the valve. Dorsal striae number 17–19 in 10 µm, ventral striae number 28–30 in 10 µm.

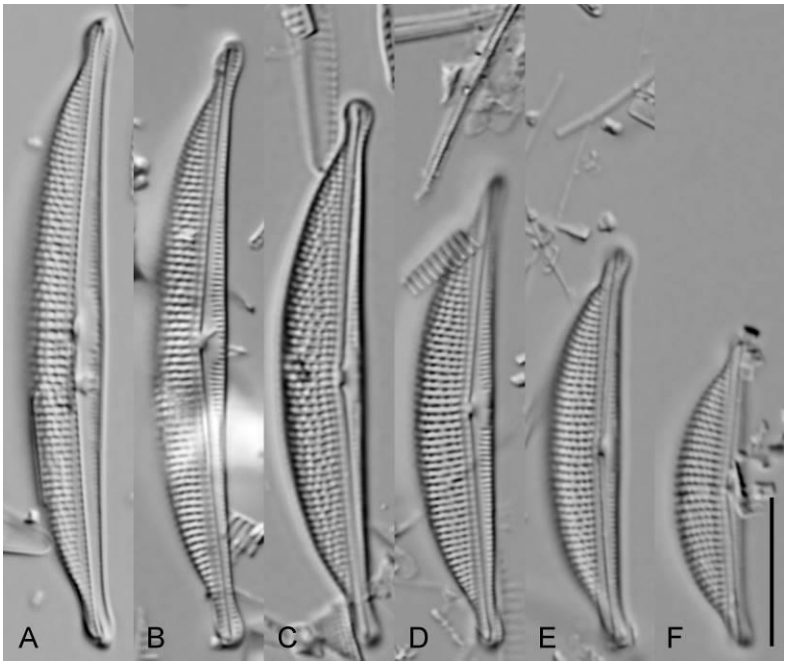

Figure 4.150. A–F. Light micrographs of *Halamphora pertusa* Amph121/123 showing observed size range. Scale bar = 10 µm.

In SEM, externally, the raphe branches are straight with dorsally deflected proximal and distal ends. The dorsal raphe ledge is well developed and continuous along the length of the valve. A dorsal marginal ridge is not present. The dorsal striae are composed of numerous round to elongate areolae separated by thick virgae. Each dorsal areolae is internally biseriate, a feature that is most distinct in the axial areolae. The ventral striae are composed of a single row of small areolae, more or less continuous through the central portion of the valve depending on the specimen imaged. The ventral axial area is centrally expanded. Internally, the proximal raphe ends terminate in a small fused central helictoglossa. The dorsal striae are separated by thick virgae crossed by thin vimines to create small biseriate areolae. An axial band of silica runs the longitudinal length of the valve.

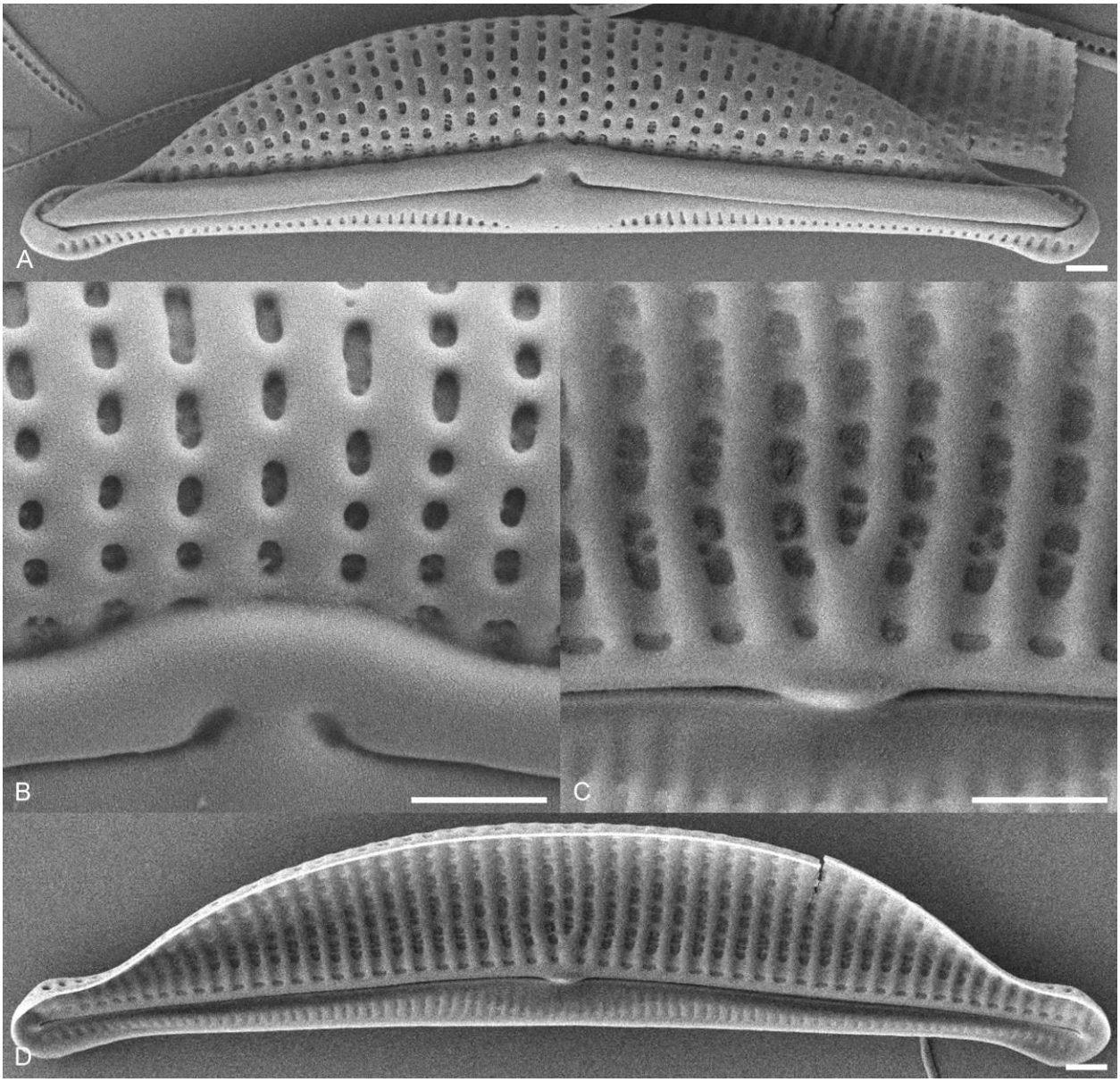

Figure 4.151. Scanning electron micrographs of *Halamphora pertusa* Amph121/123. **A.** External whole valve. **B.** Detail of external valve center. **C.** Detail of internal valve center. **D.** Internal whole valve. Scale bar = 1 µm.

Halamphora subtropica (Wachnicka & Gaiser) Stepanek & Kociolek comb. nov. Amph168 (Figs 4.153, 4.154)

Valves semi-elliptical and strongly dorsiventral. The dorsal margin is smoothly arched, the ventral margin is straight to slightly concave. The valve ends are protracted, narrowly rounded to subcapitate and ventrally deflected. Valve length 12.0–19.0 µm, valve breadth 3.0–4.0 µm. The raphe is

weakly arched with straight branches and proximal ends. The axial area is narrow throughout dorsally and difficult to distinguish ventrally. The dorsal striae are areolate, parallel at the valve center, becoming radiate near the apices. The ventral striae are difficult to image in the LM. Striae number 19–20 in 10 µm.

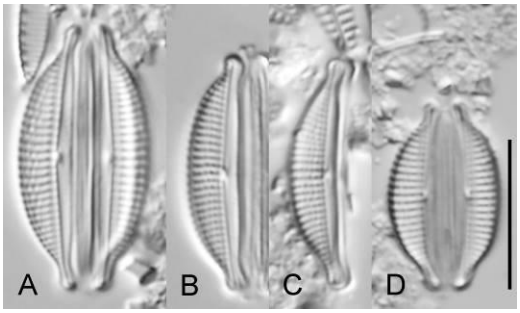

Figure 4.152. A–D. Light micrographs of *Halamphora subtropica* Amph168 showing observed size range. Scale bar = 10 µm.

In SEM, externally, the raphe branches are straight with slightly dorsally deflected proximal ends and dorsally deflected distal ends. The dorsal raphe ledge is well developed and continuous along the length of the valve. The dorsal striae composed of numerous relatively large round to elongate areolae. A dorsal marginal ridge is not present. The ventral striae are composed of a single row of small elongate areolae and are more or less continuous through the central portion of the valve depending on the specimen imaged. The ventral axial area is narrow near the apices, expanding at the valve center. Internally, the proximal raphe ends terminate in a small fused central helictoglossa. The dorsal striae are separated by virgae crossed by thin vimines to produce round to elongate areolae. An axial band of silica runs the longitudinal length of the valve.

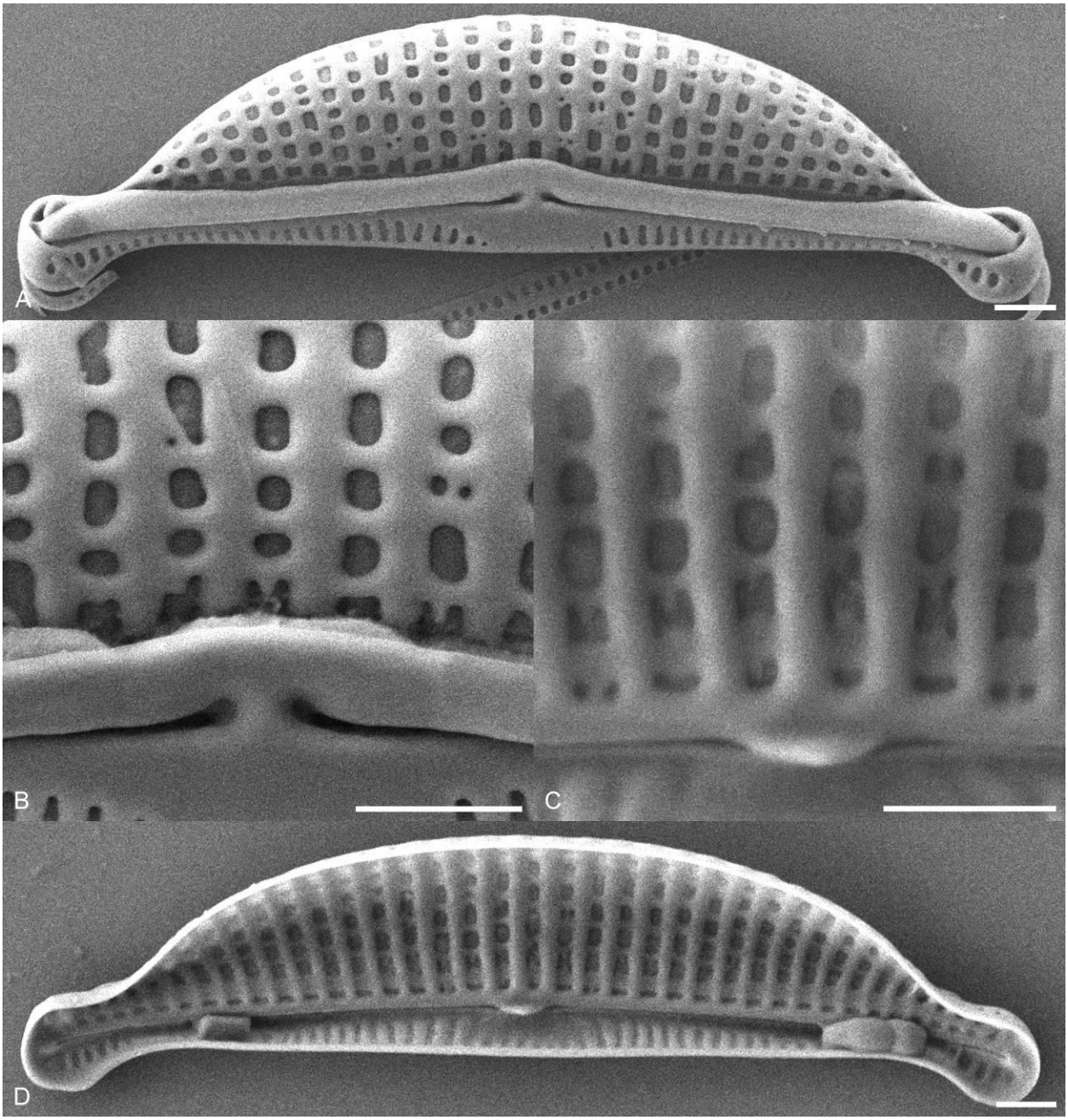

Figure 4.153. Scanning electron micrographs of *Halamphora subtropica* Amph168. **A.** External whole valve. **B.** Detail of external valve center. **C.** Detail of internal valve center. **D.** Internal valve center. Scale bars = 1 µm.

Halamphora subtropica (Wachnicka & Gaiser) Stepanek & Kociolek comb. nov. Amph051/054 (Figs 4.155, 4.156)

Valves semi-elliptical and strongly dorsiventral. The dorsal margin is smoothly arched, the ventral margin is straight. The valve ends are protracted, narrowly rounded to subcapitate and ventrally deflected. Valve length 20.0–24.0 µm, valve breadth 3.5–4.5 µm. The raphe is weakly arched with straight branches and proximal ends. The axial area is narrow dorsally and centrally expanded on the ventral side. The dorsal striae are finely areolae and parallel through the central portion of the valve, becoming weakly radiate towards the apices. The ventral striae are fine and appear continuous through the central portion of the valve. Striae number 20-22 in 10 µm.

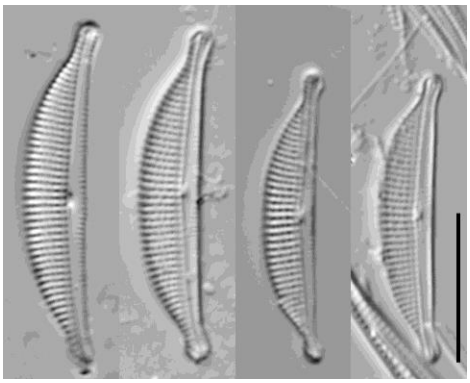

Figure 4.154. A–D. Light micrographs of *Halamphora subtropica* Amph051/054 showing observed size range. Scale bar = 10 µm.

In SEM, externally, the raphe branches are straight with slightly dorsally deflected proximal ends and dorsally deflected distal ends. The dorsal raphe ledge is continuous along the central portion of the valve. The dorsal striae are composed of numerous relatively large areolae separated by virgae. A dorsal marginal ridge is not present. The ventral striae are composed of a continuous row of small elongate areolae. The ventral axial area is centrally expanded. Internally, the proximal raphe ends terminate in a small fused central helictoglossa. The dorsal striae are separated by thick virgae crossed by thin vimines to form round to elongate areolae. The central virgae appear slightly thickened. An axial band of silica runs the longitudinal length of the valve.

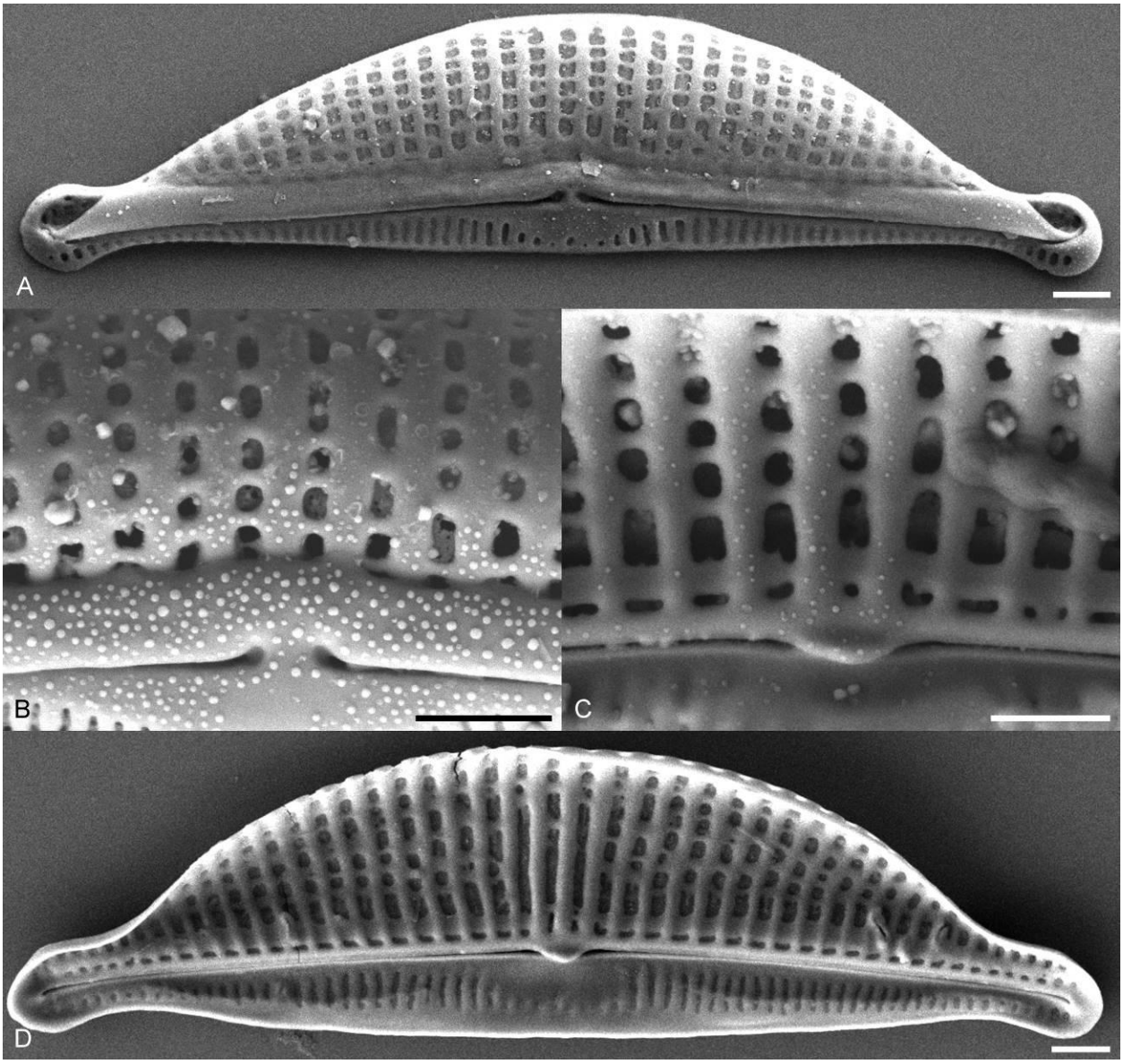

Figure 4.155. Scanning electron micrographs of *Halamphora subtropica* Amph051/054. **A.** External whole valve. **B.** Detail of external valve center. **C.** Detail of internal valve center. **D.** Internal whole valve. Scale bars = 10 µm.

Halamphora sp. nov. Amph158 (Figs 4.157, 4.158)

Valves semi-elliptical and strongly dorsiventral. The dorsal margin is smoothly arched the ventral margin is straight. The valve ends are protracted, narrowly rounded to subcapitate and ventrally deflected. Valve length 16–17 µm, valve breadth 3.0–3.5 µm. The raphe is weakly arched with straight branches and proximal ends. The axial area is narrow dorsally and difficult to distinguish along the ventral side. The

dorsal striae do not appear areolate and are parallel through the central portion of the valve, becoming weakly radiate near the apices. A dorsal marginal ridge is visible in the LM. The ventral striae are difficult to image in the LM. Striae number 20–22 in 10 µm.

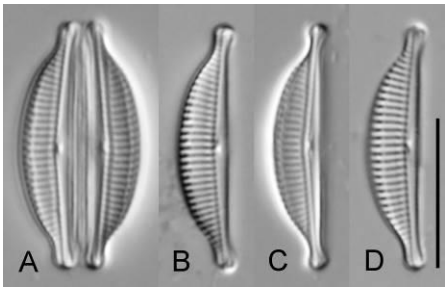

Figure 4.156. A–D. Light micrographs of *Halamphora sp. nov.* Amph158 showing observed size range. Scale bar = 10 µm.

In SEM, externally, the raphe branches are straightly with nearly straight proximal ends and dorsally deflected distal ends. The dorsal raphe ledge is broad and continuous along the length of the valve. The dorsal striae are biseriate separated by relatively thin virgae. A marginal ridge runs the length of the valve. Unlike the striae on the valve face, the mantle striae are irregularly crossed by vimines creating biseriate areolae. The ventral striae are composed of a single continuous row of small elongate areolae. Internally, the proximal raphe ends terminate in a small fused central helictoglossa. The dorsal striae are biseriate and separated by thin virgae. An axial band of silica runs the longitudinal length of the valve.

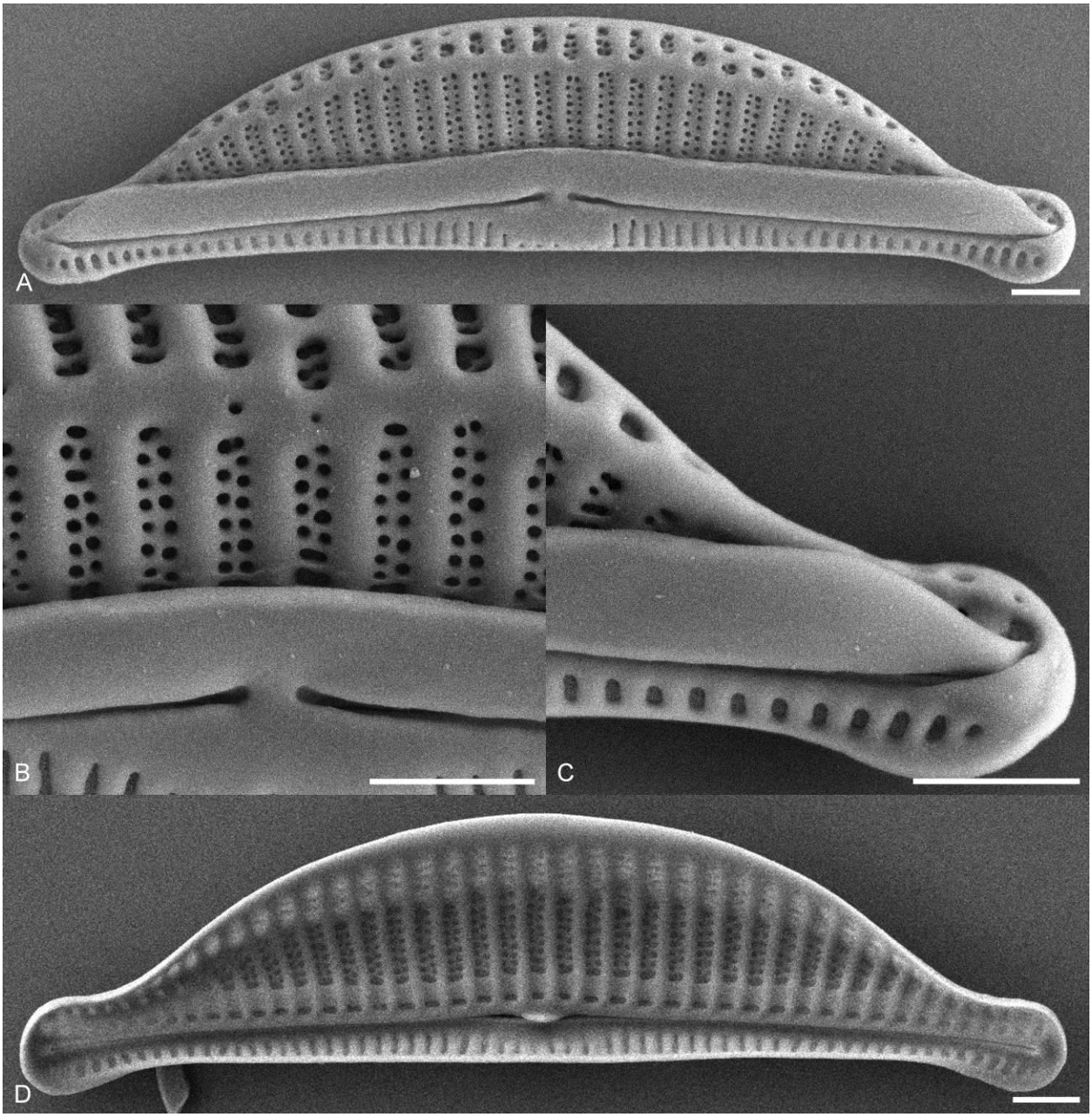

Figure 4.157. Scanning electron micrographs of *Halamphora sp. nov.* Amph158. **A.** External whole valve. **B.** Detail of external valve center. **C.** Detail of external valve end. **D.** Internal whole valve. Scale bars = 10 µm.

Halamphora sp. nov. Amph063 (Figs 4.159, 4.160)

Valves broadly semi-elliptical and strongly dorsiventral. The dorsal margin is smoothly arched, the ventral margin is straight to slightly convex. The valve ends are protracted, subcapitate and ventrally deflected. Valve length 17.0–18.0 µm, valve breadth 4.0–4.5 µm. The raphe is weakly arched with

straight branches and proximal ends. The axial area is narrow dorsally and difficult to distinguished ventrally. The dorsal striae are finely areolate, a feature that is more apparent towards the dorsal margin. The dorsal striae are parallel at the valve center, becoming radiate towards the apices. The ventral striae are difficult to image in the LM. Striae number 21–22 in 10 µm.

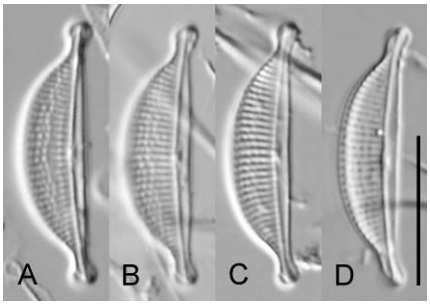

Figure 4.158. A–D. Light micrographs of *Halamphora sp. nov.* Amph063 showing observed size range. Scale bar = 10 µm.

In SEM, externally, the raphe branches are straight with weakly dorsally deflected proximal and distal ends. The dorsal raphe ledge is broad and continuous along the length of the valve. The dorsal striae are biseriate near the axial area, transitioning to small round to elongate areolae towards the dorsal margin. A dorsal marginal ridge cannot be distinguished from the vimines creating the dorsal areolae. The ventral striae are fine and composed of a single row of thin areolae. The ventral striae are continuous through the central portion of the valve. The ventral axial area is narrow near the apices, becoming expanded near the valve center. Internally, the proximal raphe ends terminate in a small fuse central helictoglossa. The dorsal striae are separated by relatively thick virgae. The dorsal striae are biseriate near the axial area before being crossed by thin vimines towards the dorsal margin.

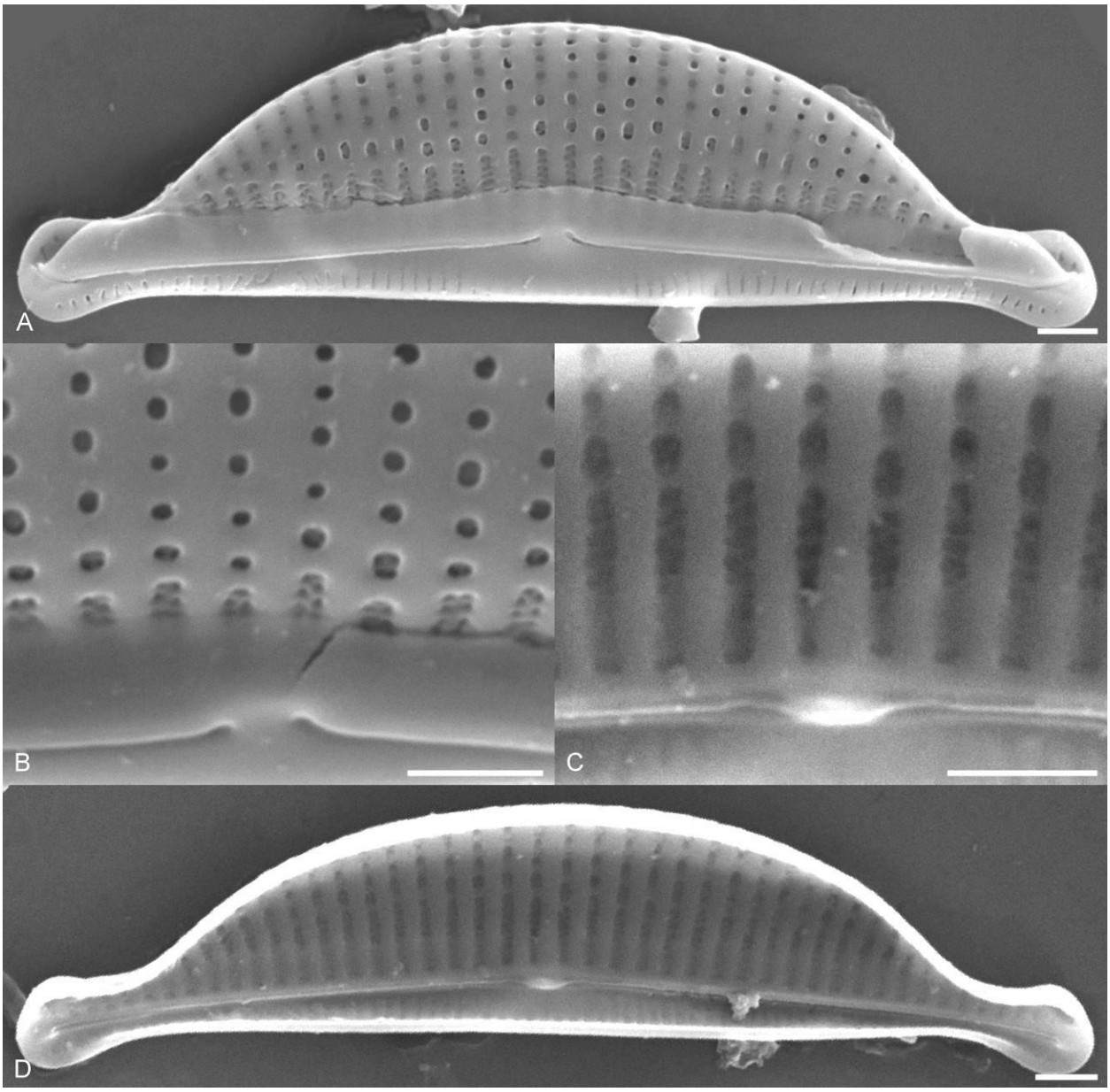

Figure 4.159. Scanning electron micrographs of *Halamphora sp. nov.* Amph063. **A.** External whole valve. **B.** Detail of external valve center. **C.** Detail of internal valve center. **D.** Internal whole valve. Scale bars = 1 µm.

HALAMPHORA CLADE K

Halamphora sp. nov. Amph093 (Figs 4.161, 4.162)

Valves are semi-elliptical and strongly dorsiventral. The dorsal margin is smoothly arched, somewhat flattened over the valve center in larger specimens, the ventral margin is straight to slightly convex. The valve ends are strongly protracted, subcapitate and ventrally deflected. Valve length 43.0–65.0 µm, valve breadth 7.5–10.5 µm. The raphe is arched with straight branches. The proximal raphe ends are straight to slightly dorsally deflected. The axial area is narrow dorsally, appearing slightly expanded near the ventral valve center. A distinct longitudinal line is visible near the dorsal axial area and runs the length of the valve. The dorsal striae are uninterrupted, parallel at the valve center becoming radiate towards the apices. The ventral striae are fine and do not appear continuous through the valve center. Striae number 15–16 in 10 µm.

In SEM, externally, the proximal raphe ends are slightly deflected dorsally, the distal ends are strongly deflected dorsally. The dorsal raphe ledge is broad and continuous through the central valve. The dorsal striae are opened externally as a single uninterrupted foramen slit running from the axial area through the dorsal mantle. The ventral striae are not continuous through the valve center and are composed of a single row of small areolae. Internally, the proximal raphe ends terminate in a fused central helictoglossa. The dorsal striae are biseriate throughout. An axial band of silica runs the longitudinal length of the dorsal valve.

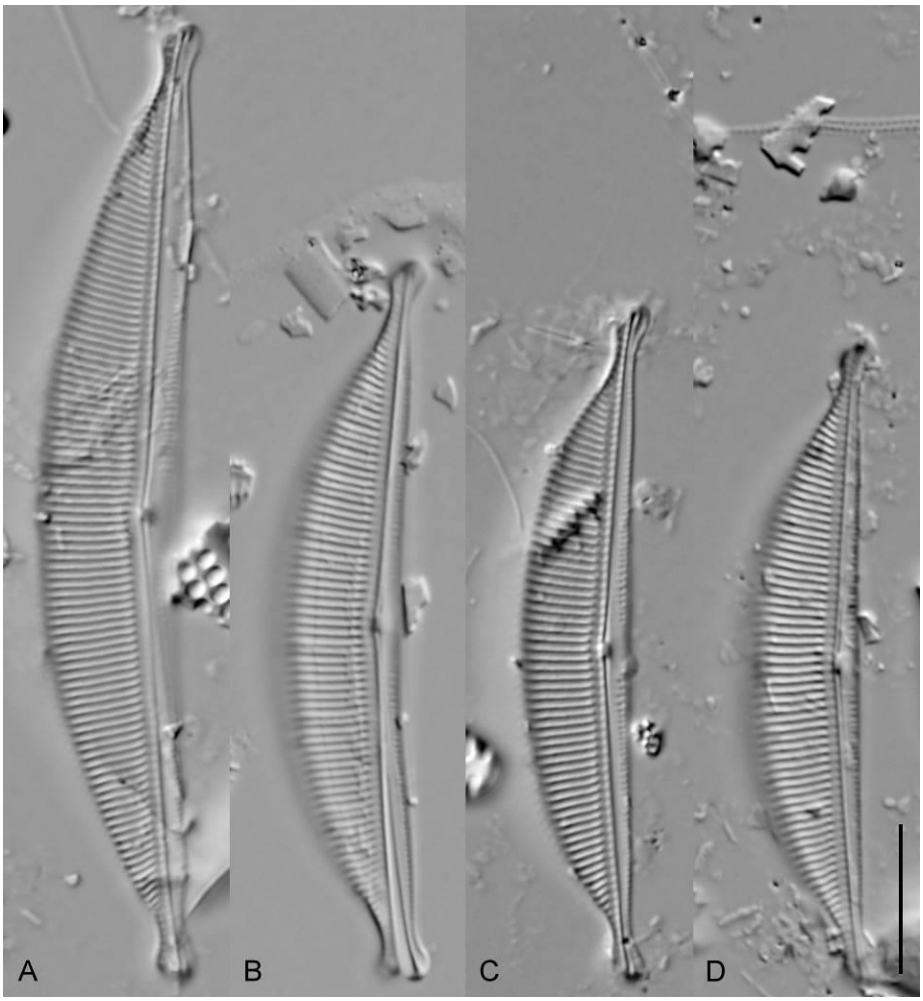

Figure 4.160. A–D. Light micrographs of *Halamphora sp. nov.* Amph093 showing observed size range. Scale bar = 10 µm.

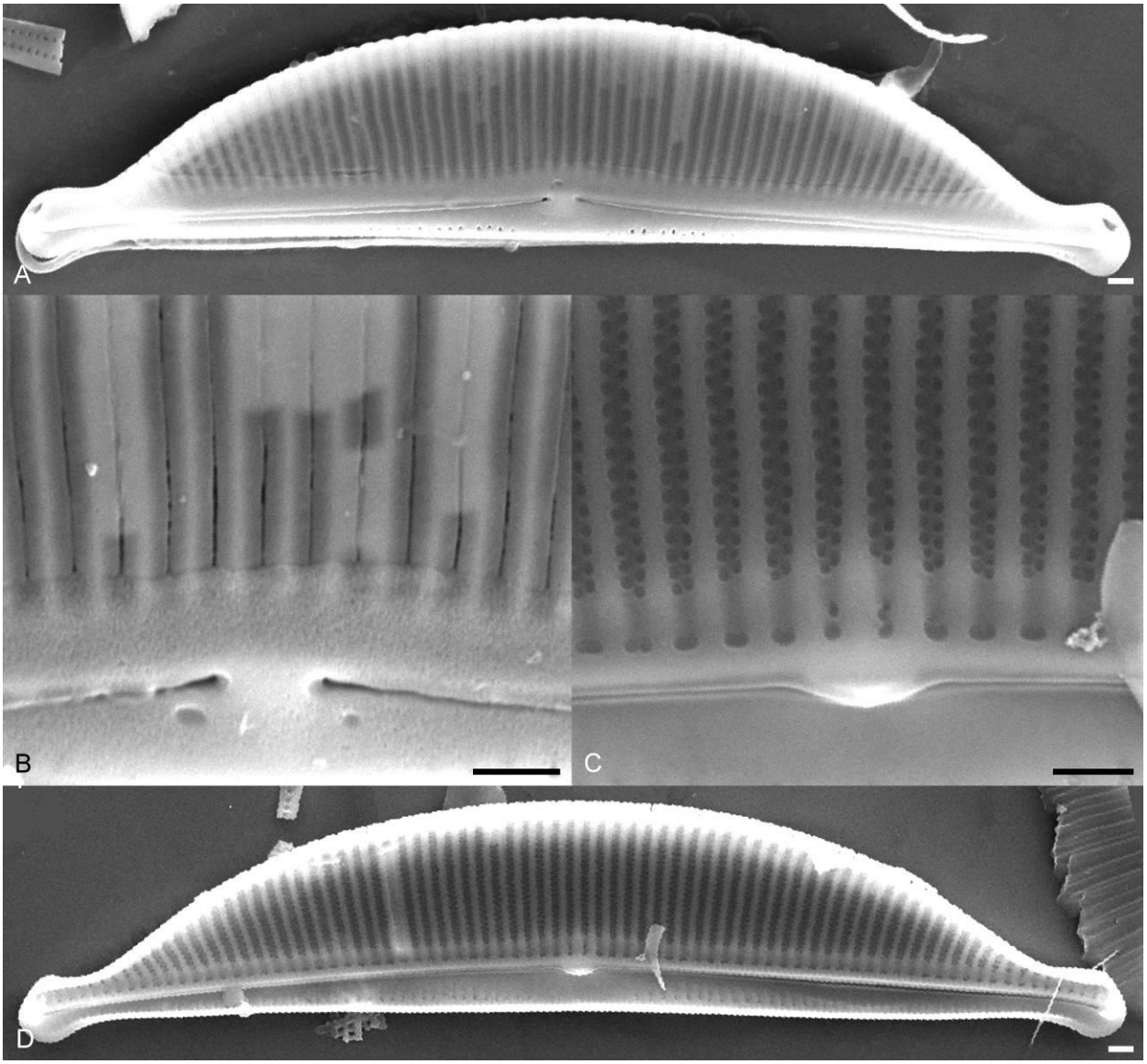

Figure 4.161. Scanning electron micrographs of *Halamphora sp. nov.* Amph093. **A.** External whole valve. **B.** Detail of external valve center. **C.** Detail of internal valve center. **D.** Internal whole valve. Scale bars = 1 µm.

Halamphora sydowii (Cholnoky) Levkov Amph028 (Figs 4.163, 4.164)

Valves are broadly semi-elliptical and strongly dorsiventral. The dorsal margin is arched near the apices, becoming somewhat flattened at the valve center. The ventral margin is slightly concave. The valve ends are strongly protracted, subcapitate and ventrally deflected. Valve length 37.0–45.0 µm, valve breadth 6.0–7.0 µm. The raphe is arched with straight branches. The proximal raphe ends terminate

closely and are slightly dorsally deflected. The axial is narrow throughout. The dorsal raphe ledge is often visible in the LM as a faint longitudinal line. The dorsal striae are areolate, parallel only at the valve center and radiate throughout the rest of the valve. The ventral striae are fine and difficult to image in the LM due to the narrow ventral valve face exhibited by this species. Striae number 16–17 in 10 µm.

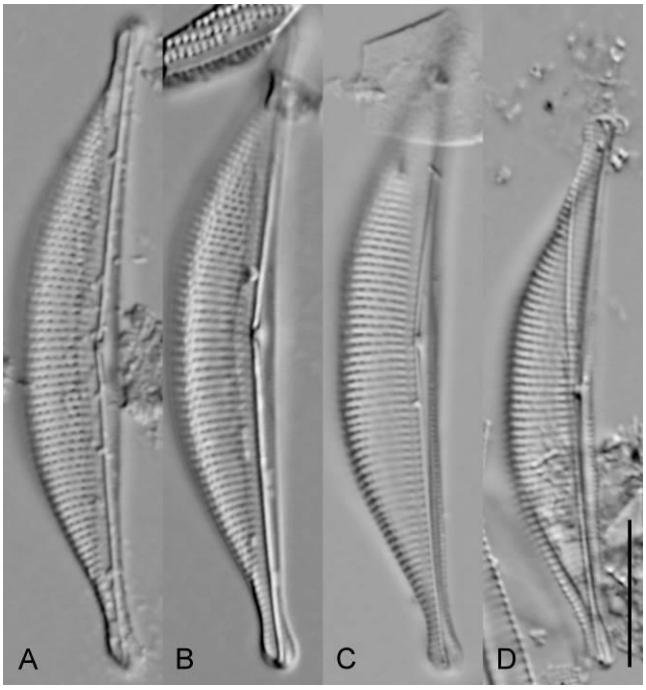

Figure 4.162. A–D. Light micrographs of *Halamphora sydowii* Amph028 showing observed size range. Scale bar = 10 µm.

In SEM, externally, the proximal raphe ends terminate closely and are deflected dorsally and the distal ends are deflected dorsally. The dorsal raphe ledge is very broad and continuous along the length of the valve. A dorsal marginal ridge is not present. The dorsal striae are biseriate near the axial area. The biseriate striae extend past the raphe ledge before transitioning to small elongate areolae that continue though the dorsal mantle. The ventral axial area is narrow at the apices becoming expanded at the valve center creating a semi-lanceolate hyaline area. Internally, the proximal raphe ends terminate in a small fused central helictoglossa. The dorsal striae are biseriate, becoming less obviously so as they transition to the small elongate areolae. An axial band of silica runs the length of the dorsal valve.

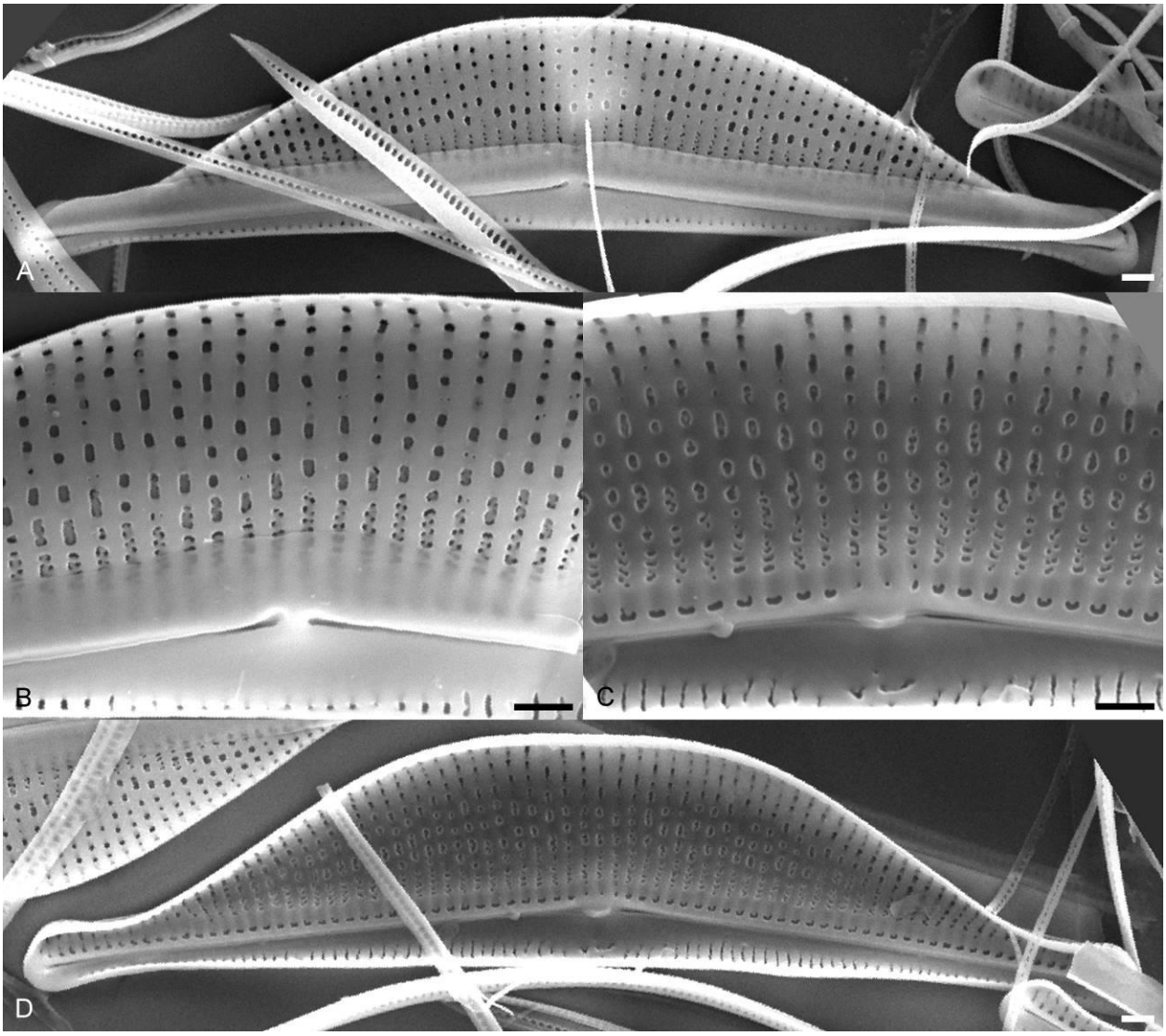

Figure 4.163. Scanning electron micrographs of *Halamphora sydowii* Amph028. **A.** External whole valve. **B.** Detail of external valve center. **C.** Detail of internal valve center. **D.** Internal whole valve. Scale bar = 1 µm.

Halamphora sydowii (Cholnoky) Levkov Amph045 (Figs 4.165, 4.166)

Valves are semi-elliptical and strongly dorsiventral. The dorsal margin is smoothly arched, the ventral margin is slightly concave. The valve ends are protracted, rounded to subcapitate and ventrally deflected. Valve length 20.0–33.0 µm, valve breadth 5.0–6.5 µm. The raphe is arched with straight branches. The proximal raphe ends terminate closely and are slightly dorsally deflected. The axial area is

narrow, appearing slightly expanded near the ventral valve center in some specimens. The dorsal raphe ledge is visible in many specimens as a faint longitudinal line. The dorsal striae are areolate and parallel at the valve center, becoming radiate towards the apices. The ventral striae are fine and appear continuous through the valve center, although they can be difficult to image in the LM depending on the valve angle. Striae number 19–22 in 10 µm.

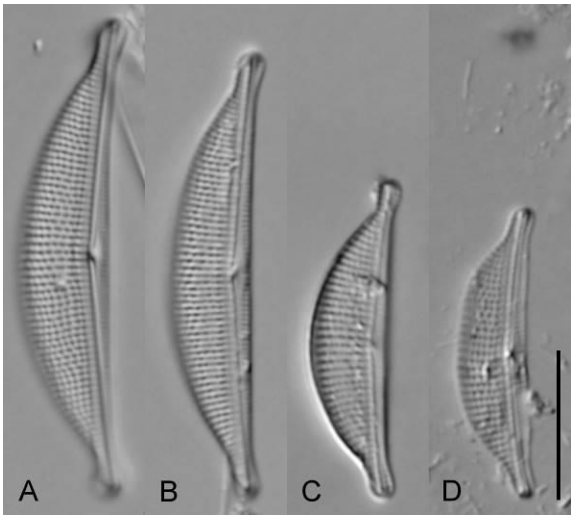

Figure 4.164. A–D. Light micrographs of *Halamphora sydowii* Amph045 showing observed size range. Scale bar = 10 µm.

In SEM, externally, the proximal raphe ends terminate closely and are dorsally deflected, the distal ends are dorsally deflected. The dorsal raphe ledge is very broad and continuous along the length of the valve. The dorsal striae are biseriate near the axial area transitioning to small elongate areolae towards the margin. The ventral striae are continuous through the valve center and are fine and composed of a single row of thin elongate areolae. The ventral axial area is narrow throughout the majority of the valve, expanded near the valve center. Internally, the proximal raphe ends terminate at a very small fused central helictoglossa. The dorsal striae are biseriate, becoming less obviously biseriate as they transition to the small elongate areolae that make up the majority of the valve face. A distinct axial band of silica runs the length of the dorsal valve.

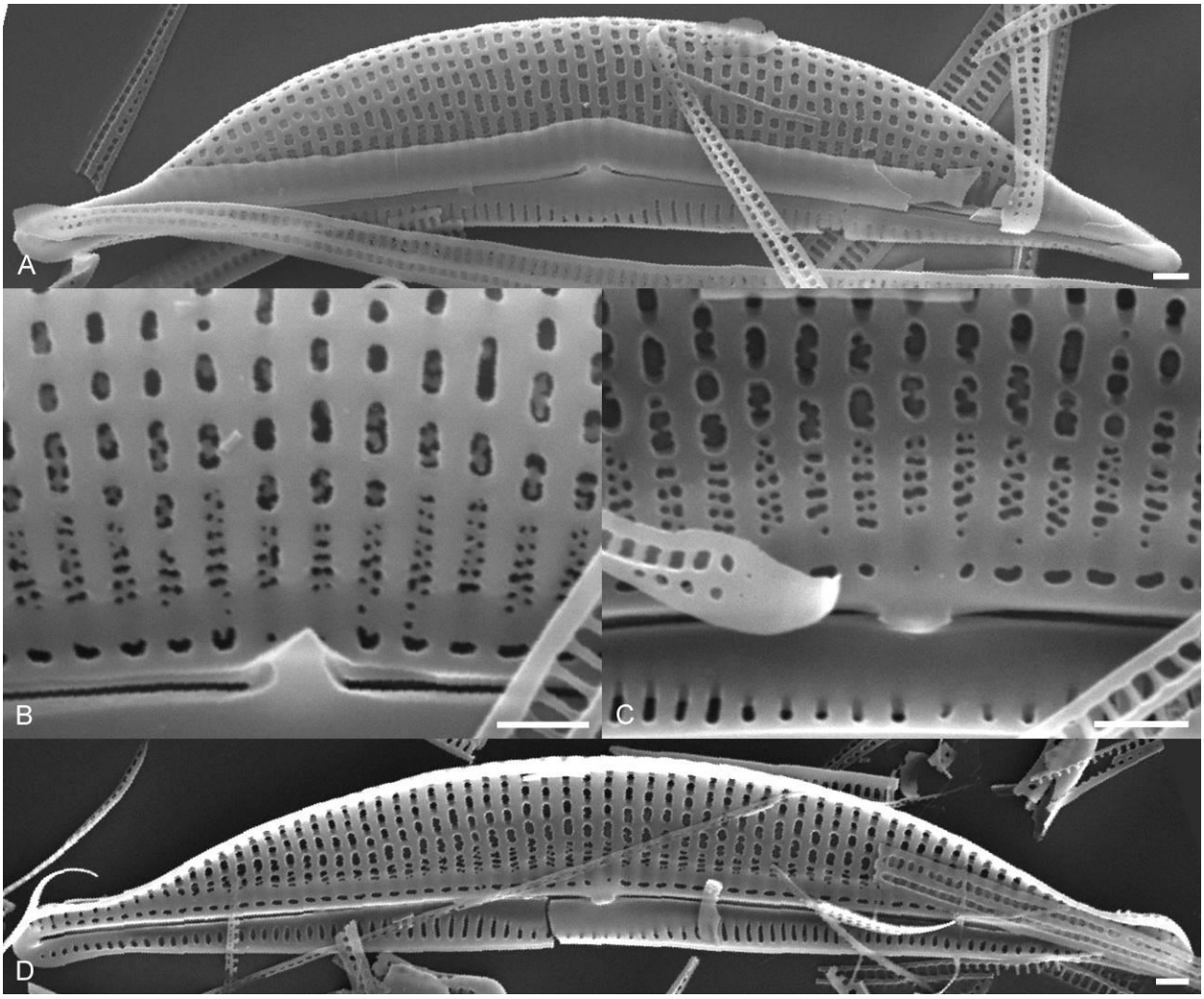

Figure 4.165. Scanning electron micrographs of *Halamphora sydowii* Amph045. **A.** External whole valve. **B.** Detail of external valve center. **C.** Detail of internal valve center. **D.** Internal whole valve. Scale bar = 1 µm.

Halamphora tumida (Hustedt) Levkov Amph149 (Figs 4.167, 4.168)

Valves semi-elliptical and strongly dorsiventral. The dorsal margin is arched near the apices becoming somewhat flattened over the valve center, the ventral margin is straight to slightly tumid at the valve center. The valve ends are weakly protracted and rounded to subcapitate in larger specimens. Valve length 18.0–27.0 µm, valve breadth 4.5–5.5 µm. The raphe is straight with weakly dorsally deflected proximal ends. The axial area is narrow throughout. A dorsal axial longitudinal line is visible in the LM.

The dorsal striae do not appear areolate and are slightly more widely spaced at the valve center. The dorsal striae are parallel at the valve center becoming radiate towards the apices. The ventral striae are fine and do not appear continuous through the valve center. Striae number 16–18 in 10 µm.

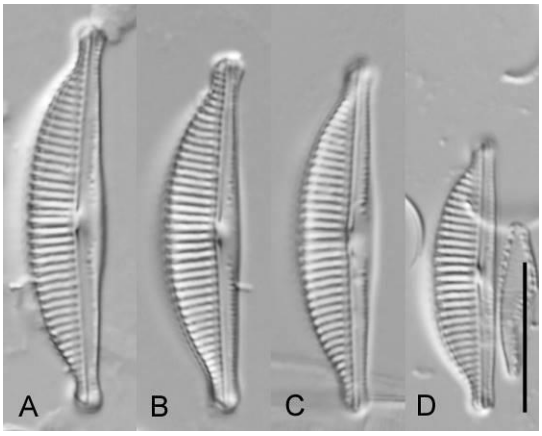

Figure 4.166. A–D. Light micrographs of *Halamphora tumida* Amph149 showing observed size range. Scale bar = 10 µm.

In SEM, externally, the proximal and distal raphe ends are dorsally deflected. The dorsal raphe ledge is very broad and expanded at the valve center and apices. The dorsal striae are finely biseriate and separated by thick virgae for the majority of the valve face, becoming areolate and internally biseriate near the margin. Although there is a distinct transition from the valve face to the dorsal mantle, a marginal ridge is difficult to distinguish. The ventral striae are fine, uniseriate and are not continuous through the valve center. Internally, the proximal raphe ends terminate in a weakly developed fused central helictoglossa. The dorsal striae are biseriate and separated by thick virgae. The dorsal central virgae are distinctly thickened becoming slightly fused at the central area. A dorsal axial band of silica runs the length of the valve.

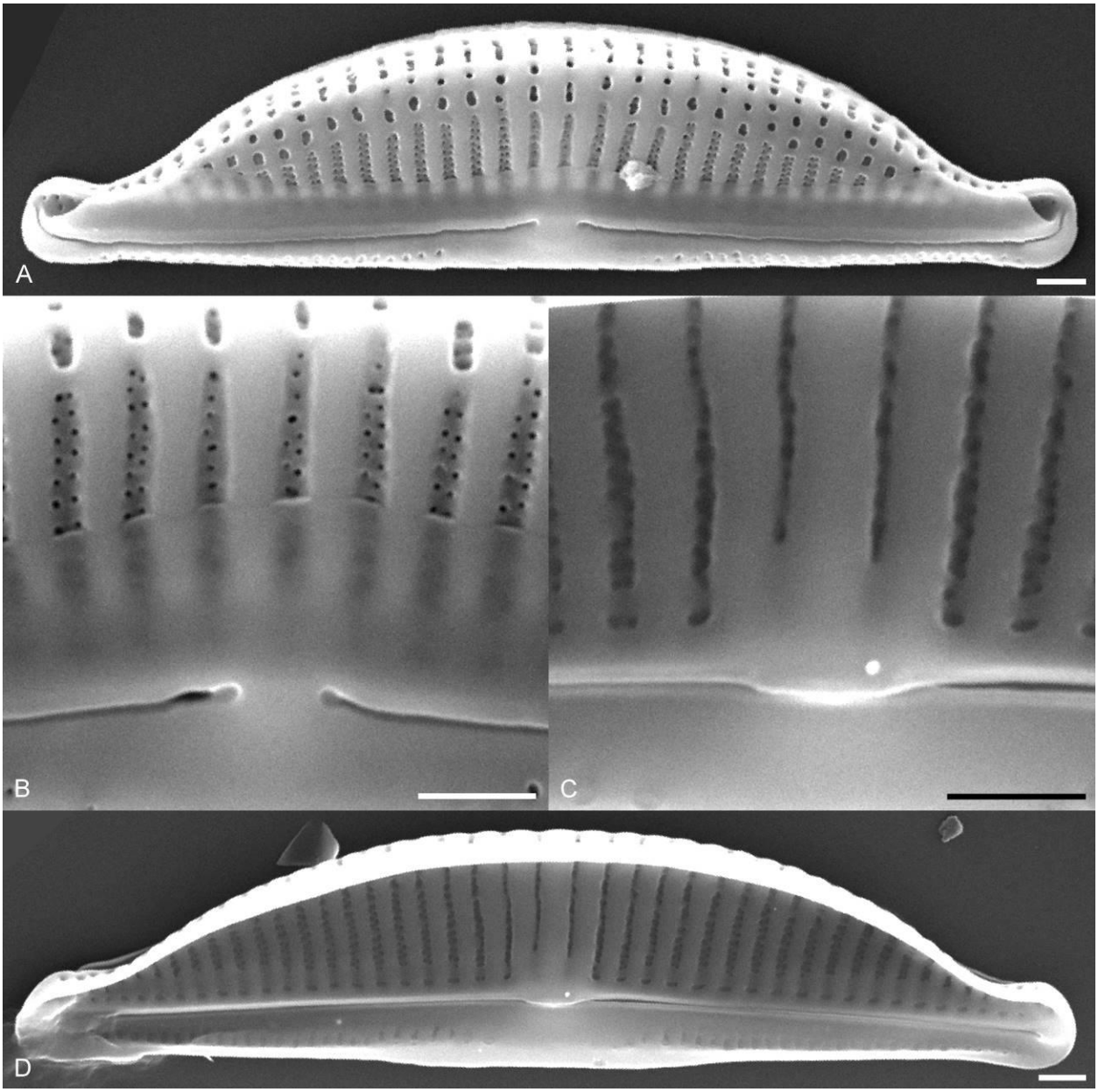

Figure 4.167. Scanning electron micrographs of *Halamphora tumida* Amph149. **A.** External whole valve. **B.** Detail of external valve center. **C.** Detail of internal valve center. **D.** Internal whole valve. Scale bars = 1 µm.

Halamphora sp. nov. Amph115 (Figs 4.169, 4.170)

Valves narrowly semi-elliptical and dorsiventral. The dorsal margin is smoothly arched, the ventral margin is straight to slightly convex. The valve ends are protracted, subcapitate and ventrally

deflected. Valve length 31.0 µm, valve breadth 4.0–5.0 µm. The raphe is weakly arched with straight branches and straight proximal raphe ends. The dorsal axial area is narrow, the ventral axial area is slightly expanded, more so at near the valve center. The dorsal striae are areolate with the first row of µaxial areolae distinctly elongate compared to the rest of the areolae. The dorsal striae are slightly radiate throughout. The ventral striae are fine and marginally positioned. The ventral striae appear continuous through the valve center. Dorsal striae number 18–19 in 10 µm, ventral striae number 24–25 in 10 µm.

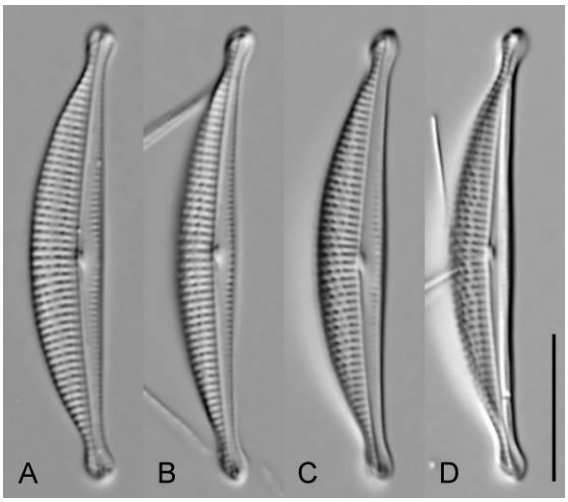

Figure 4.168. A–D. Light micrographs of *Halamphora sp. nov.* Amph115 showing observed size range. Scale bar = 10 µm.

In SEM, externally, the proximal raphe ends are dilated and dorsally deflected, the distal ends are dorsally deflected. The dorsal raphe ledge is broad, completely obscuring the axial row of elongate areolae, and is continuous along the length of the valve. A dorsal marginal ridge is absent. The dorsal striae are composed of small round to ovoid areolae with no external occlusions. The ventral striae are fine and are difficult to image in some valve orientations due to their marginal position. The ventral striae are continuous through the valve center and are composed of a single row of small elongate areolae. Internally, the proximal raphe ends terminate in a fused central helictoglossa. The dorsal striae are biseriate and are composed of an axial row of elongate areolae, transitioning to small ovoid areolae towards the dorsal margin.

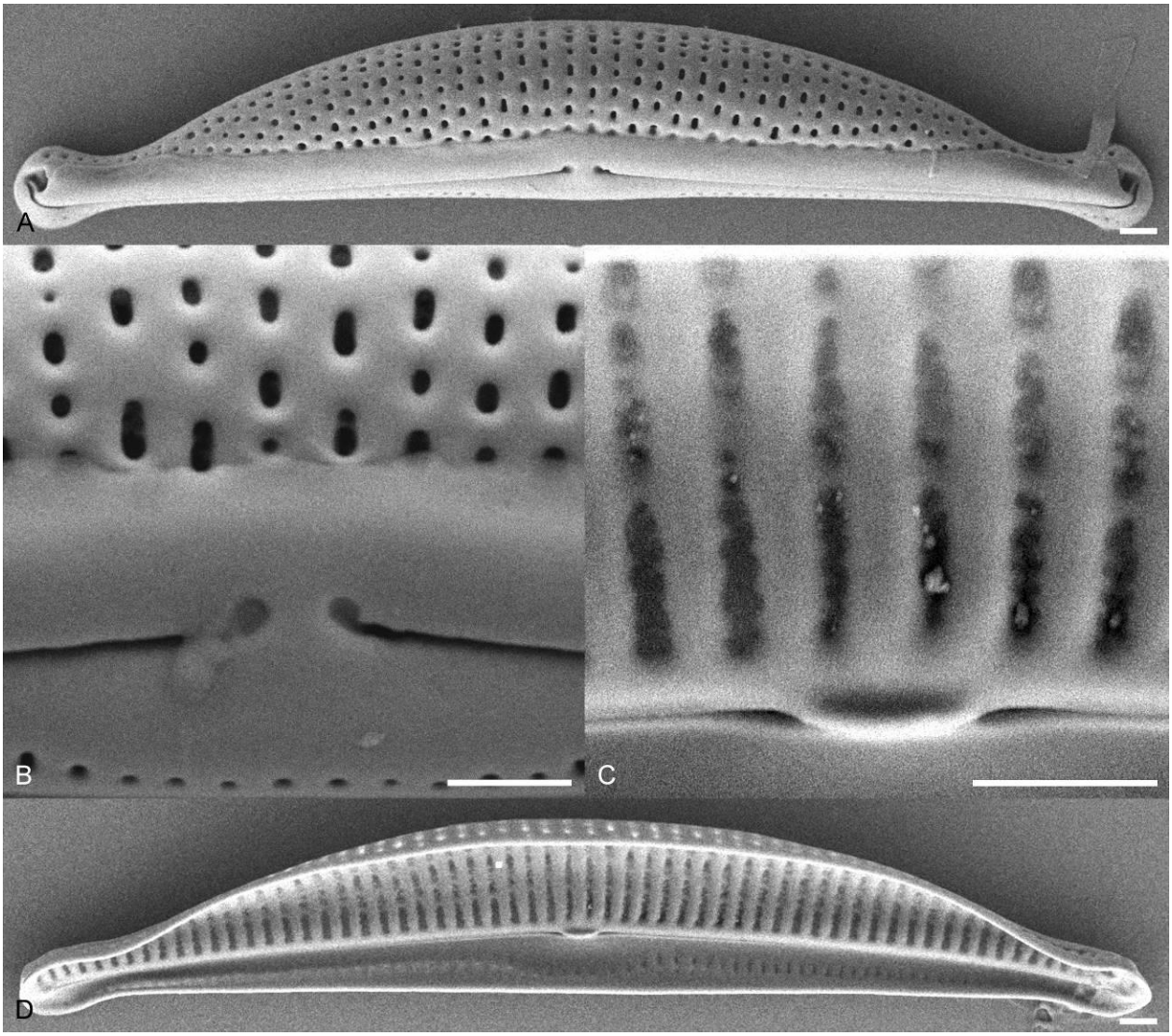

Figure 4.169. Scanning electron micrographs of *Halamphora sp. nov.* Amph115. **A.** External whole valve. **B.** Detail of external valve center. **C.** Detail of internal valve center. **D.** Internal whole valve. Scale bars = 1 µm.

Halamphora americana Kociolek Amph022/100 (Figs 4.171, 4.172)

Valves semi-elliptical and moderately dorsiventral. The dorsal margin is smoothly arched, the ventral margin is straight to slightly convex. The valve ends are protracted, narrowly rounded to subcapitate and slightly ventrally deflected. Valve length 23.0–30.0 µm, valve breadth 4.0–5.0 µm. The raphe is arched with closely terminating straight proximal raphe ends. The dorsal axial area is narrow, the

ventral axial area is expanded at the valve center. The dorsal striae are weakly areolate, more distinctly so near the dorsal margin and weakly radiate throughout. The ventral striae are fine and continuous along the length of the valve. Striae number 19 in 10 µm.

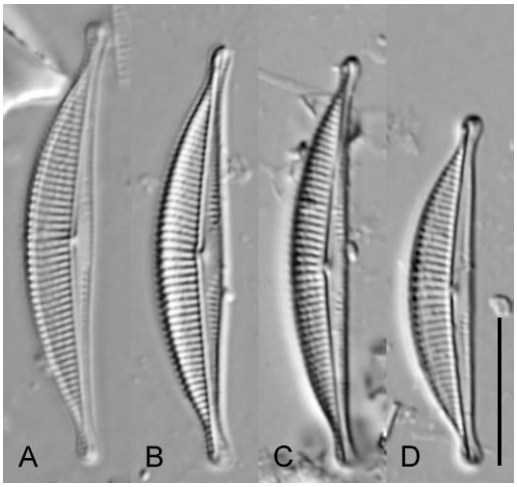

Figure 4.170. A–D. Light micrographs of *Halamphora americana* Amph022/100 showing observed size range. Scale bar = 10 µm.

In SEM, externally, the proximal raphe ends terminate closely, are dilated and slightly dorsally deflected. The dorsal raphe ledge is narrow and continuous along the length of the valve. The dorsal striae are biseriate near the axial area, becoming coarsely areolate near the margin. A dorsal marginal ridge is absent. The ventral striae are composed of a single row of elongate areolae. The ventral axial area is expanded at the valve center. Internally, the proximal raphe ends terminate in a fused central helictoglossa. The dorsal striae are biseriate near the axial area, becoming areolate near the margin. The dorsal central virgae are slightly thickened, becoming fused near the central area.

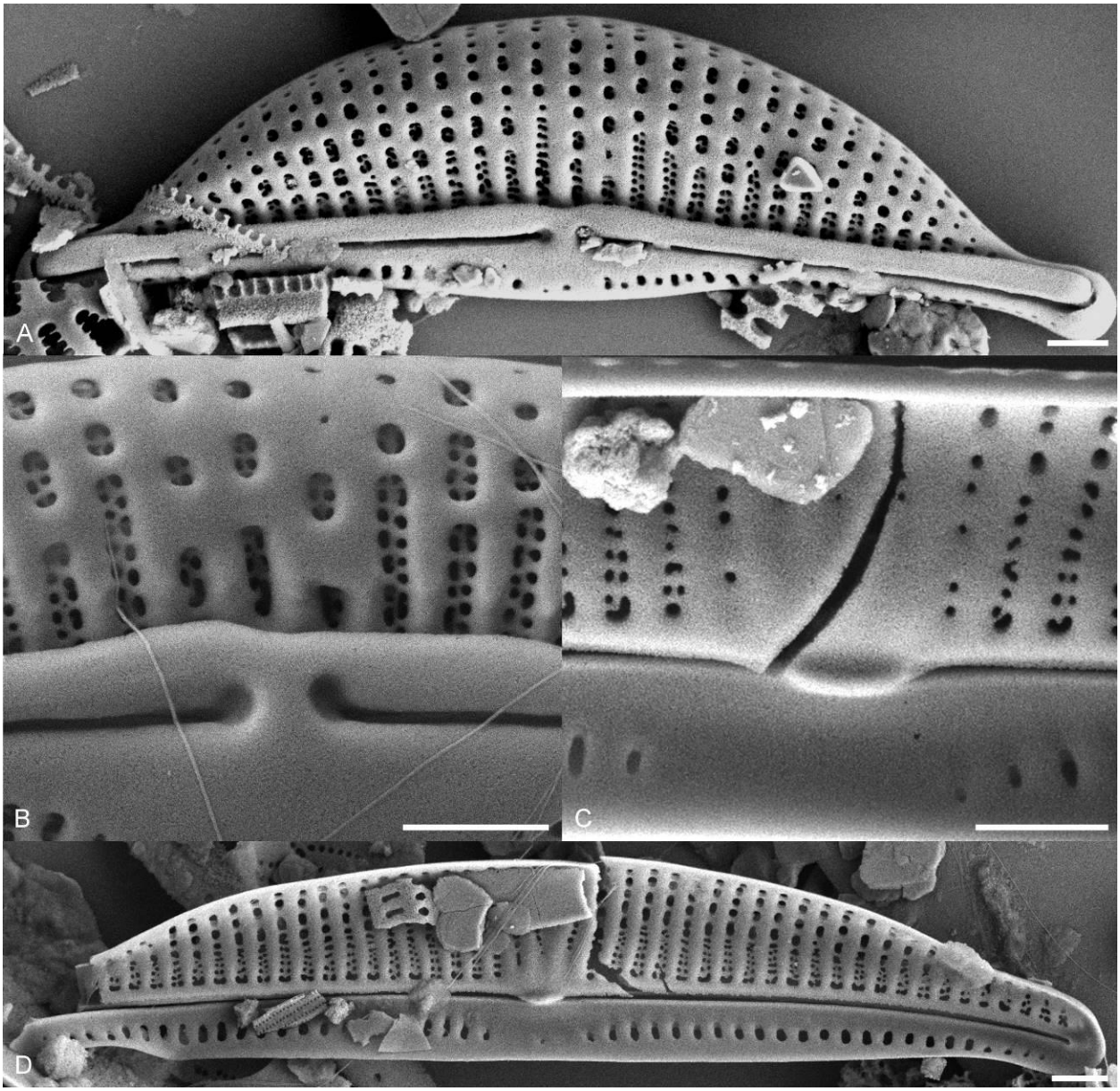

Figure 4.171. Scanning electron micrographs of *Halamphora americana* Amph022/100. **A.** External whole valve. **B.** Detail of external valve center. **C.** Detail of internal valve center.. **D.** Internal whole valve. Scale bars = 1 µm.

Halamphora sp. nov. Amph043 (Figs 4.173, 4.174)

Valves are semi-elliptical strongly dorsiventral. The dorsal margin is flatly arched, the ventral margin is straight to slightly concave. The valve ends are protracted, narrowly rounded and deflected ventrally. Valve length 19.0–29.0 µm, valve breadth 4.0–4.5 µm. The dorsal axial area is narrow throughout, the ventral axial area is slightly expanded at the valve center. The dorsal striae are finely

areolate, nearly parallel at the valve center, becoming weakly radiate near the apices. The ventral striae are fine and continuous through the valve center. Dorsal striae number 20–21 in 10 µm, ventral striae number 32 in 10 µm.

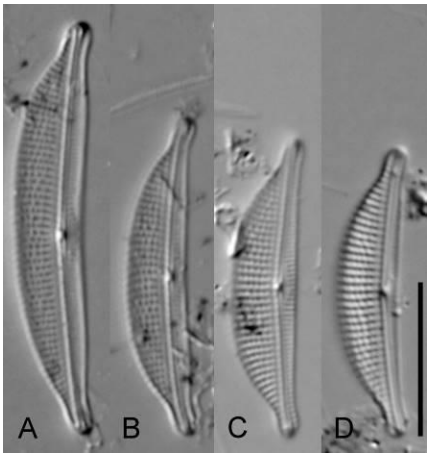

Figure 4.172. A–D. Light micrographs of *Halamphora sp. nov.* Amph043 showing observed size range. Scale bar = 10 µm.

In SEM, externally, the proximal raphe ends terminate closely and are slightly deflected dorsally. The distal ends are deflected dorsally. The dorsal raphe ledge is broad and continuous along the length of the valve. The dorsal striae are biseriate near the axial are becoming coarsely areolate towards the margin. A marginal ridge is absent. The ventral striae are fine and composed of a single row of elongate areolae. The ventral striae are continuous along the length of the valve. The ventral axial area is slightly expanded at the valve center. Internally, the proximal raphe ends terminate in a small fused central helictoglossa. The dorsal striae are biseriate near the axial area becoming areolate towards the margin.

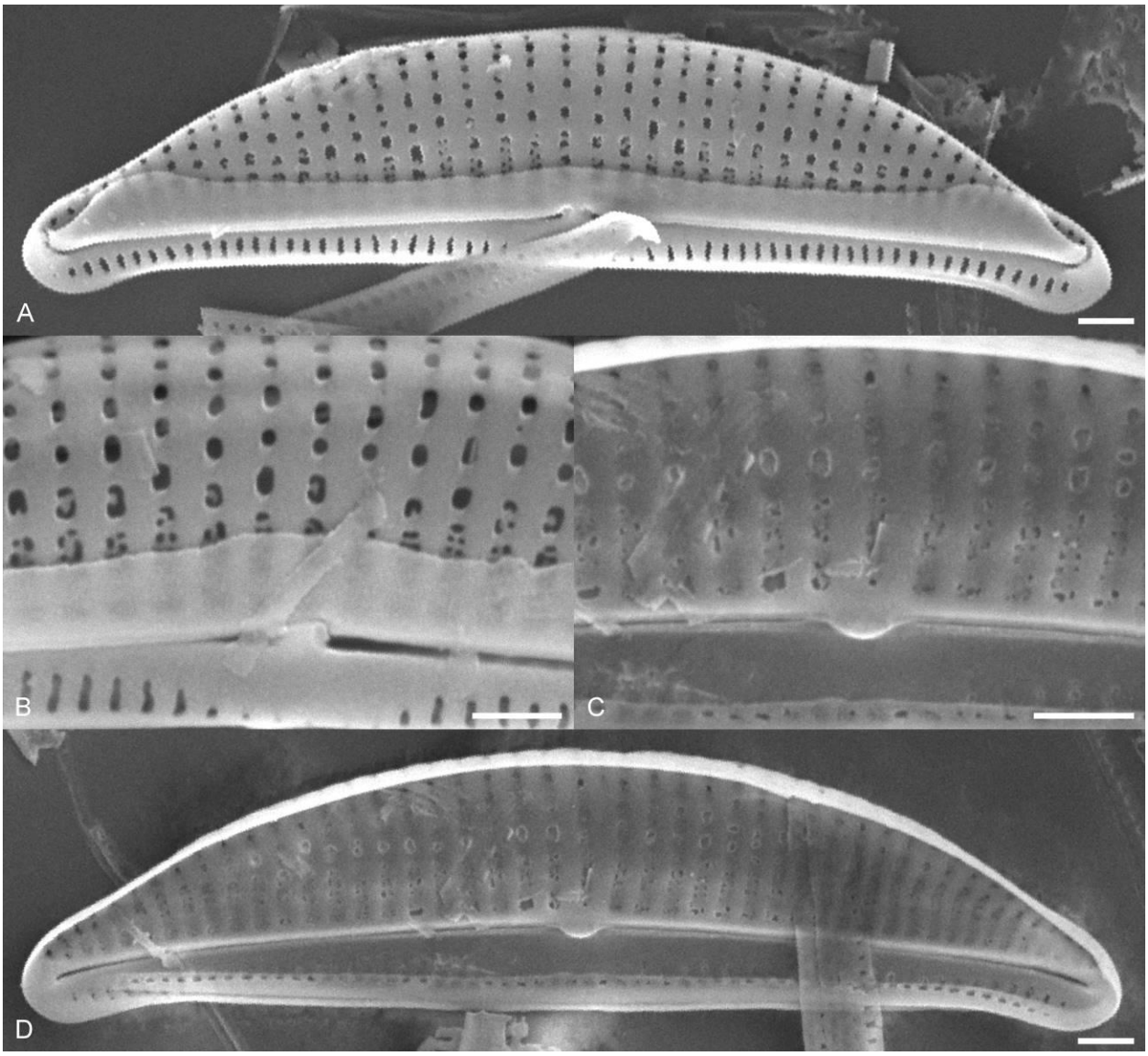

Figure 4.173. Scanning electron micrographs of *Halamphora sp. nov.* Amph043. **A.** External whole valve. **B.** Detail of external valve center. **C.** Detail of internal valve center. **D.** Internal whole valve. Scale bars = 1 µm.

Halamphora sp. nov. Amph118 (Figs. 4.175, 4.176)

Valves are semi-elliptical and strongly dorsiventral. The dorsal margin is smoothly arched, the ventral margin is straight. The valve ends are highly protracted and rounded to subcapitate. Valve length 36.0–46.0 µm, valve breadth 6.5–8.0 µm. The raphe is arched with straight raphe branches with straight closely terminating proximal ends. The axial area is narrow dorsally and expanded near the valve center on the ventral side. The dorsal striae are areolate, more distinctly so as the striae near the dorsal margin.

The dorsal striae are parallel at the valve center, becoming radiate towards the apices. The ventral striae are fine and composed of a single row of areolae. Striae number 16–17 in 10 µm.

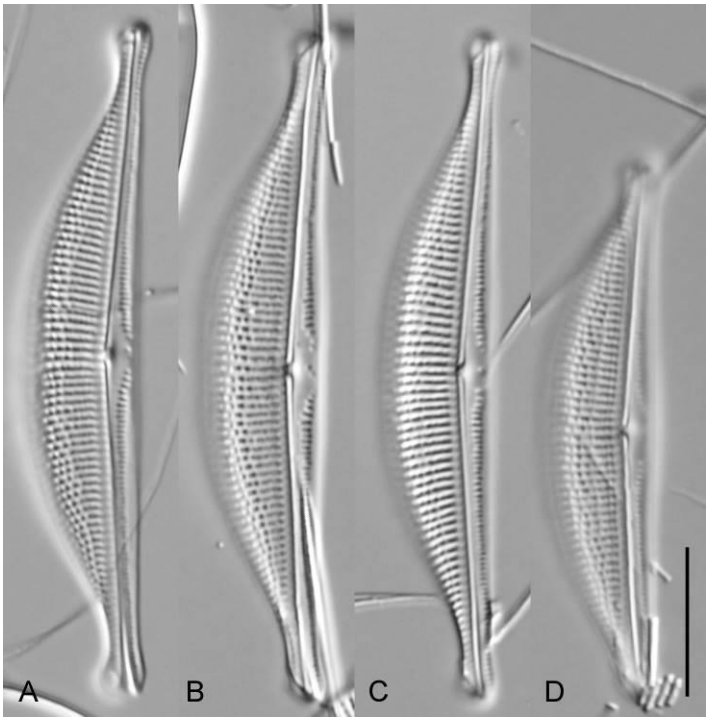

Figure 4.174. A–D. Light micrographs of *Halamphora sp. nov.* Amph118 showing observed size range. Scale bar = 10 µm.

In SEM, externally, the raphe is straight with closely terminating and dorsally deflected proximal raphe ends. The dorsal raphe ledge is broad and continuous along the length of the valve. The dorsal striae begin biseriate near the axial area then transition to large elongate areolae towards the dorsal margin. A marginal ridge is absent. The ventral striae are composed of a single row of elongate areolae and are more or less continuous through the valve center. Internally, the proximal raphe ends terminate in a small fused central helictoglossa. The dorsal striae are irregularly biseriate near the axial area becoming areolate towards the dorsal margin. An axial silica band runs the longitudinal length of the valve.

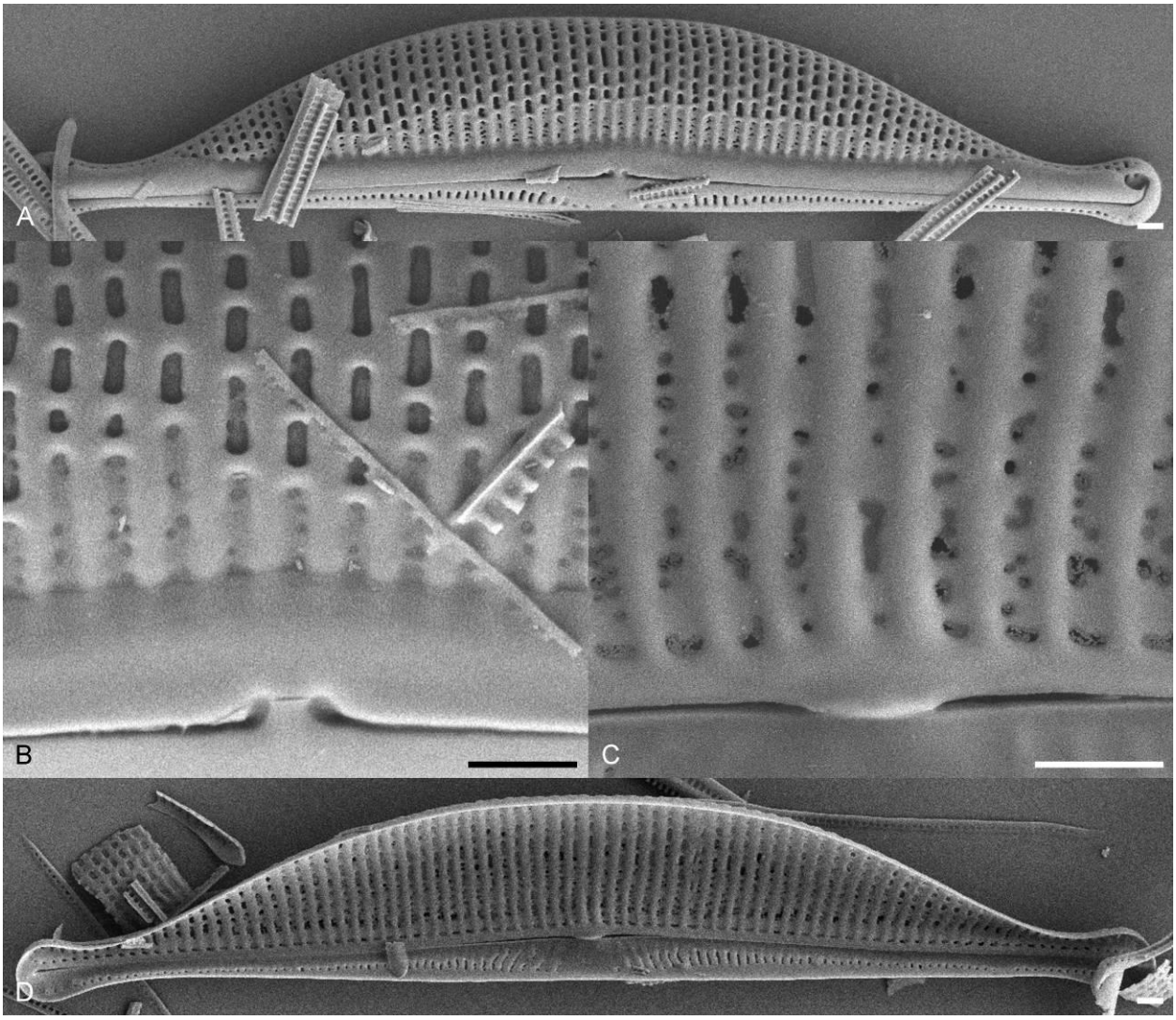

Figure 4.175. Scanning electron micrographs of *Halamphora sp. nov.* Amph118. **A.** External whole valve. **B.** Detail of external valve center. **C.** Detail of internal valve center. **D.** Internal whole valve. Scale bars = 1 µm.

Halamphora sp. nov. Amph089 (Figs 4.177, 4.178)

Valves semi-elliptical and strongly dorsiventral. The dorsal margin is smoothly arched, the ventral margin is straight to slightly concave in some specimens. The valve ends are weakly protracted, narrowly rounded and slightly ventrally deflected. Valve length 25.0–35.0 µm, valve breadth 5.0–6.5 µm. The raphe is arched with straight raphe branches. The proximal raphe ends are straight and terminate closely. The axial are is narrow dorsally, slightly expanded at the ventral valve center. The dorsal striae appear weakly areolate, more distinctly areolate near the dorsal margin. The dorsal striae are parallel at

the valve center, becoming radiate towards the apices. The ventral striae are fine and continuous along the ventral margin. Striae number 16–18 in 10 µm.

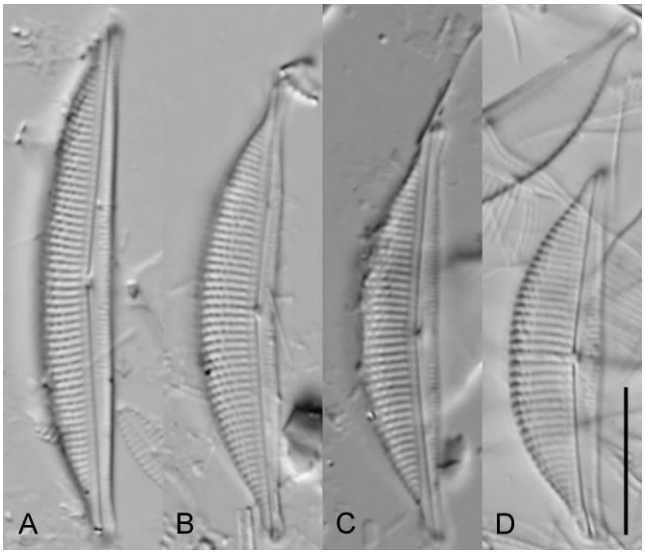

Figure 4.176. A–D. Light micrographs of *Halamphora sp. nov.* Amph089 showing observed size range. Scale bar = 10 µm.

In SEM, externally, the proximal raphe ends are slightly dilated and slightly deflected dorsally, the distal ends are dorsally deflected. The dorsal raphe ledge is broad and continuous along the length of the valve. The dorsal striae are biseriate near the axial area becoming coarsely areolate approximately half way to the dorsal margin. A dorsal marginal ridge is absent. The ventral striae are composed of a single row of areolae. The ventral axial area is expanded near the valve center. Internally, the proximal raphe ends terminate in a small fused central helictoglossa. The dorsal striae are biseriate near the axial area becoming areolate towards the dorsal margin. A weakly developed axial siliceous band is more or less visible.

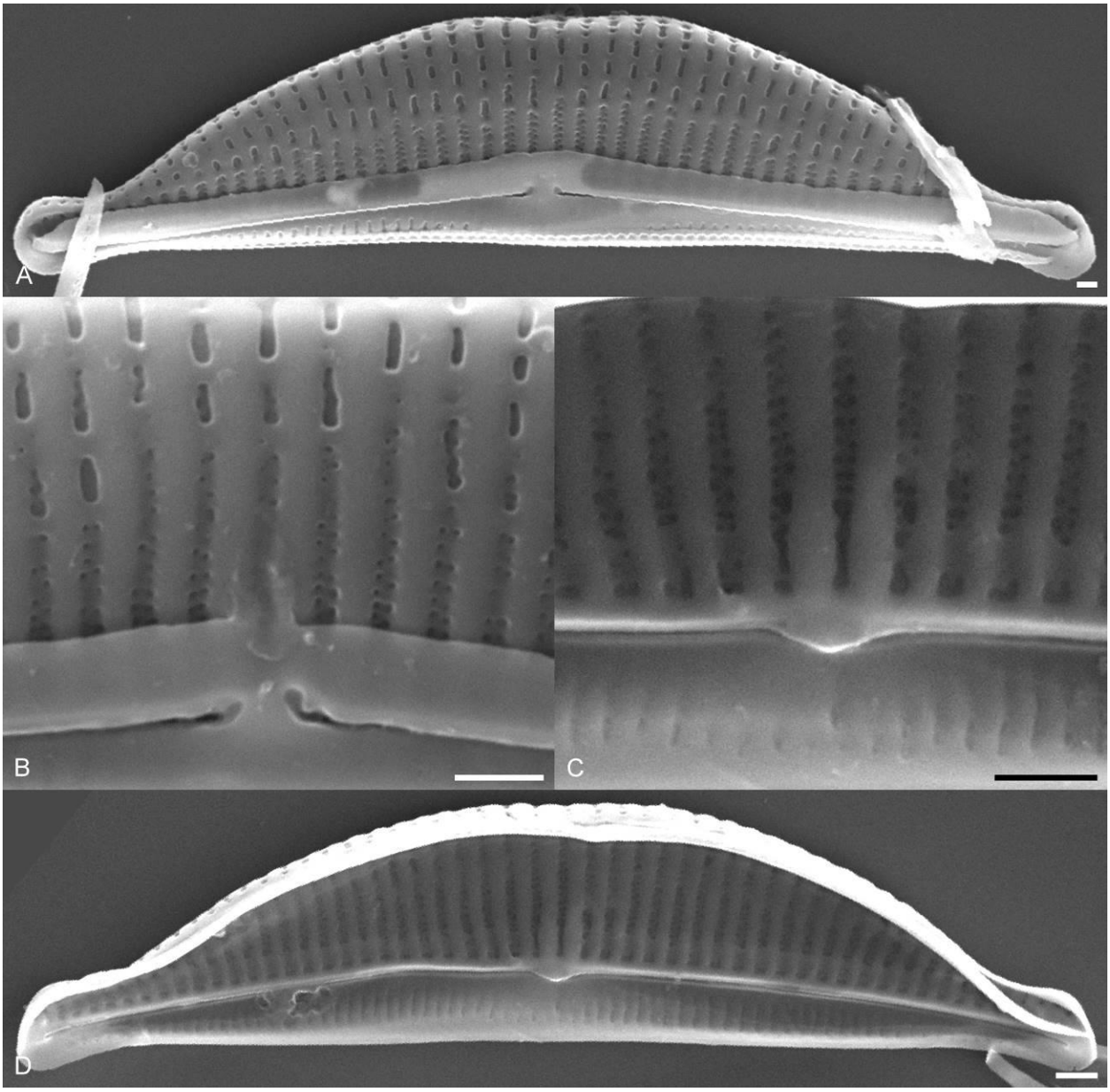

Figure 4.177. Scanning electron micrographs of *Halamphora sp. nov.* Amph089. **A.** External whole valve. **B.** Detail of external valve center. **C.** Detail of internal valve center. **D.** Internal whole valve. Scaler bars = 1 µm.

SECTION II

SYSTEMATICS OF THE AMPHOROID DIATOMS

CHAPTER V

MOLECULAR PHYLOGENY OF *AMPHORA SENSU LATO* (BACILLARIOPHYTA): AN INVESTIGATION INTO THE MONOPHYLY AND CLASSIFICATION OF THE AMPHOROID DIATOMS

Adapted from: Stepanek, J.G. & Kociolek, J.P. 2014. Molecular phylogeny of *Amphora sensu lato* (Bacillariophyta): an investigation into the monophyly and classification of the amphoroid diatoms. *Protist* 165: 177–195.

ABSTRACT

Amphora sensu lato encompasses a large group of raphid diatoms, diverse in both form and ecology. The defining feature of this group has been an extreme asymmetry, bringing both faces of the cell onto a single plane. Although this 'amphoroid' structure has long been the diagnostic feature and thus considered 'conservative' for the group, many have argued that the diversity of forms assigned to *Amphora* likely does not represent a monophyletic group. With the exception of several taxonomic transfers and the recent elevation of *Halamphora* to the level of genus, much of *Amphora* classification has remained unchanged for over 100 years. This study presents a phylogenetic analysis of *Amphora s.l.* based on a molecular phylogenetic analysis including the nuclear marker SSU rDNA and the chloroplast markers *rbc*L and *psb*C. These results are discussed within the framework of the current classification system of *Amphora* and *Halamphora* and lay the groundwork for a taxonomic revision of the group based on monophyly. This analysis demonstrates that the genus *Amphora* is polyphyletic with lineages distributed widely across the raphid diatom tree of life. We discuss the nature of conservative characters in the raphid diatoms and their usefulness as a guide to phylogenetic relationships

INTRODUCTION

Amphora Ehrenberg ex Kützing *sensu lato* is a large (>800 species; Fourtanier & Kociolek 2009; Levkov 2009) and morphologically diverse group of raphid diatoms found in fresh, brackish and salt water habitats from the tropics to the poles (Bérard-Therriault et al. 1986, Hohn & Hellerman 1966, Patrick & Freese 1961, Stepanek & Kociolek 2013, Stoermer & Yang 1971, Wachnicka & Gaiser 2007). Partially due to this morphological diversity, the genus is primarily defined by a distinct asymmetry in the valve mantle and girdle bands. This asymmetry, which places both valve faces on the same plane, is distinct in the light microscope and has been the single feature unifying the genus since its description by Kützing in 1844. (Cleve 1895, Kützing 1844. Smith 1873). For nearly as long there have been concerns as to whether the genus *Amphora,* as defined by this asymmetry, represented a natural group (Cleve 1895, Krammer 1980, Mann 1994) and early attempts at a comprehensive *Amphora* classification proved difficult (Cleve 1895, Mereschkowsky 1903). Now, over 100 years after these concerns were first raised, questions regarding the monophyly of the genus *Amphora* have yet to be fully resolved.

In a classification system that largely persists today, Cleve (1895) separated the genus into nine subgenera (*Amphora, Diplamphora, Halamphora, Oxyamphora, Amblyamphora, Psammamphora, Cymbamphora, Calamphora,* and *Archiamphora*) based on a number of morphological characters such as a ‘simple’ or ‘complex’ connecting zone (girdle area), the presence or absence of ‘longitudinal lines’, as well as several raphe and striae features. In creating his classification, Cleve struggled with the relationships between the subgenera and their position within the larger diatom classification system. Cleve recognized frustular asymmetry as a feature shared by members of the genus, but unlike previous authors (Smith 1873) he did not believe this characteristic was appropriate for the formation of a natural group (Cleve 1895, p. 99). A notable aspect of Cleve’s treatment was his assertion that his subgenera likely represented a number of distinct and potentially unrelated genera, though he was hesitant to elevate his new subgenera because of nomenclatural concerns as well as affording an “opportunity of testing my views, which are entirely new, before admitting the proposed new genera” (Cleve 1895, p. 100).

Mereschkowsky (1903) put forth the first challenge to Cleve's classification system, in which he proposed a new classification based on plastid number and morphology. Mereschkowsky separated *Amphora* into four large groups based on plastid number, and within these groups the taxa were further divided into nine subgroups based on the position and shape of the chloroplast. This new classification system was not widely adopted and the genus *Amphora* continued to be recognized for this entire group of species by most taxonomists.

With the increased use of electron microscopy came new investigations and revisions to groups and taxa within *Amphora s.l.* Paddock and Sims (1980) where the first to transfer taxa from the genus *Amphora* to other genera, transferring taxa from the subgenus *Oxyamphora*, to the newly created genus *Undatella* Paddock and Sims. Several other transfers based on scanning electron microscope (SEM) observations followed, including several taxa to the genus *Biremis* Mann and Cox (Mann & Cox in Round et al. 1990) and *Colliculoamphora* Williams and Reid (Williams & Reid 2006), as well as the elevation of the *Amphora* subgenus *Halamphora* to generic status (Levkov 2009) and the transfer of the subgenus *Cymbamphora* to the newly created genus *Seminavis* Mann (Mann in Round et al. 1990).

In addition to the morphological investigations, several molecular phylogenetic studies, while not specifically focusing on *Amphora*, have included *Amphora s.l.* in their analyses (Bruder & Medlin 2008, Medlin & Kaczmarska 2004, Ruck & Theriot 2011, Sorhannus 2004). The molecular markers used varied between studies from single marker alignments (Medlin & Kaczmarska 2004, Sorhannus 2004) to three marker concatenated alignments (Bruder & Medlin 2008, Ruck & Theroit 2011). Although these studies included few *Amphora s.l.* taxa (2–10) and produced somewhat variable results, trends that emerged included the non-monophyly of *Amphora* + *Halamphora* and a close association of some of these taxa and the canal raphid orders Rhopalodiales Mann and Surirellales Mann (Bruder & Medlin 2008, Medlin & Kaczmarska 2004, Ruck & Theriot 2011, Sorhannus 2004). Although provocative, the small taxon sampling and continued low support has done little to advance our understanding of the systematics of this group.

In the most extensively sampled phylogeny to date, and the first to include taxa outside *Amphora s.s.* and *Halamphora,* Sato et al. (2013) recently published a phylogeny based exclusively on SSU data that includes 22 *Amphora* taxa: nine from *Amphora s.s.*, nine from *Halamphora*, three from the subgenus *Diplamphora*, and one from the subgenus *Oxyamphora*. This analysis supported the non-monophyly of *Amphora s.l.*, with *Halamphora* and the lone representative from the subgenus *Oxyamphora* most closely related to the Rhopalodiales and Surirellales, and *Amphora s.s.* most closely related to taxa from the subgenus *Diplamphora*. Although returning a result supporting the hypothesis of a paraphyletic *Amphora s.l.*, hypothesis testing performed on the single marker alignment was unable to reject the hypothesis of monophyly of *Amphora s.l.* at a 0.05 significance level (Sato et al. 2013, p. 233).

This investigation presents a molecular phylogeny of *Amphora s.l.* inferred from a three marker dataset that includes the largest sampling of *Amphora s.l.* taxa and subgenera. Taxa presented here include representatives from *Amphora s.s.* and *Halamphora* as well as taxa from the subgenera *Oxyamphora*, *Diplamphora* and *Amblyamphora*. The aims of this study are to 1) investigate hypotheses concerning the monophyly of *Amphora s.l.* and of the represented subgenera, and 2) discuss the systematic implications of the phylogenetic analysis within the framework of the hypotheses preceding it, most notably Cleve's (1895) and Mereschkowsky's (1903) classification, and offer insights towards a revised classification of the group.

MATERIALS AND METHODS

Taxon collections

This analysis includes 30 representatives from *Amphora s.l.* and sequence data, obtained from Genbank, for an additional 70 taxa. The taxa from *Amphora s.l.* include ten representatives from the genus *Halamphora*, seven from *Amphora s.s.*, ten from the subgenus *Oxyamphora*, two from the subgenus *Diplamphora* and one from the subgenus *Amblyamphora* (Appendix 1, 2).

All *Amphora s.l.* taxa were isolated into monoculture via micro-pipette serial dilution from collections made in Colorado, North Dakota and Florida, USA, from February to November 2011.

Isolated taxa were grown in one of three media based on the conductivity of the collection site, WC medium (Guillard & Lorenzen 1972) for freshwater taxa, and one of two f/2 media (Guillard 1975) with conductivities of 15 or 40 mS cm^{-1} for brackish water and saltwater isolates respectively. Conductivity at the collection sites was determined using a calibrated YSI 556 multi-probe (YSI Incorporated, Yellow Springs, Ohio). Appropriate conductivity for the brackish and saltwater media were obtained using distilled water and the artificial sea salts Instant Ocean (United Pet Group, Blacksburg, Virginia). After isolation, the cultures were maintained at a temperature of ca. 25°C, with a 12:12 light dark cycle at an irradiance of 50 µmol cm^{-2} s^{-1}.

Materials were cleaned for LM and SEM observations by boiling in nitric acid followed by repeated rinses with distilled water until a neutral pH was reached. Cleaned material was permanently mounted in Naphrax® mounting medium for LM observations. All LM observations were performed using an Olympus BX-51 light microscope (Olympus America Inc., Center Valley, Pennsylvania, USA) with 100x oil immersion objective (N.A. 1.40). Light microscope images were taken using an Olympus DP 71 digital camera. For SEM observations, cleaned material was dried onto glass cover slips and sputter coated using a Cressington 108 auto sputter coater (Cressington Scientific Instruments Ltd., Watford, UK) with 1 nm gold. Electron micrographs were taken using a JEOL JSM 7401 field emission SEM (JEOL Ltd., Tokyo, Japan) at an acceleration voltage of 3 kV. Valve ultrastructure terminology follows that of Cox and Ross (1981), Levkov (2009) and Nagumo (2003).

DNA extraction amplification and sequencing

Extraction of DNA from *Amphora* monocultures was performed using either a DNeasy Plant Mini Kit (Qiagen Sciences, Germantown, Maryland) following the manufacturer's protocol, or a Chelex 100® extraction method (Richlen & Barber 2005). We utilized a combination of conserved (SSU) and more variable (*rbc*L, *psb*C) molecular markers, previously shown to provide order (Bruder & Medlin 2008, Ruck & Theriot 2011, Theriot et al. 2010) and species (Alverson et al. 2007, Hamsher et al. 2012, Souffreau et al. 2011) level resolution. In addition, these markers are commonly used in diatom

phylogenetics (Alverson et al. 2007, Bruder & Medlin 2008, Medlin & Kaczmarska 2004, Ruck & Theriot 2011, Souffreau et al. 2011, Theriot et al. 2010), allowing for the inclusion of non-*Amphora s.l.* GenBank sequences from the greatest breadth of raphid diatom lineages. Primers used for the amplification and sequencing of these markers is listed in Appendix 3.

All markers were amplified by polymerase chain reaction (PCR) using GE Healthcare illustra Ready-To-Go™ PCR beads (GE Healthcare Biosciences, Pittsburg, Pennsylvania) following the manufacturer's instructions. Polymerase chain reaction was carried out in an Eppendorf Mastercycler using the following program: 94°C for 3:30, followed by 36 cycles of 94°C for 50 seconds, 52°C for 50 seconds, 72°C for 80 seconds, with a final extension at 72°C for 15 minutes. After amplification, the PCR products were purified using the PCR clean-up product ExoSap-it (Affymetrix, Santa Clara, California) following the manufacturers recommended protocol. Purified PCR product was sequenced by Functional Biosciences, Inc. (Madison, Wisconsin) and returned sequences were assembled and edited using Geneious ver. 5.6 (Drummond et al. 2012). Obtained sequences for the 30 *Amphora s.l.* taxa included in this analysis are deposited in GenBank and accession numbers for SSU, *rbc*L and *psb*C sequences are listed in Appendix 2.

Sequence alignment and phylogenetic analysis

Sequences were edited and aligned in Geneious using a muscle alignment algorithm (Edgar 2004). Each DNA region was aligned separately before concatenation in the three-marker alignment (total of 4 alignments). The ends of the each of the alignments were trimmed to minimize missing characters. A variable 67 bp region of SSU, corresponding to region 650–717 in the initial alignment, was removed because of ambiguity in the alignment, creating a final trimmed length of 1471 sites. The markers *rbc*L and *psb*C had a final trimmed length of 1283 and 1031 bp respectively. The three-marker concatenated alignment for 66 taxa was 3925 sites.

The SSU alignment included 70 non-*Amphora* taxa with representatives from all raphid diatom orders (*sensu* Round et al. 1990) except the Dictyoneidales, for which no sequence data was available.

The *rbc*L, *psb*C and concatenated alignments included 36 non-*Amphora* taxa, for which end-to-end full sequence of each region was available.

All four datasets (SSU, *rbc*L, *psb*C and concatenated three-marker) were analyzed using the general time reversible (GTR) model with a gamma distribution (Γ) and a proportion of invariable sites (I) as selected using jModelTest ver. 0.1.1 (Guindon & Gascuel 2003, Posada 2008) implementing the Akaike Information Criterion (AIC). Maximum likelihood (ML) analysis was performed using PhyML version 3.0 (Guindon et al. 2010) implemented in SeaView version 4.3.4 (Gouy et al. 2010) using the GTR+ Γ+I model with six rates classes and branch support estimated using 500 bootstrap replicates. Bayesian analysis was conducted using Mr.Bayes version 3.2.1 (Ronquist et al. 2011). Analysis was run using the default priors and a GTR+ Γ +I model with six rate classes. Single marker datasets were run for 15 million generations with a burn-in of 1.5 million generations. The concatenated three-marker alignment was run for 30 million generations with a burn-in of 3 million generations. All alignments were analyzed using two runs of four MCMC chains sampled every 1000 generations.

Hypothesis testing

Hypotheses concerning the monophyly of *Amphora s.l.* were tested using tree likelihoods and the approximately unbiased (AU) test (Shimodaira 2002). For the test, an unconstrained tree was tested against three constrained alternative topologies: **H_1:** the clades containing *Halamphora* and *Amphora* form a monophyletic group, **H_2:** the clades containing *Halamphora*, *Amphora* and the *Oxyamphora lineolata* + *securicula* + *sulcata* clade form a monophyletic group, and **H_3:** *Amphora s.l.* forms a monophyletic group. RAxML ver. 7.3.2 (Stamatakis 2006) and the graphical user interface raxmlGUI ver. 1.2 (Silvestro 2012) were used to generate maximum likelihood trees from the unconstrained and constrained datasets corresponding to the hypotheses above. The probability that the alternative topologies were as likely as the null (unconstrained tree) topology was tested by calculating per site log likelihood values using RAxML and implementing the AU in the program Consel using default settings (Shimodaira and Hasegawa 2001). In the AU test, Consel compares a hypothesized tree topology to a set

of trees generated through a multi-scale bootstrap technique of per site log likelihoods. If the hypothesized tree topology falls outside the 95% confidence interval of the generated trees the hypothesis can be rejected.

RESULTS

Maximum likelihood and bayesian analyses were performed on the concatenated three-marker alignment (SSU + *rbc*L + *psb*C) as well as on individual markers. Presented are the ML phylograms. Node labels correspond to maximum likelihood bootstrap values (BS)/bayesian posterior probability (BPP) reported as a percentage. Incongruence between the ML and bayesian trees is denoted as (-) in the bayesian node support. The results from the analysis of the three marker concatenated matrix is shown in Figure 5.1.

There was congruence between the ML and Bayesian analysis in both the relationships within *Amphora* clades, as well as the positions of these clades within the larger tree. The analysis of the three-marker alignment indicates that *Amphora s.l.* is polyphyletic, both including and excluding the genus *Halamphora*, and has members distributed widely across raphid diatom lineages.

Trees inferred from single marker alignments are largely congruent with the major patterns shown in the concatenated analysis. The results of the ML analyses are presented in supplementary material figures S1, S2 and S3 for the markers SSU, *rbc*L and *psb*C, respectively. All three markers indicate *Amphora s.l.* is polyphyletic. As in the three-marker analysis, *Amphora* and *Diplamphora* were consistently monophyletic, *Halamphora* was monophyletic, and *Oxyamphora* was polyphyletic. Support for the deeper nodes was low in the single markers analyses, making the position of these groups within the larger raphid diatom lineage somewhat ambiguous. Only the sister relationship between *Amphora s.s.* and the *Diplamphora* + *Oxyamphora* clade was consistently well supported (95/100, 86/100 and 48/97 for SSU, *rbc*L and *psb*C, respectively). Only the *psb*C analysis returned a tree in which *Amphora s.l.* was largely monophyletic with a large clade including *Amphora s.s.*, the *Diplamphora* + *Oxyamphora* clade, and the *Halamphora* + *Oxyamphora* clade, although support for this relationship was low (16/56).

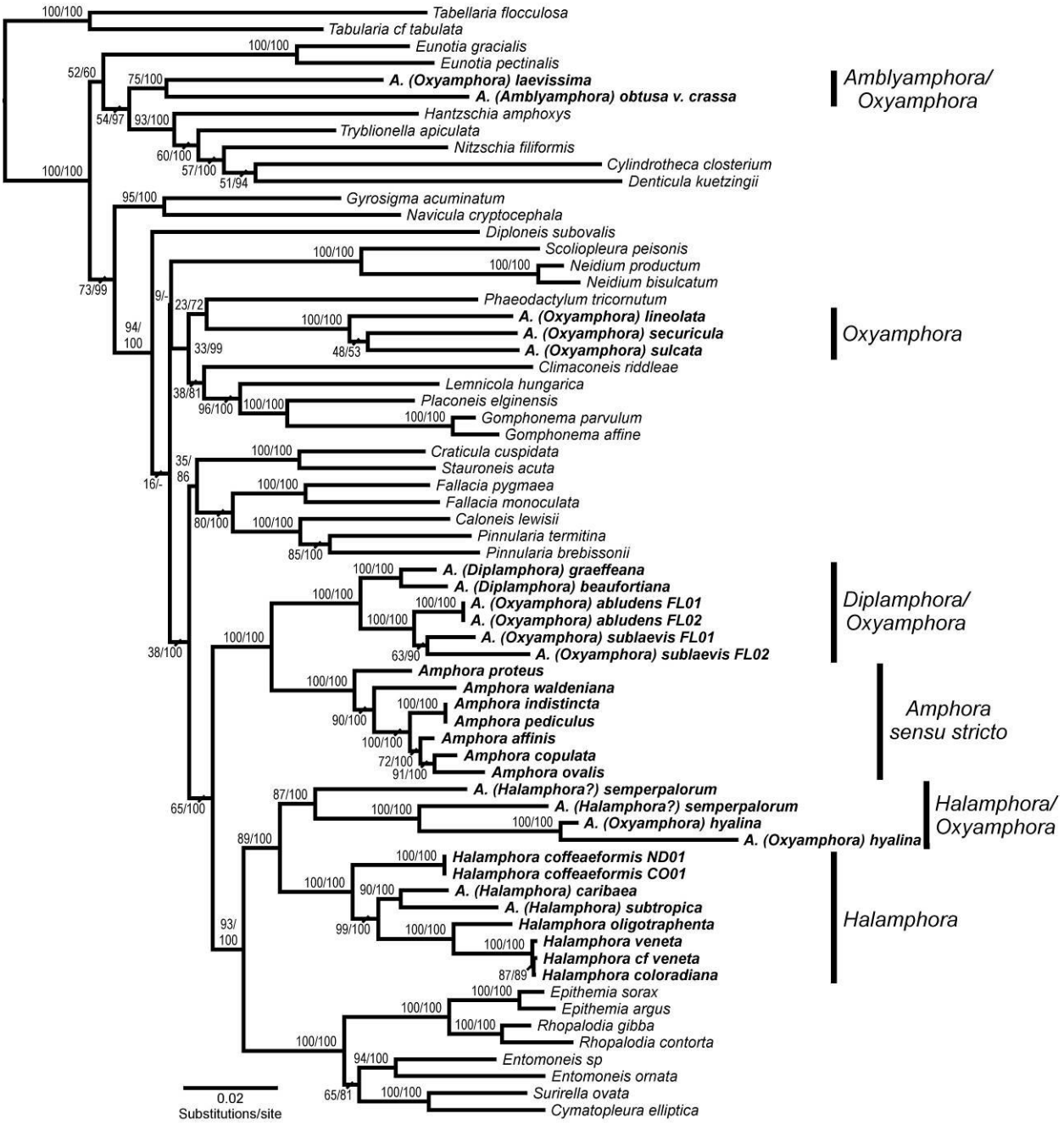

Figure 5.1. Maximum likelihood phylogram inferred from a concatenated three molecular marker alignment, including the nuclear marker SSU rDNA, and the chloroplast markers *rbc*L and *psb*C. Node labels are given as maximum likelihood bootstrap values (500 bootstrap replicates)/bayesian posterior probability (as a percentage). Incongruence between the maximum likelihood and bayesian analyses are denoted with a (-) as a bayesian support value. *Amphora sensu lato* taxa are presented in bold and include the subgenus name in parenthesis. Major clades are labeled with bars and corresponding subgenus or order names. Major chloroplast types, based on Mereschkowsky's (1903) classification, are bracketed.

The results of the hypothesis testing using tree likelihoods and the AU test are listed in Table 5.1. All alternative topologies constrained for monophyly returned AU $p \leq 0.01$, and therefore were rejected given the current data.

Table 5.1. Results from the testing of monophyletic hypotheses using the approximately unbiased (AU) test statistic. OBS = the unconstrained ML tree score subtracted from the constrained tree score. P_{AU} = p-values from the AU test. H0: unconstrained topology from the maximum likelihood analysis. H1: Large *Amphora* and *Halamphora* clades form a monophyletic group. H2: Large *Amphora, Halamphora* and *Oxyamphora lineolata* clades form a monophyletic group, H3: *Amphora sensu lato* is monophyletic.

Hypothesis	OBS	P_{AU}
H_0	-19.3	0.991
H_1	19.3	**0.010**
H_2	70.2	**<0.001**
H_3	162.1	**<0.001**

Amphora sensu stricto

Amphora s.s., containing the generitype *A. ovalis*, is monophyletic with strong node support (100/100) (Figs 5.1, 5.2), and is part of a well-supported (100/100) larger monophyletic group containing the subgenus *Diplamphora* and taxa from the subgenus *Oxyamphora* (Figs 5.1, 5.2). The included taxa conform well to Cleve's (1895) morphological definition, having a semi-elliptical to semi-lanceolate valve outline (Figs 5.2G–M), a biarcuate (Figs 5.2G–H, K–M) to nearly straight (Figs 5.2I–J) raphe, unornamented girdle bands (Fig. 5.5C), and striae composed of more or less elongate areolae in the LM (Figs 5.2G–M). Taxa in this clade correspond to Mereschkowsky's (1903) type 1 chloroplast, having a single, ventrally appressed, plastid with four lobes wrapping up the sides of the frustule (Fig. 5.8A).

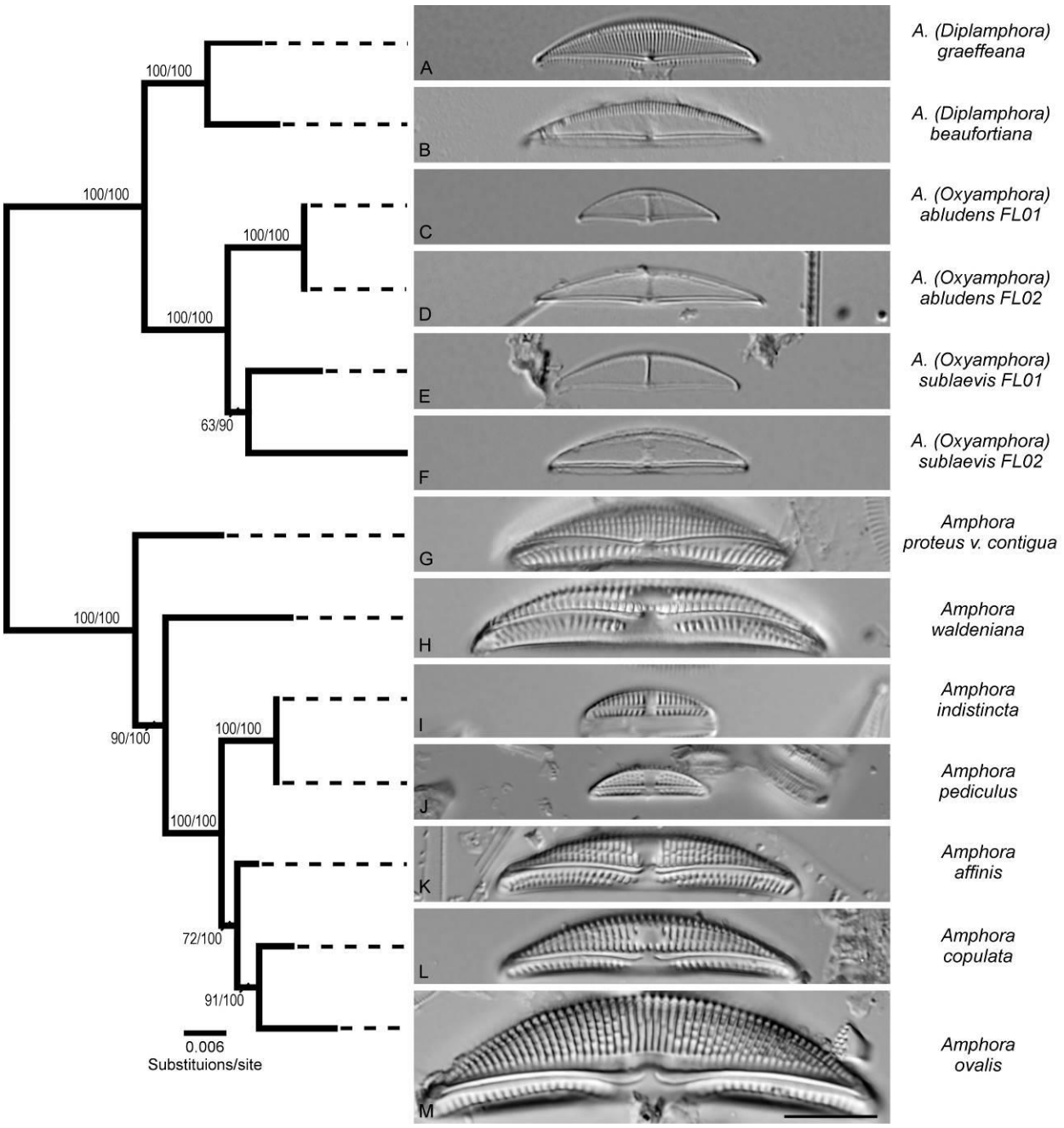

Figure 5.2. Enlarged view of the *Diplamphora* + *Oxyamphora* + *Amphora* clade, with light microscope images of the included taxa, taken from the concatenated maximum likelihood analysis shown in Figure 5.1. Branch lengths correspond to substitutions per site as inferred by the maximum likelihood analysis. Node support is reported as maximum likelihood bootstrap values (500 bootstrap replicates)/bayesian posterior probabilities (shown as a percentage). Dashed lines are for visualization purposes only. **A**–**B**. *Diplamphora* clade. **C**–**F**. *Amphora* (*Oxyamphora*) *abludens* + *sublaevis* clade. **G**–**M**. *Amphora sensu stricto* clade. Scale bar = 10 µm.

Amphora subgenus Diplamphora

The sister clade to *Amphora s.s*. contains taxa from the subgenera *Diplamphora* and *Oxyamphora*. The *Diplamphora* taxa included in this analysis conform well to Cleve's concept of the subgenus, both having semi-elliptical to semi-lanceolate valves (Figs 5.2A, B), a distinct marginal ridge (Fig. 5.5E, arrow) and a more or less distinct hyaline area on the dorsal side (Fig. 5.5E, thin arrow) that correspond to the two longitudinal lines described by Cleve (Figs 5.2A, B), and girdle bands with a row of elongate areolae (Fig. 5.5F). As with *Amphora s.s*., the included *Diplamphora* taxa have a type 1 chloroplast (Fig. 5.8B).

Amphora subgenus Oxyamphora

The ten *Oxyamphora* strains, representing seven species, included in the concatenated analysis fall into four distinct clades: 1) four strains representing two species sister to the *Diplamphora* clade, 2) two strains representing one species within a clade sister to the *Halamphora* clade, 3) a clade containing three species with a poorly supported (23/72) position sister to *Phaeodactylum tricornutum* Bohlin, and 4) a single species with a moderately supported (75/100) relationship with *Amphora* (*Amblyamphora*) *obtusa* var. *crassa* Tempère and Paragallo sister to taxa from the order Bacillariales Hendey.

Of these seven *Oxyamphora* taxa, four of them including, *Amphora abludens* Simonsen, *Amphora sublaevis* Hustedt, *Amphora hyalina* Kützing and *Amphora laevissima* Gregory, although phylogenetically disparate, appear quite similar in the LM (Figs 5.2C–F, 5.3A, 5.4C, D).

In the SEM, *A. laevissima* is distinguished by having striae composed of very small areolae arranged in transverse rows, and lacking both a raphe-ledge and a dorsal marginal ridge (Fig 5.5G, J), features shared with its sister taxon, *A. obtusa* var. *crassa* (Figs 5.5I, K). Although similar in frustule morphology, they differ in chloroplast structure with *A. laevissima* having a single dorsally appressed plastid (Mereschkowsky's type 4) (Fig. 5.8G), and *A. obtusa* var. *crassa* having two dorsally appressed plastids (Mereschkowsky's type 6) (Fig. 5.8H). Additionally, the two taxa differ from each other in the

position and direction of the raphe along the valve (Figs 5.3A, B) and the direction of the deflection of the distal raphe ends (Figs 5.5J, K, arrows).

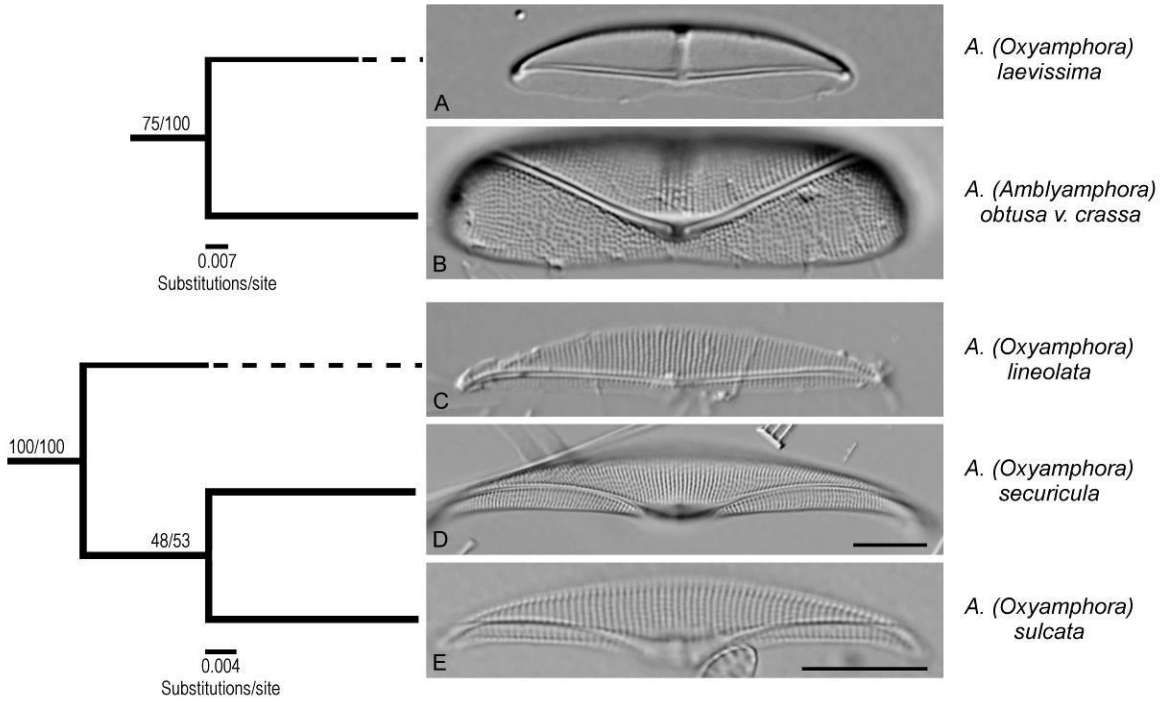

Figure 5.3. Enlarged view of the *Oxyamphora* + *Amblyamphora* and *Amphora* (*Oxyamphora*) *lineolata* + *securicula* + *sulcata* clades, with light microscope images of the included taxa, taken from the concatenated maximum likelihood analysis shown in Figure 5.1. Branch lengths correspond to substitutions per site as inferred by the maximum likelihood analysis. Node support is reported as maximum likelihood bootstrap values (500 bootstrap replicates)/bayesian posterior probabilities (shown as a percentage). Dashed lines are for visualization purposes only. **A–B**. *Oxyamphora* + *Amblyamphora* clade. **C–E**. *Amphora* (*Oxyamphora*) *lineolata* + *securicula* + *sulcata* clade. Scale bars = 10 µm.

Amphora abludens and *A. sublaevis*, positioned sister to the *Diplamphora* clade, share a continuous dorsal raphe-ledge (Figs 5.6A, B, arrows), small and somewhat irregular round to oblong areolae, and a distinct dorsal marginal ridge bordered by elongate areolae (Fig. 5.6A, thin arrow). The continuous dorsal raphe-ledge and marginal ridge bordered by a row of elongate areolae are very similar to members of the sister group, *Diplamphora* (Fig. 5.5E). These groups also share girdle band punctation consisting of a single row of elongate areolae running the length of the band (Fig. 5.6C) and a type 1 plastid (Fig. 5.8C).

The *Oxyamphora* clade containing the taxa *Amphora lineolata* Ehrenberg, *Amphora securicula* Peragallo and Peragallo, and *Amphora sulcata* Brébisson form a well-supported (100/100) monophyletic group and this close relationship is reflected in their similar morphologies (Figs 3C–E). These taxa lack a raphe-ledge and a marginal ridge (Figs 6D, F), and all have many areolate girdle bands (Fig. 6E, arrow) and four chloroplasts, two positioned dorsally and two positioned ventrally (Mereschkowsky's type 8) (Figs 8I). Although support for this clade is strong, its phylogenetic position remains ambiguous with a weakly supported sister relationship (23/72) with *P. tricornutum*.

Finally, two *A. hyalina* strains, from the subgenus *Oxyamphora*, are positioned within a clade that includes *Amphora* (*Halamphora*?) *semperpalorum* (87/100) and is sister to the genus *Halamphora*. Although these taxa differ from *A. semperpalorum* in the biseriate nature of the striae and their lack of axial longitudinal lines, their continuous dorsal raphe-ledge, more or less distinct marginal ridge, and biseriate dorsal striae (Figs 5.6G, H) are all suggestive of an affinity to members of the genus *Halamphora* (Figs 5.7C–E). Additionally, the plastid morphology of *A. hyalina* and *A. semperpalorum* (Figs 5.8E, F) are similar to the type 2 plastid seen in *Halamphora*, which have a single ventrally appressed H-shaped plastid (Fig 5.8D).

Halamphora

This study lends strong support (93/100) to the previously reported (Ruck and Theriot 2011; Sato et al. 2013) phylogenetic position of the genus *Halamphora* as sister to the Rhopalodiales and Surirellales. *Halamphora* is described as having dorsiventral linear, semi-lanceolate to semi-elliptical valves with variable but often protracted valve ends, striae composed of round, elliptical to transversely elongate areolae, the raphe lying on a raphe ledge near the ventral margin with dorsally curved distal ends and numerous girdle bands with one to two rows of pores (Levkov 2009). As these taxa are currently classified, the genus *Halamphora* forms a monophyletic group (100/100), sister to a clade containing the taxa *A. semperpalorum* and *A. hyalina* (89/100), two taxa that are phylogenetically and morphologically distinct from *Amphora s.s.*, the genus to which they are currently assigned.

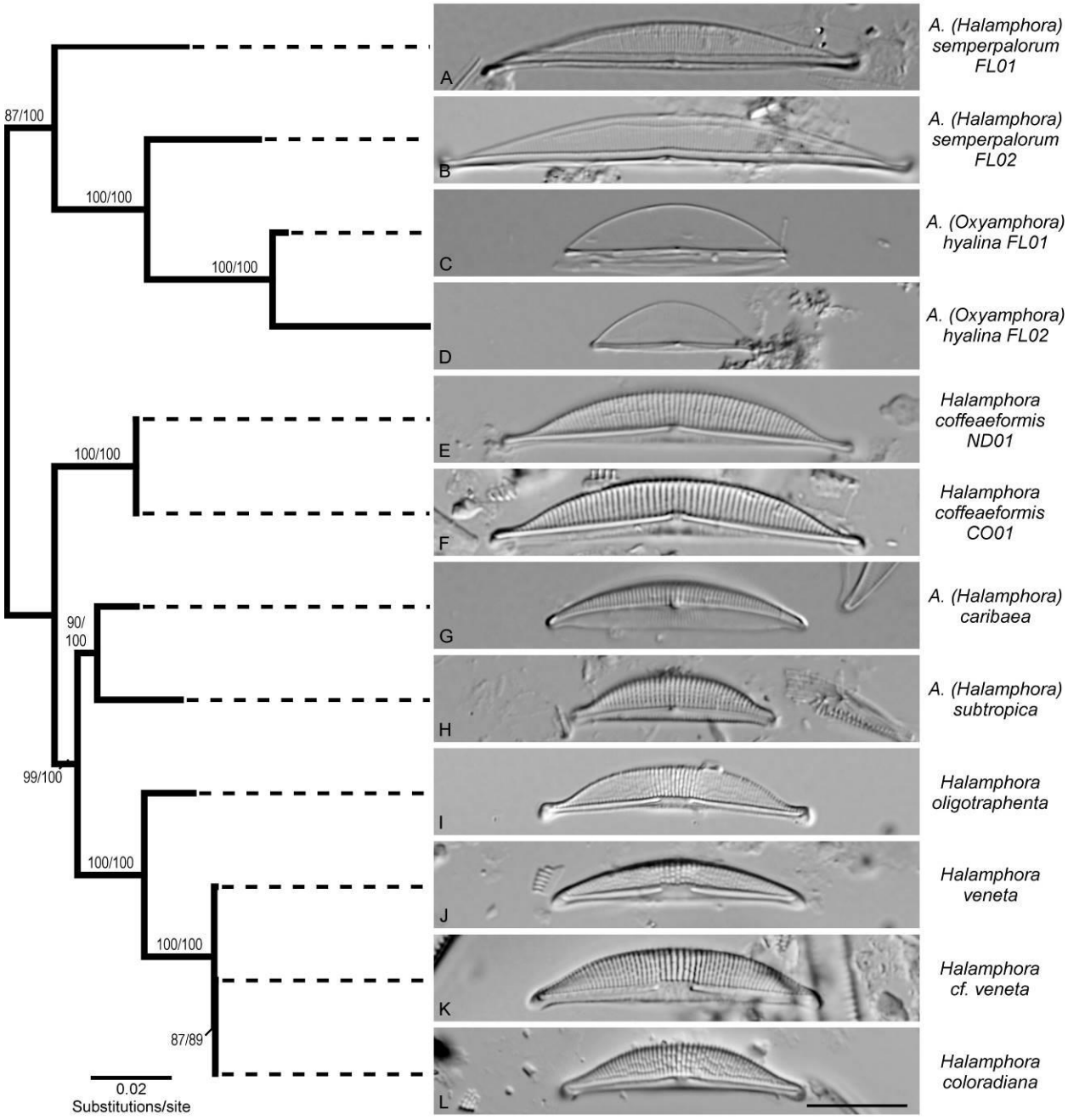

Figure 5.4. Enlarged view of the *Halamphora* + *Oxyamphora* clade, with light microscope images of the included taxa, taken from the concatenated maximum likelihood analysis shown in Figure 5.1. Branch lengths correspond to substitutions per site as inferred by the maximum likelihood analysis. Node support is reported as maximum likelihood bootstrap values (500 bootstrap replicates)/bayesian posterior probabilities (shown as a percentage). Dashed lines are for visualization purposes only. **A–D**. *Amphora* (*Halamphora*?) *semperpalorum* + *Amphora* (*Oxyamphora*) *hyalina* clade. **E–L**. *Halamphora* clade. Scale bar = 10 µm.

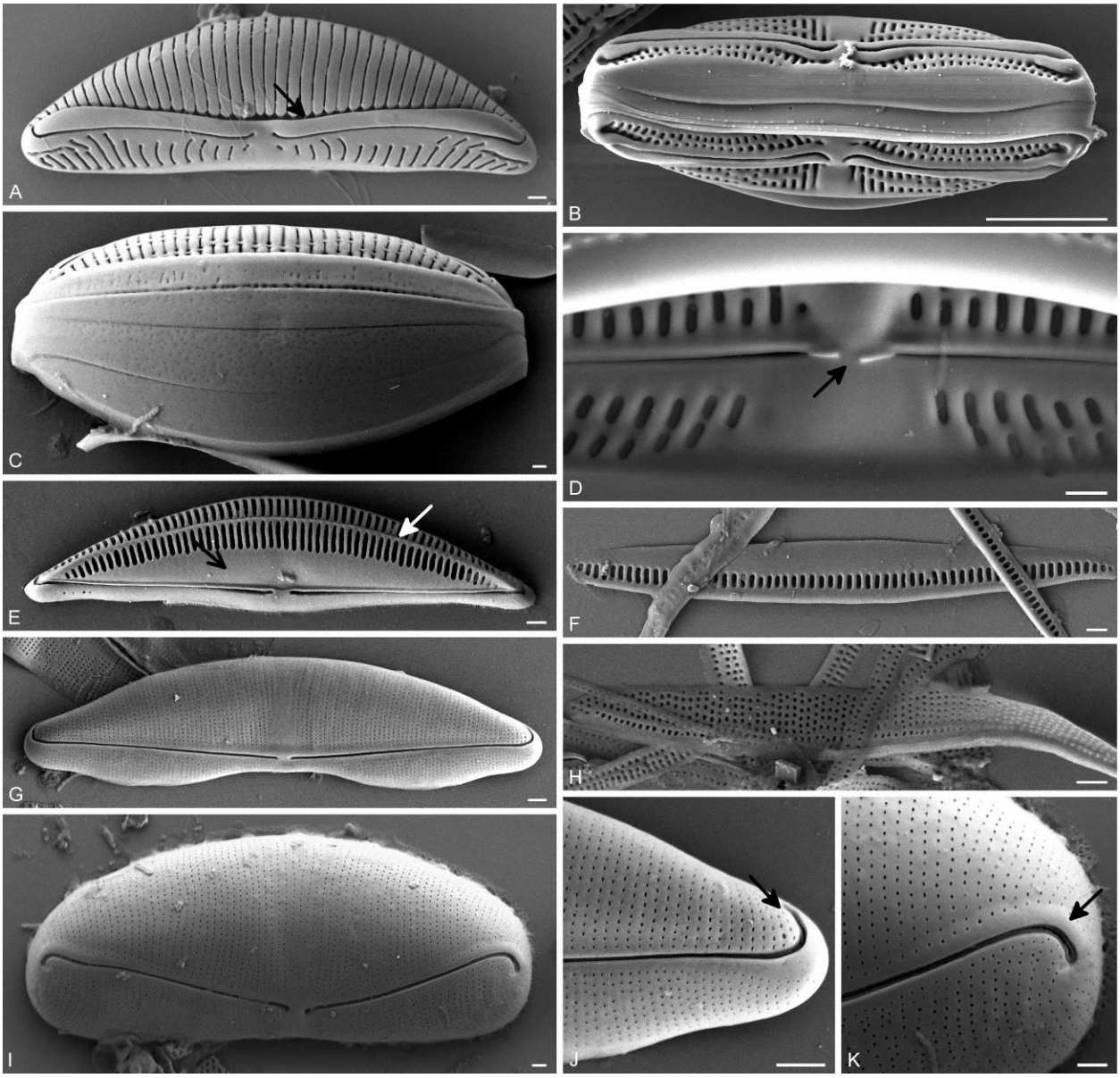

Figure 5.5. Scanning electron micrographs of select taxa included in the phylogenetic analysis. **A–D**. Taxa from the *Amphora sensu stricto* clade. **E, F**. Taxa from the *Diplamphora* clade. **G–K**. taxa from the *Oxyamphora* + *Amblyamphora* clade. **A**. External valve view of *Amphora proteus* var. *contigua* showing the continuous raphe ledge (arrow). **B**. External whole frustule view of *Amphora affinis*. **C**. Dorsal whole frustule view of *Amphora copulata* showing non-areolate girdle bands. **D**. Internal detail of *A. affinis* showing separated central helictoglossae (arrow). **E**. External valve view of *Amphora* (*Diplamphora*) *beaufortiana* showing the marginal ridge (white arrow) and dorsal hyaline area (thin arrow). **F**. Girdle band of *A. beaufortiana*. **G**. External valve view of *Amphora* (*Oxyamphora*) *laevissima*. **H**. Girdle band of *A. laevissima*. **I**. External valve view of *Amphora* (*Amblyamphora*) *obtusa* var. *crassa*. **J**. Detail of *A. laevissima* external valve showing finely areolate striae and dorsally bent distal valve ends. **K**. Detail of *A. obtusa* var. *crassa* external valve showing finely areolate striae and ventrally bent distal valve ends. Scale bars A, C–K = 1 µm, B = 10 µm.

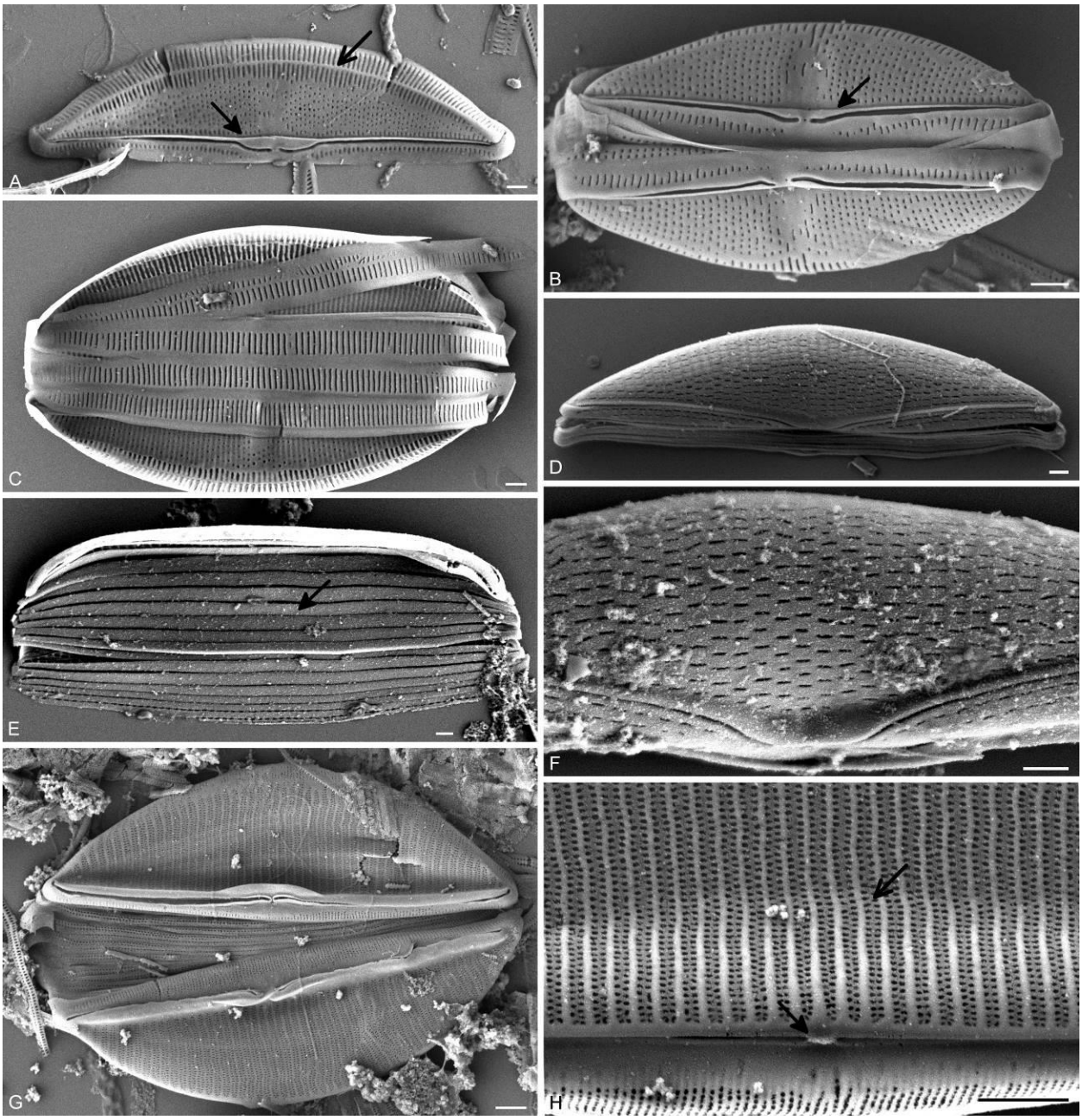

Figure 5.6. Scanning electron micrographs of select taxa included in the phylogenetic analysis. **A–C**. Taxa from the *Amphora* (*Oxyamphora*) *abludens* + *sublaevis* clade. **D–F**. Taxa from the *Amphora* (*Oxyamphora*) *lineolata* + *securicula* + *sulcata* clade. **G, H**. *Amphora* (*Oxyamphora*) *hyalina*. **A**. External valve view of *A. sublaevis* showing the continuous dorsal raphe ledge (arrow), and a distinct marginal ridge (thin arrow). **B**. External whole frustule view of *A. abludens* showing marginal ridge (arrow). **C**. Internal whole frustule view of *A. sublaevis* with areolate girdle bands. **D**. External valve view of *A. sulcata*. **E**. External dorsal view of *A. sulcata* showing numerous thin girdle bands (arrow). **F**. Detail of *A. sulcata* external central valve. **G**. External whole frustule view of *A. hyalina*. **H**. Detail of *A. hyalina* internal central valve showing fused central helictoglossae (arrow) and biseriate dorsal striae (thin arrow). Scale bars = 1 μm.

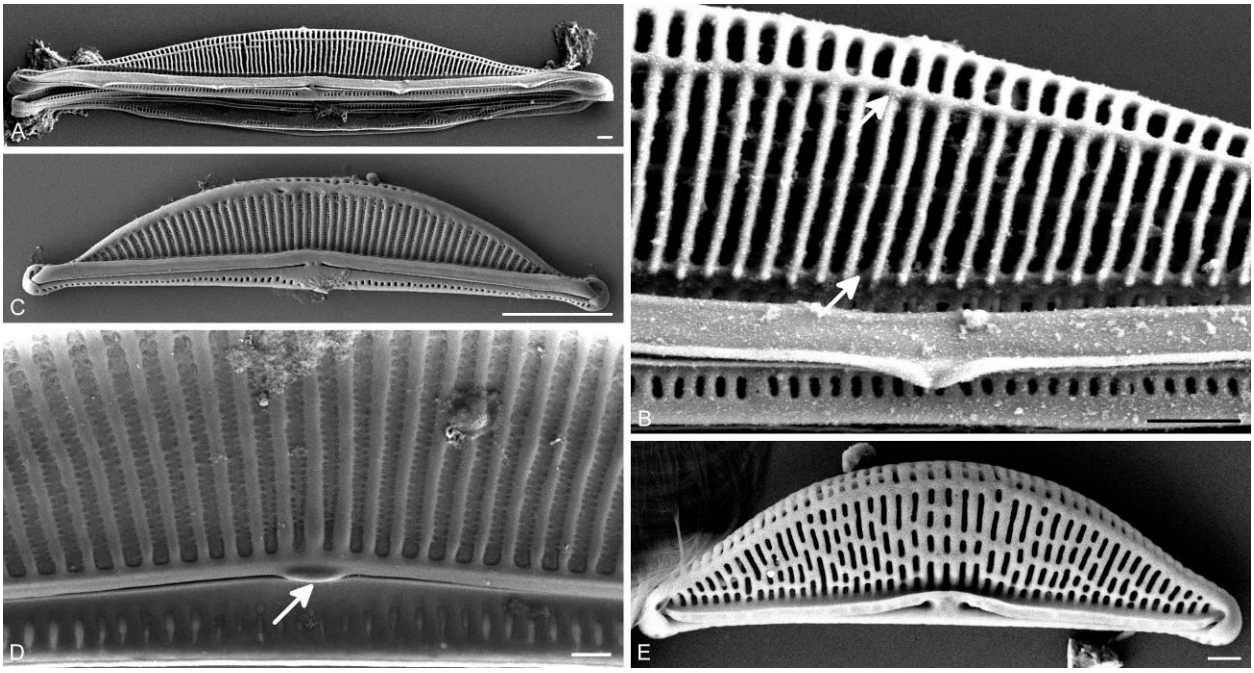

Figure 5.7. Scanning electron micrographs of select taxa included in the phylogenetic analysis. **A, B**. *Amphora* (*Halamphora*?) *semperpalorum*. **C–E**. Taxa from the *Halamphora* clade. **A**. External valve view of *Amphora* (*Halamphora*?) *semperpalorum*. **B**. Detail of *A. semperpalorum* external valve showing two dorsal longitudinal lines (arrows). **C**. External valve view of *Halamphora coffeaeformis*. **D**. Detail of *H. coffeaeformis* showing fused central helictoglossae (arrow). **E**. External valve view of *Halamphora coloradiana*. Scale bars A, B, D, E = 1 μm, Scale bar C = 10 μm.

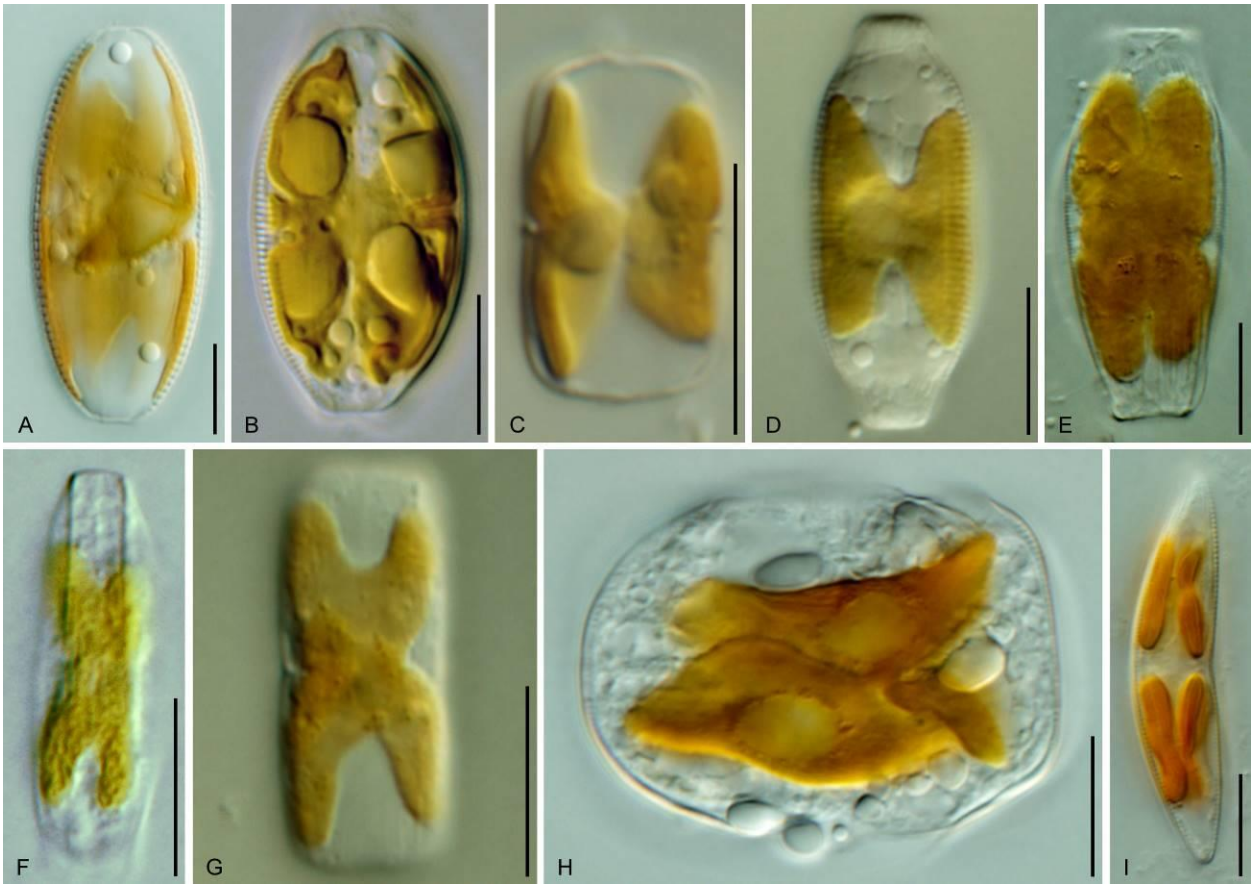

Figure 5.8. Light micrographs showing the plastid morphology and diversity across included taxa. **A–C**. Taxa corresponding to Mereschkowsky's (1903) type 1 plastid. **D–F**. Mereschkowsky's type 2 plastid. **G**. Mereschkowsky's type 4 plastid. **H**. Mereschkowsky's type 6 plastid. **I**. Mereschkowsky's type 8 plastid. **A**. *Amphora proteus*. **B**. *Amphora* (*Diplamphora*) *graeffeana*. **C**. *Amphora* (*Oxyamphora*) *abludens*. **D**. *Halamphora coffeaeformis*. **E**. *Amphora* (*Halamphora*?) *semperpalorum*. **F**. *Amphora* (*Oxyamphora*) *hyalina*. **G**. *Amphora* (*Oxyamphora*) *laevissima*. **H**. *Amphora* (*Amblyamphora*) *obtusa* var. *crassa*. **I**. *Amphora* (*Oxyamphora*) *sulcata*. Scale bars = 10 μm.

DISCUSSION

The aim of this investigation was to examine the monophyly of *Amphora s.l.* and its overall position within raphid diatoms utilizing three molecular markers and extensive taxon sampling. These results will be discussed within the context of Cleve's (1895) classification, which divided *Amphora* into nine subgroups, of which six extant groups remain under the current classification.

The most recent studies (Ruck & Theriot 2011, Sato et al. 2013) have indicated *Amphora s.l.* is paraphyletic with *Halamphora* sister to the Rhopalodiales and Surirellales, although the support for this relationship has not been strong enough to reject outright the monophyly of *Amphora s.s.* + *Halamphora*

(Sato et al. 2013). The results of this study have both strengthened support for the paraphyly of the groups (hypothesis of monophyly was rejected p = 0.01) and the systematic position of *Halamphora* as sister to the Surirellales and Rhopalodiales. Additionally, inclusion of taxa from the subgenera *Oxyamphora* and *Amblyamphora* have shown several groups classified within the genus *Amphora* fall well outside these clades. Although not monophyletic as a whole, we can now begin to examine the subgroups within *Amphora s.l.* as work continues toward a natural classification system.

Suggestions for a revised classification

The implications of this investigation moving forward within *Amphora* systematics are numerous. As has been suggested previously, *Amphora s.l.* is polyphyletic and distributed widely throughout raphid diatom lineages. It would appear that in order to create a classification system that reflects monophyletic groups within *Amphora s.l.*, new genera will need to be erected that do not necessarily correspond to Cleve's subgenera.

Amphora s.s., including the generitype *A. ovalis*, remains a monophyletic group. Although morphologically and phylogenetically distinct from *Amphora s.s.*, the sister clade containing taxa from the subgenera *Diplamphora* and *Oxyamphora* are included in a larger monophyletic *Amphora s.l.* In light of the results from Sato et al. (2013), additional taxon sampling from the subgenus *Diplamphora* may be necessary to determine whether *Amphora s.s.* and taxa from the subgenus *Diplamphora* remain as distinct monophyletic groups or whether *Diplamphora* is non-monophyletic as in Sato et al.'s (2013) analysis. Likewise, whether the *Diplamphora* and *Oxyamphora* taxa will remain as two distinct monophyletic groups as more morphological diversity within the *Diplamphora* and *Oxyamphora* subgenera are included requires further investigation. What is clear is that as part of a large clade that includes *Amphora s.s.*, these and there closely related taxa are taxonomically stable as currently classified within the genus *Amphora*.

It is apparent that *A. semperpalorum* and *A. hyalina* are not included within the genus *Amphora* to which they are currently assigned, forming a well-supported clade (87/100) sister to the genus

Halamphora. This has created a situation where the transfer of the morphologically similar *A. semperpalorum* to the genus *Halamphora* without the additional transfer of *A. hyalina* and its closely allied species would leave *Halamphora* paraphyletic. In order to maintain a monophyletic classification, these taxa and their closely allied species must either all be transferred into the genus *Halamphora* or a new genus that encompasses the morphological diversity of this clade must be erected. The genus *Halamphora* currently encompasses a large variety of forms, a situation that may certainly expand as taxa not formerly included in the subgenus are added.

A continuing challenge will be assigning evolutionarily meaningful characteristics to the *Amphora* + *Diplamphora* + *Oxyamphora* and *Halamphora* + *Oxyamphora* clades as systematic work moves forward (Fig. 5.9). Much of the difficulty in assigning synapomorphies to *Amphora* and *Halamphora* stems from the paraphyletic nature of these two large clades and the morphological diversity within them. Given the topology from this analysis, it may be inferred that many of the diagnostic features assigned to *Amphora s.s.* and *Halamphora* (asymmetry along the valvar plane, raphe ledge, dorsally bend distal raphe ends, internal areolae occlusions, central helictoglossae, a single ventrally appressed chloroplast) are symplesiomorphic within these lineages (Fig. 5.9, solid tick marks) and were subsequently lost in later lineages (although amphoroid asymmetry is observed in members of the Rhopalodiales).

With the plesiomorphic traits aside, there remains several putative synapomorphies that can be assigned to each major lineage. The most striking of these are differences in plastid morphology, with the *Amphora s.s.* + *Diplamphora* + *Oxyamphora* clade all sharing a type 1 chloroplast (Fig. 5.8A–C) and the *Halamphora* + *Oxyamphora* sharing a type 2 chloroplast (Fig. 5.8D–F). In addition to plastid morphology the *Amphora s.s.* + *Diplamphora* + *Oxyamphora* clade share separated central helictoglossae (Fig. 5.5D, arrow) (although this feature is less pronounced in *Diplamphora* and the included *Oxyamphora* taxa [Levkov 2009, Sato et al. 2013]), a marginal ridge, and a suite of somewhat variable features such as

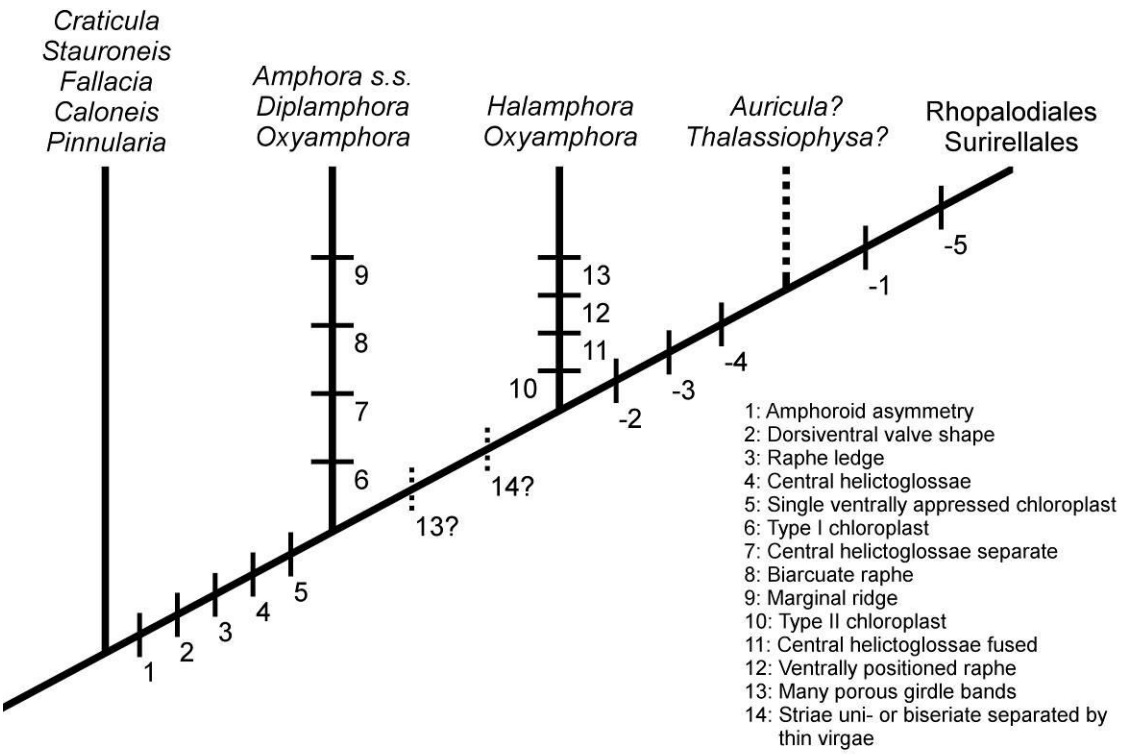

Figure 5.9. Simplified cladogram of a subsection of the phylogram presented in Figure 1. Numbers represent taxonomically important characteristics previously used with *Amphora sensu lato* taxa and correspond to the included key. Dotted lines represent currently undefined relationships.

valve outline and a biarcuate raphe. Aside from plastid morphology taxa in the *Halamphora* + *Oxyamphora* clade share a fused central helictoglossae (Figs 5.6H, 5.7D, arrows), many poroid girdle bands, and again several somewhat variable features such as valve outline, a straight ventrally placed raphe, and often protracted rostrate to capitate valve ends.

An interesting aspect of Figure 5.9 is both the loss of characters from the *Halamphora* + *Oxyamphora* clade to the Surirellales + Rhopalodiales clade, as well as a lack of features defining the larger *Halamphora* + *Oxyamphora* + Surirellales + Rhopalodiales clade. One possible explanation for this pattern is the absence of taxa (either unknown or unrepresented) that would be transitional forms between *Halamphora* and the Rhopalodiales and Surirellales. The marine genera *Thalassiophysa* Conger and *Auricula* Castracane seem obvious choices to fill this 'missing link' position in the phylogeny as they both exhibit several amphoroid characteristics and have had taxa previously assigned to the genus

Amphora. Both *Auricula* and *Thalassiophysa* exhibit amphoroid symmetry created through a deep dorsal mantle and differential thickness of their many poroid girdle bands (see Paddock and Sims [1980] for a thorough morphological treatment of both genera), features potentially shared with *Amphora s.s.* + *Halamphora* and *Halamphora*, respectively. Additionally, both genera have a single ventrally appressed chloroplast and biseriate striae separated by thin virgae (Paddock & Sims 1980) that are not unlike stria features seen in the *Halamphora* + *Oxyamphora* clade (Fig. 5.6H, thin arrow, 5.7D). Although sharing several features with *Amphora* and *Halamphora*, *Auricula* and *Thalassiophysa* both have a fibulate canal raphe system similar to the Surirellales and Rhopalodiales.

As for the *Oxyamphora* and *Amblyamphora* taxa within distantly related clades, there is little question that these taxa are not closely related to *Amphora s.s.* and will, therefore, need to be either transferred to an existing genus or included in a new genus. For the clade containing *A. lineolata*, *A. securicula* and *A. sulcata* the current analysis offers few clues as to their closely allied taxa or groups, being located in a generally poorly supported portion of the tree. As these taxa are all of a marine origin, it is likely that greater taxon sampling of often under-represented coastal marine diatoms will be necessary for any definitive placement using molecular techniques.

The position of the *Amblyamphora* + *Oxyamphora* clade is one of the surprising outcomes of this study. This group is positioned within a clade sister to the majority of the raphid diatom lineages which includes members of the Bacillariales and two taxa from the genus *Eunotia* Ehrenberg. Although support for these relationships are not strong (54/97 and 52/60), the placement is none the less interesting. Mann (1994), in referring to the plastid organization and sexual reproduction of the subgenus *Psammamphora* (morphologically very similar to *Amblyamphora* but lacking poroids on its girdle bands), pointed out great differences from *Amphora s.s.* and postulated that the two may in fact be distantly related to *Amphora s.s.* Furthermore he contended that within *Amphora s.l.* may lie the closest relatives of the fibulate (canal raphid) diatoms (Bacillariales, Rhopalodiales and Surirellales) (Mann 1986), although, interestingly, he did not assume that it would necessarily be the same group of amphoroid diatoms that gave rise to each. This analysis lends strong evidence for both the polyphyletic nature of the genus

Amphora as well as to the close association between amphoroid taxa and the, also polyphyletic (Ruck & Theriot 2011) canal raphid diatoms, with *Amphora* taxa sister to the two independent occurrences of the canal raphe in the Bacillariales and the clade containing the Rhopalodiales and Surirellales.

The close association with the taxa from the genus *Eunotia*, from the raphid diatom order Eunotiales Silva, is also of interest as the genera *Amphorotia* Williams and Reid and *Eunophora* Vyverman, Sabbe and Mann from this order exhibit strong amphoroid asymmetry (Vyverman et al. 1998, Williams & Reid 2006). Additionally, members of *Eunophora* are quite similar to the subgenera *Amblyamphora* and *Psammamphora* in general morphology, differing primarily in the presence of a specialized pore (rimoportula) present in many members of *Eunophora*. The potential association between these taxa and members of *Amphora s.l.* is of special interest because of the unique systematic position the Eunotiales have historically held, what has been thought to be the first family of diatoms to have acquired a raphe system (Simonsen 1979). Because of their affinity to the non-raphe bearing diatoms, Simonsen (1979) postulated that the Enotiaceae may in fact represent an evolutionary branch independent from the rest of the raphe-bearing diatoms, and by extension may represent an independent evolution of the raphe system.

Inclusion of the taxa *A. laevissima* and *A. obtusa* var. *crassa* to the concatenated analysis has offered an expanded hypothesis for the relationship between the Eunotiaceae and raphid diatom lineages, by pulling *Eunotia*, *A. laevissima*, *A. obtusa* var. *crassa* and members of the Bacillariales (a group with a highly derived canal raphe system) into a monophyletic group sister to the remaining raphid diatoms. If this relationship stands further testing, it would expand the previous hypothesis of the parallel evolution of two independent lineages of raphid diatoms to include amphoroid lineages, and an independent occurrence of what has been considered a highly derived (Round et al. 1990, Sims & Paddock 1982) canal raphe system.

Interestingly, although he did not address all of the diversity within *Amphora s.l.*, Mereschkowsky's plastid types align well with the large clades described in this study (Fig. 5.1, brackets). Moving forward, an improved set of homologous characters, that includes features of the

frustule as well as the protoplast, will likely be necessary to develop a revised classification of *Amphora s.l.* This study lays the groundwork for just such a revision; a detailed morphological and phylogenetic reclassification of the amphoroid diatoms based on monophyly rather than symmetry.

Historically, diatom systematics has strived to define 'key' features that produced a simple classification system for a large and diverse group of organisms. What this and other studies have unequivocally demonstrated is that these defining features often have no evolutionary basis. This has certainly been the case with some of the most basic taxonomic divisions within diatoms, including between circular (centric) or elongate (pennate) cell outline (Medlin & Kaczmarska 2004, Theriot et al. 2010), having no raphe (araphid), a raphe on only one valve (monoraphid), or a raphe on both valves (biraphid) (Bruder & Medlin 2008, Kociolek & Stoermer 1986, Kociolek et al. 2013), the presence or absence of a canal raphe system (Ruck & Theriot 2011). To this can be added finer symmetry features including 'gomphonemoid' symmetry in the case of the genus *Didymosphenia* Schmidt (Kermarrec et al. 2011, Kociolek & Stoermer 1988) and now amphoroid symmetry, as well as major ecological divisions between marine and freshwater lineages (Alverson et al. 2007). Although convenient, all of these long standing systems of classification have been shown to largely define non-monophyletic groups. A diatom classification system based on monophyly will certainly be more cumbersome than the divisions mentioned above, but this cost is far outweighed by the practical benefits of a natural classification system.

This type of 'natural' classification system is becoming increasingly important as algae in general and diatoms in particular are being utilized for a number of practical applications including the quickly expanding area of biofuels production (Graham et al. 2012, Sheehan et al. 1998). Algae are of particular interest in this research as they are more productive per acre than conventional terrestrial oil crops (Chisti 2007), and can be grown in non-agricultural lands using brackish or salt waters (Groom et al. 2008, Pienkos & Darzins 2009, Sheehan et al. 1998). Within the field of algal biofuels, *Amphora* taxa have been indicated as potentially promising candidates due to their fast growth rate and high lipid production (Sheehan et al. 1998), but in light of this and other (Alverson et al. 2007, Bruder & Medlin 2008,

Kociolek & Stoermer 1986, Kociolek & Stoermer 1988, Kociolek et al. 2013, Medlin & Kaczmarska 2004, Ruck & Theriot 2011, Theriot et al. 2010) studies one is forced to ask the usefulness of making such statements about a clearly non-monophyletic group. This example plainly illustrates why a thorough understanding of the evolutionary relationships of these taxa is imperative, as claims about shared characteristics such as lipid production are meaningless if not referring to monophyletic groups. As our use of these extremely diverse organisms for practical applications increases, so must our understanding of their phylogenetic relationships if we hope to utilize them efficiently and effectively.

ACKNOWLEDGEMENTS

We would like to thank Sarah Hamsher for helpful advice throughout this project and for critical comments and suggestions in the final stages of this manuscript. This research was supported in part by a Seed Grant for Innovation from the University of Colorado, Boulder.

Figure S1. Maximum likelihood cladogram inferred from SSU sequence data. *Amphora sensu lato* taxa are presented in bold and subgenus names are in parentheses. Node support values are shown as ML bootstrap values (500 replicates)/bayesian posterior probabilities (as a percentage).

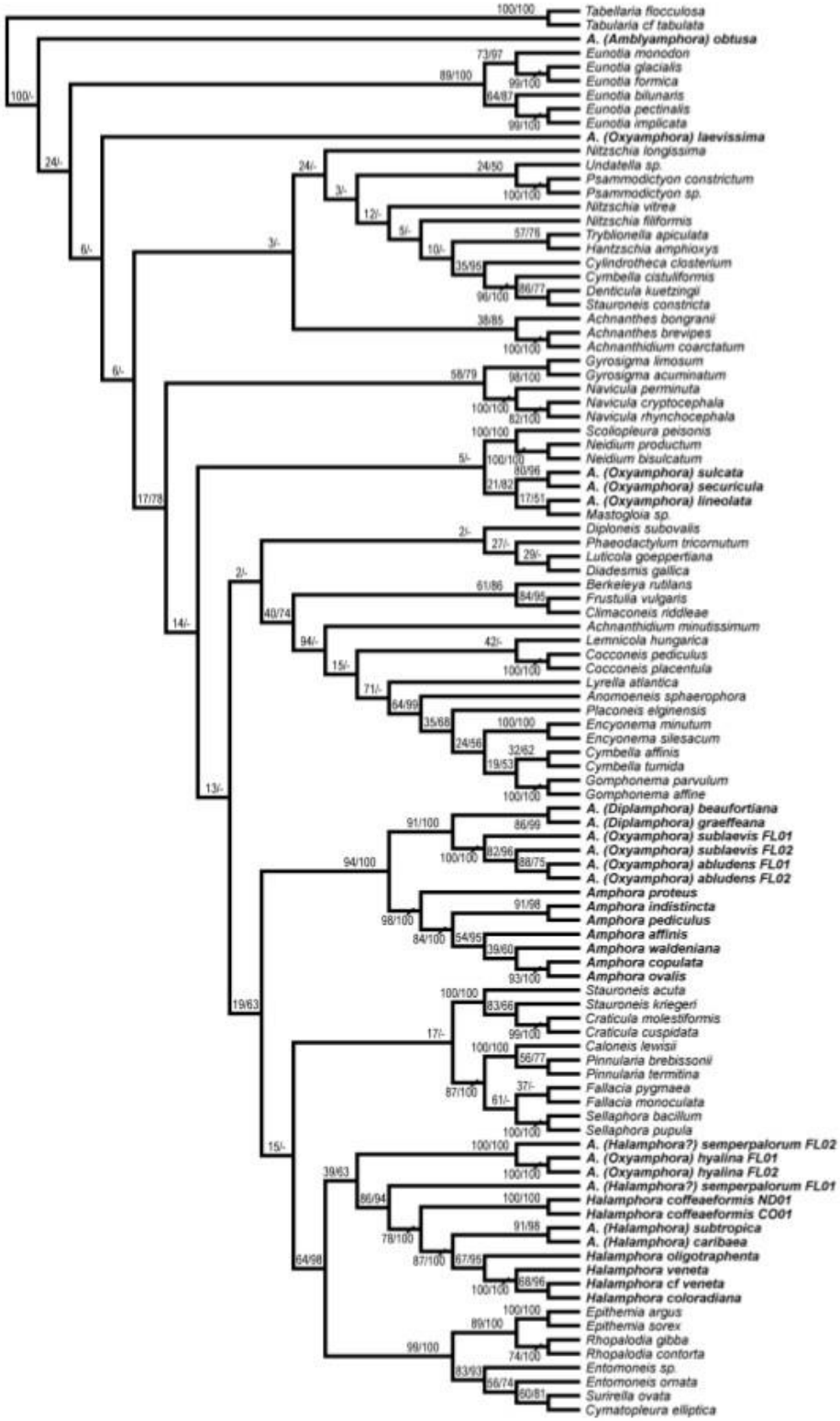

Figure S2. Maximum likelihood cladogram inferred from *rbc*L sequence data. *Amphora sensu lato* taxa are presented in bold and subgenus names are in parentheses. Node support values are shown as ML bootstrap values (500 replicates)/bayesian posterior probabilities (as a percentage).

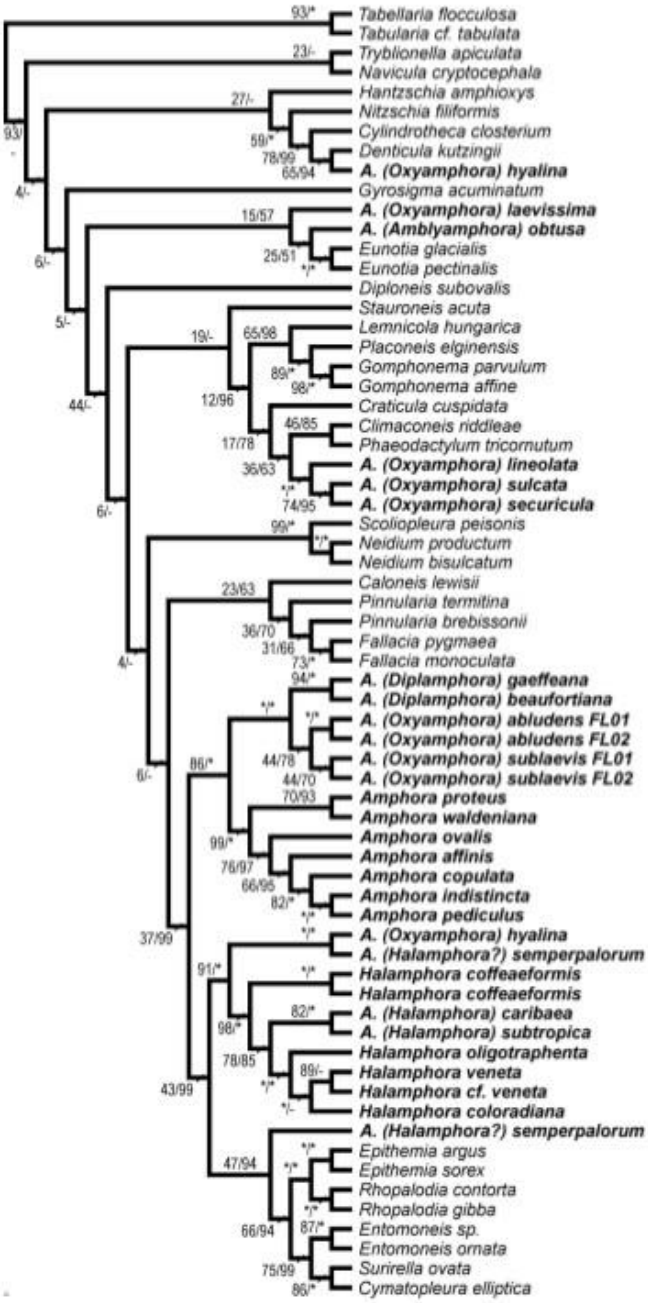

Figure S3. Maximum likelihood cladogram inferred from *psb*C sequence data. *Amphora sensu lato* taxa are presented in bold and subgenus names are in parentheses. Node support values are shown as ML bootstrap values (500 replicates)/bayesian posterior probabilities (as a percentage).

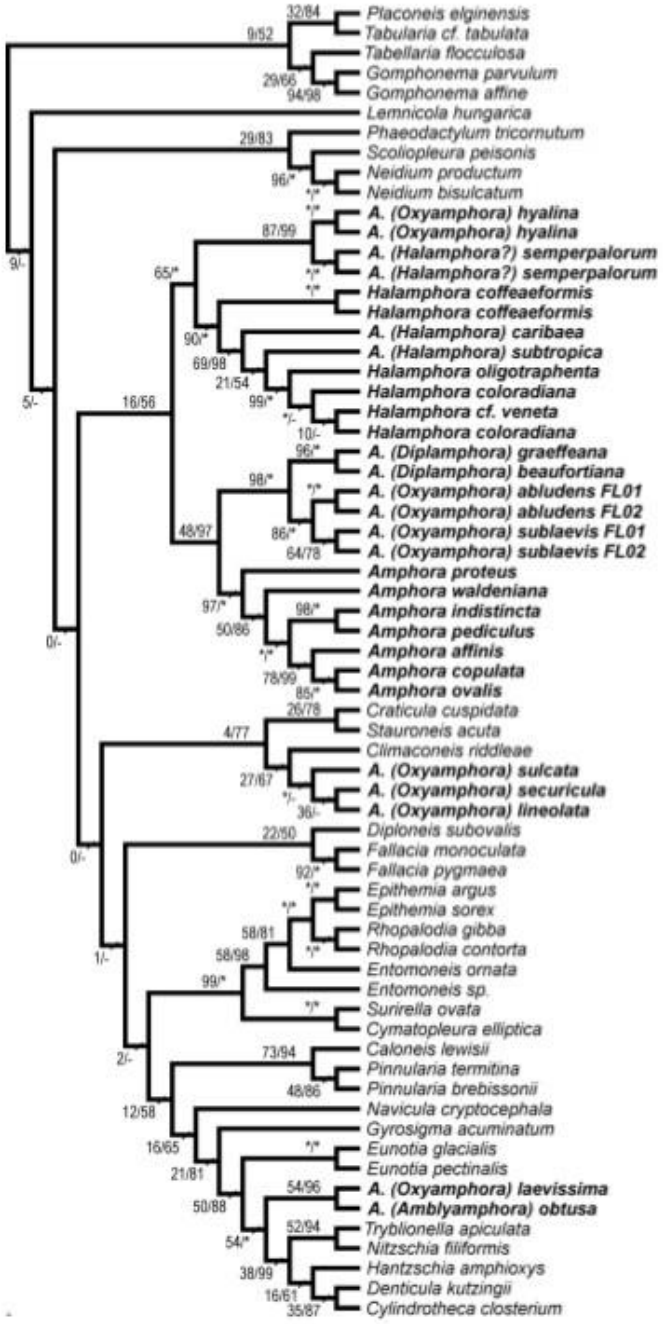

CHAPTER VI

DESCRIPTION AND PHYLOGENETIC POSITION OF *AMPHORA ALIFORMIS* (BACILLARIOPHYTA), A NEW SPECIES FROM TOKYO BAY

Adapted from: Stepanek, J.G. & Kociolek, J.P. 2015. Description and phylogenetic position of *Amphora aliformis* (Bacillariophyta), a new species from Tokyo Bay. *Phycologia* 54: 78–86.

ABSTRACT

The genus *Amphora* is a large and widely distributed group of raphid diatoms, frequently found in fresh, brackish, and saltwater environments from around the world. Presented here is the description and phylogenetic position of *Amphora aliformis*, a new species collected from the Banzu Flats, Tokyo Bay, Japan. This species has a unique morphology with features seldom or not before observed within the genus *Amphora* such as a dorsal marginal wing and ventral apical pores, as well as a unique phylogenetic position as an early diverging lineage within the genus. As with many large and diverse groups of diatoms, new evidence has called into question the validity of the long standing classification system for the genus *Amphora*. Within the previous system, *A. aliformis* would be prescribed to the subgenus *Diplamphora* based on morphological valve features. However, molecular phylogenetic analysis demonstrates that *Diplamphora* is not monophyletic and furthers evidence that *Amphora* classification is in need of revision. Included here is a description of *A. aliformis* based on light microscope, scanning electron microscope, and molecular phylogenetic data, as well as a reexamination and discussion of the current state of *Amphora* classification.

INTRODUCTION

The genus *Amphora* Ehrenberg ex Kützing *s.l.* is a large and diverse group of raphid diatoms commonly found in fresh, brackish, and saltwater environments (Stoermer & Yang 1971, Wachnicka & Gaiser 2007, Levkov 2009, Stepanek & Kociolek 2013). This morphologically diverse group has traditionally been separated into nine subgenera based on morphological features such as a 'simple' or 'complex' connecting zone (girdle area), the presence or absence of 'longitudinal lines', as well as several raphe and striae features (Cleve 1895). Although this classification stood for over 100 years, recent molecular phylogenetic data have shown the group to be non-monophyletic (Sato et al. 2013, Stepanek & Kociolek 2014, Wang et al. 2014) with members distributed across several orders of raphid diatoms (Stepanek & Kociolek 2014). Despite the polyphyly of the taxa currently assigned to *Amphora*, the beginnings of a classification based on monophyly, which does not necessarily correspond to Cleve's (1895) subgenera, is being developed (Stepanek & Kociolek 2014). One such clade includes taxa from the subgenera *Amphora s.s.* (including the generitype *Amphora ovalis* (Kützing) Kützing), *Diplamphora*, and *Oxyamphora* (Stepanek & Kociolek 2014).

The subgenus *Diplamphora* was described by Cleve (1895) to include forms that share morphological similarities with *Amphora s.s.* in having linear to semi-lanceolate valves, a dorsal valve face with one or two longitudinal lines and striae composed of transverse costae or rows of puncta (Cleve 1895). These taxa differed from *Amphora s.s.* in what Cleve termed a 'complex connecting zone' (areolate girdle bands) as opposed to the 'simple' or unornamented girdle bands in *Amphora s.s.* This rather broad definition has led to a group with a remarkable variety of forms, an issue addressed by Cleve when he remarked the subgenus *Diplamphora* "comprises a number of species, very different in appearance, but agreeing in the complex connecting zone and the longitudinal line on the dorsal side" (Cleve 1895, p. 107). Although Cleve was unsure whether the difference in girdle structure was sufficient to consider *Diplamphora* as a separate genus, he remained confident in his assertion that the group was very closely allied to *Amphora s.s.* (Cleve 1895).

Recent molecular phylogenetic studies by Sato et al. (2013) and Stepanek & Kociolek (2014) have supported the close association between the subgenera *Amphora s.s.* and *Diplamphora*. Although both demonstrate this close association, these studies differed in the taxa included in the analyses and the relationship between *Diplamphora* and *Amphora s.s.* Stepanek & Kociolek (2014) found *Diplamphora* and *Oxyamphora* taxa forming a monophyletic group sister to *Amphora s.s.*, whereas Sato et al. (2013) analyses showed *Diplamphora* taxa as a paraphyletic grade into a monophyletic *Amphora s.s.*

Presented here is the description and phylogenetic placement of *Amphora aliformis*, a new species from the genus *Amphora* collected from the Banzu Flats in Tokyo Bay, Japan, based on morphological and molecular phylogenetic data. Although exhibiting several unique morphological features, *A. aliformis* conforms to the broad concept of Cleve's (1895) subgenus *Diplamphora* and a discussion of the systematic implications of this new species in the evolving concept of the genus *Amphora* follows.

MATERIAL AND METHODS

Taxon collections

Materials containing *A. aliformis* were collected from the Banzu Flats in Tokyo Bay, Tokyo Prefecture, Japan (35.44081°N, 139.91078°E). Collections of low tide sand samples from the flats were made by Stepanek and Mayama in June 2013.

Amphora aliformis was isolated into monoculture through micropipette serial dilution into Daigo's Artificial Seawater SP medium (Nihon Pharmaceutical Co., Tokyo, Japan). Due to the epipsammic growth form of *A. aliformis*, collected sand grains were first placed into petri dishes containing growth medium, cells were allowed to divide and grow off of the sand grains onto the petri dish and these cells were then isolated into monoculture. All cultures were maintained at ca. 25°C under a 12:12 light regime with an irradiance of ca. 50 µmol m^{-2}.

Samples were cleaned of organic matter for light microscope (LM) observations by boiling in concentrated sulfuric acid with the addition of potassium permanganate, followed by repeated rinses with

distilled water until a neutral pH was reached. For LM observations, cleaned material was air dried onto glass coverslips and permanent slides were prepared using Mount Media® (Wako Pure Chemical Industries, Osaka, Japan). All LM observations were performed using an Olympus BX-51 light microscope (Olympus America Inc., Center Valley, Pennsylvania) with 100x oil immersion objective (N.A. 1.40). Light micrographs were taken with an Olympus DP 71 digital camera. For scanning electron microscope (SEM) preparation, culture material was cleaned of organic matter using a low temperature plasma treatment, previously shown to keep frustules intact for observation (Watanabe *et al*. 2010). Culture material was air dried onto glass coverslips and plasma processed for 40 minutes in a Diatom Asher Model II (Kyotodensikeisoku Co., Kyoto, Japan). For SEM images featuring cell interiors, individual valves of cultured cells were separated and cleaned of organic matter under an inverted microscope using a drop of dilute bleach solution and a fine probe. After the cleaning procedure, the separated valves were rinsed with drops of distilled water and air dried onto glass coverslips. For SEM observations, processed glass coverslips were coated with ca. 5 nm Osmium using an OPC40 Osmium Plasma Coater (Filgen, Nagoya, Japan). Electron micrographs were taken with a Hitachi S-4500 field emission SEM at an acceleration voltage of 15 kV.

Valve structure terminology follows that of Cox & Ross (1981) and Nagumo (2003).

DNA extraction, amplification and sequencing

Extraction of DNA from *A. aliformis* was performed from pelleted culture material using a Chelex 100® extraction method (Richlen & Barber 2005). For the phylogenetic analysis, two nuclear markers, the nuclear encoded small subunit ribosomal DNA (SSU) and the D1–D2 region of the nuclear encoded large subunit ribosomal DNA (LSU), and two chloroplast markers, the large subunit of RUBISCO (*rbc*L) and the photosystem II chlorophyll-*a* binding protein *psb*C, were amplified. These markers were chosen to coincide with the recently published molecular phylogeny of *Amphora s.l.* (Stepanek & Kociolek 2014) with the addition of LSU, a region that has previously been shown to resolve

species level associations within diatoms (Alverson et al. 2007, Hamsher et al. 2011). Primers used for the amplification and sequencing of these markers are listed in supplementary Appendix 3.

All markers were amplified by PCR using GE healthcare Illustra Ready-To-Go™ PCR beads (GE Healthcare Biosciences, Pittsburg, Pennsylvania) following the manufacturer's protocol. The PCR profile used for each molecular marker was: 94°C initial denaturation for 3 minutes 30 seconds, followed by 36 cycles of 94°C for 50 seconds, 52°C for 50 seconds, 72°C for 80 seconds, with a final extension at 72°C for 15 minutes. Amplified PCR product was purified using ExoSap-it (Affymetrix, Santa Clara, California) following the manufacturer's protocol. Sequencing of the purified PCR product was performed by Functional Biosciences (Madison, Wisconsin) and returned raw sequence files were edited and assembled using Geneious ver. 5.6 (Drummond et al. 2012). All newly created sequence data has been submitted to GenBank (Appendix 3).

Sequence alignment and phylogenetic analysis

Recent findings have shown members of the genus *Amphora* distributed widely across raphid diatom lineages (Stepanek & Kociolek 2014), therefore it was important to test whether *A. aliformis* belonged to the clade containing members of *Amphora s.s*. before moving forward with the analysis. To test this, sequence data for *A. aliformis* was added to the three marker (SSU, *rbc*L and *psb*C) concatenated alignment used by Stepanek & Kociolek (2014) that includes a broad sampling of raphid diatom lineages. The ML phylogram inferred from this dataset showed, with strong support (BS 99), that *A. aliformis* is part of the *Amphora s.s.* + *Diplamphora* + *Oxyamphora* clade. Because of this finding, and to allow for the inclusion of additional sequence data (LSU), all subsequent alignments and analyses included only taxa from the *Amphora s.s.* + *Diplamphora* + *Oxyamphora* clade with members of the genus *Halamphora* (from the sister clade to *Amphora*) used as outgroup taxa.

Sequences were aligned in Geneious using a muscle alignment algorithm (Edgar 2004), visually inspected and edited by hand as needed. Sequences for each of the four molecular markers were aligned individually and trimmed to minimize missing data before concatenation into an alignment consisting of

the nuclear encoded markers (SSU and LSU), an alignment consisting of the chloroplast encoded markers (*rbc*L and *psb*C), and four marker concatenated alignment. For all alignments 15 ingroup (including *A. aliformis*) taxa and four outgroup taxa from the genus *Halamphora* were included. The included markers had a final trimmed length of 1604, 559, 1369 and 1112 bps for SSU, LSU, *rbc*L and *psb*C, respectively.

Using jModelTest ver. 0.1.1 (Guindon & Gascuel 2003; Posada 2008), the general time reversible (GTR) model with a gamma distribution (Γ) and a proportion of invariable sites (I) was chosen as the best model of sequence evolution for the individual markers as well as for the concatenated alignments. For all alignments, maximum likelihood (ML) estimation was performed using PhyML version 3.0 (Guindon et al. 2010) implemented in SeaView version 4.3.4 (Gouy et al. 2010), and branch support was estimated using 500 bootstrap replicates. Bayesian estimation was conducted using MrBayes version 3.2.1 (Ronquist et al. 2012). The Bayesian estimation was run for 15 million generations, with a burn-in of 3 million generations, using two runs of four MCMC chains sampled every 1000 generations.

RESULTS

Morphological analysis

Amphora aliformis Stepanek, Mayama & Kociolek *sp. nov*. Figs 6.1–6.4.

Description: Frustule elliptical with bluntly truncated ends. Valves semi-elliptical, moderately dorsiventral, with a smoothly arched dorsal margin and a straight to slightly convex ventral margin. Valve length 12.0–24.0 µm, valve breadth 3.5–5.5 µm, although in the LM the apparent breadth can vary depending on the angle at which the valve is lying. Valve ends are narrowly rounded and slightly deflected ventrally. The raphe is nearly centrally placed on the valve, straight to slightly arched, with straight proximal raphe ends and distal raphe ends that are difficult to observe in the LM. The axial area is narrow throughout dorsally. Dorsal striae are uninterrupted, nearly parallel at the valve center and becoming radiate near the apices. Dorsal striae number 19–20 in 10 µm. In the LM, depending on the valve angle, the dorsal striae are often obscured near the dorsal margin by a distinct hyaline area. Ventral striae are absent, although a broad unornamented ventral area is present.

GenBank accession numbers: KP229525 (SSU), KP229544 (LSU), KP229546 (*rbc*L), KP229548 (*psb*C).

Holotype: TNS-AL-56400s, slide deposited at the National Museum of Nature and Science, Tsukuba, Japan (TNS). Collected 23 June 2013.

Isotypes: TNS-AL-56400m, cleaned material deposited at the National Museum of Nature and Science, Tsukuba, Japan (TNS). JPK10169, slide and material deposited at the University of Colorado Boulder, Kociolek collection at COLO. Collected 23 June 2013.

Type locality: 35.44081°N, 139.91078°E, epipsammic, Banzu Flats, Tokyo Bay, Japan.

Etymology: *aliformis* (Latin = wing-shaped) refers to the prominent dorsal marginal wing exhibited by this taxon.

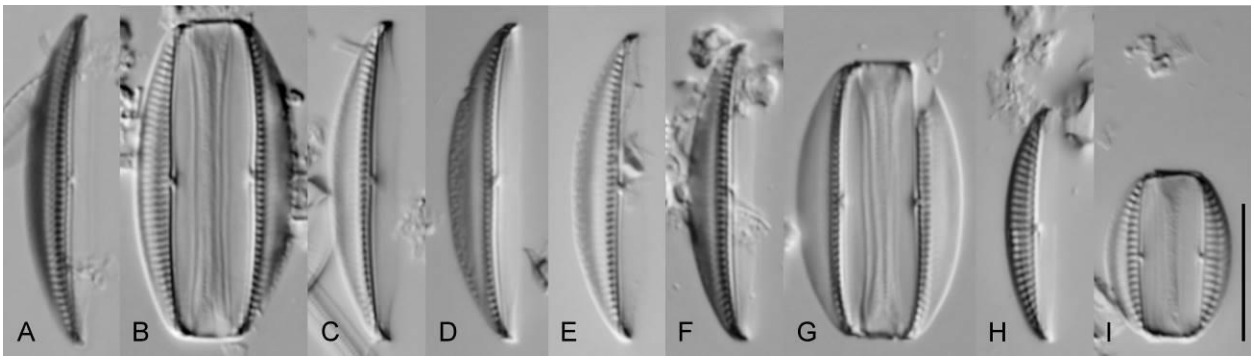

Figure 6.1. A–I. Light micrographs of whole frustules and valves of *Amphora aliformis* showing observed size range. Cleaned collection material, JPK 10105. Scale bar = 10 µm.

In the SEM, the most prominent feature of *A. aliformis* is a dorsal marginal ridge that extends into a broad 'wing' running the length of the dorsal margin (Fig. 6.2A–D). When the whole frustule is viewed from the dorsal margin side, this wing lies flush against the substrate (Fig. 6.2A). The wing is broad and unornamented except for small depressions or dimples irregularly spaced throughout the structure (Fig. 6.2 B). When viewed from the ventral mantle side, the dorsal valve face quickly falls away from the valvar plane before meeting the dorsal wing (Fig. 6.2C). The wing then comes back to the valvar plane creating a deep depression or valley between the axial area and the dorsal edge of the wing (Fig. 6.2C).

The steep curvature of the dorsal valve face combined with the broad unornamented dorsal wing creates the obscured dorsal striae seen in the LM (Fig. 6.1).

The striae are alveolate with the external areolae openings consisting of a narrow slit interrupted only by the dorsal marginal wing (Fig. 6.2 A–E). The external areolae openings extend some way onto the protracted wing, past the internal occlusions that make up the internal valve structure (Fig. 6.2D, arrow). This feature is seen in both the valve face and marginal striae creating a hollow chamber at the base of the wing that is open via the external striae but is closed to the valve interior by the internal striae coverings (Fig. 6.2 D, E, arrows). In cross-section this chamber is open connecting the dorsal and marginal alveoli but is partitioned between each stria by virgae and does not continue the longitudinal length of the valve (Fig. 6.3A).

Externally, the raphe is weakly arched with proximal ends slightly deflected dorsally. The distal raphe ends are sharply deflected dorsally past the distal end of the raphe ledge and dorsal marginal wing, continuing onto the dorsal margin (Fig. 6.2A, arrow). The raphe ledge is continuous on the dorsal side, not apparent on the ventral side. The ventral valve is broad and unornamented aside from several large pores positioned near the valve apices (Fig. 6.2E).

The girdle bands are somewhat irregularly areolated, varying between small pores to more complex crescent and horseshoe shaped openings. Along with the pores, many irregular depressions are visible throughout the girdle area (Fig. 6.2A, C, F).

Internally, the striae are composed of a single elongate areolae interrupted only at the valve margin by a band of silica (Fig. 6.3B, C). The internal raphe terminates proximally at a weakly developed central helictoglossae (Fig. 6.3C). The ventral apical pores are occluded internally by a sieve plate anchored in several places to the ventral valve (Fig. 6.3D). Although in the fully developed cell the ventral striae are absent, in early valve development ventral virgae are initially formed and must be filled in later development (Fig. 6.3E, F, arrows).

Living cells of *A. aliformis* contains a single ventrally appressed chloroplast consisting of four lobes extending up the valve sides towards the dorsal girdle area (Fig. 6.4). This chloroplast arrangement

is consistent with Mereschkowsky's (1903) type 1 *Amphora* chloroplast, shown by Stepanek & Kociolek (2014) to be shared within the *Amphora s.s.* + *Diplamphora* + *Oxyamphora* clade.

Taxonomic remarks

Amphora aliformis is similar in valve outline and stria features to other members previously placed in the subgenus *Diplamphora* such as *Amphora graeffeana* Hendey (Schoemann & Archibald 1986; Levkov 2009), *Amphora beaufortiana* Hustedt (Hustedt 1955) and *Amphora australiensis* John (John 1981). However, *A. aliformis* is easily distinguished from *A. graeffeana* and *A. beaufortiana* in the LM by the distinct hyaline area created by the dorsal marginal wing and its lack of ventral striae. *Amphora australiensis* (considered a synonym of *Amphora polita* Krasske by Levkov 2009), along with sharing valve outline striae features with *A. aliformis*, has been shown to have a distinct siliceous flap extending from the dorsal marginal ridge (John 1981). *Amphora aliformis* can be distinguished from *A. australiensis* by its lack of ventral striae and broad dorsal axial area, both evident in *A. australiensis*. Cleve (1895) reports *Amphora truncata* Cleve, a member of the subgenus *Diplamphora*, as having a structureless ventral side, however *A. truncata* is larger (50–55 µm), has a broad dorsal axial area, and no mention is made of a dorsal hyaline area.

Phylogenetic analysis

The results from the ML estimation of the four marker concatenated alignment are shown in Figure 6.5. Both the ML and Bayesian estimation returned identical topologies with log likelihood values of −15500.69 and −15517.67 for the ML and Bayesian estimations, respectively. The resulting tree strongly supports (100/100) *A. aliformis* sister to a clade containing the remaining *Amphora* taxa, including representatives from the subgenera *Amphora s.s.*, *Diplamphora*, and *Oxyamphora*. In this tree *A. aliformis* and *Amphora commutata* Grunow in Van Heurck represent early branching lineages within the genus *Amphora*, however, there was not congruence in the position of *A. aliformis* between the trees

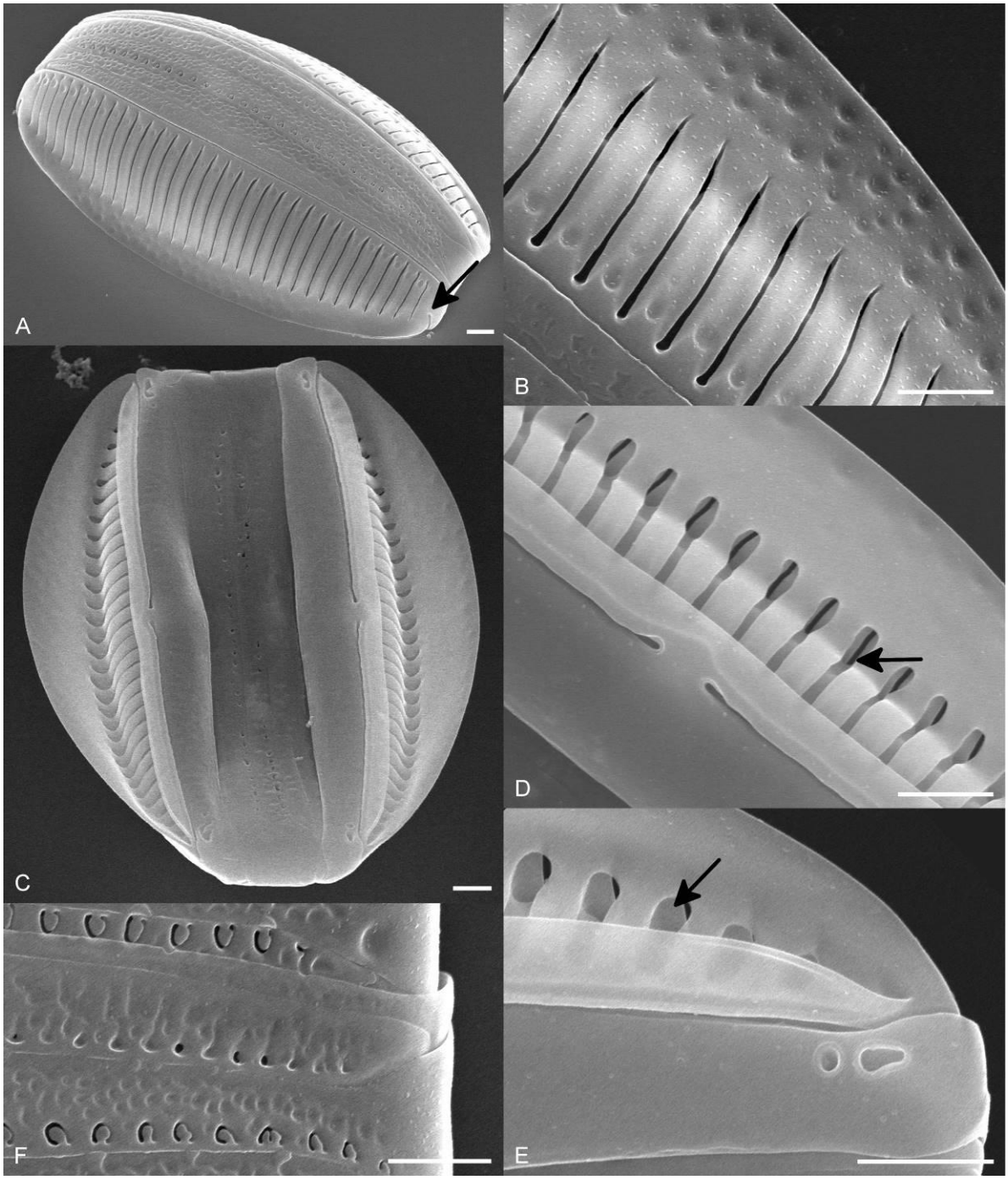

Figure 6.2. Scanning electron micrographs of *Amphora aliformis*. Cleaned culture material, JPK culture 10105-AMPH177. **A.** External dorsal view of the whole frustule, showing marginal wing, areolate girdle bands, and distal raphe end extending onto the dorsal mantle (arrow). Scale bar = 1 µm. **B.** Detail of the external dorsal mantle showing irregularly spaced depressions on the marginal wing. Scale bar = 1 µm. **C.** External ventral view of the whole frustule showing sharply curved dorsal valve face, marginal wing, and absence of ventral striae. Scale bar = 1 µm. **D.** Detail of the external valve center showing raphe ledge and hollow chamber created by the marginal wing (arrow). Scale bar = 1 µm. **E.** Detail of the areolate girdle bands. Scale bar = 1 µm. **F.** Detail of the external valve end showing the ventral apical pores and hollow chamber created by the marginal wing (arrow). Scale bar = 1 µm.

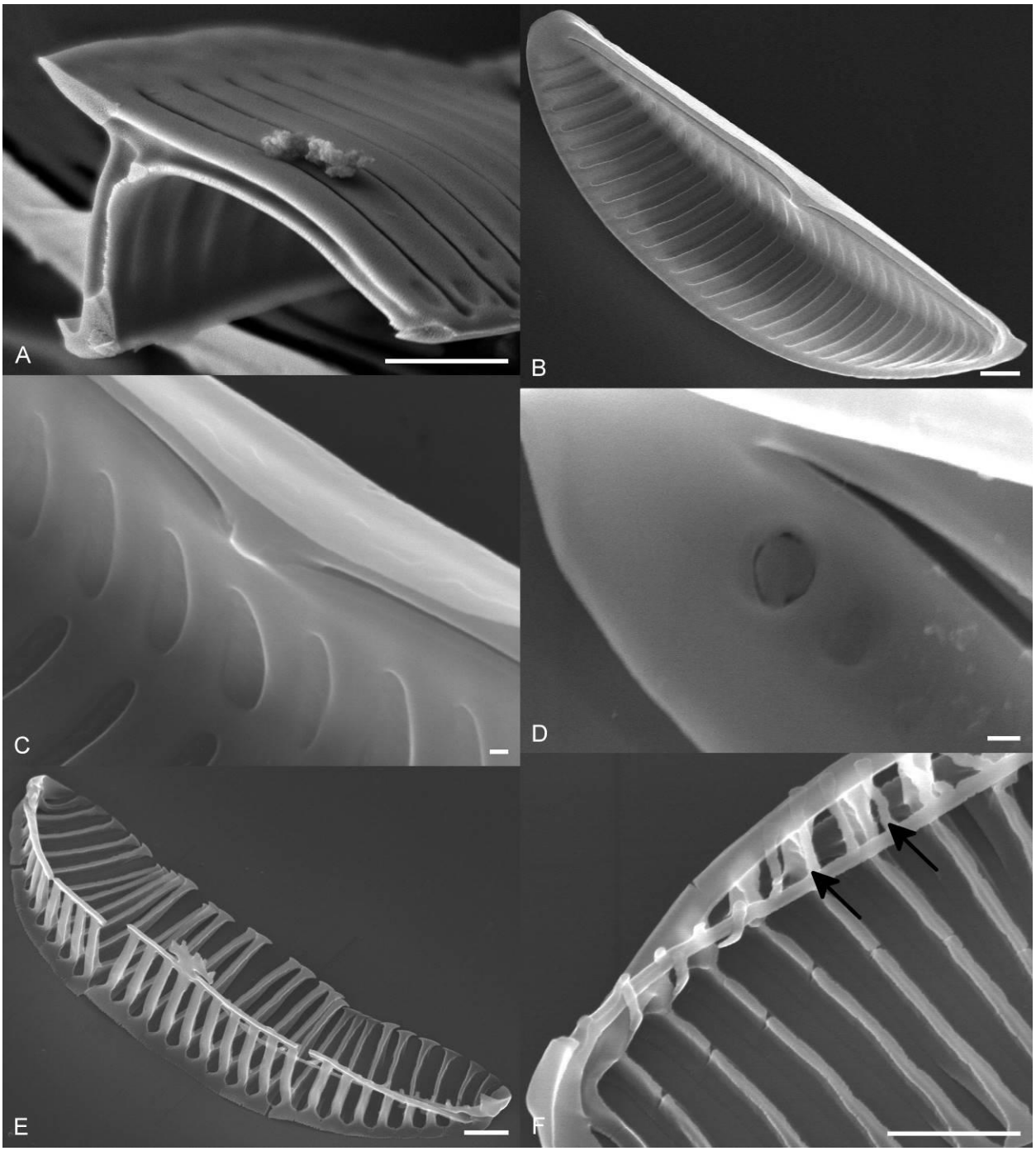

Figure 6.3. Scanning electron micrographs of *Amphora aliformis*. Cleaned culture material, JPK culture 10105-AMPH177. **A.** Valve cross-section showing alveolate dorsal and marginal striae extending into the marginal wing. Scale bar = 1 µm. **B.** Internal view of single valve showing internal striae. Scale bar = 1 µm. **C.** Detail of internal valve center showing internal marginal ridge and weakly developed central helictoglossae. Scale bar = 100 nm. **D.** Detail of internal valve end showing ventral apical pore occluded by a sieve plate anchored to the valve with struts. Scale bar = 100 nm. **E.** Developing valve. Scale bar = 1 µm. **F.** Detail of developing valve showing early development of ventral virgae (arrows). Scale bar = 1 µm.

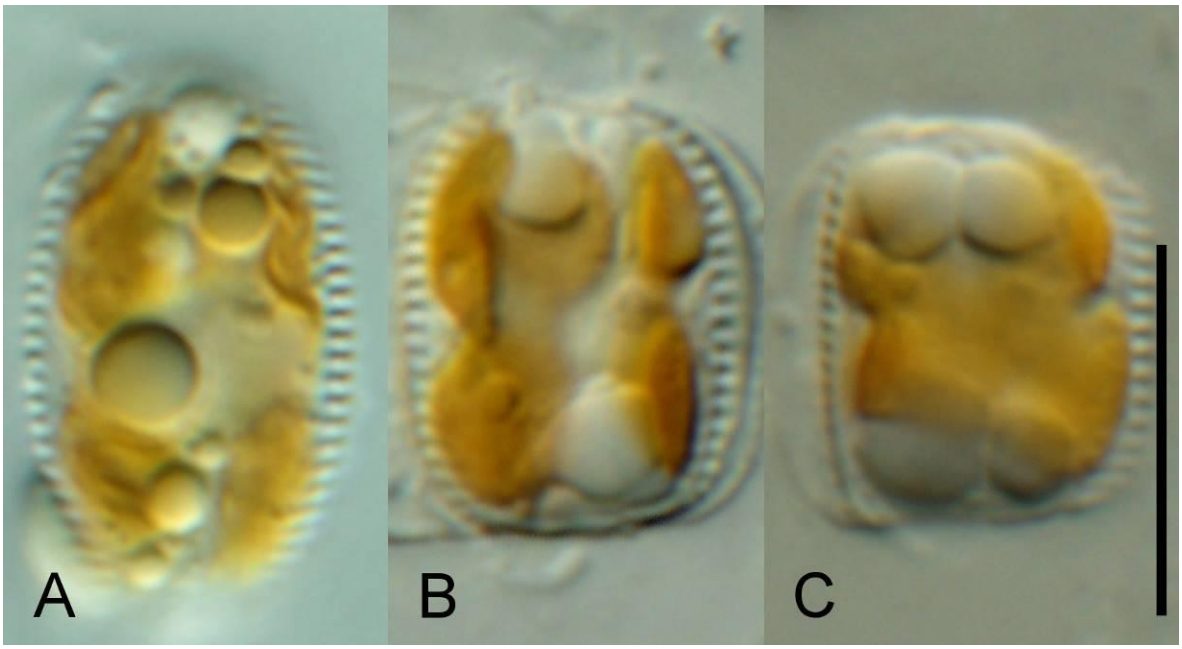

Figure 6.4. A–C. Light micrographs of living cells of *Amphora aliformis* showing chloroplast structure. Live culture material, culture JPK 10105-AMPH177. Scale bar = 10 µm.

inferred from the nuclear encoded markers (Fig. 6.6) and the chloroplast encoded markers (Fig. 6.7). The ML and Bayesian estimation of the SSU-LSU alignment returned a strongly supported (100/100) position of *A. aliformis* identical in topology to the four marker tree with *A. aliformis* positioned sister to the remaining *Amphora* representatives. The *rbc*L-*psb*C tree, however, placed *A. aliformis* in a moderately supported (85/100) position sister to the *Amphora s.s.* clade, with *A. commutata* sister to the resulting *A. aliformis* + *Amphora s.s.* clade. In this tree the remaining *Diplamphora* taxa form a separate clade sister to the *Oxyamphora* taxa.

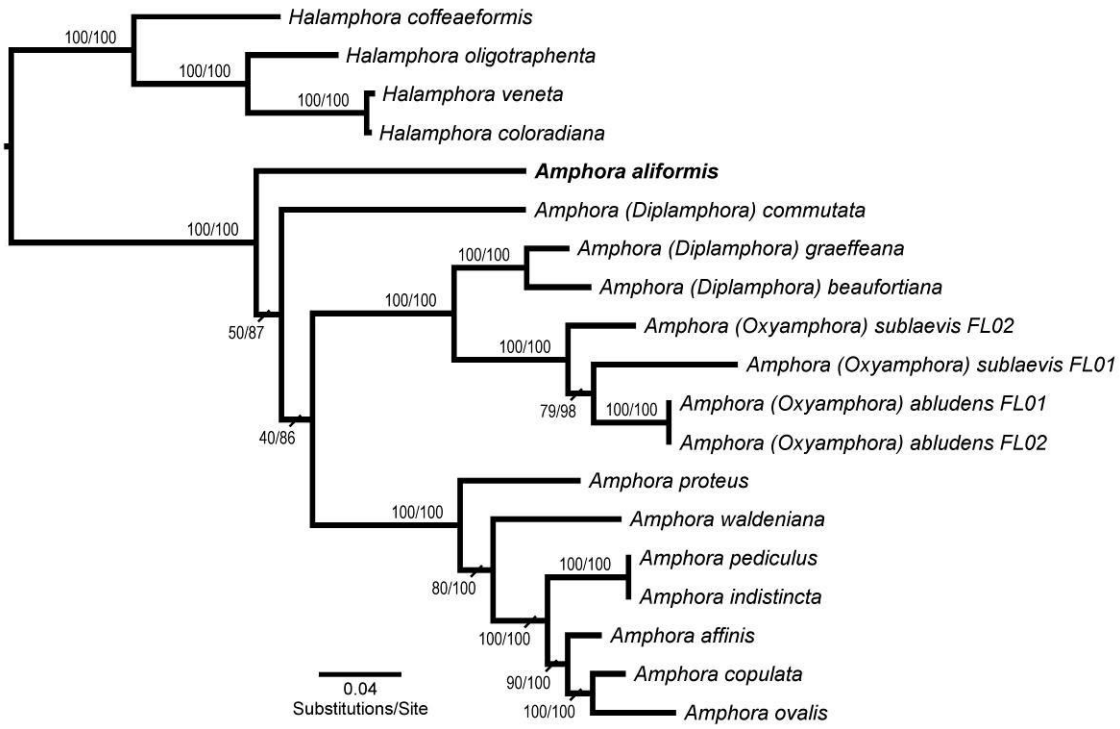

Figure 6.5. Maximum likelihood phylogram inferred from a concatenated four molecular marker alignment, including the nuclear markers SSU rDNA and LSU rDNA, and the chloroplast markers *rbc*L and *psb*C. Node support is given on the branches as maximum likelihood bootstrap values (500 replicates)/Bayesian posterior probability (as a percentage). Cleve's (1895) subgenus names are in parentheses where applicable.

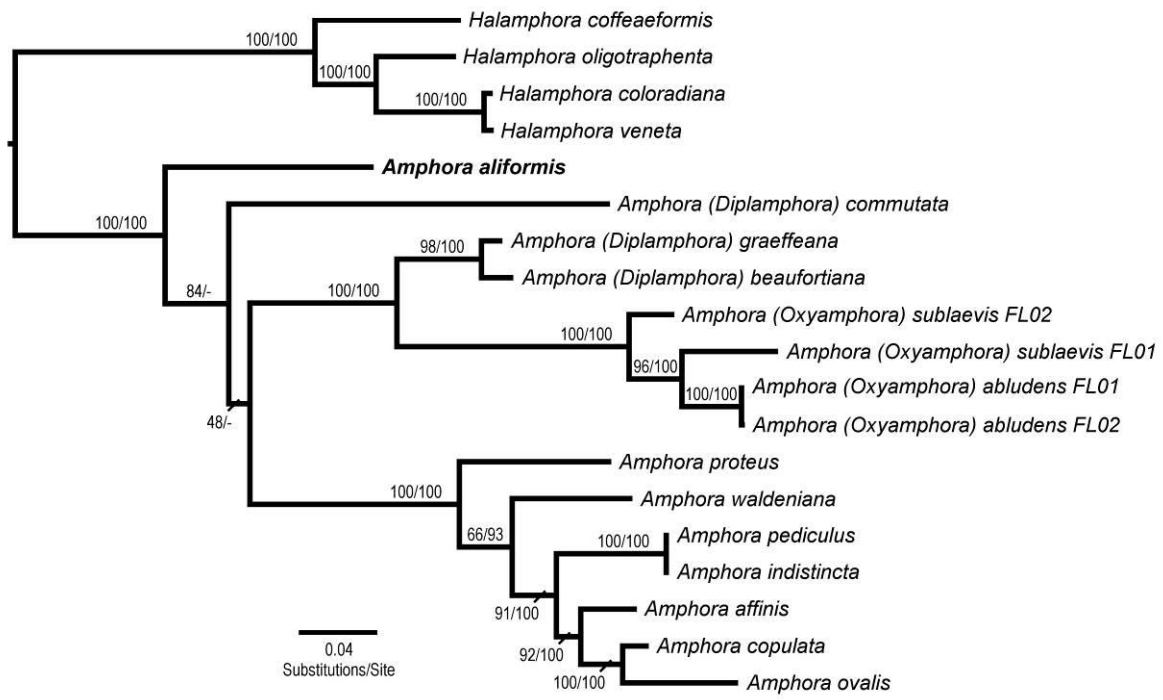

Figure 6.6. Maximum likelihood phylogram inferred from a concatenated alignment of the nuclear encoded markers SSU rDNA and LSU rDNA. Node support is given on the branches as maximum likelihood bootstrap values (500 replicates)/Bayesian posterior probability (as a percentage). Posterior probabilities shown as (-) indicate unresolved relationships in the Bayesian phylogram. Cleve's (1895) subgenus names are in parentheses where applicable.

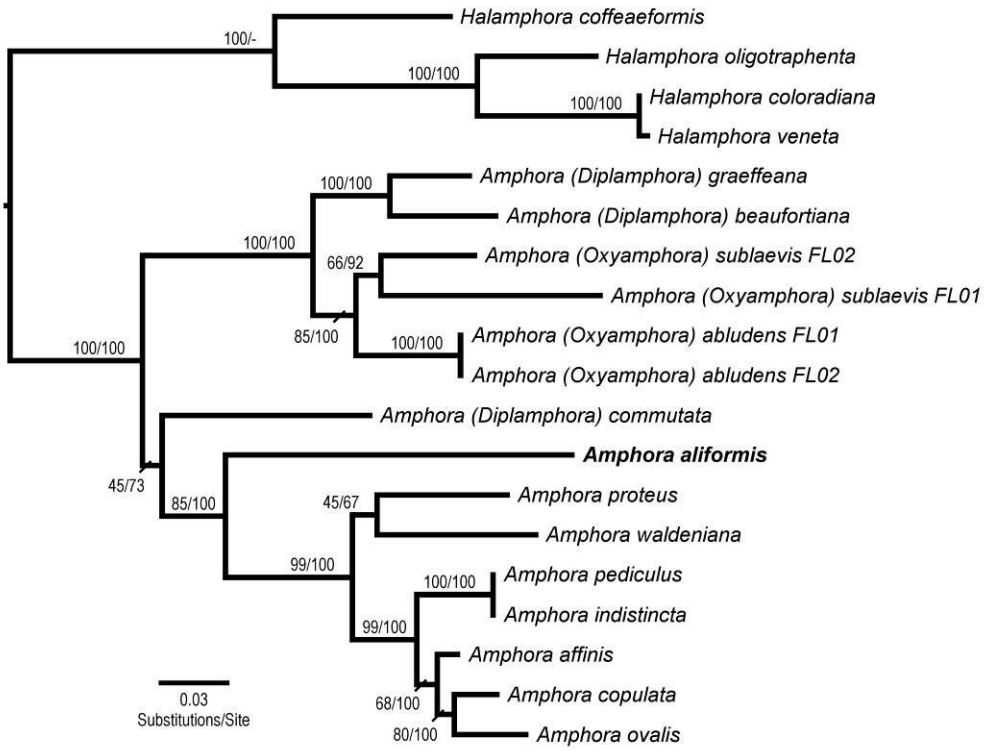

Figure 6.7. Maximum likelihood phylogram inferred from a concatenated alignment of the chloroplast encoded markers *rbc*L and *psb*C. Node support is given above the branches as maximum likelihood bootstrap values (500 replicates)/Bayesian posterior probability (as a percentage). Cleve's (1895) subgenus names are in parentheses where applicable.

DISCUSSION

Cleve (1895) described the subgenus *Diplamphora* as being most closely related to *Amphora s.s.*, differing only in the 'complex connecting zone' seen in *Diplamphora* taxa. Morphologically, *A. aliformis* fits this definition in terms of general valve outline, raphe ledge, and chloroplast structure that ally this taxon with the *Amphora s.s.* clade. Conversely, the areolate girdle bands, slit like alveolate dorsal striae, infilling of the ventral striae, and the highly reduced central helictoglossae (see images in Sato et al. 2013; Stepanek & Kociolek 2014), all point to its inclusion in the subgenus *Diplamphora*.

Additionally, *A. aliformis* shares several morphological features with the unusual *Diplamphora* taxon *A. commutata* (see Sato et al. 2013 for a detailed morphological treatment). The presence of the

distinct pore found near the ventral apices has only previously been reported in *A. commutata* (Sato et al. 2013), although *Amphora micrometra* Giffen shows a small pore near the dorsal apices (Ács et al. 2011). Although the distal pores in *A. aliformis* and *A. commutata* differ externally, with *A. aliformis* much larger and more prominent, internally the sieve plate occlusion suspended by what Sato et al. (2013) termed 'marginal struts', may indicate these are related features and would suggest an affinity between these two species.

The most prominent morphological feature of *A. aliformis* is the conspicuous dorsal marginal wing. Many *Amphora* taxa, including *Amphora absoluta* Levkov, *Amphora rotunda* Skvortzow, *Amphora serrataeformis* Levkov, and *Amphora sibirica* Skvortzow & Meyer exhibit a distinct marginal ridge (see Nagumo 2003; Levkov 2009), and in some taxa, such as *A. australiensis*, *Amphora calumetica* (Thomas in Thomas & Chase) Peragallo, *Amphora calumeticoides* Cocquyt, and *Amphora dentata* Edlund & Levkov in Levkov, siliceous flaps may extend from the marginal ridge (John 1981, Levkov 2009). In contrast to these marginal features, the degree to which the marginal wing is developed in *A. aliformis* has not been previously illustrated in the SEM. Cleve (1895) observed several taxa with a 'broad hyaline limbus' that may correspond to a dorsal marginal wing structure, including: *Amphora limbata* Cleve & Grove that Cleve assigned to the subgenus *Calamphora*; *Amphora schleinitzii* Janisch that was assigned to the subgenus *Amphora*; *Amphora weissflogii* Schmidt that was assigned to the subgenus *Diplamphora*; and *Amphora wittsteinii* Schmidt that Cleve was unable to assign to any of his nine newly created subgenera (Schmidt et al. 1874–1959 and Peragallo & Peragallo 1897–1908 for illustrations). Their classification across many subgenera make it difficult to make any comparisons between these taxa and *A. aliformis*, and to our knowledge no modern morphological treatment has been performed on any of these potentially winged taxa.

Although not extended into a wing, *A. commutata* exhibits a broad marginal ridge (Sato et al. 2013). Interestingly, Sato et al. (2013, Fig. 39) show that this ridge is not a solid band of silica, but is chambered, a structure that may be homologous with the chambered wing of *A. aliformis*. How widespread this chambered dorsal marginal ridge is within the genus is difficult to say, as, with the

exception of Nagumo (2003), SEM investigations of *Amphora* taxa seldom examine valves in cross-section.

Phylogeny and systematic implications

Although *A. aliformis* shares several morphological features with *A. commutata*, none of the phylogenetic analyses performed indicate they form a monophyletic group. Instead, the nuclear and full concatenated trees indicates that *A. aliformis* and *A. commutata* represent early branching lineages within the *Amphora* + *Diplamphora* + *Oxyamphora* clade, and the chloroplast tree shows *A. aliformis* and *A. commutata* as early branching lineages grading into the *Amphora s.s.* clade. Although the inferred position of *A. aliformis* and *A. commutata* was not congruent between the nuclear encoded and plastid encoded markers nor between individual marker trees (data not shown), it is important to note that no individual marker (SSU, LSU, *rbc*L or *psb*C) or concatenation of markers (nuclear, chloroplast or four marker) returned a tree in which *Diplamphora* or *Diplamphora* + *Oxyamphora* was monophyletic. In addition, these results indicating the non-monophyly of *Diplamphora* taxa support the findings of Sato et al. (2013), which was based on SSU sequence data and included *A. graeffeana*, *A. commutata* and an unnamed *Diplamphora* species. In their analysis Sato et al. (2013) also found the subgenus *Diplamphora* non-monophyletic, and instead were early branching lineages grading into *Amphora s.s.*

The non-monophyly of *Diplamphora*, with *A. aliformis* and *A. commutata* as either sister to *Amphora s.s.* or as sister to the entire *Amphora* + *Diplamphora* + *Oxyamphora* clade, has implications for our changing concept of *Amphora s.l.* classification. First, it is becoming clear that Cleve's (1895) subgenera are largely inappropriate for continued use in *Amphora* systematics (Sato et al. 2013, Stepanek & Kociolek 2014, this study). Although *Amphora s.s.* continues to be recovered as monophyletic, the non-monophyly of the taxa previously placed in the subgenera *Diplamphora* and *Oxyamphora* (Sato et al. 2013, Stepanek & Kociolek 2014, this study) requires a reexamination of the defining features of the genus *Amphora* as it now stands.

A majority of the commonly cited characteristic features of *Amphora* such as 'amphoroid' symmetry, dorsiventral valve shape, presence of a raphe ledge, central helictoglossae, and a single ventrally appressed chloroplast, have been shown to be symplesiomorpic (Stepanek & Kociolek 2014). Our results indicate areolate girdle bands (Cleve's 1895 important 'complex connecting zone') were likely the ancestral condition within the *Amphora* clade, shared by the *Diplamphora* and *Oxyamphora* taxa and were subsequently lost in the *Amphora s.s*. clade. Additionally, the distinctly separate central helictoglossae seen in most *Amphora s.s*. taxa (Stepanek & Kociolek 2014) appears to be a synapomorphy of the *Amphora s.s*. clade and not the genus as a whole.

The remaining commonly cited *Amphora* traits that are synapomorphic for the genus is relatively small. Mereschkowsky's (1903) type 1 chloroplast remains the best feature unifying the group (Sato et al. 2013, Stepanek & Kociolek 2014, this study). Others could loosely include a dorsal marginal ridge and a biarcuate raphe, although these features are quite variable across this morphologically diverse group. Certainly, as our understanding of how the remaining uninvestigated '*Diplamphora*' and '*Oxyamphora*' taxa fit into this new view of the genus increases, it may be possible to further differentiate these groups based on shared derived features. This remains a daunting task with the vast majority of *Amphora* diversity not currently included in any analysis, morphological or molecular. This study highlights the importance of including the greatest taxonomic breadth possible in future studies, as the addition of new taxa continues to change our view of the systematics of *Amphora s.l.*

ACKNOWLEDGEMENTS

This research was partially funded through a joint National Science Foundation and Japanese Society for the Promotion of Science East Asia and Pacific Summer Institute fellowship award No. 1316805 and a student research grant from the University of Colorado Boulder Department of Ecology and Evolutionary Biology. The authors would also like to thank Sarah Hamsher for helpful comments and discussion.

CHAPTER VII

RE-EXAMINATION OF MERESCHKOWSKY'S GENUS *TETRAMPHORA* (BACILLARIOPHYTA) AND ITS SEPARATION FROM *AMPHORA*

Adapted from: Stepanek, J.G. & Kociolek, J.P. *Accepted*. Re-examination of Mereschkowsky's genus *Tetramphora* (Bacillariophyta) and its separation from *Amphora*. *Diatom Research*.

ABSTRACT

The raphid diatom genus *Amphora* has been subject to considerable revision over the previous 30 years, with many species transferred to newly-created or existing genera. Despite these efforts, recent work has demonstrated that taxa presently assigned to the genus continue to be non-monophyletic and further revision is required. This investigation re-examines Mereschkowsky's genus *Tetramphora*, which includes all *Amphora* species with four chloroplasts. Although largely ignored over the last 100 years, recent work has shown that taxa aligning with *Tetramphora* are monophyletic and distinct from *Amphora sensu stricto*. Presented here are illustrations and descriptions of nine species belonging to *Tetramphora*, based on light and scanning electron microscope observations, as well as a preliminary molecular phylogeny for the group. From these observations, we lectotypify *Tetramphora* based on Mereschkowsky's *T. ostrearia*, recognize *T. lineolata*, and transfer the *Amphora* taxa *A. decussata*, *A. sulcata*, *A. rhombica*, *A. intermedia* and *A. securicula*, and the *Halamphora* taxon *H. chilensis* to *Tetramphora*. In addition, three new species, *T. fontinalis*, *T. lineolatoides* and *T. robusta* are described.

INTRODUCTION

The genus *Amphora* Ehrenberg ex Kützing, characterized by a distinct asymmetry of the apical and valval planes, has long been speculated to be non-monophyletic (Cleve 1895, Krammer 1980, Mann 1994). The morphological diversity in features, other than symmetry, have hampered efforts at a natural classification, as evidenced by many early, and largely unsuccessful, attempts (Smith 1873, Cleve 1895, Mereschkowsky 1903, Gusylakov 1985). Of these early attempts, Cleve's (1895) was, and remains, the most comprehensive and influential classification system. Cleve (1895) divided the genus into nine subgenera, *Archiamphora*, *Amblyamphora*, *Amphora*, *Calamphora*, *Cymbamphora*, *Diplamphora*, *Halamphora*, *Oxyamphora* and *Psammamphora* based on valve and girdle morphological characteristics. Cleve's (1895) revision was noteworthy for another reason, as he was the first to postulate that the genus was composed of several unrelated groups, and that amphoroid symmetry is likely a product of shared growth form rather than shared evolutionary history. Although he believed his subgenera should be separate genera, he was reluctant to make these changes at the time.

Of these early researchers, Mereschkowsky (1903) alone examined plastid morphology across the genus. From these observations he identified nine chloroplast types based on the number, shape, and position within the cell. Although not addressing all of the chloroplast categories, from these observations Mereschkowsky proposed two new genera separated from the genus *Amphora*, *Clevamphora* containing all of the species with a Type 1 chloroplast (single four lobed ventrally appressed chloroplast) corresponding to Cleve's *Amphora s.s.*, and *Tetramphora* for species with a Type 8 chloroplast (two dorsally and two ventrally appressed chloroplasts connected by pyrenoids) that includes some, but not all, members of Cleve's *Oxyamphora* (Mereschkowsky 1903). Of these proposed genera, *Clevamphora* referring to species within *Amphora s.s.* is considered nomenclaturally superfluous (Fourtanier & Kociolek 2011) and *Tetramphora* was largely ignored by later taxonomists, with most adopting Cleve's (1895) nine *Amphora* subgenera.

Although concerns of the non-monophyly of the genus were first raised 120 years ago (Cleve 1895), it has only been recently that an effort has been made to revise the classification of *Amphora*. Recent changes have included the transfer of taxa to existing and newly-created genera such as *Undatella* Paddock and Sims (Paddock & Sims 1980), *Biremis* Mann and Cox (Mann & Cox in Round et al. 1990), and *Colliculoamphora* Williams and Reid (Williams & Reid 2006), as well as the transfer of Cleve's subgenus *Cymbamphora* to the newly created genus *Seminavis* Mann (Mann in Round et al. 1990) and the elevation of the subgenus *Halamphora* to generic status (Levkov 2009).

Although a considerable number of taxa have been transferred out of the genus *Amphora*, recent molecular phylogenetic work has demonstrated that the genus, as it is currently assigned, continues to be non-monophyletic and dispersed widely across raphid diatom lineages (Stepanek & Kociolek 2014). Although non-monophyletic as a whole, Stepanek & Kociolek (2014) demonstrated that several monophyletic groups exist outside of *Amphora s.s.* One such group corresponds to Mereschkowsky's genus *Tetramphora* and includes several members still classified within the genus *Amphora*. Presented here is a re-examination of genus *Tetramphora*, using light microscope (LM) and scanning electron microscope (SEM) observations of taxa collected from coastal and inland waters of the United States and Japan. In addition, a preliminary, molecular phylogeny is presented to understand the position of *Tetramphora* within the raphid diatom lineages.

MATERIALS AND METHODS

Taxon collection and isolation

Material was collected from coastal and inland waters of Florida, New Jersey and Utah, USA, and Japan from 2011–2013 (Appendix 1). When reported, pH and conductivity measurements were taken near shore at the time of collection using a YSI 556 multi-probe (YSI Incorporated, Yellow Springs, Ohio, USA). To remove the organic portions of samples for LM and SEM observations, the collected material was boiled in concentrated nitric acid followed by repeated rinses with distilled water until a neutral pH was reached. For LM observations, cleaned material was air dried onto glass coverslips and mounted onto

permanent slides using Naphrax mounting medium (Brunell Microscopes, Chippenham, UK). All LM observations were conducted using an Olympus BX-51 light microscope (Olympus America Inc., Center Valley, Pennsylvania, USA) with a 100x oil immersion objective (N.A. 1.40). Light micrographs were captured with an Olympus DP 71 digital camera. For SEM observations, cleaned material was air dried onto glass coverslips and mounted onto aluminum stubs. The stubs were coated with ca. 1.5 nm of gold using a Cressington 108 auto sputter coater (Cressington Scientific Instruments Ltd., Watford, UK). All SEM images were taken using a JEOL JSM 7401 field emission SEM at an acceleration voltage of 3 kV.

Tetramphora chilensis was isolated into monoculture via micro-pipette serial dilution. This taxon was grown in a modified f/2 artificial saltwater medium using the marine sea salts Instant Ocean (United Pet Group, Blacksburg, Virginia, USA). The salt concentration was decreased to a conductivity of 10 mS cm^{-1} to match the measured conductivity at the collection site, Blue Lake, UT. The culture was maintained under fluorescent illumination at ca. 25°C with a 12:12 light cycle at an illumination of ca. 50 µmol m^{-2}.

DNA extraction, amplification, and sequencing

DNA was extracted from *Tetramphora chilensis* monocultures using a Chelex 100 extraction method (Richlen & Barber 2005). The nuclear encoded 18S small subunit rDNA (SSU) and the chloroplast encoded large subunit of RUBISCO (*rbc*L) and photosystem II chlorophyll-a binding protein *psb*C were chosen as phylogenetic markers to coincide with previous published sequence data from this group (Stepanek & Kociolek 2014). Amplification and sequencing primers are listed in supplementary Appendix 3.

All markers were amplified by polymerase chain reaction (PCR) using GE healthcare Illustra Ready-To-Go PCR beads (GE Healthcare Biosciences, Pittsburgh, Pennsylvania, USA) following the manufacturers' protocol. The PCR profile used for all markers was a 94°C initial denaturation for 3 minutes 30 seconds, followed by 36 cycles of 94°C for 50 seconds, 52°C for 50 seconds, 72°C for 80 seconds, with a final extension period of 72°C for 15 minutes. The amplified PCR product was purified

using ExoSap-it (Affymetrix, Santa Clara, California, USA) following the manufacturers' protocol. Sequencing was performed by Functional Biosciences (Madison, Wisconsin, USA) and returned sequence files were assembled and edited in Geneious ver. 5.6 (Drummond et al. 2012).

Sequence alignment and phylogenetic analysis

Sequences were aligned in Geneious using a muscle alignment algorithm (Edgar 2004) and edited by hand as needed. Each marker was aligned individually and the ends were trimmed to minimize missing data before concatenating. Although trees inferred from individual markers may give conflicting results, alignment concatenation has been shown to be a successful strategy for returning the most accurate tree within diatoms (Theriot et al. 2015). Single marker alignment lengths were 1602, 1328 and 1059 bp for SSU, *rbc*L and *psb*C, respectively. Due to variable sequence availability between markers, a SSU-*rbc*L-*psb*C and a SSU-*rbc*L alignment was created in an effort to maximize taxon coverage. For the concatenated alignments, *Tetramphora* sequences were combined with sequence data for an additional 53 and 77 taxa obtained from GenBank for the three marker and SSU-*rbc*L alignments, respectively, and includes taxa from most major lineages of raphid diatoms (*sensu* Round et al. 1990). Four araphid diatom species were chosen as outgroup taxa.

For tree inference, maximum likelihood (ML) estimation was performed in RAxML ver. 7.3.2 (Stamatakis 2006) with the graphical user interface raxmlGUI ver. 1.2 (Silvestro & Michalak 2012) using the general time reversible (GTR) model of sequence evolution with a gamma rate distribution (Γ) and a proportion of invariable sites (I). For the ML estimation, three alignment partitioning strategies were employed, partition by marker, partition by marker and third codon position for the protein coding genes (*rbc*L and *psb*C) and partition by marker and all codon positions for the protein coding genes. For all alignment partitions, the final tree was chosen as the most likely tree from 100 independent tree searches and node support was estimated on the most likely tree with 500 bootstrap (BS) replicates. Bayesian inference was conducted using MrBayes ver. 3.2.1 (Ronquist et al. 2012). The bayesian estimation was run on an alignment partitioned by marker for 15 million generations, with a burn-in of 3 million

generations, using two runs of four chains sampled every 1000 generations. MCMC run and posterior probability convergence was evaluated using AWTY (Nylander et al. 2008).

RESULTS

Amended description of the genus *Tetramphora* Mereschkowsky 1903, p. 149

Lectotype (here designated): *Tetramphora ostrearia* (Brébisson) Mereschkowsky

Basionym: *Amphora ostrearia* Brébisson ex Kützing 1849, p. 94.

MERESCHKOWSKY C. 1903. Les types de l'endochrome chez les diatomées. Botanicheskiia Zhurnal 21: 1–106.

Literature. Schoeman & Archibald 1986, Figs 57–65; Levkov 2009, Pl. 275, Figs 5–11.

Cells elliptical with a strong valvar asymmetry creating a frustule with both valve faces on a single plane. Valves semi-elliptical to semi-lanceolate and moderately to strongly dorsiventral. The raphe is more or less biarcuate. The distal raphe ends are dorsally deflected, the proximal ends are either ventrally deflected or completely obscured by a prominent hyaline area or siliceous flap at the dorsal central area. In the LM this hyaline area gives the appearance of highly dilated to abruptly undulate proximal raphe ends. The striae are typically composed of small apically or transapically oriented areolae with thin slit-like external openings. Internally, the raphe terminates distally in helictoglossae and is often continuous through the central area. Internally, the raphe branches are flanked by more or less developed axial costae, often becoming a distinct siliceous projection at the dorsal central area. The girdle area is composed of numerous thin girdle bands. Each band exhibits a single row of large areolae along one margin, a feature that is clearly visible in the LM but often is obscured in the SEM by band overlap. Living cells exhibit Mereschkowsky's type 8 amphoroid chloroplast, containing two pairs of plate-like plastids one of each pair dorsally and ventrally appressed and bridged by large pyrenoids. Species are only known from marine, brackish and high conductivity inland waters.

Previously described Tetramphora species

Tetramphora ostrearia (Brébisson) Mereschkowsky (Figs 7.2, 7.3)

Basionym: *Amphora ostrearia* Brébisson ex Kützing 1849, p. 94.

Description. Valves dorsiventral and semi-elliptical. The dorsal margin is smoothly arched, becoming nearly flat at the valve center in some views, the ventral margin is straight to concave. Valve length 58.0–66.0 µm, valve breadth 7.0–8.0 µm. Valve ends are narrowly rounded and deflected ventrally. The raphe is highly biarcuate and is difficult to view in a single focal plane due to the curvature of the valve face. The axial area is narrow throughout. Although no dorsal fascia is present, thickened central virgae are observable in the LM. Striae are parallel near the valve center, becoming radiate near the apices on the dorsal side, convergent on the ventral side. Striae number 13–14 in 10µm.

In SEM, the striae, dorsally and ventrally, are separated by thin internal virgae (Fig. 7.2) and are crossed by fine vimines to form areolate striae. The striae are opened externally by thin longitudinally oriented slits. Internally, the central dorsal virgae are distinctly thickened (Fig. 7.2B) and a small protruding thickening is visible on the dorsal side of the central area (Fig. 7.2B, thin arrow). The raphe appears continuous through the internal central area and is bordered dorsally and ventrally by raised axial costae creating a narrow trough in which the raphe lies (Fig. 7.2B). Although difficult to see on the imaged specimens, the external distal raphe ends appear to terminate on the dorsal mantle of the valve (Fig. 7.2 A, C, arrows). The girdle area is composed of many thin, alternating, open girdle bands.

Taxonomic remarks. Although Mereschkowsky failed to designate a type for *Tetramphora* when the genus was proposed, *A. ostrearia* is one of two species that he originally transferred (along with *A. lineolata*). Of these taxa, *T. ostrearia* is the only taxon of which the type material has been extensively investigated and illustrated (Schoeman & Archibald 1986, Figs 57–65; Levkov 2009, Pl. 275, Figs 5–11). For this reason we are designating *T. ostrearia* as the lectotype of the genus *Tetramphora*. Schoemann and Archibald (1986) give length 58–95 µm, breadth 9–16 µm, and 12–14 striae in 10 µm for the

population on the type slide (BM 18948). The population examined here, although agreeing in length and striae counts, exhibits narrower valves, with valve breadth 7.0–8.0 µm. It is worth noting that Schoeman & Archibald (1986) cautioned that the shape of the valve in this taxon "varies considerably depending on the plane of viewing", and several images illustrated by Levkov (2009, Pl. 275, Figs 5–6), also from BM 18948, seem to correspond well to the proportions and valve angle of the specimens presented here.

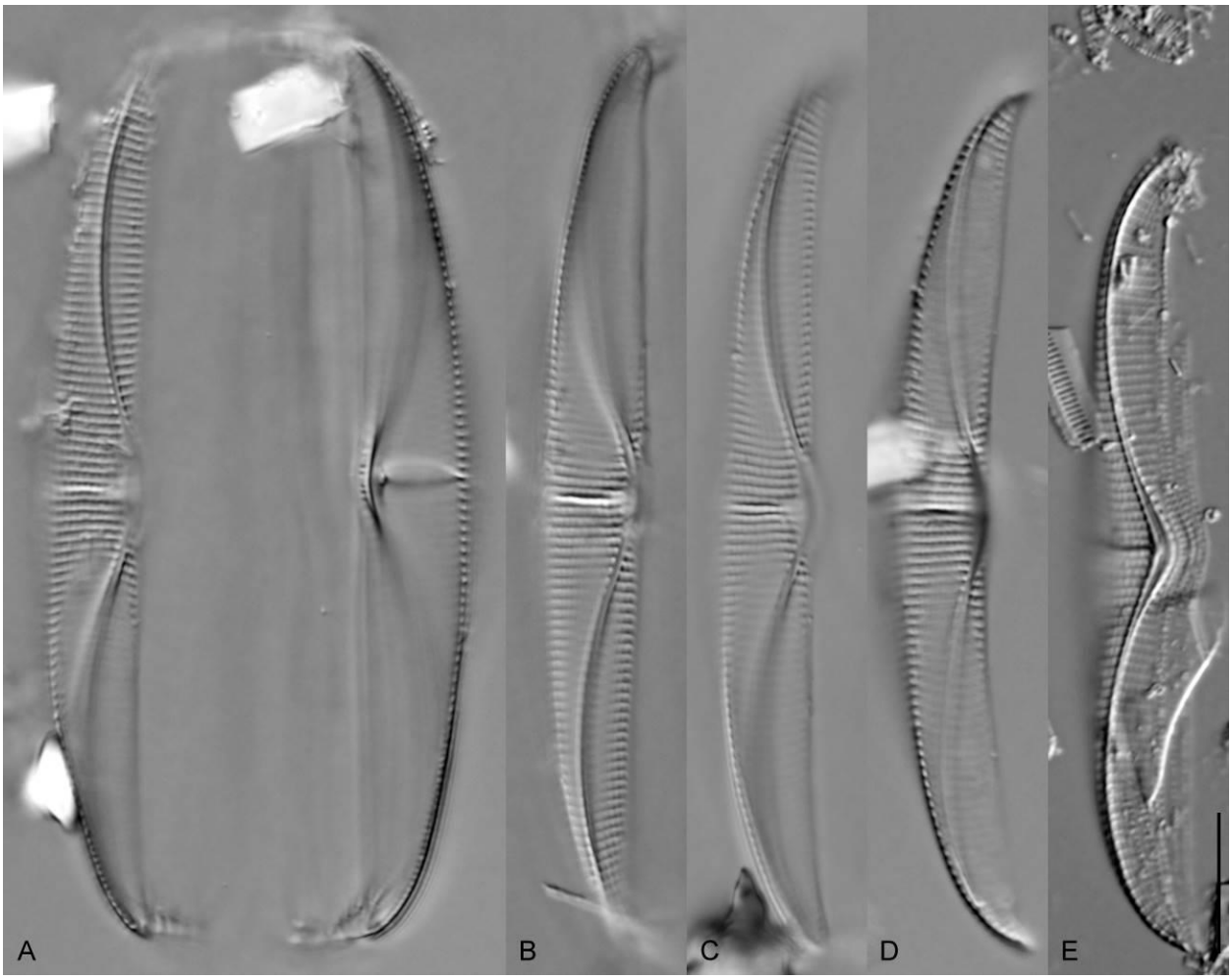

Figure 7.1. *Tetramphora ostrearia* whole frustule and valves showing size range, LM. **A.** Whole frustule. **B–E.** Single valves. Scale bar = 10 µm.

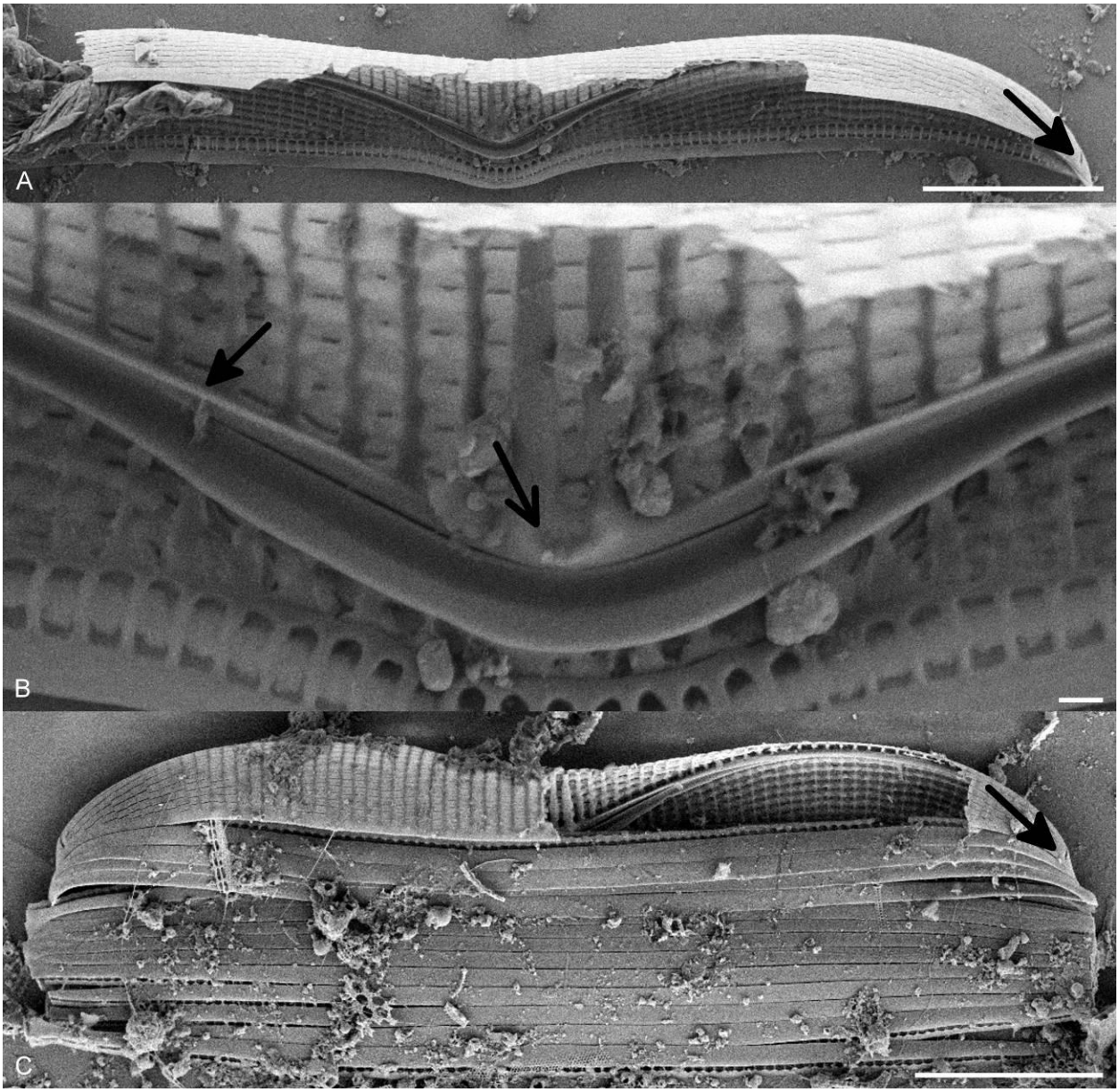

Figure 7.2. *Tetramphora ostrearia*, SEM. **A.** Internal whole valve showing distal raphe ends. **B.** Detail of the internal central valve showing thickened central virgae (arrow), protruding central thickening (thin arrow), and axial ribs. **C.** Dorsal view showing distal raphe ends (arrow) and girdle bands. Scale bars = 10 µm (Figs A, C), 1 µm (Fig. B).

Tetramphora lineolata (Ehrenberg) Mereschkowsky (Figs 7.3, 7.4)

Basionym: *Amphora lineolata* Ehrenberg 1838, p. 189.

Description. Valves semi-elliptical and strongly dorsiventral. The dorsal margin is smoothly arched, the ventral margin is straight to slightly convex. Valve ends are rounded and slightly ventrally deflected. Valve length 25.0–48.0 µm, valve breadth 5.5–8.0 µm. The raphe, which is largely visible in a single focal plane, is positioned near the ventral margin and is weakly biarcuate. The axial area is narrow, although a slight dilation is visible at the central area. The striae are fine and not obviously areolate, parallel at the valve center, becoming slightly radiate near the apices. Striae number 21–23 in 10 µm.

In SEM, the valves are much less flexed than in other members of the genus making observations of the raphe clearer in both the LM and SEM. Externally, the raphe is weakly biarcuate with distal ends hooking dorsally and proximal ends dipping ventrally near the central area and terminating, closely, in simple pores (Fig. 7.4A, B). Although a small, unornamented area is present dorsal to the proximal raphe ends, this structure is highly reduced when compared to the large siliceous flap that often obscures the proximal raphe ends in other *Tetramphora* taxa. The areolae are opened externally by thin, longitudinally oriented slits. Internally, the raphe is continuous through the central area (Fig. 7.4C) and is bordered by well-developed axial costae (Fig. 7.4D). Near the central area the dorsal axial costa diminishes before forming a small dorsally positioned siliceous projection (Fig. 7.4C, D). The striae are separated by thin virgae, more or less crossed by weakly developed vimines.

Taxonomic notes. *Tetramphora lineolata* is easily identified by its distinctly flat valve face (nearly the entire raphe system is visible in a single focal plane), and fine parallel striae (21–23 in 10 µm). It has been noted that the current concept of *T. lineolata* may differ from Ehrenberg's (1838) account of the species in which he describes a larger cell than is currently reported for this taxon (Jahn & Kusber 2004). Here we present the concept adopted by Cleve (1895) and Peragallo and Peragallo (1897–1908), in which they present a length of 32–45 um and a striae count of 20–23 in 10 µm (Peragallo & Peragallo 1897–1908

give a striae count of 19–23 in 10 µm) for *T. lineolata*. This concept for *T. lineolata* has been widely adopted in current literature (Krammer & Lange-Bertalot 1986, Witkowski et al. 2000).

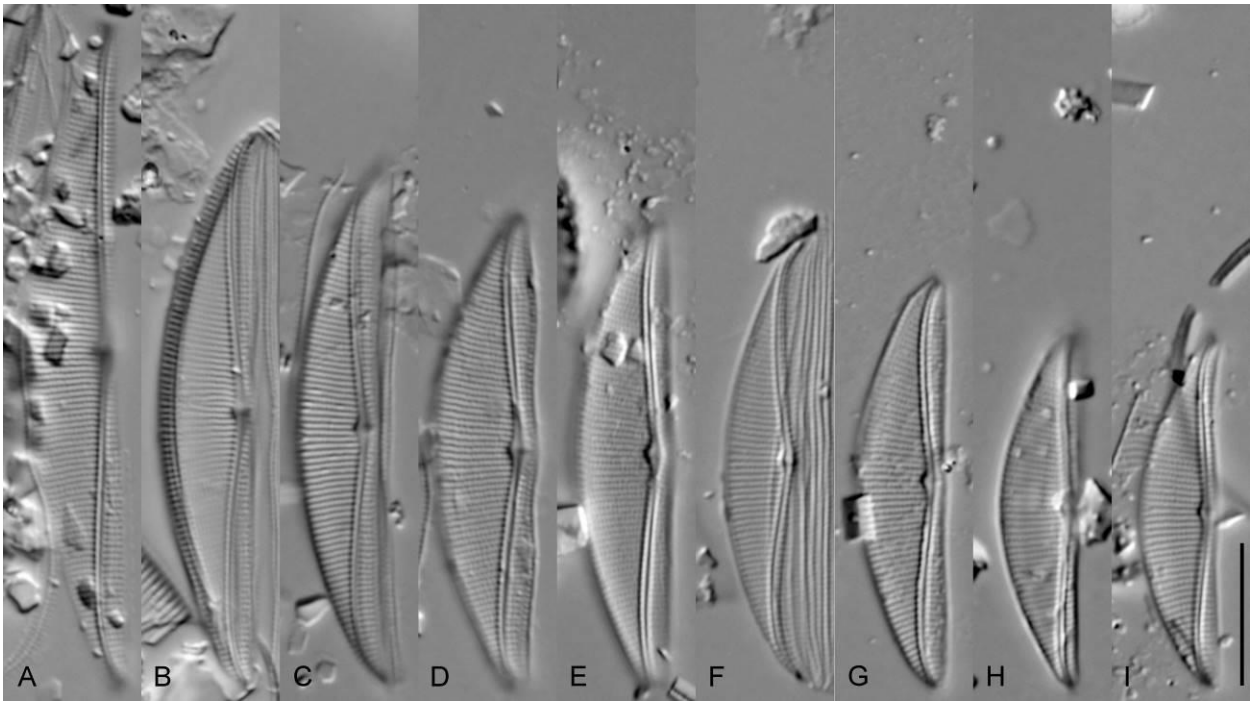

Figure 7.3 A–I. *Tetramphora lineolata*, single valves showing size range, LM. Scale bar = 10 µm.

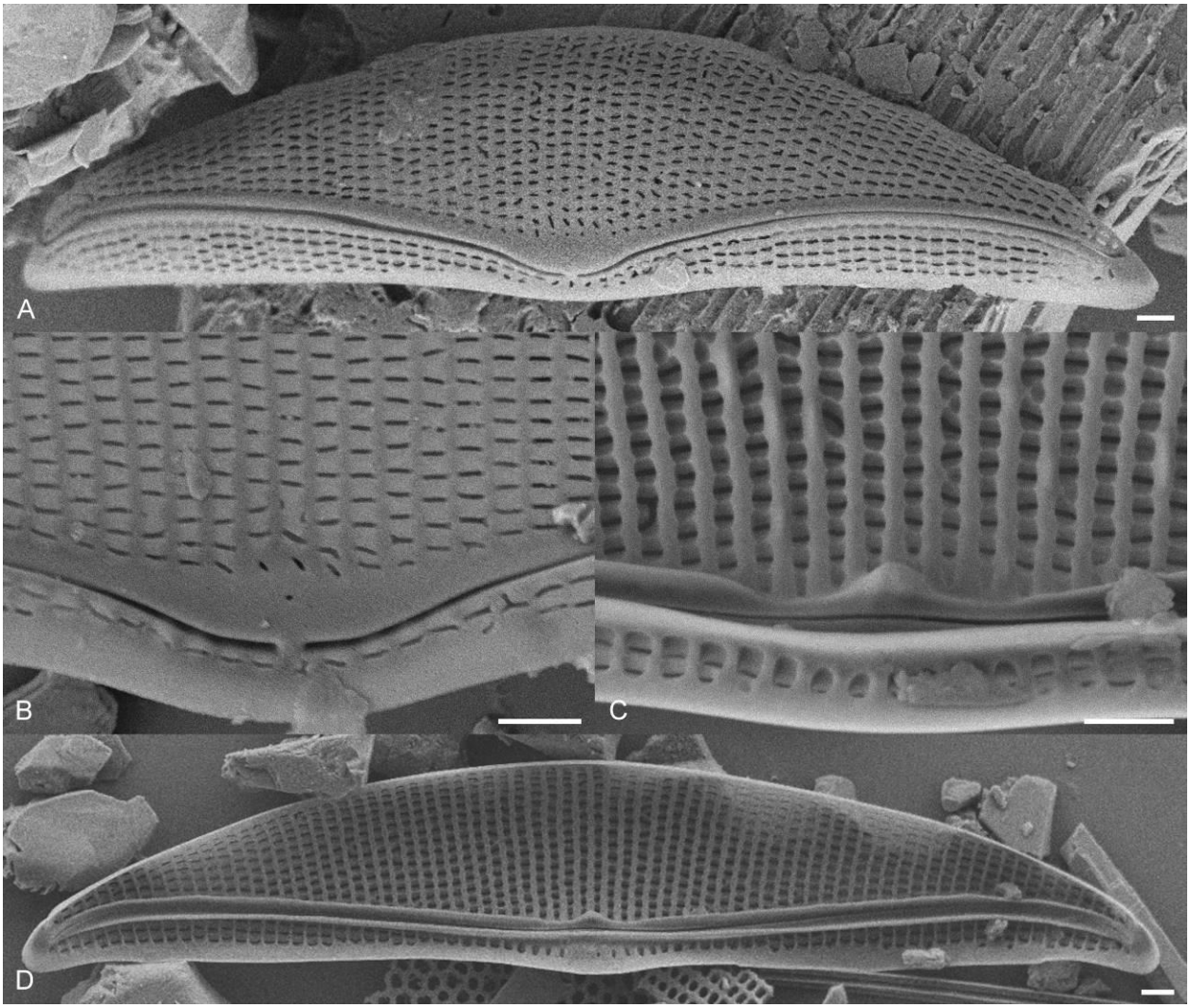

Figure 7.4. *Tetramphora lineolata*, SEM. **A.** External whole valve. **B.** Detail of the external valve center showing longitudinally oriented areolae, central hyaline area and closely spaced proximal raphe ends. **C.** Detail of internal valve center showing axial ribs and protruding central thickening. **D.** Internal whole valve. Scale bars = 1 µm.

Transfer of previously described species to Tetramphora

Tetramphora sulcata (Brébisson) Stepanek & Kociolek, comb. nov. (Figs 7.5, 7.6)

Basionym: *Amphora sulcata* Brébisson 1854, p.256; pl. 1, fig. 8

BRÉBISSON, A. 1854. Note sur quelques diatomées marines rares ou peu connues, du littoral de Cherbourg. *Mémoires de la Société des Sciences Naturelles de Cherbourg*. Paris. 2: 241–258, 1 pl.

Description. Valves semi-elliptical and dorsiventral. The dorsal margin is smoothly arched, becoming flat over the central portion of the valve in some specimens, the ventral margin is biarcuate. Valve apices are acute, narrowly rounded and ventrally deflected. Valve length 35.0–58.0 µm, valve breadth 5.5–7.5 µm. The raphe is highly biarcuate and the proximal ends are difficult to view due to the valve curvature. The axial area is narrow throughout. The striae are distinctly areolate and nearly parallel throughout. Striae number 18–19 in 10 µm.

In SEM, externally, the raphe is biarcuate with distal ends deflecting dorsally and proximal ends dipping towards the ventral margin before terminating, closely, in simple endings (Fig. 7.6A, B). An unornamented area is present at the dorsal central area but is not extended into a flap (Fig. 7.6B). The areolae are opened externally as thin longitudinally oriented slits. Internally, the raphe is continuous through the central area (Fig. 7.6C) and is bordered by axial costae. Near the central area the ventral axial costa is thickened and the dorsal costa is reduced until forming a small, projecting thickening (Fig. 7.6C, D). The striae are separated by thin virgae more or less crossed by weakly developed vimines.

Taxonomic notes. Although Cleve (1895) treats *A. sulcata* as a variety of *A. arcus* Gregory, he notes that the variety *sulcata* is akin to *A. lineolata* and gives a striae count of 14–20 in 10 µm. *Tetramphora sulcata* is similar to *T. lineolata* and *T. lineolatoides* Stepanek & Kociolek sp. nov. in having more or less parallel

striae, lack of a central raphe flap and longitudinal orientation of the external areolar slits. This taxon is distinguished from *T. lineolata* and *T. lineolatoides* by its distinctly flexed and biarcuate valve shape.

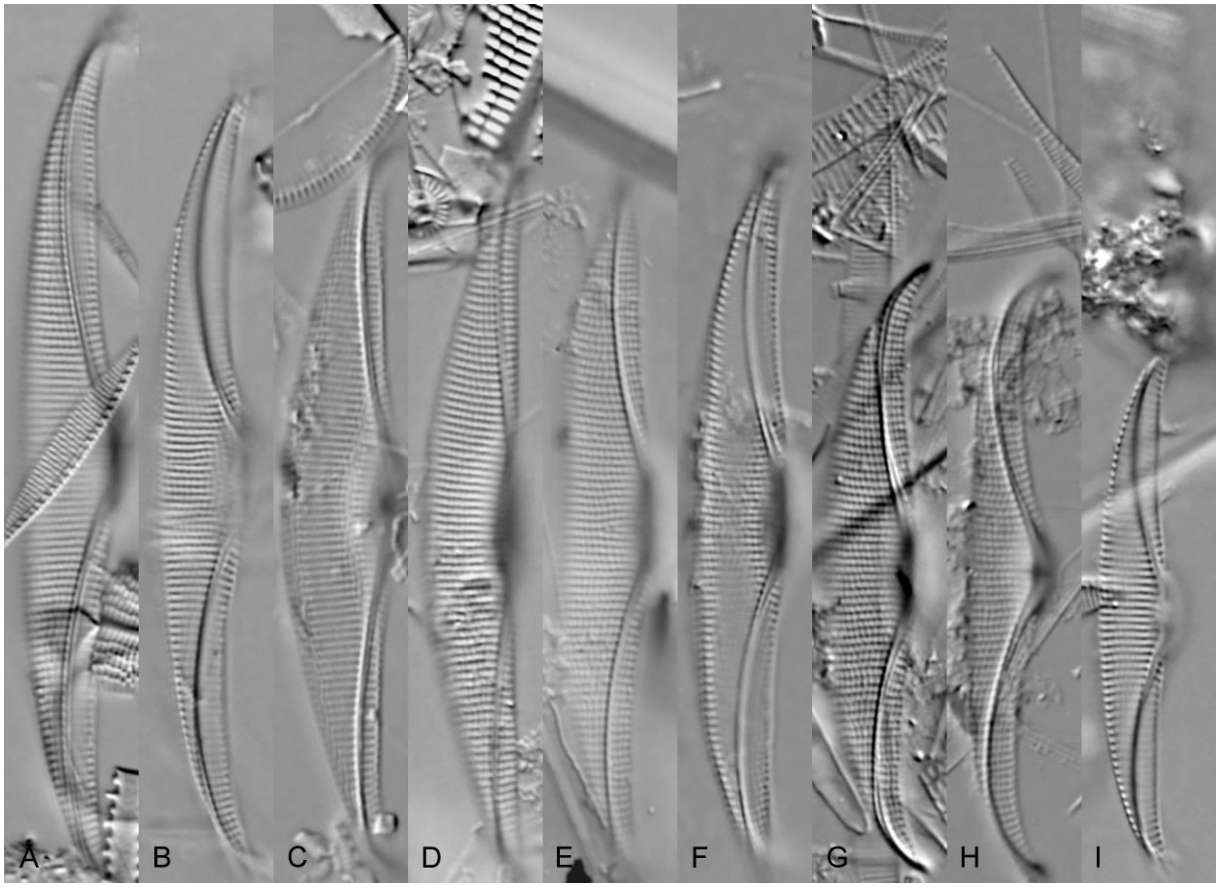

Figure 7.5. A–I. *Tetramphora sulcata* comb. nov., single valves showing size range, LM. Scale bar = 10 µm.

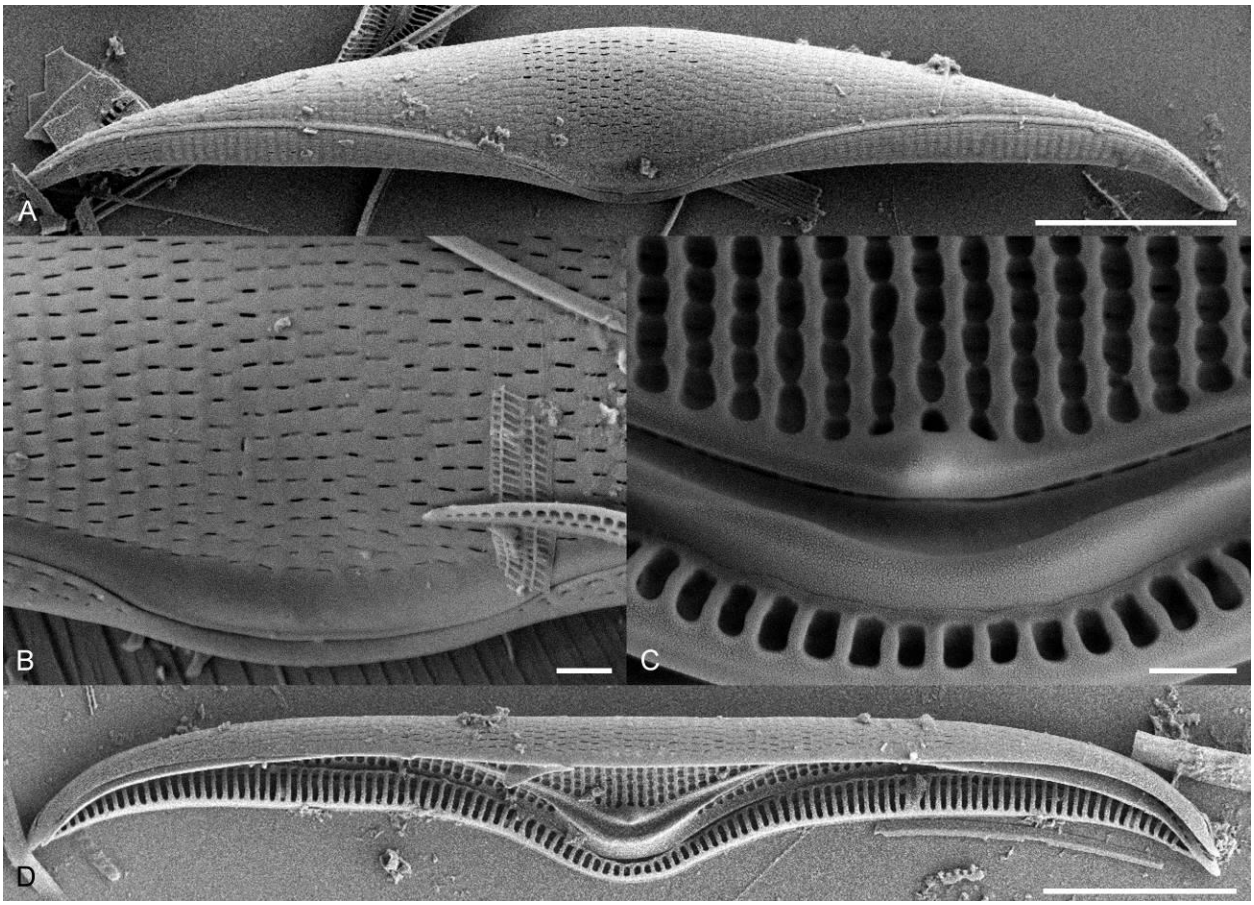

Figure 7.6. *Tetramphora sulcata* comb. nov., SEM. **A.** External whole valve. **B.** Detail of external valve center showing longitudinally oriented areolae, central hyaline area and closely spaced proximal raphe ends. **C.** Detail of internal valve center showing continuous raphe and protruding central thickening. **D.** Internal whole valve. Scale bars = 10 µm (A, D), 1 µm (B, C).

Tetramphora intermedia (Cleve) Stepanek & Kociolek, comb. nov. *stat. nov*. (Figs 7.7, 7.8)

Basionym: *Amphora rhombica* var. *intermedia* Cleve 1895, p. 127.

CLEVE P.T. 1895. Synopsis of naviculoid diatoms. II. *Kongliga Svenska-Vetenskaps Akademiens Handlingar* 27: 1–219.

Description. Valves broadly semi-lanceolate and strongly dorsiventral. The dorsal margin is arched, the ventral margin is nearly straight. Valve ends are acutely rounded and weakly ventrally deflected. Valve length 80.0–105.0 µm, valve breadth 17.0–19.0 µm. The raphe is weakly biarcuate and positioned near the ventral margin. The proximal and distal raphe ends are difficult to view due to the valve curvature. The axial area is narrow throughout. The dorsal and ventral striae are areolate and radiate throughout. Striae number 14–17 in 10 µm.

In SEM, externally, the raphe is biarcuate with distal ends deflected dorsally and the proximal ends ending at a large flap of unornamented silica partially obscuring the raphe ends (Fig. 7.8A). A thin weakly developed rib runs along either side of the raphe (Fig. 7.8A, arrow). This rib appears more prominent near the apices. The striae are areolate and opened externally by single, narrow, transapically oriented slits. A weakly developed marginal ridge appears to interrupt the striae as they continue onto the dorsal margin (Fig. 7.8A, thin arrow). Internally, the striae are separated by very thin virgae, vimines are not well developed (Fig. 7.8B). The raphe system is bordered by moderately developed axial costae and ends distally at a helictoglossae (Fig 7.8C, D). A small thickened projection is apparent at the internal central area (Fig. 7.8B).

Taxonomic remarks. This taxon is easily distinguished from other *Tetramphora* species by its large broad valves. It is separated from the nominate variety by its relatively smaller size and finer striation (Cleve 1895 gives length 130–260 µm, breadth 21–50 µm, and 10–12 striae in 10 µm for *A. rhombica* Kitton and length 90–100 µm, breadth 17 µm and 14 striae in 10 µm for *A. rhombica* var. *intermedia*).

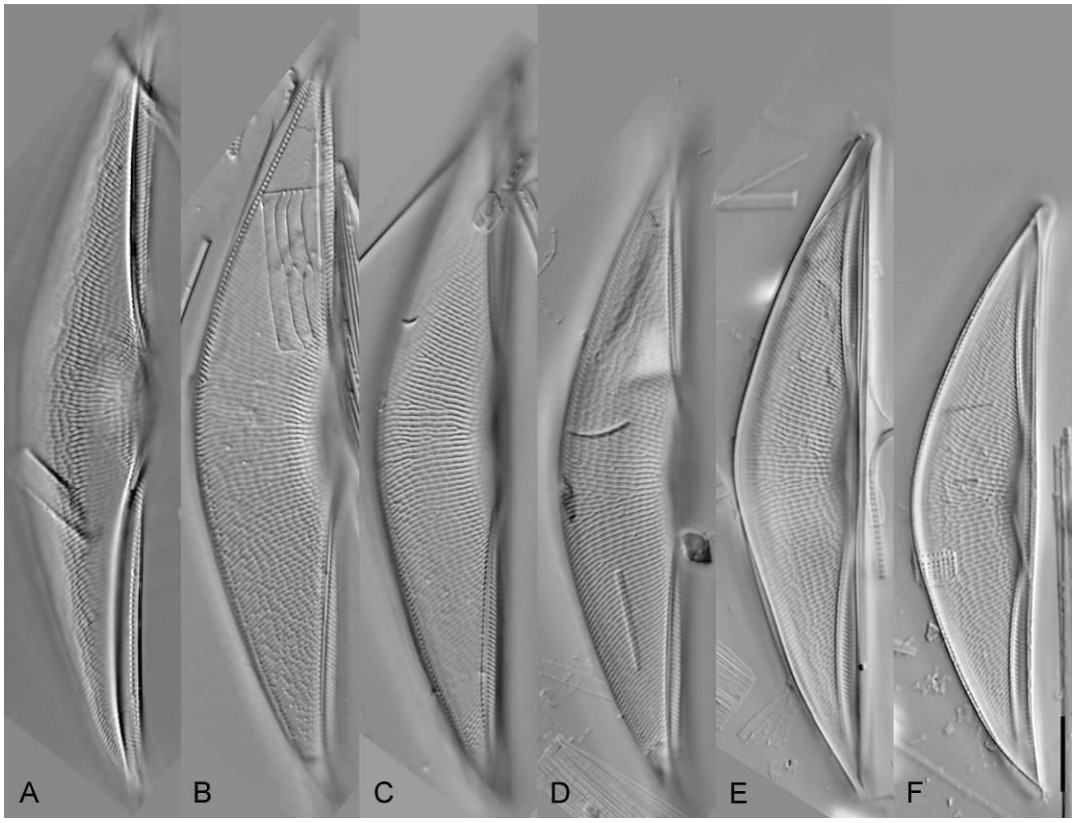

Figure 7.7. A–F. *Tetramphora intermedia* comb. nov. stat. nov., single valves showing size range, LM. Scale bar = 10 µm.

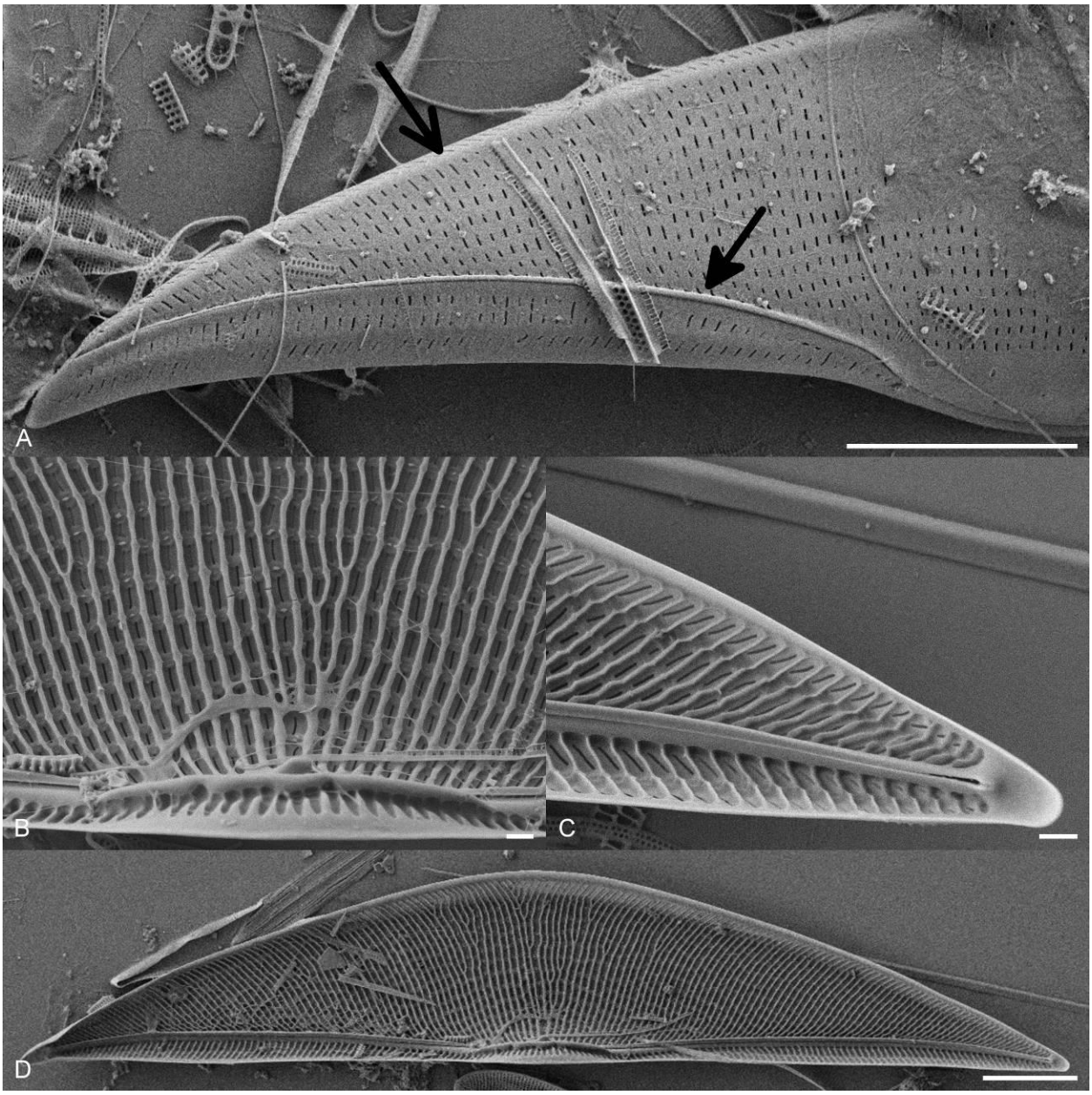

Figure 7.8. *Tetramphora intermedia* comb. nov. stat. nov., SEM. **A.** External valve showing axial rib (arrow) and marginal ridge (thin arrow). **B.** Detail of internal valve center showing thin virgae and protruding central thickening. **C.** Detail of internal valve end showing axial rib and distal raphe ends ending in a helictoglossa. **D.** Internal whole valve view. Scale bars = 10 µm (A, D), 1 µm (B, C).

Tetramphora securicula (Peragallo & Peragallo) Stepanek & Kociolek, comb. nov. (Figs 7.9, 7.10)

Basionym: *Amphora securicula* Peragallo & Peragallo 1897–1908, p. 224; pl. 50, fig. 2.

PERAGALLO H. & PERAGALLO M. 1897–1908. *Diatomées marines de France et des districts maritimes voisins.* M.J. Tempère micrographe-éditeur, Grez-sur-Loing. 492 pp.

Description. Valves semi-elliptical and dorsiventral. The dorsal margin is smoothly arched, the ventral margin is straight to biarcuate. Valve ends are acutely rounded and ventrally deflected. Valve length 55.0–75.0 µm, valve breadth 8.0–10.0 µm. The raphe is strongly biarcuate and the proximal and distal endings are obscured by the curvature of the valve face. The axial area is narrow throughout. The dorsal striae are areolate, nearly parallel near the valve center, becoming radiate towards the apices. Ventral striae are obscured near the valve center, radiate throughout. Striae number 16 in 10 µm.

In SEM, externally, the raphe is biarcuate and bordered by a weakly developed axial rib (Fig. 7.10A). The distal raphe ends deflect dorsally and the proximal raphe ends are obscured by a large, unornamented siliceous flap (Fig. 7.10B). The areolae are opened externally by small transapically oriented slit-like openings. Internally, the striae are separated by thin virgae crossed by poorly developed vimines. Internally, the raphe is bordered by axial costae and a small siliceous projection is present at the dorsal central area (Fig. 7.10 C, D).

Taxonomic remarks. This taxon can be distinguished by its large size, coarse striae and prominent highly biarcuate raphe. Although this taxon has not been extensively illustrated, the population reported here conforms well to Wachnicka and Gaiser's (2007) observations of *A. securicula* from southern Florida, who reported valve metrics as length 55–59 µm, breadth 9–10, and 16–17 striae in 10 µm for their specimens. In SEM, the specimens presented here corresponds to the taxon illustrated by Levkov (2009, Pl. 282, Figs 1–6) as *A. securicula* based on material from the British Museum of Natural History, both populations agreeing in with ours in overall valve shape, the prominent central siliceous flap, and the transapically-oriented external areolar slits.

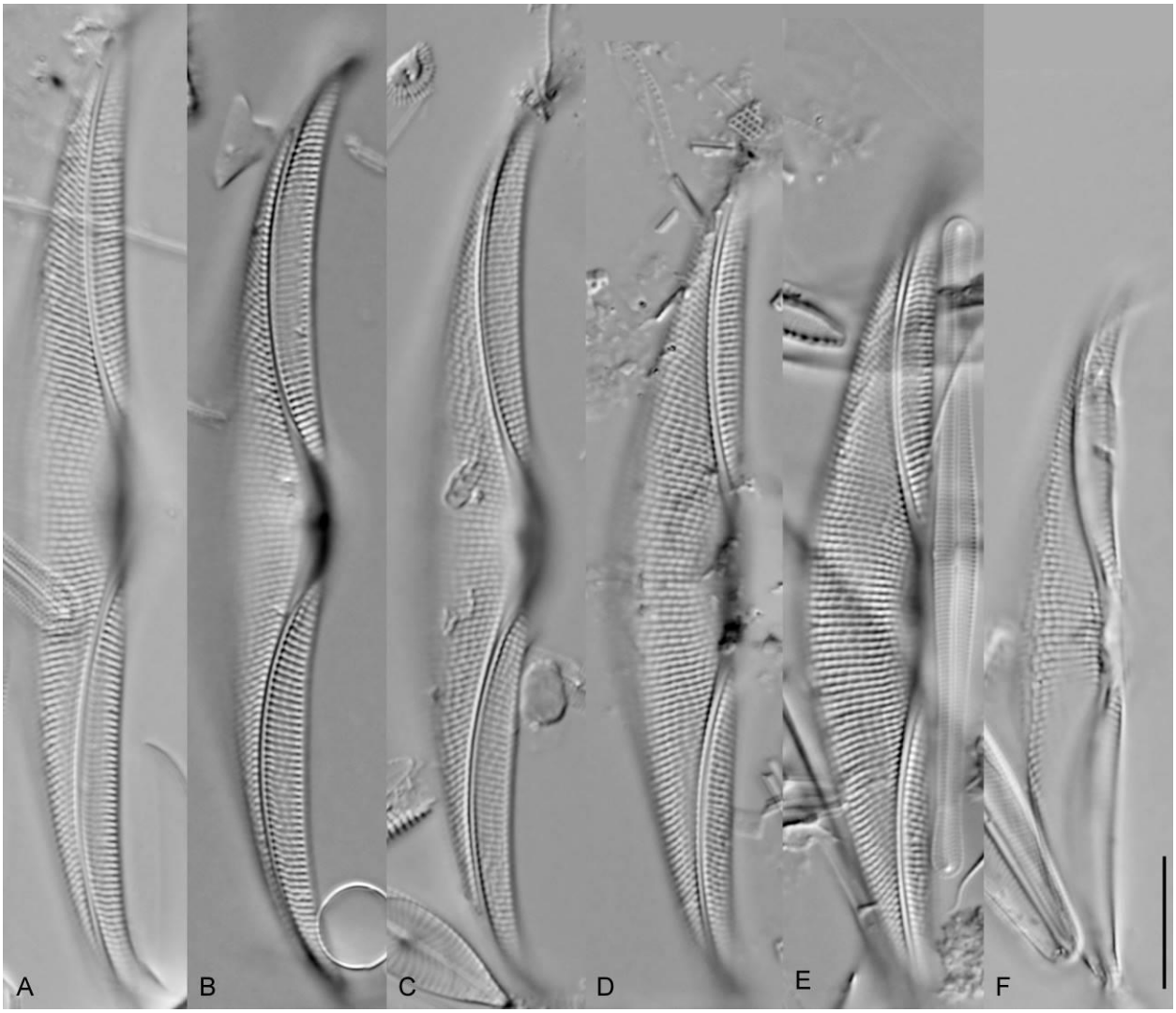

Figure 7.9. A–F. *Tetramphora securicula* comb. nov., single valves showing size range, LM. Scale bar = 10 µm.

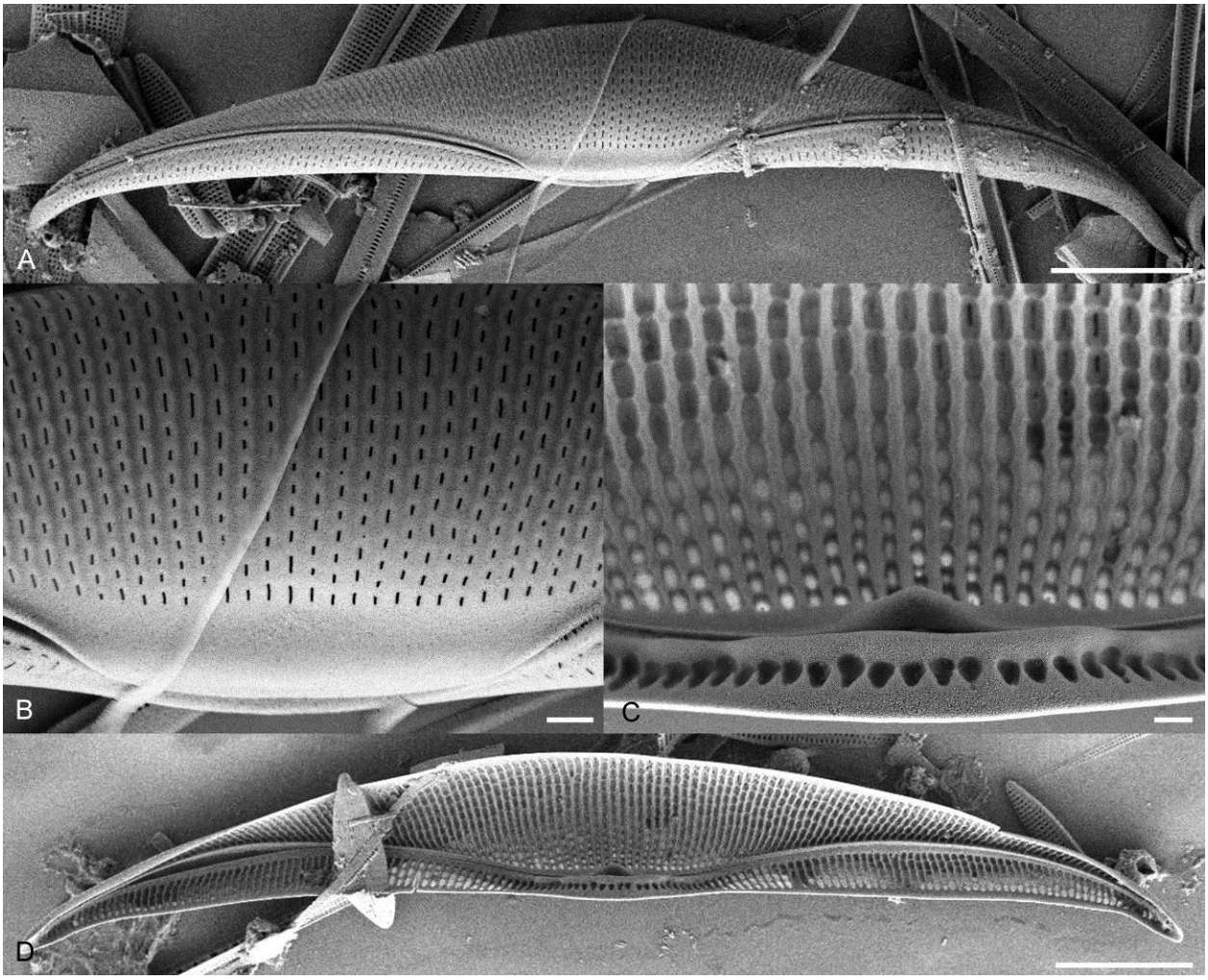

Figure 7.10. *Tetramphora securicula* comb. nov., SEM. **A.** External whole valve showing axial ribs. **B.** Detail of external valve center showing transapically oriented areolae and central siliceous flap obscuring the proximal raphe ends. **C.** Detail of internal valve center showing protruding central thickening. **D.** Internal whole valve showing axial ribs. Scale bars = 10 µm (A, D), 1 µm (B, C)

Tetramphora chilensis (Hustedt) Stepanek & Kociolek, comb. nov. (Figs 7.11, 7.12)

Basionym: *Amphora chilensis* Hustedt 1927, p. 239; pl. 7, figs 8–10.

HUSTEDT, F. 1927. Fossile bacillariaceen aus dem Loa-Becken in der Atacama-Wüste, Chile. *Archiv für Hydrobiologie* 18 (2): 224–251, Tafs 7–9.

Synonym: *Halamphora chilensis* (Hustedt) Levkov

Description. Valves are narrowly semi-elliptical and strongly dorsiventral. The dorsal margin is smoothly arched, the ventral margin is straight to slightly concave. The valve ends are narrowly rounded to rostrate and ventrally deflected. Valve length 20.0–42.0 µm, valve breadth 4.5–6.0. The raphe is straight to slightly arched and positioned very near the ventral margin. The distal raphe ends are dorsally bent and the proximal raphe ends become suddenly and distinctly deflected ventrally as they near the central area. The striae are areolate and weakly radiate throughout. Dorsal striae number 20–23 in 10 µm, ventral striae are finer, numbering 26–30 in 10 µm.

In SEM, externally, the raphe is nearly straight with dorsally-deflected distal raphe ends (Fig. 7.12A). The proximal raphe ends dip towards the ventral margin as they approach the central area before terminating, closely, in simple raphe ends (Fig. 7.12A, B). A broad unornamented dorsal central area is present but not extended into a flap (Fig. 7.12B). The external areolar openings consist of small transapically oriented dash-like openings. Internally, the raphe is straight with each distal end terminating as a helictoglossa and the proximal ends straight and terminating close to one another (Fig. 7.12C, D). Both the highly developed axial costae and dorsal central swelling seen in other *Tetramphora* taxa are absent in *Tetramphora chilensis* (Fig. 7.12D). The striae are separated by relatively thick virgae crossed by weakly developed vimines.

Taxonomic remarks. *Tetramphora chilensis* is quite unique and easily identified within the genus *Tetramphora* given its small flat valves and nearly strait raphe. Although it was noted that *A. chilensis* lacked several features common in *Halamphora* taxa (raphe ledge and internal central helictoglossa),

Levkov (2009) transferred this taxon to *Halamphora* based on girdle band and areolae structure. Although overall valve shape, striae and areolae structure in this taxon are quite similar to taxa such as *Halamphora veneta* (Kützing) Levkov, the external central hyaline area, and resulting deflected proximal raphe ends, as well as molecular data clearly place this species within *Tetramphora*.

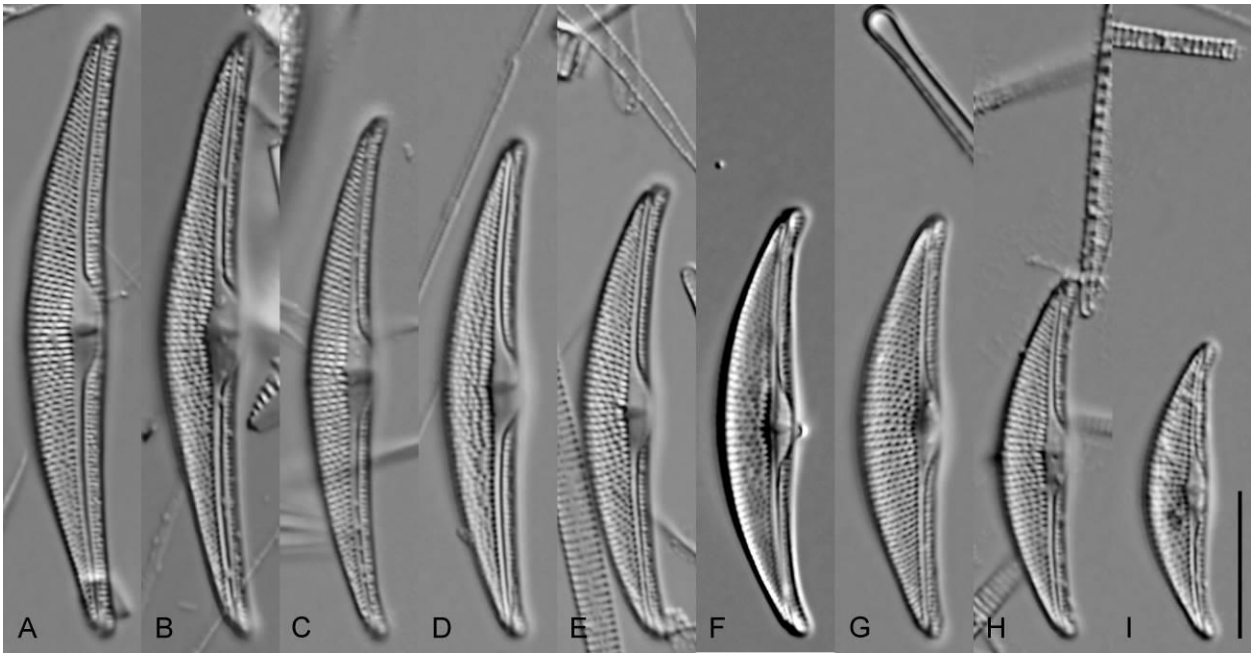

Figure 7.11. A–I. *Tetramphora chilensis* comb. nov., single valves showing size range, LM. Scale bar = 10 µm.

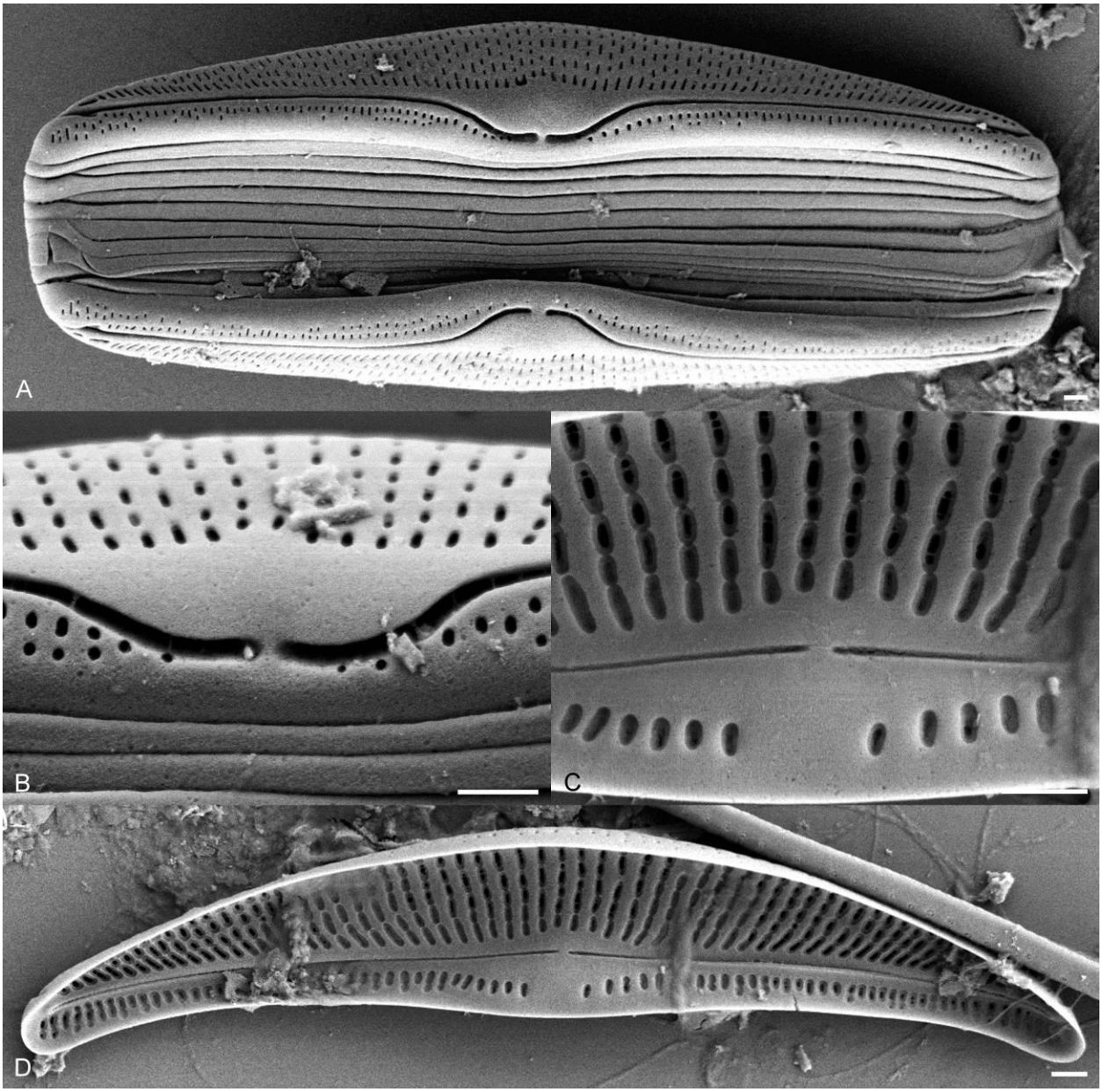

Figure 7.12. *Tetramphora chilensis* comb. nov., SEM. **A.** Whole frustule dorsal view showing girdle bands. **B.** Detail of external valve center showing transapically oriented dash-like areolae, central hyaline area and closely spaced proximal raphe ends. **C.** Detail of internal valve center showing closely spaced proximal raphe ends. **D.** Internal whole valve. Scale bars = 1 µm.

Newly described species

Tetramphora lineolatoides Stepanek & Kociolek (Figs 7.13, 7.14)

Description. Valves strongly dorsiventral and semi-elliptical. The dorsal margin is rounded, nearly flat through the central portion of the valve, the ventral margin is nearly straight to slightly convex. The valve ends are narrowly rounded and ventrally deflected. Valve length 28.0–45.0 µm, valve breadth 5.0–8.0 µm. The raphe is moderately biarcuate and positioned near the ventral margin. The valve face is weakly flexed, obscuring the proximal raphe endings in some views. The axial area is narrow, although a slight inflation is visible at the central area in some orientations. The striae are areolate and nearly parallel throughout. Striae number 18–19 in 10 µm.

In SEM, the valves are only moderately flexed. The raphe is biarcuate with dorsally deflected distal raphe ends and proximal ends dipping towards the ventral margin before terminating in simple endings (Fig 7.14A–C). An unornamented area is present on the dorsal side of the proximal raphe ends, but it does not extend into a flap (Fig. 7.14C). The external areolae openings consist of thin longitudinally oriented slits. Internally, the raphe is continuous through the central area, bordered by weakly developed axial costae and ending distally in helictoglossae (Fig. 7.14D–F). A small protruding central thickening is present on the dorsal central area (Fig. 7.14F). The striae are separated by thin virgae crossed by very weakly developed vimines.

Holotype. Slide ANSP GC 36356, deposited at the Academy of Natural Sciences, Philadelphia, USA. Holotype specimen illustrated in Fig. 7.14C.

Isotype. Cleaned material ANSP GC 24052, deposited at the Academy of Natural Sciences, Philadelphia, USA. Slide and cleaned material JPK10929, deposited at the University of Colorado Boulder, Kociolek Collection at COLO.

Type locality. 35.61063°N, 135.90234°E. Epiphytes, Wakasa Bay, Toyama, Japan.

Etymology. *lineolatoides* refers to the close morphological affinity to the species *T. lineolata*.

Taxonomic notes. *Tetramphora lineolatoides* shares several features with *T. lineolata*, including a relatively flat valve face, lack of a central raphe flap, and orientation of the external areolar slits. However, *T. lineolatoides* can be easily distinguished by its distinctly coarser striae and, in the SEM, its more widely spaced proximal raphe ends. *Tetramphora lineolatoides* is distinguished from *T. sulcata*, for which it shares similar size, striae counts, and SEM features by its less flexed and biarcuate valve shape.

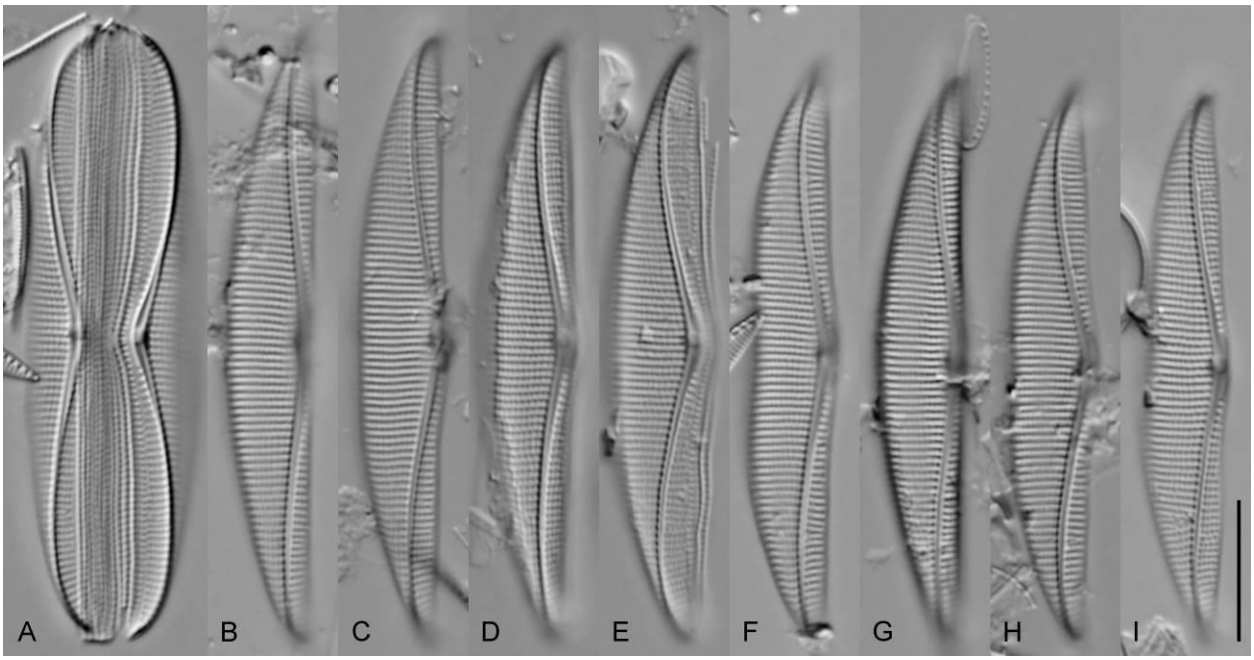

Figure 7.13. *Tetramphora lineolatoides* sp. nov., whole frustule and single valves showing size range, LM. **A.** Whole frustule. **B–I.** Single valves. **C.** Holotype specimen. Scale bar = 10 µm.

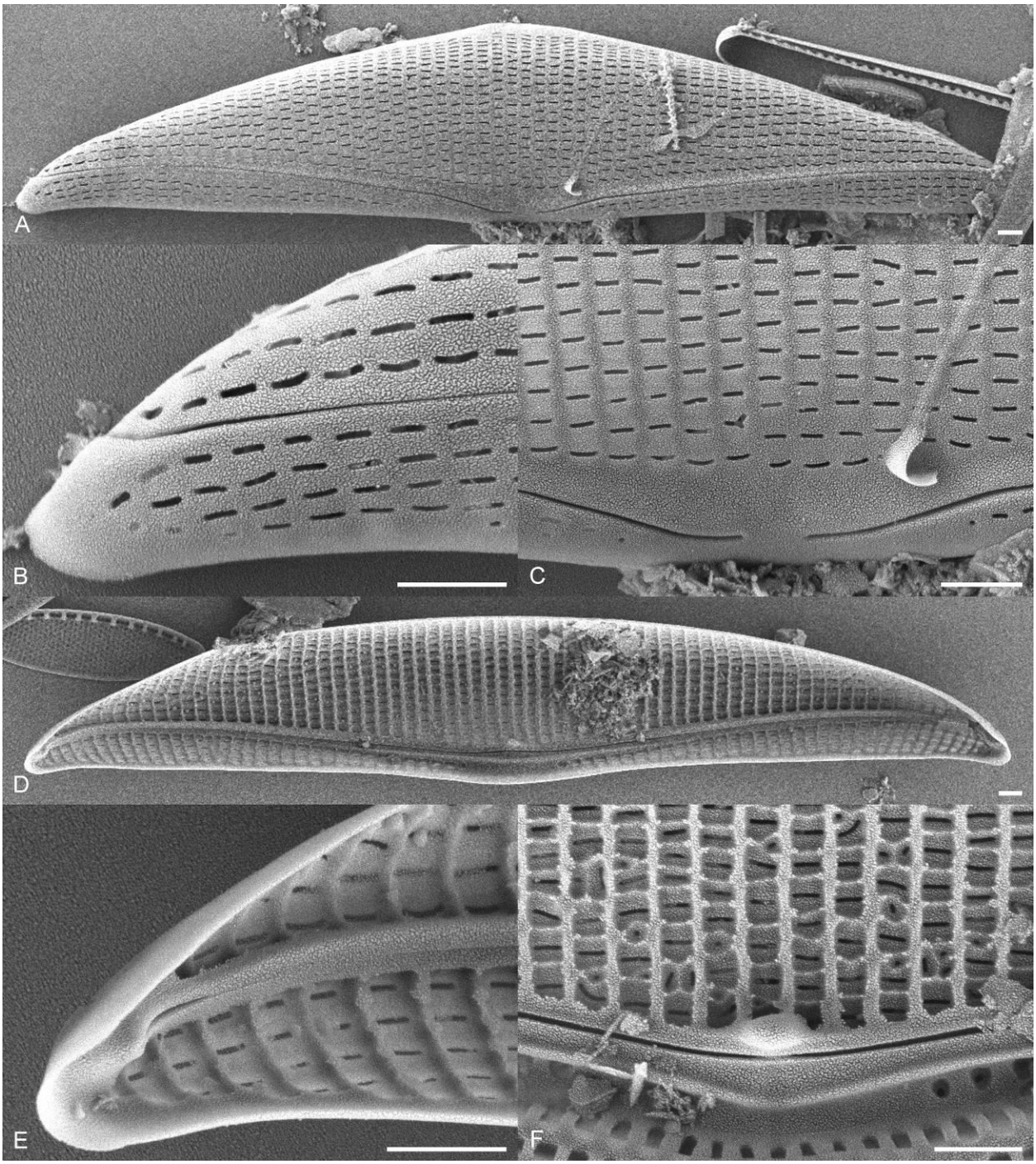

Figure 7.14. *Tetramphora lineolatoides* sp. nov., SEM. **A.** External whole valve. **B.** Detail of external valve end showing dorsally deflected dorsal raphe ends and longitudinally oriented areolae. **C.** Detail of external valve center showing central hyaline area and proximal raphe ends. **D.** Internal whole valve. **E.** Detail of internal valve end showing distal helictoglossa. **F.** Detail of internal valve center showing continuous raphe and protruding central thickening. Scale bar = 1 µm.

Tetramphora fontinalis Stepanek & Kociolek sp. nov. (Figs 7.15, 7.16)

Description. Valves dorsiventral and narrowly semi-elliptical becoming linear through the central portion of the valve. The dorsal margin is arched, becoming flat over the valve center, the ventral margin is more or less straight. Valve ends are narrowly rounded and ventrally deflected. Valve length 38.0–60.0 µm, valve breadth 6.0–8.0 µm. The raphe is highly biarcuate and both the proximal and distal ends are difficult to view due to the valve curvature. The striae are distinctly areolate, near parallel at the valve center, weakly radiate across the rest of the valve. Striae number 17–21 in 10 µm.

In SEM, externally, the raphe is biarcuate with dorsally bent distal raphe ends and appears continuous through the central area (Fig. 7.16A–C). The unornamented, dorsal, central area is well developed into a siliceous flap obscuring the proximal raphe ends (Fig. 7.16B). The external areolae openings consist of small transapically oriented slits. Internally, the raphe is bordered by well-developed axial costae (Fig. 7.16D). The raphe terminates distally in a helictoglossa and is continuous through the central area (Fig. 7.16E, F). A protruding central thickening is present on the dorsal side of the central area (Fig. 7.16D, F). The striae are separated by virgae crossed by weakly developed vimines.

Holotype. Slide ANSP GC 65228, deposited at the Academy of Natural Sciences, Philadelphia, USA. Holotype specimen illustrated in Fig. 7.15A.

Isotype. Cleaned material ANSP GC 5701, deposited at the Academy of Natural Sciences, Philadelphia, USA. Slide and cleaned material JPK8504, deposited at the University of Colorado Boulder, Kociolek Collection at COLO.

Type locality. 40.50257°N, 115.03359°W. Periphyton, Blue Lake warm spring, Tooele County, Utah, USA.

Etymology. *fontinalis* (Latin = growing in a spring) refers to the type locality of this taxon, Blue Lake warm spring, Utah, USA.

Taxonomic remarks. This taxon, collected from Blue Lake warm spring, Utah, appears very closely allied to the coastal marine *T. securicula*. Both exhibit a flexed valve with a highly biarcuate raphe. In SEM, they share a prominent central raphe flap and areolae orientation. *Tetramphora fontinalis* differs from *T. securicula* in its narrow distinctly linear valves (Valve breadth 8.0–10.0 µm in *T. securicula*, 6.0–8.0 µm in *T. fontinalis*), and finer dorsal striae (16 in 10 µm in *T. securicula* and 17–21 in 10 µm in *T. fontinalis*). *Tetramphora fontinalis* shares a similar valve outline, size and striae count with *T. sulcata*, but can be distinguished from this taxon in the LM by its more distinct areolae and radiate striae. In SEM, *T. fontinalis* is distinguished from *T. sulcata* by its prominent central siliceous flap obscuring the proximal raphe ends and by its transapically oriented areolae slits.

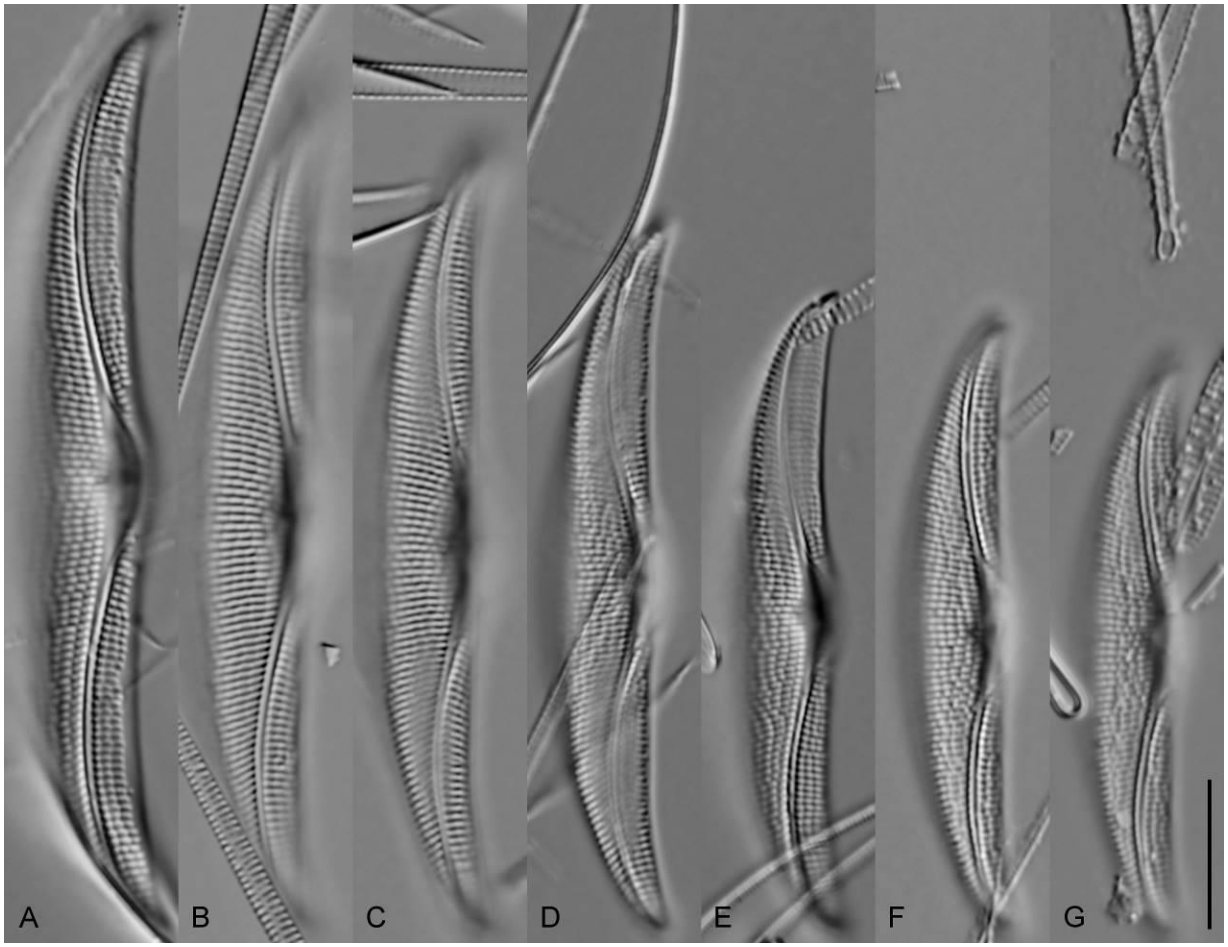

Figure 7.15. A–G. *Tetramphora fontinalis* sp. nov., single valves showing size range. **A.** Holotype specimen. Scale bar = 10 µm.

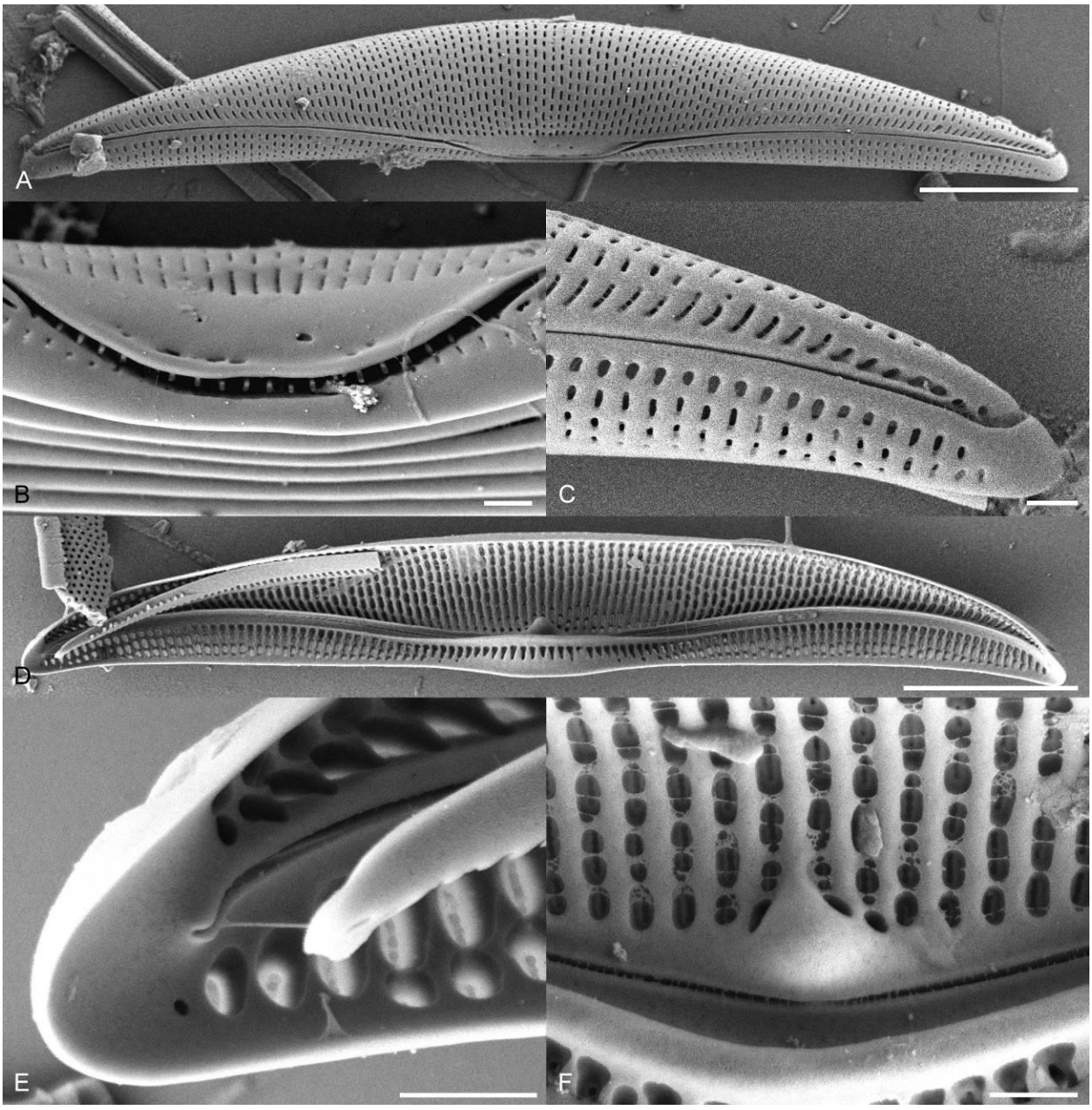

Figure 7.16. *Tetramphora fontinalis* sp. nov., SEM. **A.** External whole valve showing transapically oriented areolae. **B.** Detail of external valve center showing central siliceous flap and continuous raphe. **C.** Detail of external valve end showing dorsally deflected distal raphe end. **D.** Internal whole valve. **E.** Detail of internal valve end showing distal helictoglossa. **F.** Detail of internal valve center showing continuous raphe and protruding central thickening. Scale bars = 10 µm (A. D), 1 µm (B, C, E, F).

Tetramphora robusta Stepanek & Kociolek sp. nov. (Figs 7.17, 7.18)

Description. Valves broadly semi-elliptical and strongly dorsiventral. The dorsal margin is smoothly arched, the ventral margin appears straight to slightly convex depending on the angle of the specimen. The valve ends are narrowly rounded. Valve length 45.0–65.0 µm, valve breadth 8.0–10.0 µm. The raphe is weakly biarcuate and positioned near the ventral margin. The valve is highly flexed near the apices and central area making much to the raphe system difficult to image in a single focal plane. The axial area is narrow throughout. The striae are coarse and distinctly areolate, parallel near the valve center and becoming radiate near the apices. Striae number 13–14 in 10 µm.

In SEM, externally, the raphe is biarcuate with dorsally deflected distal ends and proximal ends that dip towards the ventral margin before terminating closely in simple endings (Fig. 7.18A–C). An unornamented area is present at the dorsal central area, but is not extended into a flap (Fig. 7.18C). The external areolar openings consist of small transapically oriented slits. Internally, the raphe is bordered by well-developed axial costae (Fig. 7.18D, E). The distal raphe ends terminate in a helictoglossa. In the imaged specimens the central area is obscured by the flexure of the valve. Although the majority of the central area is obscured, a protruding central thickening is visible (Fig. 7.18D, E). The striae are separated by thin virgae, the vimines are not well developed.

Holotype. Slide ANSP GC 59143, deposited at the Academy of Natural Sciences, Philadelphia, USA. Holotype specimen illustrated in Fig. 7.17B.

Isotype. Cleaned material ANSP GC 4859, deposited at the Academy of Natural Sciences, Philadelphia, USA. Slide and cleaned material JPK8566, deposited at the University of Colorado Boulder, Kociolek Collection at COLO.

Type locality. 24.64167°N, 81.33877°W. Benthos, Long Beach Backwater, Big Pine Key, Florida Keys, Florida, USA.

Etymology. *robusta* refers to the large coarsely striated valves of this species.

Taxonomic remarks. *Tetramphora robusta* is distinguished from *T. securicula* with which it shares similar length and breadth by the more ventral position of its weakly biarcuate raphe, and its coarser striae (*T. robusta* 13–14 striae in 10 µm, *T. securicula* 16 striae in 10 µm). *Tetramphora robusta* is similar in valve outline and raphe position to the large-celled *T. rhombica* and *T. rhombica* var. *intermedia*. *Tetramphora robusta* is distinguished from both by its smaller size (Cleve 1895 gives lengths of 130–260 µm and 90–100 µm for *A. rhombica* and *A. rhombica* var. *intermedia*, respectively) and more flexed valves.

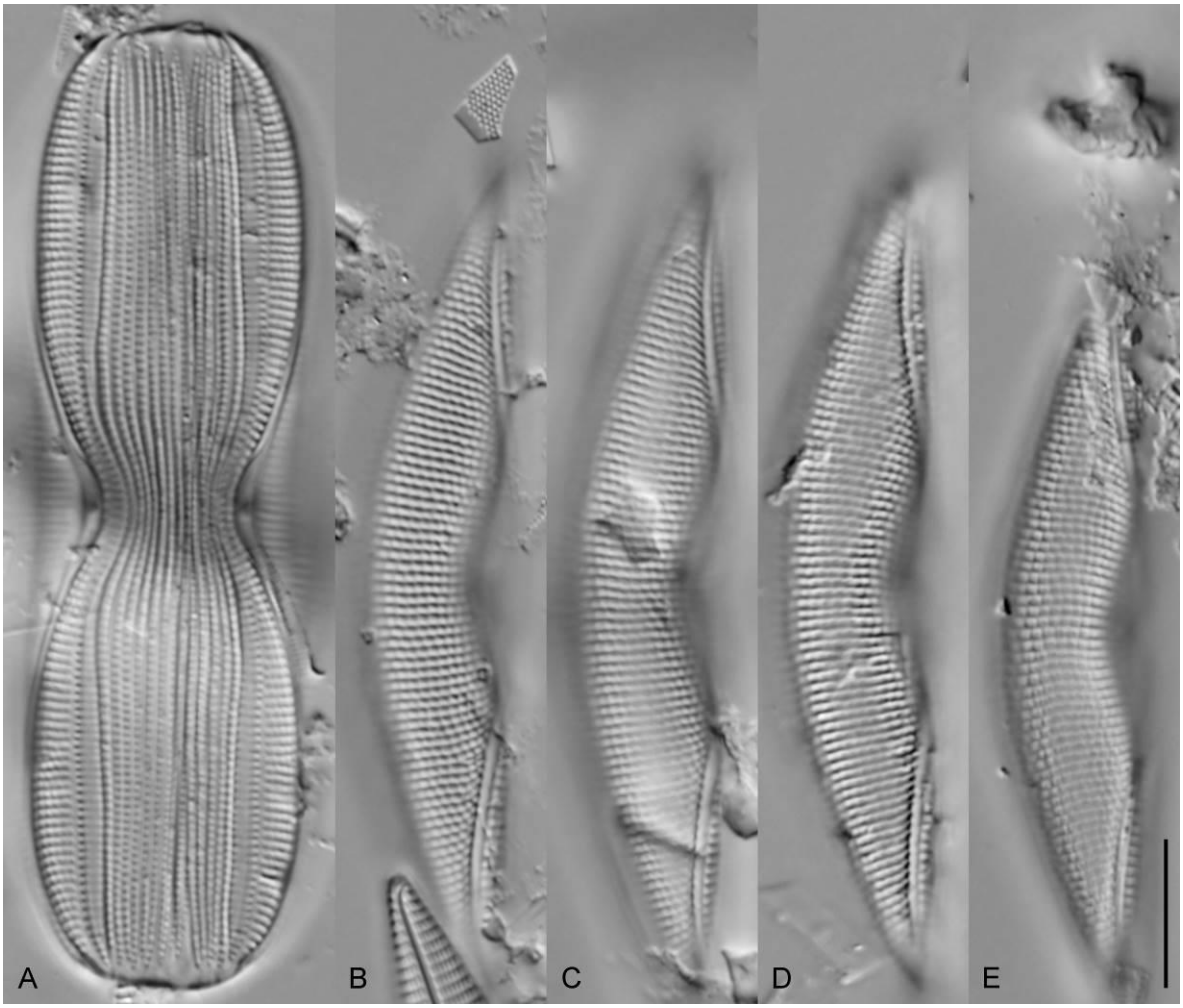

Figure 7.17. *Tetramphora robusta* sp. nov., whole frustule and single valves showing size range. **A.** Whole frustule. **B–E.** Single valves. **B.** Holotype specimen. Scale bar = 10 µm.

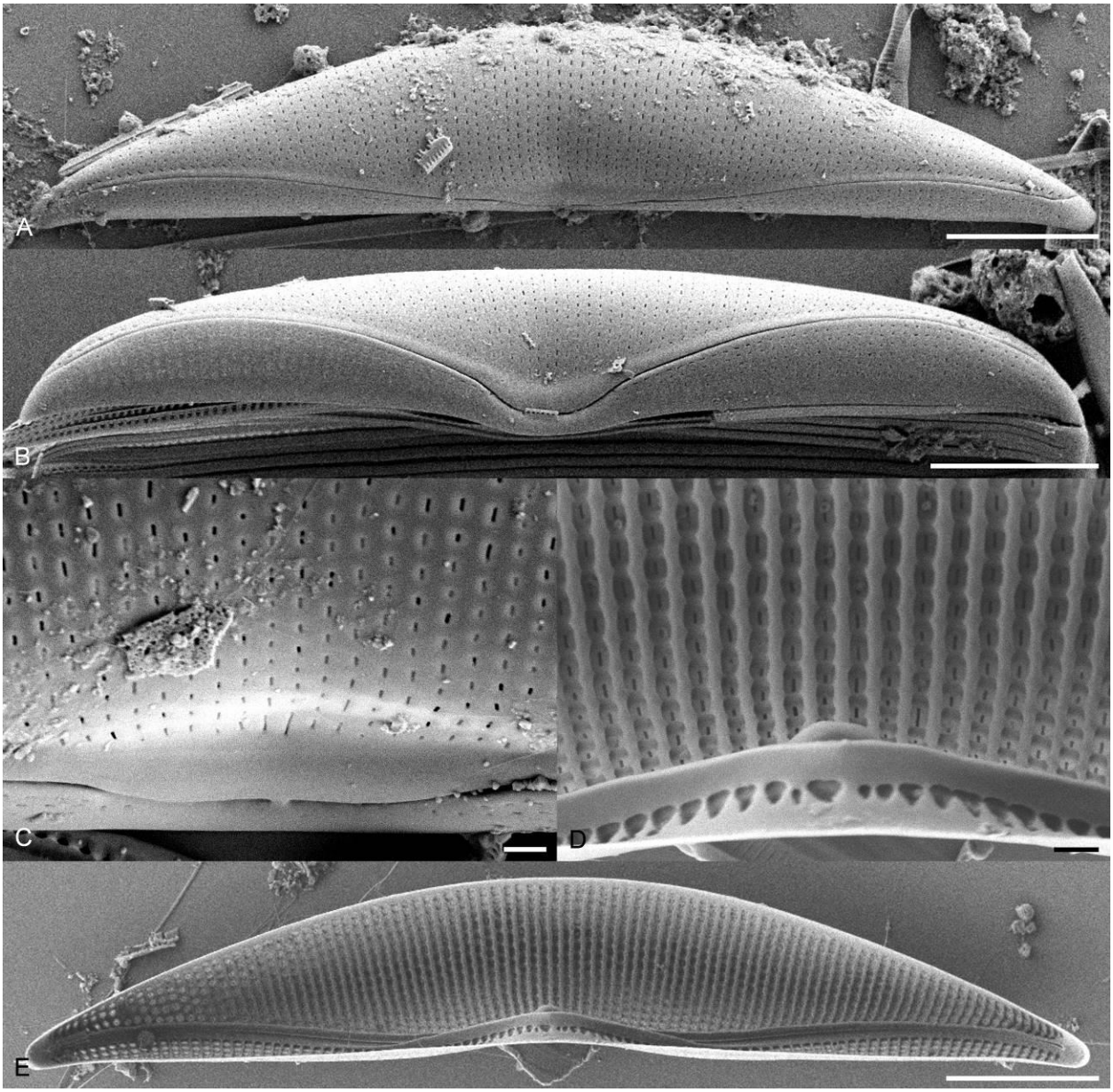

Figure 7.17. *Tetramphora robusta* sp. nov., SEM. **A.** External whole valve. **B.** External whole valve showing ventral margin. **C.** Detail of external valve center showing transapically oriented areolae, central hyaline area and closely spaced proximal raphe ends. **D.** Detail of internal valve center showing axial ribs and protruding central thickening. **E.** Internal whole valve. Scale bars = 10 µm (A, B, E), 1 µm (C, D).

Taxa transferred to Tetramphora but not illustrated here

Tetramphora rhombica (Kitton in Schmidt) Stepanek & Kociolek comb. nov.

Basionym. *Amphora rhombica* Kitton *in* Schmidt *et al*. 1874–1959, pl. 40 Fig. 39.

SCHMIDT A., SCHMIDT M., FRICKE F., HEIDEN H., MÜLLER O. & HUSTEDT F. 1874–1959. *Atlas der Diatomaceen-Kunde.* O.R. Reisland, Leipzig. 460 pls.

Literature. Schmidt et al. 1874–1959, pl. 40, Fig. 39; Peragallo & Peragallo 1897–1908, pl. 50, Fig. 4; Cleve 1895, p. 127; Navarro 1982, Figs 24–37.

Taxonomic remarks. Although not extensively imaged, the type drawing in Schmidt *et al*. (1874–1959) clearly illustrates features aligning *A. rhombica* with the genus *Tetramphora*. These include overall valve shape, transapically oriented slit-like areolae and characteristic flexure near the central area. Navarro (1982) illustrates, with LM and SEM, a taxon that aligns well with the description of *A. rhombica* (Cleve 1895 gives length 130–260 µm, breadth 21–50 µm and 10–12 striae in 10 µm, Navarro 1982 gives length 198 µm, breadth 36 µm and 10 striae in 10 µm for his taxon). These images show the characteristic unornamented dorsal central area, transapically oriented areolae and internal axial costae.

Tetramphora decussata (Grunow) Stepanek & Kociolek comb. nov.

Basionym. *Amphora decussata* Grunow 1867, p. 23.

GRUNOW, A. 1867. Diatomeen auf Sargassum von Honduras, gesammelt von Lindig. *Hedwigia* 6 (1–3): 1–8, 17–32, 33–37.

Literature. Peragallo & Peragallo 1897–1908, pl. 49, Figs 23–25; Cleve 1895, pl. 4, Figs 10, 11; Wachnicka & Gaiser 2007, Fig. 87; Lobban et al. 2012, pl. 1, Figs 7–9; pl. 54, Fig. 5; pl. 55, Figs 1–3.

Taxonomic notes. *Tetramphora decussata*, as previously illustrated, is both easily identifiable and morphologically unique when compared to the taxa illustrated here. In the LM the striae are parallel and run diagonally across the valve face converging on a thin semi-stauros. In SEM images presented by Lobban et al. (2012) these diagonal striae are crossed internally by thin vimines, although these vimines are not apparent externally. Although this striae structure and orientation appears unique within the genus,

the chloroplast shape and arrangement (Lobban et al. 2012, pl. 1, Figs 7–9), girdle bands, unornamented dorsal central area and internal axial costae (Lobban et al. 2012. pl. 55, Figs 1–3) clearly place this species within *Tetramphora*.

Phylogenetic analysis

The results of independent tree searches utilizing three alignment partitioning strategies returned identical topologies with the degree of alignment partition having no effect on the inferred position of *Tetramphora*. All presented phylograms are those inferred from alignments partitioned by marker. Both the ML and Bayesian estimation conducted on the three marker concatenated alignment returned a weakly supported (41/57, BS/BPP) position for the genus *Tetramphora* sister to the genus *Mastogloia* Thwaites *in* Smith, within a larger clade containing taxa from the Cymbellales Mann and Naviculales Bessey (Fig. 7.19). The ML estimation conducted on the larger SSU-*rbc*L alignment returned an identical position for *Tetramphora* as sister to the genus *Mastogloia* (BS 25) within a larger clade containing members of the Cymbellales and Naviculales (Fig. 7.20). The Bayesian estimation conducted on the SSU-*rbc*L alignment was the only analysis to return a tree with *Tetramphora* not sister to *Mastogloia* (Fig. 7.21). In this case, *Mastogloia* was sister to *Phaeodactylum tricornutum* Bohlin (BPP 83), which was part of a polytomy with a monophyletic *Tetramphora* and a clade containing taxa from the Cymbellales and Naviculales (Fig. 7.21). These analyses supports earlier findings that *Tetramphora* is distantly related to *Amphora s.s.* (Stepanek & Kociolek 2014) and lends strong support for the transfer of *H. chilensis* as part of an early branching lineage within this genus (100/100).

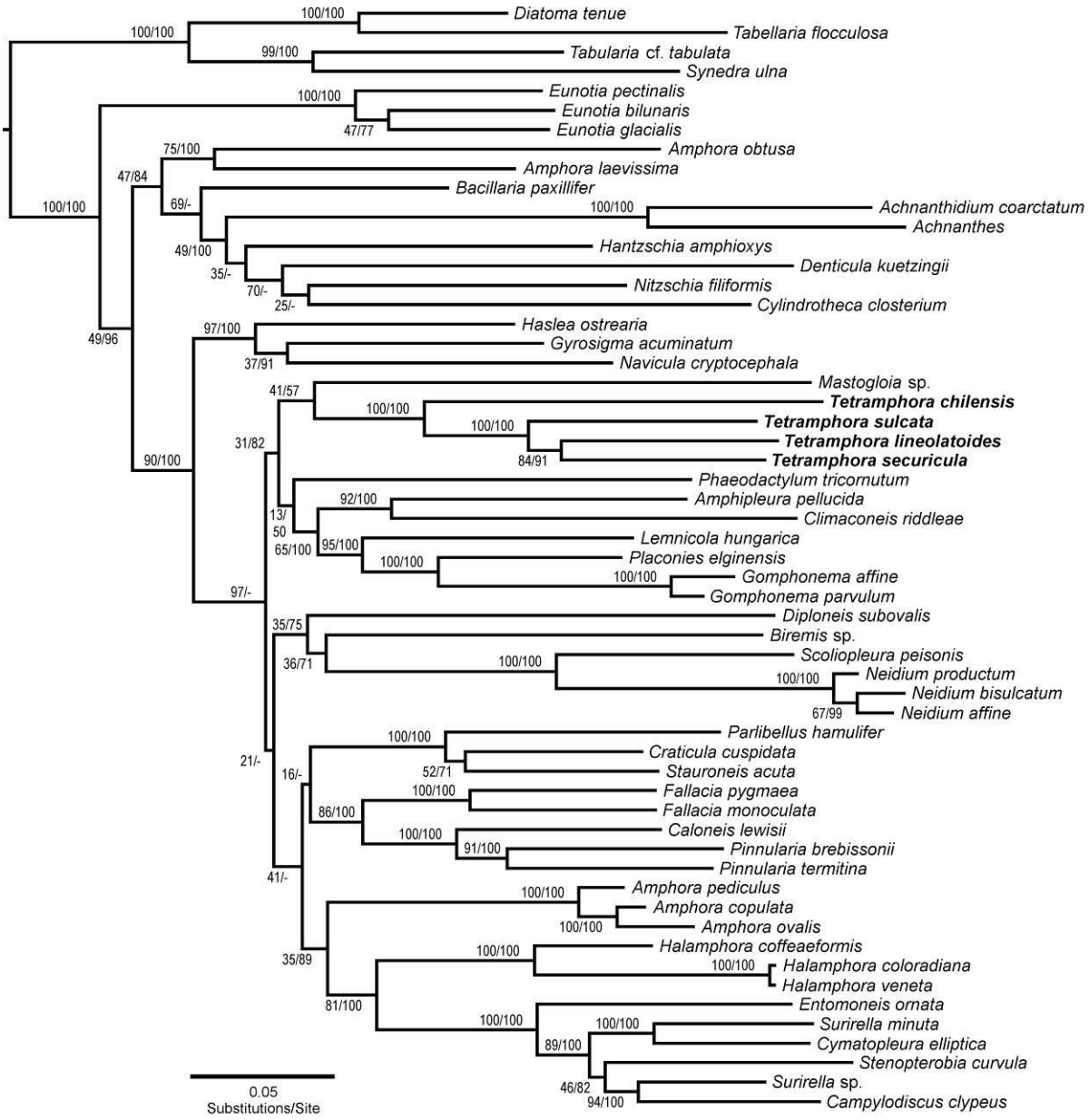

Figure 7.19. Maximum likelihood phylogram inferred from a three marker concatenated alignment including the nuclear encoded marker SSU and the chloroplast encoded markers *rbc*L and *psb*C. Node support is position above or below the branch and is given as ML bootstrap value/Bayesian posterior probability (as a percent). A Bayesian posterior probability of (-) indicates incongruence between the maximum likelihood and bayesian trees. *Tetramphora* taxa are given in bold.

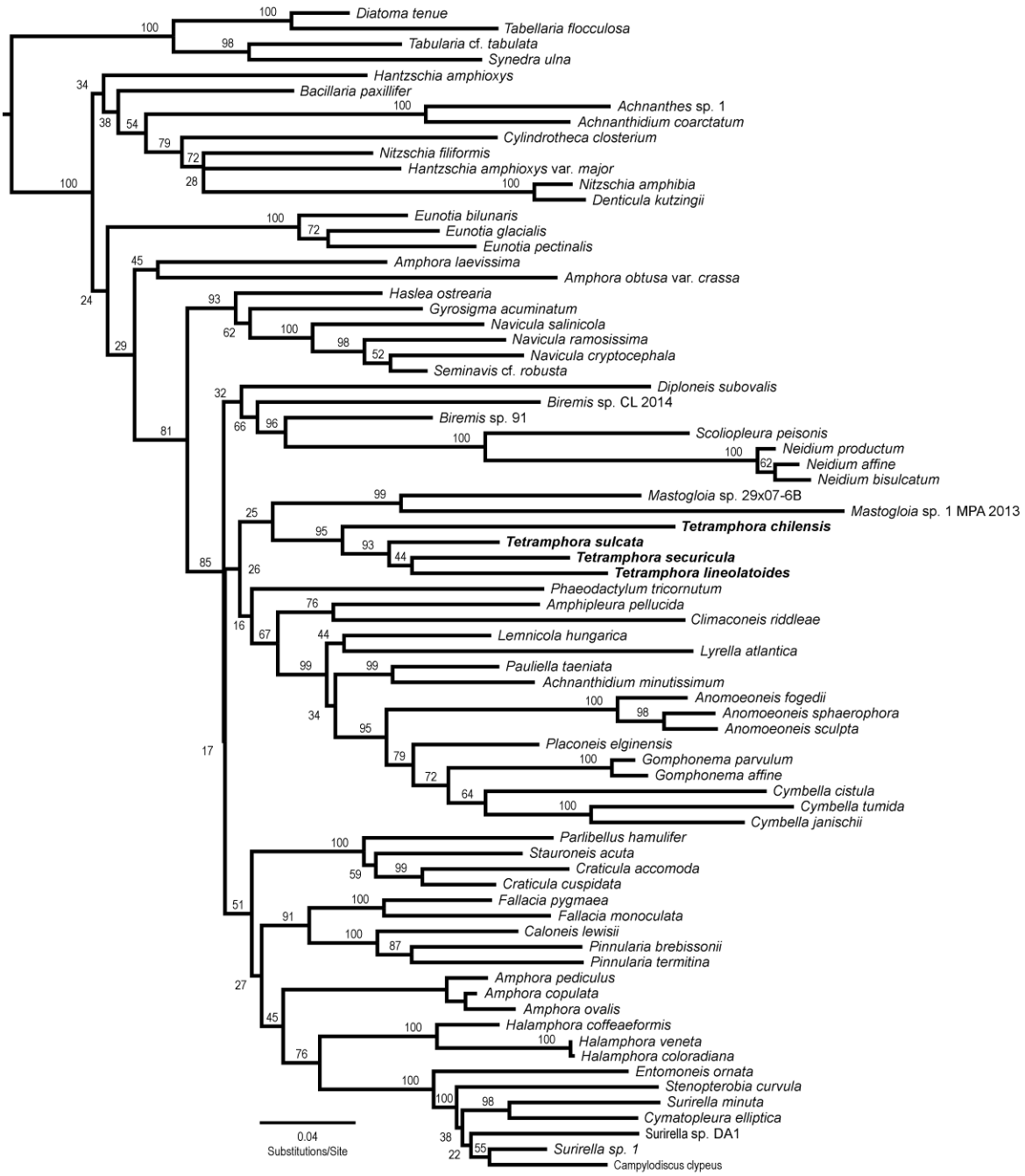

Figure 7.20. Maximum likelihood phylogram inferred from a two marker concatenated alignment including the nuclear encoded marker SSU and the chloroplast encoded *rbc*L. Node support is given as ML bootstrap values. *Tetramphora* taxa are given in bold.

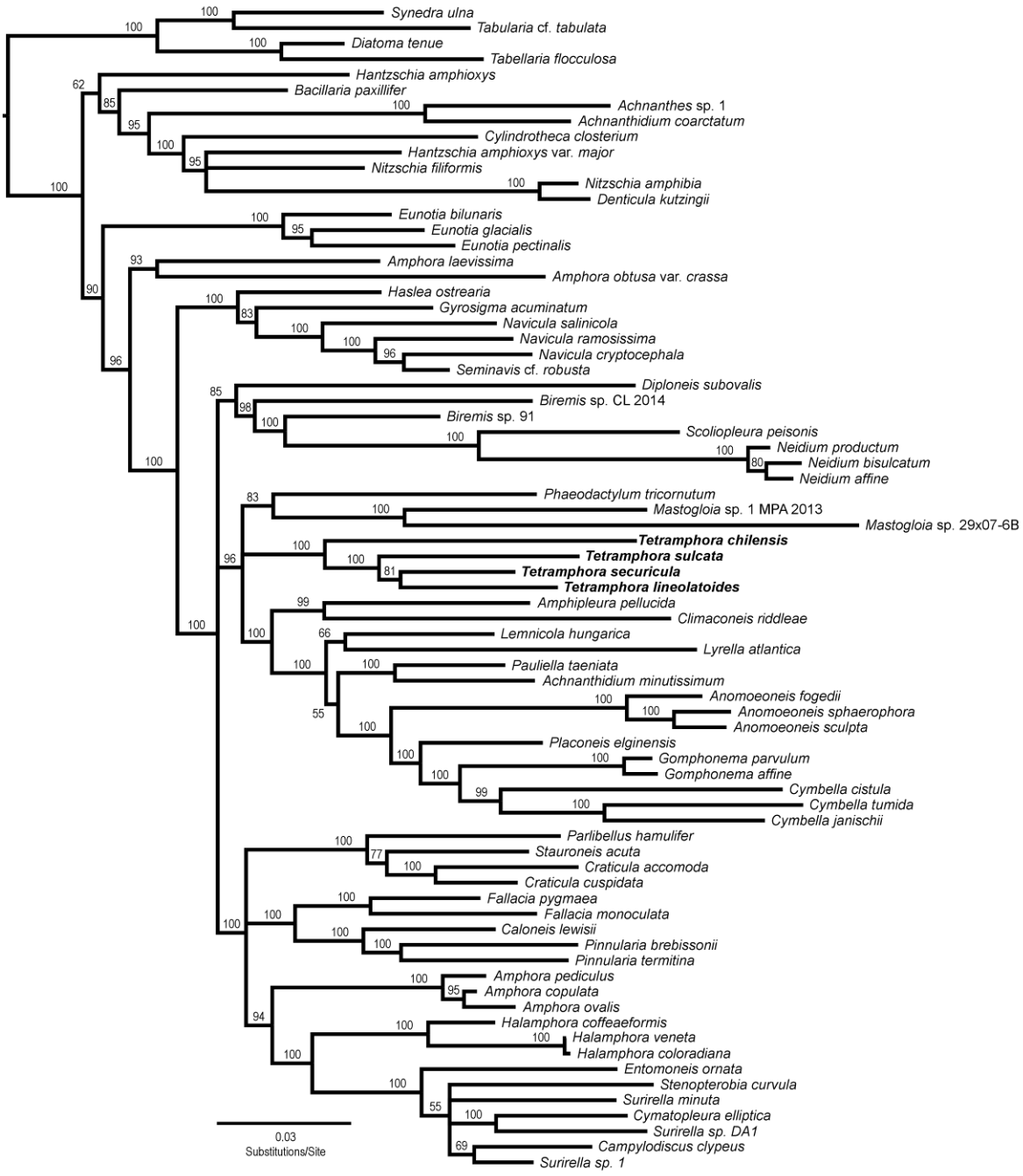

Figure 7.21. Bayesian phylogram inferred from a two marker concatenated alignment including the nuclear encoded marker SSU and the chloroplast encoded *rbc*L. Node support is given as Bayesian posterior probabilities as a percent. *Tetramphora* taxa are given in bold.

Chloroplast arrangement

Live cells of *T. lineolatoides* (Fig. 7.22A–C) and *Mastogloia* sp. (Fig. 7.22D, E) were imaged to illustrate the number and arrangement of the chloroplasts. *Tetramphora lineolatoides* exhibits Mereschkowsky's type 8 *Amphora* chloroplast with four plastids paired dorsally and ventrally by large pyrenoids. *Mastogloia* sp. exhibits a similar plastid structure when viewed in girdle view, with four reticulate chloroplasts paired by large pyrenoids.

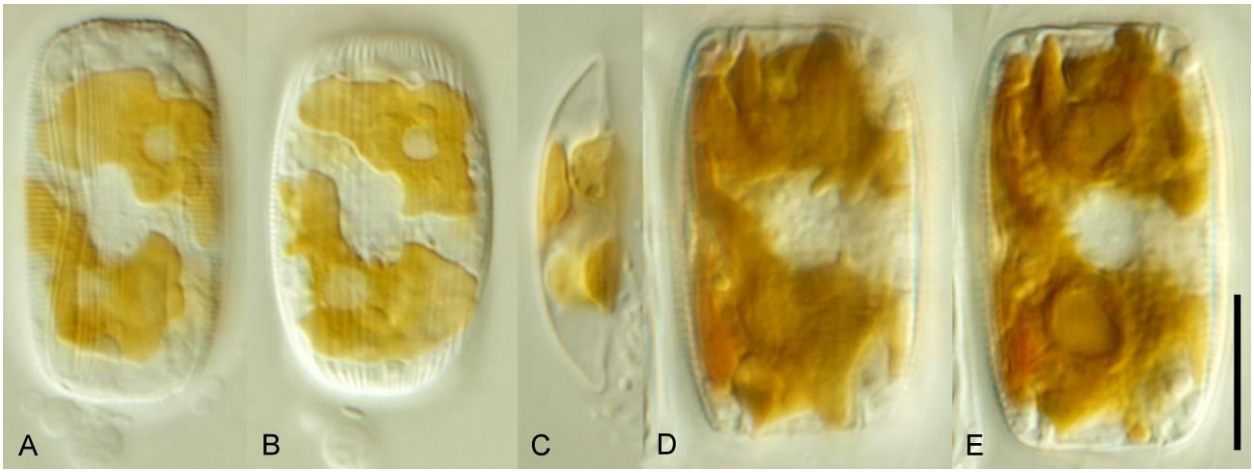

Figure 7.22. Live cells showing plastid arrangement. **A–C.** *Tetramphora lineolata*. **D–E.** *Mastogloia* sp. **A.** *Tetramphora lineolata*, ventral focal plane showing two ventrally appressed plastids. **B.** *Tetramphora lineolata*, dorsal focal plane showing two dorsally appressed plastids. **C.** *Tetramphora lineolata*, valve view showing four plastids, two ventrally and two dorsally appressed. **D.** *Mastogloia* sp., lower focal plane showing two plastids. **E.** *Mastogloia* sp., upper focal plane showing two plastids. Scale bar = 10 µm.

DISCUSSION

With the possible exception of *T. chilensis*, the taxa currently included in *Tetramphora* share the general features: strong "amphoroid" frustule symmetry; a moderately to strongly dorsiventral valve with a biarcuate raphe; a central hyaline area that creates undulate proximal raphe ends; slit-like external areolae openings; axial costae; a protruding dorsal central thickening; and Mereschkowsky's (1903) type 8 chloroplast with four paired plastids (Fig. 7.22). Of these features, taxa appear to group,

morphologically, based on striae and raphe structure. Several of the taxa presented here (*T. fontinalis*, *T. rhombica* var. *intermedia*, *T. robusta* and *T. securicula*) share the features of transapically oriented areolar slits and a highly developed central hyaline area that extends into a prominent siliceous flap. Conversely, the taxa sharing longitudinally oriented areolar slits (*T. lineolata*, *T. lineolatoides*, *T. ostrearia* and *T. sulcata*), when imaged (no external valve orientation was found for *T. ostrearia*), have a reduced central hyaline area with clearly visible proximal raphe ends and, typically, a less flexed valve through the central area.

Although morphological similarities would indicate these relationships, they are not supported by the molecular phylogeny as it is currently sampled (Figs 7.19, 7.20, 7.21). In the three marker concatenated analysis, *T. lineolatoides* was more closely related to *T. securicula* (84/91) than to the more morphologically similar *T. sulcata*. Certainly, this discrepancy between the morphological and molecular evidence may be the result of the small number of taxa currently included in the molecular phylogeny, or, as is often the case, these features may not in fact be synapomorphies but instead symplesiomorpic or homoplastic within the genus.

How additional, morphologically diverse, taxa such as *T. decussata* will fit into this classification remains to be seen. *Tetramphora decussata* departs dramatically from the taxa illustrated here in striae and areolae features (see Lobban et al. 2012 for live LM, cleaned LM and SEM illustrations of *T. decussata*). Although these features differ greatly, typical *Tetramphora* plastid structure and prominent central hyaline area extended into a siliceous flap (Lobban et al. 2012) firmly place this taxon within the genus *Tetramphora*. It is likely, with further observations, other taxa included in this genus will expand the morphological boundaries presented here.

Although there are likely other described species that are in need to transfer to *Tetramphora*, at the present time only taxa that have been directly observed or illustrated well by others are being treated. Taxa such as *Amphora acuta* Gregory, *Amphora arcus* Gregory and *Amphora aspera* Petit, although classified within Cleve's (1895) subgenus *Oxyamphora* and having original illustrations that would seem to ally them with *Tetramphora*, have upon further analysis been shown to exhibit features more closely

aligning them with the genus *Halamphora* (Levkov 2009, Sato et al. 2013). Moving forward, Mereschkowsky's type 8 chloroplast and undulate proximal raphe ends produced by a distinct central hyaline area will be important features for the positive inclusion into *Tetramphora*.

Systematic placement of Tetramphora

Although monophyletic and distinct from the genus *Amphora* (no marker or analysis has placed *Tetramphora* within *Amphora* or *Halamphora*) from which these species were described, the systematic placement of *Tetramphora* based on the molecular phylogenetic analysis is far from conclusive, with node support of 41/57 and 25 for the sister relationship with *Mastogloia* in the three marker and SSU-*rbc*L ML trees, respectively. This low support may be indicative of the overall poor taxon sampling across the diverse raphid diatom lineages, an issue that has led to low backbone support in many diatom molecular systematic studies. This issue is particularly acute when working with marine raphid lineages, which are severely underrepresented in sequence archives like GenBank. Although the relationship with *Mastogloia* does not have strong support, the molecular evidence gives little indication for an alternative placement. Within the Bayesian estimation of the SSU-*rbc*L alignment, although not sister to *Mastogloia*, *Tetramphora* is in an unresolved relationship with the other members of the *Mastogloia*, Cymbellales, Naviculales clade in which it has consistently been placed (Fig. 108). In addition, when a similar analysis was conducted without the inclusion of *Mastogloia* taxa (Stepanek & Kociolek 2014) the *Tetramphora* taxa remained associated with this clade, sister to *P. tricornutum* Stepanek & Kociolek 2014, Fig. 1).

Although frustule morphology differs greatly between *Tetramphora* and *Mastogloia*, the distinct axial costae seen in most *Tetramphora* taxa is a feature also observed in many *Mastogloia* and *Decussata* (Patrick) Lange-Bertalot species (see Lee et al. 2014 for an illustration of this feature in *Mastogloia* and Edlund et al. 2006 for *Decussata*). Plastid morphology provides additional support for this grouping. In Mereschkowsky's (1903) treatment of diatom plastid types, in which he proposed the genus *Tetramphora*, he placed this genus within a larger group of diatoms containing four plastids, the Tetraplacatae, into which was also included the genus *Mastogloia* (Mereschkowsky 1903, p. 149). A comparison between

the chloroplast structure of *Tetramphora* and *Mastogloia* (Fig. 7.22) demonstrates the similarity in structure with both exhibiting four reticulate plastids linked in pairs by pyrenoids. Additionally, a very similar arrangement was observed by Edlund et al. (2006) in the genus *Decussata* and was, in part, cited as evidence for its placement within the Mastogloiales Mann. Given the phylogenetic, chloroplast and structural evidence available, it seems appropriate to place *Tetramphora* within the order Mastogloiales..

The early history of the genus *Amphora* saw it defined by overall frustule symmetry alone, creating a non-monophyletic grouping that has persisted for 150 years. With modern imaging and molecular techniques employed in the last 30 years this situation is slowly being resolved with the transfer of taxa, historically classified within *Amphora*, to other genera. The recognition of the genus *Tetramphora* is one more step in this effort to create a natural classification system for the "amphoroid" diatoms.

ACKNOWLEDGEMENTS

This research was funded, in part, by a joint National Science Foundation and Japanese Society for the Promotion of Science East Asia and Pacific Summer Institute fellowship NSF EAPSI No. 1316805 and a Seed Grant for Innovation from the University of Colorado Boulder. The authors would like to thank Drs. Shigeki Mayama and Sam Rushforth for assistance in the selection of collection sites in Japan and Utah, respectively, and Dr. Sarah Hamsher for the Jenkins Sound collections and for helpful comments in the final stages of this manuscript.

CHAPTER VIII

MOLECULAR PHYLOGENY AND SYSTEMATIC REVISION OF THE AMPHOROID DIATOM (BACILLARIOPHYTA) GENERA *AMPHORA* AND *HALAMPHORA*

ABSTRACT

The systematic history of the diatom genus *Amphora* is one of a broad early concept, based on frustule symmetry, leading to the description and inclusion of a large number of morphologically diverse taxa, followed by an extended period of revision and taxonomic refinement of the genus in an effort to create a more natural classification. The introduction of molecular systematic techniques has increased the pace of revision and has shed light on the relationships between the major lineages of amphoroid diatoms. Within the two largest lineages, the genus *Halamphora* and those taxa still included within the genus *Amphora*, the intrageneric morphological and ecological relationships and have yet to be explored in any detail. Presented here is a four marker molecular phylogeny for the genera *Amphora* and *Halamphora*. This phylogenic investigation includes 31 taxa from the genus *Amphora* and 77 taxa from the genus *Halamphora* collected from fresh, brackish and salt waters from coastal and inland habitats. Based on the phylogenetic relationships presented here, as well as detailed morphological examination, five new species of *Amphora* and 26 new species of *Halamphora* are described and eight species are transferred into the genus *Halamphora*. In addition to the newly described diversity, the phylogenetic relationships will be used examine morphological character evolution and habitat preference across the genera in an effort to understand the diversity within the genera as well as build a stable classification system for the amphoroid diatoms.

INTRODUCTION

Amphora Ehrenberg ex Kützing has historically been a morphologically and ecologically diverse group of raphid diatoms and has proven systematically difficult since its description by Kützing in 1844 (Kützing 1844, Smith 1873, Cleve 1895, Peragallo & Peragallo 1897–1908, Mereschkowsky 1903). These early authors struggled with the relationships within the genus, which by the beginning of the 20th century included 221 named species (De Toni 1891). Although significant efforts were attempted (Cleve 1895, Mereschkowsky 1903), it was not until modern imaging (scanning and transmission electron microscopy) and systematic methods were employed that significant progress was achieved in revising the genus to reflect a more natural classification.

The genus *Amphora*, originally diagnosed by a distinct 'amphoroid' symmetry (Stepanek & Kociolek 2014) has long been considered a heterogeneous collection of taxa (Cleve 1895, Mereschkowsky 1903, Krammer 1980, Mann 1994). Because of this, the early systematic revisions largely involved the transfer of taxa and lineages out of *Amphora* into existing or newly created genera (Paddock & Sims 1980, Mann & Cox in Round et al. 1990, Mann in Round et al. 1990, Vyvermann et al. 1998, Williams and Reid 2006, Levkov 2009). Although this work resulted in a significant narrowing of the morphological concept of the genus, the application of molecular phylogenetic techniques demonstrated that *Amphora* continued to be non-monophyletic with members scattered widely across raphid diatom lineages (Stepanek & Kociolek 2014). This molecular dataset led to the resurrection and separation of the genus *Tetramphora* (Stepanek & Kociolek *in review*) for the *Amphora* taxa with Mereschkowsky's Type 8 chloroplast (Mereschkowsky 1903) and separation of the members of Cleve's (1895) *Amphora* subgenera *Amblyamphora* and *Psammamphora* (*in preparation*).

Following these transfers, the two closely related genera *Amphora* and *Halamphora* (Cleve) Levkov now represented monophyletic lineages containing taxa once classified within the *Amphora* subgenera *Amphora*, *Diplamphora*, *Halamphora* and *Oxyamphora* (Stepanek & Kociolek 2014). Additionally, this phylogeny indicated the genus *Amphora* was comprised of two major clades, one which was comprised of taxa from *Amphora s.s.* and one which was comprised of taxa from the *Amphora*

subgenera *Diplamphora* and *Oxyamphora*. A phylogeny of the genus *Amphora* presented around the same time by Sato et al. (2013) indicated that *Amphora s.s.* may not represent a distinct clade but may be nested within a clade containing early branching *Diplamphora* lineages, a contention that was further supported by Stepanek et al. (2015) with the addition of a newly described *Amphora* species corresponding to the *Diplamphora* morphology. Although returning a monophyletic *Amphora* clade, it was found that most of the historically used diagnostic features were either plesiomorphic or diagnostic of only the *Amphora s.s.* clade (Stepanek & Kociolek 2014, Stepanek et al. 2015). It was further presented that the presence of a Type 1 amphoroid chloroplast (Mereschkowsky 1903) may be one of the few synapomorphies for the genus as a whole (Stepanek & Kociolek 2014).

This preliminary phylogenetic work also indicated two major clades within the monophyletic *Halamphora* lineage. One clade that corresponds well to Levkov's (2009) description of the newly elevated genus *Halamphora*, including the type of the genus *H. coffeaeformis* (Agardh) Levkov. The second major clade contained a taxon previously assigned to the subgenus *Oxyamphora*, *A. hyalina* Kützing, and the taxonomically problematic taxon *A. semperpalorum* Wachnicka & Gaiser (Stepanek & Kociolek 2014). Due to its non-monophyly with the genus *Amphora* and its exhibited morphological diversity, assigning synapomorphies to *Halamphora* was equally difficult. As with *Amphora*, chloroplast type (Type 2 amphoroid chloroplast, Mereschkowsky 1903) was indicated as the most stable diagnostic character.

In addition to the great morphological breadth present within *Amphora* and *Halamphora*, these genera are also unique given their great ecological breadth which spans conductivities from fresh to hypersaline waters and latitudes from the tropics to the poles (Patrick & Freese 1961, Hohn & Hellerman 1966, Stoermer & Yang 1971, Wachnicka & Gaiser 2007, Stepanek & Kociolek 2013, 2015, Van de Vijver et al. 2014). It has been discussed that many diatom genera are found only in either freshwater or saltwater environments and are rarely found in both (Round & Sims 1980). This observation had led to the idea that this salinity gradient is a significant barrier to the dispersal of diatoms and that lineages crossing this barrier would be a rare event in diatom evolutionary history (Round & Sims 1980, Mann

1999a). By extension, it would be expected that these transitions would represent major divergences within the diatom phylogeny. Although this salinity barrier hypothesis has been challenged recently (Alverson et al. 2007, 2011, Potapova 2011), within diatom classification there remains a distinction between freshwater diatoms and marine diatoms, the validity of which has been recently called into question (Stepanek & Kociolek 2015).

Amphora and *Halamphora* offer a unique opportunity to explore the pattern of lineage movement between freshwater and saltwater habitats. Both genera are taxonomically large and are found extensively in coastal marine, saline inland and freshwater inland habitats. Given this variety of habitats along a salinity gradient and inferred phylogenetic relationships the following questions can be addressed: is the ancestral habitat for each genus freshwater or marine? Has the diversity in habitat been generated by few transitions followed by diversification or by many independent movements across this salinity barrier? Have saline inland habitats been an intermediate step between freshwater and marine systems? Is the movement between habitats more common in one direction than another?

Although Stepanek & Kociolek (2014) provided the overall relationships between the remaining groups of amphoroid diatoms, systematic questions remain within these separate monophyletic clades. Presented here is a detailed phylogeny of the genera *Amphora* and *Halamphora*. This phylogenetic analysis includes 31 taxa from the genus *Amphora* and 77 taxa from the genus *Halamphora*, corresponding to species previously classified within the subgenera *Amphora*, *Diplamphora*, *Halamphora* and *Oxymaphora*. In addition to the amphoroid taxa included, sequence data for *Thalassiophysa hyalina* (Greville) Paddock & Sims (*Amphora* and *Halamphora* are currently classified within the order Thalassiophysales Mann in Round et al.) is also presented in an effort to provide a larger taxonomic context for the amphoroid diatoms. The inferred phylogeny will be used to examine the morphological diversity within the group with a focus on historical characters utilized in amphoroid taxonomic investigations. Based on detailed light microscope (LM) and scanning electron microscope (SEM) observations and the phylogenetic results, 31 new species of *Amphora* and *Halamphora* have been

described as well as the transfer of eight species from *Amphora* to *Halamphora* laying the groundwork for a taxonomically stable amphoroid diatom classification.

MATERIALS AND METHODS

Isolation and culturing

The *Amphora* and *Halamphora* strains examined here were collected from coastal marine, estuarine, inland saline and freshwaters of Colorado, Florida, Hawaii, Michigan, North Carolina, North Dakota and Utah, USA and Japan from 2011–2014 (see Appendix 1 for collection site information). When available, pH and conductivity measurements were taken near shore at the time of collection using a YSI 556 multi-probe (YSI Incorporated, Yellow Springs, Ohio, USA), and these are presented with the collection information. Examined taxa were isolated into monoculture through micropipette serial dilution under an inverted microscope. Taxa were grown in one of five liquid media depending on the measured conductivity of the collection site. Freshwater taxa were grown in WC medium (Guillard & Lorenzen 1972) with the Na_2SiO_3 concentration increased to 56.84 mg l^{-1}. The brackish and saltwater taxa were grown in one of four artificial saltwater media using the artificial sea salts Instant Ocean (Spectrum Brands, Inc., Blacksburg, Virginia, USA) with WC medium nutrient levels. The sea salt concentration was adjusted to create media with conductivities of 10, 15, 40 and 50 mS cm^{-1} to match the major collection conductivity groups. Cultures were maintained at ca. 25°C under fluorescent lights (illumination ca. 50 µmol m^{-2} S^{-1}) with a 12:12 light:dark cycle.

All light microscope (LM) observations were made with an Olympus BX-51 light microscope (Olympus America Inc., Center Valley, Pennsylvania, USA) and LM images were captured using an Olympus DP71 digital camera. Scanning electron microscope (SEM) images were taken using either a JEOL 6060LV SEM or a JEOL JSM 7401 field emission SEM (JEOL Ltd., Tokyo, Japan).

DNA extraction, amplification and sequencing

DNA was extracted from *Amphora* and *Halamphora* monocultures using either a DNeasy Plant Mini Kit (Qiagen Sciences, Germantown, Maryland, USA) following the manufacturer's protocol or a Chelex 100 extraction method (Richlen & Barber 2005). Four molecular markers were chosen for polymerase chain reaction (PCR) amplification, the nuclear encoded 18S small subunit rDNA (SSU) and partial 28S large subunit rDNA (LSU), and the chloroplast encoded large subunit of RUBISCO (*rbc*L) and photosystem II chlorophyll-a binding protein *psb*C. These markers were chosen for their demonstrated utility in diatom phylogenetic studies (Alverson et al. 2007, Bruder & Medlin 2008, Theriot et al. 2010, Stepanek & Kociolek 2014, Stepanek & Kociolek *accepted*, Stepanek et al. 2015). Primers used in the amplification and sequencing of these markers are listed in Appendix 3.

All markers were amplified by PCR using GE Healthcare Illustra Ready-To-Go PCR beads (GE Healthcare Biosciences, Pittsburg, Pennsylvania, USA) following the manufacturers protocol. For all markers the PCR was carried out under the following conditions: 94°C for 3:30, followed by 36 cycles of 94°C for 50 seconds, 52°C for 50 seconds, 72°C for 80 seconds, and a final extension at 72°C for 15 minutes. Amplified PCR products were purified with ExoSap-it (Affymetrix, Santa Clara, California, USA) following the manufacturer's instructions. Sequencing services were provided by Functional Biosciences (Madison, Wisconsin, USA) and returned sequences were assembled and edited in Geneious ver. 5.6 (Drummond et al. 2012). All sequences used in this study have been or previously were uploaded to GenBank and a list of all taxa examined and GenBank accession numbers can be found in Appendix 2.

Sequence alignment and phylogenetic analysis

Sequences were aligned in Geneious using a muscle alignment algorithm (Edgar 2004) and alignments were visually inspected and edited as necessary. Each of the four markers were aligned, edited and trimmed to minimize missing data individually before concatenation into one of three alignments. The individual alignments had final trimmed lengths of 1591 bp for SSU, 517 bp for LSU, 1286 for *rbc*L and 1047 for *psb*C. These individual alignments were combined to form a concatenated nuclear marker

alignment (2109 bp), a chloroplast encoded alignment (2334 bp) and a four marker concatenated alignment (4444 bp). All alignments contained 123 taxa, 31 taxa from the genus *Amphora*, 77 taxa from the genus *Halamphora* and 11 species from the sister group to *Halamphora* the Rhopalodiales and Surirellales (Ruck & Theriot 2011, Stepanek & Kociolek 2014). Included in this analysis is a single member of the genus *Thalassiophysa* for which the order that *Amphora* and *Halamphora* belong (Thalassiophysales) is named and four outgroup taxa from the genus *Tetramphora* that has been shown to be separate from *Amphora* and *Halamphora* and for which identical molecular markers are available (Stepanek & Kociolek *accepted*).

Tree inference was based on maximum likelihood (ML) and Bayesian estimation and was conducted on the concatenated nuclear, chloroplast and four marker alignments. For the ML estimation, the concatenated alignments were partitioned by marker and tree inference was conducted using RAxML ver. 7.3.2 (Stamatakis 2006) with the graphical user interface raxmlGUI ver. 1.2 (Silvestro & Michalak 2012). The general time reversible model (GTR) of sequence evolution with gamma rate distribution (Γ) with a proportion of invariable sites (I) was used as the model of evolution. The most likely tree was chosen from 20 independent searches and node support for this topology was estimated with 1000 thorough bootstrap replicates. Bayesian estimation was conducted on the four marker concatenated alignment using MrBayes ver. 3.2.1 (Ronquist et al. 2012). The alignment was partitioned by marker and the Bayesian inference using a GTR+Γ+I model of evolution and utilizing two runs of four MCMC chains was run for 25 million generations sampling topologies every 1000 generations with a burn-in of 5 million generations.

Phylogenetic comparative methods

Topological hypothesis testing was conducted to compare the unconstrained four marker *Halamphora* tree to topologies recovered under topological constraints designed to approximate more parsimonious morphological hypotheses. Most likely trees and per-site log likelihoods were generated in RAxML on the unconstrained alignment and under three alternative monophyly constraints (Clades C, D,

F), (Clades B, H, I, J, K) and a fully constrained tree with both constraints in effect. Probabilities of the three alternative topologies compared to the unconstrained topology were generated using the approximately unbiased (AU) test (Shimodaira 2002) implemented in the program Consel (Shimodaira & Hasegawa 2001) using 100,000 topological replicates.

Ancestral state reconstruction was used to infer valve morphological and habitat character states at the internal nodes of the phylogeny. Valve morphological characters were coded as discrete binary data gathered from SEM observations of the included taxa (Chapter 4). The ancestral states of these discrete features was estimated and visualized in Mesquite ver. 3.4 (Maddison & Maddison 2015) using ML methods and an equal rates model of trait evolution. Habitat type was divided into either a coastal habitat, which was defined as any coastal or estuarine waters that had a direct connectivity to the ocean and exhibited some tidal influence, or inland waters which had no direct connectivity. The habitat conductivity was taken from the measured conductivity values from the collection sites. If original collection conductivities were unavailable, the conductivity of the medium in which the cultures were grown was used. The majority of the taxa without measured collection site conductivity data were collected from freshwater habitats, with four saltwater, one brackish water and 12 freshwater cultures lacking conductivity data. The ancestral node states for both the continuous habitat conductivity and the discrete habitat type where estimated using maximum likelihood methods. The continuous habitat conductivity values were estimated and visualized using the 'contMap' function in the R phylogenetics package phytools (Revell 2012). The discrete habitat type values where estimated using the 'rerootingMethod' function in the R phylogenetic package phytools (Revell 2012), using an equal rates model of evolution. All ancestral habitat reconstructions were performed in RStudio v. 0.99.473.

RESULTS

The general topology of the ML estimation based on the four marker concatenated alignment is illustrated in Figure 8.1. Both *Amphora* and *Halamphora* were returned as monophyletic groups, and the large relationships between *Amphora*, *Halamphora* and the Surirellales + Rhopalodiales clade agrees with

previously published work (Ruck & Theriot 2011, Sato et al. 2013, Stepanek & Kociolek 2014). Within *Amphora*, two major clades are distinguished, Clade A and Clade B. Within *Halamphora*, 11 major clades have been distinguished, Clades A–K. A member of the genus *Thalasiophysa*, the type genus of the order Thalassiophysales for which the genera *Amphora* and *Halamphora* belong, was included in the analysis and was positioned outside of either *Amphora* or *Halamphora* being most closely related to the Surirellales and Rhopalodiales clades.

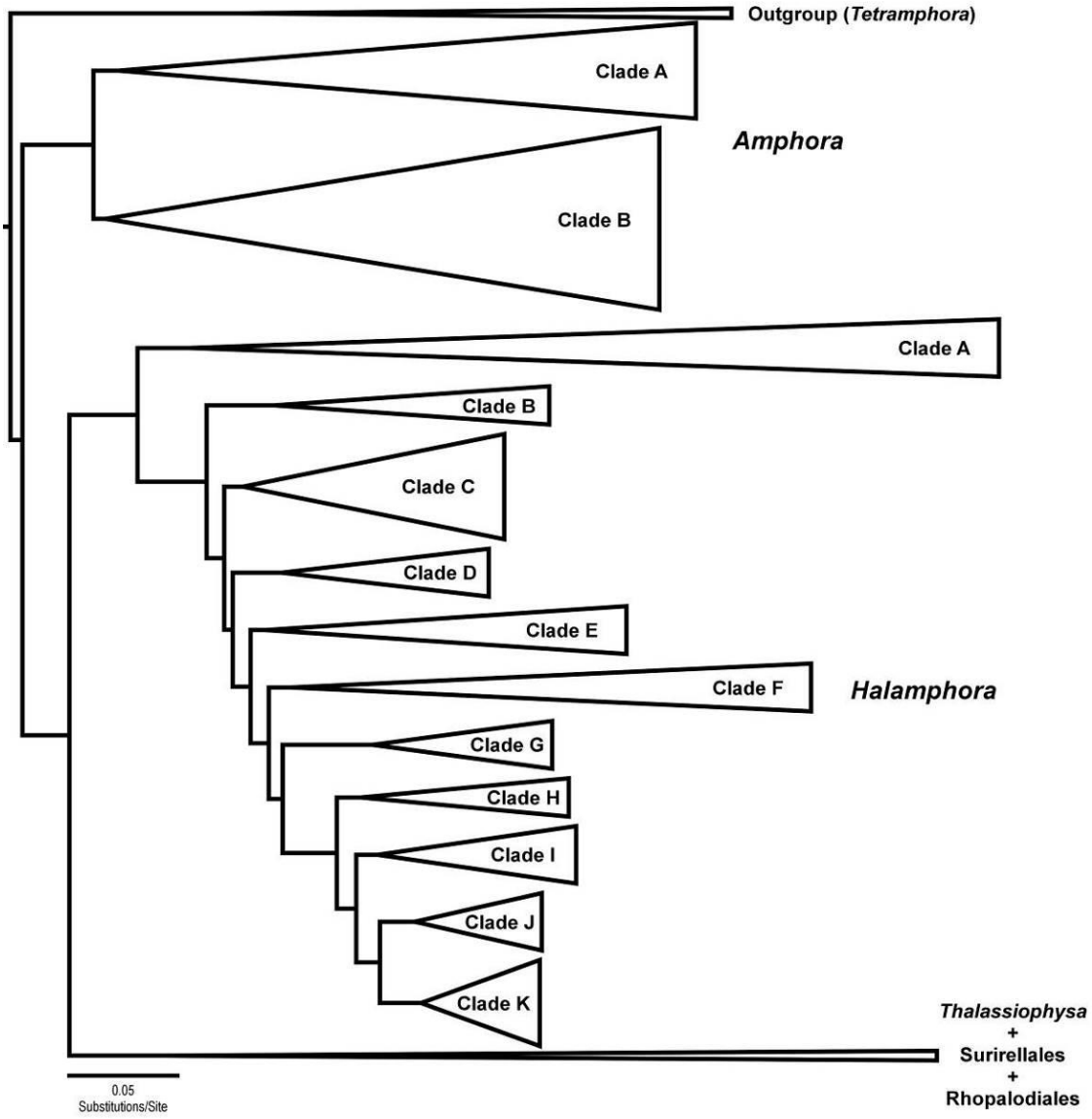

Figure 8.1. Simplified maximum likelihood phylogram showing overall relationships between *Amphora*, *Halamphora* and the canal raphid diatoms. Phylogram inferred from a four marker (SSU, LSU, *rbc*L and *psb*C) concatenated alignment.

Amphora phylogeny

Figure 8.2 shows the detailed phylogeny of the monophyletic *Amphora* group containing 31 sequenced taxa. Within this group two major clades emerge. Clade A contains taxa originally assigned to the *Amphora* subgenera *Diplamphora* and *Oxyamphora* (Cleve 1895, Stepanek & Kociolek 2014). These taxa fall into two primary forms, taxa that would be associated with *A. graeffeana* Hendey (*A. australiensis*, *A. sp. nov.* Amph026/066 and *A. graeffeana*) and taxa associated with *A. abludens* Simonsen (*A. sp. nov.* Amph044/038, *A. abludens* and *A. sp. nov.* Amph135) (Stepanek & Kociolek 2014, Chapter 4, Figs 4.1–4.14). Although distinct, these morphological groups do not form monophyletic subgroups within Clade A, with the *A. graeffeana* form is paraphyletic into the *A. abludens* form.

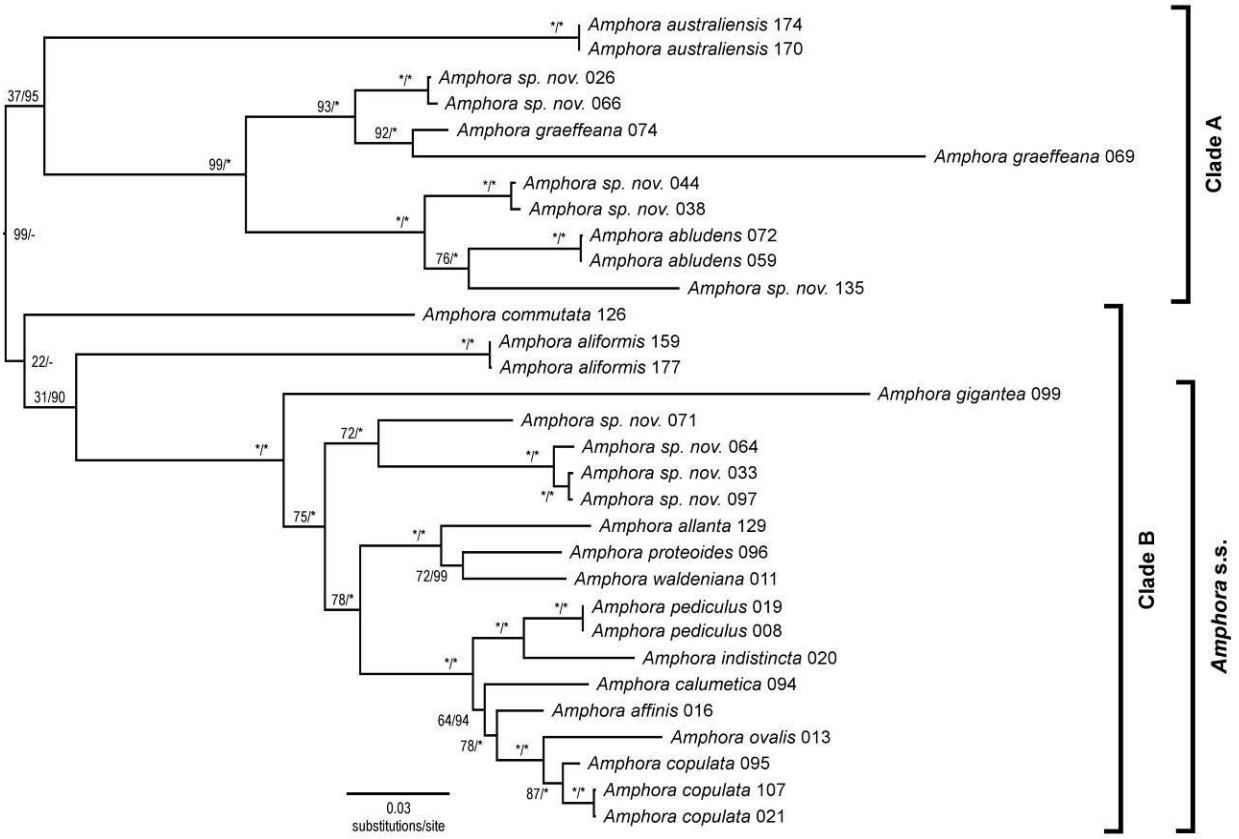

Figure 8.2. Maximum likelihood phylogram of the *Amphora* clade inferred from a four marker (SSU, LSU, *rbc*L, *psb*C) concatenated alignment. Node support is given as ML bootstrap (500 replicates)/Bayesian posterior probability (as a percent). Node support (*) indicates 100, (-) indicates incongruence between the ML and Bayesian estimations.

Clade B contains a well-supported monophyletic *Amphora* s.s. (100/100) as well as two early branching lineages within this clade (*A. commutata* Grunow in Van Heurck and *A. aliformis* Stepanek, Mayama & Kociolek) that, although sharing many features with *Amphora s.s.* (Stepanek et al. 2015), would historically have been included in the *Diplamphora* subgenus based on their areolate girdle bands (Sato et al. 2013, Stepanek et al. 2015). The early branching lineages in both of these clades (*A. australiensis* John in Clade A, *A. commutata* and *A. aliformis* in Clade B) have positions that are not well supported in the phylogeny (37/95, 22/- and 31/90 for the three taxa, respectively) and their position between markers and analyses is somewhat variable with *A. commutata* in a polytomy with Clade A and B in the Bayesian four marker estimation and considerable variability in these early lineages between the nuclear and chloroplast markers (Figs 8.3, 8.4).

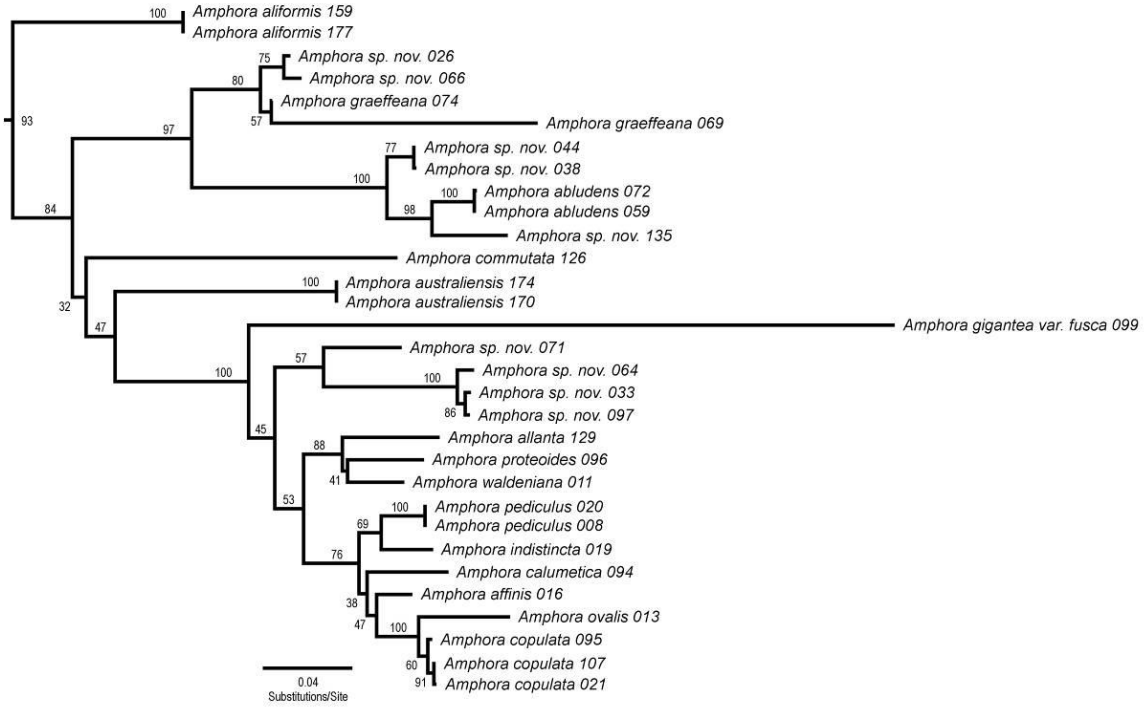

Figure 8.3. Maximum likelihood phylogram of *Amphora* inferred from a concatenated alignment of the nuclear markers (SSU, LSU). Node support is given as ML bootstrap (500 replicates) values. Node support (*) indicates 100.

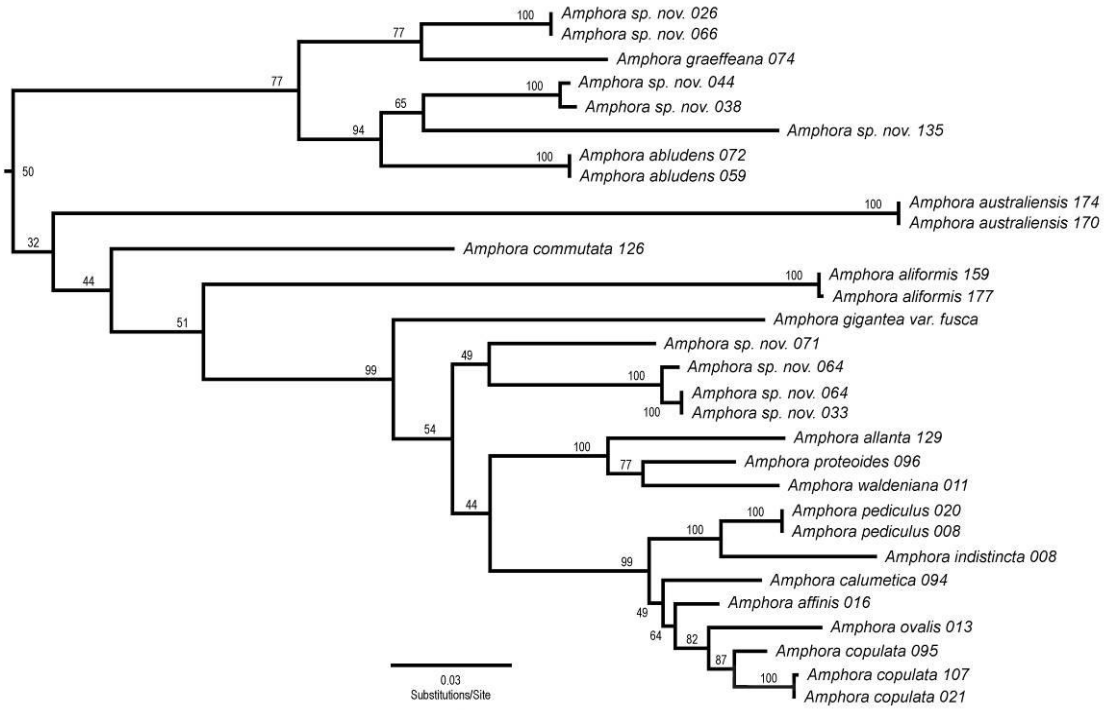

Figure 8.4. Maximum likelihood phylogram of *Amphora* inferred from a concatenated alignment of the nuclear markers (SSU, LSU). Node support is given as ML bootstrap (500 replicates) values. Node support (*) indicates 100.

The difficulty in assigning synapomorphies to the genus *Amphora* was discussed in detail by Stepanek & Kociolek (2014) and ancestral state reconstruction of commonly used *Amphora* morphological characters (Levkov 2009, Stepanek & Kociolek 2013, Stepanek & Kociolek 2014, Stepanek et al. 2015) demonstrates an equal difficulty in assigning synapomorphies to the major clades within *Amphora* (Supplemental Figures S8.1–S8.3). Many of the typical '*Amphora*' features, such as areolate striae, non-areolate girdle bands, ventral raphe ledge and separated central helictoglossa are synapomorphies for only the *Amphora* s.s. clade within Clade B and do not include the *A. commutata* and *A. aliformis* lineages (Fig. 8.5). Additionally, external areolae occlusions and the presence of areolate girdle bands are plesiomorphic to Clades A and B, as is a fused central helictoglossa for Clade A, and are of little help in classification (Fig. 8.5).

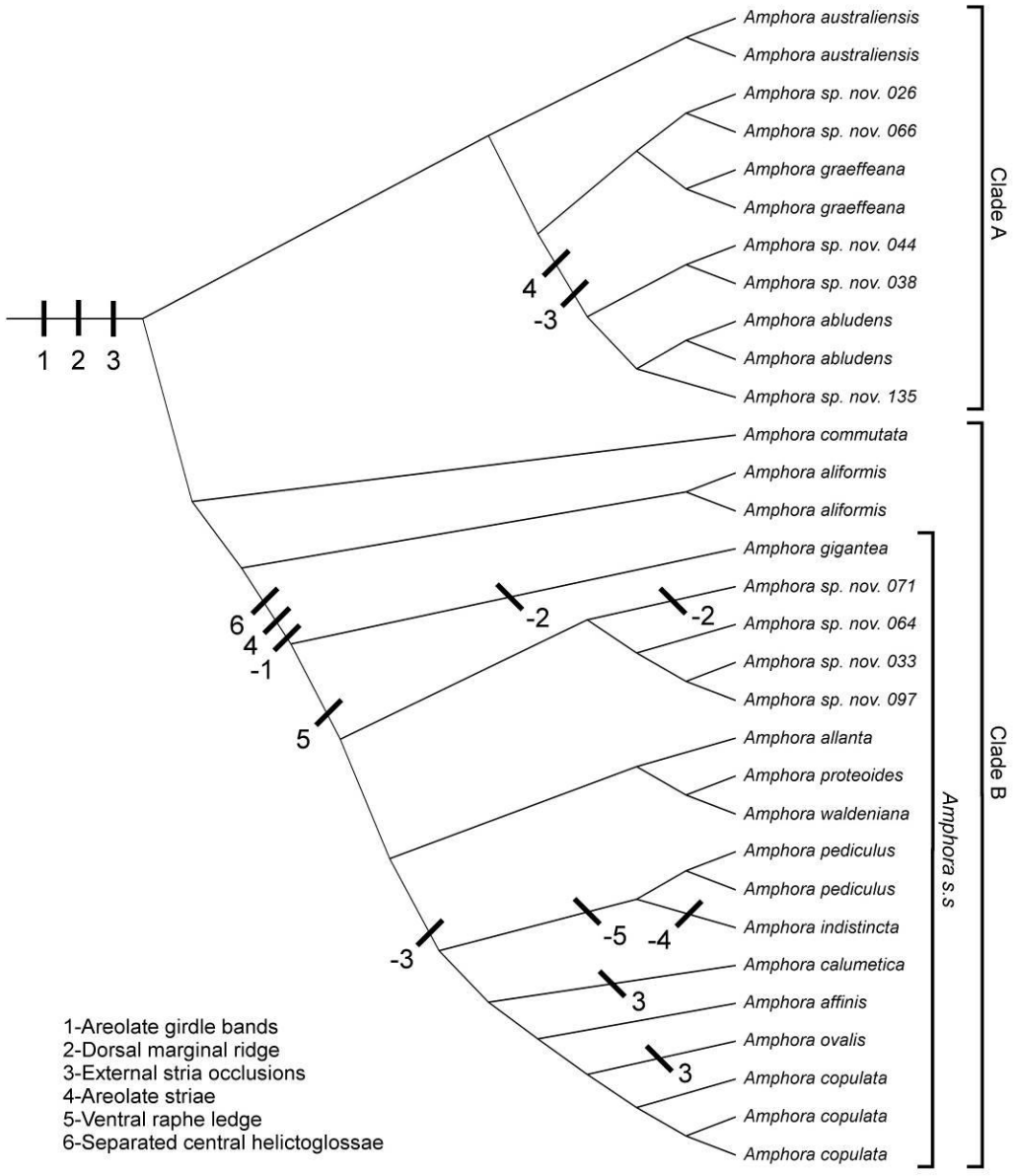

Figure 8.5. Common *Amphora* morphological traits mapped onto a maximum likelihood cladogram inferred from a four marker (SSU, LSU, *rbc*L, *psb*C) concatenated alignment. (-) indicates the secondary loss of a trait.

Halamphora phylogeny

The detailed *Halamphora* phylogeny inferred from the four marker concatenated alignment ML estimation is presented in Figure 8.6. Within *Halamphora*, 11 major clades are identified (Clades A–K). The ML and Bayesian estimations were largely congruent, with the exception that the Bayesian estimation placed Clades C and D, which are in a weakly supported paraphyletic relationship in the ML estimation (BS 34 and 20), as sister to each other. Although many of the early backbone relationships are weakly supported, the major clades are largely well supported (an exception would be the BS support of 21 for Clade E).

Within the genus, Clade A contains taxa not historically associated with the genus *Halamphora*. Although exhibiting significant molecular diversity, as currently described, Clade A only contains three taxa, *H. hyalina* (Kützing) Stepanek & Kociolek, *H. sp. nov.* 081 and *H. semperpalorum* (Wachnicka & Gaiser) Stepanek & Kociolek. *Halamphora hyalina* and *H. sp. nov.* 081 were until this study classified within the genus *Amphora* and would, historically, have been included in Cleve's (1895) *Amphora* subgenus *Oxyamphora*. *Halamphora semperpalorum* has a suite of morphological features that makes it quite difficult to place within the amphoroid diatoms (Stepanek & Kociolek 2014), and previously was also classified within the genus *Amphora* (Wachnicka & Gaiser 2007).

Clades B–K correspond to taxa belonging to a morphological concept of *Halamphora s.s.*, but as was noted by Levkov (2009) when he separated *Halamphora* from the genus *Amphora*, this genus remains very large and morphologically diverse. Unlike within *Amphora*, there is no large dichotomy within the genus *Halamphora*, instead, at the present level of taxon coverage, the clades within the genus appear as a step-like grade of individual lineages. In particular, given the current topology, most of the morphological features used to describe taxa appear to be either plesiomorphic and secondarily lost several times (dorsal marginal ridge) or homoplasious, having evolved independently between and within lineages (axial longitudinal line, areolate dorsal striae, biseriate striae occlusions) (Figs S8.4–S8.6). General morphological trends within *Halamphora* are that a marginal ridge and non-areolate biseriate striae are characteristic of a paraphyletic grade of early branching lineages within the genus. More derived

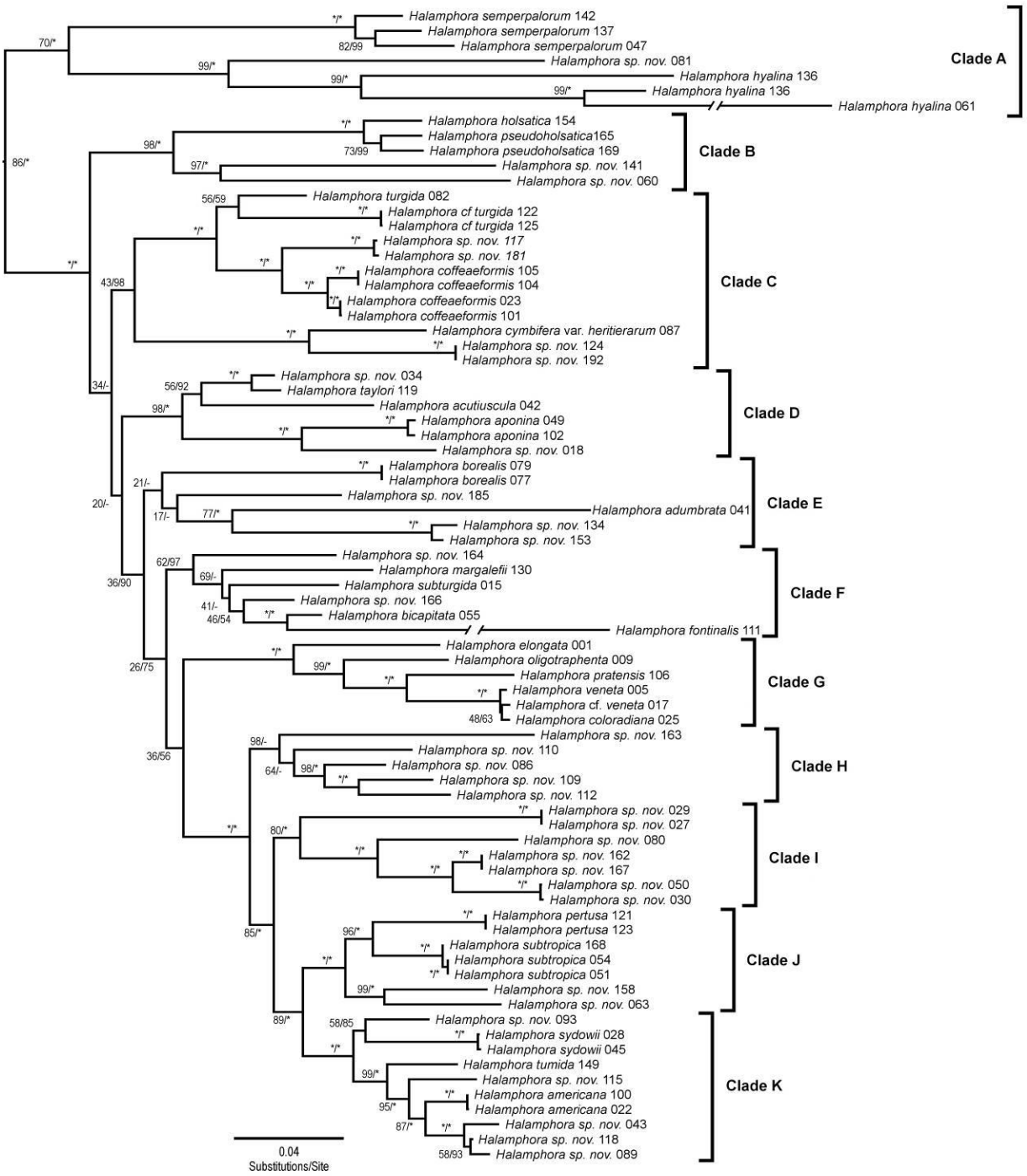

Figure 8.6. Maximum likelihood phylogram of the *Halamphora* clade inferred from a four marker (SSU, LSU, *rbc*L, *psb*C) concatenated alignment. Node support is given as ML bootstrap (500 replicates)/Bayesian posterior probability (as a percent). Node support (*) indicates 100, (-) indicates incongruence between the ML and Bayesian estimations.

features (although see Clade B for early branching exceptions) appear to be the loss of the marginal ridge, areolate dorsal striae, sieve-like areolar occlusions and biseriate areolate dorsal striae (Fig. 8.7).

Although the composition of the major clades was generally consistent between the nuclear and chloroplast markers there was a lack of congruence in the relationships between the major lineages in the ML estimations of the separate and concatenated alignments (Figs 8.8, 8.9). In general, the most derived lineages (Clades H–K) are in agreement across all three phylogenies. Alternatively, aside from the positions of Clade A and B as the earliest branching lineages within *Halamphora*, there is considerable disagreement as to the relationships between the lineages Clades C–G, with a less hierarchal structure in the chloroplast encoded tree (Fig. 8.9) and some newly created clades in the nuclear encoded tree (Fig. 8.8).

Canal raphid diatom clade

Although the genus *Amphora* is classified within the order Thalassiophysales (Round et al. 1990), Stepanek and Kociolek (2014), based on morphological features, speculated that genera also included within this order that were once included in *Amphora*, such as *Auricula* Castracane and *Thalassiophysa* Conger may represent intermediate lineages between the amphoroid lineages (*Amphora* and *Halamphora*) and the canal raphid lineages Rhopalodiales and Surirellales (Stepanek & Kociolek 2014, Fig. 8.9). This arrangement would have an important effect on the higher classification system within raphid diatoms as the amphoroid diatoms could no longer be placed in the Thalassiophysales without the inclusion of the canal raphid orders. The taxon *Thalassiophysa hyalina* was included in the present analysis and had a position sister to the Rhopalodiales and Surirellales clade in all examined alignments (Fig. 8.1). Figure 8.10 shows the detailed ML phylogeny inferred from the concatenated alignment of the *Thalassiophysa* + Rhopalodiales + Surirellales clade. Within this clade *T. hyalina* is in a well-supported (95/100) position sister to the remainder of the canal raphid diatoms.

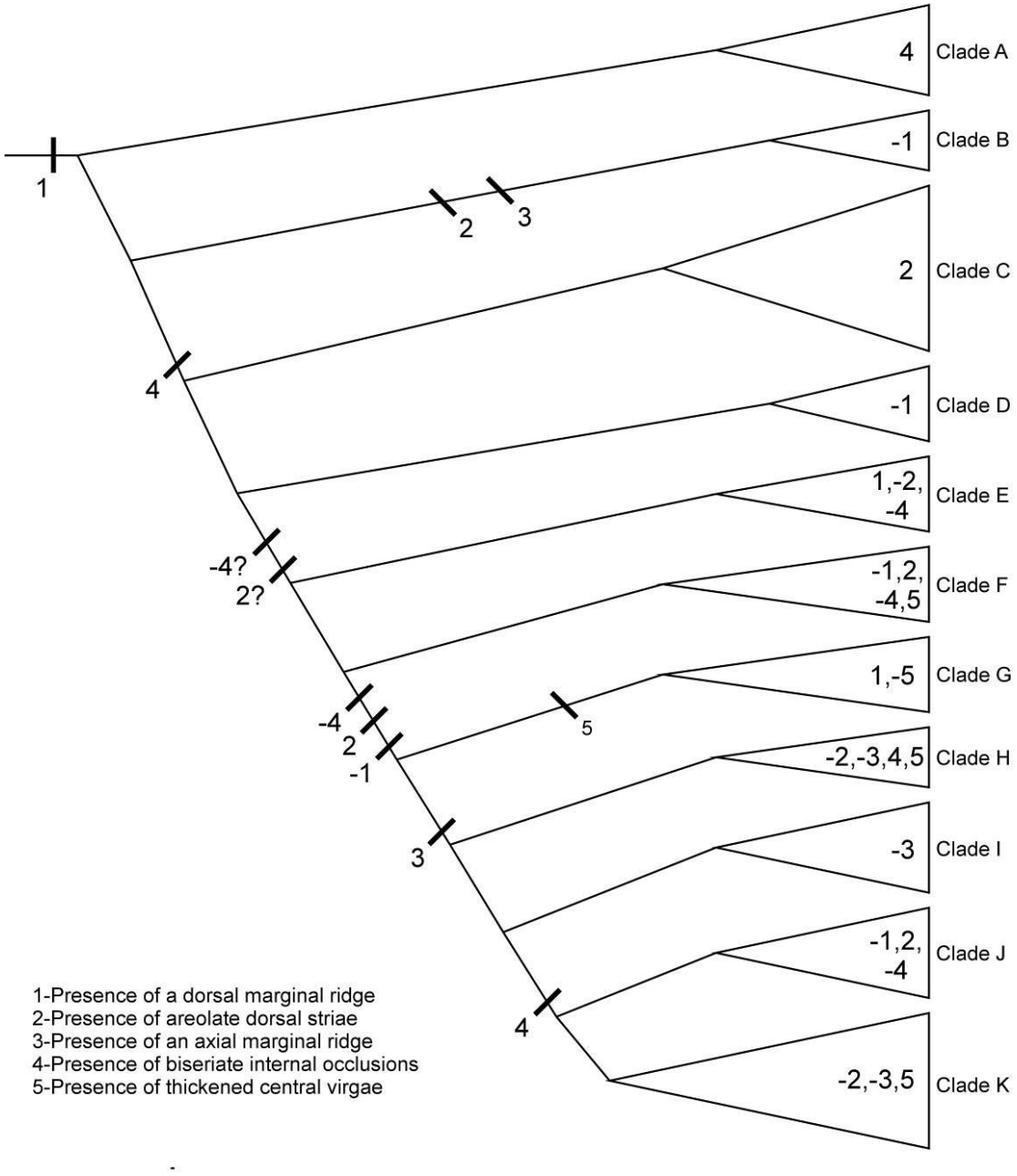

Figure 8.7. Common *Halamphora* morphological traits mapped onto a maximum likelihood cladogram inferred from a four marker (SSU, LSU, *rbc*L, *psb*C) concatenated alignment. (-) indicates the secondary loss of a trait.

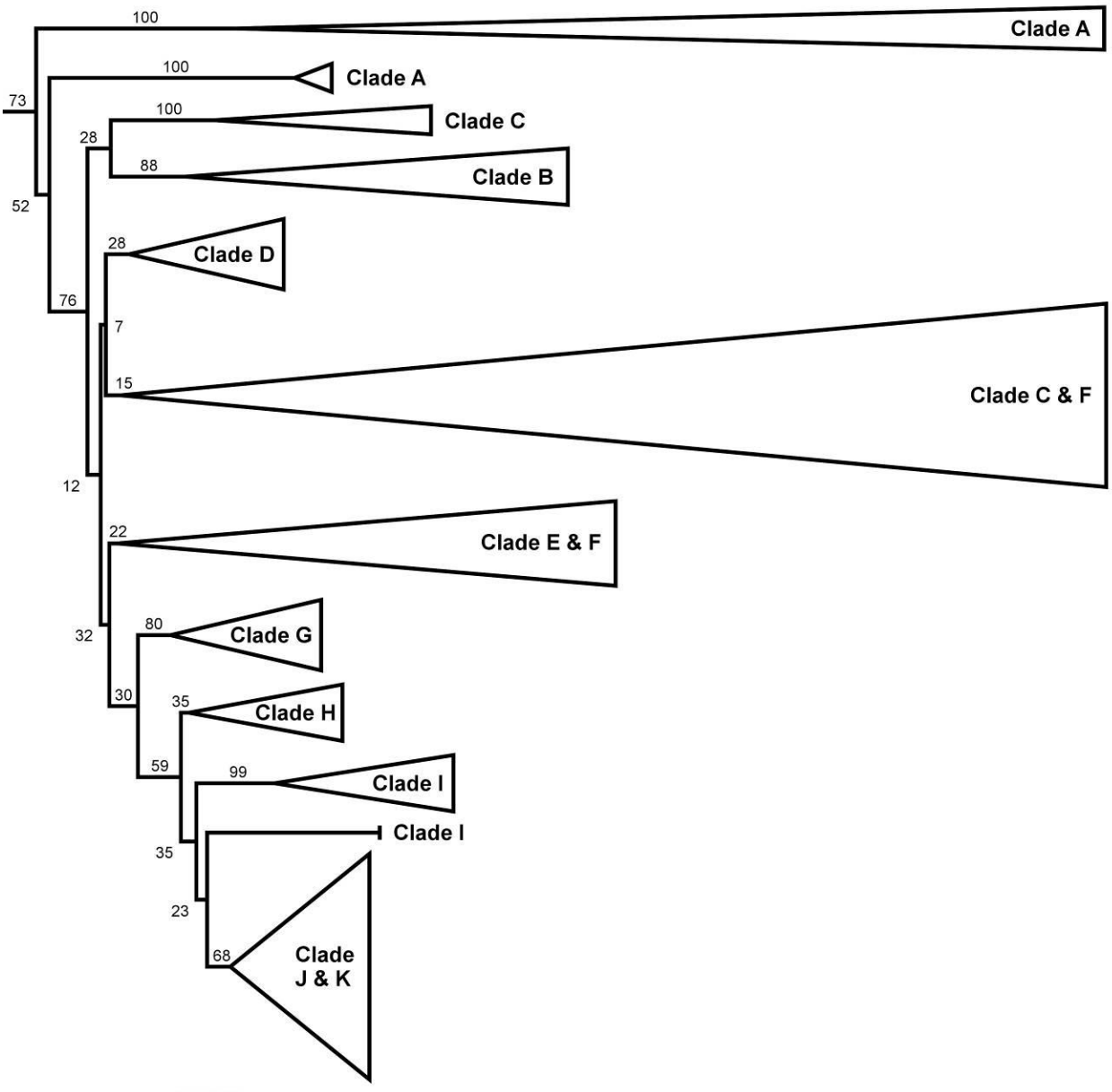

Figure 8.8. Simplified maximum likelihood phylogram showing the relationships between the major subclades within *Halamphora*. Phylogram inferred from a nuclear marker (SSU, LSU) concatenated alignment. Node support is given as ML bootstrap values.

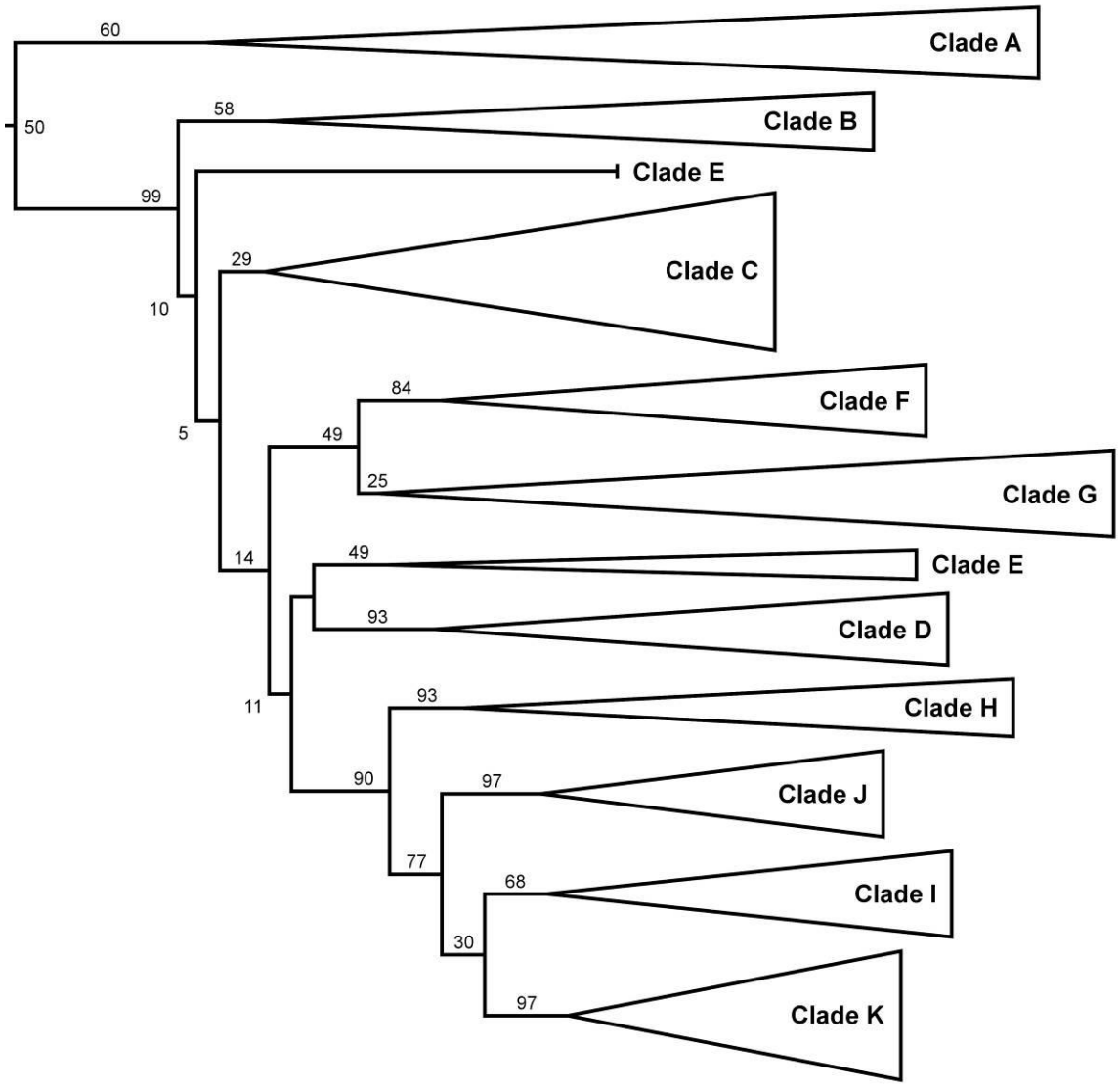

Figure 8.9. Simplified maximum likelihood phylogram showing the relationships between the major subclades within *Halamphora*. Phylogram inferred from a chloroplast marker (*rbc*L, *psb*C) concatenated alignment. Node support is given as ML bootstrap values.

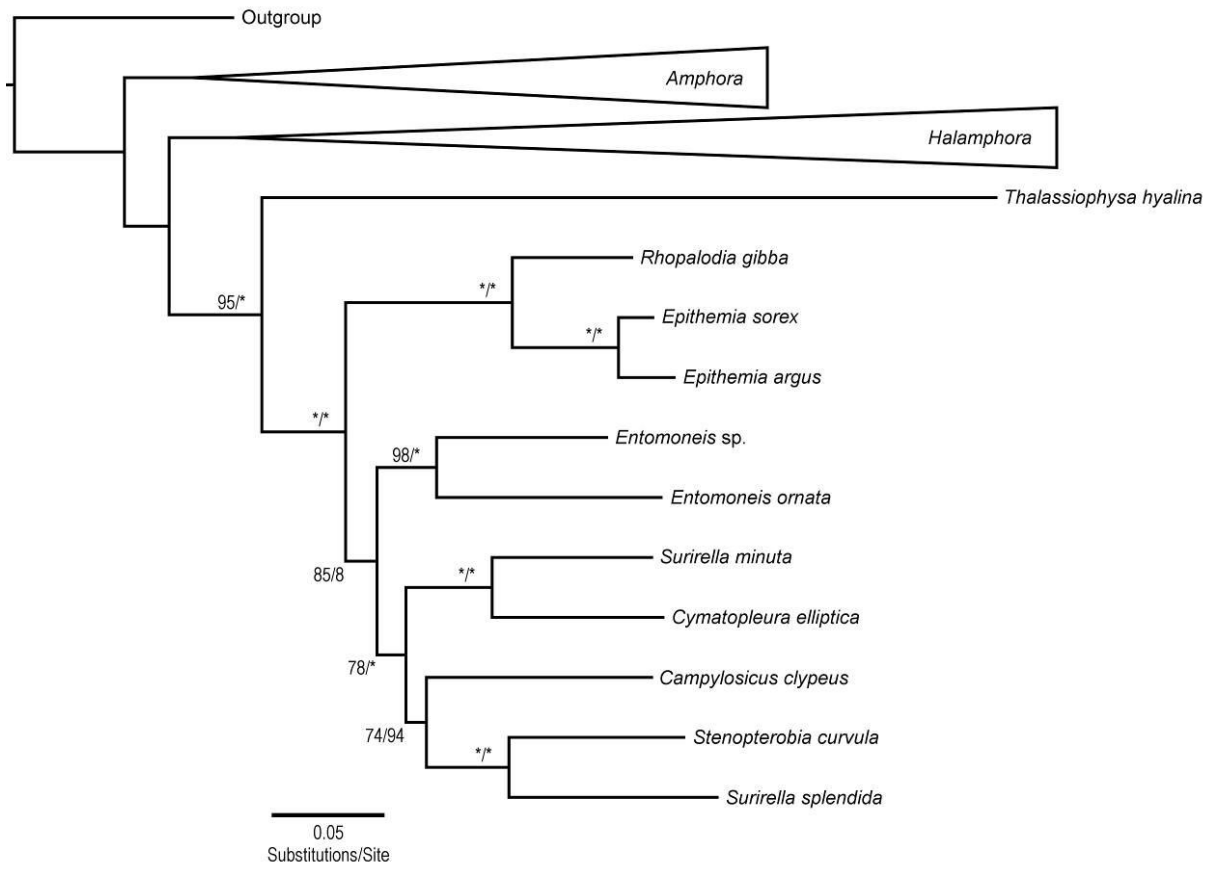

Figure 8.10. Maximum likelihood phylogram of the Surirellales + Rhopalodiales + *Thalassiophysa* clade. Phylogram inferred from a four marker (SSU, LSU, *rbc*L, *psb*C) concatenated alignment. Node support is given as ML bootstrap/Bayesian posterior probability (as a percent). (*) represents a value of 100.

Topological hypothesis testing

Three topologically constrained hypotheses where tested against the unconstrained topology inferred from the four marker concatenated alignment. The three constraints where chosen to reduce incongruence between the topology inferred from the molecular data and the most parsimonious arrangement of major lineages within *Halamphora s.s.* based on five common taxonomically important morphological characteristics (Fig. 8.11). Constraint one consisted of the monophyly of all of the biseriate striae taxa (Clades C, D and F). This topology was less likely than the unconstrained topology (log likelihood −10.9), but based on the approximately unbiased (AU) topology test this alternative topology cannot be statistically rejected (p=0.390). Constraint two forced the monophyly of all of the areolate striae

and axial longitudinal line bearing taxa (Clades B, H–K). As with constraint one, although returning a less likely solution (likelihood −23.7) this alternative topology could not be statistically rejected given the data (p=0.151). The third constraint combines constraints one and two and fully conforms to the most parsimonious topology given the five investigated morphological features (Fig. 8.11). The most likely tree given these two constraints is illustrated in Figure 8.12. This constrained topology returned a less likely tree than the unconstrained topology (likelihood −39.3), and this morphologically congruent hypothesis was statistically rejected by the AU topological test (p=0.003).

Movement between fresh and salt waters

Figures 8.13 and 8.14 illustrate the ancestral habitat states for *Amphora* and *Halamphora*, respectively, inferred from a ML ancestral state reconstruction of collection site conductivity (branch color) and collection habitat type (node pie color). These reconstructions were based on the concatenated ML tree topology. In both figures cooler branch color indicates more saline waters and warmer branch color indicates less saline waters with freshwaters in red.

The *Amphora* reconstruction indicates that, given the current taxon coverage, the genus is ancestrally coastal marine (Fig. 8.13). This coastal marine habitat is shared by all of the Clade A taxa, as well as the early branching lineages within Clade B and the *Amphora* s.s. clade. Within *Amphora* there appears to be a single large movement into inland waters from the marine environment. This transition was followed by a diversification into a clade containing the saline inland taxa *A. allanta* Hohn & Hellerman and *A. waldeniana* Stepanek & Kociolek (as well as an apparent move back to the coastal marine environment in *A. proteoides* Hustedt) and into a large clade that contains many of the common cosmopolitan freshwater *Amphora* species. The only other movement from coastal to inland environments is in the taxon *A. commutata* which is commonly found in high conductivity inland habitats (Levkov 2009, Sato et al. 2013).

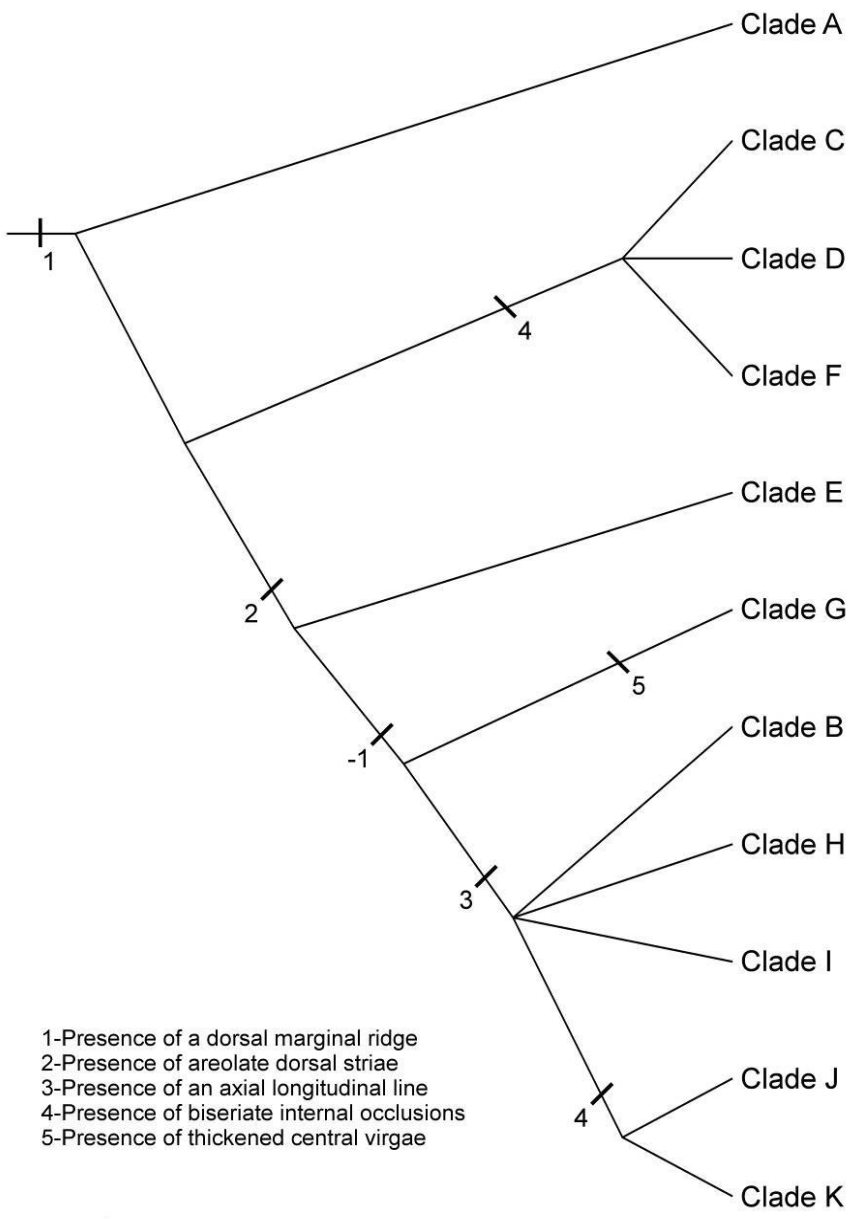

Figure 8.11. Most parsimonious relationships of the major subclades within *Halamphora* inferred from maximum parsimony analysis of five common morphological traits. (-) indicates the secondary loss of a trait.

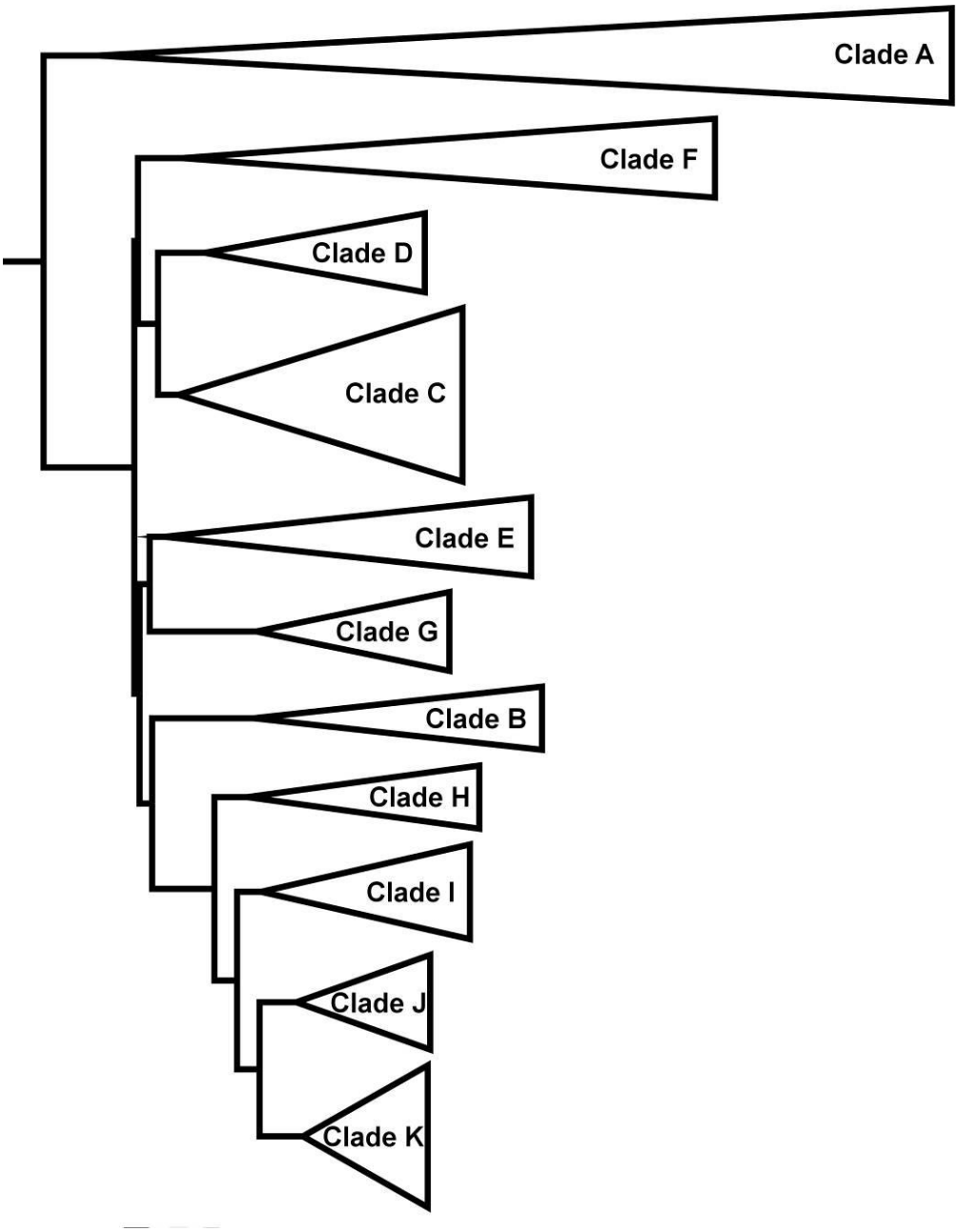

Figure 8.12. Simplified maximum likelihood phylogram inferred from a constrained four marker (SSU, LSU, *rbc*L and *psb*C) concatenated alignment. Two monophyletic constraints were enforced, constraint 1 (B, H, I, J, K), constraint 2 (F, D, C).

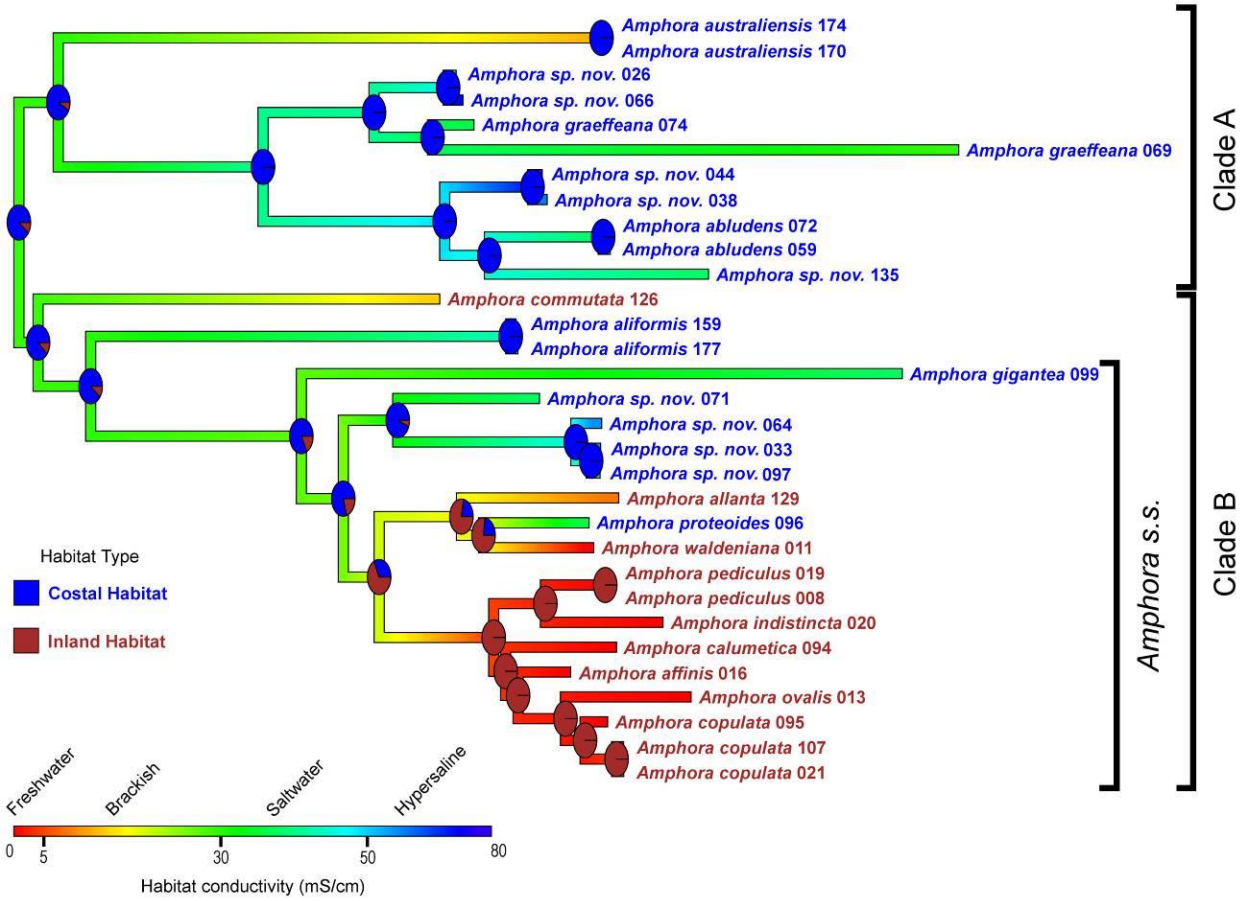

Figure 8.13. Ancestral trait reconstruction of habitat conductivity and type for the genus *Amphora* inferred from ML methods. The phylogeny is taken from Fig. 8.2. Branch colors indicate inferred ancestral habitat conductivity based on the measured conductivity at the taxon collection site. Taxon colors and node pies indicate habitat type coded as either inland or coastal.

As with *Amphora*, the inferred ancestral habitat for the genus *Halamphora* is coastal marine (Fig. 8.14). Unlike *Amphora*, the sampled *Halamphora* taxa show several independent incursions into inland and freshwater systems. Major movements from coastal to inland habitats appear to have occurred within Clades C, F, G and K with at least single taxon incursions in all major clades except Clades A, B and I. Many of these taxa are found in inland waters with elevated conductivities of 5-15 mS cm^{-1} (*H. turgida* (Gregory) Levkov, *H. sp. nov.* 117/181, *H. sp. nov.* 124/192, *H. taylori* (Grunow in Van Heurck) Stepanek & Kociolek, *H. sp. nov.* 018, *H. margalefii* (Tomàs in Sabater et al.) Stepanek & Kociolek, *H. pertusa* Stepanek & Kociolek, *H. sp. nov.* 115, *H. americana* Kociolek, *H. sp. nov.* 118). The only large

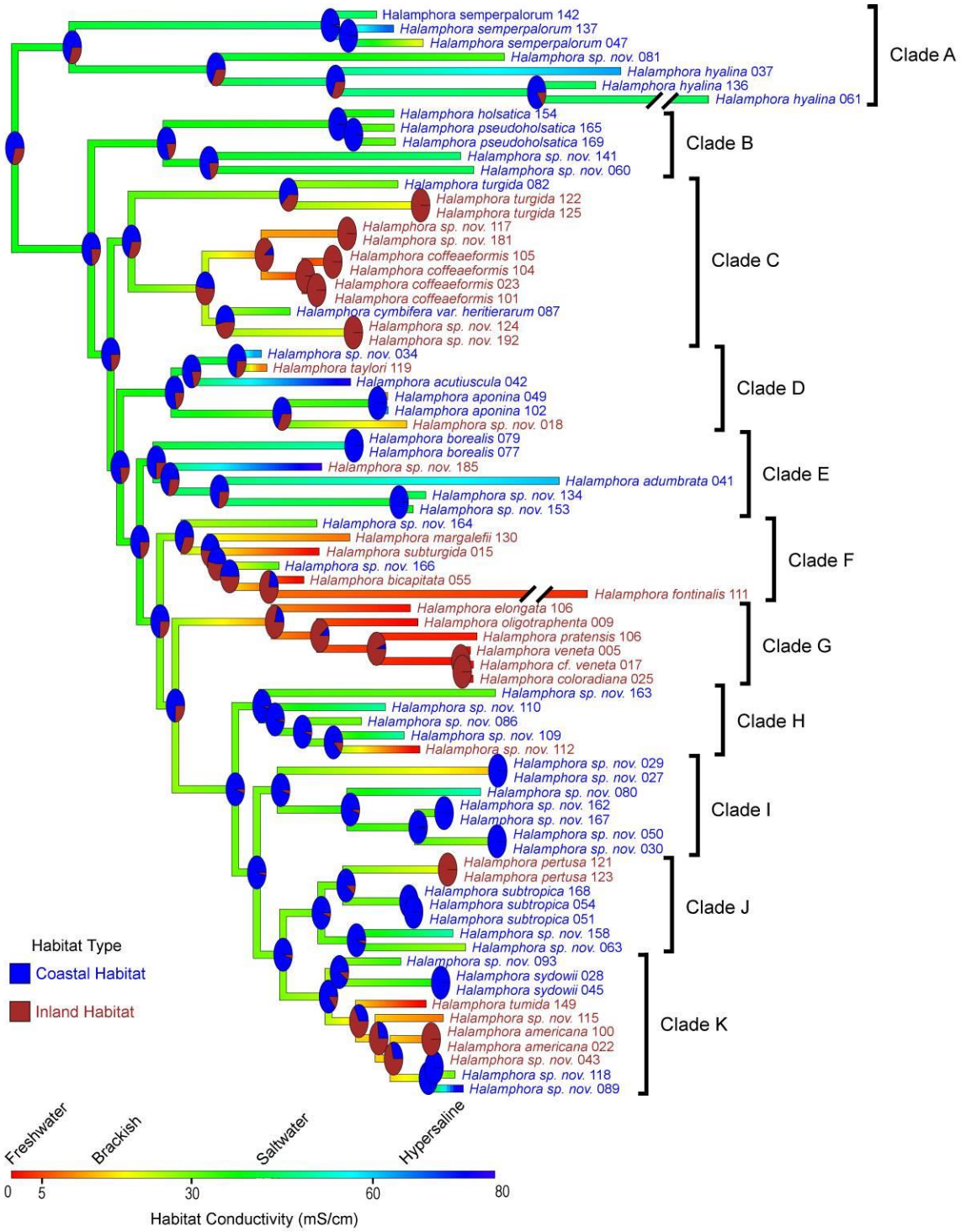

Figure 8.14. Ancestral trait reconstruction of habitat conductivity and type for the genus *Halamphora* inferred from ML methods. The phylogeny is taken from Fig. 8.6. Branch colors indicate inferred ancestral habitat conductivity based on the measured conductivity at the taxon collection site. Taxon colors and node pies indicate habitat type coded as either inland or coastal.

diversification within freshwaters sampled here was within Clade G which is entirely comprised of freshwater forms from the common and widespread *H. veneta* (Kützing) Levkov morphological group. As with the *Amphora* taxa, movement from coastal to inland habitats and from high conductivity to low conductivity appears far more common than in the other direction. A notable exception appears in Clade K where *H. sp. nov.* 043 and *H. sp. nov.* 089 have moved back to a coastal marine environment.

DISCUSSION

The overall relationships between the amphoroid diatom groups and the canal raphid diatoms agree with previous investigations utilizing multi-gene phylogenies (Ruck & Theriot 2011, Stepanek & Kociolek 2014). As with the previous works, this investigation returned strong support (91/100) for a sister relationship between a well-supported (86/100) monophyletic *Halamphora* and a strongly supported (95/100) monophyletic canal raphid diatom clade plus the genus *Thalassiophysa*. Sister to this *Halamphora* + canal raphid diatom clade (100/100) is a strongly supported (99/100) clade containing the genus *Amphora*. With this new data a stable concept of the classification and relationships within this group, are beginning to emerge.

Systematics of the genus Amphora

The genus *Amphora*, here defined as only those amphoroid taxa that contain a Type 1 chloroplast (Mereschkowsky 1903) (see Stepanek & Kociolek 2014), and based on this feature now contains taxa that once belonged to Cleve's (1895) subgenera *Amphora s.s.*, *Diplamphora* and *Oxyamphora*. While *Amphora* is diagnosed by chloroplast structure, there is significant incongruence between the relationships inferred from the molecular data and the most parsimonious interpretation of valve morphological features (Stepanek et al. 2015). Within the taxa examined here, three distinct morphological groups emerge. There are taxa that have historically belonged to *Amphora s.s.* (Chapter 4, Figs 4.19–4.47), the subgenus *Diplamphora* (Chapter 4, Figs 4.1–4.9, 4.15–4.18) and the *A. abludens* morphological group within the subgenus *Oxyamphora* (Chapter 4, Figs 4.10–4.14). Although three

distinct morphological groups are present, these morphological distinctions are not fully returned in the molecular phylogeny (Fig. 8.5). The relationships inferred by the four marker concatenated alignment returns two major clades within *Amphora*, Clade A which contains the *Diplamphora* taxa that are morphologically allied with *A. graeffeana* and the *Oxyamphora* taxa that are morphologically allied with *A. abludens*. Within Clade B is the clade that contains *Amphora s.s.* taxa as well as two early branching lineages represented by taxa that, although similar to *Amphora s.s.* in overall valve appearance, would have historically also been classified within *Diplamphora* on account of their areolate girdle bands (Sato et al. 2013, Stepanek et al. 2015).

If one presumes that the present molecular phylogeny is an accurate reflection of the actual relationships between the represented species of *Amphora,* then the morphological features most commonly used in *Amphora* taxonomy have little utility in separating the major groups within the genus. Figure 5 demonstrates that these features are largely plesiomorphic to the entire genus (Fig. 8.5, features 1, 2, 3) or are diagnostic to the *Amphora s.s.* clade to the exclusion of the early branching *Diplamphora* lineages (Fig. 8.5, features -1, 4, 6). From a morphological cladistic perspective, this arrangement between the major morphological groups is clearly not the most parsimonious.

The most parsimonious solution to this phylogeny, given the limited number of morphological characters examined here, is to have three monophyletic lineages corresponding to the three large morphological groups. Given these six morphological traits and these three morphological lineages all possible topologies A(BC), (AB)C and (AC)B are equally parsimonious with each fully resolving the phylogenetic relationships in 8 steps. For the sake of comparison, the topology in Figure 8.15 has been chosen because, although equally parsimonious, Figure 8.15 requires the least number of plesiomorphic traits and reversals, making it the most appealing if attempting a morphological classification of the group. In this classification a dorsal marginal ridge and externally occluded striae are traits diagnostic of the entire clade, areolate striae, a ventral raphe ledge and separate central helictoglossae are shared features of the *Amphora s.s.* clade, areolate girdle bands are shared within the *Diplamphora* + *Oxyamphora* clade with the *Oxyamphora* clade secondarily losing external areolar occlusions and

independently gaining areolate striae. While this is appealing as it allows for diagnostic synapomorphies (or a secondary loss of a feature in the case of the *A. abludens* Clade) for the major divisions within the genus, it is not supported by the molecular evidence, an incongruence that is worth further attention.

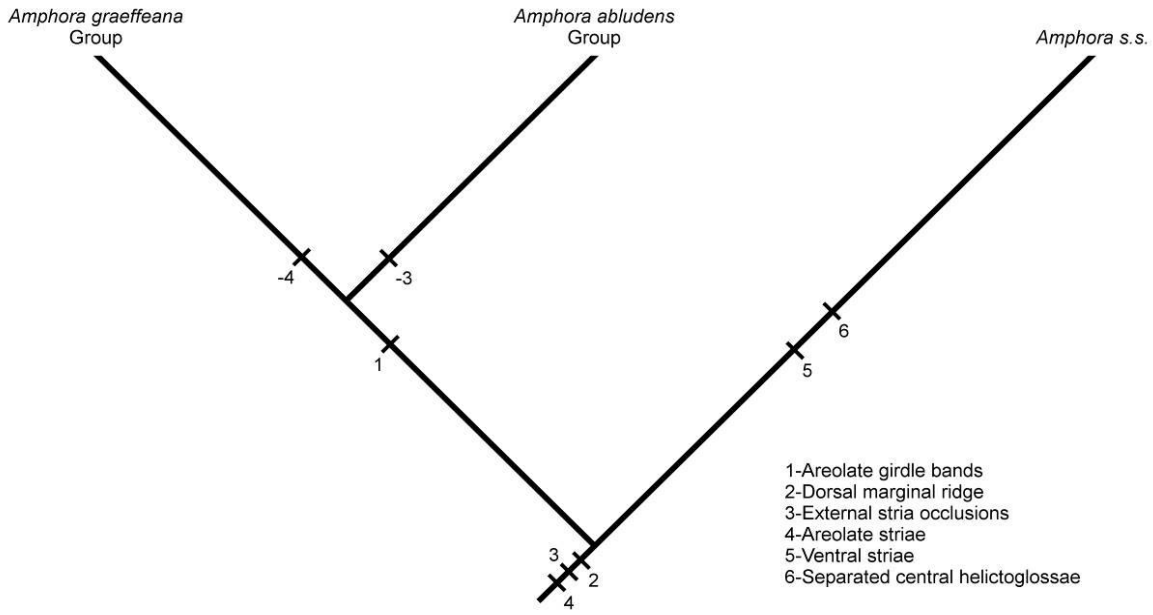

Figure 8.15. One of three most parsimonious relationships between the major morphological groups within the genus *Amphora*. Common morphological characters are mapped onto the branches. (-) indicates the secondary loss of a trait.

As phylogenetic trees inferred from molecular data are in fact gene trees rather than species trees (Doyle 1992, Maddison 1997), it is worth considering the possibility that incomplete lineage sorting or unrecognized paralogy within early branching lineages may be creating the morphological paraphyly seen in the *Diplamphora* taxa of Clades A and B (Doyle 1992, Maddison 1997, Funk & Omland 2003, Maddison & Knowles 2006). Although the tree topology between the phylogenetic estimations performed on the three alignments (nuclear markers, chloroplast markers, four marker concatenated) is not in total agreement, it is important to examine what is congruent (Figs 8.2–8.4). First, *Amphora s.s.* is monophyletic in all three trees. Second, in no returned tree are the *Diplamphora* taxa monophyletic. Third, in all returned trees, some combination of *Diplamphora* taxa are basal and paraphyletic into

Amphora s.s. The fact that independent markers, from the nuclear and chloroplast genomes, support the non-monophyly of the *Diplamphora* morphological groups and their early branching positions within Clade B greatly reduces the probability that these inferred relationships are an artifact of an early gene duplication (or even genome duplication) and incomplete lineage sorting (Doyle 1992, Maddison 1997, McCracken & Sorenson 2005). It is more likely in this case that the typical *Diplamphora* morphology of non-areolate externally occluded striae, areolate girdle bands and a fused internal central helictoglossa were the ancestral morphological states within the genus *Amphora* and that the *A. abludens* and *Amphora s.s.* morphological groups represent morphologically derived groups nested within the genus.

Systematics of the genus Halamphora

Although there was some question as to the appropriateness of Levkov's (2009) elevation of the *Amphora* subgenus *Halamphora* to generic status without any corresponding phylogenetic evidence as to its monophyly or distinctness from *Amphora* (Sar et al. 2010), the genus as described by Levkov continues to be returned as a monophyletic and distinct lineage of diatoms. In contrast to *Amphora*, which has seen a dramatic narrowing of its morphological concept given molecular evidence, the morphological concept of the already diverse *Halamphora* has expanded given the phylogenetic evidence and corresponding taxonomic transfers presented here (Clade A).

Clades B–K represents taxa belonging to *Halamphora s.s.* as prescribed by Levkov (2009). Sister to this large and diverse clade is a molecularly diverse (if not morphologically diverse) clade that is comprised of two very distinct morphological forms. Within Clade A are several taxa from a morphological species, *H. hyalina*, that was first described from coastal waters in 1841 (Ehrenberg 1841) and which has been classified within the *Amphora* subgenus *Oxyamphora* since 1895 (Cleve 1895). Sister to this species complex is a group of taxa belonging to the morphological species concept of *H. semperpalorum* which is unique in morphology (see Stepanek & Kociolek 2014) and was unknown to science until its description from coastal Florida, USA in 2003 (Wachnicka & Gaiser 2003). Although morphologically and phylogenetically distinct from *Halamphora s.s.*, given our limited knowledge of

additional forms that may reside in this clade, its morphological diversity and lack of synapomorphies, the least taxonomically disruptive course is the transfer of these taxa into the genus *Halamphora*.

When considering the taxa assigned to *Halamphora s.s.* (Clades B–K), similar morphological issues arise as were seen in *Amphora*. One distinct feature of the topology inferred from the concatenated alignment is that *Halamphora* is separated into many small clades grading through morphological features (Fig. 8.2, Chapter 4, Figs 4.48–4.178). This is in contrast to a general morphological dichotomy with lineages either exhibiting biseriate (Clades C, D and F) or areolate dorsal striae (Clades E, G, B, H, I, J and K).

This incongruence between morphology and the inferred molecular phylogeny can be seen when mapping five morphological traits commonly used in *Halamphora* taxonomic investigations onto the molecular phylogeny (Fig. 8.7). To help illustrate the incongruence between these characters and the molecular phylogeny, a maximum parsimony cladogram of the major lineages was produced using these six features. Figure 8.11 represents the single most parsimonious tree based on morphology. As with the *Amphora* morphological tree, the *Halamphora* tree, although not fully resolved as a very parsimonious morphological solution requiring only seven steps to for the five examined characters compared to the twelve steps required in the molecular tree. In this classification there is a dichotomous split within *Halamphora s.s.* with an unresolved clade containing all of the biseriate striae lineages (Clades C, D and F) and a large partially resolved clade containing all of the areolate striae lineages (Fig. 8.11). Several additional features are diagnostic within the areolate striae clade creating further subdivisions, including the loss of the dorsal marginal ridge (Clades G, B, H, I, J and K), the presence of thickened central virgae (Clade G), the presence of an axial longitudinal line (Clades B, H, I, J and K) and an independent evolution of biseriate internal striae occlusions (Clade J and K).

The positions of Clades B and F are primary cause of incongruence between the molecular and morphological phylogenies. Clade B has a strongly supported position as the sister lineage to the remaining *Halamphora s.s.* taxa (100/100) although morphologically it exhibits what would appear to be two derived features of areolate striae and an axial marginal longitudinal line that would ally it with

lineages H and I, although it does retain the plesiomorphic character of a dorsal marginal ridge that has been lost in these later branching lineages. Unlike the strong node support for the position of Clade B, Clade F has a poorly supported (26/75) position sister to the areolate striae Clades G–H, with the areolate striae Clade E sister (36/90) to this larger group. In the context of the relationships between these early branching relationships it is worth noting that, although the relationships between the later branching lineages (Clades H–K) are well-supported, the relationships between Clades C–G suffer from low support and incongruence between the ML and Bayesian analysis (Figs 8.6, 8.8, 8.9).

With this in mind, the question becomes what weight to give the molecular topologies that are in direct conflict with the inferred morphological tree. When examining the trees inferred from the four marker (Fig. 8.6), nuclear (Fig. 8.8) and chloroplast (Fig. 8.9) markers, it is apparent that there is a great deal of variability in the inferred relationships between these early branching lineages. Although this variability exists, some general statements regarding the relationships between these lineages can be made. First, there are some areas of the tree that are supported across marker types. Clade A as the sister lineage to *Halamphora s.s.* is consistent across trees, although it is not monophyletic in the nuclear tree (Fig. 8.8). The other well supported relationship is in the later branching lineages, Clades H–K. These clades contain all of the areolate taxa without a marginal ridge and with an axial longitudinal line. Although some topological differences exist, these four clades form a monophyletic group across all of the trees.

Other important topological themes include that the biseriate striae clades (Clades C, D and F) are non-monophyletic in all estimations, although the tree inferred from the nuclear analysis has many of these taxa grouped together (Fig. 8.8) and the Bayesian inferred tree from the concatenated alignment has Clade C in a monophyletic group with Clade D. Finally, in all trees the areolate striae Clade B is distinct from the well supported (100/100) Clade H–K for which it shares a close morphological affinity. In both the concatenated and chloroplast trees Clade B is in a strongly supported (100/100, BS 99 for the concatenated and chloroplast marker trees, respectively) position as the first branching lineage within the *Halamphora s.s.* group (Figs 8.6, 8.9). In the nuclear marker tree Clade B is also contained within the

earliest branching lineage within *Halamphora s.s.* (BS 76), although within this lineage it is sister (BS 28) to several biseriate striae taxa from Clade C (Fig. 8.8).

Given the low backbone support for many of the deeper relationships within the *Halamphora s.s.* clade it is difficult to rule out the relationships inferred by morphology. In an effort to estimate the likelihood of the alternative morphological topological hypotheses, a ML tree was generated under topological constraints designed to approximate the most parsimonious morphological topology shown in Figure 8.11. Two monophyletic constraints were enforced, one in which Clades C, D and F, corresponding to the biseriate striae lineages, and one in which the areolate striae lineages (Clades B, H–K) are under a monophyletic constraint. Within these constraints the tree topology is free to arrange in the most likely topology. These constraints require Clade B to associate with the morphologically similar areolate striae taxa and requires Clade F to associate with the morphologically similar biseriate taxa, all other associations are left unconstrained. The most likely tree given these topological constraints and inferred from the concatenated alignment is shown in Figure 8.12 and closely resembles the morphological tree (Fig. 8.11). Although aligning with the morphological hypothesis, given the molecular data, hypothesis testing rejected this alternative topology ($p=0.003$)

As with the *Amphora* phylogeny, given the agreement across markers from both the nuclear and chloroplast genomes it is difficult to attribute this incongruence between molecular and morphological phylogenetic hypotheses to unrecognized paralogy and incomplete lineage sorting (Doyle 1992, Maddison 1997). The seemingly well supported morphological split between the areolate striae taxa aside, the generally low backbone node support for the relationships between clades C–G is somewhat surprising given the evolutionary scales under investigation and the strong support for within clade relationships. Marker saturation, especially in the third codon position of the protein encoding chloroplast genes *rbc*L and *psb*C, could be one possible explanation. Given the small evolutionary breadth examined here this seems unlikely as recent work has demonstrated that evolutionary signal outweighs noise in these same markers over evolutionary scales of classes of diatoms (Theriot et al. 2015) and the identical

markers have produced well resolved and supported phylogenies across several orders of diatom diversity (Li et al. 2015), as well as for genus level relationships in this analysis (Fig. 8.1).

Furthermore, this seems to be an unusual case in which greater taxon sampling, considered important for greater phylogenetic resolution and support (Pollock et al. 2002, Zwickl & Hillis 2002, Heath et al. 2008), has decreased support to the well supported *Halamphora* clade presented in Stepanek & Kociolek (2014) that included taxa from Clades C, G and J and returned strong support throughout. If the phylogenetic ambiguity is not caused by a shortcoming in the data used for the inference (e.g., resolving power of the markers, poor taxon coverage), an alternative possibility could be either extensive hybridization or horizontal gene flow deep in the early branching lineages within *Halamphora*. Both of these processes could lead to the poorly supported relationships along the early backbone of the phylogeny. Although these processes have been believed to have occurred within diatom lineages, until recently very little work has been dedicated to their investigation (Armbrust et al. 2004, Bowler et al. 2008, Casteleyn et al. 2009, D'Alelio et al. 2009).

A final scenario that cannot be ruled out is that the ambiguity in the relationships between Clades C–G is the result of an extremely rapid early diversification within the *Halamphora s.s.* group, essentially creating a hard polytomy and leading to poorly resolved relationships between these early lineages (Hoelzer & Melnick 1994). Although not often cited in diatom phylogenetics, dramatic early radiations have been implicated in the persistent poor deep node support in many other morphologically diverse groups of organisms (Hoelzer & Melnick 1994, Malcomber 2002, Gavrilets & Losos 2009, Harmon et al. 2010, Straub et al. 2014).

Morphological and molecular variability within Amphora and Halamphora

Although molecular phylogenetic and molecular barcoding studies within diatoms continues to increase, the vast majority of taxonomic and ecological investigations within the field continues to use morphological valve features as the basis for taxonomic identification. This is driven in part by convenience, as no culturing or molecular analysis is required and a permanent morphological voucher

record is produced, partially because of the rich morphological diversity exhibited by diatoms when compared to other algal groups, and partially by historical precedent as the morphological description and classification of diatoms extends back to the late 18th century (Müller 1786, Gmelin 1791).

Within this morphological taxonomic framework is the implicit assumption that morphological diversification tracks organismal diversification. In morphologically based ecological investigations this assumption is taken a step further in that, ideally, morphological groups are assumed to be monophyletic with an associated shared set of ecological traits (ten Cate et al. 1993, Cox 1995, Pan et al. 1996). The phylogeny presented here allows some insight into the variable degree to which molecular and morphological diversification are linked. Figure 8.16 shows the *Amphora* Clade A and the freshwater group within *Amphora* Clade B with the associated morphological diversity based on LM imaging of cleaned valves. Figure 8.17 shows *Halamphora* Clade A and *Halamphora* Clade G with corresponding morphological diversity. Tables 8.2–8.5 show the genetic distances between the taxa included in Figs 8.16 and 8.17 based on branch lengths inferred from the concatenated alignment.

A striking feature of *Amphora* Clade A and *Halamphora* Clade A is the minimal morphological diversity given the amount of genetic diversity in the four markers examined here. Using historical taxonomic references it is likely that the seven distinct lineages represented in *Amphora* Clade A would be classified into three species, *A. australiensis*, *A. graeffeana* and *A. abludens*. Whereas the same number of distinct lineages (seven) in the Clade B subclade would easily be separated morphologically into six previously described species. A similar situation is observed between *Halamphora* Clades A and G. Purely based on a historical morphological species concept, the seven distinct lineages within *Halamphora* Clade A would likely be placed into only two species, *H. semperpalorum* and *H. hyalina*. Whereas the six lineages within Clade G are clearly morphologically distinct and are currently prescribed to five previously described species.

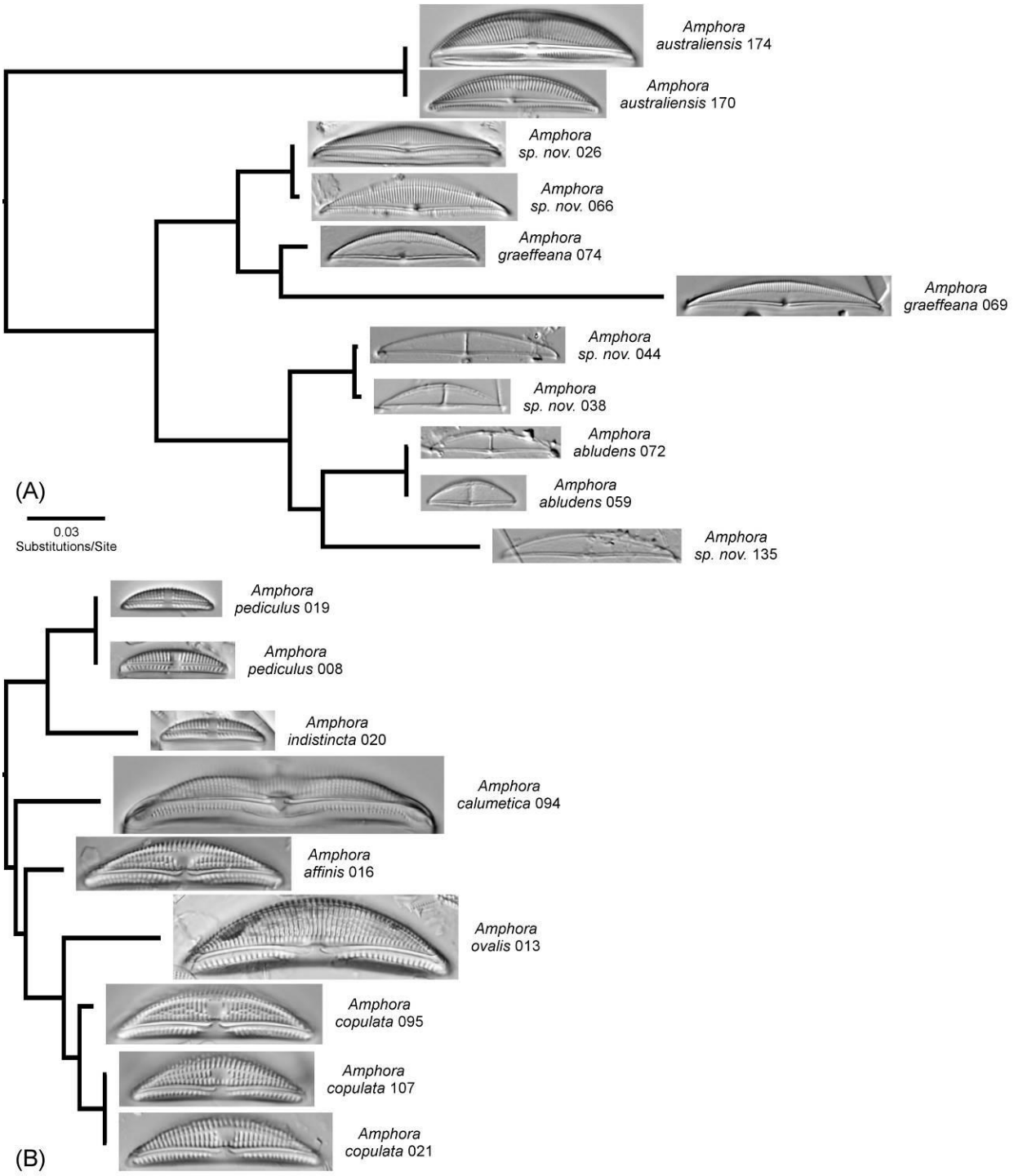

Figure 8.16. Phylograms taken from Fig. 8.2 illustrating the relationship between molecular diversity and morphological diversity within two *Amphora* clades. **A.** Taxa from *Amphora* Clade A. **B.** Taxa from the freshwater Clade of *Amphora* clade B.

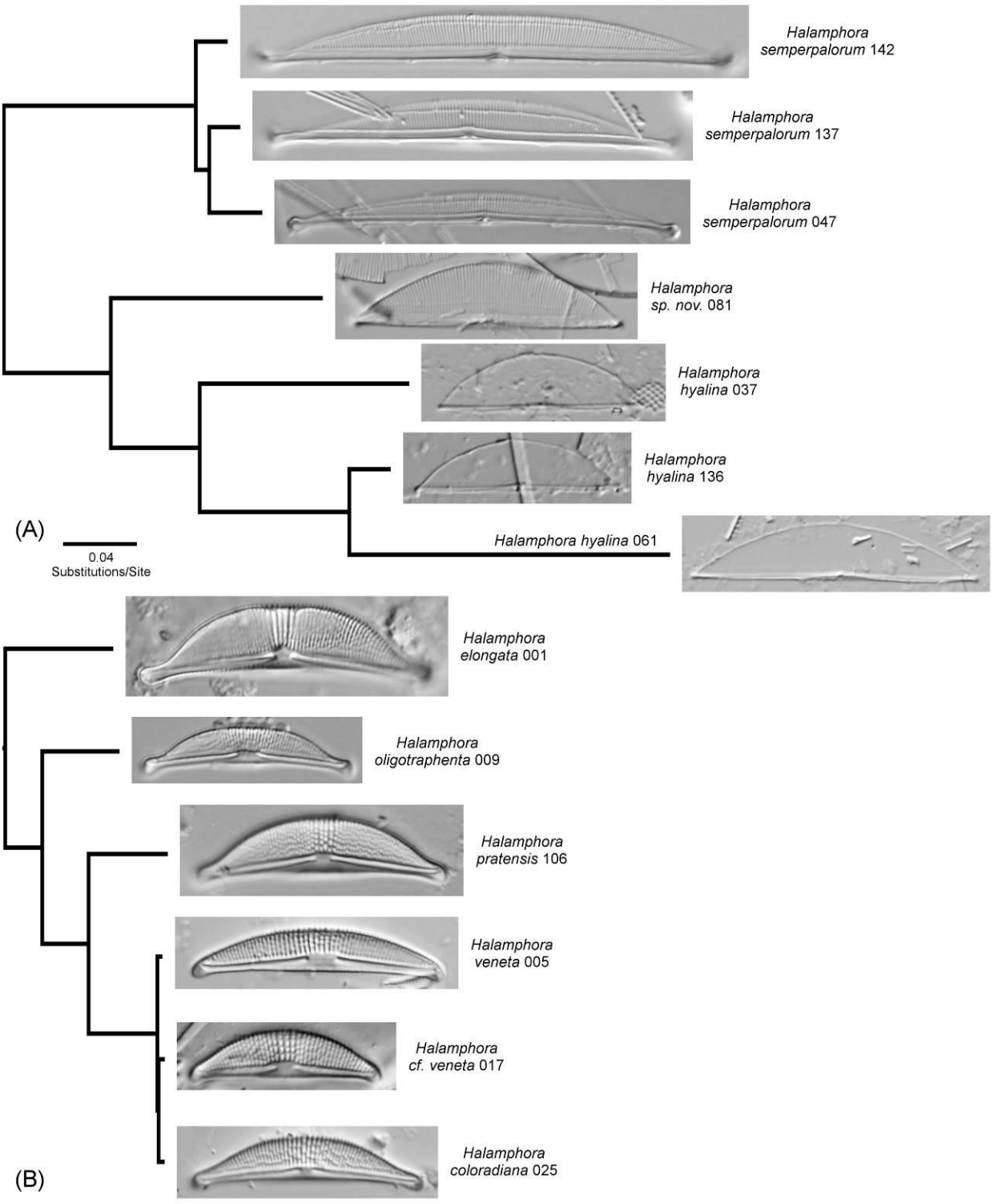

Figure 8.17. Phylograms taken from Fig. 8.6 illustrating the relationship between molecular and morphological diversity within two *Halamphora* clades. **A.** Taxa from *Halamphora* Clade A. **B.** Taxa from *Halamphora* Clade G.

Table 8.1. Phylogenetic distances between taxa from *Amphora* Clade A based on branch lengths from the four marker phylogram. Lower decimal values represent branch length distances between taxa. Upper whole numbers represent inferred base differences between taxa (4444 total bases).

A. australiensis 174	0	0	1217	1208	1857	1231	1326	1319	1407	1405	1534
A. australiensis 170	0	0	1217	1208	1857	1231	1326	1319	1407	1405	1534
A. sp. nov. 066	0.2739	0.2739	0	16	856	231	612	605	693	690	820
A. sp. nov. 026	0.2719	0.2719	0.0037	0	848	222	603	597	684	682	811
A. graeffeana 069	0.4179	0.4179	0.1927	0.1907	0	720	1252	1245	1333	1330	1460
A. graeffeana 074	0.2771	0.2771	0.0519	0.0499	0.1619	0	626	620	707	705	834
A. sp. nov. 038	0.2983	0.2983	0.1376	0.1357	0.2816	0.1409	0	18	333	330	460
A. sp. nov. 044	0.2969	0.2969	0.1362	0.1342	0.2802	0.1394	0.0042	0	327	324	453
A. abludens 072	0.3167	0.3167	0.1560	0.1540	0.3000	0.1592	0.0749	0.0735	0	3	426
A. abludens 059	0.3161	0.3161	0.1554	0.1534	0.2994	0.1586	0.0743	0.0729	0.0006	0	423
A. sp. nov. 135	0.3452	0.3452	0.1845	0.1825	0.3285	0.1877	0.1035	0.1020	0.0958	0.0952	0
	A. australiensis 174	*A. australiensis* 170	*A. sp. nov.* 066	*A. sp. nov.* 026	*A. graeffeana* 069	*A. graeffeana* 074	*A. sp. nov.* 038	*A. sp. nov.* 044	*A. abludens* 072	*A. abludens* 059	*A. sp. nov.* 135

Table 8.2. Phylogenetic distances between taxa from the *pediculus-copulata* clade based on branch lengths from the four marker phylogram. Lower decimal values represent branch length distances between taxa. Upper whole numbers represent inferred base differences between taxa (4444 total bases).

A. pediculus 020	0	0	223	296	237	285	305	305	392
A. pediculus 008	0	0	223	296	237	285	305	305	392
A. pediculus 019	0.0501	0.0501	0	364	305	353	373	373	460
A. calumetica 094	0.0666	0.0666	0.0819	0	214	262	282	282	369
A. affinis 016	0.0533	0.0533	0.0686	0.0481	0	170	191	191	278
A. copulata 095	0.0640	0.0640	0.0793	0.0589	0.0383	0	66	66	204
A. copulata 107	0.0687	0.0687	0.0840	0.0635	0.0430	0.0148	0	5	224
A. copulata 021	0.0687	0.0687	0.0840	0.0635	0.0430	0.0148	0.0012	0	224
A. ovalis 013	0.0883	0.0883	0.1036	0.0831	0.0626	0.0458	0.0505	0.0505	0.0
	A. pediculus 020	*A. pediculus* 008	*A. pediculus* 019	*A. calumetica* 094	*A. affinis* 016	*A. copulata* 095	*A. copulata* 107	*A. copulata* 021	*A. ovalis* 013

Table 8.3. Phylogenetic distances between taxa from *Halamphora* Clade A based on branch lengths from the four marker phylogram. Lower decimal values represent branch length distances between taxa. Upper whole numbers represent inferred base differences between taxa (4444 total bases).

H. hyalina 061	0	881	1655	1877	2166	2197	2250
H. hyalina 136	0.1983	0	975	1196	1486	1517	1570
H. hyalina 037	0.3724	0.2193	0	1242	1531	1562	1616
H. sp. nov. 081	0.4223	0.2692	0.2795	0	1321	1351	1405
H. semperpalorum 142	0.4874	0.3344	0.3446	0.2972	0	186	239
H. semperpalorum 137	0.4943	0.3413	0.3515	0.3041	0.0418	0	204
H. semperpalorum 047	0.5064	0.3533	0.3635	0.3161	0.0538	0.0460	0.0000
	H. hyalina 061	*H. hyalina* 136	*H. hyalina* 037	*H. sp. nov.* 081	*H. semperpalorum* 142	*H. semperpalorum* 137	*H. semperpalorum* 047

Table 8.4. Phylogenetic distances between taxa from *Halamphora* Clade G based on branch lengths from the four marker phylogram. Lower decimal values represent branch length distances between taxa. Upper whole numbers represent inferred base differences between taxa (4444 total bases).

H. oligotraphenta 009	0	449	437	442	443	492
H. pratensis 106	0.1011	0	339	344	344	599
H. veneta 005	0.0984	0.0763	0	27	28	587
H. coloradiana 025	0.0995	0.0774	0.0061	0	27	592
H. cf. veneta 017	0.0996	0.0775	0.0062	0.0061	0	593
H. elongata 001	0.1108	0.1348	0.1321	0.1332	0.1333	0
	H. oligotraphenta 009	*H. pratensis* 106	*H. veneta* 005	*H. coloradiana* 025	*H. cf. veneta* 017	*H. elongata* 001

These two examples clearly illustrate very different degrees of linkage between molecular and morphological divergence within *Amphora* and *Halamphora* lineages. In the case of *Amphora* genetic distances between taxa that have been classified within the same species (0.0735 and 0.0499 between *A. sp. nov.* 044 and *A. abludens* 072 and between *A. sp. nov.* 026 and *A. graeffeana* 074, respectively), are as great or greater than what is seen in extremely morphologically divergent forms such as *A. affinis* and *A. calumetica* (0.0481). *Taxa* within *Halamphora* provide an even more striking example with molecular divergence within the nearly morphologically identical *H. hyalina* group (0.1983 between *H. hyalina* 061 and *H. hyalina* 163) orders of magnitude greater than the molecular divergences within the clearly morphologically defined *H. veneta* clade (0.0061 between *H. coloradiana* and *H. veneta*). How this understanding of molecular diversity within diatoms translates into a taxonomic system that is still largely based and dependent on morphological identifications remains to be seen. One difficulty arises from the fact that no standards have been set for molecular separation of new species within diatoms, although molecular techniques have been used for the identification of so-called 'cryptic species' (Beszteri et al. 2005, Amato et al. 2007, Evans et al. 2007, Poulíčková et al. 2010) Although not the primary consideration in systematic investigations, the utility of these splits and how they will be received and utilized by the broader community must none-the-less be considered, as well as how to describe and voucher such specimens (Alverson 2008, Tripp & Lendemer 2014).

This variability between molecular and morphological divergence will no doubt be a continuing issue as the species concept within diatoms continues to evolve from a largely morphological concept (Mann 1999b) into one which will likely rely to a greater extent on molecular characterization (Beszteri et al. 2005, Alverson 2008, Evans et al. 2008, Poulíčková et al. 2010, Hamsher et al. 2013, Hamsher & Saunders 2014). A more immediate challenge is the assumed monophyly of morphological groups. Molecular phylogenetic analyses have consistently demonstrated that morphological features long considered important synapomorphies within diatoms, including general valve symmetry (Alverson et al. 2006, Theriot et al. 2010, 2015), amphoroid symmetry (Stepanek & Kociolek 2014), the presence or absence of a raphe (Kociolek et al. 2013, Li et al. 2015) and the canal raphe system (Sorhannus 2004,

Ruck & Theriot 2011) among others, have been found to be paraphyletic or homoplasious. Given the current phylogenetic understanding of the genera *Amphora* and *Halamphora* this trend appears to extend to intrageneric morphological features as well (Figs 8.5, 8.7). Although most the lineages within *Amphora* and *Halamphora* are well supported molecularly, the challenge moving forward will be in assigning taxa to these lineages given the apparent lack of synapomorphies available.

This disjunct between morphology and phylogeny at many evolutionary scales highlights a great challenge and important area for future diatom research. Although morphology has played the primary role in diversity and ecological research, the genetic basis for the incredible morphological diversity seen within the group remains unknown. Because of this, there is an equal lack of knowledge concerning the regulatory controls that may lead to dramatic changes in morphological appearance and how drift and selection may act on these controls to produce the variety of forms seen. Until the basis of morphological diversity within the group is understood, reconciling these two lines of evidence will be difficult, as will the debate over which, molecules or morphology, has the greatest utility in cataloging and classifying the diversity of this important group of micro-algae.

Movement between fresh and salt waters

The prevalence, timing and direction of movements of diatom lineages between freshwater and marine systems continues to be an active area of investigation (Round and Sims 1980, Mann 1999a, Alverson et al. 2007, 2011, Alverson 2014). Conductivity was once considered a significant barrier to the dispersal of diatoms and the transition from one habitat to the other was thought to be a very rare evolutionary event (Round and Sims 1980, Mann 1999a). This is exemplified by the salinity barrier being referred to as a ‘Rubicon’ (Mann 1999a). Although this fundamental ecological split was based on the observation that very few diatom genera are found in both habitats, a growing body of research is beginning to indicate that the frequency of these crossing events is greater than previously thought (Alverson et al. 2007, 2011, Alverson 2014). *Amphora* and *Halamphora* are interesting subjects for studying this phenomenon as both genera have considerable diversity in marine, brackish and freshwater

environments. In addition to the inland freshwater and coastal marine habitats, both genera are also well represented in elevated conductivity inland habitats (Stepanek & Kociolek 2013, Stepanek & Kociolek 2015) and it has been postulated that these inland environments may be an intermediate step between marine and freshwater habitats (Stepanek & Kociolek 2015).

A reconstruction of the ancestral habitat type and conductivity indicates two different patterns of lineage movement in *Amphora* and *Halamphora* (Figs 8.13, 8.14). Given the currently investigated taxa, *Amphora* demonstrates a pattern of habitat preference that more closely aligns with what would be predicted in the 'Rubicon' model. In this case it appears that there is a single transition from a coastal marine to into inland habitats followed by a diversification within freshwaters (Fig. 8.13). In this scenario, the reconstruction indicates the ancestor of the *A. allanta–A. copulata* clade likely moved from a coastal marine habitat to an elevated conductivity inland habitat leading to two inland clades. One clade includes two taxa still found in elevated conductivity inland habitats, *A. allanta* and *A. waldeniana*, and what may represent a move back into a coastal marine habitat in *A. proteoides*. The second clade, *A. pediculus–A. copulata* represents a diversification within inland freshwaters and includes many of the most widely reported freshwater *Amphora*.

The taxa sampled here clearly indicate that the genus is primarily and ancestrally coastal marine, and a freshwater habitat preference is a derived state (Fig. 8.13). Although the sampling of freshwater *Amphora* in this analysis is far from comprehensive, with many large lake forms not represented (Levkov 2009), the majority of the freshwater morphologies correspond well to the morphological forms presented here in the freshwater *Amphora* clade and for this reason although the number of freshwater incursions may change the ancestral condition may not.

Whereas *Amphora* was characterized by a single major move into inland habitats and then fresh waters, the habitat reconstruction for *Halamphora* indicates many independent transitions between these habitats (Fig. 8.14). As with *Amphora*, a coastal marine habitat is the estimated ancestral type for *Halamphora*. Unlike *Amphora*, the data presented here indicates as many as 12 independent incursions into inland waters from coastal habitats, with the majority of these inland lineages (7) confined to

elevated conductivity inland waters. Within the five transitions into fresh waters, most are single lineages or include a small amount of sampled freshwater diversity within predominantly and ancestrally high conductivity clades (see Clades F, H and K). Only Clade G shows a pattern of single move into inland freshwater environments followed by species diversification within these habitats.

Although Alverson et al. (2007) found that movement between saltwater and freshwater habitats in the Thalassiosirales was evident in both directions, the pattern in *Halamphora* seems to support the idea that there is a common directionality to these transitions (Round & Sims 1981, Mann 1999a). In this case, although there were as many as 12 moves from coastal marine habitats into inland habitats (freshwater or elevated conductivity), there are only two instances where an ancestrally inland lineage moved back into coastal marine waters (Clades F and K) with the ancestral habitat type rather ambiguous in Clade F. This pattern is somewhat surprising given the notion that, in general, freshwater environments are thought to be the more osmotically challenging habitat (Alverson et al. 2007) for what is an ancestrally marine lineage of micro-algae (Sims et al. 2006). With the physiological adaptations required to cross the saltwater/freshwater salinity barrier still poorly understood within diatoms (Alverson 2007), hypotheses concerning this directionality have centered around the availability of open niche space and lack of competition in derived freshwater habitats (Round & Sims 1981, Mann 1999) as well as the general directional trend seen in other organisms (Lovejoy et al. 1998, Lee & Bell 1999, Lovejoy & Collette 2001, Betancur-R. et al. 2012).

Given the number of coastal–inland and saltwater–freshwater transitions that have taken place within this genus it provides an excellent opportunity to better understand and characterize these habitat shifts within diatoms. Although, given fossil evidence, it appears that diatoms as a whole are ancestrally marine (Sims et al. 2006) and therefore all of the freshwater diversity is the result of incursions of freshwaters from marine lineages, the physiological adaptation that make the move into more osmotically challenging fresh waters is still not understood (Alverson 2007). The genus *Halamphora* provides ample opportunity for future study of the adaptations that make this possible including whether there is a single

best strategy for coping with this osmotic stress, or if there are as many strategies as there are independent colonizations.

Implications for the higher classification of raphid diatoms

With the namesake of the order for which *Amphora* and *Halamphora* belong, *Thalassiophysa hyalina*, being more closely related to the orders Rhopalodiales and Surirellales than it is to either of the amphoroid lineages it is clear that dramatic changes will be necessary to the larger classification of these taxa. This corresponds to a time when, due to large-scale molecular phylogenetic work (Theriot et al. 2010, 2015) the diatom classification system as a whole is in a state of flux. The challenge with the Thalassiophysales taxa currently represented in molecular phylogenies is that *Amphora*, *Halamphora* and *Thalassiophysa* represent a grade of lineages into the Rhopalodiales and Surirellales. Given the limited utility of making *Amphora* and *Halamphora* monotypic orders of diatoms, which would be necessary to keep the Rhopalodiales and Surirellales as orders, a more inclusive system will be necessary.

The simplified cladogram presented as Figure 9 in Stepanek and Kociolek (2014) may serve as an appropriate guide for such a system. In this classification *Amphora* + *Halamphora* + *Thalassiophysa* + Rhopalodiales + Surirellales would be a single taxonomic unit with each of these lineages becoming families with corresponding genera. This organization would not only create a series of monophyletic hierarchal groups but would have a series of morphological synapomorphies that could be assigned to the order and families within (Stepanek & Kociolek 2014).

Proposed classification system

Phylogenetic and taxonomic information from Round et al. (1990), Ruck and Theriot (2011), Stepanek and Kociolek (2014) and this study.

Order: Thalassiophysales Mann

Family: Amphoraceae fam. nov.

Amphora, Catenula?

Family: Halamphoraceae fam. nov.

Halamphora

Family: Thalassiophysaceae Mann

Thalassiophysa, *Undatella*?

Family: Rhopalodiaceae (Karsten) Topachevs'kyj & Oksiyuk

Epithemia, *Rhopalodia*, *Tetralunata*

Family: Auriculaceae Hendey

Auricula

Family: Entomoneidaceae Reimer in Patrick & Reimer

Entomonies

Family: Surirellaceae Kützing

Hydrosilicon, *Petrodictyon*, *Plagiodiscus*, *Stenopterobia*, *Campylodiscus*, *Cymatopleura*

ACKNOWLEDGEMENTS

This research was funded, in part, by a joint National Science Foundation and Japanese Society for the Promotion of Science East Asia and Pacific Summer Institute fellowship NSF EAPSI No. 1316805, a Seed Grant for Innovation from the University of Colorado Boulder and a grant from Prairie Biotic Research.

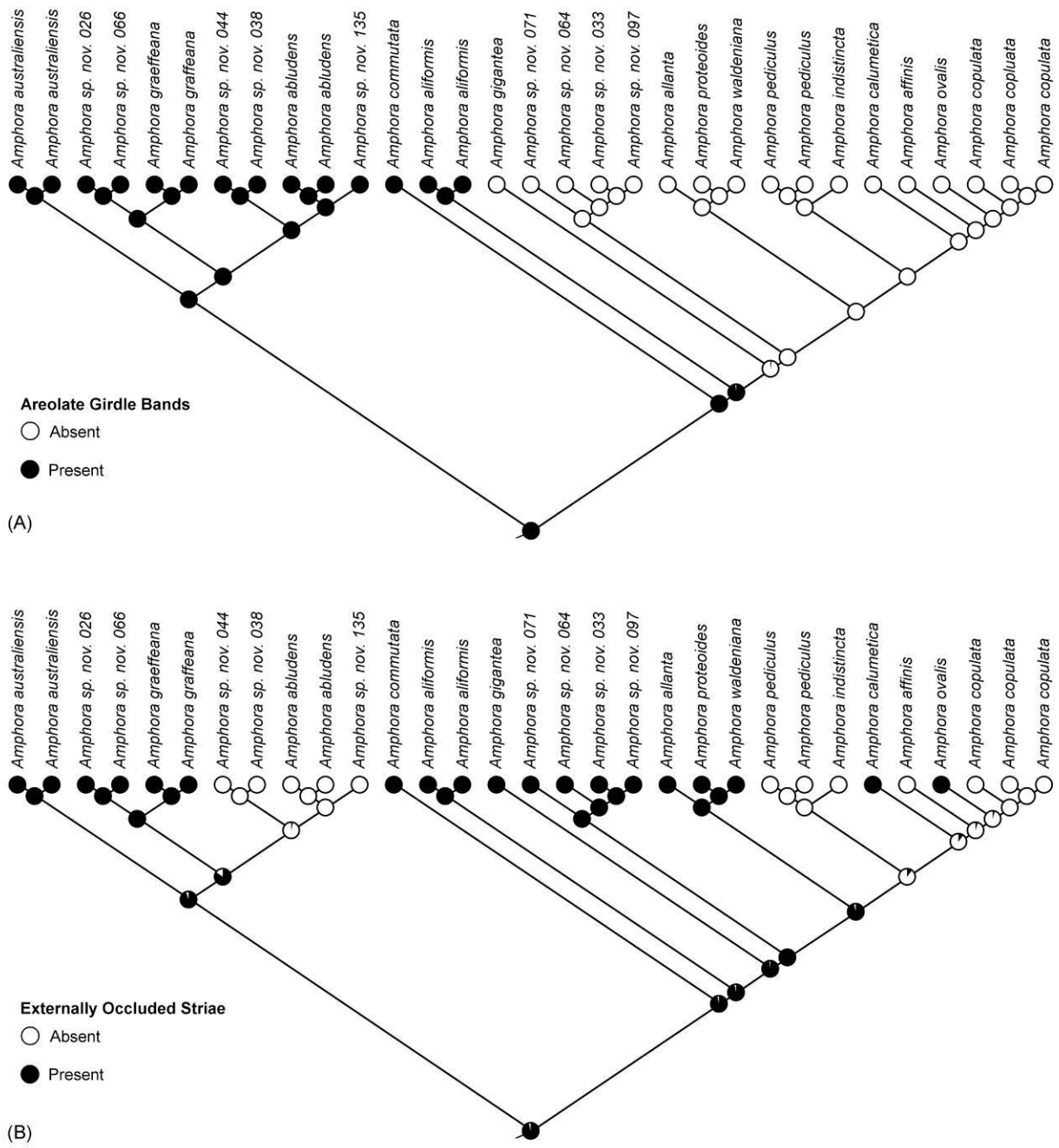

Figure 8.S1. Ancestral state reconstruction of morphological traits within the genus *Amphora* estimated with ML methods. Phylogeny is taken from Fig. 8.2. **A.** Presence or absence of areolae on the girdle bands. **B.** Presence or absence of striae with externally occluded areolae.

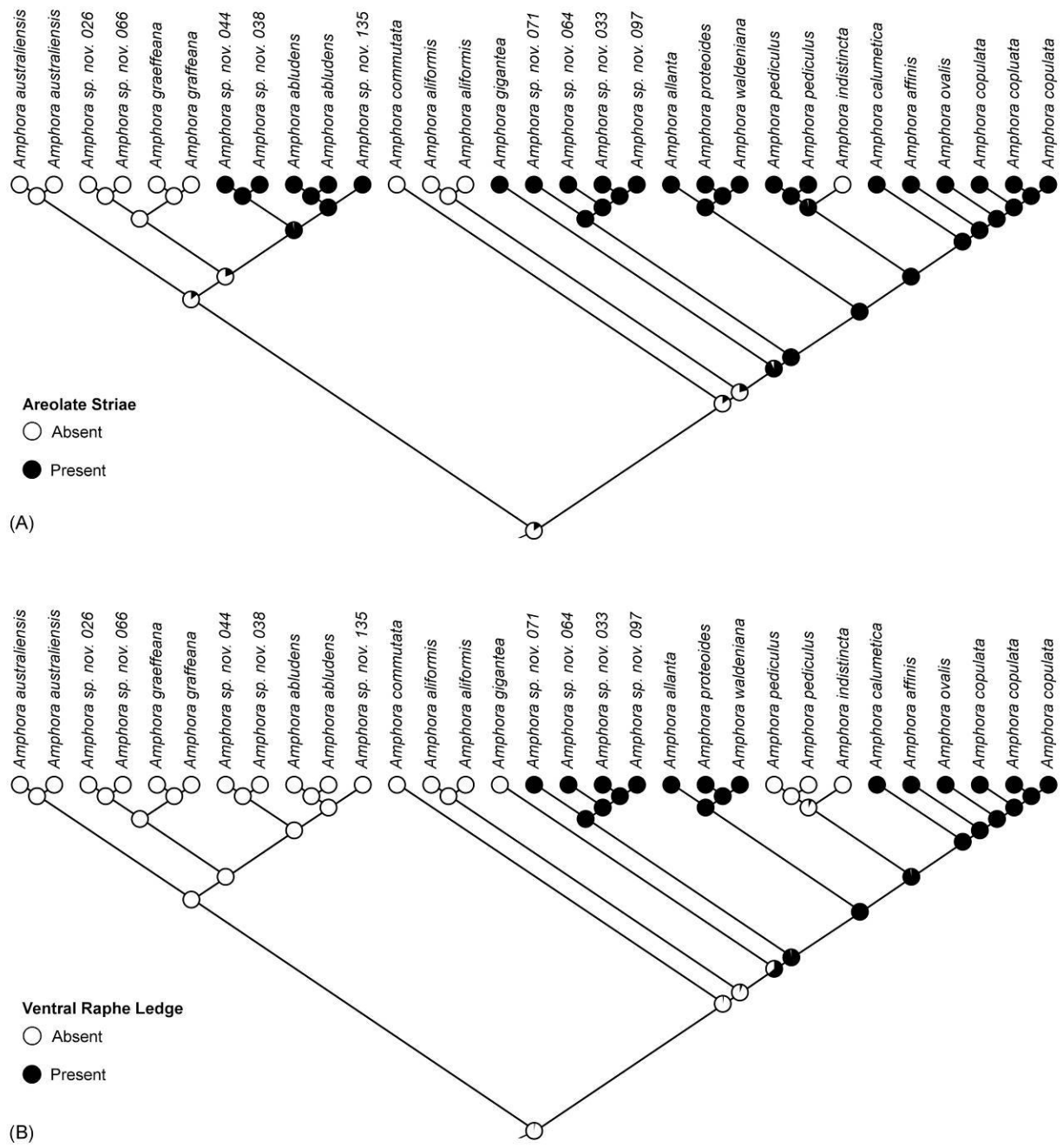

Figure 8.S2. Ancestral state reconstruction of morphological traits within the genus *Amphora* estimated with ML methods. Phylogeny is taken from Fig. 8.2. **A.** Presence or absence of areolate striae. **B.** Presence or absence of a ventral raphe ledge.

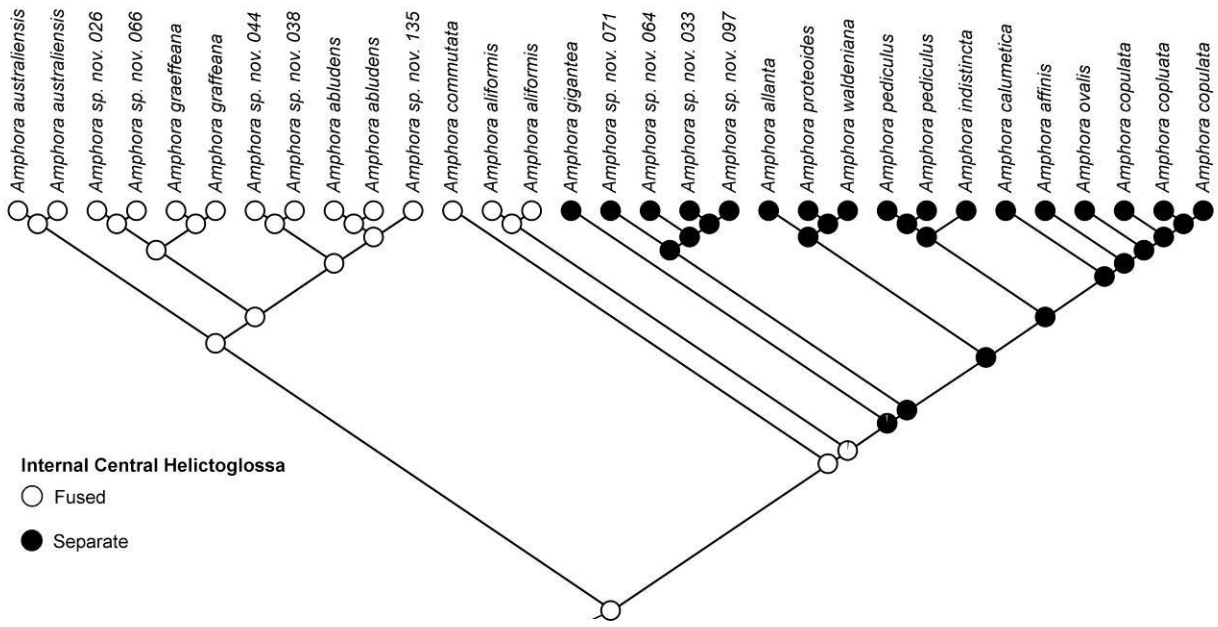

Figure 8.S3. Ancestral state reconstruction of morphological traits within the genus *Amphora* estimated with ML methods. Phylogeny is taken from Fig. 8.2. Presence of a fused or separate central helictoglossae.

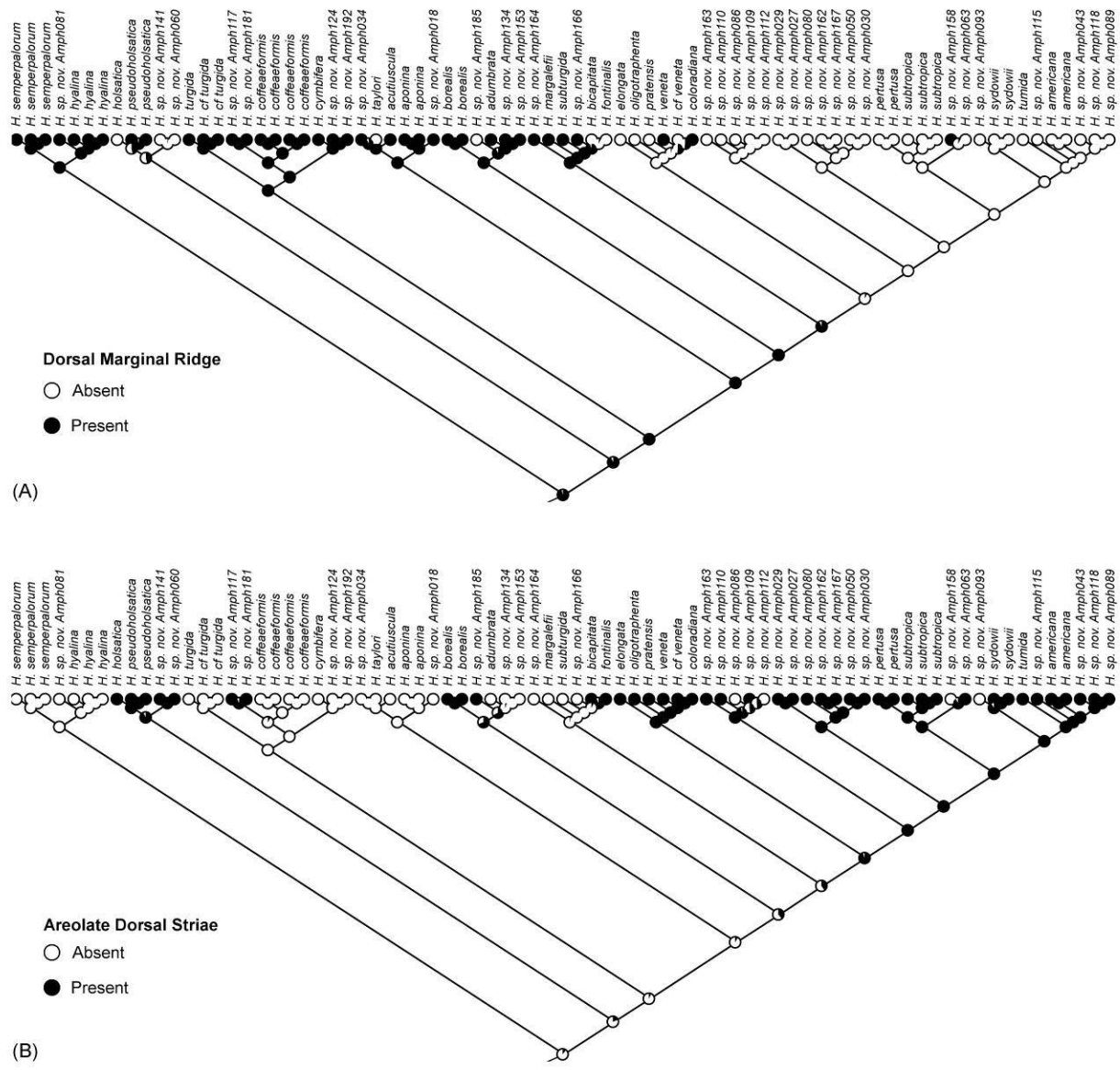

Figure 8.S4. Ancestral state reconstruction of commonly cited morphological traits within the genus *Halamphora* estimated with ML methods. Phylogeny is taken from Fig. 8.6.

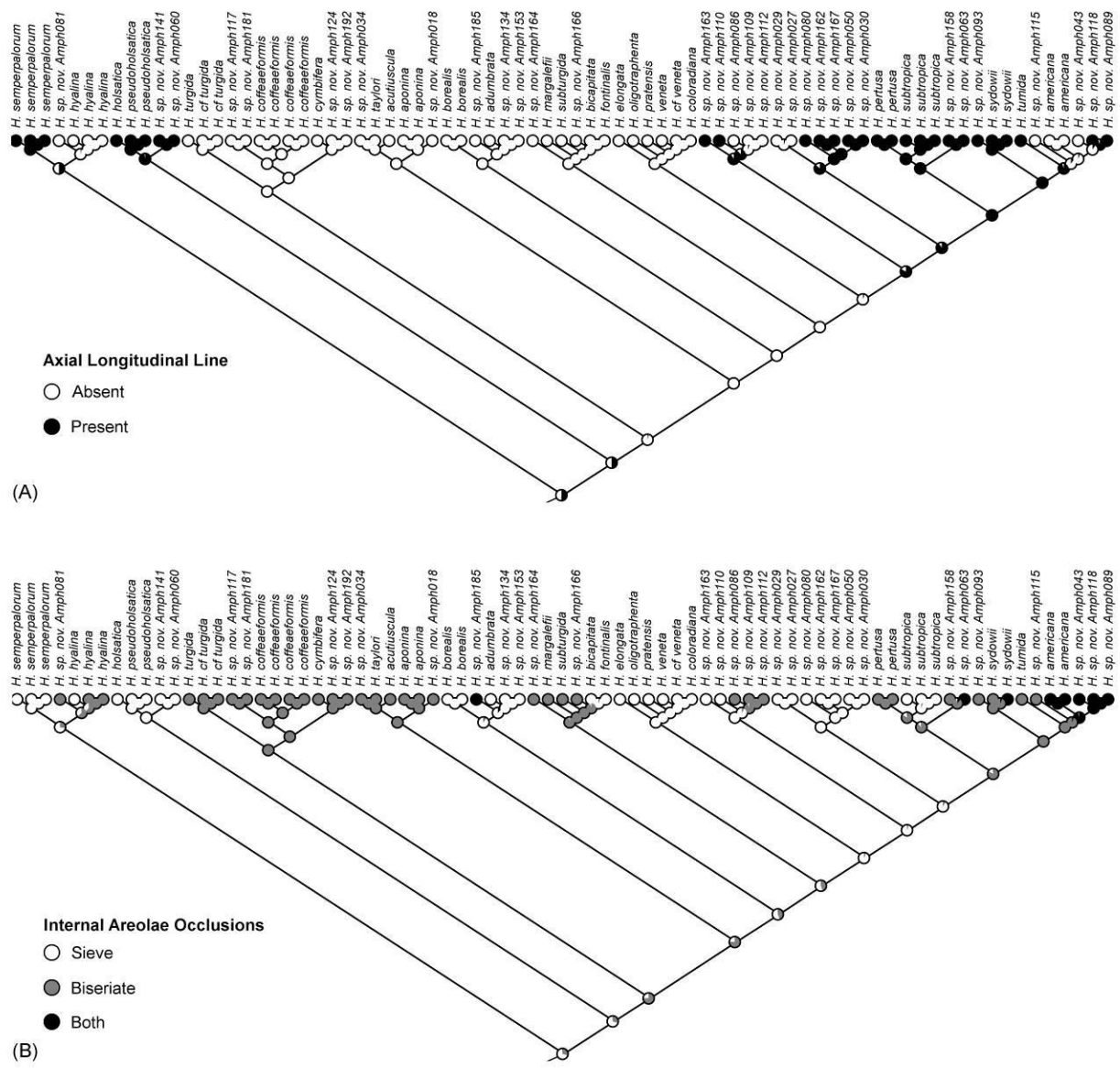

Figure 8.S5. Ancestral state reconstruction of commonly cited morphological traits within the genus *Halamphora* estimated with ML methods. Phylogeny is taken from Fig. 8.6. **A.** Presence or absence of an axial longitudinal line. **B.** Internal areolae occlusions as either a sieve plate only, biseriate occlusions or both occlusion types.

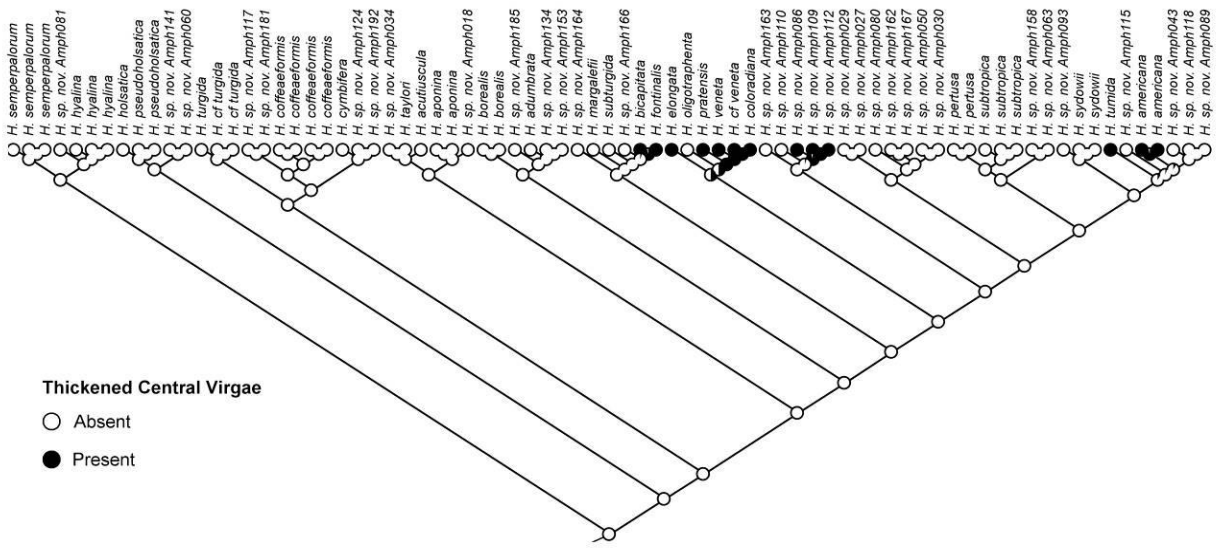

Figure 8.S6. Ancestral state reconstruction of commonly cited morphological traits within the genus *Halamphora* estimated with ML methods. Phylogeny is taken from Fig. 8.6. Presence of absence of thickened central helictoglossae.

SECTION III

LIPID ACCUMULATION WITHIN THE GENUS HALAMPHORA

CHAPTER IX

A COMPARISON OF LIPID CONTENT METRICS USING SIX SPECIES FROM THE GENUS *HALAMPHORA* (BACILLARIOPHYTA)

Adapted from: Stepanek, J.G., Fields, F.J. & Kociolek, J.P. 2016. A comparison of lipid content metrics using six species from the genus *Halamphora* (Bacillariophyta). *Biofuels*. doi:10.1080/17597269.2016.1163216

ABSTRACT

The potential for algal-derived lipid products has been well documented and, therefore, has garnered considerable research attention over the last 30 years. Although promising, hurdles remain in strain selection, optimization and enhancement for commercial production. As this field moves away from the coarse screening efforts that characterized early research and into focused investigations of strain evolution, comparative genetics and genetic engineering, measures of lipid accumulation that are directly comparable and biologically relevant will become increasingly important. Presented here is a comparison of lipid content from six species from the diatom genus *Halamphora*, *H. cf. borealis*, *H. coffeaeformis*, *H. oligotraphenta*, *H. pertusa*, *H. subturgida* and *H. turgida*, utilizing four lipid reporting methods. Methods examined include percent dry weight and milligrams per liter, as well as newly proposed metrics of lipid per cellular volume and lipids per cell per day. The results demonstrate that the method chosen has a dramatic effect on the conclusions drawn concerning promising strains. Furthermore, commonly used metrics may be inappropriate for interspecific comparisons due to confounding effects outside cellular lipid accumulation. The newly proposed methods offer a biologically relevant alternative to the commonly reported lipids as a percent of dry weight.

INTRODUCTION

The great potential for algal derived products, including food (Becker 2007), fuels (Sheehan et al. 1998, Graham et al. 2012, Scholz & Liebezeit 2013), pharmaceuticals (Lincoln et al. 1990, Berge et al. 1997, Desbois et al. 2009, Prestegard et al. 2009), and other high value products (Jin et al. 2003, Singh & Gu 2010, Scranton et al. 2015) have been well documented and reviewed (Chisti 2007, Brennen & Owende 2010, Griffiths & Harrison 2009). The advantage of utilizing microalgae is largely driven by the high per acre lipid productivity and broad ecological tolerances exhibited by many examined algal strains (Sheehan et al. 1998), as well as the ability of some to dedicate a considerable proportion of their mass to the storage of lipids when compared to terrestrial feedstocks (Chisti 2007).

Within this evolutionarily diverse group of organisms, diatoms (Bacillariophyta), characterized by their primary photosynthetic pigments being chlorophylls *–a* and *–c* and highly ornate silica cell wall (termed a frustule), are often referenced as one of the most promising groups for continued lipid production research (Sheehan et al. 1998, Graham et al. 2012, Hildebrand et al. 2012, Fields & Kociolek 2015). This attention is not unwarranted as many diatom strains have been shown to grow well in culture, have broad ecological tolerances, exhibit high productivity, and accumulate large amounts of cellular lipids under nutrient-replete and stressed conditions (Sheehan et al. 1998, Graham et al. 2012, Hildebrand et al. 2012, Scholz & Liebezeit 2013, Chtourou et al. 2015, d'Ippolito et al. 2015. Fields & Kociolek 2015). Although promising, many challenges yet remain for large scale production of diatom products, and screening for high lipid producing strains continues to be an area of active research.

As the number of studies examining lipid production, not only for diatoms but across all algal groups, continues to increase, a critical examination of lipid reporting methods seems appropriate. Persistent questions remain concerning how reliable currently reported lipid values can be compared across and within algal groups that may differ vastly in size, morphology and cellular composition (Hildebrand et al. 2012, Fields & Kociolek 2015). This is of special concern when attempting to compare taxa and draw generalizations using the most prevalent reporting method (see Griffiths & Harrison 2009 and Fields & Kociolek 2015 for references), lipid as a percent dry weight (%DW). Putting aside issues

concerning methodological differences between studies, it has been suggested that the silica cell wall of diatoms, by substantially increasing the inorganic biomass of the organism, leads to the dramatic underrepresentation of the actual cellular lipid accumulation (Ramachandra et al. 2009, Hildebrand et al. 2012, Fields & Kociolek 2015). Although this effect would be most pronounced when comparing diatoms to non-siliceous algal lineages such as green algae (Chlorophyta), evidence for variation in silica content and frustule weight between diatom lineages (Martin-Jézéquel et al. 2000, Scholz & Liebezeit 2013) make comparisons within diatoms equally problematic.

While this inconsistency between previously reported data is a concern, looking towards the future, larger issues involve how existing measures fit into the changing landscape of diatom lipid research. Given the incredible diversity present within diatoms (Mann & Vanormelingen 2013 estimate as many as 100,000 extant species) large scale screening efforts epitomized by the aquatic species program (Sheehan et al. 1998) are giving way to more focused strategies to discover high lipid content diatoms and enhance lipid production capabilities. Fields and Kociolek (2015) have proposed an evolutionary approach to diatom strain selection and there is evidence that evolutionary relationships are predictors of lipid content (Fields & Kociolek 2015) as well as fatty acid composition (Galloway & Winder 2015) across large taxonomic groups. These studies have helped guide a better understanding of the basic biology of these organisms and allowed the identification of lineages with high lipid content. Along with the evolutionary approach, genetic engineering and comparative genetics/genomics of algal strains continues to be a robust area of research (Roessler et al. 1994, Dunahay et al. 1996, Rosenberg et al. 2008, Beer et al. 2009, Radakovits et al. 2010, Cheng et al. 2014, Ma et al. 2014, Tanaka et al. 2015) and is likely to increase in diatoms as the number of sequenced full and chloroplast genomes continues to increase (Armbrust et al. 2004, Bowler et al. 2008, Green 2011, Ruck et al. 2014). As research in all these areas continue, it will help focus efforts in molecular labs towards sequencing and genetically modifying more robust strains for commercial production.

All of these strategies (phylogenetic screening, genetic modification, and comparative genetics/genomics) inherently deal with organismal level biology of diatom strains and may not be well

served by the most commonly reported lipid measures. To progress our understanding of the biology behind lipid accumulation at the organismal level, not just general trends across broad taxonomic groups and cultures, requires the ability to make accurate comparisons of lipid content between strains and requires a biologically relevant method of reporting lipid accumulation and production.

This study will use newly generated lipid accumulation data for six species from the diatom genus *Halamphora* (Kützing) Levkov, including *H. cf. borealis* (Kützing) Levkov, *H. coffeaeformis* (Agardh) Levkov, *H. oligotraphenta* (Lange-Bertalot) Levkov, *H. pertusa* Stepanek & Kociolek, *H. subturgida* (Hustedt) Levkov and *H. turgida* (Gregory) Levkov (Figure 9.1), to compare previously reported and newly proposed lipid reporting methods.. These taxa were chosen as they represent the range of ecological setting in which *Halamphora* taxa are typically found, including fresh (*H. oligotraphenta* and *H. subturgida*), brackish (*H. coffeaeformis*) and saltwater (*H.* cf. *borealis*, *H. pertusa*, *H. turgida*) habitats and members of this genus have been previously shown to exhibit high lipid accumulation (Sheehan et al. 1998, Graham et al. 2012, Scholz & Liebezeit 2013, Chtourou et al. 2015). The reporting methods compared will include the previously used measures %DW, milligrams of lipid per liter of culture (mg l^{-1}) and percent organic dry weight (%ODW), as well as newly proposed measures lipid mass 100 μm^{-3} of cellular volume (pg 100 μm^{-3}) and lipid production $cell^{-1}$ day^{-1} (pg $cell^{-1}$ day^{-1}).

The results from these comparisons will be used to 1) assess variation in lipid accumulation between closely related species and reporting methods, 2) demonstrate how reporting method choice affects conclusions drawn concerning high lipid accumulating strains, 3) critically evaluate the reliability and potential confounding factors of commonly used methods, 4) propose lipid accumulation per cellular volume as a biologically meaningful alternative to previous methods for reporting lipid accumulation.

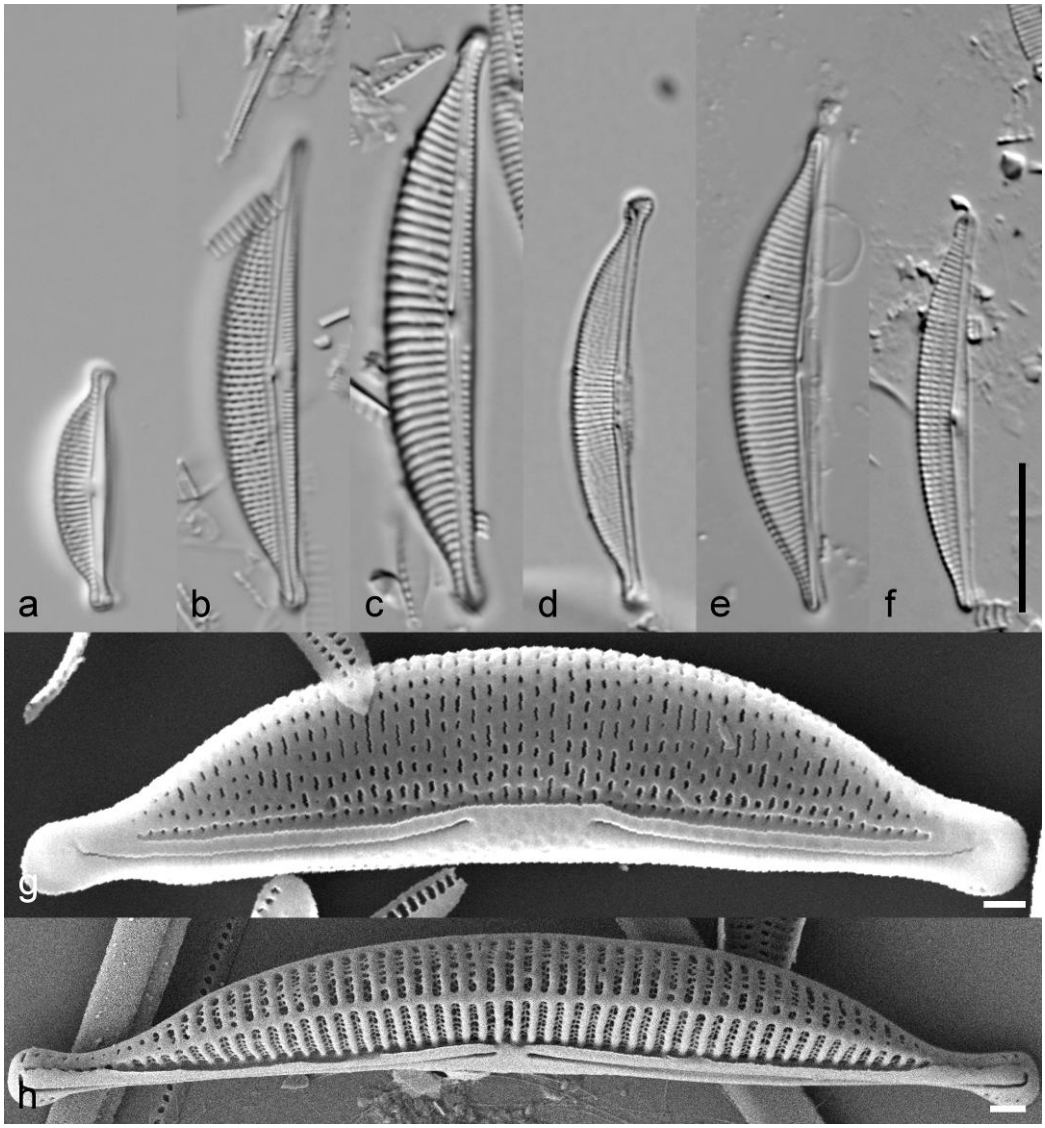

Figure 9.1. Light micrographs (A–F) and scanning electron micrographs (G, H) of cleaned frustules of the *Halamphora* species included in this investigation. (A) *Halamphora subturgida*. (B) *Halamphora pertusa*. (C) *Halamphora turgida*. (D) *Halamphora oligotraphenta*. (E) *Halamphora coffeaeformis*. (F) *Halamphora* cf. *borealis*. (G) *Halamphora oligotraphenta* showing heavily silicified features. (h) *Halamphora coffeaeformis* showing more lightly silicified features. Scale bars a–f = 10 µm, g, h = 1 µm.

MATERIALS AND METHODS

Isolation and culturing

The algal strains used in this study were collected from waters in Colorado, Florida, North Dakota and Utah from 2012 to 2014 with representatives from fresh, brackish and saltwater environments (Appendix 1). Strains were isolated into monoculture via micro-pipette serial dilution. Taxa were grown and maintained in one of three culture media depending on the conductivity of the of the collection site. Media used include WC medium (Guillard & Lorenzen 1972) for freshwater taxa or an artificial saltwater medium using the artificial sea salts Instant Ocean (Spectrum Brands, Inc., Blacksburg, Virginia, USA) with the addition of WC nutrients. The silica concentration, often a limiting nutrient for diatoms and demonstrated to affect productivity and stationary phase cell densities (Graham et al. 2012, Hildebrand et al. 2012), was doubled from the original recipe to Na_2SiO_3 56.84 mg l^{-1} in all media. The conductivity of the artificial saltwater medium was tailored to the collection site with conductivities of 15 and 50 mS cm^{-1} for the brackish and saltwater media, respectively. Cultures were maintained at ca. 25°C under fluorescent lights (illumination ca. 50 µmol m^{-2} S^{-1} total irradiance) with a 12:12 light:dark cycle.

All light microscope (LM) images were taken using an Olympus BX-51 light microscope (Olympus America Inc., Center Valley, Pennsylvania, USA) and captured with an Olympus DP71 digital camera. Scanning electron microscope (SEM) images were taken using a JEOL JSM 7401 field emission SEM (JEOL Ltd., Tokyo, Japan).

Growth and lipid accumulation experiments

In order to maintain consistent nutrient levels across media of differing conductivity (Instant Ocean contains measurable concentrations of macro- and micro-nutrients), UTEX Artificial Seawater Medium (UTEX Culture Collection, University of Texas, Austin, USA) was used for all lipid production experiments. As with the Instant Ocean media, nutrient levels were based on the WC medium concentrations with double the silica levels. Stock cultures were allowed to acclimate to the experimental medium for a minimum of two weeks before lipid production experiments were performed. All growth

and lipid production experiments were performed, in triplicate, in 250 ml Erlenmeyer flasks. Initial inoculations consisted of 5 ml of actively growing stock culture added to 220 ml of growth medium. The experiments were conducted in a VWR Signature Diurnal Growth Chamber (VWR International, Radnor, Pennsylvania, USA) at 25°C, at an irradiance of ca. 120 μmol m^{-2} S^{-1} and a 12:12 light:dark cycle. Although growth conditions were not optimized for each taxon, similar standard conditions have been extensively used when comparing lipid production across multiple diverse taxa (Dempster & Sommerfeld 1998, Nascimento et al. 2013, Cheng et al. 2014, Fields & Kociolek 2015). During the experimental growth period, the cultures were continuously stirred with small stir bars in each flask and bubbled continuously with humidified filtered air (0.2 μm inline filter).

Growth was monitored daily by counting a full transect on a Palmer counting cell at 40x magnification. Maximum growth rate (μ) and divisions per day were calculated over the 48 hours that exhibited the fastest growth. As the exponential growth phase began to slow but while the cultures were still actively growing (typically between five and ten days), a 50 percent exchange of the growth medium with fresh medium was performed and repeated on consecutive days before cell harvest. This was done to help ensure that the results were not affected by nutrient limitation at the time of cell harvest. For each experimental replicate a 10 ml subsample for final cell count and biovolume measurement was taken, preserved in glutaraldehyde and stored in the dark at ca. 2°C. For lipid extraction, 200 ml of culture was filtered onto pre-weighed 47 mm Whatmann GF/C glass fiber filters (GE Healthcare Biosciences, Pittsburg, Pennsylvania, USA) and stored at −20°C until extraction.

Before lipid extraction, filtered diatoms were dried overnight in a drying oven and placed in a desiccator under vacuum for a minimum of two hours before weighing with a Mettler Toledo ML204 analytical balance (Mettler-Toledo International Inc., Columbus, Ohio, USA) with readability to 0.0001 grams. The original filter mass was subtracted from the mass of the filter plus diatoms to obtain the total dry mass of each replicate. Lipid extractions were performed using a Soxhlet extraction method, using 80 ml of a 2:1 chloroform methanol mixture for an 18 hour extraction period. After extraction, the solvent was evaporated using a Kuderna-Danish Concentrator to a volume less than 3 ml where the sample was

transferred to a pre-weighed glass vials and allowed to further air dry. To ensure that the final lipid mass was not affected by any residual salts from the growth medium, the dried lipid was re-dissolved in chloroform and transferred to a new vial for final lipid mass. Before final weighing, the vials with extracted lipids were held in a desiccator under vacuum for a minimum of two hours.

Final cell counts and cell biovolumes were measured using the preserved subsamples. Final cell counts were calculated using the same method as the growth rate cell counts. To estimate mean culture biovolume, 20 images were captured for each taxon at 100x magnification. Cellular measurements were made on the imaged cells in Gimp 2.8.10 (www.gimp.org) and biovolumes were estimated using Hillebrand et al.'s (2012) equation for the genus *Amphora*.

Ash free dry mass

For quantification of ash free dry weight (AFDW), cultures were grown as in the lipid production experiments. To minimize the number of dead cells included, cells for AFDW were harvested near the end of the exponential growth phase when growth had begun to slow but cells were continuing to divide. Cultures were pelleted by centrifugation in 50 ml centrifuge tubes and the pellets were rinsed with distilled water and re-centrifuged two times to remove residual salt from the pelleted cells. The culture pellets were re-suspended in distilled water and filtered onto pre-weighed and incinerated 47 mm Whatmann GF/C glass fiber filters. These filters were dried overnight in a drying oven and weighed after a minimum of two hours under vacuum in a desiccator. Filters were then placed in a muffle furnace for 1.5 hours at 550°C to burn off the organic portions of the cell and re-weighed.

Lipid production and accumulation calculations

Lipid production and accumulation values were calculated as follows:

Percent dry weight: % DW = Total extracted lipid weight / Total dry cellular weight * 100

Milligrams lipid per liter: mg l^{-1} = Total extracted lipid from 200 ml at time of harvest * 5

Lipid mass per cell: Lipid $cell^{-1}$ = Total extracted lipid / Cell count at harvest

Lipid mass per 100 μm^{-3} of cellular volume: Lipid $100\mu m^{-3}$ = Lipid $cell^{-1}$ / cell volume * 100

Lipid production per cell per day: Lipid day−1 = Lipid $cell^{-1}$ * Divisions day^{-1}

Significant differences in the reported data were determined by one-way ANOVA performed in RStudio ver. 0.99.473.

RESULTS

Lipid content

The results for all of the calculated lipid reporting methods are listed in Table 9.1. The most commonly reported measure, %DW, shows a significant difference between the mean accumulation values ($p=0.001$), with values ranging from 12–25% (Figure 9.2A). Within this measure, *H. subturgida* and *H. pertusa* were the top accumulators with 25% and 24%, respectively. These taxa exhibited significantly higher yields than the lowest three producers ($p<0.05$ for all comparisons) and the lowest two producers ($p<0.04$ for all comparisons) for *H. subturgida* and *H. pertusa*, respectively.

The other commonly reported measure of lipid content, mg l^{-1}, shows a very different pattern from %DW (Figure 9.2B). While also exhibiting a significant difference between means ($p<0.001$), this measure shows over an order of magnitude difference between the lowest (*H. subturgida*, 6.0 mg l^{-1}) and highest (*H. turgida*, 77.7 mg l^{-1}) values. In this measure *H. turgida*, *H. coffeaeformis* and *H. pertusa* were the top accumulators with *H. turgida* significantly greater than the other five taxa ($p<0.001$ for all comparisons) and *H. coffeaeformis* significantly greater than the lowest performing three taxa ($p<0.001$ for all comparisons).

The proposed measure, pg 100 μm^{-3} of cellular volume, gives an indication of how much cellular space is being dedicated towards lipid storage, taking into account not only lipid accumulated but also the size of the cell (Figure 9.2C). Values for this measure showed a significant difference between means ($p<0.001$), with values ranging from 7.3–51.2 pg 100 μm^{-3}. Within this measure *H. turgida* and *H. cf. borealis* were the highest accumulators having significantly greater lipid content than the remaining four taxa ($p<0.04$ and $p<0.003$ for all comparisons, respectively).

Table 9.1. Results from growth and lipid accumulation experiments for six *Halamphora* species, including growth rate, biovolume, inorganic fraction of cell weight and six measures of lipid accumulation. Bold values highlight the two taxa that would be considered the top producers under each method.

Taxon	Growth Rate (μ)	Biovolume (μm^3)	Percent Inorganic	pg/Cell		% DW		mg/l		pg/100 μm^3		pg/Cell/Day		% ODW	
				Mean	SE	Mean	SE	Mean	SE	Mean	SE	Mean	SE	Mean	SE
H. subturgida	0.26	94	46	34.3	5.5	**25.1**	2.9	6.0	1.0	36.7	5.8	12.9	2.1	**46.0**	5.2
H. pertusa	1.33	365	31	**82.2**	2.7	**24.1**	0.4	46.2	4.6	22.5	0.7	**157.8**	5.1	35.2	0.6
H. turgida	1.16	278	30	**142.5**	6.7	18.8	0.7	**77.7**	3.2	**51.2**	2.4	**238.5**	11.2	26.8	1.1
H. oligotraphenta	0.33	178	55	39.2	4.9	17.1	2.3	6.5	1.5	22.0	2.7	18.6	2.3	**37.8**	5.2
H. coffeaeformis	1.01	864	30	63.0	3.9	15.8	1.2	**50.3**	1.7	7.3	0.5	91.8	5.7	22.6	1.7
H. cf. borealis	0.98	62	35	27.8	1.1	12.1	0.3	30.3	1.9	**44.9**	1.8	39.3	1.6	18.4	0.4

Finally, the measure of pg of lipid produced cell^{-1} day^{-1} takes into account the lipid accumulated within a cell as well as how many times per day the cell divides (Figure 9.2D). Again, there was a significant difference between the means ($p<0.001$) with values spanning over an order of magnitude from 12.9–238.5 pg cell^{-1} day^{-1}. Within this measure *H. turgida* and *H. pertusa* were the highest producers with *H. turgida* having significantly greater lipid production than the other five taxa ($p<0.001$ for all comparisons) and *H. pertusa* having significantly greater lipid production than the lowest four producers ($p<0.001$ for all relationships).

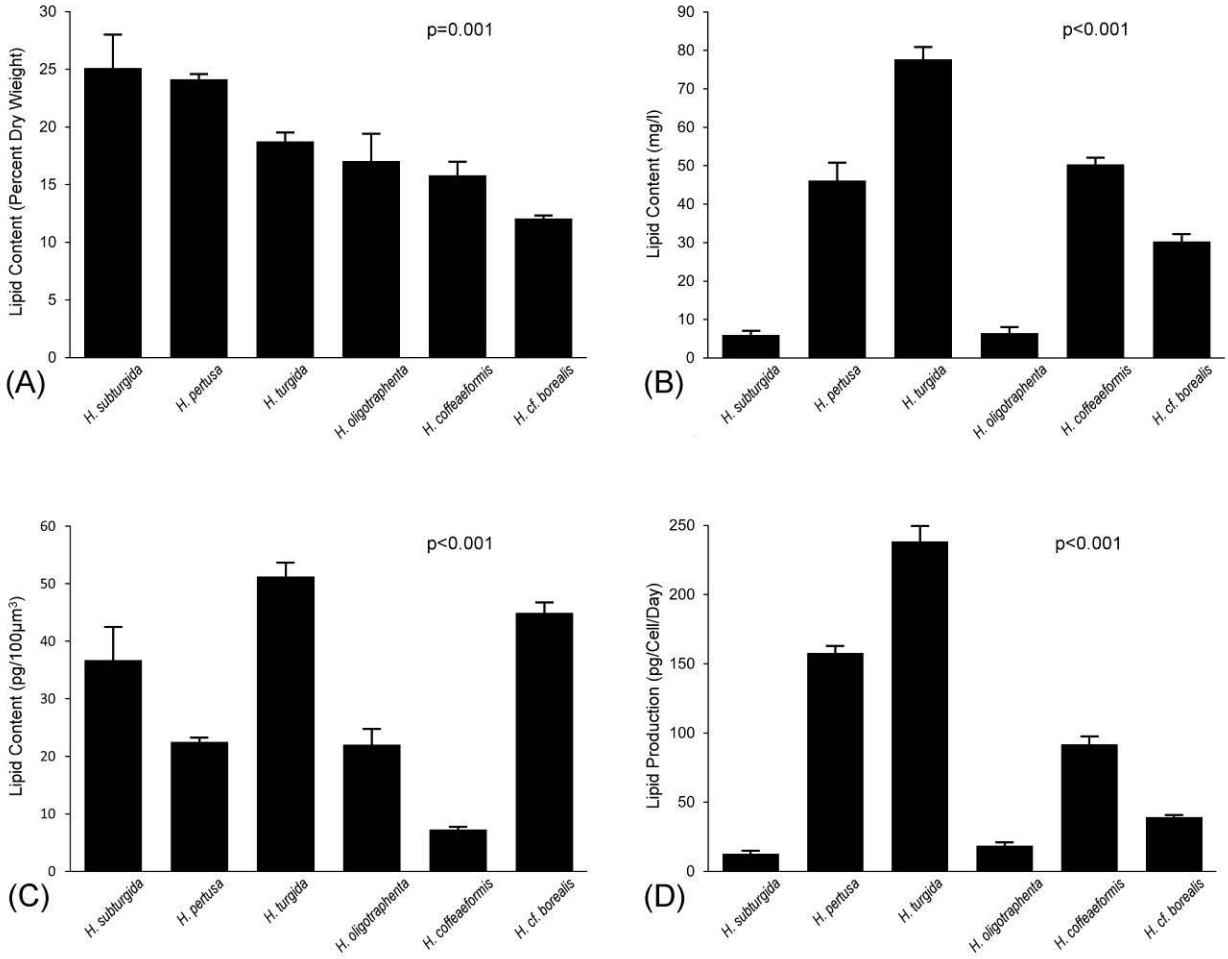

Figure 9.2. Results from lipid accumulation experiments reported using four different metrics. (A) Mean lipid content reported as a percent of dry cell weight. (B) Mean lipid production reported as mg lipid per liter of culture. (C) Mean lipid content reported as pg lipid per 100 µm^{-3} of cellular volume. (D) Mean lipid production reported as pg lipid produced per cell per day. Error bars represent standard error of the mean. P-values indicate a significant difference between means as determined by one-way ANOVA.

Percent inorganic dry mass

The silica cell wall of diatoms has been cited as a potentially confounding factor in accurately representing lipid accumulation in diatoms. Table 9.1 lists the percent of dry weight of the included taxa that was attributed to inorganic materials. The average percent inorganic for all six taxa was 38% with a range of values from 30–55%. Additionally, there appears to be a relationship between conductivity and the percent inorganic dry weight, similar to a pattern described by Martin-Jézéquel et al. (2000). The brackish and marine taxa (*H. cf. borealis*, *H. coffeaeformis*, *H. pertusa* and *H. turgida*) exhibit a range of 30–35%, whereas the freshwater taxa (*H. oligotraphenta* and *H. subturgida*) show considerably higher proportions of their biomass as inorganic material at 55% and 47%, respectively.

With these percent inorganic dry weight values it is possible to estimate lipids as a percent dry weight of only the organic portion of the cell biomass (%ODW) (Table 9.1). These values range from 18–46%, with *H. oligotraphenta*, *H. pertusa* and *H. subturgida* exhibiting over 30% of their organic dry weight as lipids.

DISCUSSION

The conclusions drawn from this experiment vary dramatically depending upon the measure of lipid content reported for these six closely related species of diatoms (Table 9.1). When viewed through the common lipid measure of %DW, the range of values, 12–25%, are fairly consistent with other reported values for diatoms grown in a nutrient replete environment (Scholz & Liebezeit 2013, Fields & Kociolek 2015, Chtourou et al. 2015). In this case, although the range of values is not extreme, there is significant variation in lipid production across these taxa ($p=0.001$), with *H. subturgida* and *H. pertusa* exhibiting greater lipid production than the remaining four taxa.

Although %DW continues to be the standard reporting method, researchers have also used the lipid content per volume measure mg l^{-1} to report lipid yields for a given culture (Dempster & Sommerfeld 1998, Graham et al. 2012, Cheng et al. 2014, d'Ippolito et al. 2015). This strategy produces very different results than % DW with a nearly ten-fold difference in lipid content between the lowest (*H.*

subturgida) and the highest (*H. turgida*) accumulator. If using these data to select promising strains, the conclusions arrived at are heavily dependent on the methods used to report lipid yield (Figs 9.2A,B). In this case, not only do the taxa with the greatest lipid content differ between reporting methods, but the taxon with the highest %DW (*H. subturgida*) exhibits the lowest mg l^{-1} values.

The discrepancy between these values arises due to inherent problems with each. Percent dry weight is a popular reporting measure since it relies on relatively simple measurements (measured lipid mass / measured cellular mass) that give some indication as to the amount of lipid that could be harvested from a specific amount of biomass. From a biological perspective, however, this value has the potential to be heavily influenced by any confounding factor that alters the dry weight of the harvested cells but is not related to the allocation of carbon within the cell. This could include variations in the inorganic portions of the cell such as frustule weight and cellular salts or unintended non-culture weight such as bacterial contamination and residual salt or water from the growth media. In addition, it has been noted that, within diatoms, some cell death often occurs under nutrient stress which would underestimate the lipid content during these conditions (Fields & Kociolek 2015).

As was previously stated, this bias will be most acutely seen when comparing diatoms to other non-silicified algal groups that have a much lower proportion of inorganic cellular mass (Hildebrand et al. 2012). However, even when comparing six species from within a single genus of diatoms, the inorganic portion of the cellular weight ranges from 30–55%, and may reflect species-level differences in frustule morphology and silicification across a diatom lineage (Fig. 9.1). We would expect even greater differences as comparisons were made across broader taxonomic categories. Because of this, %DW may not be an accurate reflection of the amount of lipid actually being accumulated within a diatom cell. A more appropriate measure would be %ODW (Table 9.1), in which all of the currently studied taxa show a substantial increase in lipid content from 12–25% to 18–46% in %DW and %ODW, respectively. Additionally, the increase in reported lipid content is not uniform between species, with the two most heavily silicified taxa as indicated from the percent inorganic measurements, *H. oligotraphenta* and *H.*

subturgida, showing the greatest corresponding increase in lipid content and becoming top producers in %ODW.

From a practical standpoint, as is demonstrated in the difference in values in Figures 9.2A and 2B, the ability of a taxon to yield a substantial proportion of its dry weight as lipids, does not necessarily translate into high lipid yield during culturing. The measure of mg l^{-1} is appealing because it inherently combines lipid content with culture density and indicates which species are capable of the highest yields in a commercial setting, but does not take into account the length of time it took to reach those culture densities. Those species with high mg l^{-1} values are likely to have either higher cell densities or higher lipid content. In this case both *H. oligotraphenta* and *H. subturgida* exhibited very slow growth under experimental conditions ($\mu = 0.26$ and 0.33, respectively), leading to low cellular density cultures at the time of cell harvest and the extremely low mg l^{-1} values. Those species with high mg l^{-1} values are likely to have either higher cell densities or higher lipid content.

An alternative to %DW is the measure pg 100 μm^{-3} (Figure 9.2C). This is a biologically-relevant measure of lipid content and is comparable across lineages regardless of size, morphology and cellular composition. This measure essentially illustrates the average proportion of cellular volume that is being dedicated to lipid storage. In this case the measure is illustrated as a weight per volume, but if the average fatty acid composition was known one could calculate a volume of lipid per cellular volume that would describe the proportion of the cell volume that was dedicated to lipid storage. This measure removes the confounding elements of culture weight, and because it is standardized to a measure of cellular volume it removes the cell size bias seen in pg $cell^{-1}$ estimations (e.g. one would expect larger cells to have the ability to store more lipid on a per cell basis than smaller cells simply based on their greater cell volume). In this case, the six *Halamphora* species presented here exhibited substantial variation in lipid stored per cellular unit, with values ranging from 7 pg 100 μm^{-3} for the large celled (864 μm^3) *H. coffeaeformis* to 51 pg 100 μm^{-3} for the moderately sized (278 μm^3) *H. turgida*. Within this measure *H. cf. borealis*, *H. subturgida* and *H. turgida* all exhibit the propensity to dedicate more of their intracellular space to the storage of lipids. This measure will not only allow for comparison across taxa and lineages, but will be a

biologically relevant measure for understanding differences in lipid accumulation between species and accurately reporting differences in lipid accumulation within a single lineage under varied growth conditions.

Although relevant for understanding cellular lipid accumulation, the measure lipid 100 μm^{-3} from a practical standpoint does not indicate potential lipid production in an applied setting. For this measure pg $cell^{-1}$ day^{-1} is appropriate (Fig. 9.2D). This measure is calculated by multiplying the lipids accumulated per cell by the average cellular divisions per day of the taxon. This measure is both biologically and practically relevant as it combines lipid production per cell with overall productivity of the diatom strain to estimate a lipid production value not dependent on culture density at the time of harvest. Because it is scaled per cell and not to biomass, this measure could be used to calculate lipid production at any period within the growth cycle or at any carrying capacity, which is often more dependent on nutrient input than the taxon being grown (Graham et al. 2012, Hildebrand et al. 2012).

The values returned for lipid production per day show a nearly ten-fold difference between the highest and lowest values (Fig. 9.2D). When compared to the lipid per volume measurements it is clear that growth rate is the largest driver of these differences. This will allow for a useful comparison between taxa as it demonstrates not only the amount of lipid that could potentially be produced but parses out the factors leading to this production. Enhancement options would include maximizing the growth rate of taxa that dedicate a large proportion of their cellular space to lipid storage but exhibit low productivity (*H. cf. borealis* and *H. subturgida*), or enhancing the lipid production in highly productive but low lipid producing taxa (*H. coffeaeformis*). Given the diversity of diatom lineages available the best strategy may be to select the taxon that exhibits both traits under the specific culturing conditions required (Sheehan et al. 1998, U.S. DOE 2010). Under the conditions of this experiment, although not exceptional in %DW, *H. turgida* both produced the greatest amount of lipid per cellular volume (51 pg 100 μm^{-3}) while also exhibiting high productivity ($\mu = 1.16$), which led to this taxon surpassing the next closest species in lipid production by 52%.

It is likely that the future of algal lipid research will continue to move away from the large-scale screening of diverse algal taxa that has characterized early efforts (Sheehan et al. 1998). Although these investigations were important for general characterization of algal lipids across broad groups, the scope of the diversity within even the most promising groups (ca. 100,000 extant diatom species) precludes the possibility of even the most basic comprehensive screening. Although this tremendous diversity will be a continuing challenge to bioprospecting efforts, it is also a great asset for the identification of algal strains adapted to site specific growth conditions. Biological approaches to the discovery and enhancement of high accumulating strains, including the phylogenetic, comparative genetics/genomics and genetic engineering approaches previously discussed, will continue to increase. All of these fields will require a measure of lipid content that is comparable between lineages as well as biologically meaningful to the organism under study. Lipid per volume and lipid per cell per day measurements exhibit these characteristics, while at the same time not being mutually exclusive with %DW, allowing these new measures to be included along with the production data generated over the last 30 years of algal lipid research.

ACKNOWLEDGEMENTS

This research was funded in part by a Seed Grant for Innovation from the University of Colorado Boulder.

CHAPTER X

A COMPARATIVE PHYLOGENETIC APPROACH FOR THE EVALUATION OF LIPID ACCUMULATION WITHIN THE DIATOM (BACILLARIOPHYTA) GENUS *HALAMPHORA*

ABSTRACT

Commercial products derived from algal lipids have long been touted as a promising alternative to the petroleum, plant and animal based options currently in wide scale production. Although promising, commercial algal lipid production has not reached predicted levels and current screening efforts may not be meeting the needs of a new generation of algal biomass research. An alternative to the broad based screening efforts that characterized early research is a systematic phylogenetic approach. This method uses a known phylogeny to create an evolutionarily representative taxa subsample for further investigation. Lipid content values can then be compared through a meaningful evolutionary context and predictive conclusions can be drawn. In this investigation, 32 taxa from the diatom genus *Halamphora* where investigated for growth and lipid accumulation under nutrient replete and silica deplete conditions. These measured values were evaluated within the context of the evolutionary relationships between taxa, based on a four marker molecular phylogeny of the genus. Results presented here indicate that there is significant variation within habitat conductivity and lipid accumulation between *Halamphora* taxa and that this variation exhibits a significant phylogenetic signal, in that more closely related taxa resemble each other more than randomly assembled taxa. Because significant signal exists, the *Halamphora* phylogeny can be used as a predictive roadmap for the selection of high lipid accumulating taxa that can be grown under specific conditions.

INTRODUCTION

Algal derived products have been receiving considerable attention recently as an efficient and renewable source for fuels (Sheehan et al. 1998, Graham et al. 2012, Scholz & Liebezeit 2013), nutritional supplements (Becker 2007) and other high value products (Lincoln et al. 1990, Berg et al. 1997, Jin et al. 2003, Desbois et al. 2009, Prestegard et al. 2009, Scranton et al. 2015). Although research into higher-value products continues to grow, the majority of the algal biomass research over the last 40 years has focused on the potential for renewable liquid biofuels produced from micro-algae, an objective that will require highly productive algal strains. Biofuels as a whole are often touted as a promising alternative to fossil fuels as they are renewable, have a lower net release of greenhouse gasses, and can be processed and burned in conventional infrastructure (Gavrilescu & Chisti 2005, Pienkos & Darzins 2009, Scott et al. 2010). Algae are of particular interest as a biomass feedstock as they are more productive per acre than conventional terrestrial oil crops (Chisti 2007), and can be grown in non-agricultural lands using brackish or salt waters (Sheehan et al. 1998, Groom et al. 2008, Pienkos & Darzins 2009).

Although promising, microalgae as a lipid biomass crop have not yet achieved the high yields predicted from early investigations (Sheehan et al. 1998, Gordon & Polle 2007, Chist 2007, Dismukes et al. 2008). Although technical research and process engineering continues to increase, basic biological research and screening have lagged behind (Sheehan et al. 1998, Radakovits et al. 2010, U.S. DOE 2010). Current biofuels literature reports a range of micro-algal cellular lipid levels of between 2 and 75 percent of the total dry weight of the cells (Chisti 2007, Huerliman et al. 2010, Singh et al. 2011, Fields & Kociolek 2015), demonstrating the extreme variability between algal taxa and lineages. In the context of total algal diversity this variation is not surprising, given the typical definition of ‘algae’ as all aquatic chlorophyll-a containing organisms that are not ‘higher plants’. To put algal diversity into perspective, ‘algae’ as previously defined spans two domains, 15 divisions, and 54 classes of life (Guiry 2012). This diversity when combined with the observed variability in lipid production creates enormous challenges in taxon selection for the biomass industry.

Much of the early screening in algal biomass research centered on the production of triacylglycerols (TAG's) for liquid biofuel's production (Sheehan et al. 1997) and this still remains an active area of research today. The most comprehensive early screening effort was the U.S. Department of Energy's Aquatic Species Program (ASP), which from 1978–1996 examined over 3000 strains of micro-algae including taxa from the green algae (Chlorophyta), diatoms (Bacillariophyta), golden-brown algae (Chrysophyta), haptophyte algae (Haptophyta), and the cyanobacteria (Cyanophyta). After examining 3000 algal strains, the authors concluded that diatoms were one of the best choices for continued biofuels research (Sheehan et al. 1998).

Diatoms are a lineage of single celled and colony forming primary producers found in virtually all aquatic habitats. The group is characterized by the primary photosynthetic pigments chlorophyll's -*a* and -*c*, and the presence of a glass cell wall (SiO_2) termed a frustule. Diatoms are particularly important in the aquatic ecosystem as they potentially account for over 40% of all aquatic primary production (Werner 1977, Nelson et al. 1995) and are the preferred food source for many aquatic grazers (Werner 1977, Round et al. 1990). The recommendation of Sheehan et al. (1998) for continued focus on diatoms as a feedstock was based on diatoms high productivity, ability to grow in large-scale culture, wide ecological breadth and high cellular oil accumulation consisting primarily of 16 and 20 carbon fatty acids (Orcutt & Patterson 1975, Mortensen et al. 1988) in the form of TAG's (accounting for 40-60% of the cell's mass in some taxa). This recommendation for continued research with diatoms over other algal groups has been regularly echoed by subsequent authors (Ramachandra et al. 2009, Graham et al. 2012, Hildebrand et al. 2012, d'Ippolito et al. 2015, Fields & Kociolek 2015).

With nearly 40 years of general screening performed, the question becomes where the field moves from here. Clearly the time has come for a more focused approach to these screening efforts, as the number and diversity of extant diatoms precludes an exhaustive survey (current estimates place diatom diversity at around 100,000 extant species, Mann & Vanormelingen 2013). With many studies moving away from screening and towards more focused organismal approaches including genetic engineering and comparative genetics research (Roessler et al. 1994, Dunahay et al. 1996, Rosenber et al. 2008, Beer et al.

2009, Radakovits et al. 2010, Cheng et al. 2014, Ma et al. 2014, Scranton et al. 2015, Tanaka et al. 2015), it is important for a new generation of screening efforts to not only explore taxonomic diversity but also examine this diversity in a way that has application to the entire field of algal biomass research.

Within diatoms (and most other large groups of algae) non-systematic sampling and screening has led to limited understanding of species level variation in lipid accumulation and the drivers of this variation. The diatom genus *Navicula* Bory de Saint-Vincent, with six species examined by a single author, is the best characterized genus and exhibits lipid accumulation values ranging from 17.3–25.5% (Scholz & Liebezeit 2013). To truly understand patterns of lipid variation, a phylogenetic appraisal of lipid accumulation will need to be undertaken across the known evolutionary breadth of a group. This type of investigation has revealed a phylogenetic basis for variation in a variety of traits across diverse organisms including plant morphological and ecological traits (Ackerly 2009), bird habitat (Rheindt et al. 2004) and song (Päckert et al. 2003), animal body size (Ashton 2004) and bone microstructure (Cubo et al. 2005) and even in mammalian extinction risk (Fritz & Purvis 2010). Although lipid accumulation and ecological preference are of critical importance to biomass research, this type of investigation has rarely been attempted in microalgae.

Early efforts at this type of investigation include Galloway and Winder (2015) who demonstrated that within marine phytoplankton variation in fatty acid profiles are explained more by phylogeny (in this case large algal groups) than by environmental factors. At a finer taxonomic scale, Fields and Kociolek (2015) concluded that major lineages within diatoms have some degree of predictive power as it pertains to cellular lipid accumulation. While these studies begin to frame the possibility that observed variation in lipid accumulation may exhibit a phylogenetic signal, which here is defined as more closely related organisms exhibiting more similar trait values than a random selection of organisms due to their shared evolution, neither deals with the process at the level in which most applications are performed, at the level of species.

From this species level appraisal across a single genus several fundamental questions concerning algal lipid accumulation can be addressed: first, how much variation in lipid accumulation actually occurs

within a genus and whether genus level assumptions concerning high lipid content are appropriate? Second, if there is significant variation in lipid accumulation within a genus and whether this variation is best explained by the phylogenetic relationships between the species? Third, if a phylogenetic signal in the data is established, can this data be used to better understand drivers of higher lipid accumulation in some taxa and lower accumulation in others?

The diatom genus *Halamphora* (Cleve) Levkov, which until recently was part of the genus *Amphora* Ehrenberg ex Kützing (Levkov 2009), is particularly well suited for a phylogenetic study of lipid accumulation. Of the diatom taxa examined, *Halamphora* strains have shown to accumulate some of the highest levels of cellular oils (Sheehan et al. 1998, Chen 2012, Chtourou et al. 2015), exhibit high productivity (Sheehan et al. 1998), and are found in a wide range of habitat types and conductivities from the arctic to the tropics (Patrick & Freese 1961, Hohn & Hellerman 1966, Stoermer & Yang 1971, Wachnicka & Gaiser 2007, Stepanek & Kociolek 2013, Stepanek & Kociolek 2015). More importantly, the group (*Amphora s.l.*) has been the focus of considerable recent taxonomic (Stepanek & Kociolek 2013, Stepanek & Kociolek 2015, Chapter 4) and molecular phylogenetic (Stepanek & Kociolek 2014, Stepanek et al. 2015, Stepanek & Kociolek *In Review*, Chapter 8) work.

From this previous work a phylogenetic cross-section of taxa from all major subclades within *Halamphora* has been investigated for growth and lipid accumulation under standardized conditions. Lipid accumulation experiments were conducted under nutrient replete and silica deplete conditions, with silica depletion having been shown to increase lipid accumulation within some diatom strains (Sheehan et al. 1998, Griffiths & Harrison 2009, Fields & Kociolek 2015). Measured growth, lipid and habitat data were evaluated in the context of phylogenetic relationships between species to determine if a significant phylogenetic signal exists in one or more parameters, and similarly, whether phylogenetic relationships and clade membership can be used as a predictor of trait values. Taken together this combined dataset will create a predictive evolutionary roadmap for the selection of high lipid accumulating members of *Halamphora*.

MATERIALS AND METHODS

Isolation and culturing

Halamphora taxa included in this study were collected from coastal marine, estuarine, inland saline and fresh waters of Colorado, Florida, Hawaii, North Carolina, North Dakota and Utah, USA and Japan from 2011–2014 (see Appendix 1 for collection and site information). When available, pH and conductivity measurements were taken near shore at the time of collection using a YSI 556 multi-probe (YSI Incorporated, Yellow Springs, Ohio, USA). *Halamphora* taxa were isolated into monoculture through micropipette serial dilution under an inverted microscope. Taxa were grown in one of five liquid media depending on the measured conductivity at the collection site. Freshwater taxa were grown in WC medium (Guillard & Lorenzen 1972) with the Na_2SiO_3 concentration increased to 56.84 mg l^{-1} from the original recipe. The brackish and saltwater taxa were grown in one of four artificial saltwater media created using the artificial sea salts Instant Ocean (Spectrum Brands, Inc., Blacksburg, Virginia, USA) and using WC medium nutrient levels. The sea salt concentrations were adjusted conductivities of 10, 15, 40 and 50 mS cm^{-1} to match the major conductivity categories at collection sites. Cultures were maintained at ca. 25°C under fluorescent lights (illumination ca. 50 µmol m^{-2} S^{-1}) with a 12:12 light:dark cycle.

All light microscope (LM) observations were made with an Olympus BX-51 light microscope (Olympus America Inc., Center Valley, Pennsylvania, USA) and LM images were captured using an Olympus DP71 digital camera. Scanning electron microscope (SEM) images were taken using either a JEOL 6060LV SEM or a JEOL JSM 7401 field emission SEM (JEOL Ltd., Tokyo, Japan).

Growth and lipid accumulation

In an effort to keep nutrient levels consistent across growth media of differing conductivities (Instant Ocean contains measurable levels of macro- and micronutrients as well as silica), UTEX Artificial Seawater Medium (UTEX Culture Collection, University of Texas, Austin, USA) was used in all experiments. As with the media used for culture maintenance, the silica concentrations were increased

in the experimental media. Stock cultures were allowed to acclimate to the experimental medium for a minimum of two weeks prior to experimental trials.

Growth and lipid accumulation experiments were performed in a VWR Signature Diurnal Growth Chamber (VWR International, Radnor, Pennsylvania, USA) at 25°C and at an illumination of ca. 120 µmol m^{-2} S^{-1} with a 12:12 light:dark cycle. Although growth conditions were not optimized for each *Halamphora* taxon, similar standard conditions have been extensively used when examining multiple diverse algal taxa (Dempster & Sommerfeld 1998, Nascimento et al. 2013, Cheng et al. 2014, Fields & Kociolek 2015). Experiments were performed, in triplicate, in 250 ml Erlenmeyer flasks. Initial inoculation consisted of 5 ml of stock culture added to 220 ml of experimental growth medium. Throughout the course of the experiment, flasks were individually stirred by small stir bars and humidified filtered air (0.2 µm sterile inline filter) was continuously bubbled through the flasks.

Cell growth was monitored daily from a 1 ml extracted subsample. From this subsample living cells were manually counted using a Palmer counting cell at 40x magnification. Maximum growth rate (µ) and divisions per day were calculated over the 48 hours of most rapid cell growth.

For lipid accumulation under non-nutrient limitation experiments, a 50 percent exchange of the growth medium was conducted as the exponential growth phase began to slow but as cells were continuing to divide. This exchange was repeated for two consecutive days before cell harvest. For lipid accumulation under silica limitation, cultures were initially grown in full silica growth medium. As the exponential growth phase began to slow but while cells were continued to actively divide, cells were allowed to settle and a full media exchange with experimental media containing no added silica was performed. Cells were maintained in silica deplete medium under standard experimental conditions for three days before cell harvest. At harvest, for each experimental replicate, a 10 ml subsample was extracted and preserved in glutaraldehyde for final cell count and biovolume calculations. The preserved samples were stored in the dark at 2°C. For lipid extraction, 200 ml of culture was filtered onto pre-weighed 47 mm Whatmann GF/C glass fiber filters (GE Healthcare Biosciences, Pittsburg, Pennsylvania, USA) and stored at −20°C until extraction.

Before lipid extraction, filtered cells were dried overnight in a drying oven and placed in a vacuum desiccator for a minimum of two hours before weighing with a Mettler Toledo ML204 analytical balance (Mettler-Toledo International Inc., Columbus, Ohio, USA) with readability to 0.0001 grams. The original filter mass was subtracted from the mass of the filter plus cells to obtain the total dry mass of each replicate. Lipid extractions were performed using a Soxhlet extraction method, using 80 ml of a 2:1 chloroform:methanol mixture for an 18 hour extraction period. After extraction, the solvent was evaporated using a Kuderna-Danish Concentrator to a volume less than 3 ml, transferred to a pre-weighed 3 dram glass vial where the last of the solvent was allowed to evaporate. Once dried, to ensure that the final lipid mass was not affected by any residual salts from the growth medium, the lipid was re-dissolved in chloroform and transferred to a new vial (leaving the crystalized salts behind). The final lipid vials were held in a desiccator under vacuum for a minimum of two hours before obtaining the final lipid mass.

Final cell counts were calculated on the preserved subsamples using the same method as with the growth rate calculations. To estimate the mean cellular volume of the experimental cultures, 20 images were captured for each taxon at 100x magnification. From these images, cellular measurements were taken in Gimp 2.8.10 (www.gimp.org) and biovolumes were estimated using Hillebrand et al.'s (1999) equation for calculating cellular volume of *Amphora* species.

Lipid production and accumulation calculations

Lipid production and accumulation values were calculated as follows:

Percent dry weight: % DW = Total extracted lipid weight / Total dry weight of cells * 100

Lipid mass per cell: Lipid $cell^{-1}$ = Total extracted lipid / Cell count at harvest

Lipid mass per 100 μm^{-3} of cellular volume: Lipid $100\mu m^{-3}$ = Lipid $cell^{-1}$ / cell volume * 100

Lipid production per cell per day: Lipid day−1 = Lipid $cell^{-1}$ * Divisions day^{-1}

Significant differences in the reported data were determined by one-way ANOVA performed in RStudio ver. 0.99.473.

Phylogenetic analysis

The molecular phylogeny for the genus *Halamphora* was generated using the four marker concatenated alignment of Stepanek & Kociolek (Chapter 8). This alignment utilized the nuclear encoded 18S small subunit rDNA (SSU) and the 28S large subunit rDNA (LSU) and the chloroplast encoded large subunit of RUBISCO (*rbc*L) and photosystem II chlorophyll-a binding protein *psb*C. Included in the alignment are 31 taxa from the genus *Amphora*, 77 taxa (including all the taxa presented here) from the genus *Halamphora*, 11 species from the sister group to *Halamphora* the Surirellales Mann in Round et al. and Rhopalodiales Mann in Round et al. and four outgroup taxa from the genus *Tetramphora* Mereschkowsky. Tree inference was based on maximum likelihood (ML) estimation conducted in RAxML ver. 7.3.2 (Stamatakis 2006) using the graphical user interface raxmlGUI ver. 1.2 (Silvestro & Michalak 2012) and Bayesian inference using MrBayes ver. 3.2.1 (Ronquist et al. 2012). Both estimations used a GTR+Γ+I model of sequence evolution and the alignments were partitioned by marker. For the ML estimation, the final tree was chosen as the most likely tree from 20 independent searches. Node support was estimated with 1000 thorough bootstrap replicates. For the Bayesian inference, 25 million generations were run with tree sampling every 1000 generations and a burn-in of 5 million generations. In order to ensure the most accurate phylogenetic tree given the data, the full tree was estimated after which the monophyletic *Halamphora* subtree was extracted from the larger analysis. Although pruned, the relationships between the represented taxa are identical to the original phylogenetic estimation.

Phylogenetic comparative methods

Habitat type and conductivity for the internal nodes and branches of the *Halamphora* phylogeny were estimated from an ancestral state reconstruction performed on the entire *Halamphora* phylogeny. For the reconstruction of the habitat conductivity, tip values corresponded to the measured collection site conductivity at the time the samples were taken (Appendix 1). Habitat type was coded as binary data and was divided into either a coastal habitat, which was defined as any coastal or estuarine waters that had a direct connectivity to the ocean and exhibited some tidal influence, or inland waters with no direct

connectivity. The ancestral node states for both the continuous habitat conductivity and the discrete habitat type where estimated using a maximum likelihood method. The continuous habitat conductivity values were estimated and visualized using the 'contMap' function in the R phylogenetics package phytools (Revell 2012). The discrete habitat type values where estimated using the 'rerootingMethod' function in the R phylogenetic package phytools (Revell 2012), using an equal rates model of evolution. All ancestral state reconstructions were performed in RStudio v. 0.99.473.

Tests for a phylogenetic signal in the habitat conductivity data utilized the entire available *Halamphora* phylogeny with the topology returned from the ML estimation. The tip values correspond to the measured sample site conductivity values as in the ancestral state reconstruction. For the analysis of the lipid accumulation and growth data, a reduced tree including only the experimental *Halamphora* taxa was used. This tree was constructed from the full phylogeny by dropping the tips of taxa with no associated data. This allowed for the topology as well as the relative branch lengths to be preserved from the full, and presumably most reliable, phylogenetic tree. The tests for phylogenetic signal were performed using the 'phylosignal' function in the R phylogenetics package picante (Kembel et al. 2010) and was run in RStudio v. 0.99.473. This function utilizes the methods of Blomberg et al. (2003) and returns a p-value describing how well the tree topology fits the tip data based on phylogenetic independent contrasts (PIC's) (Felsenstein 1985) and tip reshuffling, and a k-value which describes the degree to which the tip data fits a model of Brownian trait evolution given the tree topology (k=1 is a perfect Brownian fit). All analyses utilized 100,000 tip reshufflings to calculate the p-value for significant phylogenetic signal. Tree transformations were performed using the 'rescale' function in the phylogenetics package geiger (Harmon et al. 2008). All tests were also run on the tree topology returned from the Bayesian analysis with no loss of significant detected signal, for this reason only the ML topology is illustrated for the remainder of the manuscript.

RESULTS

Phylogenetic analysis

The *Halamphora* subtree from the ML estimation conducted on the four marker concatenated alignment is illustrated in Figure 10.1. Support values are given as ML bootstrap values and Bayesian posterior probabilities as a percent, support given as (*) indicates a value of 100. Bayesian node support of (-) indicates incongruence between the ML and Bayesian trees. From this analysis the *Halamphora* clade has been subdivided into 11 subclades (Clades A–K). The subset of taxa included in the lipid accumulation experiments have been highlighted in bold. The principle incongruence between the ML and Bayesian trees is that the returned Bayesian tree places Clades C and D into a single monophyletic group. This difference in topology was shown to have minimal effect on the comparative analyses and the ML tree will be shown throughout.

Habitat conductivity

The test for phylogenetic signal in habitat conductivity across *Halamphora* returned mixed results with p=0.00009 and a k=0.061. These results indicate that there is significant phylogenetic signal in the conductivity data (p=0.00009), in that the given tree topology fits the conductivity data significantly better than alternative arrangements of the tip data, although the low k-value (k=0.061) indicates that this pattern is not well described by a model of Brownian trait evolution.

Figure 10.2 shows a ML ancestral state reconstruction of both the measured habitat conductivity (colored branches with cool colors correspond to saline environments hotter colors more fresh) as well as coastal or inland habitat type (node pies and taxon names). The reconstruction indicates that *Halamphora* is an ancestrally coastal marine genus that has undergone several independent incursions into inland environments, often with a corresponding move into lower conductivity waters. This transition in habitat type appears directional, with few well supported instances of taxa moving from an inland habitat to a marine habitat (Clade K). The shifts in habitat within the included taxa indicate this transition most commonly occurs with lineages moving from a coastal marine habitat to an inland elevated conductivity or inland freshwater habitat, with the only well supported move from an inland low conductivity habitat back to a coastal marine environment occurring in Clade K.

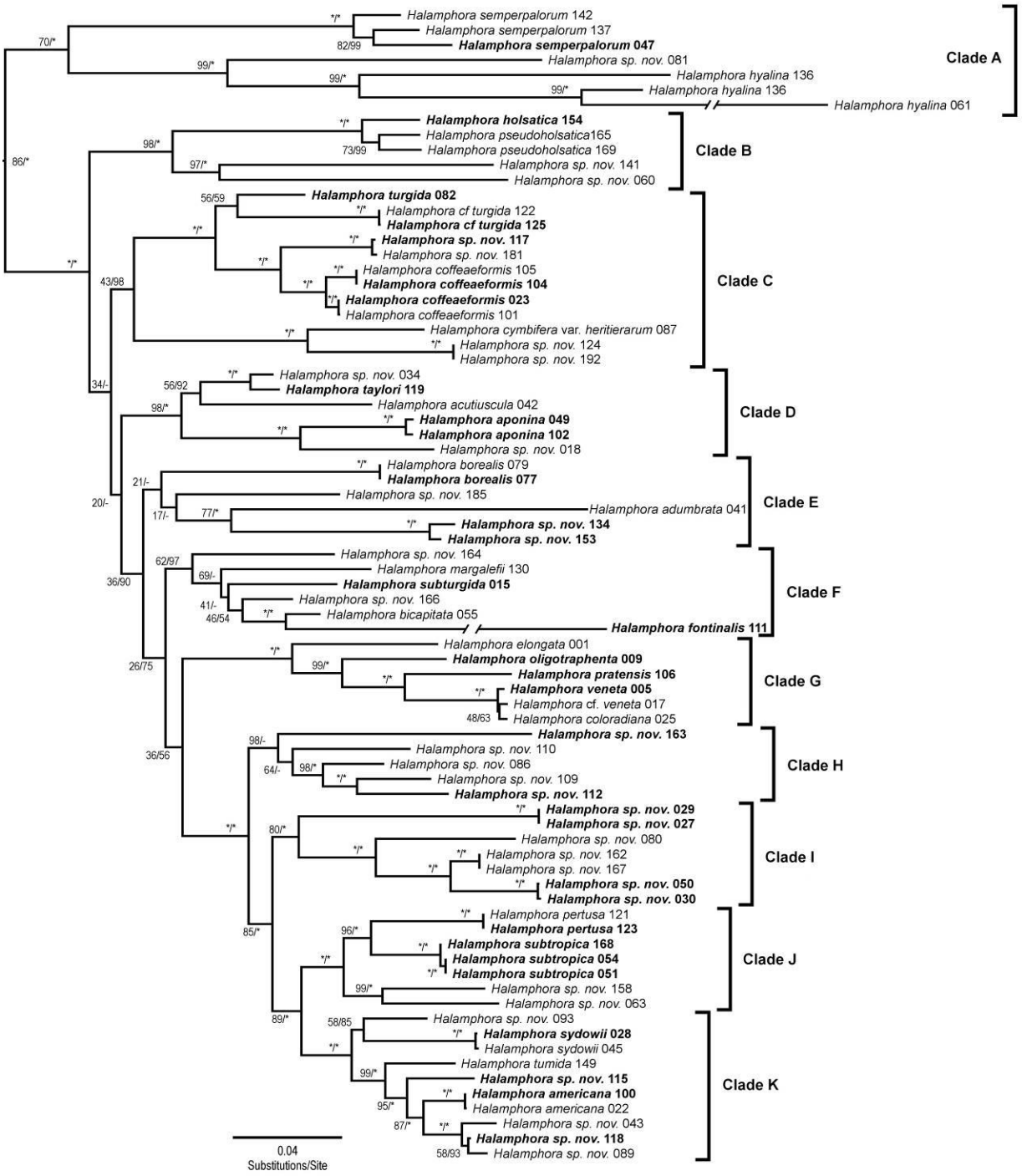

Figure 10.1. Maximum likelihood phylogram of the genus *Halamphora* inferred from a concatenated four marker (SSU, LSU, *rbc*L and *psb*C) alignment. Node support is presented as ML bootstrap (1000 replicates)/Bayesian posterior probability (as a percent). The taxa included in the lipid accumulation experiments are highlighted in bold.

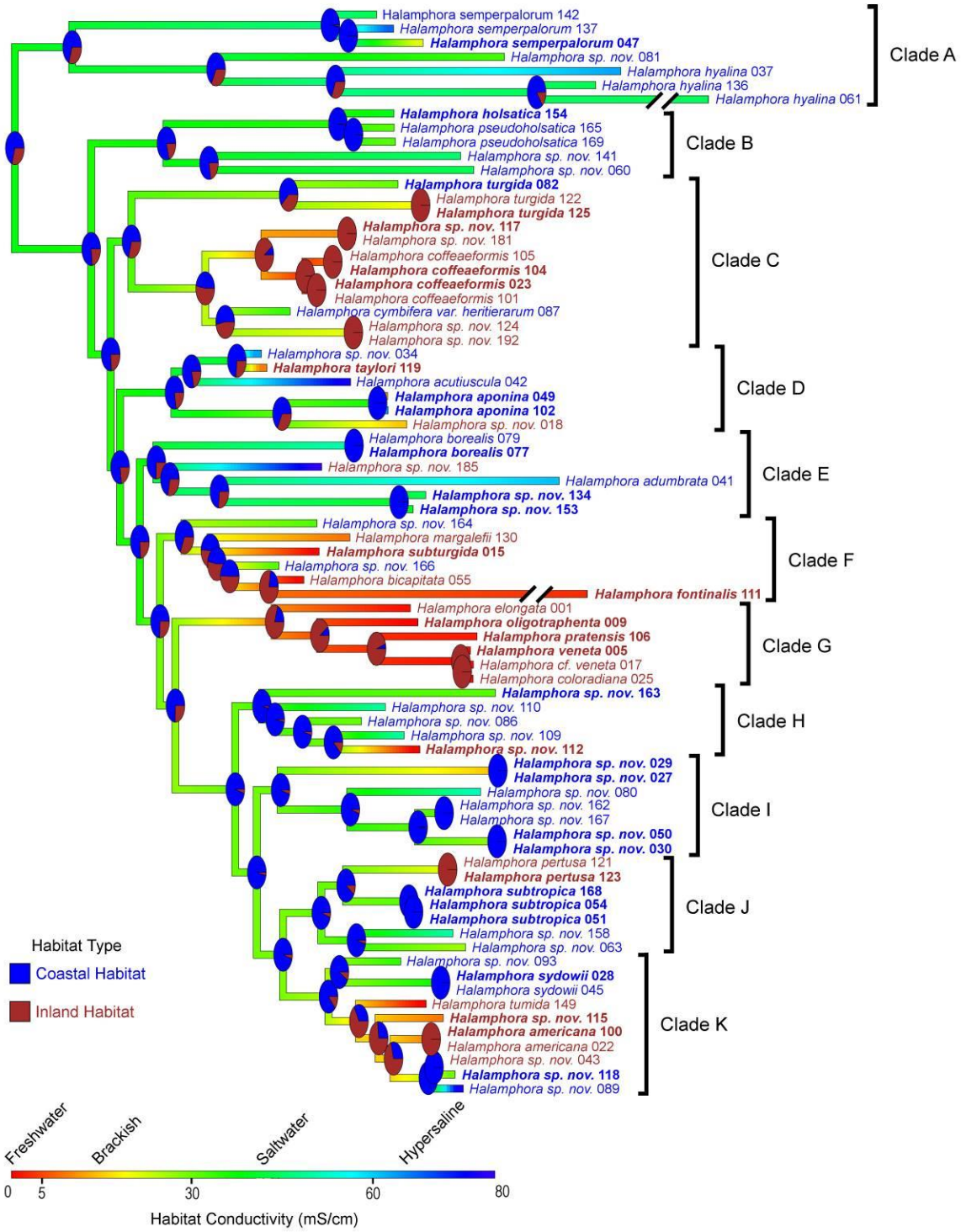

Figure 10.2. Ancestral character state reconstruction of habitat conductivity and habitat type across the genus *Halamphora* based on taxon collection site measurements and the four marker concatenated ML phylogeny. Branch color corresponds to estimated ancestral habitat conductivity with warmer colors lower conductivity water, cooler colors higher conductivity waters. Habitat type (coastal or inland) is indicated by taxon name color and node pies. Red indicates inland habitat, blue indicates coastal habitat.

Lipid accumulation

All measured parameters, including biovolumes, growth rate and lipid accumulation are listed in Table 10.1. Figures 10.3 and 10.4 show the lipid accumulation values across the included subset of *Halamphora* taxa, grouped according to their phylogenetic relationships. The tree branches are colored to reflect habitat conductivity for each lineage as inferred by the ML ancestral state reconstruction illustrated in Figure 10.2. Green branches indicate saltwater, yellow indicate brackish water and red indicate freshwater habitats. Solid horizontal red lines correspond to the mean value across all taxa and the dotted red lines correspond to one standard deviation from this mean. Yellow colored bars indicate clades that, on average, performed better than one standard deviation from the mean. Asterisks above clades indicate whether the top performing clades accumulated significantly greater lipids than the below average performing clades as indicated by a one-way ANOVA.

Percent dry weight

Figures 10.3A, B show the results of the lipid accumulation in nutrient replete (Fig. 10.3A) and silica deplete (Fig. 10.3B) experiments as a percent of cellular dry weight (PDW). For nutrient replete experiments, across the examined taxa, the mean lipid accumulation was 18.1% with a standard deviation of 4.9%. Within these lineages, *Halamphora turgida* (Gregory) Levkov of Clade C was the lowest accumulator with a mean PDW of 7.7% and *Halamphora fontinalis* (Hustedt) Levkov of Clade F accumulated the greatest amount of lipid by weight with a mean PDW of 32.2%. Two clades (Clade F and Clade H) had an average accumulation of over one standard deviation above the overall mean and both were significantly greater than all below average clades ($p<0.001$ and $p<0.01$ for Clade F and Clade H, respectively). Although two clades had significantly higher lipid accumulation, no significant phylogenetic signal was detected with $p=0.371$ and $k=0.024$.

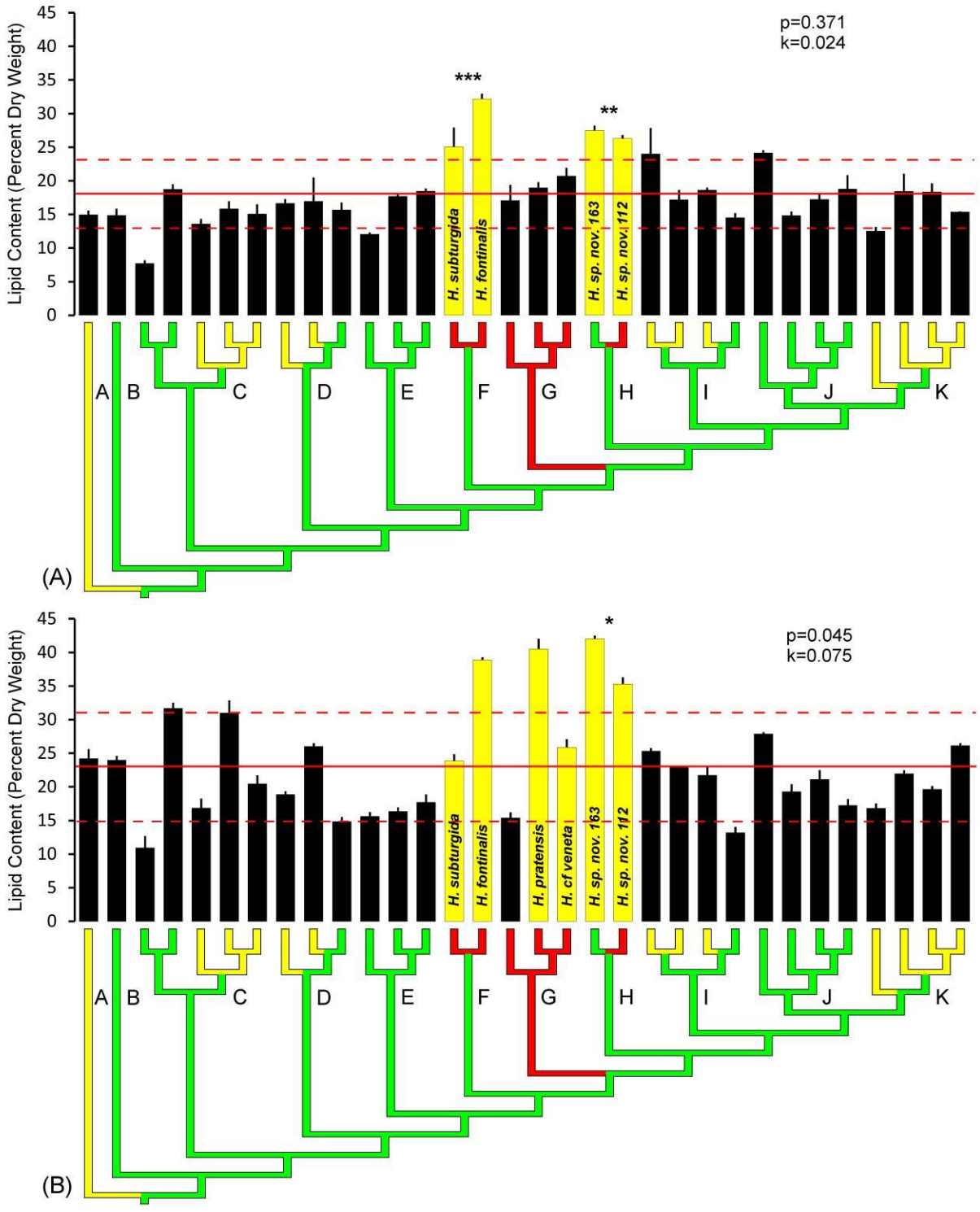
Lipid Content (Percent Dry Weight)
p=0.371
k=0.024
***
**
H. subturgida
H. fontinalis
H. sp. nov. 163
H. sp. nov. 112
A B C D E F G H I J K
(A)
Lipid Content (Percent Dry Weight)
p=0.045
k=0.075
*
H. subturgida
H. fontinalis
H. pratensis
H. cf veneta
H. sp. nov. 163
H. sp. nov. 112
A B C D E F G H I J K
(B)

Figure 10.3. Lipid content as a percent of cellular dry weight. **A.** Cultures grown under nutrient replete conditions. **B.** Cultures grown under silica deplete conditions. Branch color indicates lineage habitat conductivity as estimated from ancestral state reconstruction. Green = saltwater, yellow = brackish and red = freshwater habitat. Solid red line shows the mean lipid content across all taxa. The dashed red line shows one standard deviation from the mean. Yellow bars indicate clades that have an average lipid content greater than one standard deviation above the mean. Asterisks indicate that the clade had a significantly greater average lipid content than all below average clades. P-value indicates whether a significant phylogenetic signal in the lipid data. K-values indicates how well the variation in lipid data fits a model of Brownian trait evolution. * = $p<0.05$, ** = $p<0.01$, *** = $p<0.001$.

In the silica deplete experiments the mean lipid accumulation across all taxa was 23.2% with a standard deviation of 7.9%. Within lineages, *Halamphora turgida* from Clade C accumulated the least amount of lipid per weight with a mean of 11.0% and *Halamphora sp. nov.* 163 accumulated the most lipid with a mean PDW of 42.0%. Three clades had a mean lipid accumulation over one standard deviation from the overall mean, Clade F, partial Clade G and Clade H. Of these three top performing clades, only Clade H was found to be significantly greater than all of the below average clades ($p<0.05$). Signal testing showed a significant signal in the silica deplete PDW values with $p=0.045$. However, as with the conductivity measurements, the test returned a low k-value of 0.075 indicating that the pattern significantly deviates from a Brownian model of trait evolution.

Lipid per cellular volume

Figures 10.4A, B show the lipid accumulation results from nutrient replete (Fig. 10.4A) and nutrient deplete (Fig. 10.4B) experiments as picograms of lipid per 100 μm^3 of cellular volume. In the nutrient replete experiments there was a high degree of variation in lipid accumulation across the taxa examined with a mean accumulation of 20.2 pg $100\mu m^{-3}$ with a standard deviation of 15.2 pg $100\mu m^{-3}$. *Halamphora sydowii* (Cholnoky) Levkov from Clade K had the smallest proportion of cellular volume as lipids with 4.3 pg $100\mu m^{-3}$ and *Halamphora sp. nov.* 112 had the greatest proportion of cellular volume as lipids with 61.3 pg $100\mu m^{-3}$. Two clade had mean accumulation greater than one standard deviation from the mean, partial Clade C and Clade H. Both of these clades had a mean lipid accumulation significantly greater than all below average clades with $p<0.01$ and $p<0.001$ for partial Clade C and Clade

H, respectively. A significant phylogenetic signal was detected in the nutrient replete results with p=0.005 and k=0.222.

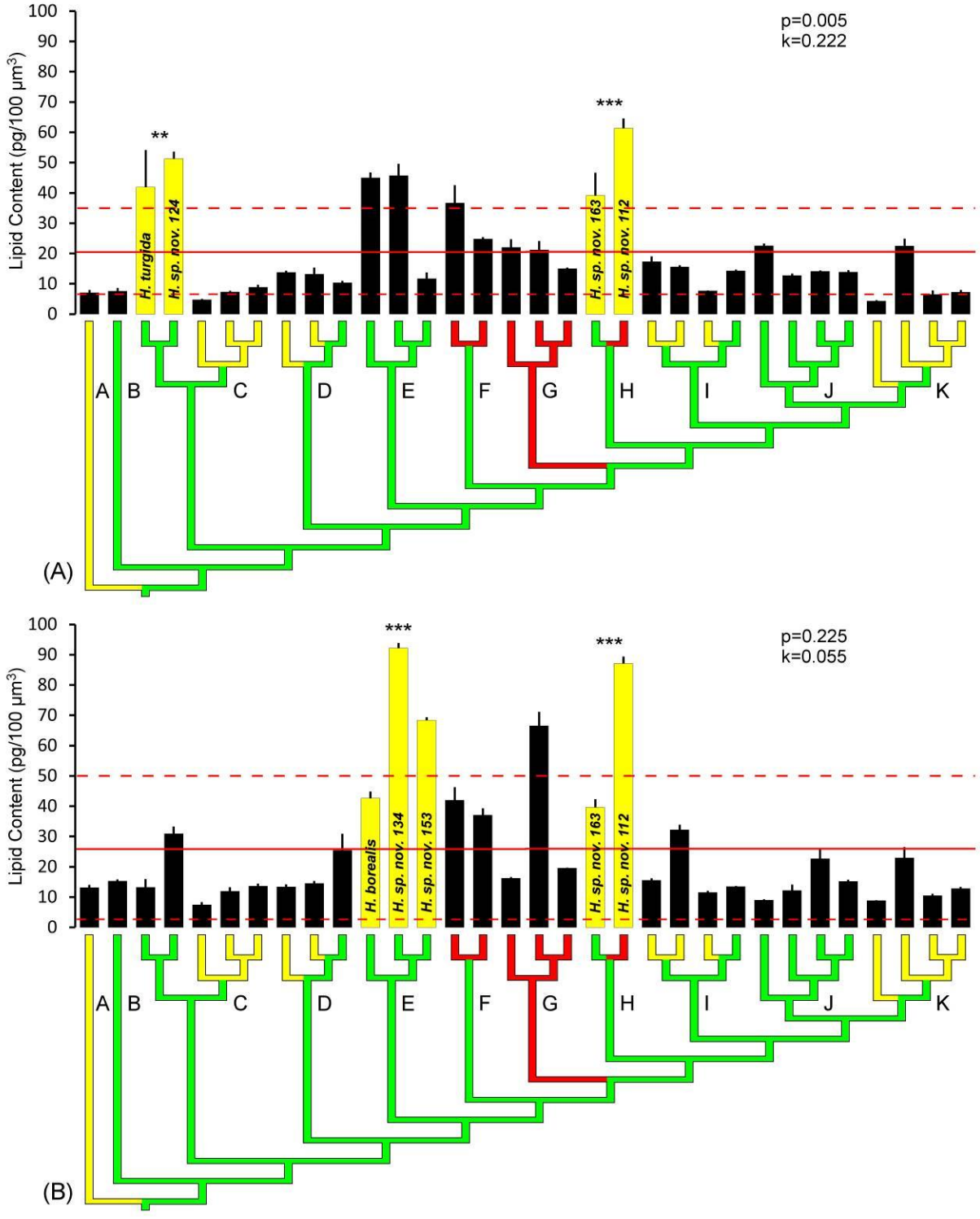

Figure 10.4. Lipid content as a picograms of lipid per 100 μm^3 of cellular volume. **A.** Cultures grown under nutrient replete conditions. **B.** Cultures grown under silica deplete conditions. Cladogram branch color indicate lineage habitat conductivity as estimated from ancestral state reconstruction. Green branches indicate a saltwater habitat, yellow branches indicate a brackish water habitat and red branches indicate a freshwater habitat. Solid red line shows the mean lipid content across all taxa. The dashed red line shows one standard deviation from the mean. Yellow bars indicate clades that have an average lipid content greater than one standard deviation above the mean. Asterisks indicate that the clade had a significantly greater average lipid content than all below average clades. P-value indicates whether a significant phylogenetic signal in the lipid data. K-values indicates how well the variation in lipid data fits a model of Brownian trait evolution. * = $p<0.05$, ** = $p<0.01$, *** = $p<0.001$.

As with the nutrient replete results, there was considerable variation between taxa in the silica deplete results. The mean lipid accumulation across all taxa was 26.8 pg 100μm^{-3} with a standard deviation of 22.6 pg 100μm^{-3}. *Halamphora sp. nov.* 117 had the lowest proportion of cellular volume as lipid with 7.4 pg 100μm^{-3} and *Halamphora sp. nov.* 134 had the greatest proportion with 92.2 pg 100μm^{-3}. Two clades had mean lipid accumulation greater than one standard deviation from the mean, Clade E and Clade H. Both clades had mean accumulations significantly greater than the below average clades with $p<0.001$ for both. Although clades were shown to have significantly greater lipid accumulation, a significant phylogenetic signal was not detected with $p=0.225$ and $k=0.055$.

Tree transformations

Although clades were found to have significantly higher mean values for the nutrient replete PDW and silica deplete lipid per volume datasets, no significant phylogenetic signal was apparent. An examination of the PIC's (Felsenstein 1985), with which the phylogenetic signal test is based (Blomberg 2003), demonstrates that much of the PIC variation within these two datasets is produced by variation between strains from single species clades with near zero branch lengths (data not shown). Because PIC's are essentially scaled to branch lengths, any variation between phylogenetically identical taxa create extremely large contrasts that can have a disproportionate effect on signal testing. To demonstrate this, the nearly molecularly identical single species groups (*Halamphora subtropica* (Wachnicka & Gaiser) Stepanek & Kociolek, *Halamphora sp. nov.* 030-050, *Halamphora sp. nov.* 027-029) were collapsed into a single lineages with the species mean used for the lipid accumulation value. The resulting tree and lipid

content values are illustrated in Fig. 10.5. Although this transformation had no effect on the top performing clades, it had a dramatic effect on the test for phylogenetic signal. After collapsing the zero branch length clades the nutrient replete PDW dataset showed a significant phylogenetic signal with p=0.016 and k=0.523, and the silica deplete lipid per volume dataset also showed a significant phylogenetic signal with p=0.0034 and k=0.744.

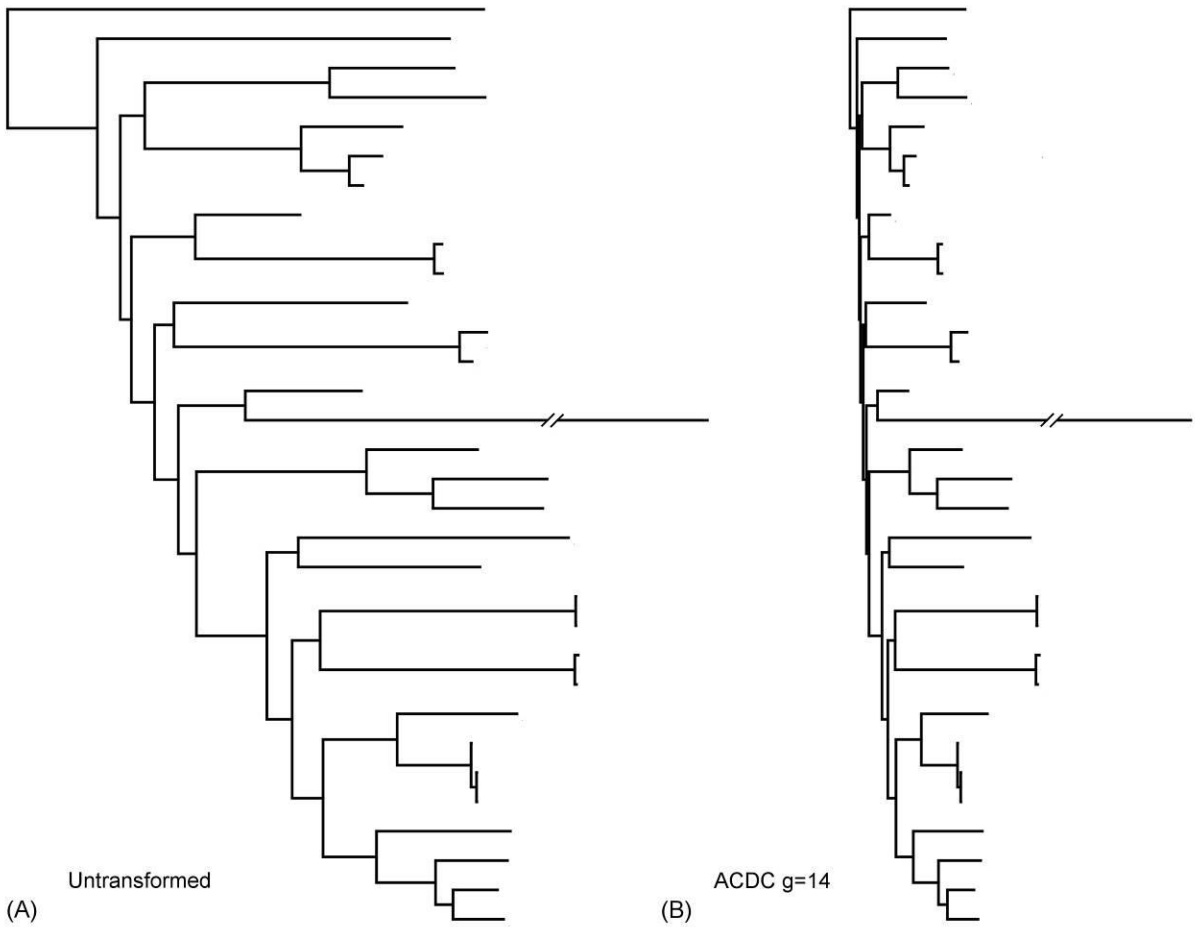

Figure 10.5. Illustration of the best fit ACDC tree branch transformation for the lipid accumulation data. **A.** Untransformed tree inferred from four marker concatenated alignment. **B.** Tree branch lengths after an ACDC transformation g=14.

Although a significant phylogenetic signal was detected in the conductivity, nutrient deplete PDW and nutrient replete lipid per volume datasets, low k-values throughout indicate that the pattern of trait evolution deviates substantially from a Brownian model of evolution along the given phylogeny. In an effort to better understand the process of trait evolution within these datasets two commonly utilized and biologically relevant tree transformations were performed, the Ornstein-Uhlenbeck (OU) transformation which attempts to model stabilizing selection and the acceleration or deceleration (ACDC) (sometimes called an early burst model) transformation that changes the weight of early shared history by lengthening or condensing early branches (Blomberg 2003). An ACDC transformation of the collapsed zero clade tree gave the best fit for all of the lipid datasets with a transformation of g=11 returning k=0.553 for the nutrient replete PDW dataset, g=13 returning K=0.3672 for the silica deplete PDW, g=14 returning k=0.331 for the nutrient replete lipid per volume and g=10 returning k=0.768 for the silica deplete dataset. These transformations decrease the length of the deep branches within the phylogeny (see Fig. 10.6 for the largest ACDC transformation of g=14), essentially reducing the shared evolutionary history between major clades while maintaining the shared evolutionary history within clades. In the case of these datasets, this indicates that the signal is largely explained by the more recent relationships (recent shared evolutionary history) and less by the deeper shared evolutionary history between major clades.

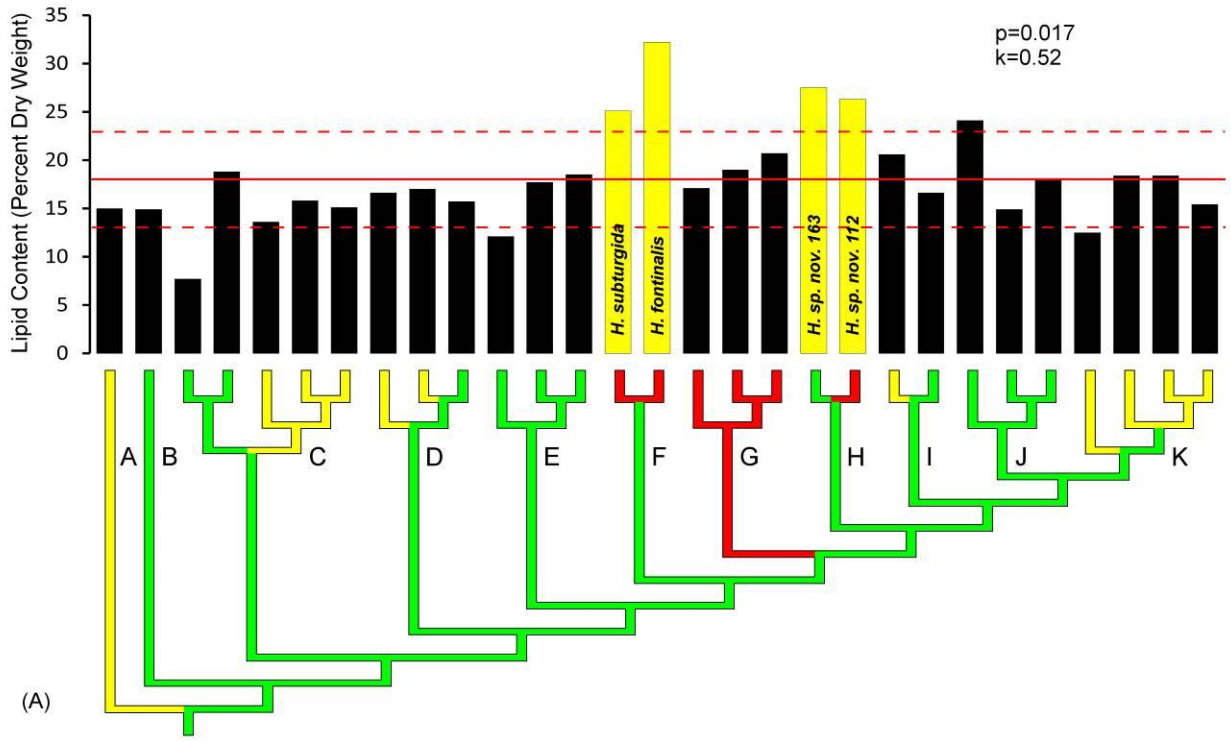
Lipid Content (Percent Dry Weight)
35
30
25
20
15
10
5
0
p=0.017
k=0.52
H. subturgida
H. fontinalis
H. sp. nov. 163
H. sp. nov. 112
A
B
C
D
E
F
G
H
I
J
K
(A)

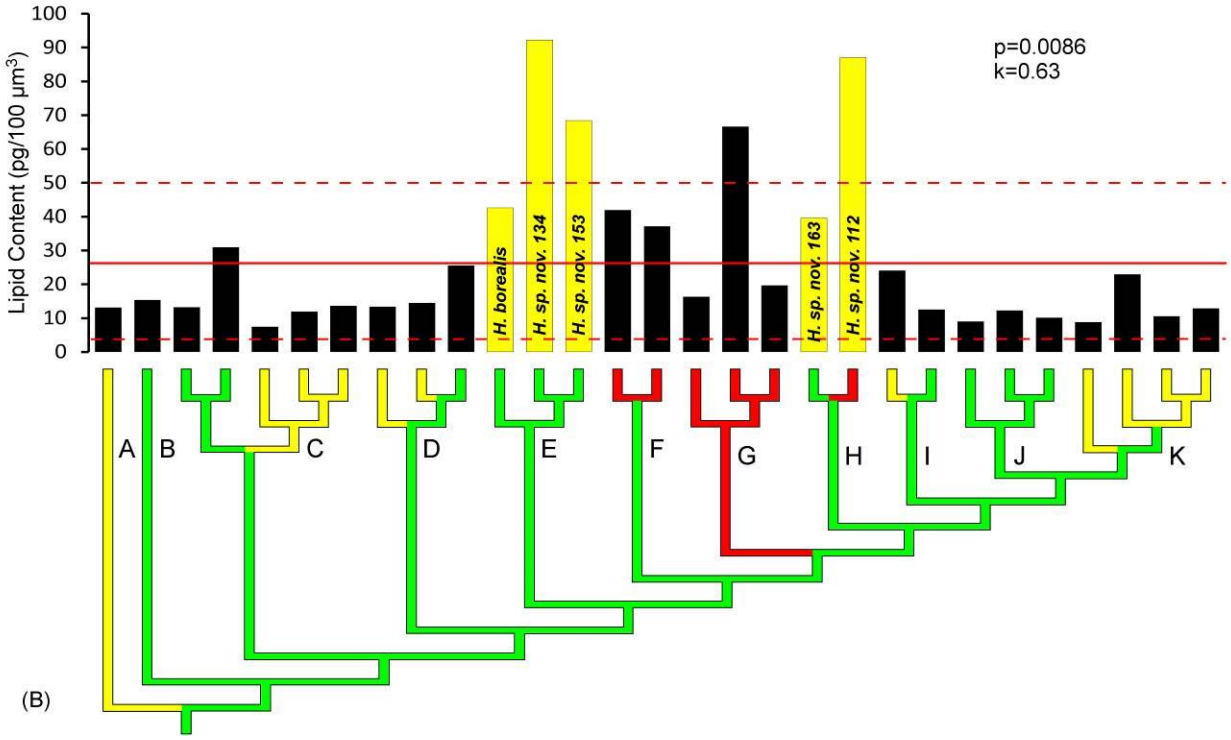
Lipid Content (pg/100 µm3)
100
90
80
70
60
50
40
30
20
10
0
p=0.0086
k=0.63
H. borealis
H. sp. nov. 134
H. sp. nov. 153
H. sp. nov. 163
H. sp. nov. 112
A
B
C
D
E
F
G
H
I
J
K
(B)

Figure 10.6. Lipid content after near zero branch lengths have been collapsed. **A.** Lipid content as a percent dry weight grown under nutrient replete conditions. **B.** Lipid content as picograms of lipid per 100 μm^3 of cellular volume. Cladogram branch color indicate lineage habitat conductivity as estimated from ancestral state reconstruction. Green branches indicate a saltwater habitat, yellow branches indicate a brackish water habitat and red branches indicate a freshwater habitat. Solid red line shows the mean lipid content across all taxa. The dashed red line shows one standard deviation from the mean. Yellow bars indicate clades that have an average lipid content greater than one standard deviation above the mean. Asterisks indicate that the clade had a significantly greater average lipid content than all below average clades. P-value indicates whether a significant phylogenetic signal in the lipid data. K-values indicates how well the variation in lipid data fits a model of Brownian trait evolution. * = $p<0.05$, ** = $p<0.01$, *** = $p<0.001$.

Correlated trait evolution

As a result of phylogenetic signal being found in the lipid accumulation and habitat data, regression analyses examining correlations between lipid accumulation and other measured traits were conducted using PIC's. This strategy allows the removal of correlation due to shared evolutionary history (Felsenstein 1985). The results of the PIC correlations examining lipid accumulation as a function of cell size, conductivity and growth rate are shown in Figure 10.7. Due to the large contrast generated from near zero branch lengths discussed earlier, the collapsed zero branch length tree was used for all correlations. Although it has been speculated that cell size and growth rate have an effect on algal lipid production (Graham et al. 2011, Sheehan et al. 1998), aside from a weak trend of faster growing cells actually having a greater PDW (Fig. 10.7E), no correlations appear between any of these factors. This finding is similar to one recently presented by Fields and Kociolek (2015) where they found no correlation between cell size and lipid accumulation across several orders of diatoms.

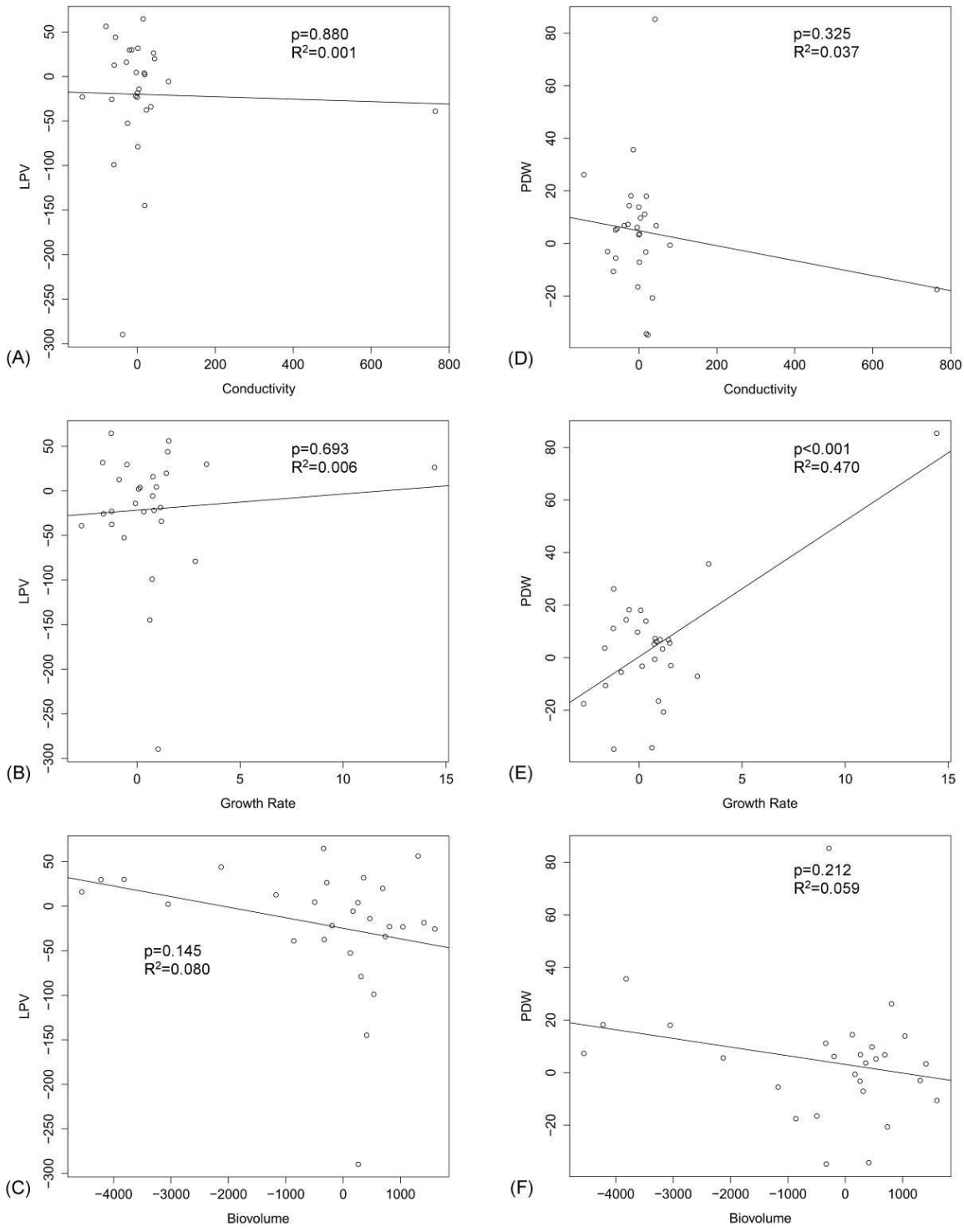

Figure 10.7. Linear regression analysis of correlations between phylogenetic independent contrasts of lipid content and habitat conductivity, growth rate and cellular biovolume. **A.** LPV as a function of habitat conductivity. **B.** LPV as a function of maximum growth rate. **C.** LPV as a function of average cellular biovolume. **D.** PDW as a function of habitat conductivity. **E.** PDW as a function of maximum growth rate. **F.** PDW as a function of average cellular biovolume. LPV = lipid content as picograms of lipid per 100 μm^3 of cellular volume. PDW = lipid content as a percent of cellular dry weight.

DISCUSSION

Lipid production within Halamphora

When taken as a whole, lipid accumulation as a percent dry weight within the genus *Halamphora* corresponds well to previously published reports. Although, as has been discussed by previous authors (Hildebrand 2012, Fields and Kociolek 2015), significant methodological differences make comparisons of lipid accumulation across studies questionable, the published reports summarized in Fields and Kociolek (2015) give a mean nutrient replete percent dry weight across all examined diatoms of 20.8% with a standard deviation of 7.3% and in nutrient limiting studies a mean of 32.3% with a standard deviation of 12.6%. The nutrient replete *Halamphora* mean of 18.1% is near the overall diatom average of 20.8% and the highest accumulating clade (Clade F) is well above average within diatoms with a mean PDW of 28.7%. Additionally, the highest accumulating taxon, *Halamphora fontinalis*, with a PDW of 32.2% has the fourth highest levels of lipid accumulation measured in a nutrient replete experiment following *Chaetoceros calcitrans* (Paulsen) Takano (39.8%) (Rodolfi et al. 2008), *Gyrosigma spenceri* (Ehrenberg) Frenguelli (34.5%) (Scholz & Liebezeit 2013) and *Pleurosigma angulatum* (Quekett) Smith (33.5%) (Scholz & Liebezeit 2013).

The comparison of silica stressed lipid accumulation is more difficult as the number of species examined is considerably smaller than in nutrient replete experiments (58 and 33 species examined for nutrient replete and nutrient limited experiments, respectively) and more importantly the nutrients limited and the methods used for nutrient limitation vary considerably between studies (Fields & Kociolek 2015). Lipid accumulation taken from Fields and Kociolek (2015) across all diatom taxa give a mean of 32.3% with a standard deviation of 12.6%. This mean is higher than the mean across *Halamphora* of 23.2%, although the top accumulating clade within *Halamphora* (Clade H) with a mean of 38.7% is within this range. As under nutrient replete experiments, the highest accumulating *Halamphora* taxon, *Halamphora sp. nov.* 163 at 42.0%, is in the upper range of lipid accumulating taxa with only six other species reported to accumulate more lipid as a percent dry weight (Fields & Kociolek 2015).

Previously, the greatest taxon coverage within a genus from a single study was conducted by Scholz and Liebezeit (2013) in which they examined six different species (among others) from the genus *Navicula*. Even given this small sample, the authors found a range of lipid accumulation under nutrient replete conditions of 17.3–25.5% (Scholz & Liebezeit 2013). Between the *Halamphora* taxa examined here, the range is even greater with accumulation ranging from 7.7–32.2% in nutrient replete conditions and 11.0–42.0% in nutrient deplete conditions. This clearly demonstrates that the taxonomic level of genus is not an appropriate level of hierarchy for making statements concerning lipid production.

Further complicating genus level statements of lipid accumulation is poor taxonomy and a generally poor understanding of the phylogenetic relationships within many diatom groups. The amphoroid diatoms are an excellent example. Previous reports have indicated the genus *Amphora* as a promising diatom genus for continued lipid study due to ecological breadth, fast growth and high lipid accumulation (Sheehan et al. 1998, Chtourou et. al. 2015). At the time that many of these statements were made the genus *Amphora* was considered a large and morphologically diverse group of diatoms. It was not until recent work that genera have begun to be separated from the genus (Paddock & Sims 1980, Mann & Cox in Round et al. 1990, Mann in Round et al. 1990, Williams & Reid 2006, Levkov 2009, Stepanek & Kociolek *in review*) with the most important separation being Levkov's (2009) elevation of the *Amphora* subgenus *Halamphora* to generic status. Equally important was the finding by Stepanek and Kociolek (2014) that many of the groups remaining in the genus *Amphora* were not monophyletic and were distributed widely across raphid diatom lineages.

Given our current understanding of amphoroid systematics, we can critically evaluate previously reported lipid accumulation within the group. To date, lipid accumulation as a percent dry weight has been reported for nine *Amphora* taxa, *A. angusta* Schmidt in Schmidt et al. (Scholz & Liebezeit 2013), *A. arenaria* Donkin (Scholz & Liebezeit 2013), *A. bigibba* Grunow in Schmidt et al. (Chen 2012), *A. exigua* (Gregory) Levkov (Orcutt & Patterson 1975, Chen 2012, Scholz & Liebezeit 2013), *A. graeffii* Cleve (Scholz & Liebezeit 2013), *A. hyalina* Ehrenberg (Sheehan et al. 1998), *A.* sp. (Orcutt & Patterson 1975), *A.* sp. (de la Peña 2007) and *A.* sp. (Chtourou et al. 2015). Although all reported were from the genus

Amphora in the literature, only *A. graeffii* (synonym of *A. graeffeana*) is currently classified within the genus *Amphora* and this taxon is not within *Amphora s.s.* (that is, the clade containing the type species of the genus), but instead was previously classified within the subgenus *Diplamphora* and is currently within *Amphora* Clade A (Stepanek & Kociolek 2014, Chapter 8). Of the remaining '*Amphora*' taxa, *A. bigibba* and *A. exigua* are part of *Halamphora s.s.*, *A. hyalina* is part of *Halamphora* Clade A (Stepanek & Kociolek 2014, Chapter 8), *A. arenaria* is part of Cleve's (1895) subgenus *Amblyamphora* which has been shown to be part of an early branching lineage within raphid diatoms (Stepanek & Kociolek 2014), and *A. angusta* is now classified within the genus *Seminavis* Mann in Round et al. and has been shown to be more closely related to the genus *Navicula* than to the genus *Amphora* (Round et al. 1990). These six named '*Amphora*' species actually belong to four different lineages spanning several orders of raphid diatoms. Even more difficult are the three taxa referred to only as *Amphora* sp. (Orcutt & Patterson 1975, de la Peña 2007, Chtourou et al. 2015) with no provided images. Because Chtourou et al. (2015) included a molecular phylogeny including their '*Amphora*' taxon it appears that at the very least this species can be assigned to the genus *Halamphora*, but given the polyphyletic nature of *Amphora s.l.* (Stepanek & Kociolek 2014), the data associated with the other two studies have little utility outside of a general description of raphid diatom lipid production. Although the genus *Amphora* is likely a particularly dramatic case, given how rapidly diatom taxonomy and systematics are changing with the introduction of molecular systematics, one would expect similar issues in other large and diverse genera.

Phylogenetic basis for lipid accumulation within Halamphora

At least to some degree (with or without collapsed near zero branches) phylogenetic signal was detected in the lipid accumulation data in both nutrient replete and silica deplete conditions either measured as a percent dry weight or as a lipid per cellular volume (Figs 10.3, 10.4, 10.6). When based on untransformed trees, there was significant phylogenetic signal in the lipid per volume data under nutrient replete conditions (Fig. 10.4A, $p=0.005$, $k=0.22$) and in the percent dry weight data under nutrient deplete conditions (Fig. 10.3B, $p=0.045$, $k=0.075$). When near zero branch lengths were collapsed a significant

signal was detected in the percent dry weight under nutrient replete conditions data (Fig. 10.6A, p=0.016, k=0.52) and in the lipid per volume under silica deplete conditions data (Fig. 10.6B, p=0.003, k=0.74).

This trend is evident when examining the highest lipid accumulators within *Halamphora*. Under nutrient replete conditions Clades F and H both averaged over one standard deviation greater lipid content as a percent of their cellular dry weight, with both significantly greater than the below average clades (Fig. 10.3A). When examining lipid content as a proportion of cellular volume, under the same conditions a subclade within Clade C and Clade H were significantly greater than the below average clades (Fig. 10.4A). Under silica deplete conditions Clades F, a subclade within Clade G, and Clade H all averaged over one standard deviation greater lipid content as percent of dry weight, but due to high performing taxa in other clades only Clade H was significantly greater than all below average clades (Fig. 10.3B). When examined as a proportion of cellular volume, Clades E and H were top accumulators and were significantly greater than all below average clades (Fig. 10.4B).

Several general trends can be taken from this. First, that Clade H is a top lipid accumulator in both nutrient replete and silica deplete conditions as measured as either percent dry weight or as a lipid per cellular volume. Second, that the taxa with the largest proportion of their cellular volume dedicated to lipid storage are not always the same taxa that have the highest lipid as a percent of dry weight. While this has been demonstrated to be the case in the taxa of Clade H, this is not a pattern uniformly seen within *Halamphora*. Although still useful as an easy comparative measure of lipid content the many potential issues with lipid reporting as a percent of dry weight has been discussed in detail by Stepanek et al. (*in review*). Third, although there is a general trend towards greater lipid accumulation with nutrient stress, this response is not consistent across taxa. This finding mirrors findings by Fields & Kociolek (2014) and Chtourou et al. (2015) in which they reported similar responses to silica deprivation in lipid as a percent dry weight. Although silica deprivation is presented as an appealing alternative to nitrogen deprivation used in non-siliceous algae (Sheehan et al. 1998), some cell death often begins around the third day of silica deprivation in some examined *Halamphora* taxa (personal observation). This cell death could mask additional lipid accumulation as PDW as even after death diatoms silica cell wall remains and adds to the

total dry weight. Although this should not affect lipid per volume measurements as only living cells are measured, cultures in which cell death is occurring are likely stressed to an unhealthy point. Although moderate stress may provide the desired increase in lipid production, too much stress may create the opposite reaction and result in a net less oil being produced. One of the many advantages of diatoms as a biomass feedstock is that they produce significant lipid even in nutrient replete conditions. Although accumulations may not be as great for some taxa, this could be outweighed by reduced negative reactions and continuous culture growth (Fields & Kociolek 2015, Stepanek & Kociolek *accepted*).

Phylogeny as a predictive tool

The utility of combining phylogeny, morphology, ecology and lipid production is in the development of a flexible predictive tool for the selection of clades that express a trait of interest. If an application requires a high lipid accumulating strain to be grown in high conductivity waters, taxa from Clade H would likely be a good place to begin. The power of this approach is that it extends well beyond the taxa examined in this or future studies. Because of the significant signal in lipid and conductivity data, one can predict that all members of the clade, whether they are currently known or not, would share similar trait characteristics. In this case, taxa within this clade have either biseriate dorsal striae with no marginal ridge, thickened central virgae and a prominent ventral valve with ventral striae composed of fine areolate striae, or if the dorsal striae are areolate they lack a marginal ridge but have an axial longitudinal line (Chapter 4) (Fig. 10.8). Taxa that morphologically align with this clade can be expected to share the traits of growth in marine salinities and the accumulation of high amounts of lipid. If high lipid accumulating fresh or brackish water taxa are required, Clade F contains taxa from a variety of habitats and exhibit biseriate dorsal striae with a prominent marginal ridge and no axial longitudinal line in the marine and brackish water taxa with areolate dorsal striae and thickened central virgae in the freshwater members (Chapter 4) (Fig. 10.9). For hypersaline forms Clade E would be an appropriate group for investigation (see Chapter 4 for a thorough morphological description of all *Halamphora* subgroups).

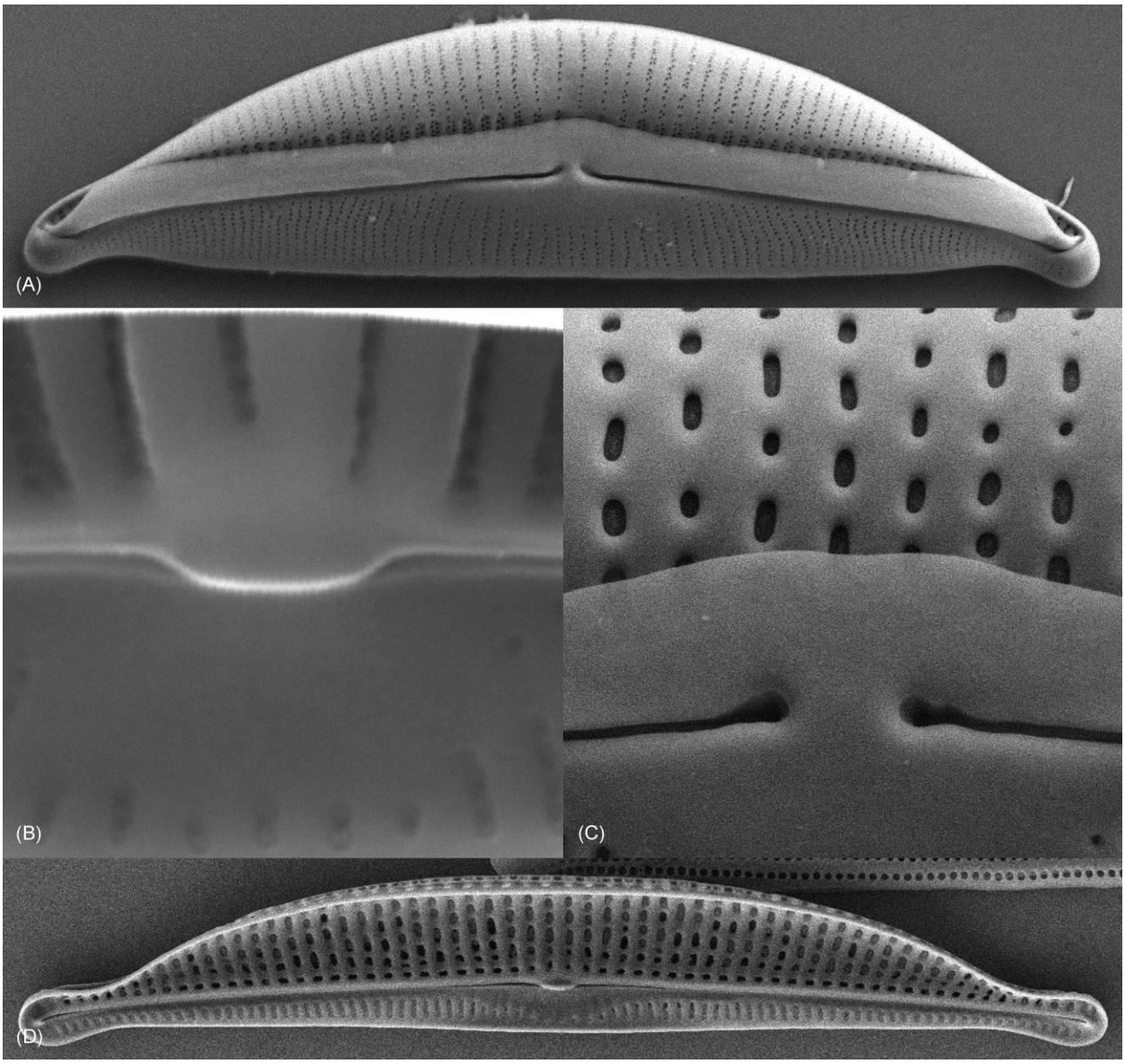

Figure 10.8. Scanning electron micrographs of *Halamphora* Clade H taxa demonstrating common morphological features. **A.** *Halamphora sp. nov.* 086 whole external valve showing biseriate dorsal striae, lack of a dorsal marginal ridge, fine ventral striae and prominent ventral valve. **B.** *Halamphora sp. nov.* 112 detail of internal valve center showing thickened central virgae. **C.** *Halamphora sp. nov.* 163 detail of external valve center showing areolate dorsal striae. **D.** *Halamphora sp. nov.* 163 whole internal valve showing areolate striae and axial longitudinal line.

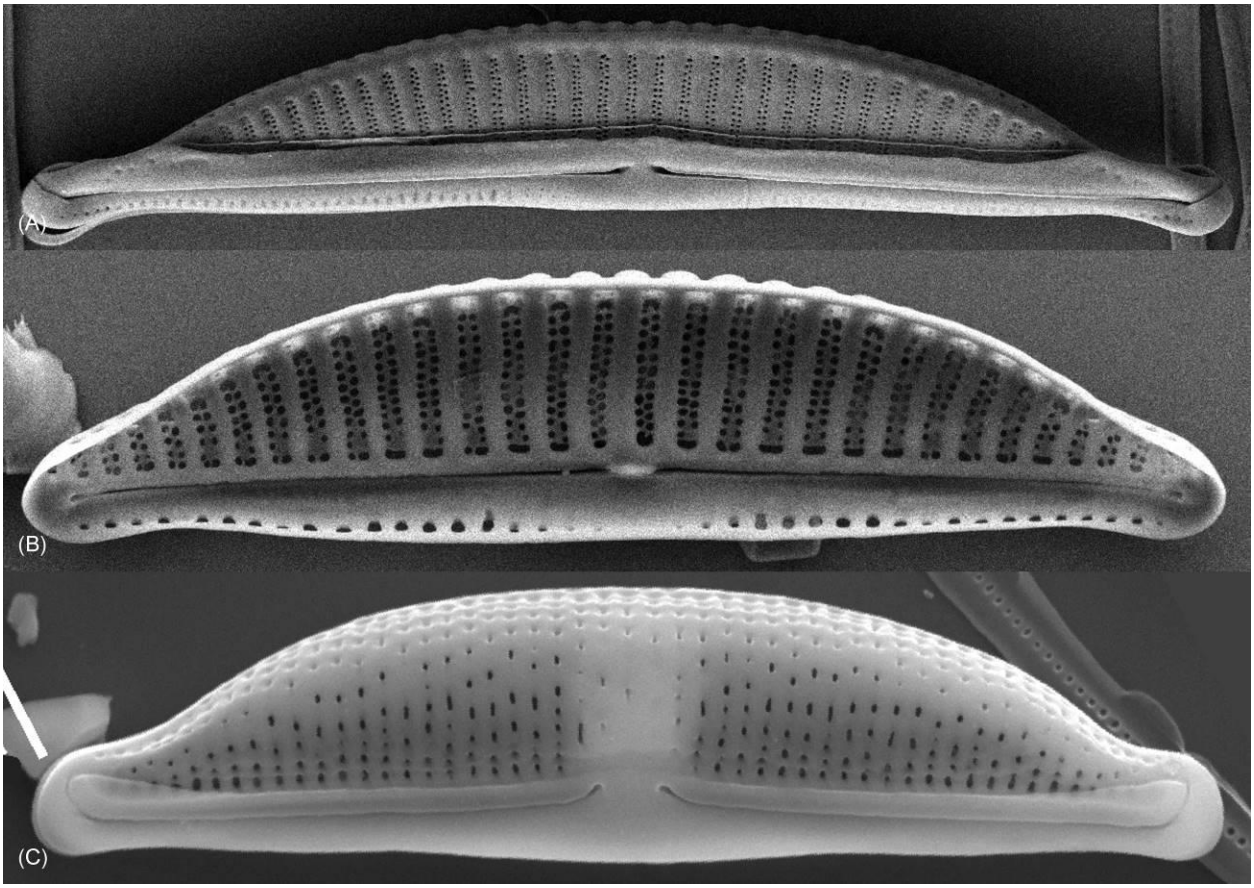

Figure 10.9. Scanning electron micrograph of *Halamphora* Clade F taxa demonstrating common morphological features. **A.** *Halamphora sp. nov.* 164 whole external valve showing biseriate dorsal striae and dorsal marginal ridge. **B.** *Halamphora sp. nov.* 166 whole internal valve showing biseriate striae and lack of an axial longitudinal line. **C.** *Halamphora fontinalis* whole external valve showing areolate striae and thickened central virgae.

The information contained within this phylogenetically organized dataset goes beyond the utility of taxon selection and can guide research into the evolution and physiological basis underlying these traits. Lipid accumulation per volume under nutrient replete conditions for Clade C (Fig. 10.4A) provides an example. This is a clade of morphologically similar taxa that includes the type of the genus, *H. coffeaeformis* (Agardh) Levkov, and can be distinguished by broad valves with biseriate dorsal striae a prominent dorsal marginal ridge and no axial longitudinal line (Chapter 4) (Fig. 10.10). Within the examined taxa, there are sister clades with significantly different lipid accumulation values. One clade that includes coastal marine and high conductivity inland taxa dedicates some of the greatest proportion of its cellular volume to lipid production and a second clade of lower conductivity inland taxa dedicates

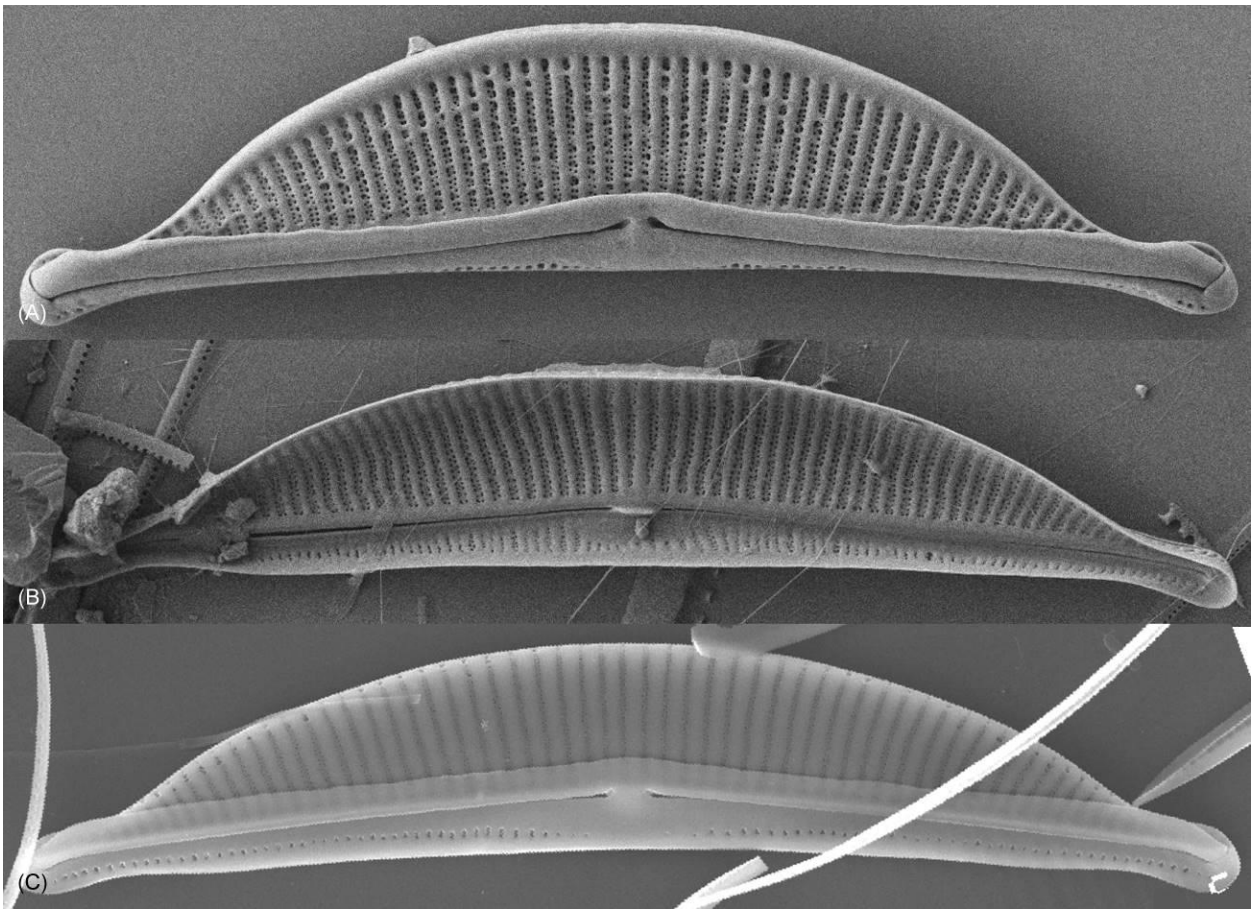

Figure 10.10. Scanning electron micrograph of *Halamphora* Clade C taxa demonstrating common morphological features. **A.** *Halamphora cf. turgida* whole external valve showing biseriate dorsal striae and dorsal marginal ridge. **B.** *Halamphora coffeaeformis* whole external valve showing biseriate dorsal striae and lack of an axial longitudinal line. **C.** *Halamphora turgida* showing biseriate dorsal striae.

some of the smallest proportion of their cellular volume to lipid storage. As sister clades, their common ancestor either exhibited high lipid production that was subsequently lost in one clade or exhibited low lipid production with one clade gaining high lipid accumulation. Overlaid onto this is a shift in ecology from what was likely an ancestral high conductivity environment into a low conductivity to nearly freshwater habitat in the low accumulating clade. Known trait difference between sister clades allows for comparative biological and genomic questions that would not be approachable without this information. Questions concerning differences in gene expression and differential adaptation are the next step to understanding the process behind the demonstrated pattern in ecological shifts as well as lipid production.

With current and future algal biomass research requiring a more detailed biological understanding of traits of interest and with the scale of the algal diversity available, hunt and peck screening (Mahapatra et al. 2013, Chtourou et al. 2015), or on the other extreme, expecting a handful of 'lab rat' algal strains to provide viable feedstocks (Dayananda et al. 2006, Scranton et al. 2015) for all applications seems unrealistic. Understanding the evolutionary relationships between organisms and the evolutionary histories of the traits they exhibit will provide a firm and predictive foundation for effective selection of lineages to meet the wide and ever changing needs of this evolving area of biomass research.

ACKNOWLEDGEMENTS

This research was funded, in part, by a joint National Science Foundation and Japanese Society for the Promotion of Science East Asia and Pacific Summer Institute fellowship NSF EAPSI No. 1316805 and a Seed Grant for Innovation from the University of Colorado Boulder.

CHAPTER XI

CONCLUSIONS AND FUTURE RESEARCH DIRECTIONS

The evolution of algal biomass research has progressed through several distinct stages, including the early exploration and characterization of algal lipids (De Mort et al. 1972, Orcutt & Patterson 1975, Anderson & Sweeny 1977), an externded period of widespread taxon screening (Sheehan et al. 1998), a period of general excitement but little progress in strain screening and selection outside of hunt and peck style localized efforts (Chelf 1990, Chisti 2007, Pienkos & Darzins 200, Brennan & Owende 2010), now into a period of genetic manipulation of model taxa (Rosenber et al. 2008, Beer et al. 2009, Radakovits et al. 2010, Cheng et al. 2014, Ma et al. 2014, Scranton et al. 2015, Tanaka et al. 2015). Although varied in approach, all of these methods are predicated on the idea that there is a best biomass taxon that will have the right combination of features to make large scale production profitable. Although considerable research has been dedicated to this process over the previous 40 years, these approaches have failed to produce yields predicted by early investigators (Sheehan et al. 1998, Gordon & Polle 2007, Chist 2007, Dismukes et al. 2008). Given the great diversity present within algal lineages, this ‘silver bullet’ model of strain selection seems unlikely to produce a taxon that is adapted and appropriate for all required applications. An alternative approach is to use the diversity present within a lineage of algae to select taxa that are most appropriate for individual applications.

The concept of creating a diverse pool of algal candidates is not a new one (Sheehan et al. 1998, DOE 2010), although this call for screening and basic biological research has gone unheeded by most subsequent researchers. The most important aspect of this candidate pool is the notion that the best algal strain is likely to be different for each production site and will require an alga that is adapted to the unique

conditions at hand (Sheehan et al. 1998). This becomes especially important in open pond systems where contamination and competition with native algal strains can severely limit the production of desired products (Posten & Schaub 2009, Williams & Laurens 2010). This has led to a disconnect between benchtop characterization and large scale production of strains, with many of the most promising laboratory strains unable to maintain production levels when grown at actual sites (Sheehan et al. 1998). The solution presented in this research is to move away from single strain investigations into a systematic appraisal of lipid production across a widespread group of known high lipid accumulating algae that are commonly found in the areas in which algal biomass operations are likely to be conducted.

This work is distinguished from previous screening efforts in that evolutionary relationships are used as the backbone for all analyses, comparisons and conclusions. This feature allows for the predictive flexibility required in the selection of promising algal strains. The diatom genus *Amphora s.l.* was chosen because it is a large and diverse group (>700 species) that is commonly found in a range of coastal and inland environments from fresh to hypersaline waters (Patrick & Freese 1961, Hohn & Hellerman 1966, Stoermer & Yang 1971, Wachnicka & Gaiser 2007, Stepanek & Kociolek 2013, Stepanek & Kociolek 2015). Additionally, members of *Amphora* have been previously shown to exhibit fast growth in culture (> 2.5 divisions per day) (Sheehan et al. 1998) and have been consistently shown to accumulate large amounts of cellular lipid (Sheehan et al. 1998, Chen 2012, Chtourou et al. 2015). Although promising, as with many algal groups, the diversity present and phylogenetic relationships within *Amphora* were poorly understood. This work represents the most extensive systematic investigation into a potential biomass feedstock, and as such, the results clearly illustrate the challenges of working with a group of organisms as diverse and understudied as microalgae. Although challenging, this work also presents a clear way forward to deal with this diversity in a biologically and evolutionarily relevant manner.

Although often overlooked, accurate and stable taxonomy must be the foundation of successful applied research. Unfortunately, even a basic level of taxonomic consistency and voucher has not been the norm for the majority of algal biofuels research. Images of taxa under investigation are rarely, if ever, included within published reports of lipid accumulation, severely limiting the usefulness and scope of the

published findings. Illustrations of investigated taxa are even more critical given the current state of flux within algal taxonomy with the inclusion of a greater number of molecular systematic studies. Nowhere is this taxonomic deficit more apparent than in the amphoroid diatoms (Section I). Of the 115 *Amphora* and *Halamphora* taxa collected from coastal and inland waters of the United States and Japan, species names could not be assigned to 50 collected taxa (Appendix 1). Although sampling was far from exhaustive, these results indicate that as much as 40% of the extant diversity of a group singled out for biofuels applications was previously unknown to science. This level of unknown diversity not only raises questions as to the diversity of lipid traits within the group, but also calls into question previous taxonomic identifications that have largely reported only a handful of commonly cited *Amphora* species if species names were given at all (Orcutt & Patterson 1975, Sheehan et al. 1998, de la Peña 2007, Csavina et al. 2011, Scholz & Liebezeit 2013).

A more confounding issue than taxonomic ambiguity is our general lack of a phylogenetic understanding of species and higher order relationships within microalgal groups, including diatoms. This is evidenced by the incongruence between historical classification systems and the relationships inferred by recent molecular phylogenetic studies within diatoms (Medlin & Kaczmarska 2004, Theriot et al. 2010, Alverson et al. 2011, Ruck & Theriot 2011, Souffreau et al. 2011, Ashworth et al. 2013, Nakov et al. 2014). The phylogeny presented here represents the most extensively sampled investigation of a single group of diatoms and illustrates the difficulty in the continued use of historical classifications in most applied diatom studies (Section II). This phylogeny demonstrates that the genus *Amphora*, for which all previous lipid accumulation data was assigned, is non-monophyletic with groups distributed across lineages that span several diatom orders. From a practical standpoint this calls into question all previous reports of high lipid production within the genus '*Amphora*' and highlights the need for a phylogenetic basis for such claims. Within the nine *Amphora* species for which lipid data has been published, only one species is included in *Amphora* as it is now prescribed. The remaining eight species are members of amphoroid groups now known to be distributed widely across the raphid diatom tree of life.

As opposed to previous screening efforts, with a firm taxonomic and phylogenetic foundation, a monophyletic subgroup within the amphoroid diatoms was selected for an evolutionary based appraisal of lipid production. Although only a subset of amphoroid diversity, the *Halamphora* group exhibited all of the characteristics that made *Amphora s.l.* a promising group for continued research. These include taxonomic and habitat diversity, fast growth rate in culture and previously reported high lipid accumulation (Sheehan et al. 1998, Scholz & Liebezeit 2013). By selecting taxa with known relationships from across the sampled evolutionary breadth the genus, important conclusions concerning lipid accumulation were made. First, there is significant species level variation in cellular lipid accumulation, making genus level characterizations inappropriate. Second, this variation in lipid accumulation exhibits a phylogenetic signal in that closely related taxa tend to have similar levels of lipid accumulation. The novelty and power of this result is that it moves away from the 'silver bullet' model of strain selection into one where evolutionary relationships are used for the predictive selection of well performing lineages.

This evolutionary based dataset has practical application for current biomass production and lays the groundwork for future comparative research. Lipid accumulation per cellular volume within *Halamphora* Clade C clearly illustrates both of these points with subclades representing some of the highest and lowest accumulators (Fig. 11.1). From the perspective of lineage selection for lipid production, the marine lineages within Clade C are promising as top accumulators within *Halamphora* and can be diagnosed as all marine taxa corresponding to the biseriate Clade C.

Although practically useful, a comparison of lipid production between clades can guide research into the evolutionary history and physiological basis underlying these traits. Much of the practical usefulness of this dataset is in the inferred similarity between closely related taxa, but for understanding drivers of the observed variation in lipid accumulation the dramatic differences between closely related lineages may be more informative. An outstanding question includes to what degree ecology plays in the variation seen in lipid accumulation. It has been shown that increased culture medium conductivity can act as a stressor to increase lipid accumulation with microalgal strains (Pugh 1971), but what is not clear

is the effect habitat transitions seen throughout the *Halamphora* phylogeny may have on lipid accumulation. This includes whether greater or lesser lipid accumulation is more adaptive to one type of habitat or if these differences may be caused by stress factors from these transitions. The results shown in Figure 11.1 Clade C as well as other areas of the phylogeny provides opportunities to test these questions through common garden style experiments. By experimentally determining the range of conductivities that the high and low accumulating lineages can survive and their lipid accumulation along this gradient, it can be determined whether there is significant overlap between lineages and to what extent divergence in ecology (Clade C is a ancestrally coastal marine group with the low accumulating lineages having moved into elevated conductivity inland waters) may be driving variation in lipid production.

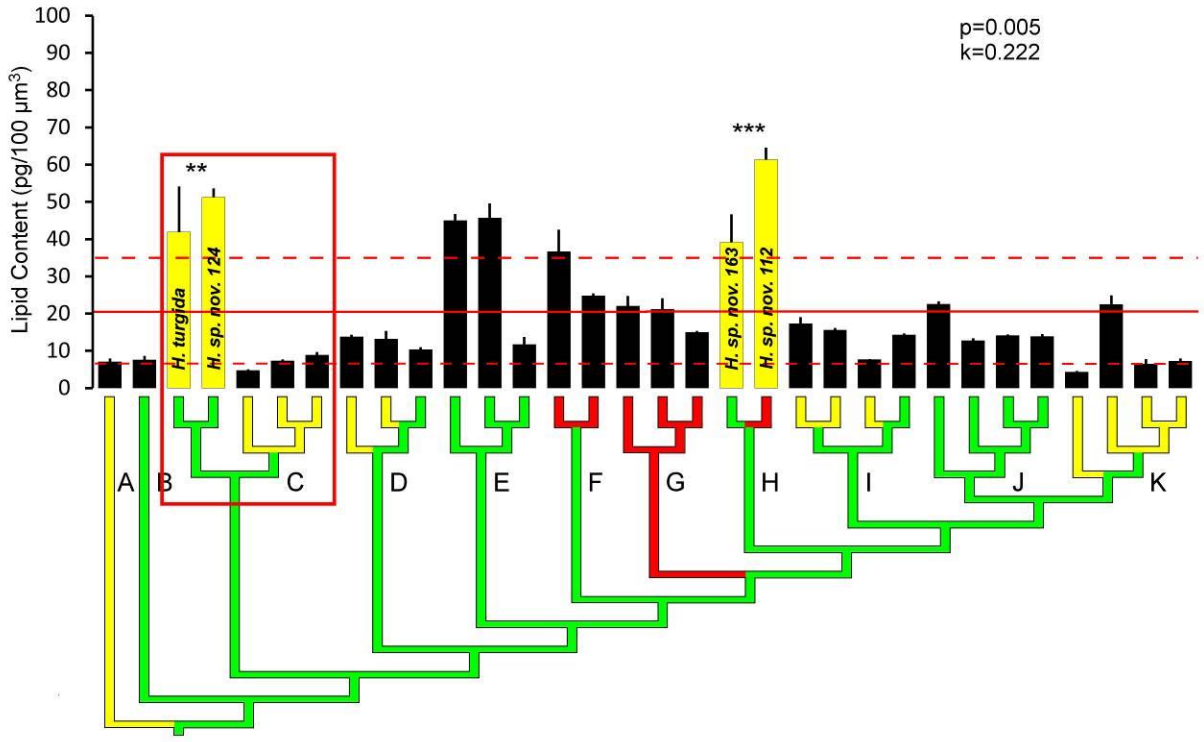

Figure 11.1. Lipid content per 100 µm^3 of cellular volume under nutrient replete growth conditions. *Halamphora* Clade C has been single out (red square) as both a potential source of high lipid accumulating taxa as well as a source of future research as a lineage with both some of the highest and lowest accumulating taxa.

If not fully attributable to habitat diverge, the known evolutionary relationships and lipid accumulation values presented here offer a unique opportunity for comparative genomic approaches towards the understanding of these habitat transitions and the regulatory mechanisms that are driving variation in lipid accumulation. Although the lipid production pathway has been extensively studied in microalgae (Sheehan et al. 1998, Gong et al. 2013, Huerlimann & Heimann 2013, Ge et al. 2014, Ma et al. 2014) the mechanisms regulating the degree of lipid accumulation remain poorly understood (Tanaka et al. 2015). The only comparative genomics investigation into diatom lipid accumulation (Tanaka et al. 2015), while an important step, relied on comparisons between published genomes of distantly related taxa to attempt to understand high lipid accumulation within *Fistulifera solaris* Mayama et al. By exploring gene expression between lineages with a known evolutionary relationship but with differing lipid expression over the range of their growth parameters provides the best opportunity to understand the genomic mechanisms behing lipid accumulation within diatoms. Taken together, this holistic biological approach of combining taxonomic, phylogenetic and applied research produces an evolutionary roadmap to both the current selection of high lipid producing lineages within *Halamhora* as well as one to guide future research into the mechanisms responsible for them.

REFERENCES

Ackerly D. 2009. Conservatism and diversification of plant functional traits: evolutionary rates versus phylogenetic signal. *Proceedings of the National Academy of Sciences*. 106: 19699–19706.

Ács É., Ector L., Kiss K.T., Cserháti C., Morales E.A. & Levkov Z. 2011. Morphological observations and emended description of *Amphora micrometra* from the Bolivian Altiplano, South America. *Diatom Research* 26: 199–212.

Admiraal W. 1977. Influence of light and temperature on the growth rate of estuarine benthic diatoms in culture. *Marine Biology*. 39: 1–9.

Agardh C.A. 1827. Aufzählung einiger in den östereichischen Ländern gefundenen neuen Gattungen und Arten von Algen nebst ihrer Diagnostik und beigefügten Bemerkungen. *Flora oder Botanische Zeitung* 2: 625–640.

Alverson A.J. 2008. Molecular systematics and the diatom species. *Protist* 159: 339–353.

Alverson A.J. 2014. Timing marine-freshwater transitions in the diatom order Thalassiosirales. *Paleobiology* 40: 91–101.

Alverson A.J., Beszteri B. Julius M.L. and Theriot E.C. 2011. The model marine diatom *Thalassiosira pseudonana* likely descended from a freshwater ancestor in the genus *Cyclotella*. *BMC Evolutionary Biology*. 11: 125.

Alverson A.J., Cannone J.J., Gutell R.R. & Theriot E.C. 2006. The evolution of elongate shape in diatoms. *Journal of Phycology* 42: 655–668.

Alverson A.J., Jansen R.K., and Theriot E.C. 2007. Bridging the Rubicon: Phylogenetic analysis reveals repeated colonizations of marine and fresh waters by thalassiosiroid diatoms. *Molecular Phylogenetics and Evolution*. 45:193-210.

Amato A., Kooistra W.H.C.F., Ghiron J.H.L., Mann D.G., Pröschold T. & Montressor M. 2007. Reproductive isolation among sympatrick cryptic speceis in marine diatoms. *Protist* 158: 193–207.

Archibald R.E.M. & Barlow D.J. 1983. On the raphe ledge in the genus *Amphora* (Bacillariophyta). *Bacillaria* 6: 257–266

Armbrust E.V., Berges J.A., Bowler C., Green B.R., Martinez D., Putnam N.H., Zhou S., Allen A.E., Apt K.E., Bechner M., Brzezinski M.A., Chaal B.K., Chiovitti A., Davis A.K., Demarest M.S., Detter J.C., Glavina T., Goodstein D., Hadi M.Z., Hellsten U., Hildebrand M., Jenkins B.D., Jurka J., Kapitonov V., Kröger N., Lau W.W.Y., Lane T.W., Larimer F.W., Lippmeier J.C., Lucas S., Medina M., Montsant A., Obornik M., Parker M.S., Palenik B., Pazour G.J., Richardson P.M., Rynearson T.A., Saito M.A., Schwartz D.C., Thamatrakoln K., Valentin K., Vardi A., Wilkerson F.P. & Rokhsar D.S. 2004. The genome of the diatom *Thalassiosira pseudonana*: ecology, evolution, and metabolism. *Science*. 306: 79–86.

Ashton K.G. 2004. Comparing phylogenetic signal in intraspecific and interspecific body size datasets. *Journal of Evolutionary Biology* 17: 1157–1161.

Badger M.R., Andrews T.J., Whitney S.M., Ludwig M., Yellowees D.C., Leggat W. & Price G.D. 1998. The diversity and co-evolution of Rubisco, plastids, pyrenoids and chloroplast-based CCMs in algae. *Canadian Journal of Botany* 76: 1052–1071.

Bajpai R., Zappi M., Dufreche S., Subramaniam R. & Prokop A. 2014. Status of algae as vehicles for commercial production of fuels and chemicals. In: *Algal Biorefineries Volume I: Cultivation of Cells and Products* (Eds. R. Bajpai, A. Prokop & M. Zappi), pp. 3–24. Springer Dordiecht, Heidelberg, London, New York.

Barclay W., Johansen J., Chelf P., Nagle N., Roessler R. & Lemke P. 1986. Microalgae culture collection 1986–1987. Solar Energy Research Institute, Golden, Colorado, SERI/SP-232-3079. 147 pp.

Bassi A., Saxena P. & Aguirre A. 2014. Mixotrophic algae cultivation for energy produciton and other applications. In: *Algal Biorefineries Volume I: Cultivation of Cells and Products* (Eds. R. Bajpai, A. Prokop & M. Zappi), pp. 177–202. Springer Dordiecht, Heidelberg, London, New York.

Baurain D., Brinkmann H., Petersen J., Rodríguez-Ezpeleta N., Stechmann A., Demoulin V., Roger A.J., Burger G., Lang B.F. & Philippe H. 2010. Phylogenetic evidence for the separate acquisition of

plastids in Cryptophytes, Haptophytes, and Stramenopiles. *Molecular Biology and Evolution* 27: 1698–1709.

Becker E.W. 2007. Micro-algae as a source of protein. *Biotechnology Advances* 25: 207–210.

Beer L.L., Boyd E.S. Peters J.W. & Posewitz M.C. 2009. Engineering algae for biohydrogen and biofuel production. *Current Opinion in Biotechnology*. 20: 264–271.

Bérard-Therriault L., Cardinal A. & Poulin M. 1986. Les diatomées (Bacillariophyceae) benthiques de substrats durs des eaux marines et saumâtres du Québec. 6. Naviculales: Cymbellaceae et Gomphonemaceae. *Le Naturaliste Canadien*. 113: 405–429.

Berge J.P., Bourgougnon N., Carbonnelle D., Le Bert V., Tomasoni C., Durand P. & Roussakis C. 1997. Antiproliferative effects of an organic extract from the marine diatom *Skeletonema costatum* (Grev.) Cleve against a non-small-cell bronchopulmonary carcinoma line (NSCLC-N6). *Anticancer Research*. 17: 2115–2120.

Beszteri B., Ács E & Medlin L.K. 2005. Ribosomal DNA sequence variation among sympatric strains of the *Cyclotella meneghiniana* complex (Bacillariophyceae) reveals cryptic diversity. *Protist* 156: 317–333.

Betancur-R R., Ortí G., Stein A.M., Marceniuk A.P. & Pyron R.A. 2012. Apparent signal of competition limiting diversification after ecological transitions from marine to freshwater habitats. *Ecology Letters* 15: 822–830.

Blinn D.W. 1993. Diatom community structure along physicochemical gradients in saline lakes. *Ecology* 74: 1246–1263.

Blomberg S.P., Garland T. & Ives A.R. 2003. Testing for phylogenetic signal in comparative data: behavioral traits are more labile. *Evolution*. 57: 717–745.

Bowler C., Allen A.E., Badger J.H., Grimwood J., Jabbari K., Kuo A., Maheswari U., Martens C., Maumus F., Otillar R.P., Rayko E., Salamov A., Vandepoele K., Beszteri B., Gruber A., Heijde M., Katinka M., Mock T., Valentin K., Verret F., Berges J.A., Brownlee C., Cadoret J., Chiovitti A., Choi C.J., Coesel S., De Martino A., Detter J.C., Durkin C., Falciatore A., Fournet J., Haruta

M., Huysman M.J.J., Jenkins B.D., Jiroutova K., Jorgensen R.E., Joubert Y., Kaplan A., Kröger N., Kroth P.G., La Roche J., Lindquist E., Lommer M., Martin–Jézéquel V., Lopez P.J., Lucas S., Mangogna M., McGinnis K., Medlin L.K., Montsant A., Oudot–Le Secq M., Napoli C., Obornik M., Parker M.S., Petit J., Porcel B.M., Poulsen N., Robison M., Rychlewski L., Rynearson T.A., Schmutz J., Shapiro H., Siaut M., Stanley M., Sussman M.R., Taylor A.R., Vardi A., von Dassow P, Vyverman W., Willis A., Wyrwicz L.S., Rokhsar D.S., Weissenbach J., Armbrust E.V., Green B.R., Van de Peer Y. & Grigoriev I.V. 2008. The *Phaeodactylum* genome reveals the evolutionary history of diatom genomes. *Nature*. 456: 239–244.

Boyer C.S. 1914. A new diatom. *Proceedings of the Academy of Natural Sciences of Philadelphia* 66: 219–221.

Brennen L, Owende P. 2010. Biofuels from microalgae – a review of thechnologies for production, and extractions of biofuels and co-products. *Renewable and Sustainable Energy Reviews* 14, 557–577.

Bruder K. & Medlin L.K. 2008. Morphological and molecular investigations of naviculoid diatoms. II. Selected genera and families. *Diatom Research.*23: 283-329.

Carter J.R. & Round F.E. 1993. Studies on freshwater *Amphora* species V. *A. montana* and *A. normanii*. *Diatom Research* 8: 1–11.

Casteleyn G., Adams N.G., Vanormelingen P., Debeer A., Sabbe K. & Vyverman W. 2009. Natural hybrids in the marine diatom *Pseudo-nitzschia pungens* (Bacillariophyceae): genetic and morphological evidence. *Protist* 160: 343–354.

Chen Y.C. 2012. The biomass an total lipid content and composition of twelve species of marine diatoms cultured under various environments. *Food Chemistry* 131: 211–219.

Cheng J., Feng J., Sun J., Huang Y., Zhou J. & Cen K. 2014. Enhancing the lipid content of the diatom *Nitzschia sp*. by ^{60}Co-ɣ irradiation mutation and high-salinity domestication. *Energy*. 78: 9–15.

Chisti Y. 2007. Biodiesel from microalgae. *Biotechnology Advances.* 25: 294–306.

Chtourou H., Dahmen I., Jebali A., Karray F., Hassairi I., Abdelkafi S. Ayadi H. Sayadi S. & Dhouib A. 2015. Characterization of *Amphora* sp., a newly isolated diatom wild strain, potentially usable for biodiesel production. *Bioprocesses and Biosystems Engineering*. 38: 1381–1392.

Cirulis J.T., Strasser B.C. Scott J.A. & Ross G.M. 2012. Optimization of staining conditions for microalgae with three lipophilic dyes to reduce precipitation and fluorescence variablility. *Cytometry Part A*. 81A: 618–626.

Clavero E., Grimalt J.O. & Hernández-Mariné M. 2000. The fine structure of two small *Amphora* species. *A. tenerrima* Aleem & Hustedt and *A. tenuissima* Hustedt. *Diatom Research* 15: 195–208.

Cleve P.T. 1895. Synopsis of naviculoid diatoms. II. KongligaSvenska-Vetenskaps Akademiens Handlingar, Vol: 27, Issue: 3, 1-219.

Cobelas M.A. & Lechado J.Z. 1989. Lipids in microalgae. A review I. Biochemistry. *Grasas y Aceites*. 40: 118–145.

Cox E.J. 1995. Morphological variation in widely distributed diatom taxa: taxonomic and ecological implications. Proceedings of the thirteenth international diatom symposium, Bristol: Biopress LTD.

Cox E.J. & Ross R. 1981. The striae of pennate diatoms. Proceedings of the 6th international symposium on recent and fossil diatoms, Budapest. pp. 115–133

Csavina J.L., Stuart B.J., Riefler R.G. & Vis M.L. 2011. Growth optimization of algae for biodiesel production. *Journal of Applied Microbology* 11: 312–318.

Cubo J., Ponton F., Laurin M., De Margerie E. & Castanet J. 2005. Phylogenetic signal in bone microstructure of sauropsids. *Systematic Biology* 54: 562–574.

D'Alelio D., Amato A., Kooistra W.H.C.F., Procaccini G., Casotti R. & Montresor M. 2009. Internal transcribed spacer polymorphism in *Pseudo-nitzschia multistriata* (Bacillariophyceae) in the Gulf of Naples: recent divergence or intraspecific hybridization? *Protist* 160: 9–20.

d'Ippolito G., Sardo A., Paris D., Vella F.M., Adelfi M.G., Botte P., Gallo C. & Fontana A. 2015. Potential of lipid metabolism in marine diatoms for biofuel production. *Biotechnology for Biofuels*. DOI 10.1186/s13068-015-0212-4.

Da Silva T.L., Reis A., Medeiros R., Oliveira A.C. & Gouveia L. 2009. Oil production towards biofuel from autotrophic microalgae semicontinuous cultivations monitorized by flow cytometry. *Applied biochemistry and Biotechnology*. 159: 568–578.

Dahl T.E. 1990. Wetland losses in the United States 1780's to 1980's. *U.S. Department of the Interior, Fish and Wildlife Service*. Washington D.C. 13 pp.

Daugbjeg N. & Andersen R.A. 1997. A molecular phylogeny of the heterokont algae based on analysis of chloroplast-encoded rbcL sequence data. *Journal of Phycology* 33: 1031–1041.

Dayananda C., Sarada R., Usha Rani M., Shamala T.R. & Ravishankar G.A. 2007. Autotrophic cultivation of *Botryococcus braunii* for the production of hydrocarbons and exopolysaccharides in various media. *Biomass and Bioenergy* 31: 87–93.

de la Peña M.R. 2007. Cell growth and nutritive value of the tropical benthic diatom, *Amphora* sp., at varying levels of nutrients and light intensity, and different culture locations. *Journal of Applied Phycology* 19: 647–655.

De Toni G.B. 1891. Sylloge algarum omnium hucusque cognitarum. Vol. II. Sylloge Bacillariearum. Sectio I. Rhaphideae.

Dempster T.A. & Sommerfeld M.R. 1998. Effects of environmental conditions on growth and lipid accumulation in *Nitzschia communis* (Bacillariophyceae). *Journal of Phycology*. 34: 712-721.

Desbois A.P., Mearns-Spragg A. & Smith V.J. 2009. A fatty acid from the diatom *Phaeodactylum tricornutum* is antibacterial against diverse bacteria including multi-resistant *Staphylococcus aureus* (MRSA). *Marine Biotechnology* 11: 45–52.

Dismukes G.C., Carrieri D., Bennette N., Ananyev G.M. & Posewitz M.C. 2008. Aquatic phototrophs: efficient alternatives to land-based crops for biofuels. *Current opinion in biotechnology* 19: 235–240.

Doherty K.E., Ryba A.J., Stemler C.L., Niemuth N.D. & Meeks W.A. 2013. Conservation planning in an era of change: state of the U.S. prairie pothole region. *Wildlife Society Bulletin* 37: 546–563. doi:10.1371/journal.pone.0130053.

Doucha J. & Lívanský K. 2014. High density outdoor microalgal culture. In: *Algal Biorefineries Volume I: Cultivation of Cells and Products* (Eds. R. Bajpai, A. Prokop & M. Zappi), pp. 147–173. Springer Dordiecht, Heidelberg, London, New York.

Doyle J.J. 1992. Gene trees and species trees: molecular systematics as one-character taxonomy. *Systematic Botany* 17: 144–163.

Drum R.W. & Hopkins J.T. 1966. Diatom locomotion: an explanation. *Protoplasm* 62: 1–33.

Drummond A.J., Ashton B., Buxton S., Cheung M., Cooper A., Duran C., Heled J., Kearse M., Markowitz S., Moir R., Stones-Havas S., Sturrock S., Swidan F., Thierer T., Wilson A. 2012. Geneious v5.6, Available from http://www.geneious.com

Dunahay T.G., Jarvis E.E., Dais S.S. & Roessler P.G. 1996. Manipulation of microalgal lipid production using genetic engineering. *Applied Biochemistry and Biotechnology*. 57/58: 223–231.

Edgar C. 2004. MUSCLE: multiple sequence alignment with high accuracy and high throughput. *Nucleic Acids Research* 32: 1792–1797.

Edgar S.M. & Theriot E.C. 2004. Phylogeny of *Aulacoseira* (Bacillariophyta) based on morphology and molecules. *Journal of Phycology* 40: 772–788.

Edlund M.B. & Stoermer E.F. 1999. Taxonomy and morphology of *Amphora calumetica* (B.W. Thomas *ex* Wolle) Perag., an episammic diatom from post-Pleistocene large lakes. In: *Proceedings of the fourteenth international diatom symposium* (Ed. by S. Mayama, M. Idei & I. Koizumi), pp. 63–74. Koeltz Scientific Books, Koenigstein.

Edlund M.B., Brant L.A., Levkov Z. & Nakov T. 2006. An emended description of *Decussata* (Patrick) Lange-Bertalot & Metzeltin that includes protoplast organization and detailed valve and cingulum ultrastructure. *Diatom Research* 21: 269–280.

Ehrenberg C.G. 1838. Die infusionsthierchen als vollkommene Organismen. Verlag von Leopold Voss, Leipzig. 548 pp.

Ehrenberg C.G. 1841 Verbreitung und Einflufs des mikroskopischen Lebens in Süd-und Nord-Amerika. *Abhandlungen der Königlichen Akademie der Wissenschaften zu Berlin* 1: 291–445.

Elmore C.J. 1921. The diatoms (Bacillarioideae) of Nebraska. *University Studies, January-October, The University of Nebraska, Lincoln* 21: 22–214.

Evans K.M., Wortley A.H. & Mann D.G. 2007. An assessment of potential diatom "barcode" genes (*cox*1, *rbc*L, 18S and ITS rDNA) and their effectiveness in determining relationships in *Sellaphora* (Bacillariophyta). *Protist* 158: 349–364.

Evans K.M., Wortley A.H., Simpson G.E., Chepurnov V.A. & Mann D.G. 2008. A molecular systematic approach to explore diversity within the *Sellaphora pupula* species complex (Bacillariophyta). *Journal of Phycology* 44: 215–231.

Felsenstein J. 1985. Phylogenies and the comparative method. *The American Naturalist* 125: 1–15.

Fields F.J. & Kociolek J.P. 2015. An evolutionary perspective on selecting high-lipid-content diatoms (Bacillariophyta). *Journal of Applied Phycology*. 27: 2209–2220.

Foged N. (1964) Freshwater diatoms from Spitsbergen. *Tromsö Museums Skrifter, Universitetsførlaget* 11: 1–204.

Fourtanier E. & Kociolek J.P. 2009. Catalogue of diatom names part II: *Abas* through *Bruniopsis*. Occasional papers of the California Academy of Sciences No. 156: Part II

Fourtanier E. & Kociolek J.P. 2011.Catalogue of Diatom Names, California Academy of Sciences, On-line at http://www.calacademy.org/research/diatoms/names/index.asp.

Frenguelli G. 1929. Algae Bacillariales. In: Chiovenda, E. (ed.) *Flora Somala*. Sindacato Italiano Arti Graphiche Editore in Roma. 1: 371–408.

Fritz S.C. & Battarbee R.W. 1988. Sedimentary diatom assemblages in freshwater and saline lakes of the Northern Great Plains, North America: Preliminary results. In: *Proceedings of the ninth*

international diatom symposium (Ed. by F.E. Round), pp. 246–252. Biopress Ltd, Bristol and Koeltz Scientific Books, Koenigstein.

Fritz S.C. 1990. Twentieth-century salinity and water-level fluctuations in Devils Lake, North Dakota: Test of a diatom-based transfer function. *Limnology and Oceanography* 35: 1771–1881.

Fritz S.A. & Purvis A. 2010. Selectivity in mammalian extinction risk and threat types: a new measure of phylogenetic signal strength in binary traits. *Conservation Biology*. 24: 1042–1051.

Fritz S.C., Ito E., Yu Z., Laird K.R & Engstrom D.R. 2000. Hydrologic variation in the northern great plains during the last two millennia. *Quaternary Research* 53: 175–184.

Funk D.L. & Omland K.E. 2003. Species-level paraphyly and polyphyly: frequency, causes, and consequences, with insights from animal mitochondrial DNA. *Annual Review of Ecology, Evolution and Systematics* 34: 397–423.

Galloway A.W.E. & Winder M. 2015. Partitioning the relative importance of phylogeny and environmental conditions on phytoplankton fatty acids. *PLoS ONE* 10: e0130053. doi:10.1371/journal.pone.0130053.

Gavrilescu M. & Chisti Y. 2005. Biotechnology–a sustainable alternative for chemical industry. *Biotechnology Advances*. 23: 471–499.

Gavrilets S. & Losos J.B. 2009. Adaptive radiation: contrasting theory with data. *Science* 323: 732–737.

Ge F., Huang W., Chen Z., Zhang C., Xiong Q., Bowler C., Yang J., Xu J. & Hu H. 2014. Methylcrotonyl-CoA carboxylase regulates triacylglycerol accumulation in the model diatom *Phaeodactylum tricornutum*. *The Plant Cell* doi: http://dx.doi.org/10.1105/tpc.114.124982

Gmelin J.F. 1791. In *Systema Naturae* Edition 13, 1(6). Lipsiae.

Gong Y., Zhang J., Guo X., Wan X., Liang Z., Hu C.J. & Jiang M. 2013. Indentification and characterization of PtDGAT2B, an acyltransferase of the DGAT2 acyl-Coenzyme A: Diacylglycerol acyltransferase family in the diatom *Phaeodactylum tricornutum*. *FEBS Letters* 587: 481–487.

Gordon J.M. & Polle J.E.W. 2007. Ultrahigh bioproductivity from algae. *Applied Microbial Biotechnology* 76: 969–975.

Gouy M., Guindon S. & Gascuel O. 2010. SeaView version 4: a multiplatform graphical user interface for sequence alignment and phylogenetic tree building. *Molecular Biology and Evolution* 27: 221–224.

Graham J.M., Graham L.E., Zulkifly S.B. Pfleger B.F. Hoover S.W. & Yoshitani J. 2012. Freshwater diatoms as a source for biofuels. *Journal of Industrial Microbiology and Biotechnology*. 39: 419–428.

Green B.R. 2011. Chloroplast genomes of photosynthetic eukaryotes. *The Plant Journal* 66, 34–44.

Griffiths M.J. & Harrison T.L. 2009. Lipid productivity and a key characteristic for choosing algal species for biodiesel production. *Journal of Applied Phycology*. 21: 493–507.

Groom M.J., Gray E.M. & Townsend P.A. 2008. Biofuels and biodiversity: principles for creating better policies for biofuel production. *Conservation Biology* 22: 602–609.

Gross F. & Zeuthen E. 1948. The buoyancy of planktonic diatoms: a problem of cell physiology. *Proceedings of the Royal Society B.* vol. 135.

Guillard R.R.L. & Lorenzen C.J. 1972. Yellow-green algae with chlorophyllide. *Journal of Phycology*. 8: 10–14.

Guillard R.R.L. 1973. Division rates. J.R. Stein (Ed.), Handbook of phycological methods, culture methods and growth measurements. Press Syndicate of the University of Cambridge, New York, pp. 289–312.

Guindon S., Dufayard J.F., Lefort V., Anisimova M., Hordijk W. & Gascuel O. 2010. New algorithms and methods to estimate maximum-likelihood phylogenies: assessing the performance of PhyML 3.0. *Systematic Biology* 59: 307–321.

Guindon S. & Gascuel O. 2003. A simple, fast and accurate method to estimate large phylogenies by maximum-likelihood. *Systematic Biology* 52: 696–704.

Guindon S., Dufayard J.F., Lefort V., Anisimova M., Hordijk W. & Gascuel O. 2010. New algorithms and methods to estimate maximum-likelihood phylogenies: assessing the performance of PhyML 3.0. *Systematic Biology* 59: 307–321.

Guiry M.D. 2012. How many species of algae are there? *Journal of Phycology*. 48: 1057–1063.

Gusylakov N.E. 1985. 0 morfologii pantsirei nekotorykh predstabitelei roda Amphora (Bacillariophyta) iz Chernogo Morya. [On the morphology of the frustules in some representatives of genus Amphora (Bacillariophyta) from the Black Sea.] Bot. Zh. 70: 1478-1481.

Haimovich-Dayan M., Garfinkel N., Ewe D., Marcus Y., Gruber A., Wagner H., Kroth P.G. & Kaplan A. 2013. The roll of C_4 metabolism in the marine diatom *Phaeodactylum tricornutum*. *New Phytologist* 197: 177

Hamilton P.B. & Laird K.R. 2011. *Nitzschia pseudosinuata* sp. nov., a new Holocene diatom from the sediment of Moon Lake, North Dakota, U.S.A. *Diatom Research* 16: 317–324.

Hamsher S.E., Evans K.M., Mann D.G, Poulíčková A. & Saunders G.W. 2011. Barcoding diatoms: Exploring Alternatives to COI-5P. *Protist.*162: 405-422.

Hamsher S.E. & Saunders G.W. 2014. A floristic survey of marine tube-forming diatoms reveals unexpected diversity and extensive co-habitation among genetic lines of the *Berkeleya rutilans* complex (Bacillariophyceae). *European Journal of Phycology* 49: 47–59.

Hamsher S.E., LeGresley M.M., Martin J.L. & Saunders G.W. 2013. A comparison of morphological and molecular-based surveys to estimate the species richness of *Chaetoceros* and *Thalassiosira* (Bacillariophyta), in the Bay of Fundy. *PLOS ONE* 8: e73521. doi:10.1371/journal.pone.0073521.

Harmon L.J, Weir J.T, Brock C.D. Glor R.E. & Challenger W. 2008. GEIGER: investigating evolutionary radiations. *Bioinformatics* 24: 129–131.

Harmon L.J., Losos J.B., Davies T.J., Gillespie R.G., Gittleman J.L., Jennings W.B., Kozak K.H., McPeek M.A., Moreno-Roark F., Near T.J., Purvis A., Ricklefs R.E., Schluter J.A., Seehausen

O., Sidlauskas B.L., Torres-Carvajal O., Weir J.T. & Mooers A.Ø. 2010. Early bursts of body size and shape evolution are rare in comparitive data. *Evolution* 64: 2385–2396.

Heath T.A., Hedtke S.M. & Hillis D.M. 2008. Taxon sampling and the accuracy of phylogenetic analyses. *Journal of Systematics and Evolution* 46 : 239–257.

Hildebrand M., Davis A.K., Smith S.R., Traller J.C. & Abbriano R. 2012. The place for diatoms in the biofuels industry. *Biofuels*. 3: 221–240.

Hillebrand H., Dürselen C., Kirschtel D., Pollingher U. & Zohary T. 1999. Biovolume calculation for pelagic and benthic microalgae. *Journal of Phycology*. 35: 403–424.

Hoelzer G.A. & Melnick D.J. 1994. Patterns of speciation and limits to phylogenetic resolution. *Tree* 9: 104–107.

Hohn M.H. & Hellerman J. 1966. New diatoms from the Lewes-Rehoboth Canal, Delaware and Chesapeake Bay area of Baltimore, Maryland. *Transactions of the American Microscopical Society* 85: 115–130.

Hohn M.H. 1961. The relationship between species diversity and population density in diatom populations from Silver Springs, Florida. *Transactions of the American Microscopical Society* 80: 140–165.

Hohn M.H. & Hellerman J. 1963. The taxonomy and structure of diatom populations from three eastern North American rivers using three sampling methods. *Transactions of the American Microscopical Society* 82: 250–329.

Holland A.D. & Dragavon J.M. 2014. Algal reactor design based on comprehensive modeling of light and mixing. In: *Algal Biorefineries Volume I: Cultivation of Cells and Products* (Eds. R. Bajpai, A. Prokop & M. Zappi), pp. 25–68. Springer Dordiecht, Heidelberg, London, New York.

Huang G., Chen G. & Chen F. 2009. Rapid screening method for lipid production in alga based on Nile red fluorescence. *Biomass and Bioenergy*. 33: 1386–1392.

Hudek K., Davis L.C., Ibbini J. & Erickson L. 2014. Commercial products from algae. In: *Algal Biorefineries Volume I: Cultivation of Cells and Products* (Eds. R. Bajpai, A. Prokop & M. Zappi), pp. 275–295. Springer Dordiecht, Heidelberg, London, New York.

Huerlimann R. & Heimann K. 2013. Comprehensive guide to acetyl-carboxylases in algae. *Critical Reviews in Biotechnology* 33: 49–65.

Huerlimann R., de Nys R. & Heimann K. 2010. Growth, lipid content, productivity, and fatty acid composition of tropical microalgae for scale-up production. *Biotechnology and Bioengineering*. 107: 245–257.

Hustedt F. 1955. Marine littoral diatoms of Beaufort, North Carolina. *Duke University Marine Station, Bulletin* 6: 1–67.

Hustedt F. 1925. Bacillariales aus den Salzgewässern bei Oldesloe in Holstein. *Mitteilungen der geographischen Gesellschaft und der Naturhistorischen Museums in Lubeck, zweite Reihe* 30: 84–121.

Jahn R. & Kusber W. 2004. Algae of the Ehrenberg collection: 1. Typification of 32 names of diatom taxa described by C.G. Ehrenberg. *Wildenowia* 34: 577–595.

Jin E., Polle J.E.W., Lee H.K., Hyun S.M. & Chang M. 2003. Xanthophylls in microalgae, from biosynthesis to biotechnological mass production and application. *Journal of Microbiology and Biotechnology*. 13: 165–174.

John J. 1981. *Amphora australiensis* sp. nov. *Nova Hedwigia* 31: 39–53.

Johnson R.R. & Higgins K.F. 1997. *Wetland resources of eastern South Dakota*. South Dakota State University, Brookings, South Dakota, 120 pp.

Julius M.L. & Tanimura Y. 2001. Cladistic analysis of plicated *Thalassiosira* (Bacillariophyceae). *Phycologia* 40: 111–122.

Julius M.L., Stepanek J., Tedrow O. Gamble C. & Schoenfuss H.L. 2007. Estrogen-receptor independent effects of two ubiquitous environmental estrogens on *Melosira varians* Agardh, a common component of the aquatic primary production community. *Aquatic Toxicology*. 85: 19–27.

Kaczmarska I. & Rushforth S.R. 1983. The diatom flora of Blue Lake Warm Spring, Utah, U.S.A. *Bibliotheca Diatomologica*. 2: 1–123.

Kembel S.W., Cowan P.D., Helmus M.R., Cornwell W.K., Morlon H., Ackerly D.D., Blomberg S.P. & Webb C.O. 2010. Picante: R tools for integrating phylogenies and ecology. *Bioinformatics* 26: 1463–1464.

Kermarrec L., Ector L., Bouchez A., Rimet F., Hoffmann L. 2011. A preliminary phylogenetic analysis of the Cymbellales based on 18S rDNA gene sequencing. *Diatom Research* 26: 305–315

Khozin-Goldberg I. & Cohen Z. 2006. The effect of phosphate starvation on the lipid and fatty acid composition of the fresh water eustigmatophyte *Monodus subterraneus*. *Phytochemestry*. 67: 696–701.

Kociolek J.P. 2006. Some thoughts on the development of a diatom flora for freshwater ecosystems in the continental United States and a listing of recent taxa described from U.S. freshwaters. *Proceedings of the California Academy of Sciences* 57: 561–586.

Kociolek J.P. & Stoermer E.F. 1986. Phylogenetic relationships and classification of monoraphid diatoms based on phonetic and cladistic methodologies. *Phycologia* 25: 297–303.

Kociolek J.P. & Stoermer E.F. 1988. A preliminary investigation of the phylogenetic relationships among the freshwater, apical pore field bearing cymbelloid and gomphonemoid diatoms (Bacillariophyceae). *Journal of Phycology* 24: 337–385.

Kociolek J.P. & Stoermer E.F. 1993. Freshwater gomphonemoid diatom phylogeny: Preliminary results. *Hydrobiologia* 269-270: 31–38.

Kociolek J.P., Laslandes B., Benett D., Thomas E., Brady M. & Graeff C. 2014. Diatoms of the United States 1 taxonomy, ultrastructure and descriptions of new species and other rarely reported taxa from lake sediments in the western U.S.A. *Bibliotheca Diatomologica* 61: 1–188.

Kociolek J.P., Stepanek J.G., Lowe R.L., Johansen J.R. & Sherwood A.R. 2013. Molecular data show the enigmatic cave-dwelling diatom *Diprora* (Bacillariophyceae) to be a raphid diatom. *European Journal of Phycology* 48: 474–484.

Krammer K. & Lange-Bertalot H. 1986. Bacillariophyceae. I. Teil. Naviculaceae. In *Süsswasserflora von Mitteleuropa. Band 2/1.* 876 pp.

Krammer K. 1997. Die cymbelloiden Diatomeen. Eine Monographie der weltweit bekannten Taxa. Teil 2. *Encyonema* part., *Encyonopsis* and *Cymbellopsis*. *Bibliotheca Diatomologica* 37: 1–463.

Krammer K. 1980. Morphologic and taxonomic investigations of some freshwater species of the diatom genus *Amphora* Ehr. *Bacillaria* 3: 197–225.

Kützing F.T. 1844. *Die Kieselschaligen. Bacillarien oder Diatomeen.* Nordhausen. 152 pp.

Kumar A., Ergas S., Yaun X., Sahu A., Zhang Q., Dewulf J., Malcata F.X. & van Langenhove H. 2010. Enhanced CO2 fixation and biofuel production via microalgae: recent developments and future directions. *Trends in Biotechnology* 28: 371–380.

Lancelot C. & Mthot S. 1985. Biochemical fractionation of primary production by phytoplankton in Belgian coastal waters during short-term and long-term incubations with ^{14}C-bicarbonate. 1. Mixed diatom population. *Marine Biology*. 86: 219–226.

Lang I. & Kaczmarska I. 2011. A protocol for a single-cell PCR of diatoms from fixed samples: method validation using *Ditylum brightwellii* (T. West) Grunow. *Diatom Research*. 26: 43–49.

Lange-Bertalot H. & Metzeltin D. 1996. Indicators of oligotrophy, 800 taxa representative of three ecologically distinct lake types, carbonate buffered – oligodystrophic – weakly buffered soft water. In: Lange-Bertalot, H. (ed.) *Iconographia Diatomologica*. Annotated Diatom Monographs. Vol. 2. Ecology, Diversity, Taxonomy. Koeltz Scientific Books. Königstein, Germany, 390 pp.

Laurens L.M.L., Quinn M., Van Wychen S., Templeton D.W. & Wolfrum E.J. 2012. Accurate and reliable quantification of total microalgal fuel potential as fatty acid methyl esters by *in situ* transesterification. *Analytical and Bioanalytical Chemistry*. 403: 167–178.

Lebeau T. & Roberts J. 2003. Diatom cultivation and biotechnologically relevant products. Part 1: cultivation at various scales. *Applied Microbiology and Biotechnology*. 60: 612–623.

Lee C.E. & Bell M.A. 1999. Causes and consequences of recent freshwater invasions by saltwater animals. *Trends in Ecology and Evolution* 14: 284–288.

Lee K. & Round F.E. 1987. Studies on freshwater *Amphora* species. I. *Amphora ovalis. Diatom Research* 2: 193–203.

Lee K. & Round F.E. 1988. Studies on freshwater *Amphora* species. II. *Amphora copulata* (Kütz.) Schoeman & Archibald. *Diatom Research* 3: 217–225.

Lee K. & Round F.E. 1989. Studies on freshwater *Amphora* species. III. *Amphora pediculus* (Kütz.) Grun. and some possibly related forms. *Diatom Research* 4: 79–87.

Lee S.S., Gaiser E.E., Van De Vijver B., Edlund M.B. & Spaulding S.A. 2014. Morphology and typification of *Mastogloia smithii* and *M. lacustris*, with descriptions of two new species from the Florida Everglades and the Caribbean region. *Diatom Research* 29: 325–350.

Levkov Z. 2009. *Amphora* sensu lato. In: Lange-Bertalot, H. (ed.) *Diatoms of Europe, Volume 5*. A.R.G. Gantner Verlag K.G., Ruggell, 916 pp.

Li C.L., Ashworth M.P., Witkowski A., Dabek P., Medlin L.K., Kooistra W.H.C.F., Sato S., Zglobicka I., Kurzydloski K.J., Theriot E.C., Sabir J.S.M., Khiyamai M.A., Mutwakil M.H.Z., Sabir M.J., Alharbi N.S., Hajarah N.H., Qing S. & Jansen R.K. 2015. New insights into Plagiogrammaceae (Bacillariophyta) based on multigene phylogenies and morphological characteristics with the description of a new genus and three new species. *PLOS ONE* 10: e0139300. doi: 10.1371/journal.pone.0139300.

Lincoln R.A., Strupinski K. & Walker J.M. 1990. Biologically active compounds from diatoms. *Diatom Research* 5: 337–349.

Lobban C.S., Schefter M., Jordan R.W., Arai Y., Sasaki A, Theriot E.C., Ashworth M., Ruck E.C. & Pennesi C. 2012. Coral-reef diatoms (Bacillariophyta) from Guam: new records and preliminary checklist, with emphasis on epiphytic species from farmer-fish territories. *Micronesica* 43: 237–479.

Lodge D.M. 1986. Selective grazing on periphyton: a determinant of freshwater gastropod microdistributions. *Freshwater Biology* 16: 831–841.

Lovejoy N.R., Bermingham E. & Martin A.P. 1998. Marine incursion into South America. *Nature* 396: 421–422.

Lovejoy N.R. & Collette B.B. 2001. Phylogenetic relationships of new world needlefishes (Teleostei: Belonidae) and the biogeography of transitions between marine and freshwater habitats. *Copeia* 2001: 324–338.

Lowe R.L., Kociolek J.P., Johansen J.R., Van de Vijver B., Lange-Bertalot H. & Kopalová K. 2014. *Humidophila* gen. nov., a new genus for a group of diatoms (Bacillariophyta) formerly within the genus *Diadesmis*: species from Hawai'I, including one new species. *Diatom Research* 29: 351–360.

Ma Y., Wang X., Niu Y., Yang Z., Zhang M., Wang Z., Yang W., Liu J. & Li H. 2014. Antisense knockdown of pyruvate dehydrogenase kinase promotes the nuetral lipid accumulation in the diatom *Phaeodactylum tricornutum. Microbial Cell Factories*. 13: 100–109.

Maddison W.P. 1997. Gene trees in species trees. *Systematic Biology* 46: 523–536.

Maddison W.P. & Knowles L.L. 2006. Inferring phylogeby despite incomplete lineage sorting. *Systematic Biology* 55: 21–30.

Maddison W. P. & Maddison D.R. 2015. Mesquite: a modular system for evolutionary analysis. Version 3.04 http://mesquiteproject.org.

Mahapatra D.M., Chanakya H.N. & Ramachandra T.V. 2013. *Euglena* sp. as a suitable source of lipids for potential use as biofuel and sustainable wastewater treatment. *Journal of Applied Phycology* 25: 855–865.

Malcomber S.T. 2002. Phylogeny of *Gaertnera* Lam. (Rubiaceae) based on multiple DNA markers: evidence of a rapid radiation in a widespread, morphologically diverse genus. *Evolution* 56: 42–57.

Mann D.G. 1984. Observations on copulation in *Navicula pupula* and *Amphora ovalis* in relation to the nature of diatom species. *Annals of Botany* 54: 429–438.

Mann D.G. 1994. The systematics amphoroid diatoms: the life history of *Amphora arcus*. *Nova Hedwigia*. 58: 335–352.

Mann D.G. & Vanormelingen P. 2013 An inordinate fondness? The number, distributions and origins of diatom species. *Journal of Eukaryotic Microbiology.* 60: 414–420.

Mann D. G. 1999a. Crossing the Rubicon: the effectiveness of the marine/freshwater interface as a barrier to the migration of diatom germplasm. *In* S. Mayama, M. Idei & I. Koizumi (Eds) *Proceedings of the 14th International Diatom Symposium*. Koeltz Scientific Books, Koenigstein, pp. 1–21.

Mann D.G. 1999b. The species concept in diatoms. *Phycologia* 38: 437-495.

Martin-Jézéquel V, Hildebrand M, Brzezinski M.A. 2000. Silicon metabolism in diatoms: implications for growth. *Journal of Phycology* 36, 821–840.

McCracken K.G. & Sorenson M.D. 2005. Is homoplasy or lineage sorting the source of incongruent mtDNA and nuclear gene trees in the stiff-tailed ducks (*Nomonyx-Oxyura*)? *Systematic Biology* 54: 35–55.

McGinnis K.M., Dempster T.A. & Sommerfeld M.R. 1997. Characterization of the growth and lipid content of the diatom *Chaetoceros muelleri*. *Journal of Applied Phycology*. 9: 19–24.

McLellan M.R. 1989. Cryopreservation of diatoms. *Diatom Research* 4: 301–318.

Medlin L.K. & Kaczmarska I. 2004. Evolution of the diatoms: V. Morphological and cytological support for the major clades and a taxonomic revision. *Phycologia* 43: 245–270.

Medlin L.K., Ellwood K.J., Stickel S. & Sogin M.L. 1988. The characterization of enzymatically amplified eukaryotic 16S-like rRNA-coding regions. *Gene* 71: 491–499.

Meier R.L. 1955. Biological cycles in the transformation of solar energy into useful fuels. In Solar energy research (Daniels, F. & Duffie, J.A. Eds). Madison, WI: University of Wisconsin Press, pp. 179–183.

Mereschkowsky C. 1903. Les types de l'endochrome chez les diatomées. BotanicheskiiaZapiski 21:1-106.

Metzgar P. & Largeau C. 2005. *Botryococcus braunii*: a rich source for hydrocarbons and related ether lipids. *Applied Microbiology and Biotechnology*. 66: 486–496.

Moniz M.B.J. & Kaczmarska I. 2009. Barcoding diatoms: is there a good marker? *Molecular Ecology Resources* 9: 65–74.

Montgomery R.T. 1978. Environmental and ecological studies of the diatom communities associated with the coral reefs of the Florida Keys. Ph.D. Dissertation, Florida State University, Tallahassee, FL, USA.

Mortensen S.H., Børsheim K.Y., Rainuzzo J.R. & Knutsen G. 1988. Fatty acid and elemental composition of the marine diatom *Chaetoceros gracilis* Schütt. Effest of silicate deprivation, temperature and light intensity. *Journal of Experimental Marine Biology and Ecology*. 122: 173–185.

Müller O.F. 1786. *Animalcula infusoria fluviatilia et marina*. 367 pp. Havniae: N. Moller.

Münkemüller T., Lavergne S., Bzeznik B., Dray S., Jombart T. Schiffers K. & Thuiller W. 2012. How to measure and test phylogenetic signal. *Methods in Ecology and Evolution*. 3: 743–756.

Nagumo T. 2003. Taxonomic studies of the subgenus *Amphora* Cleve of the genus *Amphora* (Bacillariophyceae) in Japan. *Bibliotheca Diatomologica*. 49: 1–265.

Nascimento I.A., Marques S.S.I., Cabanelas I.T.D., Pereira S.A., Druzian J.I., de Souza C.O., Vich D.V., de Carvalho G.C. & Nascimento M.A. 2013. Screening microalgal strains for biodiesel production: lipid productivity and estimation of fuel quality based on fatty acid profiles as selesctive criteria. *Bioenergy Research* 6: 1–13.

Navarro J.N. 1982. A survey of the marine diatoms of Puerto Rico V. Suborder Raphidineae: families Achnanthaceae and Naviculaceae (excluding *Navicula* and *Mastogloia*). *Botanica Marina* 25: 321–338.

Nylander J.A.A., Wilgenbusch J.C., Warren, D.L. & Swofford D.L. 2008. AWTY (are we there yet?): a system for graphical exploration of MCMC convergence in Bayesian phylogenetics. *Bioinformatics* 24: 581–583.

Nelson D.M., Tréguer P., Brzezinski M.A., Leynaert A. & Quéguiner B. 1995. Production and dissolution of biogenic silica in the ocean: revised global estimates, comparison with regional data and relationship to biogenic sedimentation. *Global Biogeochemical Cycle* 9: 359–372.

Nicotri M.E. 1977. Grazing effects of four marine intertidal herbivores on the microflora. *Ecology*. 58: 1020–1032.

Orcutt D.M. & Patterson G.W. 1975. Sterol, fatty acid and elemental composition of diatoms grown in chemically defined media. *Comparitive Biochemistry and Physiology*. 50B: 579–583.

Päckert M., Martens J., Kosuch J., Nazarenko A.A. & Veith M. 2003. Phylogenetic signal in the song of crests and kinglets (Aves: *Regulus*). *Evolution* 57: 616–629.

Paddock T.B.B. & Sims P.A. 1980. Observations on the marine diatom genus *Auricula* and two new genera *Undatella* and *Proboscidea*. *Bacillaria* 3: 161–196.

Pagel M. 1999. Infering the historical patterns of biological evolution. *Nature*. 401: 877–884.

Pan Y., Stevenson R.J., Hill B.H., Herlihy A.T. & Collins G.B. 1996. Using diatoms as indicators of ecological conditions in lotic systems: a regional assessment. *North American Benthological Society* 15: 481–495.

Patrick R. & Freese L.R. 1961. Diatoms (Bacillariophyceae) from northern Alaska. *Proceedings of the Academy of Natural Sciences Philadelphia* 112: 129–293.

Patrick R.M. & Reimer C.W. 1975. The diatoms of the United States.Vol. 2, Pt. 1. Monograph 13, Academy of Natural Sciences of Philadelphia, 213p.

Peragallo H. & Peragallo M. 1897–1908. *Diatomées marines de France et des districts maritimes voisins.* M.J. Tempère micrographe-éditeur, Grez-sur-Loing. 492 pp.

Pienkos P.T. & Darzins A. 2009. The promise and challenges of microalgal-derived biofuels. *Biofuels, Bioproducts and Biorefining* 3: 431–440.

Pollock D.D., Zwickl D.J., McGuire J.A. & Hillis D.M. 2002. Increased taxon sampling is advantageous for phylogenetic inference. *Systematic Biology* 51 : 664–671.

Posada D. 2008. jModelTest: phylogenetic model averaging. *Molecular Biology and Evolution* 25: 1253–1256.

Posten C. & Schaub G. 2009. Microalgae and terrestrial biomass as source for fuels – a process view. *Journal of Biotechnology* 142: 64–69.

Potapova M. 2011. Patterns of diatom distributions in relation to salinity. *In* J. Seckbach & J. P. Kociolek (Eds) *The diatom world, cellular origin, life in extreme habitats and astrobiology*. Vol. 19. Springer, Dordrecht, pp. 313–332.

Poulíčkova A., Veselá J, Neustupa J. & Škaloud P. 2010. Pseudocryptic diversity versus cosmopolitanism in diatoms: a case study on *Navicula cryptocephala* Kütz. (Bacillariophyceae) and morphologically similar taxa. *Protist* 161: 353–369.

Prestegard S.K., Oftedal L., Coyne R.T., Nygaard G., Skjærven K.H., Knutsen G., Døskeland S.O. & Herfindal L. 2009. Marine benthic diatoms contain compounds able to induce leukemia cell death and modulate blood platelet activity. *Marine Drugs*. 7: 605–623.

Pugh P.R. 1971. Changes in the fatty acid composition of *Coscinodiscus eccentricus* with culture age and salinity. *Marine Biology* 11: 118–124.

Radakovits R., Jinkerson R.E., Darzins A. & Posewitz M.C. 2010. Genetic Engineering of algae for enhanced biofuels production. *Eukaryotic Cell*. 9: 486–501.

Ramachandra T.V., Mahapatra D.M., Karthick B. & Gordon R. 2009. Milking diatoms for sustainable energy: biochemical engineering versus gasoline-secreting diatom solar panels. *Industrial & Engineering Chemical Research*. 48: 8769–8788.

Reitan K.I., Rainuzzo J.R. & Olsen Y. 2004. Effect of nutrient limitation on fatty acid and lipid content of marine microalgae. *Journal of Phycology*. 30: 972–979.

Revell L.J. 2012. phytools: An R package for phylogenetic comparative biology (and other things). *Methods in Ecology and Evolution* 3: 217–223.

Rheindt F.E., Grafe T.U. & Abouheif E. 2004. Rapidly evolving traits and the comparative method: how important is testing for phylogenetic signal? *Evolutionary Ecology Research*. 6: 377–396.

Richlen M.L. & Barber P.H. 2005. A technique for the rapid extraction of microalgal DNA from single live and preserved cells. *Molecular Ecology Notes* 5: 688–691.

Riznyk R.Z. 1973. Interstitial diatoms from two tidal flats in Yaquina Estuary, Oregon, USA. *Botanica Marina* 16: 113–138.

Rodolfi L., Zittelli G.C. Bassi N. Padovani G., Biondi N., Bionini G. & Tredici M.R. 2008. Microalgae for oil: strain selection, induction of lipid synthesis and outdoor mass cultivation in a low-cost photobioreactor. *Biotechnology and Bioenergy* 102: 100–112.

Roessler P.G. 1988. Changes in the activities of various lipid and carbohydrate biosynthetic enzymes in the diatom *Cyclotella cryptica* in response to silicon deficiency. *Archives of Biochemistry and Biophysics* 267: 521–528.

Roessler P.G. 1990. Environmental control of glycerolipid metabolism in microalgae: commercial implications and future research directions. *Journal of Phycology* 26: 393–399.

Roessler P.G., Brown L.M., Dunahay T.G., Heacox D.A., Jarvis E.E., Schneider J.C., Talbot S.G. & Zeiler K.G. 1994. Genetic engineering approaches for enhanced production of biodiesel fuel from microalgae. *ACS symposium series*. Vol. 566. Washington, DC: American Chemical Society.

Ronquist F., Teslenko M., van der Mark P., Ayres D.L., Darling A., Höhna S., Larget B., Liu L., Suchard M.A. & Huelsenbeck J.P. 2012. MrBayes 3.2: efficient bayesian phylogenetic inference and model choice across a large model space. *Systematic Biology* 61: 539–542.

Rosenberg J.N., Oyler G.A., Wilkinson L. & Betenbaugh M.J. 2008. A green light for engineering algae: redirecting metabolism to fuel a biotechnology revolution. *Current Opinions in Biotechnology* 19: 430–436.

Round F.E. & Sims P.A. 1981. The distribution of diatom genera in marine and freshwater environments and some evolutionary considerations. *In* R. Ross (Ed.) *Proceedings of the Sixth Symposium of Recent and Fossil Diatoms*. Otto Koeltz Scientific Publishers, Hirschberg, pp. 301–320.

Round F.E., Crawford R.M. & Mann D.G. 1990. *The Diatoms. Biology and Morphology of the genera.* Cambridge Univeristy Press. 747p.

Ruck E.C., Nakov T., Jansem R.K., Theriot E.C. & Alverson A.J. 2014. Serial gene losses and foreign DNA underlie size and sequence variation in the plastid genomes of diatoms. *Genome Biology and Evolution* 6: 644–654.

Ruck E.C. & Theriot E.C. 2011. Origin and evolution of the canal raphe system in diatoms. *Protist* 162:723-37.

Ruck E.C. & Kociolek J.P. 2004. Preliminary phylogeny of the family Surirellaceae. *Bibliotheca Diatomologica* 50: 1–236.

Sala S.E., Sar E.A, Hinz F. & Sunsen I. 2006. Studies on *Amphora* subgenus *Halamphora* (Bacillariophyta): the revision of some species described by Hustedt using type material. *European Journal of Phycology* 41: 155–167.

Sar E.A., Crawford R.M., Serieyssol K., Serieyssol K. & Serieyssol K. 2010. BOOK REVIEWS. *Diatom research* 25: 227–231.

Sato S., Nagumo T. & Mann D.G. 2013. Morphology and life history of *Amphora commutata* (Bacillariophyta) I: the vegetative cell and phylogenetic position. *Phycologia* 52: 225–238.

Schenk P.M., Thomas-Hall S.R., Stephens E., Marx U.C., Mussgnug J.H., Posten C., Kruse O. & Hankamer B. 2008. Second generation biofuels: high-efficiency microalgae for biodiesel production. *Bioenergy Research*. 1: 20–43.

Schmidt A., Schmidt M., Fricke F., Heiden H., Müller O. & Hustedt F. 1874–1959. *Atlas der Diatomaceen-Kunde.* O.R. Reisland, Leipzig. 460 pls.

Schoeman F.R. & Archibald R.E.M. 1978. *The diatom flora of Southern Africa.* CSIR Special Report, WAT 50. Number 4. Graphic Arts Division of CSIR, Pretoria. 70 pp.

Schoeman F.R. & Archibald R.E.M. 1984. *Amphora delphinea* L.W. Bailey: a light-microscopical study of the type and other authenticated material. *Bacillaria* 7: 91–109.

Schoeman F.R. & Archibald R.E.M. 1986a. Observations on *Amphora* species (Bacillariophyceae) in the British Museum (Natural History) I. Some species from the subgenus *Oxyamphora* Cleve. *Nova Hedwigia* 43: 113–127.

Schoeman F.R. & Archibald R.E.M. 1986b. Observations on *Amphora* species (Bacillariophyceae) in the British Museum (Natural History) II. Some species from the subgenus *Psammamphora* Cleve. *Nova Hedwigia* 43: 473–484.

Schoeman F.R. & Archibald R.E.M. 1986c. Observations on *Amphora* species (Bacillariophyceae) in the British Museum (Natural History). V. Some species from the subgenus *Amphora. South African Journal of Botany* 52: 425–437.

Schoeman F.R. & Archibald R.E.M. 1987a. Observations on *Amphora* species (Bacillariophyceae) in the British Museum (Natural History) III. Two species from the subgenus *Amblyamphora* Cleve. *Nova Hedwigia* 44: 125–135.

Schoeman F.R. & Archibald R.E.M. 1987b. Observations on *Amphora* species (Bacillariophyceae) in the British Museum (Natural History) VI. Some species from the subgenus *Halamphora* Cleve. *Nova Hedwigia* 44: 337–398.

Schoeman F.R., Archibald R.E.M. & Sims P.A. 1986. Observations on *Amphora* species (Bacillariophyceae) in the British Museum (Natural History) IV. Some species from the subgenus *Diplamphora* Cleve. *Cryptogamie Algologie* 7: 9–21.

Scholin C.A., Herzog M., Sogin M. & Anderson D.M. 1994. Identification of group- and strain-specific markers for globally distributed *Alexandrium* (Dinophyceae). II. Sequence analysis of a fragment of the LSU rRNA gene. *Journal of Phycology* 30: 999–1011.

Scholz B. & Liebezeit G. 2013. Biochemical characterisation and fatty acid profiles of 25 benthic marine diatoms isolated from the Solthörn tidal flat (southern North Sea). *Journal of Applied Phycology*. 25: 453–465.

Scott S.A., Davey M.P., Dennis J.S., Horst I., Howe C.J., Lea-Smith D.J. & Smith A.G. 2010. Biodiesel from algae: challenges and prospects. *Current Opinion in Biotechnology* 21: 1–10.

Scranton M.A., Ostrand J.T., Fields F.J. & Mayfield S.P. 2015. *Chlamydomonas* as a model for biofuels and bio-products production. *The Plant Journal*. 82: 523–531.

Sethre P.S., Rundquist B.C. & Todhunter P.E. 2005. Remote detection of prairie pothole ponds in the Devils Lake basin, North Dakota. *GIScience & Remote Sensing* 42: 227–296.

Sheehan J., Dunahay T., Benemann J. & Roessler P. 1998. A Look Back at the US Department of Energy's Aquatic Species Program: Biodiesel from Algae Golden. National Renewable Energy Laboratory, Colorado, TP-580-24190.

Shimodaira H. & Hasegawa M. 2001. CONSEL: for assessing the confidence of phylogenetic tree selection. *Bioinformatics* 17: 1246–1247.

Shimodaira H. 2002. An approximately unbiased teat of phylogenetic tree selection. *Systematic Biology* 51: 492–508.

Shjeflo J.B. 1968. Evapotranspiration and the water budget of prairie potholes in North Dakota. *Geological Survey Professional Paper 585-B.* U.S. Government Printing Office, Washington D.C.

Sicko-Goad L.M. & Andresen N.A. 1991. Effect of growth and light/dark cycles on diatom lipid content and composition. *Journal of Phycology*. 27: 710-718.

Sicko-Goad L.M., Schelske C.L. & Stoermer E.F. 1984. Estimation of intracellular carbon and silica content of diatoms from natural assemblages using morphometric techniques. *Limnology and Oceanography*. 29: 1170–1178.

Silvestro D. & Michalak I. 2012. raxmlGUI: a graphical front-end for RAxML. *Organisms Diversity & Evolution* 12: 335–337.

Sims P.A., Mann D.G. & Medlin L.K. 2006. Evolution of the diatoms: insights from fossil, biological and molecular data. *Phycologia* 45: 361–402.

Singh A., Nigam P.S. & Murphy J.D. 2011. Mechanisms and challenges in commercialization of algal biofuels. *Bioresource Technology*. 102: 26–34.

Singh J. & Gu S. 2010. Commercialization potential of microalgae for biofuels production. *Renewable and Sustainable Energy Reviews*. 14: 2596–2610.

Sloan C.E. 1972. Ground-water hydrology of prairie potholes in North Dakota. *Geological Survey Professional Paper 585-C*. U.S. Government Printing Office, Washington D.C.

Smith H.L. 1873. Conspectus of diatomaceae. Analysis of the species of the genus *Amphora. The Lens* 2: 65–91.

Sorhannus U. 2004. Diatom phylogenetics inferred based on direct optimization of nuclear-encoded SSU rDNA sequences. *Cladistics* 20: 487–497.

Souffreau C., Verbruggen H., Wolfe A.P., Vanormelingen P., Siver P.A., Cox E.J., Mann D.G., Van de Vijver B., Sabbe K. & Vyverman W. 2011. A time-calibrated multi-gene phylogeny of the diatom genus *Pinnularia*. *Molecular phylogenetics and Evolution*. 61: 866-879.

Stamatakis A. 2006. RAxML-VI-HPC: maximum likelihood-based phylogenetic analyses with thousands of taxa and mixed models. *Bioinformatics* **22**: 2688–2690.

Stepanek J.G. & Kociolek J.P. 2013. Several new species of *Amphora* and *Halamphora* from the western USA. *Diatom Research*. 28: 61–76.

Stepanek J.G. & Kociolek J.P. 2014. Molecular phylogeny of *Amphora* sensu lato (Bacillariophyta): an investigation into the monophyly and classification of the amphoroid diatoms. *Protist* 165: 177–195.

Stepanek J.G. & Kociolek J.P. 2015. Three new species of the diatom genus *Halamphora* (Bacillariophyta) from the prairie pothole region of North Dakota, USA. *Phytotaxa* 197: 27–36.

Stepanek J.G. & Kociolek J.P. *Accepted*. Re-examination of Mereschkowsky's genus *Tetramphora* (Bacillariophyta) and its separation from *Amphora*. *Diatom Research*.

Stepanek J.G., Fields F.J. & Kociolek J.P. *Accepted*. A comparison of lipid content metrics using six species from the genus *Halamphora* (Bacillariophyta). *Biofuels.*

Stepanek J.G., Mayama S. & Kociolek J.P. 2015. Description and phylogenetic position of *Amphora aliformis* (Bacillariophyta), a new species from Tokyo Bay. *Phycologia* 54: 78–86.

Stoermer E.F. & Yang J.J. 1971. Contributions to the diatom flora of the Laurentian Great Lakes. I. New and little-known species of *Amphora* (Bacillariophyta Pennatibacillariophyceae). *Phycologia* 10: 397–409.

Stoermer E.F., Taylor S.M. & Callender E. 1971. Paleoecological interpretation of the Holocene diatom succession on Devils Lake, North Dakota. *Transactions of the American Microscopical Society* 90: 195–206.

Straub S.C.K., Moore M.J., Soltis P.S., Soltis D.E., Liston A. & Livshultz T. 2014. Phylegenetic signal detection from an ancient rapid radiation: effects of noise reduction, long-branch attraction, and model selection in crown clade Apocynaceae. *Molecular Phylogenetics and Evolution* 80: 169–185.

Tanaka T., Maeda Y., Veluchamy A., Tanaka M., Abida H., Meréchal E., Bowler C., Muto M., Sunaga Y., Tanaka M., Yoshino T., Taniguchi T., Fukuda Y., Nemoto M., Matsumoto M., Wong P.S., Aburatani S. & Fujibuchi W. 2015. Oil accumulation by the oleaginous diatom *Fistulifera solaris* as revealed by the genome and transcriptome. *The Plant Cell*. 27: 162–176.

ten Cate J.H., Maasdam R. & Roijackers R.M.M. 1993. Perspectives for the use of diatom assemblages in the water management policy of Overijssel (The Netherlands). *Hydrobiologia* 269/270: 351–359.

Theriot E.C., Ashworth M., Ruck E., Nakov T. & Jansen R.K. 2010. A preliminary multigene phylogeny of the diatoms (Bacillariophyta): challenges for future research. *Plant Ecology and Evolution*. 143: 278–296.

Theriot E.C., Ashworth M.P., Nakov T., Ruck E. & Jansen R.K. 2015. Dissecting signal and noise in diatom chloroplast protein encoding genes with phylogenetic information profiling. *Molecular Phylogenetics and Evolution* 89: 28–36.

Thomas B.W. & Chase H.H. 1886. *Diatomaceae of Lake Michigan, as collected during the last 16 years from the water supply of the City of Chicago*. Presented to the State Natural History Society of Illinois, May 14, 1886. Chicago. pp. 1–3.

Tripp E.A. & Lendemer J.C. 2014. Sleepless nights: When you can't find anything to use but molecules to describe new taxa. *Taxon* 63: 969–971.

U.S. DOE 2010. National algal biofuels technology roadmap. U.S. Department of Energy Efficiency and Renewable Energy, Biomass Program.

Van de Vijver B. & Beyens L. 1998. A preliminary study on the soil diatom assemblages from Ile de la Possession (Crozet, Subantarctica). *European Journal of Soil Biology* 34: 133–141.

Van de Vijver B., Kopalová K., Zidarova R. & Levkov Z. 2014. Revision of the genus *Halamphora* (Bacillariophyta) in the Antarctic Region. *Plant Ecology and Evolution* 147: 374–391.

Vyverman W., Sabbe K., Mann D.G., Kilroy C., Vyverman R., Vanhoutte K. & Hodgson D. 1998. *Eunophora* gen. nov. (Bacillariophyta) from Tasmania and New Zealand: description and comparison with *Eunotia* and amphoroid diatoms. *European Journal of Phycology* 33: 95–111.

Wachnicka A.H. & Gaiser E.E. 2007. Characterization of *Amphora* and *Seminavis* from South Florida,

Wagner H., Jakob T. & Wilhelm C. 2006. Balancing the energy flow from captured light to biomass under fluctuating light conditions. *New Phytologist* 169: 95–108.

Whitney S.P., Baldet P., Hudson G.S. & Andrews T.J. 2001. Form I Rubisco from non-green algae are expressed abundantly but not assembled in tobacco chloroplasts. *Plant Journal* 26: 535–547.

Wang P., Park B.S., Kim J.H., Kim J., Lee, H.L. & Han M. 2014. Phylogenetic position of eight *Amphora sensu lato* (Bacillariophyceae) species and comparative analysis of morphological characteristics. *Algae* 29: 57–73.

Watanabe T., Kodama Y. & Mayama S. 2010. Application of a novel cleaning method using low-temperature plasma on tidal flat diatoms with heterovalvy or delicate structure. *Proceedings of the Academy of Natural Sciences of Philadelphia* 160: 83–87.

Wawrik B. & Harriman B.H. 2010. Rapid, colorimetric quantification of lipid from algal cultures. *Journal of Microbiological Methods*. 80: 262–266.

Werner D. 1977. The Biology of Diatoms. Botanical Monographs, vol. 13. University of California Press, Berkeley and Los Angeles.

Whitaker T.M. & Richardson M.G. 1980. Morphology and chemical composition of a natural population of an ice-associated Antarctic diatom *Navicula glaciei*. *Journal of Phycology*. 16: 250–257.

Williams D.M. & Reid G. 2006. Fossils and the tropics, the Eunotiaceae expanded: A new genus for the upper Eocene fossil diatom *Eunotia reedii* and the recent tropical marine diatom *Amphora reichardii*. *European Journal of Phycology* 41: 147–154.

Williams D.M. 1990. Cladistic analysis of some freshwater araphid diatoms (Bacillariophyta) with particular reference to *Diatoma* and *Meridion*. *Plant Systematics and Evolution* 171: 89–97.

Williams P.J.B. & Laurens L.M.L. 2010. Microalgae as biodiesel and biomass feedstocks: review and analysis of the biochemistry, energetics and economics. *Energy and Environmental Science* 3: 554–590.

Witkowski A., Lange-Bertalot H. & Metzeltin D. 2000. Diatom flora of marine coasts I. *Iconographia Diatomologica* 7: 1–925.

Wustman B.A., Gretz M.R. & Hoagland K.D. 1997. Extracellular matrix assembly in diatoms (Bacillariophyceae) I. A model of adhesives based on chemical characterization and localization of polysaccharides from the marine diatom *Achnanthes longipes* and other diatoms. *Plant Physiology* 113: 1059–1069.

Zwickl D.J. & Hillis D.M. 2002. Increased taxon sampling greatly reduces phylogenetic error. *Systematic Biology* 51: 588–598.

APPENDIX 1

COLLECTION INFORMATION FOR EXAMINED TAXA

Culture ID	Taxon	Collection Date	Collection Site	Latitude North	Longitude West	pH	Conductivity (mS/cm)
Amph001	*Halamphora elongata* Bennett & Kociolek	9/15/2010	Cottonwood Marsh, Walden Ponds Wildlife Habitat, Boulder County, CO, USA	40.00342	105.25104	8.91	1.235
Amph005	*Halamphora veneta* (Kützing) Levkov Amph005	9/15/2010	Cottonwood Marsh, Walden Ponds Wildlife Habitat, Boulder County, CO, USA	40.00342	105.25104	8.91	1.235
Amph008	*Amphora pediculus* (Kützing) Grunow in Schmidt et al.	1/25/2011	Kittridge Pond, University of Colorado Boulder, Boulder County, CO, USA	40.002815	105.262398	n.d.	n.d.
Amph009	*Halamphora oligotraphenta* (Lange-Bertalot) Levkov	3/3/2011	Pond #1, Sawhill Ponds Wildlife Preserve, Boulder County, CO, USA	40.039606	105.185772	8.51	0.437
Amph011	*Amphora waldeniana* Stepanek & Kociolek	1/30/2011	Bass Pond, Walden Ponds Wildlife Habitat, Boulder County, CO, USA	40.045567	105.188073	7.89	0.409
Amph013	*Amphora ovalis* (Kützing) Kützing	2/13/2011	St. Vrain River, Golden Ponds Park, Boulder County, CO, USA	40.167919	105.139251	n.d.	n.d.
Amph015	*Halamphora subturgida* (Hustedt) Levkov	3/3/2011	Pond #1, Sawhill Ponds Wildlife Preserve, Boulder County, CO, USA	40.039606	105.185772	8.51	0.437
Amph016	*Amphora affinis* Kützing	4/17/2011	Sunset Lake, Pella Crossing Park, Boulder County, CO, USA	40.183508	105.176657	n.d.	n.d.
Amph017	*Halamphora* cf. *veneta* (Kützing) Levkov	3/19/2011	Pond #6, Banner Lakes State Wildlife Area, Weld County, CO, USA	40.08025	104.56507	n.d.	n.d.

Amph018	*Halamphora sp. nov.*	n.d.	Unnamed Lake, ND, USA	n.d.	n.d.	n.d.	n.d.
Amph019	*Amphora indistincta* Levkov	3/19/2011	Pond #6, Banner Lakes State Wildlife Area, Weld County, CO, USA	40.08025	104.56507	n.d.	n.d.
Amph020	*Amphora pediculus* (Kützing) Grunow in Schmidt et al.	3/19/2011	Pond #6, Banner Lakes State Wildlife Area, Weld County, CO, USA	40.08025	104.56507	n.d.	n.d.
Amph021	*Amphora copulata* (Kützing) Schoeman & Archibald	3/19/2011	Pond #9, Banner Lakes State Wildlife Area, Weld County, CO, USA	40.08834	104.57062	n.d.	n.d.
Amph022	*Halamphora americana* Kociolek	3/5/2011	Little Gaynor Lake, Boulder County, CO, USA	40.115454	105.121372	XXXX	XXXX
Amph023	*Halamphora coffeaeformis* (Agardh) Levkov	3/5/2011	Little Gaynor Lake, Boulder County, CO, USA	40.115454	105.121372	XXXX	XXXX
Amph025	*Halamphora coloradiana* Stepanek & Kociolek	3/3/2011	Cottonwood Marsh, Walden Ponds Wildlife Habitat, Boulder County, CO, USA	40.00342	105.25104	8.91	1.235
Amph026	*Amphora sp. nov.*	3/24/2011	Largo Sound, John Pennekamp Coral Reef State Park, Monroe County, FL, USA	25.156027	80.368649	7.73	46.30
Amph027	*Halamphora sp. nov.*	5/6/2011	Biscayne Bay, Black Point Park, Miami-Dade County, FL, USA	25.538954	80.327842	7.24	14.95
Amph028	*Halamphora sydowii* (Cholnoky) Levkov	5/6/2011	Biscayne Bay, Black Point Park, Miami-Dade County, FL, USA	25.538954	80.327842	7.24	14.95
Amph029	*Halamphora sp. nov.*	5/6/2011	Biscayne Bay, Black Point Park, Miami-Dade County, FL, USA	25.538954	80.327842	7.24	14.95
Amph030	*Halamphora sp. nov.*	5/6/2011	Biscayne Bay, Black Point Park, Miami-Dade County, FL, USA	25.538954	80.327842	7.24	14.95

Amph033	*Amphora sp. nov.*	5/6/2011	Biscayne Bay, Homestead Bayfront Park, Miami-Dade County, FL, USA	25.46216	80.33791	8.91	64.91
Amph034	*Halamphora sp. nov.*	5/6/2011	Biscayne Bay, Homestead Bayfront Park, Miami-Dade County, FL, USA	25.46216	80.33791	8.91	64.91
Amph035	*Tetramphora securicula* (Peragallo & Peragallo) Stepanek & Kociolek	5/6/2011	Biscayne Bay, Homestead Bayfront Park, Miami-Dade County, FL, USA	25.46216	80.33791	8.91	64.91
Amph037	*Halamphora hyalina* (Ehrenberg) Stepanek & Kociolek	5/7/2011	Florida Bay, Lower Matecumbe Key, Monroe County, FL, USA	24.862583	80.724917	8.23	63.92
Amph038	*Amphora sp. nov.*	5/7/2011	Florida Bay, Lower Matecumbe Key, Monroe County, FL, USA	24.862583	80.724917	8.23	63.92
Amph041	*Halamphora adumbrata* (Hohn & Hellerman) Stepanek & Kociolek	5/7/2011	Florida Bay, Cotton Key, Monroe County, FL, USA	24.960028	80.627139	8.34	61.90
Amph042	*Halamphora acutiuscula* (Kützing) Levkov	5/7/2011	Mangrove Swamp, No Name Key, Monroe County, FL, USA	24.69765	81.31859	7.89	77.94
Amph043	*Halamphora sp. nov.*	5/7/2011	Mangrove Swamp, No Name Key, Monroe County, FL, USA	24.69765	81.31859	7.89	77.94
Amph044	*Amphora sp. nov.*	5/7/2011	Mangrove Swamp, No Name Key, Monroe County, FL, USA	24.69765	81.31859	7.89	77.94
Amph045	*Halamphora sydowii* (Cholnoky) Levkov	5/7/2011	Mangrove Swamp, No Name Key, Monroe County, FL, USA	24.69765	81.31859	7.89	77.94
Amph046	*Tetramphora lineolatoides* Stepanek & Kociolek	5/8/2011	US1 Canal, Dade County, FL, USA	25.28829	80.44263	7.34	21.29
Amph047	*Halamphora semperpalorum* (Wachnicka & Gaiser) Stepanek & Kociolek	5/8/2011	US1 Canal, Dade County, FL, USA	25.28829	80.44263	7.34	21.29

Amph049	*Halamphora aponina* (Kützing) Levkov	5/8/2011	Mangrove Swamp, Long Key State Park, Monroe County, FL, USA	24.80735	80.83758	8.11	66.61
Amph050	*Halamphora sp. nov.*	5/9/2011	Mangrove Swamp, J.N. "Ding" Darling NWR, Sanibel Island, Lee County, FL, USA	26.45707	82.12035	7.41	33.96
Amph051	*Halamphora subtropica* (Wachnicka & Gaiser) Stepanek & Kociolek	5/9/2011	Mangrove Swamp, J.N. "Ding" Darling NWR, Sanibel Island, Lee County, FL, USA	26.45707	82.12035	7.41	33.96
Amph054	*Halamphora subtropica* (Wachnicka & Gaiser) Stepanek & Kociolek	5/9/2011	Mangrove Swamp, J.N. "Ding" Darling NWR, Sanibel Island, Lee County, FL, USA	26.45707	82.12035	7.41	33.96
Amph055	*Halamphora bicapitata* (Hohn & Hellerman) Stepanek & Kociolek	5/9/2011	Waccasassa River, Gulf Hammock Boat Ramp, Levy County, FL, USA	29.21361	82.76321	n.d.	n.d.
Amph059	*Amphora abludens* Simonsen	5/10/2011	Gulf of Mexico Canal, Dark Island, Taylor County, FL, USA	29.80402	83.58526	7.96	44.31
Amph060	*Halamphora sp. nov.*	5/10/2011	Gulf of Mexico Canal, Dark Island, Taylor County, FL, USA	29.80402	83.58526	7.96	44.31
Amph061	*Halamphora hyalina* (Ehrenberg) Stepanek & Kociolek	5/10/2011	Gulf of Mexico, Dark Island, Taylor County, FL, USA	29.80402	83.58526	7.96	44.31
Amph063	*Halamphora sp. nov.*	5/10/2011	Gulf of Mexico Tidal Flats, Dark Island, Taylor County, FL, USA	29.80402	83.58526	7.96	44.31
Amph064	*Amphora sp. nov.*	5/7/2011	Florida Bay, Lower Matecumbe Key, Monroe County, FL, USA	24.862583	80.724917	8.23	63.92
Amph066	*Amphora sp. nov.*	5/7/2011	Mangrove Swamp, No Name Key, Monroe County, FL, USA	24.69765	81.31859	7.89	77.94
Amph069	*Amphora graeffeana* Hendey	5/9/2011	Mangrove Swamp, J.N. "Ding" Darling NWR, Sanibel Island, Lee County, FL, USA	26.45707	82.12035	7.41	33.96

Amph070	*Amphora obtusa* var. *crassa* Tempère & Peragallo	5/10/2011	Gulf of Mexico, Keaton Beach, Taylor County, FL, USA	29.81911	83.59402	7.96	44.31
Amph071	*Amphora sp. nov.*	5/10/2011	Gulf of Mexico Canal, Dark Island, Taylor County, FL, USA	29.80402	83.58526	7.96	44.31
Amph072	*Amphora abludens* Simonsen	5/10/2011	Gulf of Mexico Canal, Dark Island, Taylor County, FL, USA	29.80402	83.58526	7.96	44.31
Amph074	*Amphora graeffeana* Hendey	7/12/2011	Intracoastal Waterway, Vilano Pier, St. Johns County, FL, USA	29.91674	81.29752	7.78	57.34
Amph077	*Halamphora borealis* (Kützing) Levkov	7/12/2011	Guana River, Guana River Wildlife Management Area, St. John's County, FL, USA	30.11021	81.34500	6.89	51.95
Amph079	*Halamphora borealis* (Kützing) Levkov	7/12/2011	Guana River, Guana River Wildlife Management Area, St. John's County, FL, USA	30.11021	81.34500	6.89	51.95
Amph080	*Halamphora sp. nov.*	7/12/2011	Guana River, Guana River Wildlife Management Area, St. John's County, FL, USA	30.11021	81.34500	6.89	51.95
Amph081	*Halamphora sp. nov.*	7/13/2011	Beaufort Inlet, Carteret County, NC, USA	34.72297	76.68654	7.25	33.14
Amph082	*Halamphora cymbifera* var. *heritierarum* (Wachnicka and Gaiser) Stepanek & Kociolek	7/13/2011	Backwater, Cedar Island National Wildlife Refuge, Carteret County, NC, USA	34.91625	76.36994	8.00	62.03
Amph083	*Tetramphora sulcata* (Brébisson) Stepanek & Kociolek	7/13/2011	Backwater, Cedar Island National Wildlife Refuge, Carteret County, NC, USA	34.91625	76.36994	8.00	62.03
Amph085	*Amphora laevissima* Gregory	7/15/2011	Lincolnville Saltwater Pond, St. Augustine, St. Johns County FL, USA	29.88335	81.30996	7.39	34.75
Amph086	*Halamphora sp. nov.*	7/15/2011	Saltwater Marsh, Fort Mose State Park, St. Augustine, St. Johns County, FL, USA	29.92805	81.3252	7.25	33.87

Amph087	*Halamphora turgida* (Gregory) Levkov	7/15/2011	Saltmarsh Pond, Fort Mose State Park, St. Augustine, St. Johns County, FL, USA	29.92805	81.3252	7.23	30.68
Amph089	*Halamphora sp. nov.*	7/15/2011	Saltmarsh Pond, Fort Mose State Park, St. Augustine, St. Johns County, FL, USA	29.92805	81.3252	7.23	30.68
Amph093	*Halamphora sp. nov.*	7/15/2011	Lincolnville Saltwater Pond, St. Augustine, St. Johns County FL, USA	29.88335	81.30996	7.39	34.75
Amph094	*Amphora calumetica* (Thomas in Thomas & Chase) Peragallo	5/19/2011	Lake Michigan, Silver Beach, Berrien County, MI, USA	42.11088	86.48800	n.d.	n.d.
Amph095	*Amphora copulata* (Kützing) Schoeman & Archibald	8/11/2011	South Clear Creek, Guanella Pass Road, Clear Creek County, CO, USA	39.642668	105.70722	n.d.	n.d.
Amph096	*Amphora proteoides* Hustedt	7/12/2011	Intracoastal Waterway, Vilano Pier, St. Johns County, FL, USA	29.91674	81.29752	7.78	57.34
Amph097	*Amphora sp. nov.*	7/13/2011	Intracoastal Waterway, Emerald Island, Carteret, NC, USA	34.67165	77.00514	7.25	33.14
Amph099	*Amphora gigantea* var. *fusca* (Schmidt in Schmidt et al.) Cleve	5/10/2011	Gulf of Mexico Canal, Dark Island, Taylor County, FL, USA	29.80402	83.58526	7.96	44.31
Amph100	*Halamphora americana* Kociolek	11/3/2011	Salt Alkaline Lake, Kidder County, ND, USA	46.95092	99.53915	8.89	9.811
Amph101	*Halamphora coffeaeformis* (Agardh) Levkov	11/3/2011	Salt Alkaline Lake, Kidder County, ND, USA	46.95092	99.53915	8.89	9.811
Amph102	*Halamphora aponina* (Kützing) Levkov	11/3/2011	Salt Alkaline Lake, Kidder County, ND, USA	46.95092	99.53915	8.89	9.811
Amph104	*Halamphora coffeaeformis* (Agardh) Levkov	11/5/2011	Kelley's Slough, Kelly's Slough NWR, Grand Forks County, ND, USA	47.98157	97.26046	8.61	7.975

Amph105	*Halamphora coffeaeformis* (Agardh) Levkov	11/5/2011	Kelley's Slough, Kelly's Slough NWR, Grand Forks County, ND, USA	47.98157	97.26046	8.61	7.975
Amph106	*Halamphora pratensis* Stepanek & Kociolek	11/3/2011	Long Lake, Long Lake NWR, Burleigh County, ND, USA	46.69169	100.19026	8.79	2.187
Amph107	*Amphora copulata* (Kützing) Schoeman & Archibald	11/5/2011	Kelley's Slough, Kelly's Slough NWR, Grand Forks County, ND, USA	47.98157	97.26046	8.61	7.975
Amph109	*Halamphora sp. nov.*	1/5/2012	PK-5-i-12-20:02	n.d.	n.d.	n.d.	n.d.
Amph110	*Halamphora sp. nov.*	1/5/2012	PK-5-i-12-20:03	n.d.	n.d.	n.d.	n.d.
Amph111	*Halamphora fontinalis* (Hustedt) Levkov	1/4/2012	PK-4-i-12-38:02	n.d.	n.d.	n.d.	n.d.
Amph112	*Halamphora sp. nov.*	1/10/2012	PK-10-i-12-04:01	n.d.	n.d.	n.d.	n.d.
Amph115	*Halamphora sp. nov.*	4/14/2012	Main Pool, Blue Lake Warm Spring, Tooele County, UT, USA	40.50257	114.03359	7.60	9.319
Amph117	*Halamphora sp. nov.*	4/14/2012	Main Pool, Blue Lake Warm Spring, Tooele County, UT, USA	40.50257	114.03359	7.60	9.319
Amph118	*Halamphora sp. nov.*	4/14/2012	Main Pool, Blue Lake Warm Spring, Tooele County, UT, USA	40.50257	114.03359	7.60	9.319
Amph119	*Halamphora taylori* (Grunow in Van Heurck) Stepanek & Kociolek	4/14/2012	Main Pool, Blue Lake Warm Spring, Tooele County, UT, USA	40.50257	114.03359	7.60	9.319
Amph121	*Halamphora pertusa* Stepanek & Kociolek	4/14/2012	North Shore Wetland Pool #2, Blue Lake Warm Spring, Tooele County, UT, USA	40.50257	114.03359	7.22	15.37

Amph122	*Halamphora cf. turgida (Gregory) Levkov*	4/14/2012	East Shore Wetland, Blue Lake Warm Spring, Tooele County, UT, USA	40.50257	114.03359	7.02	20.61
Amph123	*Halamphora pertusa* Stepanek & Kociolek	4/14/2012	North Shore Wetland Pool #1, Blue Lake Warm Spring, Tooele County, UT, USA	40.50257	114.03359	8.08	26.24
Amph124	*Halamphora* cf. *turgida* (Gregory) Levkov	4/14/2012	North Shore Wetland Pool #1, Blue Lake Warm Spring, Tooele County, UT, USA	40.50257	114.03359	8.08	26.24
Amph125	*Halamphora cf. turgida (Gregory) Levkov*	4/14/2012	East Shore Wetland, Blue Lake Warm Spring, Tooele County, UT, USA	40.50257	114.03359	7.02	20.61
Amph126	*Amphora commutata* Grunow in Van Heurck	4/14/2012	North Shore Wetland Pool #2, Blue Lake Warm Spring, Tooele County, UT, USA	40.50257	114.03359	7.22	15.37
Amph129	*Amphora allanta* Hohn & Hellerman	4/14/2012	Pond #2, Blue Lake Warm Spring, Tooele County, UT, USA	40.49931	114.04542	7.58	8.760
Amph130	*Halamphora margalefii* (Tomàs in Sabater et al.) Stepanek & Kociolek	4/14/2012	Pond #2, Blue Lake Warm Spring, Tooele County, UT, USA	40.49931	114.04542	7.58	8.760
Amph132	*Tetramphora chilensis* (Hustedt) Stepanek & Kociolek	4/14/2012	Inlet Stream, Blue Lake Warm Spring, Tooele County, UT, USA	40.50257	114.03359	7.22	15.37
Amph134	*Halamphora sp. nov.*	5/13/2012	905A Channel, Monroe County, FL, USA	25.27935	80.34257	7.32	44.43
Amph135	*Amphora sp. nov.*	5/13/2012	905A Channel, Monroe County, FL, USA	25.27935	80.34257	7.32	44.43
Amph136	*Halamphora hyalina* (Ehrenberg) Stepanek & Kociolek	5/13/2012	905A Channel, Monroe County, FL, USA	25.29178	80.37952	7.41	40.78
Amph137	*Halamphora semperpalorum* (Wachnicka & Gaiser) Stepanek & Kociolek	5/11/2012	Coastal Marsh, Sugarloaf Campground, Sugarloaf Key, Monroe County, FL, USA	24.65713	81.52274	8.38	69.03

Amph141	*Halamphora sp. nov.*	5/13/2012	905A Channel, Monroe County, FL, USA	25.27935	80.34257	7.32	44.43
Amph142	*Halamphora semperpalorum* (Wachnicka & Gaiser) Stepanek & Kociolek	5/13/2012	Largo Sound, John Pennekamp Coral Reef State Park, Monroe County, FL, USA	25.156027	80.36864	7.73	46.30
Amph149	*Halamphora tumida* (Hustedt) Levkov	8/16/2012	Eastern Plains 16-viii-12-44	n.d.	n.d.		
Amph153	*Halamphora sp. nov.*	12/31/2012	St. Joseph Bay, Gulf County, FL, USA	29.8114	85.30525	n.d.	n.d.
Amph154	*Halamphora holsatica* (Hustedt) Levkov	12/31/2012	St. Joseph Bay, Gulf County, FL, USA	29.8114	85.30525	n.d.	n.d.
Amph156	*Thalassiophysa hyalina* (Greville) Paddock & Sims	1/1/2013	St. Joseph Bay, Gulf County, FL, USA	29.8114	85.30525	n.d.	n.d.
Amph158	*Halamphora sp. nov.*	6/23/2013	Banzu Flats, Tokyo Bay, Tokyo, Japan	35.44081	139.91078 E	n.d.	50.36
Amph159	*Amphora aliformis* Stepanek, Mayama & Kociolek	6/23/2013	Banzu Flats, Tokyo Bay, Tokyo, Japan	35.44081	139.91078 E	n.d.	50.36
Amph162	*Halamphora sp. nov.*	7/8/2013	Isumi-Gawa at Mouth to Pacific Ocean, Chiba, Japan	35.29343	140.40558 E	n.d.	32.09
Amph163	*Halamphora sp. nov.*	7/8/2013	Isumi-Gawa at Mouth to Pacific Ocean, Chiba, Japan	35.29343	140.40558 E	n.d.	32.09
Amph164	*Halamphora sp. nov.*	7/8/2013	Isumi-Gawa at Mouth to Pacific Ocean, Chiba, Japan	35.29343	140.40558 E	n.d.	32.09
Amph165	*Halamphora pseudoholsatica* (Nagumo & Kobayasi) Stepanek & Kociolek	6/24/2013	Tama-Gawa, Mouth at Tokyo Bay, Tokyo, Japan	35.54020	139.75951 E	n.d.	32.09

Amph166	*Halamphora sp. nov.*	7/8/2013	Isumi-Gawa at Mouth to Pacific Ocean, Chiba, Japan	35.29343	140.40558 E	n.d.	32.09
Amph167	*Halamphora sp. nov.*	7/8/2013	Isumi-Gawa at Mouth to Pacific Ocean, Chiba, Japan	35.29343	140.40558 E	n.d.	32.09
Amph168	*Halamphora subtropica* (Wachnicka & Gaiser) Stepanek & Kociolek	7/8/2013	Isumi-Gawa at Mouth to Pacific Ocean, Chiba, Japan	35.29343	140.40558 E	n.d.	32.09
Amph169	*Halamphora pseudoholsatica* (Nagumo & Kobayasi) Stepanek & Kociolek	7/8/2013	Isumi-Gawa at Mouth to Pacific Ocean, Chiba, Japan	35.29343	140.40558 E	n.d.	32.09
Amph170	*Amphora australiensis* John	6/24/2013	Tama-Gawa, Kawasaki, Kanagawa, Japan	35.53596	139.70607 E	n.d.	10.61
Amph174	*Amphora australiensis* John	8/5/2013	Kugushiko, Mikatagoko, Toyama, Japan	35.61063	135.90234 E	n.d.	15.45
Amph177	*Amphora aliformis* Stepanek, Mayama & Kociolek	6/23/2013	Banzu Flats, Tokyo Bay, Tokyo, Japan	35.44081	139.91078 E	n.d.	50.36
Amph181	*Halamphora sp. nov.*	5/14/2014	Big Spring, Tooele County, UT, USA	40.73978	112.64733	7.35	12.57
Amph185	*Halamphora sp. nov.*	5/14/2014	Little Salt Spring, Elko County, Nevada, USA	40.88841	114.070587	7.87	95.7
Amph192	*Halamphora sp. nov.*	8/18/2014	Salt Alkaline Lake, Kidder County, ND, USA	46.95432	99.52351	8.72	12.19

APPENDIX 2

LIST OF PUBLISHED GENEBANK ACCESSION NUMBERS

Culture ID	Taxon	SSU	LSU	*rbc*L	*psb*C
Amph001	*Halamphora elongata* Bennett & Kociolek	TBD	TBD	TBD	TBD
Amph005	*Halamphora veneta* (Kützing) Levkov Amph005	KJ463452	KP229530	KJ463482	KJ463512
Amph008	*Amphora pediculus* (Kützing) Grunow in Schmidt et al.	KJ463438	KP229536	KJ463468	KJ463498
Amph009	*Halamphora oligotraphenta* (Lange-Bertalot) Levkov	KJ463451	KP229528	KJ463481	KJ463511
Amph011	*Amphora waldeniana* Stepanek & Kociolek	KJ463447	KP229533	KJ463477	KJ463507
Amph013	*Amphora ovalis* (Kützing) Kützing	KJ463437	KP229531	KJ463467	KJ463497
Amph015	*Halamphora subturgida* (Hustedt) Levkov	TBD	TBD	TBD	TBD
Amph016	*Amphora affinis* Kützing	KJ463424	KP229535	KJ463454	KJ463484
Amph017	*Halamphora* cf. *veneta* (Kützing) Levkov	KJ463453	TBD	KJ463483	KJ463513
Amph018	*Halamphora sp. nov.*	TBD	TBD	TBD	TBD
Amph019	*Amphora indistincta* Levkov	TBD	TBD	TBD	TBD
Amph020	*Amphora pediculus* (Kützing) Grunow in Schmidt et al.	KJ463433	KP229537	KJ463463	KJ463493
Amph021	*Amphora copulata* (Kützing) Schoeman & Archibald	KJ463429	KP229534	KJ463459	KJ463489
Amph022	*Halamphora americana* Kociolek	TBD	TBD	TBD	TBD
Amph023	*Halamphora coffeaeformis* (Agardh) Levkov	KJ463448	KP229527	KJ463478	KJ463508
Amph025	*Halamphora coloradiana* Stepanek & Kociolek	KJ463450	KP229529	KJ463480	KJ463510
Amph026	*Amphora sp. nov.*	KJ463430	KP229542	KJ463460	KJ463490
Amph027	*Halamphora sp. nov.*	TBD	TBD	TBD	TBD

Amph028	*Halamphora sydowii* (Cholnoky) Levkov	TBD	TBD	TBD	TBD
Amph029	*Halamphora sp. nov.*	TBD	TBD	TBD	TBD
Amph030	*Halamphora sp. nov.*	TBD	TBD	TBD	TBD
Amph033	*Amphora sp. nov.*	TBD	TBD	TBD	TBD
Amph034	*Halamphora sp. nov.*	TBD	TBD	TBD	TBD
Amph035	*Tetramphora securicula* (Peragallo & Peragallo) Stepanek & Kociolek	KJ463435	n.d.	KJ463465	KJ463495
Amph037	*Halamphora hyalina* (Ehrenberg) Stepanek & Kociolek	KJ463441	TBD	KJ463471	KJ463501
Amph038	*Amphora sp. nov.*	KJ463443	KP229539	KJ463473	KJ463503
Amph041	*Halamphora adumbrata* (Hohn & Hellerman) Stepanek & Kociolek	TBD	TBD	TBD	TBD
Amph042	*Halamphora acutiuscula* (Kützing) Levkov	TBD	TBD	TBD	TBD
Amph043	*Halamphora sp. nov.*	TBD	TBD	TBD	TBD
Amph044	*Amphora sp. nov.*	TBD	TBD	TBD	TBD
Amph045	*Halamphora sydowii* (Cholnoky) Levkov	TBD	TBD	TBD	TBD
Amph046	*Tetramphora lineolatoides* Stepanek & Kociolek	KJ463440	n.d.	KJ463470	KJ463500
Amph047	*Halamphora semperpalorum* (Wachnicka & Gaiser) Stepanek & Kociolek	KJ463442	TBD	KJ463472	KJ463502
Amph049	*Halamphora aponina* (Kützing) Levkov	TBD	TBD	TBD	TBD
Amph050	*Halamphora sp. nov.*	TBD	TBD	TBD	TBD
Amph051	*Halamphora subtropica* (Wachnicka & Gaiser) Stepanek & Kociolek	KJ463445	TBD	KJ463475	KJ463505
Amph054	*Halamphora subtropica* (Wachnicka & Gaiser) Stepanek & Kociolek	TBD	TBD	TBD	TBD
Amph055	*Halamphora bicapitata* (Hohn & Hellerman) Stepanek & Kociolek	TBD	TBD	TBD	TBD
Amph059	*Amphora abludens* Simonsen	KJ463425	KP229540	KJ463455	KJ463485

Amph060	*Halamphora sp. nov.*	TBD	TBD	TBD	TBD
Amph061	*Halamphora hyalina* (Ehrenberg) Stepanek & Kociolek	KJ463431	TBD	KJ463461	KJ463491
Amph063	*Halamphora sp. nov.*	TBD	TBD	TBD	TBD
Amph064	*Amphora sp. nov.*	TBD	TBD	TBD	TBD
Amph066	*Amphora sp. nov.*	TBD	TBD	TBD	TBD
Amph069	*Amphora graeffeana* Hendey	TBD	TBD	TBD	TBD
Amph070	*Amphora obtusa* var. *crassa* Tempère & Peragallo	KJ463436	n.d.	KJ463466	KJ463496
Amph071	*Amphora sp. nov.*	KJ463439	KP229532	KJ463469	KJ463499
Amph072	*Amphora abludens* Simonsen	KJ463426	KP229541	KJ463456	KJ463486
Amph074	*Amphora graeffeana* Hendey	KJ463427	KP229543	KJ463457	KJ463487
Amph077	*Halamphora borealis* (Kützing) Levkov	TBD	TBD	TBD	TBD
Amph079	*Halamphora borealis* (Kützing) Levkov	TBD	TBD	TBD	TBD
Amph080	*Halamphora sp. nov.*	TBD	TBD	TBD	TBD
Amph081	*Halamphora sp. nov.*	TBD	TBD	TBD	TBD
Amph082	*Halamphora cymbifera* var. *heritierarum* (Wachnicka and Gaiser) Stepanek & Kociolek	TBD	TBD	TBD	TBD
Amph083	*Tetramphora sulcata* (Brébisson) Stepanek & Kociolek	KJ463446	n.d.	KJ463476	KJ463506
Amph085	*Amphora laevissima* Gregory	TBD	TBD	TBD	TBD
Amph086	*Halamphora sp. nov.*	KJ463428	TBD	KJ463458	KJ463488
Amph087	*Halamphora turgida* (Gregory) Levkov	KJ463434	TBD	KJ463464	KJ463494
Amph089	*Halamphora sp. nov.*	TBD	TBD	TBD	TBD
Amph093	*Halamphora sp. nov.*	TBD	TBD	TBD	TBD

Amph094	*Amphora calumetica* (Thomas in Thomas & Chase) Peragallo	TBD	TBD	TBD	TBD
Amph095	*Amphora copulata* (Kützing) Schoeman & Archibald	TBD	TBD	TBD	TBD
Amph096	*Amphora proteoides* Hustedt	TBD	TBD	TBD	TBD
Amph097	*Amphora sp. nov.*	TBD	TBD	TBD	TBD
Amph099	*Amphora gigantea* var. *fusca* (Schmidt in Schmidt et al.) Cleve	TBD	TBD	TBD	TBD
Amph100	*Halamphora americana* Kociolek	TBD	TBD	TBD	TBD
Amph101	*Halamphora coffeaeformis* (Agardh) Levkov	KJ463449	TBD	KJ463479	KJ463509
Amph102	*Halamphora aponina* (Kützing) Levkov	TBD	TBD	TBD	TBD
Amph104	*Halamphora coffeaeformis* (Agardh) Levkov	TBD	TBD	TBD	TBD
Amph105	*Halamphora coffeaeformis* (Agardh) Levkov	TBD	TBD	TBD	TBD
Amph106	*Halamphora pratensis* Stepanek & Kociolek	TBD	TBD	TBD	TBD
Amph107	*Amphora copulata* (Kützing) Schoeman & Archibald	TBD	TBD	TBD	TBD
Amph109	*Halamphora sp. nov.*	TBD	TBD	TBD	TBD
Amph110	*Halamphora sp. nov.*	TBD	TBD	TBD	TBD
Amph111	*Halamphora fontinalis* (Hustedt) Levkov	TBD	TBD	TBD	TBD
Amph112	*Halamphora sp. nov.*	TBD	TBD	TBD	TBD
Amph115	*Halamphora sp. nov.*	TBD	TBD	TBD	TBD
Amph117	*Halamphora sp. nov.*	TBD	TBD	TBD	TBD
Amph118	*Halamphora sp. nov.*	TBD	TBD	TBD	TBD
Amph119	*Halamphora taylori* (Grunow in Van Heurck) Stepanek & Kociolek	TBD	TBD	TBD	TBD
Amph121	*Halamphora pertusa* Stepanek & Kociolek	TBD	TBD	TBD	TBD

Amph122	*Halamphora cf. turgida (Gregory) Levkov*	TBD	TBD	TBD	TBD
Amph123	*Halamphora pertusa* Stepanek & Kociolek	TBD	TBD	TBD	TBD
Amph124	*Halamphora* cf. *turgida* (Gregory) Levkov	TBD	TBD	TBD	TBD
Amph125	*Halamphora cf. turgida (Gregory) Levkov*	TBD	TBD	TBD	TBD
Amph126	*Amphora commutata* Grunow in Van Heurck	KP229526	KP229545	KP229547	KP229549
Amph129	*Amphora allanta* Hohn & Hellerman	TBD	TBD	TBD	TBD
Amph130	*Halamphora margalefii* (Tomàs in Sabater et al.) Stepanek & Kociolek	TBD	TBD	TBD	TBD
Amph132	*Tetramphora chilensis* (Hustedt) Stepanek & Kociolek	KU665638	n.d.	KU665639	KU665640
Amph134	*Halamphora sp. nov.*	TBD	TBD	TBD	TBD
Amph135	*Amphora sp. nov.*	KJ463444	KP229538	KJ463474	KJ463504
Amph136	*Halamphora hyalina* (Ehrenberg) Stepanek & Kociolek	KJ463432	TBD	KJ463462	KJ463492
Amph137	*Halamphora semperpalorum* (Wachnicka & Gaiser) Stepanek & Kociolek	TBD	TBD	TBD	TBD
Amph141	*Halamphora sp. nov.*	TBD	TBD	TBD	TBD
Amph142	*Halamphora semperpalorum* (Wachnicka & Gaiser) Stepanek & Kociolek	TBD	TBD	TBD	TBD
Amph149	*Halamphora tumida* (Hustedt) Levkov	TBD	TBD	TBD	TBD
Amph153	*Halamphora sp. nov.*	TBD	TBD	TBD	TBD
Amph154	*Halamphora holsatica* (Hustedt) Levkov	TBD	TBD	TBD	TBD
Amph156	*Thalassiophysa hyalina* (Greville) Paddock & Sims	TBD	TBD	TBD	TBD
Amph158	*Halamphora sp. nov.*	TBD	TBD	TBD	TBD
Amph159	*Amphora aliformis* Stepanek, Mayama & Kociolek	TBD	TBD	TBD	TBD
Amph162	*Halamphora sp. nov.*	TBD	TBD	TBD	TBD

Amph163	*Halamphora sp. nov.*	TBD	TBD	TBD	TBD
Amph164	*Halamphora sp. nov.*	TBD	TBD	TBD	TBD
Amph165	*Halamphora pseudoholsatica* (Nagumo & Kobayasi) Stepanek & Kociolek	TBD	TBD	TBD	TBD
Amph166	*Halamphora sp. nov.*	TBD	TBD	TBD	TBD
Amph167	*Halamphora sp. nov.*	TBD	TBD	TBD	TBD
Amph168	*Halamphora subtropica* (Wachnicka & Gaiser) Stepanek & Kociolek	TBD	TBD	TBD	TBD
Amph169	*Halamphora pseudoholsatica* (Nagumo & Kobayasi) Stepanek & Kociolek	TBD	TBD	TBD	TBD
Amph170	*Amphora australiensis* John	TBD	TBD	TBD	TBD
Amph174	*Amphora australiensis* John	TBD	TBD	TBD	TBD
Amph177	*Amphora aliformis* Stepanek, Mayama & Kociolek	KP229525	KP229544	KP229546	KP229548
Amph181	*Halamphora sp. nov.*	TBD	TBD	TBD	TBD
Amph185	*Halamphora sp. nov.*	TBD	TBD	TBD	TBD
Amph192	*Halamphora sp. nov.*	TBD	TBD	TBD	TBD

APPENDIX 3

PRIMERS USED FOR AMPLIFICATION AND SEQUENCING

Primer name	Primer sequence	Reference
SSU Primers		
SSU1[a]	AAC CTG GTT GAT CCT GCC AGT	Medlin et al. 1988
SSU515+	TGG AAT GAG AAC AAT TTA A	Alverson et al. 2007
SSU850+	GGG ACA GTT GGG GGT ATT CGT A	Ruck & Theriot 2011
SSU870−	TAC GAA TAC CCC CAA CTG TCC C	Ruck & Theriot 2011
SSU1147−	AGT TTC AGC CTT GCG ACC ATA C	Alverson et al. 2007
ITS1DR[b]	CCT TGT TAC GAC TTC ACC TTC C	Edgar & Theriot 2004
LSU Primers		
D1R[a]	ACC CGC TGA ATT TAA GCA TA	Scholin et al. 1994
D2C[b]	CCT TGG TCC GTG TTT CAA GA	Scholin et al. 1994
***rbc*L Primers**		
rbcL66+[a]	TTA AGG AGA AAT AAA TGT CTC AAT CTG	Alverson et al. 2007
rbcL404+	GCT TTA CGT TTA GAA GAT ATG	Ruck & Theriot 2011
rbcL1255−	TTG GTG CAT TTG ACC ACA GT	Alverson et al. 2007
dp7−[b]	AAA SHD CCT TGT GTW AGT YTC	Daugbjerg & Andersen 1997
***psb*C Primers**		
psbC+[a]	CAC GAC CWG AAT GCC ACC AAT G	Alverson et al. 2007
psbC221+	ACG CAT TGT TTC ACC ACC	Alverson et al. 2007
psbC857−	CTT TGG TTA TGA CTG GCG TG	Alverson et al. 2007
psbC−[b]	ACA GGM TTY GCT TGG TGG AGT GG	Alverson et al. 2007

[a]Forward amplification primer used in PCR reaction.

[b]Reverse amplification primer used in PCR reaction.